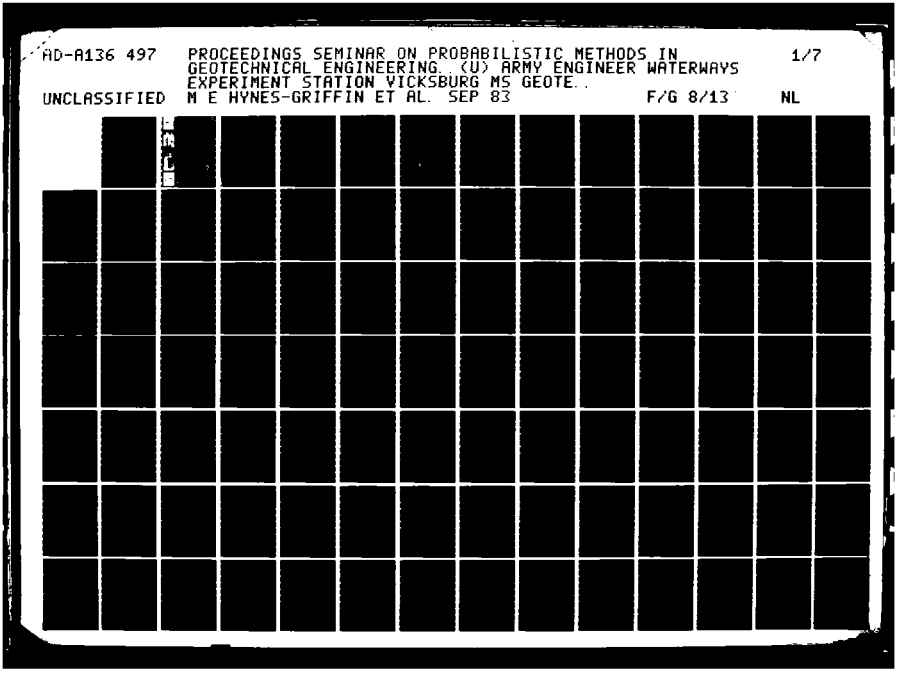
AD-A136 497
PROCEEDINGS SEMINAR ON PROBABILISTIC METHODS IN GEOTECHNICAL ENGINEERING. (U) ARMY ENGINEER WATERWAYS EXPERIMENT STATION VICKSBURG MS GEOTE..
1/7
UNCLASSIFIED
M E HYNES-GRIFFIN ET AL. SEP 83
F/G 8/13
NL

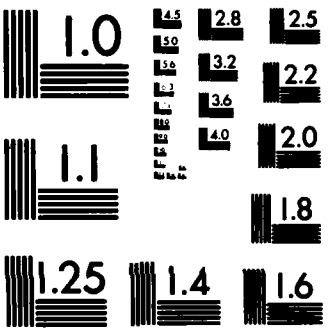

US Army Corps of Engineers

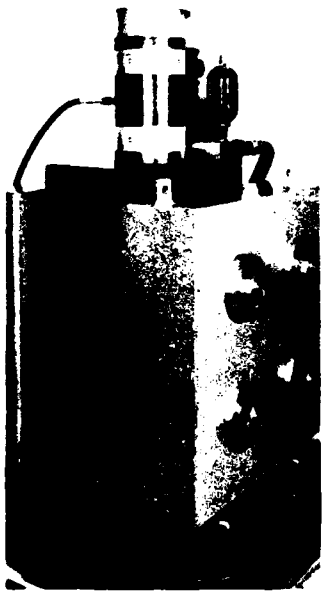

GEOTECHNICAL LABORATORY

MISCELLANEOUS PAPER GL-83-26

PROCEEDINGS, SEMINAR ON PROBABILISTIC METHODS IN GEOTECHNICAL ENGINEERING

by

Mary Ellen Hynes-Griffin, Linda L. Buege, Editors

Geotechnical Laboratory
U. S. Army Engineer Waterways Experiment Station
P. O. Box 631, Vicksburg, Miss. 39180

September 1983
Final Report

Prepared for Office, Chief of Engineers, U. S. Army
Washington, D. C. 20314
Under CWIS Work Unit 31755

Destroy this report when no longer needed. Do not return it to the originator.

The findings in this report are not to be construed as an official Department of the Army position unless so designated by other authorized documents.

The contents of this report are not to be used for advertising, publication, or promotional purposes. Citation of trade names does not constitute an official endorsement or approval of the use of such commercial products.

COMPONENT PART NOTICE

THIS PAPER IS A COMPONENT PART OF THE FOLLOWING COMPILATION REPORT:

(TITLE): Proceedings, Seminar on Probabilistic Methods in Geotechnical Engineering Held at Vicksburg, Mississippi on 21 September 1982.

(SOURCE): Army Engineer Waterways Experiment Station, Vicksburg, MS. Geotechnical Lab.

TO ORDER THE COMPLETE COMPILATION REPORT USE AD-A136 497.

THE COMPONENT PART IS PROVIDED HERE TO ALLOW USERS ACCESS TO INDIVIDUALLY AUTHORED SECTIONS OF PROCEEDINGS, ANNALS, SYMPOSIA, ETC. HOWEVER, THE COMPONENT SHOULD BE CONSIDERED WITHIN THE CONTEXT OF THE OVERALL COMPILATION REPORT AND NOT AS A STAND-ALONE TECHNICAL REPORT.

THE FOLLOWING COMPONENT PART NUMBERS COMPRISE THE COMPILATION REPORT:

AD#:		TITLE:
P002 382		Applications of Probabilistic Methods in Geotechnical Engineering. Part 1. Simplified Reliability Analyses for Geotechnical Problems.
P002 383		Applications of Probabilistic Methods in Geotechnical Engineering. Part 2. Analysis of Documented Case Histories Using a Stochastic Model for Seismically Generated Pore Pressure and Shear Strain Potential.
P002 384		Probabilistic Seismic and Geotechnical Evaluation at a Dam Site.
P002 385		Probabilistic Slope Stability Methodology.
P002 386		Probability of Liquefaction in a 3-D Soil Deposit.
P002 387		Probabilistic Design of Flood Levees.
P002 388.		Probabilistic and Statistical Methods for Determining Rock Mass Deformability Beneath Foundations: An Overview.
P002 389		Simple Statistical Methodology for Evaluating Rock Mechanics Exploration Data.
P002 390		New Development in Statistical Techniques for Analyzing Rock Slope Stability.

Unclassified

SECURITY CLASSIFICATION OF THIS PAGE (When Data Entered)

REPORT DOCUMENTATION PAGE		READ INSTRUCTIONS BEFORE COMPLETING FORM
1. REPORT NUMBER Miscellaneous Paper GL-83-26	2. GOVT ACCESSION NO. AD-A136 497	3. RECIPIENT'S CATALOG NUMBER
4. TITLE (and Subtitle) PROCEEDINGS, SEMINAR ON PROBABILISTIC METHODS IN GEOTECHNICAL ENGINEERING		5. TYPE OF REPORT & PERIOD COVERED Final report 6. PERFORMING ORG. REPORT NUMBER
7. AUTHOR(s) Mary Ellen Hynes-Griffin and Linda L. Buege, Editors		8. CONTRACT OR GRANT NUMBER(s)
9. PERFORMING ORGANIZATION NAME AND ADDRESS U. S. Army Engineer Waterways Experiment Station Geotechnical Laboratory P. O. Box 631, Vicksburg, Miss. 39180		10. PROGRAM ELEMENT, PROJECT, TASK AREA & WORK UNIT NUMBERS CWIS Work Unit 31755
11. CONTROLLING OFFICE NAME AND ADDRESS Office, Chief of Engineers, U. S. Army Washington, D. C. 20314		12. REPORT DATE September 1983 13. NUMBER OF PAGES 589
14. MONITORING AGENCY NAME & ADDRESS(if different from Controlling Office)		15. SECURITY CLASS. (of this report) Unclassified 15a. DECLASSIFICATION/DOWNGRADING SCHEDULE

16. DISTRIBUTION STATEMENT (of this Report)

Approved for public release; distribution unlimited.

17. DISTRIBUTION STATEMENT (of the abstract entered in Block 20, if different from Report)

18. SUPPLEMENTARY NOTES

Available from National Technical Information Service, 5285 Port Royal Road, Springfield, Va. 22161.

19. KEY WORDS (Continue on reverse side if necessary and identify by block number)

Geotechnical engineering
Probability theory
Rock mechanics
Soil mechanics

20. ABSTRACT (Continue on reverse side if necessary and identify by block number)

This report represents the work of eight researchers who have done extensive studies of probabilistic methods in Geotechnical Engineering. The papers were presented before OCE, Division Representatives, and WES personnel at the seminar on Probabilistic Methods in Geotechnical Engineering held in Vicksburg, Miss. on 21 September 1982, to determine whether probabilistic methods offer advantages over the deterministic approaches now used.

DD FORM 1 JAN 73 1473 EDITION OF 1 NOV 65 IS OBSOLETE

Unclassified

SECURITY CLASSIFICATION OF THIS PAGE (When Data Entered)

Preface

The seminar on Probabilistic Methods in Geotechnical Engineering was held 21 September 1982 at the Geotechnical Laboratory (GL), U. S. Army Engineer Waterways Experiment Station, Vicksburg, Miss. The seminar was sponsored by the Office, Chief of Engineers (OCE), U. S. Army, under the Civil Works Investigational Studies (CWIS), Rock Research Program (Work Unit 31755) on Probabilistic Methods in Engineering Geology, which was monitored for OCE by Mr. Paul Fisher.

The seminar was organized and coordinated by Mmes. Mary Ellen Hynes-Griffin and Linda L. Buege, Earthquake Engineering and Geophysics Division (EE&GD), GL, under the general supervision of Dr. A. G. Franklin, Chief, EE&GD, and Dr. William F. Marcuson III, Chief, GL. This report which documents the proceedings of the seminar was edited by Mmes. Hynes-Griffin and Buege.

COL Tilford C. Creel, CE, was Commander and Director of WES during the preparation of this report. Mr. Fred R. Brown was Technical Director.

Contents :

Introduction

During the past few years, researchers have developed alternative approaches based on probability and statistics to geotechnical planning, design, analysis, and performance assessments. Much of the basic research for these probabilistic methods has been done. The question now is: Are these methods sufficiently developed so that they can be tailored to conform to Corps of Engineers policies and be incorporated into Corps geotechnical activities? To address this question, researchers and practitioners met at the U. S. Army Engineer Waterways Experiment Station, Vicksburg, Miss., 21 September 1982, to present potentially useful probabilistic methods which they have applied to their own work. This report contains eight papers responding to the challenge.

The eight papers are divided into two categories: soil mechanics (five papers) and rock mechanics (three papers). The papers occur in these proceedings in the same order in which they were presented at the seminar. The participants at the seminar were informed that an attempt would be made to record the discussions that followed each paper and an open discussion towards the end of the seminar program. Unfortunately, only a small portion of the discussion was successfully recorded. This brief discussion is included next in these proceedings. The eight papers follow these discussions.

This seminar was convened and these proceedings were published to benefit the entire geotechnical community. These proceedings present the opinions of the participants and do not represent official positions of the U. S. Army Coprs of Engineers or any agency which supported work presented herein.

Discussion

Ed Pritchett: I would like to ask you for your comments on a particular subject. The Corps of Engineers, like many other Federal agencies in the dam building business, is being strongly encouraged to use "risk based analyses" and to quantify the safety of their structures. Now, I have no doubts that we can use these methods in dealing with hydrologic events such as the probability of exceeding the storage capacity of a reservoir. I also have no doubts that we can use these methods to make assessments of earthquake hazards using current state-of-the-art procedures. But, what I am concerned about is that we, in the Corps, are being asked to quantify the probability of failure of very complex structures such as an earth embankment dam that has been in existence for 50 years. We are asked to quantify geotechnical issues, in the long-term behavior and safe performance of an earth dam, such as, internal deteriorations or lack of adequate design coverage of special geologic phenomena. We are being encouraged by FEMA* and others to quantify the probability of failure of these structures. I do not personally believe that the industry is ready to do this, and I would like to hear your comments. I am not talking about hydrologic or earthquake events. I am talking about straightforward geotechnical problems. We have embankments founded on karstic terrain and a number of other conditions that constantly require costly maintenance. Large amounts of money are spent to continually evaluate and attempt to fix these problem dams. My concern is that we are being asked to determine the probability of failure for these complex structures that suffer from geotechnical problems that are difficult to quantify in terms of their threat to the overall safety of the dam. I do not believe the industry has the techniques they need to meet this demand.

David Bowles: I do not believe the necessary tools are advanced to the point where you can estimate the absolute probability of failure for the whole range of causes that affect the stability of an earth dam. But we are not too far away from the possibility of developing a relative ranking of dams in terms of their likelihood of failure or perhaps the consequences of failure. Using such techniques, you would then be able to organize dams into groups according to their relative risk of failure or the consequences of failure, distinguish those that meet established safety criteria, and to prioritize the expenditure of available funds for remedial or preventative measures on problem structures.

---

* Federal Emergency Management Association.

Ed Pritchett: Any agency involved with dams already has that reponsibility to make decisions.

Richard Davidson: I think you almost always have a problem trying to rank a whole series of dams in terms of "safe" or "unsafe." There are loads that are unsafe for hydrologic reasons as well as a number of geotechnical reasons such as slope stability, tension cracks, or piping. The only way I see that you can make a rational economic comparison between spending money on widening the spillway of a dam or flattening the slope of a dam is if the absolute probability of failure is known. . . . Even after you have assessed the potential damages resulting from each mode of failure, I do not see any rational basis for deciding between a reasonably good estimate of the actual probability of failure.

Loren Anderson: Are you talking about two different dams?

Richard Davidson: Right.

Loren Anderson: And do I spend my money on this dam or that dam?

Richard Davidson: Right.

Loren Anderson: I am familiar with a dam in the west where they have identified that they have a possible problem of liquefaction of the foundation. They are planning on spending several hundred million dollars in order to preclude the possibility of liquefaction or at least reduce the risk of liquefaction and failure by that particular means. This issue came about after the Lower San Fernando slide, when everyone became concerned about the possibility of liquefaction. Suppose you look at all your dams where liquefaction might be a problem (and it looks like it is in this particular case) and you make a decision to spend a couple hundred million dollars to reduce the risk due to liquefaction. It seems to me that the thing you also have to do is ask yourself, "Have I changed the overall risk of failure for this particular dam?" Unless you looked at some type of risk based analysis, you cannot say that. Maybe you have spent a couple hundred million dollars and you have not changed the probability of failure a significant amount, because maybe there are other mechanisms that are much more important than liquefaction.

Dimitri Grivas: I would like to make a comment. If one refers to possible mechanisms of failure for which one has no experience or which one cannot easily quantify, such as piping, it is very limited what probability theory can do. It is desirable to first have a model of the mechanics of the problem.

Ed Pritchett: We, the Corps, are being asked to quantify the safety of earth dams, excluding external stimuli such as earthquakes. These groups are interested in actually quantifying the overall safety of an embankment and all the geotechnical parameters that contribute to its safety. We are being strongly encouraged to develop a single quantity for the probability of failure. As we all know, the problem is far more complex than the experience or sufficiently developed probabilistic methods to compute the overall probability of failure for a particular earth dam.

Erik Vanmarcke: I disagree that we have no information whatsoever. We have criteria. We even have certain facts of failure. I would have to say that we are not in the position to quantify such a probability; however, I think it is clear that here we have the needed opportunity to try to solve for this probability and to quantify the risk caused by internal and external technique, which is quite powerful. This would permit more logical decision-making in terms of remedial action. I think it is the duty of research and probably also the duty of enlightened authors to try to go forward in this area, because I think there is an opportunity for making a major impact on the way that you professionally operate.

Dimitri Grivas: Certainly, but we should not start with probability theory if we do not know how a failure happened. I think we have to examine the problem from a mechanics point of view first, and then develop the probability from what we know.

Gregory Baecher: In my view, the answer to Ed Pritchett's original question is, yes. I think that useful and realistic probabilities of failures for specific dams can be estimated. On the other hand, I would put forward that there is no way we can analytically verify the probability of failure for a specific structure. By "analytically verify" I mean using probability theory to establish deductively that the probability of a certain type of failure for a particular structure is some fixed value. If we are to estimate the probability of failure for a specific structure--and I am convinced that we can--we must do so on the basis of statistics, empiricism, and judgement.

Let me suggest a familiar number. We all know that, roughly, the rate of catastrophic failure of well-built dams is on the order of 10^{-4} (per dam-year) give or take a little. Therefore, if we are considering a structure that is less well built than average, was built by less competent authority, less experienced contractor, or benefitted from less engineering analysis,

then as a first estimate the probability of failure for that structure, by all causes, should be greater than 10^{-4}. Conversely, if all such indicators are good, then the probability should be below 10^{-4}.

It is not at all out of the question to begin our attempts to establish probabilities by doing two things: First, develop a list of critical indicators of dam safety, and evaluate that list of indicators against existing dams and dam failures. This provides information on the frequency with which those indicators are associated with safe or unsafe performance, and this information can be used to judge an individual structure. Second, attempt to incorporate expert judgement within the calibration or correlation analysis. Such judgement could enter at three places: in selecting critical indicators, determining the correlation of those indicators with failed and unfailed dams, and modifying the results of final analysis to account for intangibles.

A statistical approach like this one is a vehicle for systematically combining the information we have about a particular dam. Pinning the analysis--and, therefore, the relative rankings of dams--to a historical base rate is a means for calibrating the probabilistic predictions. Approaches like these are common in other fields. They may not do everything we would like, and they may not be as precise as would be convenient, but they demonstrate that we need not be so pessimistic about what is possible. However, such a risk assessment would not come cheaply if we want the answers to mean anything. The cost of PRS's (probabilistic risk analyses) for nuclear power plants is itself empirical proof.

SOIL MECHANICS PROGRAM

APPLICATIONS OF PROBABILISTIC METHODS IN GEOTECHNICAL ENGINEERING

by

Edward Kavazanjian, Jr.
Jean-Lou Chameau
G. Wayne Clough
Tarik Hadk-Hamou

APPLICATIONS OF PROBABILISTIC METHODS IN GEOTECHNICAL ENGINEERING

PART I

SIMPLIFIED RELIABILITY ANALYSES FOR GEOTECHNICAL PROBLEMS

TABLE OF CONTENTS - PART I

LIST OF TABLES - PART I

LIST OF FIGURES - PART I

LIST OF EXAMPLES - PART I

1.0 INTRODUCTION

The increasing use of probabilistically based risk evaluation and decision analysis procedures on major Civil Engineering projects has led to a mandate for the development of probabilistic methods in Geotechnical Engineering. Because the "probability of failure" is assumed to represent an index of the safety or reliability of a system, probabilistic models can be used to assess the overall reliability or safety of a system composed of several sub-systems in series or parallel combinations and to evaluate tradeoffs between design alternatives which entail different costs and levels of risk. Originally restricted primarily to nuclear power plant design, probabilistic analyses are now used in offshore, seismic, and dam engineering and in a variety of other geotechnical problems.

Despite an increasingly strong mandate from both the public and private sectors, development and implementation of probabilistic methods in geotechnical engineering has met with substantial resistance from practioners within the field. Much of this resistance seems to stem from a lack of familiarity of the practicing engineers with probabilistic analyses and the interpretation of their results. At worst, a probabilistic method in which design is geared to a subjectively chosen probability of failure is little different from and has relatively few advantages over conventional factor of safety analyses. At best, probabilistic methods present a powerful new tool which incorporates more information into the safety assessment than factor-of-safety methods. Probabilistic methods force the engineer to quantify previously subjective judgments about parameter uncertainty, allowing him to better communicate those judgments to other engineers. Probabilistic models can be used for optimization studies, for combining modes of failure, for risk and decision analyses, and for sensitivity studies.

In general, probabilistic models in geotechnical engineering can be split into two classes, probability models and lumped parameter reliability models. In a probability model, uncertainty is assigned to each parameter at the beginning of the analysis and these uncertainties are

propagated throughout the analysis to arrive at a probabilty of failure. In a lumped parameter reliability model, uncertainty about all design parameters are lumped together into gross capacity (or resistance) and demand (or load) terms. Probability models, when available, are useful for sensitivity studies and are analytically more rigorous than lumped parameter models. The advantage of the lumped capacity-demand models are that they can be used for highly non-linear problems and that conventional factor of safety analyses can be readily converted into probabilistic analyses using this approach.

Two of the major obstacles to the use of probabilistic analyses in geotechnical engineering are the lack of well documented case studies which show the applicability of existing probabilistic methods and provide the engineer guidance in choosing model parameters and the lack of probabilistic analyses for many common geotechnical problems.

For many geotechnical problems, probabilistic design analysis are not currently available. In Part I of this report, methods for converting conventional design analyses into reliability analyses by lumping all variability into demand and capacity terms are described. Design examples in bearing capacity and slope stability analyses are presented. The advantage of these methods is not only that they allow for the calculation of probabilities of failure, but that they allow the design engineer to use methods of analysis with which he is familiar and has confidence in, allowing him to use his experience and subjective judgment in choosing design parameters.Because most geotechnical engineers are not familiar with probabilistic concepts, the subjective selection of design parameters inherent to most geotechnical analyses is a major problem in applying probabilistic design analyses. Only through the development of documented case studies in which probabilistic methods are applied can the necessary experience with choosing probabilistic parameters be accumulated. In Part II of this report, a stochastic model for the generation of seismically induced pore pressure and shear strain in cohesionless soil is used to analyze documented case histories in order to develop this requisite experience and show the validity of the model.

In the remainder of this introduction, definitions of the basic elements of probabilistic models are presented for the geotechnical engineer not familiar with the concepts of reliability and probability theory.

Definitions

Probability Density Function: Instead of characterizing parameters by deterministic values, probabilistic models use Probability Density Functions (PDF). The PDF of a continuous random variable X, $f_X(x)$, describes the relative frequency of X. The PDF is not a probability. However, $f_X(x)\,dx$ is the probability that the value of X falls between x and $x + dx$. In accordance with the axioms of probability theory, $f_X(x)$ must be non-negative and the integral of $f_X(x)$ over all values of X (the area under the PDF) must equal 1.0.

A variety of closed form mathematical functions are commonly used for PDF's, including the Gaussian or normal distribution, log-normal, exponential, extreme value, and Rayleigh distributions. Empirical distributions such as the beta distribution are also common. The reader is referred to a basic probability text for the actual form of these function (Ang and Tang, 1975; Benjamin and Cornell, 1970; Harr, 1977). These distributions are generally characterized by their mean value and standard of deviation. The mean or expected value is the centroid of the PDF and is the first moment of the PDF about the origin. The standard deviation is a measure of the dispersion of the PDF. The standard deviation is the square root of the variance of X, Var (x). The variance of X is the second moment of the PDF about the mean value and equals the mean square value of X minus the square of the mean. The coefficient of variation is the ratio of the standard deviation to the mean and is a convenient non-dimensional measure of dispersion or variability.

Cumulative Density Function: The Cumulative Density Function (CDF) of the random variable X, $F_X(x)$, is the integral of the PDF. The CDF represents the probability that X is less than or equal to x. The CDF

equals zero at minus infinity and one at plus infinity, increases monotonically with x, and is continuous with x. Any function possessing these characteristics is acceptable as a CDF, and its derivative is then the PDF.

Safety Margin: The Safety Margin, SM, of a system is defined as the capacity of the system minus the demand. If the safety margin is greater than zero, the system is expected to be safe. The probability of failure is the probability that the safety margin is less than zero, or that the factor of safety is less than 1.0.

Reliability Index: The Reliability Index, β, is the ratio of the calculated mean safety margin to the standard deviation of the safety margin. β describes how far above zero in number of standard deviations the calculated average safety margin is. If the shape of the distribution is known, β can be related to the probability of failure.

2.0 *LUMPED PARAMETER CAPACITY - DEMAND MODELING*

Introduction

While rigorous probabilistic models are most satisfying for calculating probabilities of failure from an analytical point of view, relatively few such models exist for geotechnical problems and there is little experience with using these models in design practice. Furthermore, for many non-linear numerical problems it is not feasible to develop stochastic models. To compensate for this lack of acceptable probabilistic models, techniques for using conventional discrete analyses to arrive at factors of safety have been developed. Sophisticated simulation techniques allow the engineer to determine the distribution of output variables in discrete analyses by varying the input parameters accordingly. While sophisticated simulation techniques are extremely useful, they remain too detailed for a large variety of geotechnical design problems. In this report, simple methods for estimating the moments of the probability density function of the factor of safety or safety margin from conventional analyses are described. By assuming a shape for the PDF, these moments can be used to calculate the probability of failure. Examples of the use of this method are presented for bearing capacity and slope stability problems.

Reliability - General Definitions

Design methods in geotechnical engineering usually involve comparing the capacity (resistance) of a structure to the applied demand (loading). Conventionally this is addressed through a factor of safety approach which seeks to minimize the maximum tolerable risk. Lower limits of capacity (C_{design}) and upper limits of demand (D_{design}) are compared at a critical point. The factor of safety is:

$$FS = \frac{C_{design}}{D_{design}} \quad . \tag{1}$$

In this approach the natural variability and/or uncertainty associated with material parameters is overlooked. Probabilistic techniques take

this variability into account by considering both the capacity and the demand to be random variables. These variables are defined by probability density functions $f_C(C)$ and $f_D(D)$ which describe the variations of C and D about their mean values $\bar{C}$ and $\bar{D}$, respectively. In the capacity-demand model, the probability of failure is defined as:

$$p(\text{failure}) = p\ (C - D < 0) \tag{2}$$

or

$$p(\text{failure}) = p\ (SM < 0) \tag{3}$$

where SM, the difference between the variables C and D, is called the safety margin. The complement of the probability of failure is commonly known as the reliability R:

$$R = 1 - p(\text{failure}) \quad . \tag{4}$$

Given the probability density functions of the capacity and the demand the probability of failure can be expressed as:

$$p(\text{failure}) = \int_{-\infty}^{+\infty} \int_{-\infty}^{D} f_C(C)\ f_D(D)\ dC\ dD \tag{5}$$

or

$$p(\text{failure}) = \int_{-\infty}^{+\infty} F_C(D)\ f_D\ (D)\ dD \tag{6}$$

where $F_C(D)$ is the cumulative distribution function of the capacity C.

In the case where the probability density functions of both the resistance and the loading are known and have simple analytical expressions the probability of failure may be determined analytically. The probability of failure is given in Table 1 for several common distributions, assuming C and D do have the same distribution (Grivas, 1979).

TABLE 1. PROBABILITY OF FAILURE FOR SOME EMPIRICAL MODELS

(from Grivas, 1979)

DISTRIBUTION OF C AND D	$f_C(c)$	$f_D(D)$	P_f
uniform	$\frac{1}{C_{max} - C_{min}}$	$\frac{1}{D_{max} - D_{min}}$	$\frac{1}{2}\frac{D_{max} - 2C_{min} + D_{min}}{C_{max} - C_{min}}$
exponential	$a_C \exp(-a_C C)$	$a_D \exp(-a_D D)$	$\frac{a_D}{a_C + a_D}$
normal	$\frac{1}{S_C\sqrt{2\pi}} \exp[-\frac{1}{2}(\frac{C-\bar{C}}{S_C})^2]$	$\frac{1}{S_D\sqrt{2\pi}} \exp[-\frac{1}{2}(\frac{D-\bar{D}}{S_D})^2]$	$\frac{1}{2}\,\mathrm{erf}[\frac{\bar{C} - \bar{D}}{\sqrt{(S_C^2 + S_D^2)}}]$ [A]
log-normal	$\frac{1}{CS_{\ln}\sqrt{2\pi}} \exp[-\frac{1}{2}(\frac{\ln C - \overline{\ln C}}{S_{\ln C}})^2]$	$\frac{1}{DS_{\ln D}\sqrt{2\pi}} \exp[-\frac{1}{2}(\frac{\ln D - \overline{\ln D}}{S_{\ln D}})^2]$	$\frac{1}{2}\,\mathrm{erf}[\ln(\frac{\bar{C}}{\bar{D}}\sqrt{\frac{1+V_D^2}{1+V_C^2}}) / \sqrt{\ln(1+V_C^2)(1+V_D^2)}]$ [A]
Rayleigh	$a_C C \exp(-a_C C^2/2)$	$a_D D \exp(-a_D D^2/2)$	$\frac{4a_C(a_C+2a_D)}{a_D(a_C+a_D)}$
gamma	$\frac{\lambda^n C^{n-1} e^{-\lambda C}}{\Gamma(n)}$	$\frac{\mu^m D^{m-1} e^{-\mu D}}{\Gamma(m)}$	$1 - \frac{\Gamma(m+n)}{\Gamma(m)\Gamma(n)} B_{\mu/(\mu+\lambda)}(m,n)$ [A]
beta	$\lambda_C (C-C_{min})^{\alpha_C - 1} (C_{max}-C)^{\beta_C - 1}$	$\lambda_D (D-D_{min})^{\alpha_D - 1} (D_{max}-D)^{\beta_D - 1}$	$\lambda_D \int_{D_{min}}^{D_{max}} \frac{B_u(\alpha_C,\beta_C)}{B(\alpha_C,\beta_C)} (D-D_{min})^{\alpha_D - 1} (D_{max}-D)^{\beta_D - 1}\, dD$ [A]
Weibull	$\frac{\beta_C}{\theta_C}(\frac{C-C_{min}}{\theta_C})^{\beta_C - 1} \exp[-(\frac{C-C_{min}}{\theta_C})^{\beta_C}]$	$\frac{\beta_D}{\theta_D}(\frac{D-D_{min}}{\theta_D})^{\beta_D - 1} \exp[-(\frac{D-D_{min}}{\theta_D})^{\beta_D}]$	$\int_0^\infty e^{-y} \exp[-[\frac{\theta_C}{\theta_D} y^{1/\beta_C} + (\frac{C_{min}-D_{min}}{\theta_D})]^{\beta_D}]\, dy$

[A] Note: erf [ ] = error function
B ( ) = beta function
B_u ( ) = incomplete beta function, $u = (C-C_{min})/(C_{max}-C_{min})$

When the distributions of C and D are not known, which is the most common case, a distribution must be prescribed for C - D. For analytical simplicity, the Gaussian normal distribution is usually favored for C - D. The probability of failure is:

$$p(\text{failure}) = 1 - F_u \left(\frac{\bar{C} - \bar{D}}{\sqrt{\sigma_C^2 + \sigma_D^2}} \right) \tag{7}$$

in which F_u is the tabulated CDF of the standard normal variate, and σ_C and σ_D are standard deviations of the capacity and demand, respectively.

Empirical distributions such as the beta distribution can also be used to solve the capacity-demand problem. In this case, the capacity and demand are defined by four parameters: mean value, standard deviation or coefficient of variation, lower limit, and upper limit. The probability of failure is computed by numerical integration of Eq. 5. The beta distribution has been shown to fit important soil parameters such as cohesion intercept and friction angle well (Harr, 1977). The main characteristics of this distribution are summarized in Appendix A.

An alternative approach to the capacity-demand problem is to treat the factor of safety FS (= C/D) as a random variable and define the probability of failure as:

$$P(\text{failure}) = P\left[C/D < 1\right] = p\left[FS < 1\right] \tag{8}$$

The lognormal distribution is usually prescribed for FS (Ln FS normally distributed) for analytical simplicity, but the beta-distribution between prescribed limits is also a possibility.

A design methodology can be based on requiring that the probability of failure must be below a specified value, or calculated risk. Alternatively it may be required that the average safety margin $\overline{SM} = \bar{C} - \bar{D}$ must lie at least β standard deviations above zero:

$$\overline{SM} = \beta \, \sigma_{SM} = \beta \sqrt{\sigma_C^2 + \sigma_D^2} \tag{9}$$

β is usually called the safety index or reliability index. The mean design capacity is:

$$\overline{C} = \overline{D} + \beta \sqrt{\sigma_C^2 + \sigma_D^2} \tag{10}$$

If C and D are normal variates β can be simply relted to the probability of failure by:

$$\beta = F_u^{-1}(1 - P(\text{failure})) \tag{11}$$

Alternatively a reliability index β' can be defined with respect to the safety factor (LnFS normal variate) leading to:

$$\overline{C} = \overline{D} \sqrt{\frac{1 + V_C^2}{1 + V_D^2}} \exp\left[\beta' \sqrt{\text{Ln}\,(1 + V_C^2)(1 + V_D^2)}\right] \tag{12}$$

If V_C and D_D are not large, say ≤ 0.30, Eq. 13 can be simplified to (Ang and Cornell, 1974):

$$\overline{C} = \overline{D} \exp\left[\beta' \sqrt{V_C^2 + V_D^2}\right] \tag{13}$$

The relation between β' and the probability of failure is also given by Eq. 12. A reliability index can also be established in the case of beta-variates, but its relation to the probability of failure must be obtained numerically.

Moment Estimation

The capacity C and demand D in a typical design problem are usually functions of other variables. As an example, the resistant moment of a soil slope about the center of a failure circle is a function of the cohesion intercept, angle of friction and unit weight of the soil. The basic soil parameters (angle of friction, cohesion intercept, etc.) can usually be described in terms of their mean values and coefficient of variation. Techniques are necessary to determine the statistical characteristics of the dependent variables, such as C and D, from the given moments of the

independent variables. If the moments of C and D are known, the reliability index can be calculated and, by assuming a shape for the probability distributions, the probability of failure can be estimated.

1. Taylor Series

If a random variable y is defined by a function f (x_1, x_2, .. x_n) of N independent random variables, it can be shown that the expected value and variance of y can be approximated by (Hahn and Shapiro, 1967 and Benjamin and Cornell, 1970):

$$\bar{y} = f(\bar{x}_1, \bar{x}_2, .. \bar{x}_N) + \frac{1}{2} \sum_{i=1}^{N} \frac{\partial^2 f}{\partial x_i^2} \sigma_{x_i}^2 \qquad (14)$$

$$Var(y) = \sum_{i=1}^{N} \left(\frac{\partial f}{\partial x_i}\right)^2 \sigma_{x_i}^2 \qquad (15)$$

with all the derivatives evaluated at their respective mean values. These equations are obtained from a Taylor expansion of the function about the expectations of the random variables. Equation 13 is a second-order approximation for the mean while Equation 14 is a first order approximation for the variance. These approximations require the function f(X) to be sufficiently well behaved and the derivatives to exist.

2. Point Estimates for Probability Moments

The approximate formulas obtained from the Taylor expansion require the function to be well behaved. The computation of derivatives is very often cumbersome or even impossible when the function is given by charts or graphs. These difficulties can be overcome through use of point estimates of the function (Rosenblueth, 1974 and 1975 and Guymon, Harr, Berg, and Hromadka, 1981).

2.1 Function of one random variable

Let X be a random variable with known probability moments and probability density function $f_X(x)$, and y be a random variable function of X, $y = y(x)$. The approximation for the moments of the distribution

of y can be obtained by "replacing" the distribution of X by two-point estimates, p_- and p_+, concentrated at x_- and x_+, respectively, and satisfying the following conditions:

$$p_+ + p_- = 1 \tag{16a}$$

$$p_+ x_+ + p_- x_- = \bar{X} \tag{16b}$$

$$p_+ (x_+ - \bar{X})^2 + p_- (x_- - \bar{X})^2 = \sigma_x^2 \tag{16c}$$

$$p_+ (x_+ - \bar{X})^3 + p_- (x_- - \bar{X})^3 = \gamma \sigma_x^3 \tag{16d}$$

where $\bar{X}$, σ_x, and γ are the mean, standard deviation, and coefficient of skewness of the variable X, respectively. Solution of these equations leads to:

$$p_+ = \frac{1}{2}\left[1 \mp \left(1 - \frac{1}{1 + \left(\frac{\gamma}{2}\right)^2}\right)^{1/2}\right] \tag{17a}$$

$$p_- = 1 - p_+ \tag{17b}$$

$$x_+ = \bar{X} + \sigma_X (p_+ p_-)^{1/2} \tag{17c}$$

$$x_- = \bar{X} - \sigma_X (p_-/p_X)^{1/2} \tag{17d}$$

In Equation 17a the sign preceding the radical is that of $-\gamma$. If $f_X(X)$ is approximated by the estimates p_- and p_+, the moments of y can be approximated by:

$$\bar{Y} = E(Y) = p\, y_- + p_+ y_+ \tag{18a}$$

$$E(Y^2) = p\, y_-^2 + p_- y_-^2 \tag{18b}$$

and in general:

$$E(Y^n) = p_- y_-^n + p_+ y_+^n \tag{18c}$$

with

$$y_- = Y(x_-) \text{ and } y_+ = Y(x_+) \quad .$$

When X has a symmetrical distribution, $\gamma=0$, then $p_+ = p_- = 1/2$ and $x_\pm = \bar{X} \pm \sigma_X$. It follows that:

$$\bar{Y} = \frac{y_+ + y_-}{2} \tag{18d}$$

$$\sigma_Y = \left| \frac{y_+ - y_-}{2} \right| \tag{18e}$$

2.2 Functions of several variables

The procedure has been generalized to functions of several random variables (Rosenblueth, 1974). For two variables, X_1 and X_2:

$$E(Y^n) = p_{++}\, y^n_{++} + p_{+-}\, y^n_{+-} + p_{-+}\, y^n_{-+} + p_{--}\, y^n_{--} \tag{19}$$

where

$$y_{\pm\pm} = Y\left(\bar{X}_1 \pm \sigma_{X1},\ \bar{X}_2 \pm \sigma_{X2}\right)$$

and, if X_1 and X_2 have symmetrical distributions, $p_{\pm\pm} = 1/4$. For three variables X_1, X_2, X_3:

$$E(Y^n) = p_{+++}y^n_{+++} + p_{++-}y^n_{++-} + \ldots + p_{--+}y^n_{--+} + p_{---}y^n_{---} \tag{20}$$

Equation 20 has $2^3 = 8$ terms on its right hand-side with $y_{\pm\pm\pm} = Y\left(\bar{X}_1 \pm \sigma_{X1},\ \bar{X}_2 \pm \sigma_{X2},\ \bar{X}_3 \pm \sigma_{X3}\right)$ and $p_{\pm\pm\pm} = \frac{1}{2^3} = \frac{1}{8}$. The expressions are similar for four or more random variables.

The technique can be extended to correlated random variables. As an example, Equation 20 is still valid for three correlated random variables with the magnitudes of the concentrations being:

$$p_{+++} = p_{---} = \frac{1}{2^3}\left(1 + \rho_{12} + \rho_{23} + \rho_{31}\right) \tag{21a}$$

$$p_{++-} = p_{--+} = \frac{1}{2^3}\left(1 + \rho_{12} - \rho_{23} - \rho_{31}\right) \tag{21b}$$

$$p_{+-+} = p_{-+-} = \frac{1}{2^3}\left(1 - \rho_{12} - \rho_{23} + \rho_{31}\right) \tag{21c}$$

$$p_{+--} = p_{-++} = \frac{1}{2^3}\left(1 - \rho_{12} + \rho_{23} - \rho_{31}\right) \tag{21d}$$

where ρ_{ij} is the coefficient of correlation of the random variables X_i and X_j, and the sign in front of ρ_{ij} is defined by the multiplicative rule (++ = -- = +; +- = -+ = -).

In the balance of this section, general principles of simplified lumped parameter reliability modeling and the application of these principles to slope stability and bearing capacity analyses are illustrated.

3.0 EXAMPLES OF APPLICATIONS

3.1 Shear Strength

The Mohr-Coulomb failure criteria describes the shear strength of soil, τ_f, as a function of the normal effective stress on the failure plane, σ', the angle of internal friction, ϕ', and the effective cohesion, C', as shown in Equation 17).

$$\tau_f = \sigma' \tan \phi' + C' \tag{22}$$

If the mean and variance of σ', tan ϕ', and C' are known, both the Taylor series approximation and point estimates can be used to find the mean and variance of τ_f.

Since the second derivatives of Equation 22 are zero, Equation 14 gives the Taylor series expansion for the mean of the shear strength as:

$$\bar{\tau}_f = \bar{\sigma}' \overline{\tan \phi'} + \bar{C}' \tag{23a}$$

Using Equation 15 to evaluate the variance of the shear strength, Var (τ_f), results in:

$$\text{Var}\left(\tau_f\right) = \left(\bar{\sigma}'\right)^2 \text{Var}\left(\tan \phi'\right) + \text{Var}\left(C'\right) + \left(\overline{\tan \phi'}\right)^2 \text{Var}\left(\phi'\right) \tag{23b}$$

If we assume that τ_f has a symmetrical distribution, we can use Equation 20 to estimate the moments of τ_f. Assuming the three random variables in Equation 22 to be uncorrelated leads to Equations 24 for the first and second moments of τ_f:

$$E\left(\tau_f\right) = \frac{1}{8}\left[\tau_{+++} + \tau_{++-} + \ldots + \tau_{--+} + \tau_{---}\right] \tag{24a}$$

$$E\left(\tau_f^2\right) = \frac{1}{8}\left[\tau_{+++}^2 + \tau_{++-}^2 + \ldots \tau_{--+}^2 + \tau_{---}^2\right] \tag{24b}$$

The variance of τ_f can be evaluated using Equation 24c:

$$\text{Var}\ (\tau_f) = E\ (\tau_f^2) - E^2\ (\tau_f) \tag{24c}$$

The values of the parameters $\tau_{\pm\pm\pm}$ are evaluated as

$$\tau_{\pm\pm\pm} = [(\bar{\sigma}' \pm \sigma_{\sigma'})(\overline{\tan \phi'} \pm \sigma_{\tan \phi'}) + (C' \pm \sigma_{C'})] \tag{24d}$$

where the un-superscripted σ represents the standard deviation and the superscripted variable σ' represents the normal effective stress. Table 2 presents the calculation of the moments of τ_f for one set of values of σ', tan σ', and C' using both the Taylor series approximation and point estimates. Note the very close agreement between values calculated using the two methods.

TABLE 2

Shear Strength Example

	σ'	tan ϕ	C'	Taylor Series τ_f	Point Estimates τ_f
Mean	2000 psf	.580	1000 psf	2,160 psf	2160
Variance	100^2 psf^2	.005	$(300)^2$ psf^2	113,364 psf^2	113,578 psf^2
Standard Deviation	100 psf	0.070	300 psf	3,367.7 psf	337.0 psf
Coefficient of Variation	5%	12%	30%	15.6%	15.6%

EXAMPLE 1 - SHEAR STRENGTH

$$\tau_f = \sigma' \text{ Var } \phi' + C'$$

	Mean	Variance
σ'	2000 psf	$(100)^2$ psf
Var ϕ'	.580	0.005
C'	1000 psf	$(300)^2$ psf^2

Taylor Series

$$\bar{\tau}_f = 2000\ (.580) + 1000 \qquad \left(\frac{\partial^2 \tau_f}{\partial \sigma'^2} = \frac{\partial^2 \tau_f}{\partial (\tan \phi')^2} = \frac{\partial^2 \tau_f}{\partial C'^L} = 0 \right)$$

$$\bar{\tau}_f = 2160 \text{ psf}$$

$$\text{Var } (\tau_f) = \overline{\sigma'}^2 \text{ Var } (\tan \phi') + \overline{(\tan \phi')}^2 \text{ Var } (\sigma') + \text{Var } (C')$$

$$= 2000^2\ (0.005) + (0.58)^2\ (100)^L + (300)^2$$

$$= 113{,}364 \text{ psf}^2$$

$$\sigma_{\tau_f} = \sqrt{113364} = 336.7 \text{ psf} \qquad V_{\tau_f} = \frac{336.7}{2160} = 15.6\%$$

Point Estimates

$$\sigma'_+ = \bar{\sigma}' + \sigma_{\sigma'} = 2100\ (\tan \phi)_+ = .58 + \sqrt{.005} = .651 \qquad C'_+ = 1300$$

$$\sigma'_- = \bar{\sigma}' - \sigma_{\sigma'} = 1900\ (\tan \phi')_- = .58 - \sqrt{.005} = .509 \qquad C'_- = 700$$

$$\tau_{+++} = \sigma'_+ (\tan \phi')_+ + C'_+ = 2100\ (.651) + (1300) = 2667.10$$

Similarly:

$\tau_{++-} = 2067.10 \quad \tau_{+-+} = 2368.90 \quad \tau_{+--} = 1768.9$

$\tau_{-++} = 2536.9 \quad \tau_{-+-} = 1936.9 \quad \tau_{--+} = 2267.10 \quad \tau_{---} = 1667.10$

$E(\tau_f) = \bar{\tau}_f = \frac{1}{8} \Sigma \tau_{\pm\pm\pm} = \frac{1}{8} (2667.10_{+\ldots+} 1667.10) = \frac{1}{8} 17280 = 2160 \text{ psf}$

$E(\tau_f^2) = \frac{1}{8} \Sigma \tau^2_{\pm\pm\pm} = \frac{1}{8} (2667.1^2_{+--+} 1667.1^2) = 4,779.178.4 \text{ psf}^2$

$\text{Var } (\tau_f) = E(\tau_f^2) - E^2(\tau_f) = 113578.4 \text{ psf}^2$

$\sigma_{\tau_f} = \sqrt{\text{Var } (\tau_f)} = 337.0 \text{ psf}; V_{\tau_f} = \frac{337}{2160} = 15.6\%$

3.2 Bearing Capacity

The ultimate bearing capacity of a strip footing, q_{ult}, is given by:

$$q_{ult} = \frac{\gamma B}{2} N_\gamma + \gamma D N_q + C\, N_C \tag{25}$$

where B = width of the footing

D = depth of embedment

C = cohesion

N_γ, N_q, N_C = bearing capacity factors, functions of the friction angle, ϕ

Assuming C and ϕ to be the random variables and γ, B, and D to be known, the mean and variance of q_{ult} are established using the Taylor series approximation as:

$$\bar{q}_{ult} = \frac{\gamma B}{2} \bar{N}_\gamma + \gamma D \bar{N}_q + \bar{C}\, \bar{N}_C \tag{26a}$$

$$\sigma_{qult}^2 = \left[\frac{\gamma B}{2} \frac{\partial N_\gamma}{\partial \phi} + \gamma D \frac{\partial N_q}{\partial \phi} + \bar{C} \frac{\partial N_C}{\partial \phi}\right]^2 \sigma_\phi^2 + \left(\bar{N}_C^2\right) \sigma_C^2 \tag{26b}$$

In these equations, the derivatives are evaluated at $\bar{\phi}$ and $\bar{N}_\gamma$, $\bar{N}_q$ and $\bar{N}_C$ are the Taylor series approximations of N_γ, N_g and N_C.

$$\bar{N} = (N)_{\phi=\bar{\phi}} + \frac{1}{2} \frac{\partial^2 N}{\partial \phi^2} \sigma_\phi^2 \tag{27}$$

Using point estimates and assuming a symmetrical distribution, the first two moments of q_{ult} are found to be:

$$E\left(q_{ult}\right) = \frac{1}{4}\left(q_{++} + q_{+-} + q_{-+} + q_{--}\right) \tag{28a}$$

$$E\left(q_{ult}^2\right) = \frac{1}{4}\left(q_{++}^2 + q_{+-}^2 + q_{-+}^2 + q_{--}^2\right) \tag{28b}$$

and

$$\sigma_{q_{ult}}^2 = E\left(q_{ult}^2\right) - E\left(q_{ult}^2\right) \tag{28c}$$

$$q_{\pm\pm} = q_{ult}\left(\bar{\phi} \pm \sigma_\phi,\ \bar{C} \pm \sigma_C\right) \tag{28d}$$

Table 3 presents the results for a footing 25 feet wide with a rough base embedded to a depth of 10 feet in a soil with a unit weight of 115 pcf, founded upon a soil with a friction angle of 30° with a coefficient of variation equal to 10% and a cohesion of 200 psf with a coefficient of variation of 40%. Use of the Taylor series (Equations 26) gives a mean bearing capacity of 59.2 KSF and a coefficient of variation equal to 40.6% while the point load estimates (Equations 28) yield a mean bearing capacity of 60.1 KSF and a coefficient of variation of 41.9%. These results are essentially identical, but the point estimates technique is more efficient and potentially more instructive to the engineer, as it requires him to calculate four different bearing capacities dispersed about the mean rather than plug means and variances into Taylor Series expansions.

TABLE 3

Bearing Capacity Example

	ϕ	C	Taylor Series τ_f	Point Estimates τ_f
Mean	30°	200 psf	59.2 ksf	60.1 ksf
Variance	$9(0)^2$	6400 psf	576 ksf^2	632.6 ksf^2
Standard Deviation	3°	80 psf	24 ksf	25 ksf
Coefficient of Variation	10°	40%	40.6%	41.9%

By assuming a distribution shape of q_{ult}, the results presented in Table 3 can be used to calculate the probability of failure for a specified bearing load or the allowable maximum load for a specified minimum reliability. For instance, if we assume that the ultimate bearing capacity is normally distributed we can calculate the allowable load for a minimum reliability of 95% by setting the standardized normal variable, U, equal to -1.645, the value at which the cumulative density function of U equal 0.05.

$$U = -1.645 = \left(\frac{q_{95\%} - \bar{q}_{ult}}{\sigma_{q_{ult}}}\right) \quad (29)$$

Solving for $q_{95\%}$ in Equation 29 gives a value of 19.0 KSF as the maximum allowable load for a minimum reliability level of 95%.

Alternatively, if the applied load on the footing is 15 KSF, we can calculate the probability of failure by evaluting the CDF of U at q equal to 15 KSF. If q equals 15 KSF, the value of U equals - 1.87. From Probability tables (Benjamin and Cornell, 1970), when U = 1.87 the CDF is approximately equal to 0.964, therefore the value of the CDF at U = - 1.87, and thus the probability of failure for q = 15 KSF, is equal to 3.6 percent (0.036).

Use of the beta distribution (Harr, 1977) with a minimum value of γD and a maximum value of $\bar{q}_{ult} + 3\ \sigma_{q_{ult}}$ yields a bearing capacity at the 95% level of 20 KSF. This value is contrasted to the value of 19.0 KSF arrived at using the normal distribution. Both of these values are readily calculated from standard probability tables.

Few guidelines exist to help the engineer select which distribution shape to use for the ultimate bearing capacity, or for any other geotechnical design parameters. This lack of guidance is a major hindrance to the use of probabilistic analyses. Only through active use of probabilistic methods and through analysis of documented case histories can the requisite experience be accumulated in order to provide these necessary guidelines.

EXAMPLE 2 - BEARING CAPACITY

$$q_{ult} = \frac{\gamma B}{2} N_\gamma + \gamma D\, N_q + C N_C$$

$B = 25'$, $D = 10'$, $\gamma = 115$ pcf Rough footing .

	Mean	Coefficient of variation	Standard Deviation	Variance
C	200 psf	40%	80 psf	80^2 psf^2
ϕ	30°	10%	3°	3^2 (°)^2

From DM-7, Figure 11.1

	N_γ	N_q	N_C
$\phi = 30°$	17	20	31
$\phi = 33°$	30	29	43
$\phi = 27°$	10	14	23

Taylor Series

The first and second derivatives of N_γ, N_q, N_C need to be estimated. Two possible approaches are available:

Solution 1

From Fig. 11.1 in DM-7, it is apparent that the logorithms of N_γ, N_q and N_C vary linearly with ϕ for values of ϕ ranging between 25 and 35.

The equations of these linear relationships are:

$$\text{Ln}N_\gamma = -2.641 + 0.183\,\phi$$

$$\text{Ln}N_q = -.6380 + 0.1214\,\phi$$

$$\text{Ln}N_C = .3198 + .1043\,\phi$$

From these equations the derivatives can be obtained:

	N_γ	N_q	N_C
$\frac{\partial N}{\partial \phi}\Big\vert_{\phi = 30^0}$		3.111	2.453.34
$\frac{\partial^2 N}{\partial \phi^2}\Big\vert_{\phi = 30^0}$		.569	.297.337

It follows that:

$$\bar{N}_\gamma = 17 + \frac{1}{2}\ (.569)(3^2) = 19.56$$

$$\bar{N}_q = 20 + \frac{1}{2}\ (.297)(3^2) = 21.34$$

$$\bar{N}_C = 31 + \frac{1}{2}\ (.337)(3^2) = 32.52$$

$$\bar{q}_{ult} = \frac{\gamma B}{2}\ \bar{N}_\gamma + \gamma D\ \bar{N}_q + \bar{C}\ \bar{N}_C$$

$$\bar{q}_{ult} = \frac{(115)(25)}{2}\ 19.56 + (115)(10)(21.34) + (200)(32.52)$$

$$\bar{q}_{ult} = 59.16 \text{ ksf}$$

$$\sigma_{q_{ult}}^2 = \left[\frac{\gamma B}{2}\frac{\partial N_\gamma}{\partial \phi} + \gamma D \frac{\partial N_q}{\partial \phi} + \bar{C}\frac{\partial N_C}{\partial \phi}\right]^2_{\phi=\bar{\phi}} \sigma_\phi^2 + (N_C)^2_{\phi=\bar{\phi}} \sigma_C^2$$

$$\sigma_{q_{ul}}^2 = \left[\frac{(115)(25)}{2}\ 3.11 + (115)(10)(2.45) + (200)(3.34)\right]^2 (3^2) + (31)^2(80^2)$$

$$\sigma_{qult}^2 = 5.74.85 \text{ ksf}^2$$

$$\sigma_{q_{ult}} = 24.00 \text{ ksf} \qquad V_{q_{ult}} = \frac{24}{49.16} = 40.6\%$$

Solution #2

The first and second derivatives can be approximated using finite difference:

$$\frac{\partial N}{\partial \phi} = \frac{N_{33} - N_{27}}{2 \times 3} \qquad \frac{\partial^2 N}{\partial \phi^2} = \frac{N_{33} - 2N_{30} - N_{27}}{3^2}$$

with N_{33}, N_{27}, N_{30} equal to mean values of N at ϕ=33, 27, and 30 respectively. This leads to:

	N_γ	N_q	N_C
$\frac{\partial N}{\partial \phi}$	20/6	15/6	20/6
$\frac{\partial^2 N}{\partial \phi^2}$	6/9	3/9	4/9

These values are similar but slightly higher than those obtained with the equations of LnN_γ, LnN_q and LnN_C

Then

$$\bar{N}_\gamma = 17 + 1/2\ (6/9)\ 3^2 = 20$$

$$\bar{N}_q = 20 + 1/2\ (3/9)\ 3^2 = 21.50$$

$$\bar{N}_C = 31 + 1/2\ (4/9)\ 3^2 = 33$$

$$\bar{q}_{ult} = \frac{(115)(25)}{2}\ 20 + (115)(10)(21.5) + (200)(33)$$

$$\bar{q}_{ult} = 60.07 \text{ ksf}$$

$$\sigma^2_{q_{ult}} = \left[\frac{(115)(25)}{2}\ \frac{20}{6} + (115)(10)\ \frac{15}{6} + 200\ \frac{20}{6}\right]^2 3^2 + (31)^2\ (80)^2$$

$$\sigma^2_{q_{ult}} = 631.15 \text{ ksf}^2$$

$$\sigma_{q_{ult}} = 25.12 \qquad V_{q_{ult}} = \frac{25.12}{60.07} = 41.8\%$$

Remark

A third solution could be obtained by using the following equation for N_q, N_γ and N_C (Vesic, 1973 and Harr, 1977)

$$N_q = e^{\pi \tan\phi} N_\phi \qquad N_C = (N_q - 1) \cot\phi$$

$$N_\gamma = 2 (N_q + 1) \tan\phi \text{ with } N_\phi = \tan^2 (45 + \frac{\phi}{2})$$

The derivatives can be derived using these equation (lengthy derivations).

Point Estimates

$$q_{++} = q_{ult} (\bar{\phi} + \sigma_\phi, \bar{C} + \sigma_C) = \frac{\gamma B}{2}(N_{\gamma+}) + \gamma D (N_{q+}) + C_+(N_{C+})$$

$$q_{++} = \frac{115(25)}{2} (30) + 115(10)(29) + 280(43) = 88.51 \text{ ksf}$$

$$q_{+-} = \frac{115(25)}{2} (30) + 115(10)(29) + 120(43) = 81.63 \text{ ksf}$$

$$q_{-+} = \frac{115(25)}{2} (10) + 115(10)\ 14 + 280(23) = 36.91 \text{ ksf}$$

$$q_{--} = \frac{115(25)}{2} (10) + 115(10)\ 14 + 120(23) = 33.23 \text{ ksf}$$

$$E (q_{ult}) = \frac{1}{4} (q_{++} + q_{+-} + q_{-+} + q_{--}) = 60.07 \text{ ksf}$$

$$E (q_{ult}^2) = \frac{1}{4} (q_{++}^2 + q_{+-}^2 + q_{-+}^2 + q_{--}^2) = 4241.01 \text{ ksf}^2$$

$$\text{Var } (q_{ult}) = E (q_{ult}^2) - E^2 (q_{ult}) = 632.61 \text{ ksf}^2$$

$$\sigma_{q_{ult}} = 25.15 \text{ ksf}$$

$$V_{q_{ult}} = \frac{25.15}{60.07} = 41.9\%$$

These values are identical to the results of Solution 2 of Taylor series because points at ± 1 σ were used in the finite difference approximation of the latter solution.

Reliability Analysis

Normally distributed variable

1. $R = (1 - P_f) = 0.95 \rightarrow F_u\ (-\beta) = 0.95$

   $-\beta = 1.645$ (from Benjamin and Cornell, 1970, Table A.1)

   $$-1.645 = \frac{q_{95\%} - \bar{q}_{ult}}{\sigma_{q_{ult}}}$$

Taylor Series: $\bar{q}_{ult} = 59.2$ $\sigma_{q_{lt}} = 24 \rightarrow q_{95\%} = 19.7$ ksf

Point Estimates: $\bar{q}_{ult} = 60.1$ $\sigma_{q_{ult}} = 25 \rightarrow q_{95\%} = 19.0$ ksf

2. For $q = 15$ ksf $\quad P_f = F_u\ \left(-\frac{15 - \bar{q}_{ult}}{\sigma_{q_{ult}}}\right)$

Taylor Series: $P_f = F_u\ (-1.842) = 1 - .967 = 3.3\%$

Point Estimates: $P_f = F_u\ (-1.804) = 1 - .964 = 3.6\%$

Beta Distribution

(After Harr, 1977)

$q_{min} = \gamma D = 1.15$ ksf $\quad q_{max} = \bar{q}_{ult} + 3\,(\sigma_{q_{ult}})$

Taylor Series

$$q_{max} = 131.20$$

$$\tilde{q} = \frac{59.2 - 1.15}{131.2 - 1.15} = 0.446 \qquad \tilde{V} = \left(\frac{24}{131.2 - 1.15}\right)^2 = 0.034$$

$$\alpha = \frac{\tilde{q}^2}{\tilde{V}}\left(1 - \tilde{q}\right) - \left(1 + \tilde{q}\right) = 1.795$$

$$\beta = \frac{\alpha + 1}{\tilde{q}} - (\alpha + 2) = 2.472$$

Fig. C-17 (Harr 1977)

$K = 5\%$ $\quad F = .15$ $\quad q_{95\%} = 1.15 + .15\,(131.2 - 1.15) = 20.60$

Point Estimates

$$q_{max} = 135.10$$

$$\tilde{q} = \frac{60.1 - 1.15}{135.1 - 1.15} = .440 \qquad \tilde{V} = \left(\frac{25}{135.1 - 1.15}\right)^2 = 0.035$$

$$\alpha = \frac{\tilde{q}^2}{\tilde{V}}\left(1 - \tilde{q}\right) - \left(1 + \tilde{q}\right) = 1.658$$

$$\beta = \frac{\alpha + 1}{\tilde{q}} - (\alpha + 2) = 2.382$$

Fig. C-17 (Harr, 1977)

$K = 5\%$ $\quad F = .15$ $\quad q_{85\%} = 1.15 + .15\,(135.1 - 1.15)$

$= 21.60$

3.3 Slope Stability - Cohesive Soils

The short term stability of a slope of height H in a cohesive soil of undrained shear strength S_u and unit weight γ is a function of the stability number N_C, which in turn depends on the slope angle α. In classical slope stability theory, the stability is usually expressed as a factor of safety:

$$F.S. = \frac{S_u N_C}{\gamma H} \tag{30}$$

Alternatively, the stability can be expressed in terms of the safety margin:

$$S.M. = (S_u N_C - \gamma H) \tag{31}$$

If S_u and γ are assumed to be random variables and N_C and H are fixed, then the moments of the safety margin can be evaluated as:

$$\overline{S.M.} = (\overline{S}_u N_C - \overline{\gamma} H) \tag{32a}$$

$$\sigma_{SM}^2 = (N_C^2 \ \sigma_{S_u}^2 + H^2 \ \sigma_\gamma^2) \tag{32b}$$

The parameter N_C could also be assumed random to account for analytical inaccuracies, however, this example will be used to contrast factor of safety analyses to probabilistic analyses and thus N_C will be fixed to simplify the calculations.

For this example, the slope height was fixed at 40 ft. and the slope angle was set at 30°. A slope angle of 30° corresponds to a stability number, N_C, equal to 7.8. The unit weight of the soil was assigned a mean value of 100 pcf and a coefficient of variation of 5%. Calculations were carried out for mean shear strengths of 800, 750, and 610 psf with coefficients of variation of 10% and 25%. Figure 1 shows a plot of the reliability index β versus the factor of safety. Note that β becomes asymptotic at large values of the factor of safety. This asymptotic behavior will occur whenever the variance of the load is small. The implication of this asymptotic behavior is that beyond some critical

level, increasing the factor of safety will not increase the reliability of the system. This is a non-trivial point which should be kept in mind when using factor of safety design methods.

Table 4 presents the factor of safety versus probability of failure for five different factors of safety and two different variances of the capacity variable, the shear strength. The probabilities presented in this table assume the safety margin to be normally distributed. Slopes with a higher factor of safety may actually have a lower reliability than slopes with a lower capacity variance. The slope with a factor of safety of 1.56 and a shear strength variance of 25% has a reliability of 0.92 while the slope with a factor of safety of 1.46 and a variance of 10% has a higher reliability, 0.997. Similar analysis can be performed assuming other distribution shapes for the safety margin and/or factor of safety. The results of such analyses would show the same trends described above.

TABLE 4

Probabilities of Failure, Cohesive Slope Stability

$\overline{FS}$		1.6	1.4	1.2	1.0	0.9	0.5
P_f*	V_C = 10%	0.0007	0.0034	0.062	0.50	0.84	0.999
	V_C = 25%	0.068	0.127	0.235	0.50	0.67	0.999

* Assumes capacity and demand normally distributed,, coefficient of variation of demand equal to 5%.

To account for modeling inaccuracies, the slope stability number, N_C, can also be considered as a random variable. Example 3 illustrates the calculations required to use point estimates to evaluate the probability of failure if N_C is assumed to have a coefficient of variation of 10%. With three random variables, S_u, γ, and N_C, eight point estimates of the factor of safety must be calculated. From these eight factors of safety, the mean and variance of the factor of safety is

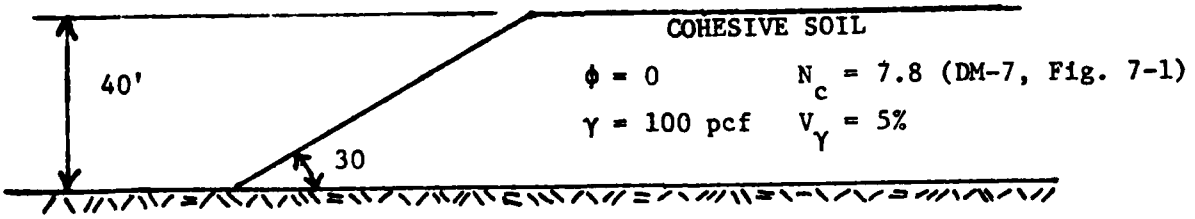

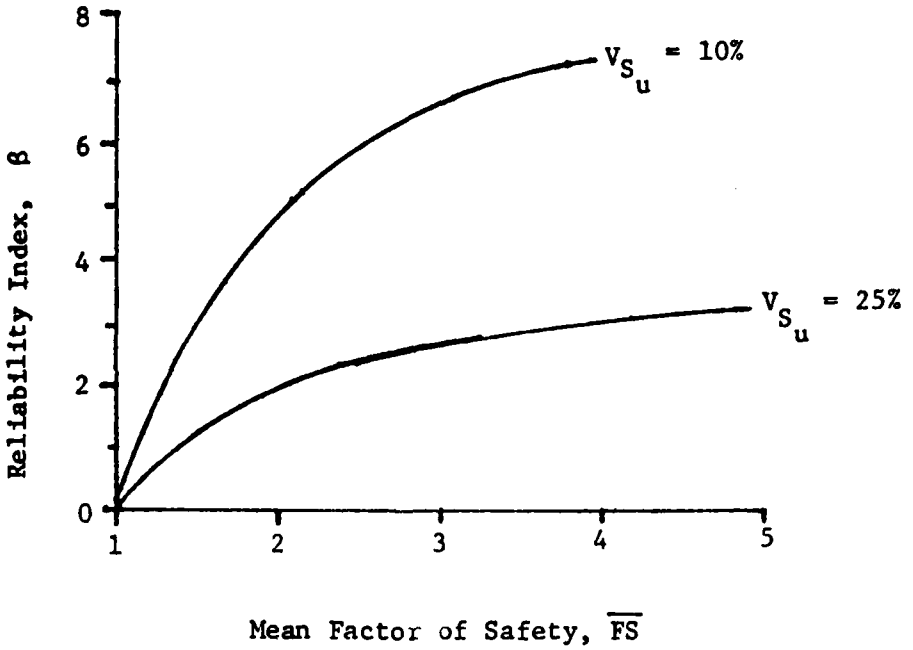

NOTE:

- Assumes Normally Distributed Variables
- Similar Plots can be prepared for all possible values of V_γ
- For F.S. > 1, slopes with lower F.S. can have lower P_F if V_{S_u} is less
- For F.S. < 1, slopes with greater V_{S_u} have lower P_F
- Slopes with same F.S. have different P_F
- For small V_γ, β (and thus P_F) become asymptotic to F.S.

Figure 1. β vs. Factor of Safety

calculated. The results yield the same mean values as the previous analyses, but a greater variance due to the additional uncertainty associated with N_C.

Even if a probabilistic analyses is not required, the calculations of point estimates would be a useful exercise for a design engineer. In calculating point estimates, the engineer is forced to quantify his subjective judgments about relative uncertainties and can graphically see the sensitivity of his analysis to these judgments. This is a major advantage of point estimates over the Taylor Series method in which the engineer plugs unfamiliar numbers into a formula to calculate the moments of the design parameter.

3.4 Slope Stability - C', ϕ' Soil

Figure 2 shows the critical slip circle for a slope in a C', ϕ' soil calculated using conventional slope stability analyses. The soil is assumed to have a dry unit weight of 110 pcf, a saturated unit weight of 120 pcf, a mean effective cohesion of 100 psf with a variance of 35% and a mean friction angle of 20° with a variance of 10% for the tangent of ϕ'. The slope height is 10 ft., the slope angle is 35°, and the water table is horizontal, two feet down from the top of the slope. Using the mean values of C' and ϕ', the conventional factor of safety is assessed as 1.35.

The total resisting and driving moments consist of six independent contributions from each of the six slices shown in Figure 2. The mean values and standard deviations of the safety margin (Resisting moment - Driving moment) and of the factor of safety (Resisting Moment/Driving moment) can be obtained from the point estimates of Taylor Series methods. The two methods give very close results (Table 5).

EXAMPLE 3 - SLOPE STABILITY, COHESIVE SOIL

Slope Height = 40 ft. Slope Angle = 30° Rigid Base at Toe of Slope

$$FS = \frac{N_c S_u}{\gamma H} \qquad SM = (N_c S_u - \gamma H)$$

1. Assume N_c, H to be deterministic; γ, S_u to be normally distributed
   Assume $\bar{\gamma}$ = 100 pcf, V_γ = 5%, V_{S_u} = 10%, 25%

$$\beta = \frac{N_c \bar{S}_u + \bar{\gamma} H}{\sqrt{\bar{N}_c^2 \sigma_{S_u}^2 + H^2 \sigma_\gamma^2}} \qquad P_f = F_u(-\beta) = 1 - F_u(\beta)$$

	V_{S_u} = 10%			V_{S_u} = 25%		
Su	σ_{S_u}	β	P_f	σ_{S_u}	β	P_f
800	80	3.42	3×10^{-4}	200	1.42	7.8×10^{-2}
720	72	2.71	3.4×10^{-3}	180	1.14	1.3×10^{-1}
610	61	1.47	7.8×10^{-2}	152.5	0.63	2.6×10^{-1}

2. S_u, γ, N_C Random

Assume V_{N_C} = 10% to account for modelling errors - use point estimates

$\bar{N}_C = 7.8$, $V_{N_C} = 10\%$; $\bar{S}_u = 800$ psf, $V_{S_u} = 10\%$' $\bar{\gamma} = 100$ pcf, $V_\gamma = 5\%$

	FS_{+++}	FS_{++-}	FS_{+-+}	FS_{+---}	FS_{-++}	FS_{-+-}	FS_{--+}	FS_{---}	$\overline{FS}$*
N_C	8.58	8.58	8.58	8.58	7.02	7.02	7.02	7.02	7.80
γ	105	105	95	95	105	105	95	95	100
S_u	880	720	880	720	880	720	880	720	800
FS	1.80	1.47	1.99	1.63	1.47	1.20	1.63	1.33	1.56

H = 40 ft.

$$\overline{FS} = 1/4 \sum FS_{\pm\pm\pm} = 1.56$$

$$\text{Var (F.S.)} = 1/4 \sum FS^2_{\pm\pm\pm} - (1.56)^2 = 0.06$$

$$\sigma_{FS} = 0.24 \qquad V_{FS} = 15\%$$

$$P_f = 7 \times 10^{-3}$$

TABLE 5
Factor of Safety and Safety Margin, Cohesive Slope Stability

	$\overline{FS}$	σ_{FS}	V_{FS}	$\overline{SM}$	σ_{SM}	V_{SM}
Taylor Series	1.33	.22	16.7%	1245	832	66.8%
Point Estimates	1.327	.225	16.9%	1245	842	67.6%

Table 6 presents values of P [F.S. < 1] and P [F.S. < 1.3] assuming F.S. to be log normally distributed, beta distributed with bounds between F.S. ± 3 $\sigma_{F.S.}$, and beta distributed between F.S. equal to zero and 3.0. The probability that the factor of safety is less than or equal to one is equal to the probability of failure, while the probability that the factor of safety is less than or equal to 1.3 is the probability that this factor of safety is unconservative.

TABLE 6
Slope Stability - C, ϕ Soil

Distribution of F.S.	Log Normal	Beta ± σ_{FS}	Beta 0 < FS < 3
P_f = P (F.S. <1)	6.7%	7%	6.5%
P (F.S. < 1.3)	44.6%	46%	45%

Note that for this example, the calculated reliability for the three distributions chosen fall in a narrow band, between 6 and 7% for the probability of failure. This relative insensitivity to the chosen distribution may not always be the case. Until more experience is obtained with respect to proper shape of distribution, the prudent engineer should investigate the sensitivity of his answer to distribution shape.

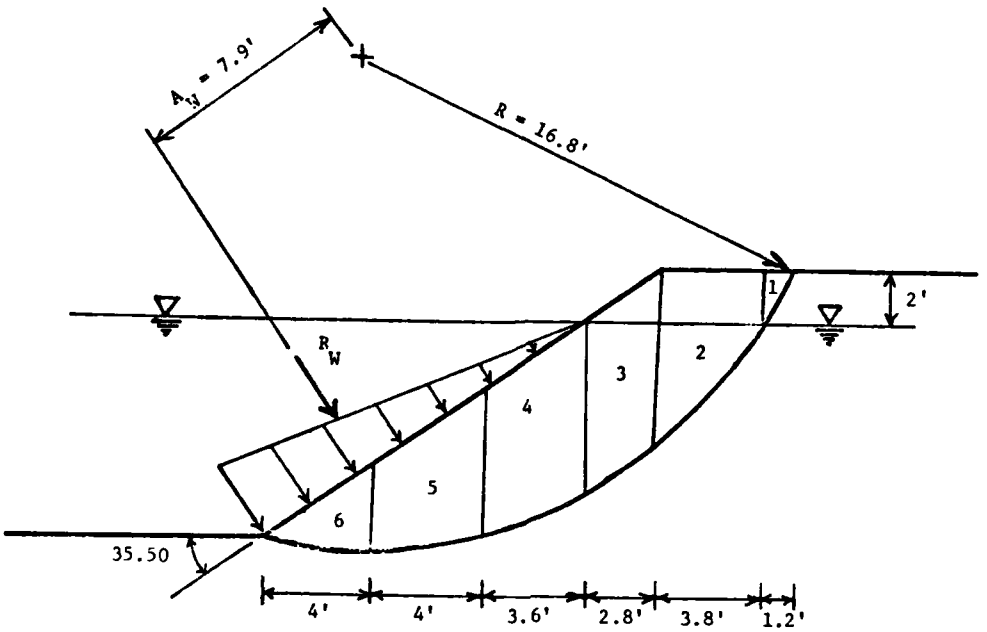

γ_{dry} = 110 pcf
$\overline{C}$ = 100 psf

V_c = 35%

γ_{SAT} = 120 pcf
$\overline{\phi}$ = 20°, V_ϕ = 15%

(Example suggested by M. E. Harr, Purdue University, 1982)

Figure 2. Critical Circle for Slope Stability

EXAMPLE 4 - SLOPE STABILITY - C, ϕ SOIL

Use ordinary method of slices. See Figure 2 for geometry of critical circle and material properties.

$$F.S. = \frac{\sum_{i=1}^{5} \left(C_i \ell_l + \left(N_i - U_i \ell_i\right) \tan \phi_i\right) + \frac{R_W}{R} A_W}{\sum_{i=1}^{5} W_i \sin \theta_i} = \frac{\bar{C}}{\bar{D}}$$

$\bar{C} = f(C, \phi)$ $\qquad$ $\bar{D}$ = Deterministic (no random variables)

Slice	ℓ	θ	w	u	uℓ	(- uℓ)	Wsin θ	$(W-W_W)$ sin θ
1	2.4	60	132	0	0	66	114	114
2	5.9	47	1839	156	920	334	1345	1345
3	3.3	33	2089	331	1092	660	1138	1138
4	3.8	22	2732	430	1634	899	1025	922
5	4.1	9	2916	499	2050	830	456	308
6	4	-4	2367	512	2048	313	-165	-50
	23.5					3102	3913	3777

$R_W = 1/2\ (62.4)\ (8)^2 = 1997$ lbs/ft.

$\frac{R_W}{R} A_W = 1680$ lbs/ft.

Given $\bar{\phi} = 20°$, $\sigma_\phi = 3°$; Find $\overline{\tan \phi}$, $\sigma_{\tan \phi}$

Taylor Series: $\overline{\tan \phi} = \tan \bar{\phi} + 1/2 \frac{\partial^2 \tan\phi}{\partial \phi^2} \sigma_\phi^2 = \tan \bar{\phi} + \frac{\sin \bar{\phi}}{\cos^2 \bar{\phi}} \sigma_\phi^2$

$\overline{\tan \phi} = 0.364 + 0.00113 = 0.365$ [Note: $\sigma_\phi = \frac{\pi}{60}$ radians]

$$\text{Var}(\tan \phi) = \left(\frac{2 \tan \phi}{\partial \phi}\right)^2 \sigma_\mu^2 = \frac{1}{\cos^4 \bar{\phi}} \sigma_\phi^2 = 0.0035$$

$$\sigma_{\tan \phi} = \sqrt{0.0035} = 0.059 \qquad V_{\tan \phi} = 16\%$$

Point Estimates: $\tan \phi_+ = \tan 23^0 = 0.424 \quad \tan \phi_- = 0.306$

$$\overline{\tan \phi} = \frac{1}{2} (\tan \phi_+ + \tan \phi_-) = 0.365$$

$$\text{Var } (\tan \phi) = \frac{1}{2} (\tan^2 \phi_+ + \tan^2 \phi_-) - (\overline{\tan \phi})^2 = 0.0035$$

$$\sigma_{\tan \phi} = \sqrt{0.0035} = 0.059$$

$$FS = \frac{(23.5)(C) + 3102 \tan \gamma + \frac{R_W}{R} a_W}{3777}$$

$$\frac{R_W}{R} a_W = 3565 \quad \frac{7.4}{17.8} = 1540$$

$$FS = 0.0062\ C + .8213\ \text{Var}\ \phi + .4077$$

$$S.M. = 23.5\ C + 3102 \tan \phi - 2237$$

Taylor Series

$$\overline{FS} = 0.0062\ \bar{C} + .8213\ \overline{\tan \phi} + .4077 = 1.33$$

$$\text{Var } (FS) = (0.0062)^2\ \text{Var } (C) + (.8213)^2\ \text{Var } (\tan \phi) = .0494$$

$$\overline{SM} = (23.5)(100) + (3102)(.365)$$

$$\text{Var } (SM) = (23.2)^2\ \text{Var } (C) + (3102)^2\ \text{Var } (\tan \phi) = 693{,}022$$

$$\sigma_{FS} = .22 \quad V_{FS} = 16.7\%$$

$$\sigma_{SM} = 832 \quad V_{SM} = 66.8\%$$

Point Estimates

$C_+ = 135 \quad C_- = 65 \quad \tan \phi_+ = .424 \quad \tan \phi_- = .306$

$FS_{++} = 1.593 \quad FS_{+-} = 1.496 \quad FS_{-+} = 1.159 \quad FS_{--} = 1.062$

$\overline{FS} = 1/4 \; \Sigma \; FS_{\pm\pm} = 1.327 \quad \overline{FS^2} = 1.8117 \quad Var\,(FS) = 0.0507$

$\sigma_{FS} = .225 \quad V_{FS} = 16.9\%$

$SN_{++} = 2250.7 \quad SN_{+-} = 1884.7$

$SN_{-+} = 605.7 \quad SN_{--} = 239.7$

$\overline{SN} = 1245 \quad \overline{SN^2} = 2260518 \quad Var(SN) = 710493$

$\sigma_{SN} = 842 \quad V_{SN} = 67.7\%$

Assume FS to be lognormally distributed

$$P_F = F_U \left(\frac{1 - 1.33}{.22}\right) = F_U \; (- 1.56) = 0.067 = 6.7\%$$

or assume SN to be normally distributed:

$$P_f = F_U \left(\frac{U - 1245}{832}\right) = F_U \; (- 1.496) = 6.7\%$$

$$P \left[FS < 1.30\right] = F_U \left(\frac{1.30 - 1.33}{.22}\right) = F_U \; (- .136)$$

$$= 1 - .554 = 44.6\%$$

Assume FS to be Beta distributed $\overline{FS} - 3 \; (\sigma_{FS}) < FS < FS + 3 \; (\sigma_{FS})$

$\sigma_{FS} = 0.22 \qquad .67 < FS < 1.99$

$$\tilde{FS} = \frac{1.33 - 0.67}{1.99 - 0.67} = 0.50 \quad \tilde{V} = \left(\frac{.22}{1.99 - .67}\right)^2 = 0.028$$

$$\alpha = \frac{0.5^2}{0.028} \; (1 - 0.5) - (1 + 0.5) = 3.00$$

$$\beta = \frac{3 +}{0.5} - (3 + 2) = 3.0$$

From Harr (1977) Fig. C-17 for $\alpha = \beta = 3$

FS*	0.77	0.86	0.97	1.04	1.17	1.33
"K" = P(FS < FS*)	0.1%	100%	5.0%	10%	25%	50%

by interpolation $P(FS < 1) = P_f = 7\%$

$P(FS < 1.3) = 46\%$

Assume F.S. to be Beta distributed between 0 and 3:

$$\tilde{FS} = \frac{1.33}{3} = 0.44 \qquad \tilde{V} = \left(\frac{0.22}{3}\right) = 0.00538$$

$$\alpha = \frac{0.44^2}{0.00538}\left(1 - .44\right) - \left(4\ .44\right) = 18.71$$

$$\beta = \frac{18.71 + 1}{.44} - (18.71 + 2) = 24.08$$

FS*	.69	.84	.97	1.05	1.17	1.33
"K" = P(FS < FS*)	0.1%	1%	5%	10%	25%	50%

By interpolation $P\ [FS < 1.0] = 6.5\%$

$P\ [FS < 1.3] = 45\%$

4.0 CONCLUSIONS

In Part II of this report, several approximate methods for determining the first and second moments of the probability density function of a random design variable have been presented. Once these moments are known, the probability of failure or reliability of the system can be calculated by assuming a distribution shape and using standard probability tables. This technique can be used on a variety of geotechnical problems to transform existing deterministic analyses into probabilistic design analyses.

Examples of the application of the methodology developed herein are presented in the areas of shear strength, bearing capacity, and slope stability. The examples are used to illustrate how a reliability type of design analyses might be performed, the influence of the choice of distribution on calculated results, and the contrasts between conventional factor of safety analyses and probabilistic analyses.

The point estimate method presented in this report is a simple and powerful tool that can be used in conjunction with any numerical analysis. By identifying the N random variables in a design analysis and assigning to them one sigma bounds to reflect subjective uncertainty or parameter variability, the mean and variances of the design parameters can be estimated from 2^n point estimates.

The primary obstacle to successful implementation of the techniques presented in this report is the lack of information on appropriate distribution shapes for various geotechnical design parameters. Only through increased use of probabilistic methods can the experience necessary to provide this information be accumulated. Until such information is available, the engineer must use his own judgment as to which type of probability distribution to use and should check the sensitivity of his result to the choice of distribution if he is in doubt as to his choice.

REFERENCES - PART I

Ang, A.H-S, and C.A. Cornell (1974), "Reliability Bases of Structural Safety and Design," ASCE, Journal of the Structural Division, Vol. 100, No. ST9, Proc. Paper 10777.

Ang, A.H-S, and W. H. Tang (1974), Probability Concepts in Engineering Planning and Design, John Wiley and Sons, New York.

Benjamin, J. R. and C. A. Cornell (1970), Probability, Statistics, and Decision for Civil Engineers, McGraw-Hill, New York.

Grivas, D. A. (1979), "Reliability Analysis of Retaining Structures," Proceedings of the 3rd International Conference on Applications of Statistics and Probability to Soil and Structural Engineering, Sydney, Australia, January.

Guymon, G. L., Harr, M. E., Berg, R. L., and Hromadka, T. V. (1981), "A Probabilistic-Deterministic Analysis of One-Dimensional Ice Segregation in a Freezing Soil Column," Cold Regions Science and Technology, Elsevier Scientific Publishing Company, Amsterdam, Vol. 5, pp. 127-140.

Hahn, G. J. and Shapiro, S. S. (1967), Statistical Models in Engineering, John Wiley and Sons, New York.

Harr, M. E. (1977) Mechanics of Particulate Media, McGraw-Hill, New York.

Rosenblueth, E. (1974), "Approximaciones de Segundos Momentos en Probabilidades," Boletin de Instituto Mexicano de Planeacon y Operacion de Sistemas, Vol. 26, Nov.-Dec., pp. 1-12.

Rosenblueth, E. (1975), "Point Estimates for Probability Moments," Proceedings of the National Academy of Science (U.S.A.), Vol. 72, No. 10, October, pp. 3812-3814.

APPENDIX A

BETA DISTRIBUTION

The beta probability density function is defined over the range [a,b] by:

$$f(x) = \frac{(b - a)^{(-1 - \alpha - \beta)}}{B(\alpha + 1, \beta + 1)}(x - a)^{\alpha}(b - x)^{\beta} \qquad (A.1)$$

where α and β are the parameters of the distribution and B (.,.) is the beta function:

$$B(\alpha + 1, \beta + 1) = \frac{\Gamma(\alpha + 1)\,\Gamma(\beta + 1)}{\Gamma(\sigma + \beta + 2)} \qquad (A.2)$$

where Γ () is the gamma funciton.

The expected mean value and variance are:

$$\bar{x} = a + \frac{\alpha + 1}{\alpha + \beta + 2}(b - a) \qquad (A.3)$$

$$\sigma_x^2 = \frac{(b - a)^2(\alpha + 1)(\beta + 1)}{(\alpha + \beta + 2)^2(\alpha + \beta + 3)} \qquad (A.4)$$

If α and β are integers, Equation A.1 reduces to:

$$f(x) = \frac{1}{C}(x - a)^{\alpha}(b - x)^{\beta} \qquad (A.5)$$

where

$$C = \frac{\alpha!\ \beta!\ (b - a)^{\alpha + \beta + 1}}{(\alpha + \beta + 1)!} \qquad (A.6)$$

A procedure has been developed (Harr, 1977) to approximate empirical data by a beta distribution. Given data ranging between a and b, and their mean $\bar{x}$ and standard deviation σ_x, the parameters α and β of the distribution can be obtained from the expressions:

$$\alpha = \frac{\tilde{x}^2}{\tilde{V}} (1 - \tilde{x}) - (1 + \tilde{x}) \qquad (A.7)$$

$$\beta = \frac{\alpha + 1}{\tilde{x}} - (\alpha + 2) \qquad (A.8)$$

where

$$\tilde{x} = \frac{\bar{x} - a}{b - a} \qquad (A.9)$$

and

$$\tilde{V} = \left(\frac{\sigma_x}{b - a}\right)^2 \qquad (A.10)$$

Expressions A.7 and A.10 can prove very useful in reliability analysis when the mean and standard deviation of C, D or F.S. are available and lower and upper limits of these parameters are known or can be assumed, based upon engineering judgment.

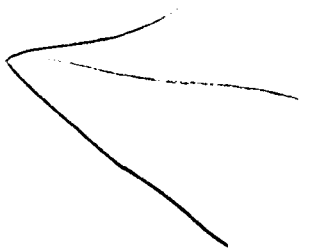

APPLICATION OF PROBABILISTIC METHODS IN GEOTECHNICAL ENGINEERING

PART II

ANALYSIS OF DOCUMENTED CASE HISTORIES USING A STOCHASTIC MODEL FOR SEISMICALLY GENERATED PORE PRESSURE AND SHEAR STRAIN POTENTIAL

E. Kavazanjian, Jr
J. L. Chameau
G. Wayne Clough
T. Hadk-Hamad

CONTENTS

LIST OF FIGURES

LIST OF TABLES

Chapter I

INTRODUCTION

Meaningful application of probabilistic design analysis in geotechnical practice is hindered by a lack of guidance for the design engineer in choosing model parameters. Decisions as to the variance of random variables and the shape of probability distribution are usually made on the basis of subjective engineering judgement, since there is rarely enough data available to compile meaningful statistics. Most engineers are unfamiliar with, and have little intuitive judgement of, probabilistic parameters, and there are few guidelines available for choosing them. Only through application of probabilistic design analysis in case history studies can the requisite experience and judgement be accumulated. Documentation of case histories in which probabilistic analyses have been successfully applied is essential to the development and dissemination of this design experience.

Part II of this report presents the basics of a new stochastic model for seismically-generated pore pressure and shear strain potential and illustrates its use for documented case histories. Model parameters are chosen according to available information on the variability of soil properties, and it is applied to sites where liquefaction was observed and where no evidence of liquefaction was observed after major seismic

events. Results of the analysis are in substantial agreement with observed field behavior, indicating that this model can be used in a predictive capacity if parameters are chosen correctly.

An application of the model to a comprehensive risk analysis of seismically induced initial liquefaction is also briefly described. An example using available seismic information for a hypothetical soil site near San Francisco is presented to illustrate the use of this type of model.

Chapter II

PROBABILISTIC PORE PRESSURE AND SHEAR STRAIN POTENTIAL MODELS

2.1 CHAMEAU PORE PRESSURE MODEL, 1980

Using the effective stress model developed by Finn and his co-workers (1975,1977), Chameau (1980) developed a stochastic model for pore pressure development that accounts for non-linear accumulation of pore pressure. The measure of pore pressure during a stress cycle depends on the stress intensity and the pore pressure accumulated during the previous cycles:

$$\Delta u_i = f(\tau_i, u_{i-1}) \tag{2.1}$$

where Δu_i is the increase in pore pressure at cycle i, τ_i the stress intensity of cycle i and u_{i-1} the pore pressure accumulated at the end of cycle i-1.

The model developed by Chameau is intended to incorporate and combine the following characteristics of the development of pore pressure under random loading:

1. Non-linear development of pore pressure under uniform and non uniform loading.

2. Uncertainties in assessing the pore pressure build-up in sands from laboratory test results, including uncertainties inherent to the test procedure such as inability to reproduce stress conditions, and uncertainties in the modelling of the in-situ conditions such as cementation and relative density.

3. Uncertainties in shear stress time history related to the earthquake motions, source mechanism, travel path and site characteristics.

2.1.1 Basic assumptions and notations

It is assumed that pore pressure development characteristics follow those observed in laboratory experiments. These characteristics are composed of a cyclic strength curve relating shear stress to the number of cycles to liquefaction (Figure 2.1a) and a set of pore pressure generation curves expressing the accumulation of pore pressure during loading (Figure 2.1b). Uncertainties in the soil resistance characteristics are taken into account by imposing a probability distribution function on the cyclic strength curve as hown on Figure 2.1c. The earthquake loading is represented by a probability density function giving for each cycle the probability of having a certain shear stress. The two probability density functions considered for the shear stresses are shown on Figure 2.1c. The following notation, used by Chameau, will also be used in this present work:

Pore pressure ratio: $R = u/\sigma_0'$

Shear stress ratio: $S = \tau/\sigma_0'$

Probability density function on number of cycles to liquefaction: $F_{N_l}(N_l)$

Probability density function and cumulative distribution function on R and S:

$$f_R(r)\ ,\ f_S(s) \quad \text{and} \quad F_R(r)\ ,\ F_S(s)$$

A functional relationship is assumed to exist between R, S and the normalized number of cycles N/N_l where N_l is the number of cycles to zero effective stress:

$$\frac{N}{N_l} = f_n(R,S) \tag{2.2}$$

2.1.2 Formulation of the model

Chameau formulated his model to answer the following question: "What is the probability of reaching a pore pressure ratio R at the end of cycle N?" Considering the first cycle of loading, the initial value of R is zero and we may write the following equation:

$$P[R \leq r] = \int_{\text{all } S} P[R \leq r \,|\, S=s] \cdot f_S(s)\,ds \tag{2.3}$$

Where $P[\ R \leq r \,|\, S=s\ ]$ is the conditional probability of R given a certain value of loading (shear stress S). Using the functional relationship in

equation 2.2 the conditional probability of R on S can be written with N=1 (First cycle, Figure 2.2):

$$P[R \leq r | S=s] = P[1/N_1 \leq f_n(R,S)] = 1 - F_{N_1}(1/f_n(R,S)) \quad (2.4)$$

Combining 2.4 and 2.3 leads to the desired results:

$$P[R \leq r] = F_R(r) = \int_{\text{all } S} [1 - F_{N_1}(1/f_n(R,S))] \cdot f_S(s)ds \quad (2.5)$$

which is the cumulative distribution of the pore pressure ratio R at the end of the first cycle. For any other cycle the same type of analysis is carried out. The main difference is in the dependence at cycle 'i' on the accumulated pore pressure ratio at the end of cycle 'i-1'. For cycle 'i' the distribution of R will be dependent on both ξ the pore pressure ratio at the end of cycle 'i-1' and the shear stress ratio S at cycle 'i'. The pore pressure ratio at the end of cycle 'i' will be less than the value of R if and only if the increase in pore pressure ratio during cycle 'i' is less than $\Delta r = r - \xi$. The mathematical development of this probability is the same as for cycle one. The increase in pore pressure Δu from cycle i-1 to cycle "i" can be related to the normalized relation in equation 2.2 (Figure 2.3).

$$\frac{i-1}{N_1} \; \frac{i}{N_1} = f_n(r,s) - f_n(\xi,s) = \Delta f_n(r,\xi,s) \quad (2.6)$$

The cumulative distribution function of R at cycle i is obtained as a function of the distribution of R at cycle i-1.

$$F_R^i(r) = \int_0^r F_{R|\xi}(r,\xi) \cdot f_R^{i-1}(\xi) d\xi \tag{2.7}$$

The conditional distribution $F(r|\xi)$ is computed as:

$$F_{R|\xi}(r,\xi) = \int_{\text{all } S} F_{R|\xi|S}(R,\xi,S) \cdot f_S(s) ds \tag{2.8}$$

where $F(r|\xi|s)$ is given by:

$$F_{R|\xi|S}(r,\xi,s) = P[1/N_1 \leq \Delta f_n(r,\xi,s)] \tag{2.9}$$

By combining 2.7, 2.8 and 2.9 the following expression for the probability of having a pore pressure ratio of R at the end of cycle "i" is obtained:

$$p[R \leq r] = F_R^i(r) = \int_0^r \int_{\text{all } S} \left[1 - F_{N_1}(1/\Delta f_n(r,\xi,s))\right] \cdot f_S(s) \cdot f_R^{i-1}(\xi)\, ds\, d\xi \tag{2.10}$$

Equations 2.5 and 2.10 give the total probabilistic distribution of the pore pressure ratio during loading.

The probability of having a pore pressure ratio less than or equal to r, $P(R \leq r)$ can be evaluated once the distribution on the shear stress $f_S(S)$, the distribution on the number of cycles $f(N_1)$ and the functional relationships between cycles and shear stress $f_n(R,S)$ are known. The probability distribution function of the shear stress $f_S(S)$ is deduced from that of the acceleration. Models have been proposed for this purpose by Vanmarcke (1976), Valera and Donovan (1977) and De Herrera (1981). The probability distribution function of the number of cycles $f(N_1)$ is chosen based on previous statistical studies. Ferrito et al. (1979) suggest that the numbers of cycles to liquefaction follows a lognormal distribution and this was adopted in the Chameau model. However, due to the generality of the mathematical derivations, the model is not limited to any particular distribution.

To allows for the non-linear development of pore pressures an empirical functional relationship is used. Seed, Martin and Lysmer (1975) first proposed an expression of the form:

$$\frac{N}{N_1} = \left[\frac{1-\cos\pi R}{2}\right]^{\theta} \qquad (2.11)$$

where θ is a shape factor function of the soil properties and the stress ratio. Chameau developed an improved version of this approach which allows for a better fit to the observed results; the equation is as follows :

$$\frac{N}{N_1} = 1 - \left[\sin\frac{\pi}{2}(1-R^{1/\beta})\right]^{2\alpha} \qquad (2.12)$$

2.1.3 Example of Application

Site and earthquakes

A hypothetical site consisting of medium dense sand is used to demonstrate the application of the model; conditions are given in Table 2.1 . Pore pressure response for the sand is taken to be that for Monterey Sand No. 0 as defined in large scale shaking tests by De Alba et al. (1975); Figure 2.5 shows the excellent fit of Equation 2.12 to the observed data.

An exponential distribution was chosen to model the amplitude of the peaks of the acceleration time history. The distribution of the shear stress is deduced from that of the acceleration and is also an exponential distribution. The exponential distribution is characterized by its mean $1/\lambda$ (Benjamin and Cornell, 1970); in the present analysis the value of $1/\lambda$ was chosen based on data published by Zsutty and De Herrera (1979). This parameter was selected as 27 cm/sec^2 , a value which corresponds roughly to that of past earthquakes which have different magnitudes, peak ground accelerations and durations expressed in number of cycles.

Results

The results of the analysis of the hypothetical site are shown on Figure 2.19 presented as the probability of exceeding a pore pressure ratio R at the end of a given cycle. The effect of the duration of the loading is dramatic. For the case of R=1.0 (liquefaction) after 90 cycles, the end of the Figueroa St. record, the probability of reaching liquefaction is about 0.5. This probability jumps to 0.7 after 120

TABLE 2.1

Hypothetical Site Properties and Earthquakes

Relative density: 54%
Total unit weight: 120 pcf
Depth of interest: 25 feet
Depth of water table: 2 feet
Cyclic strength curve: shown in Figure 2.4
Pore pressure generation: shown in Figure 2.5 [1]

Earthquake	R.M.	PGA in g's	N cycles
Hollister, 1961	5.6	.18	94
Taft, 1952	7.2	.17	320
Figueroa, 1971	6.4	.15	82
First St, 1971	6.4	.12	114

(1) note the very good fit of the curve by equation 2.12 with values of shape coefficients $\alpha = 2.0$ and $\beta = 1.05$.

cycles, representing the end of the First St record. After about 250 cycles a probability of 1 of reaching liquefaction is obtained. Although the records used are represented by the same distribution ($1/\lambda$ = 27 cm/sec^2) they have a different duration, leading to distinctly different probabilities of liquefaction . Similar conclusions are drawn for other pore pressure ratios. The model shows that earthquake ground motion needs to be characterized by more than one parameter and that duration is a very important factor.

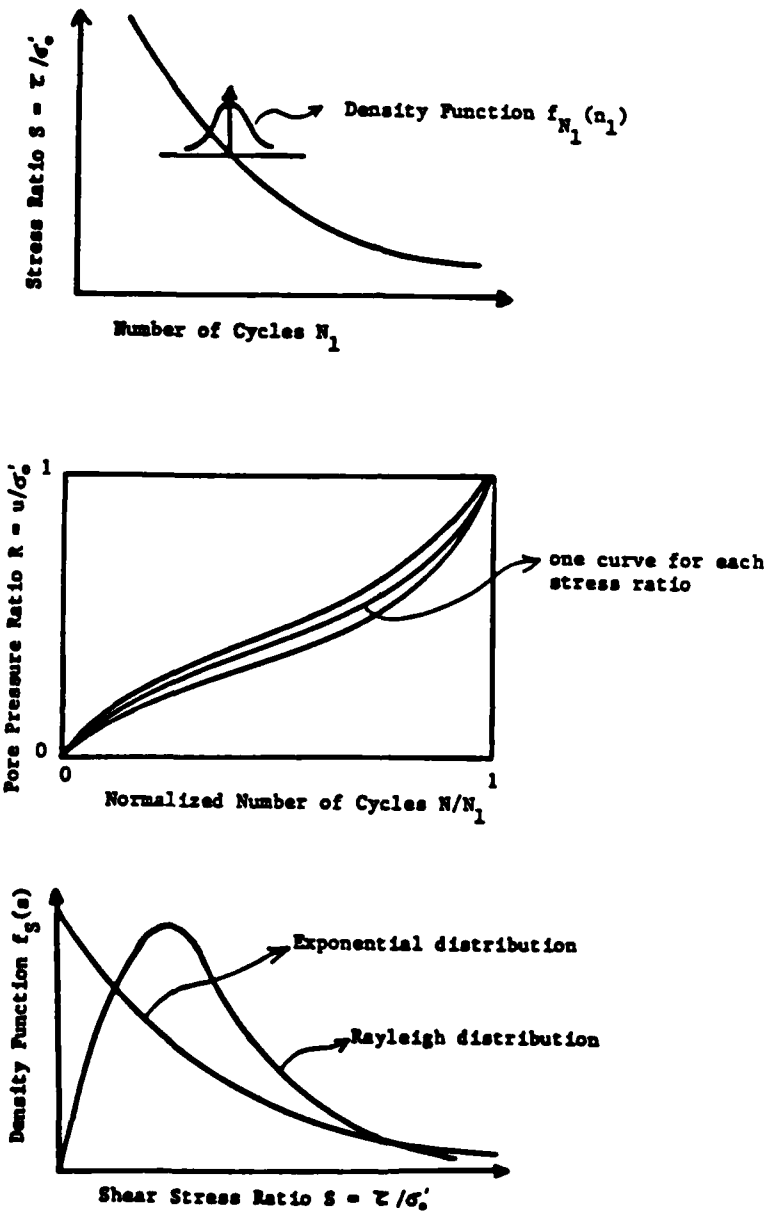

Figure 2.1: Parameters for Chameau model

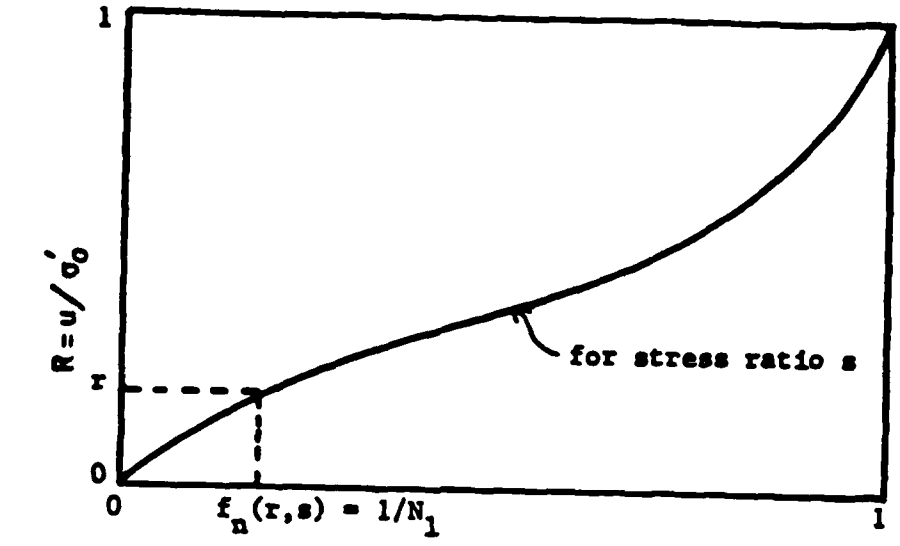

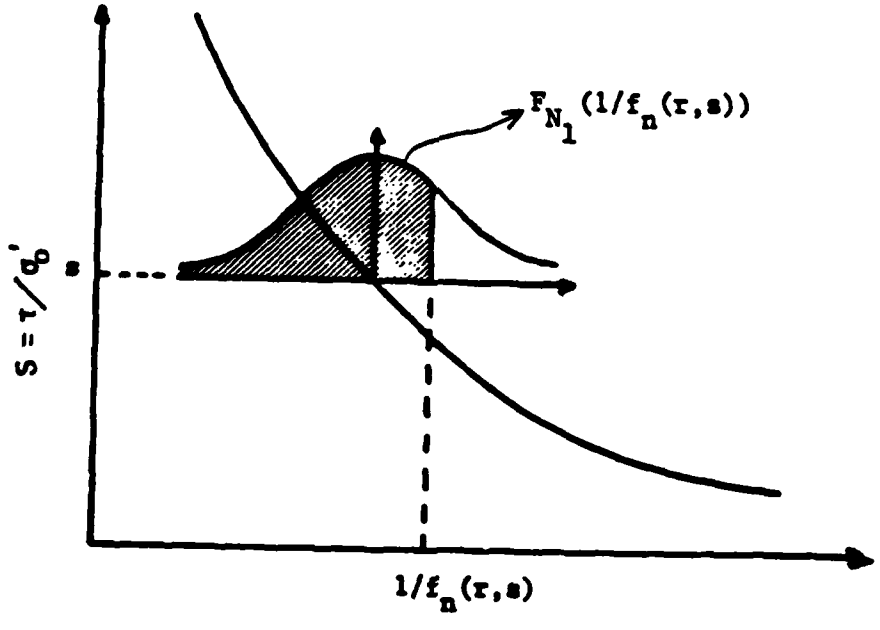

Figure 2.2: First Cycle of Loading, Chameau Model

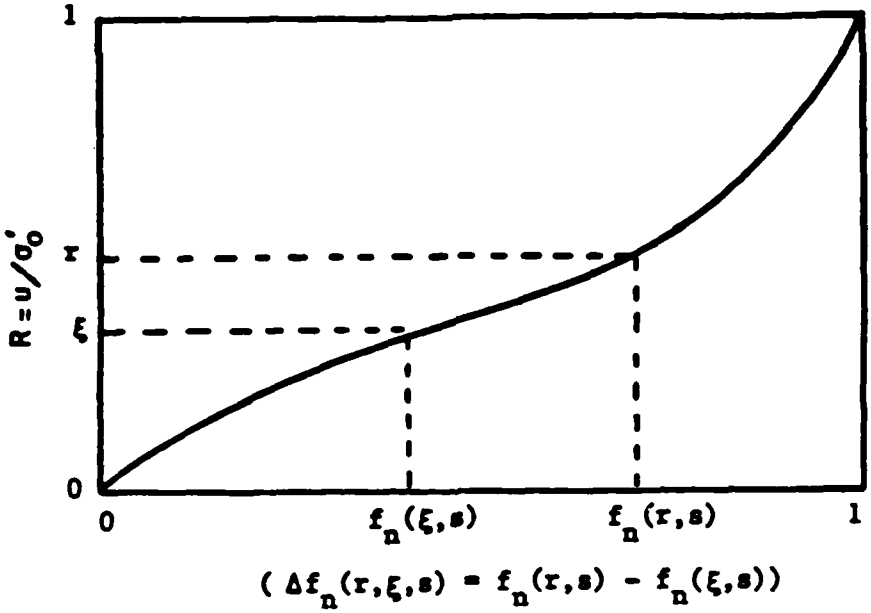

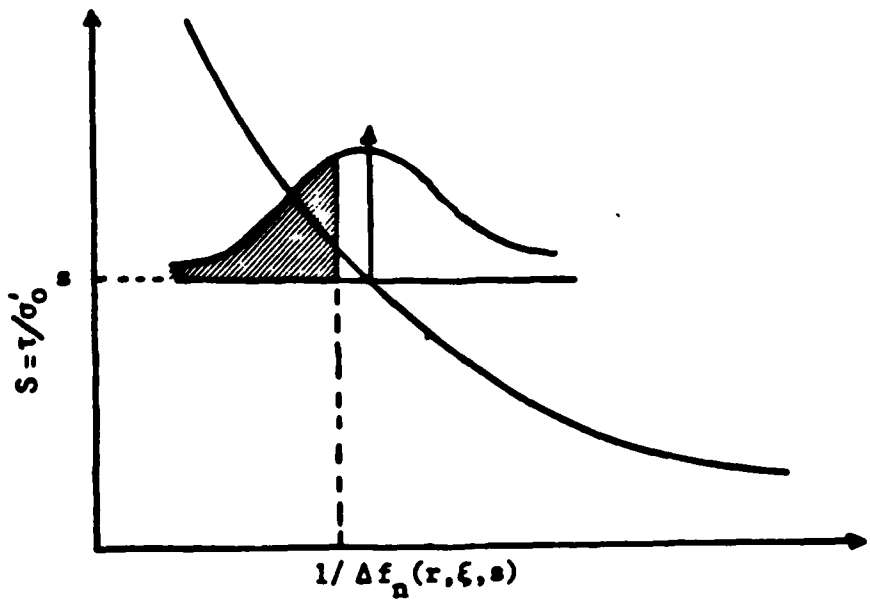

Figure 2.3: I^{th} Cycle of Loading, Chameau Model

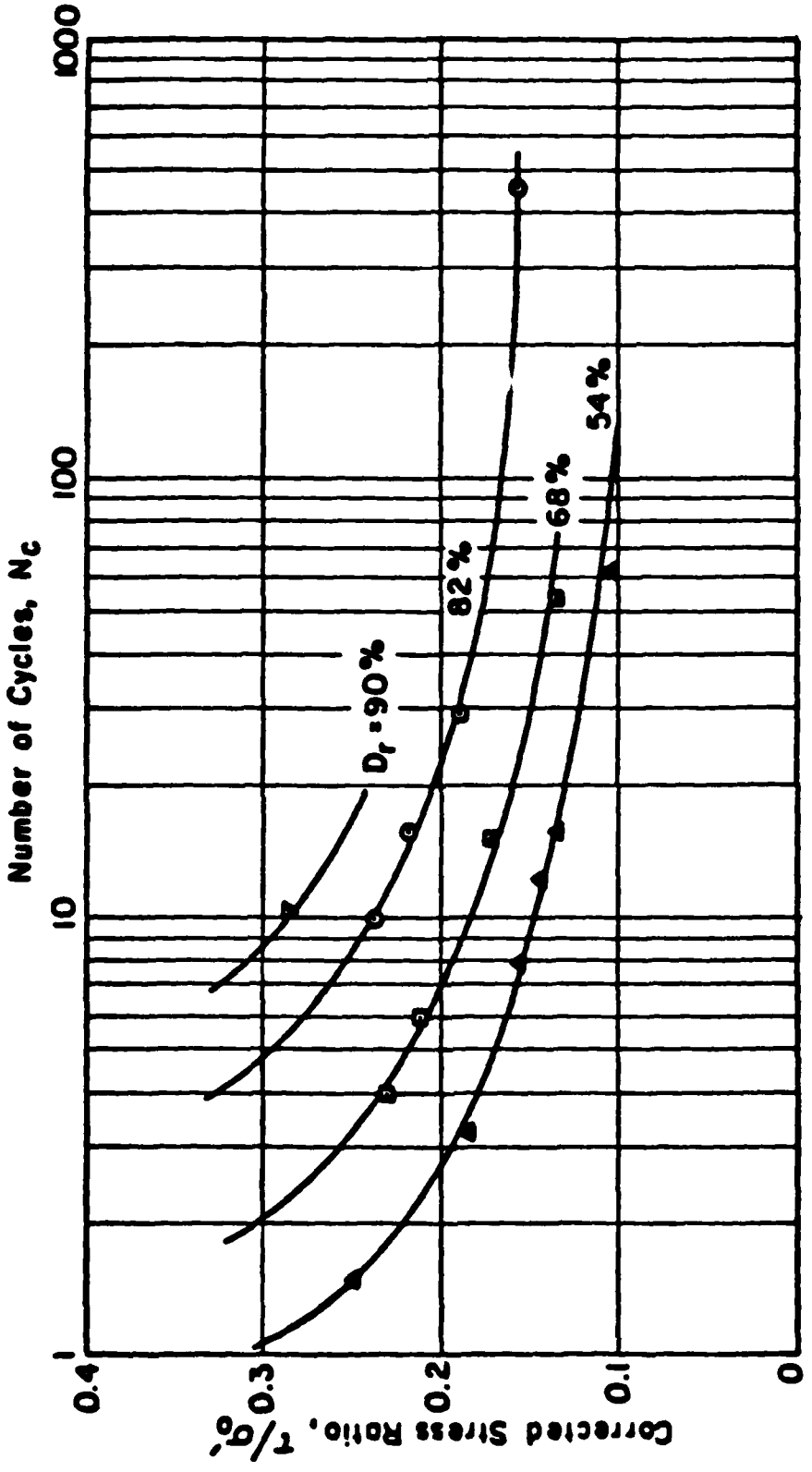

Figure 2.4: Cyclic Strength Curve

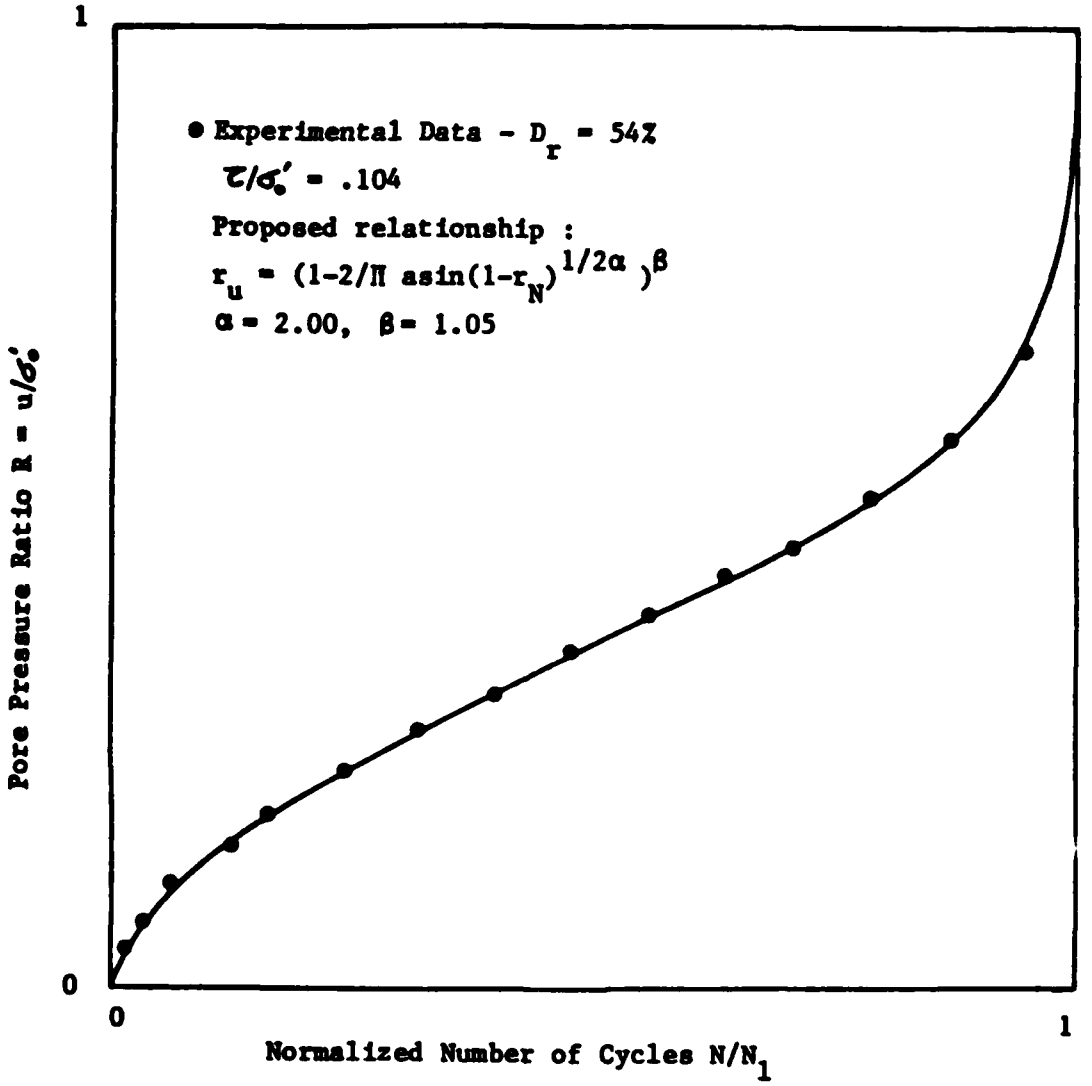

Figure 2.5: Development of Pore Pressure

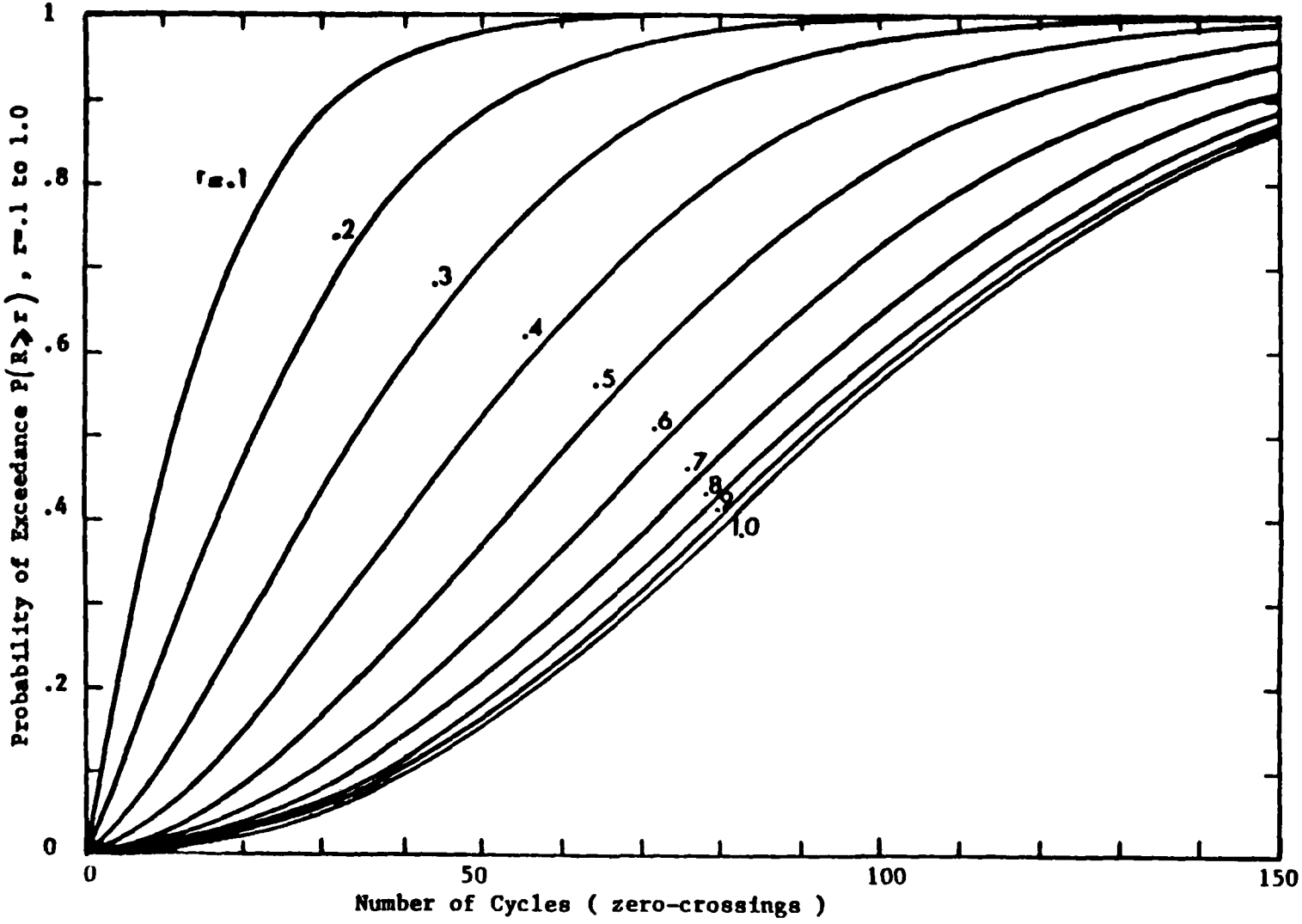

Figure 2.6: Results for Hypothetical Site

2.2 HADJ HAMOU SHEAR STRAIN POTENTIAL MODEL

2.2.1 Presentation of the model

The Chameau pore pressure model is a powerful tool to assess pore pressure development potential. However, it lacks the ability to distinguish between those cases where pore pressure build-up will and will not lead to development of shear strains in the ground. To resolve this problem the probabilistic pore pressure model developed by Chameau (1980) was transformed by Hadj Hamou (1982) to compute the probability distribution function of shear strains. One of the main inputs to the Chameau model is a cyclic strength curve relating shear stress ratios and number of cycles to liquefaction (Figure 2.4). This curve is replaced by a cyclic strain curve (Figure 2.7)in the Hadj Hamou approach. The strain analysis may then be performed for different strain levels. Uncertainties on the cyclic strain curves, loading parameters and soil parameters are accounted for in the same manner as in the pore pressure model. An application of the model to the hypothetical site used in Section 2.1.3 is presented in the following section.

2.2.2 Application

Using the data presented in table 2.1, the following two situations are analyzed:

Case 1: Relative density D_r = 54 % and exponential distribution

of shear stress with $1/\lambda$ = 27 cm/sec^2, and

Case 2: Relative density D_r = 68% and exponential distribution of shear stress with $1/\lambda$ = 53 cm/sec^2

For both cases, the depth of interest, depth of water table and other parameters are assumed the same and their values are specified in Table 2.1. The appropriate cyclic stress curve for each density is shown on Figure 2.7.

Results for Case 1

Two levels of ground strains, 10% and 15% were chosen as predictive parameters for the analysis and the results are plotted on Figure 2.8 as probability of exceeding these strain potential levels versus the number of zero-crossings. For this particular combination of site and load the probability curves are relatively close, separated only by a few percent. To emphasize the difference between strain potential and initial liquefaction, the probability curve corresponding to liquefaction was also plotted on Figure 2.8. Initial liquefaction represents the case where the pore pressure first equals the level of effective confining pressure (R=1.0). Ground strains usually develop following this event. At the end of the presumed record (150 zero crossings) the probabilities of liquefaction occurring, 10% strain and 15% strain are 85%, 76%, and 72% respectively. Those are fairly high numbers which could be used to assess the risk at this site under such a loading. One may conclude that this site is not very well suited for construction of geotechnical structures that are sensitive to ground movement.

Results for Case 2

Case 2 presents a denser, and hence stronger sand deposit loaded by a stronger event than in case 1. The same two levels of strains, 10 and 15% are adopted as a base for this analysis. Figure 2.9 shows the probability curves for development of 10% and 15% strains and initial liquefaction. The behavior for this case is quite different than that observed in Case 1. After 150 zero crossings there is a probability of one of observing liquefaction and large strains, i.e after 150 zero crossings, total ground failure could be observed. If the event should be of a much shorter duration, we will draw different conclusions. After 70 zero crossings the probability of liquefaction is one, but the probability of occurrence of large strains is 85% for 10% strains and 60% for 15% strain. For small earth structures that may withstand some movement without collapse, Case 2 may conceivably present an acceptable risk.

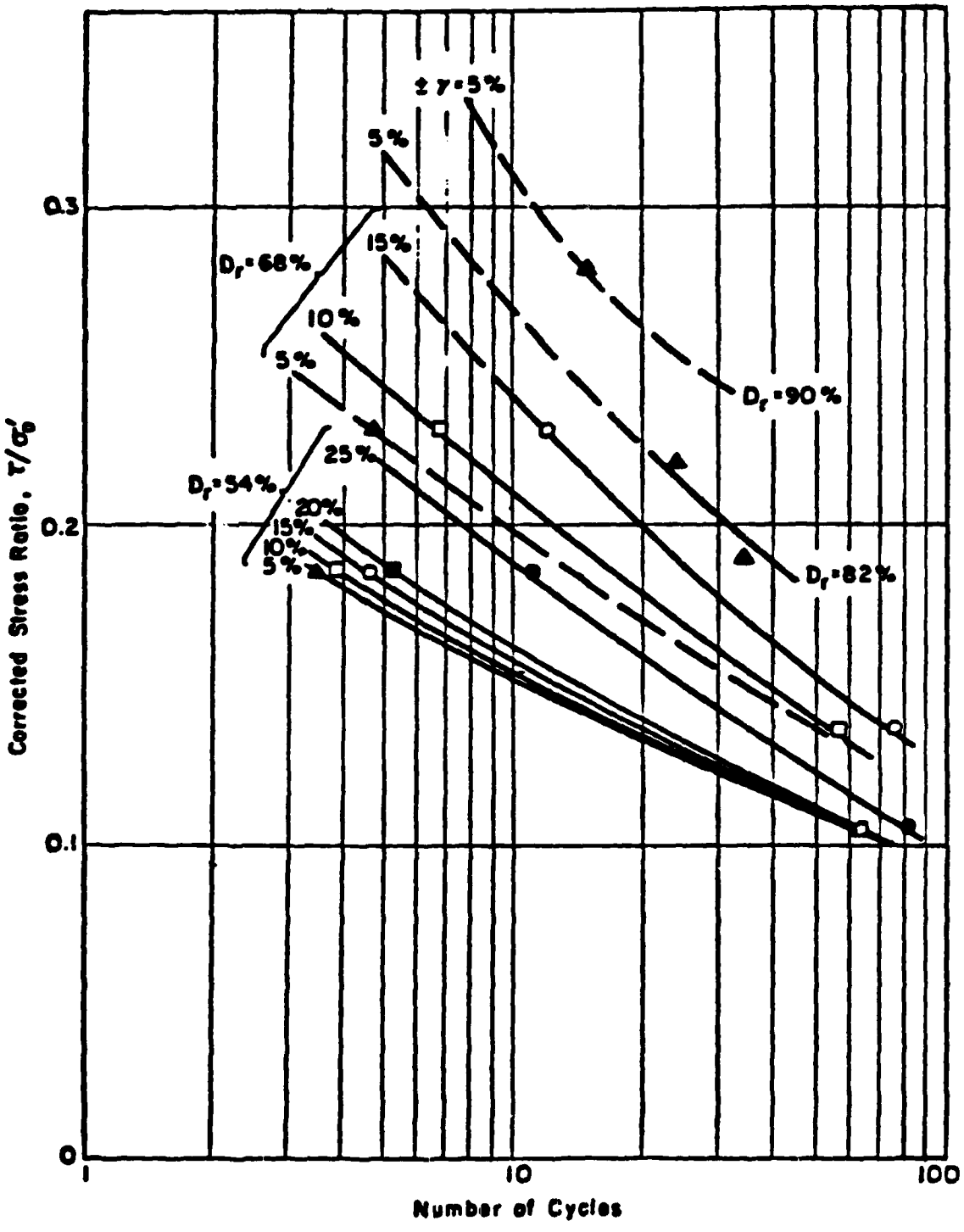

Figure 2.7: Cyclic Strength Curves for Strain Potential

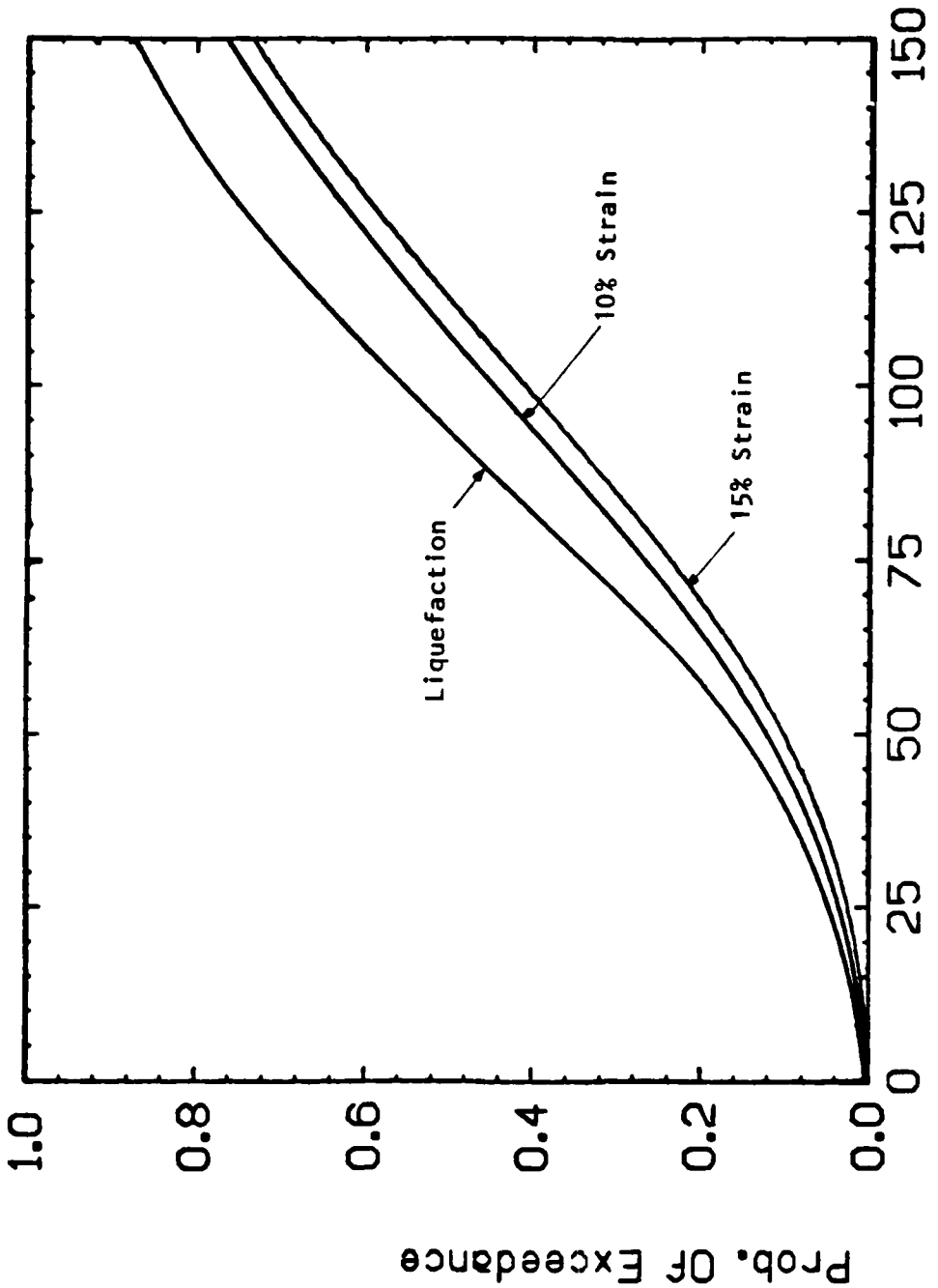

Figure 2.8: Prob. Dev. of Strain Potential Hypothetical Site, Case 1

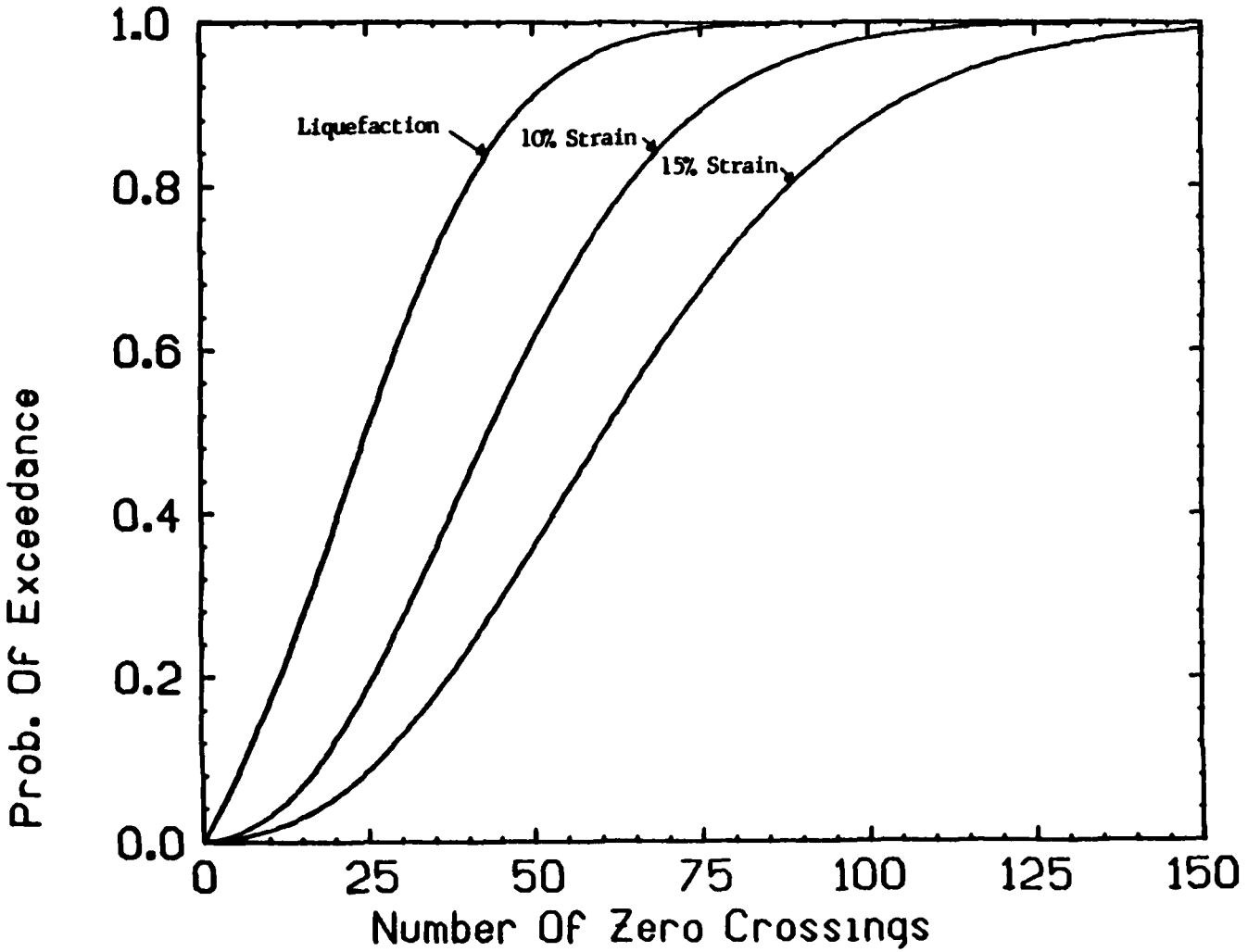

Figure 2.9: Prob. Dev. of Strain Potential Hypothetical Site, Case 2

2.3 SUMMARY

A large number of ground failures that have occurred during earthquakes have been attributed to liquefaction. Initial liquefaction of the soil mass may not in itself constitute a catastrophic failure. The consequences of initial liquefaction such as the reduction in shear strength and large strains may be the cause of dramatic failures. In this chapter, probabilistic models for the prediction of seismically induced pore pressures and shear strain potential are developed. Application of the models are illustrated for a hypothetical site and design earthquakes. In the next chapter of this report, the models are applied to documented case histories.

Chapter III

CASES HISTORY

3.1 INTRODUCTION

The previous chapter presents a probabilistic method for analyzing and predicting the development of pore pressures and strains. In this chapter these models are applied to documented case histories to demonstrate the applicability of these models and to illustrate how the probabilistic design parameters are chosen. The probabilistic pore pressure model developed by Chameau (1980) and the probabilistic shear strain model developed by Hadj Hamou (1982) are used herein to analyze the behavior of three sites where liquefaction did and did not occur during earthquakes.

3.2 LAKE AMATITLAN, GUATEMALA, 1976

On February 4, 1976, Guatemala was struck by an earthquake registering a 7.5 Richter Magnitude. One of the effects of the earthquake was extensive liquefaction which occurred near Lake Amatitlan.

3.2.1 The site and the earthquake

3.2.1.1 The site

Lake Amatitlan is located approximately 13 miles (21 km) southwest of Guatemala City and about 100 miles (160 km) south west of the epicenter (Figure 3.1) of the earthquake . Lake Amatitlan is in the central Guatemalan volcanic lineament which has been, in recent geologic time, the most volcanic segment in Central America (Stoiber and Carr, 1973). The Pacoya Volcano, located on the south shore of Lake Amatitlan, is still active. The geology around Lake Amatitlan is directly related to the volcanic activity of the area. Williams (1960) conducted a thorough geological investigation of the Guatemalan Highlands where Lake Amatitlan is located. The tertiary rocks around the lake are lavas with interbeds of tuffaceous sediments. Between Guatemala City and the north shore of the lake, only waterlaid pumice deposits are to be seen.

Following the earthquake, extensive liquefaction was reported at the settlement of La Playa on the northeast shore of the lake (Seed et al., 1979). In this area the subsurface soils are mainly composed of waterlaid pumice. Figure 3.2 shows the areas where liquefaction did and did not occur around the Lake. The general area behind the shoreline is quite flat with the ground sloping up gently at about 2 degrees away from the lake. The area of extensive liquefaction extended about 600 feet behind the nearest shoreline and is marked by the shaded zone in Figure 3.3. A second zone where evidence of liquefaction was apparent but its effects were less severe extended about 1200 feet behind the shoreline. Within the zone of extensive liquefaction there was

subsidence and severe ground disruption. The ground movement resulted in heavy damage in the resort settlement of La Playa where 29 of 32 houses were destroyed. In the zone of less severe liquefaction there was some ground cracking.

The soil conditions in the areas where liquefaction did and did not occur were explored by borings made to a depth of about 70 feet (Figure 3.2 from Seed et al., 1979). Standard penetration tests were performed in each boring at intervals of five feet and samples were extracted for some laboratory testing. From the results of the field testing program, a soil profile of the area was estimated and is presented in Figure 3.3. The area is covered by a surficial layer of brown pumice sand varying in depth from about five to ten feet. The first layer is underlain in the zone of liquefaction by medium coarse sand containing pumice fragments and in the non-liquefied area by an intermediate layer of black clayey silt above the same type of sand with pumice particles found in the liquefied zone. The water table varies in depth from about four to five feet near the shoreline to about twelve feet in the area where no liquefaction was observed. Based on the blow count data it is presumed that the pumice soils found around Lake Amatitlan have a rather low density. Also due to the volcanic activity of the region, volcanic ashes are present in the sand, making it a lightweight material leading to unusually low effective stresses in the gravity environment. The grain size distribution for samples taken from depths between 30 to 45 feet in borings 3 and 4 is shown in Figure 3.4. along with the grain size distribution of the Monterey sand No. 0 . It can be seen by comparison to the Monterey sand that the Amatitlan sands are well graded ; they are

classified primarily as medium coarse sand. Specific gravity of the Amatitlan sand was about 2.1.

In order to evaluate the resistance of the sand to cyclic loading, Seed and his co-workers conducted a serie of cyclic laboratory tests on reconstituted samples extracted at depths ranging from 30 to 40 feet in borings 3 and 4 located in the non-liquefied zone (Figure 3.3). The results of these tests are shown as the plot of the number of cycles required to reach liquefaction versus the cyclic load applied (Figure 3.5).

3.2.1.2 The earthquake

The February 4, 1976, earthquake epicenter was 90 miles (150 km) northeast of Guatemala City on the Montague Fault. There are no records of ground motion induced near Lake Amatitlan. The only strong motion records of the tremor are two seismoscope records obtained in Guatemala City. The total rupture length of the fault was estimated at 140 miles (225 km) (Espinosa, 1976). The isoseismal map, Figure 3.6, shows Lake Amatitlan on the boundary between zones VI and VII. The seismoscope records interpretation indicate that the peak ground acceleration (PGA) at Guatemala City was about 0.25g. Consideration of distances, distribution of Mercalli Intensity and local site conditions suggest that a value of PGA = 0.15 g at Lake Amatitlan is very reasonable.

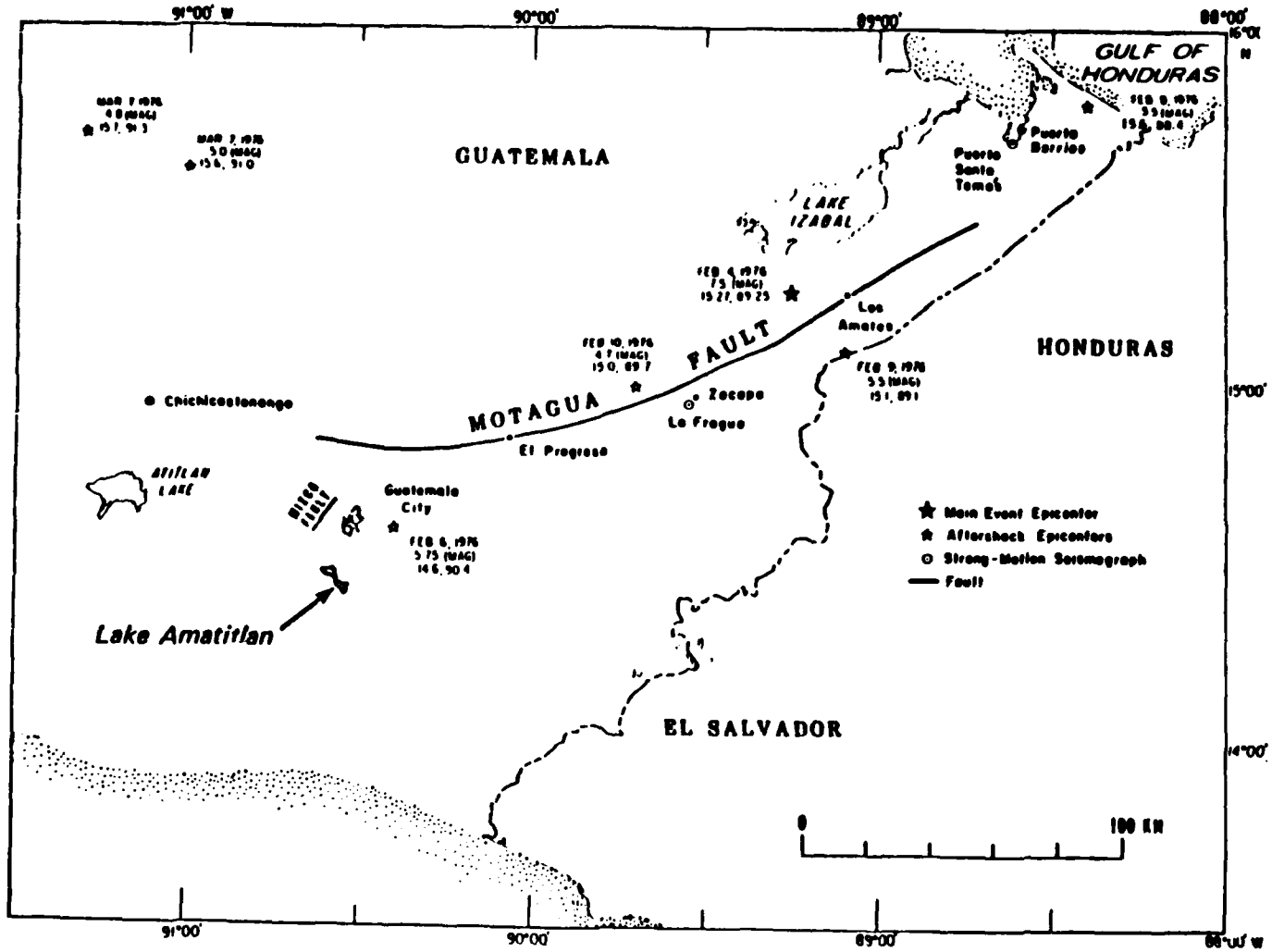

Figure 3.1: Location of Lake Amatitlan

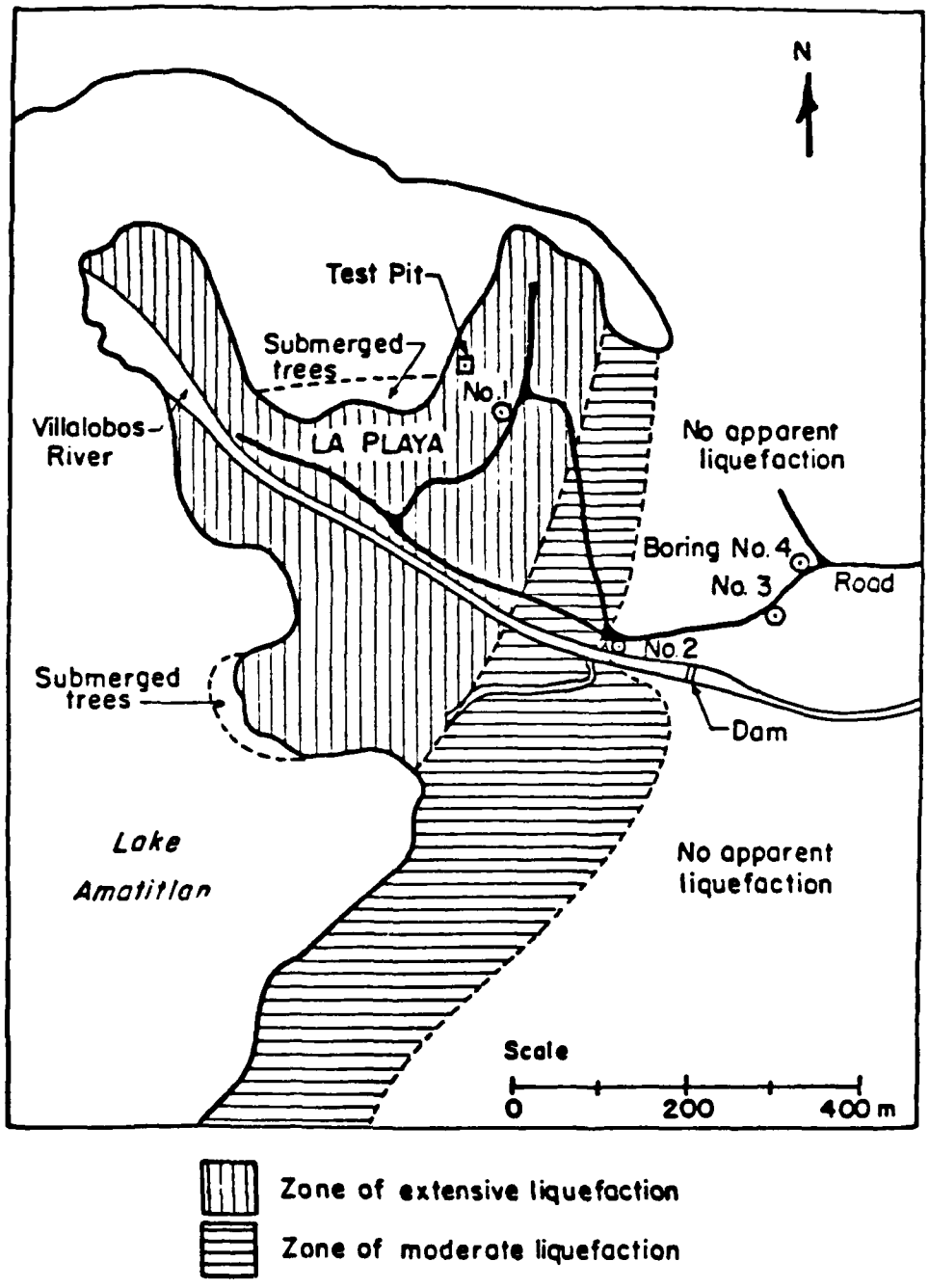

Figure 3.2: Zone of Liquefaction and Location of Borings-Amatitlan

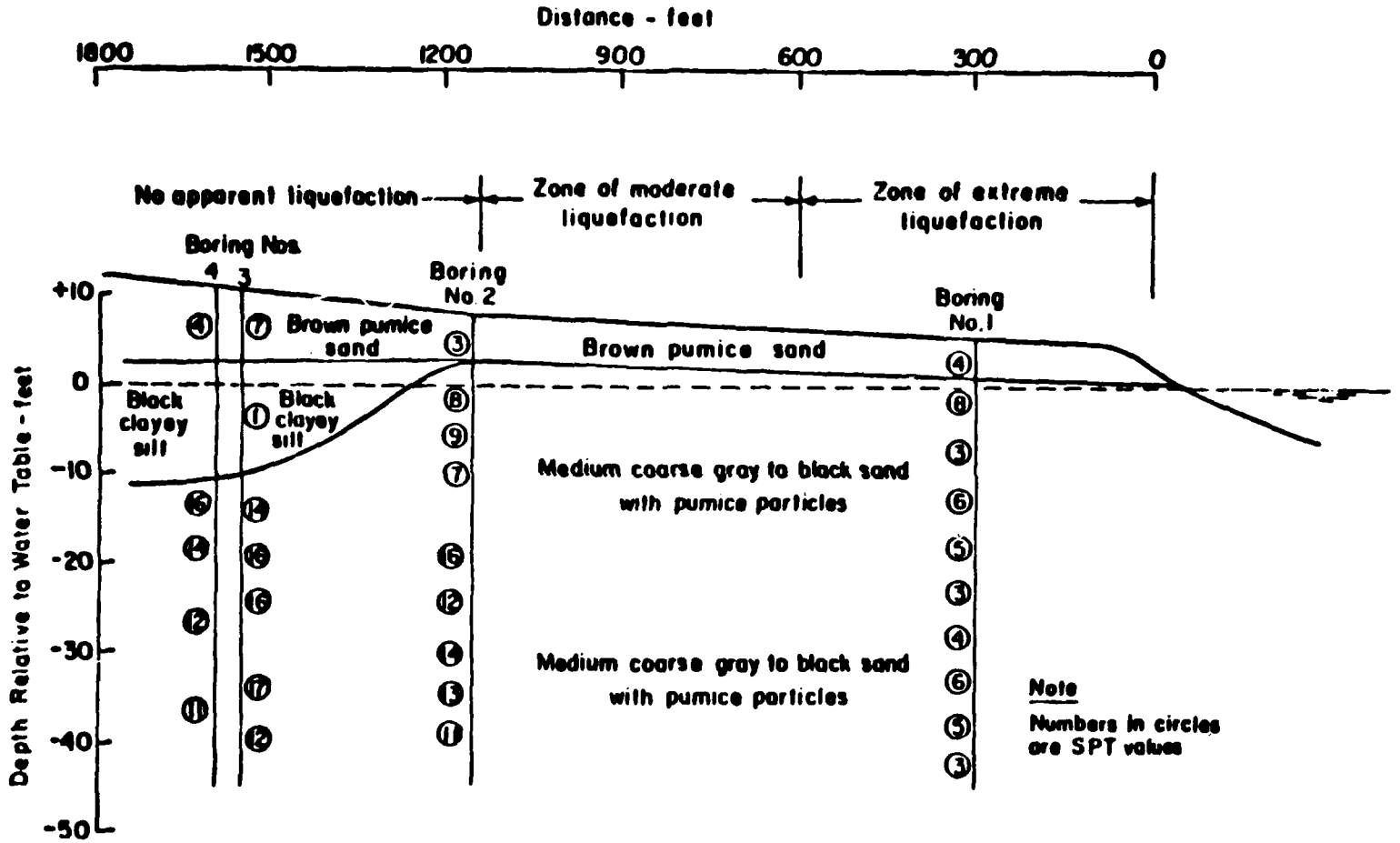

Figure 3.3: Soil Profile at Amatitlan

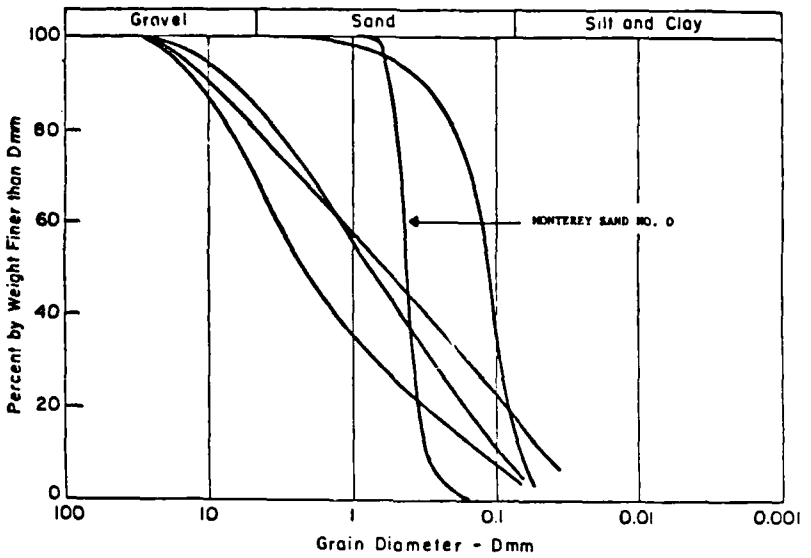

Figure 3.4: Grain Size Distribution at Amatitlan

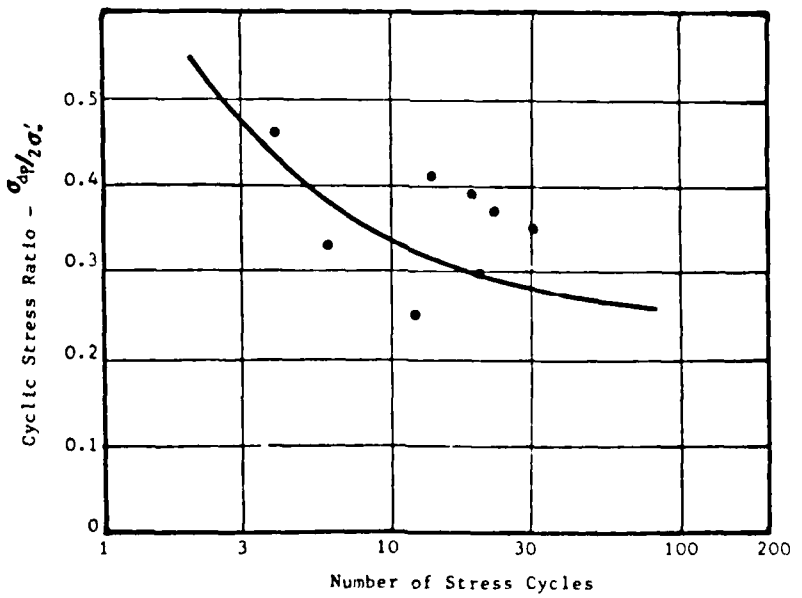

Figure 3.5: Results of Cyclic Triaxial Tests

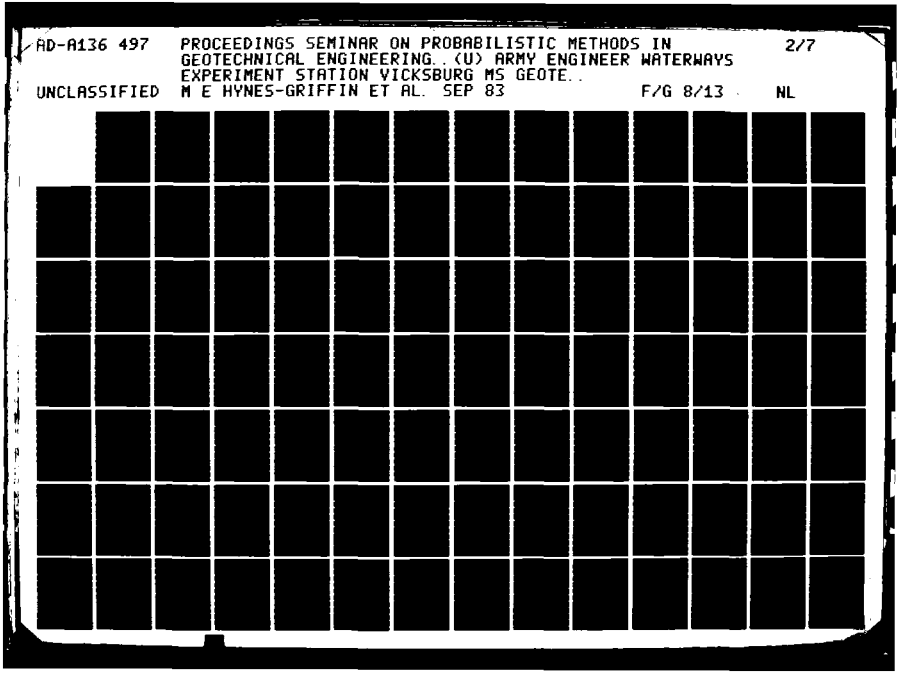
AD-A136 497 PROCEEDINGS SEMINAR ON PROBABILISTIC METHODS IN GEOTECHNICAL ENGINEERING. (U) ARMY ENGINEER WATERWAYS EXPERIMENT STATION VICKSBURG MS GEOTE..
2/7
UNCLASSIFIED M E HYNES-GRIFFIN ET AL. SEP 83
F/G 8/13
NL

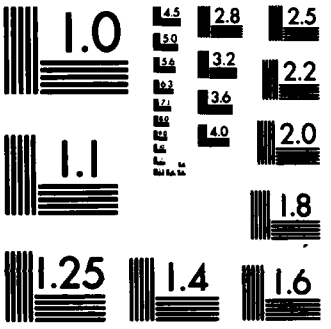

MICROCOPY RESOLUTION TEST CHART
NATIONAL BUREAU OF STANDARDS-1963-A

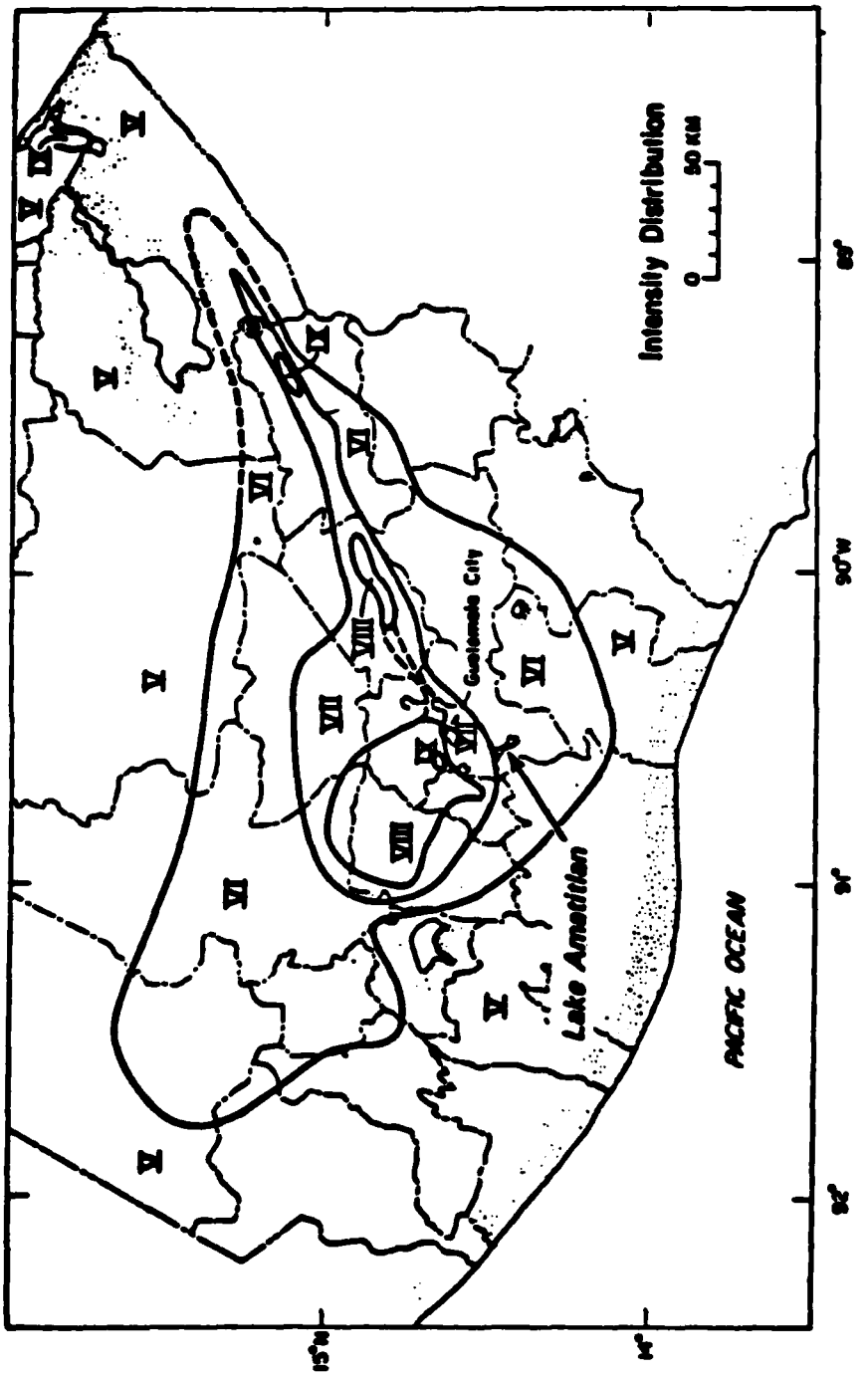

Figure 3.6: Isoseismal Map

3.2.2 Analysis

In the study of the Amatitlan site three different zones can be isolated based on observed phenomena :

Zone of extensive liquefaction : Zone I

Zone of moderate liquefaction : Zone II

Zone of no apparent liquefaction : Zone III

We will examine Zones I and III due to the extreme nature of their behavior. The soil strength and earthquake parameters necessary to the probabilistic analyses are listed in Table 3.1. The last column in the table indicates if the information is directly available through previous studies. Otherwise the best probable input is chosen for the missing parameters based on the available information , previous studies and the author's judgement.

TABLE 3.1

Parameters for Lake Amatitlan

	Parameter	
Earthquake	PGA or RMS of acceleration	Yes
	Duration	No
	Number of cycles	No
Soil	Density	Yes
	Cyclic strength curve	Yes
	Watertable Level	Yes
	Pore Pressure Curve	No

3.2.2.1 Soil strength parameters

Data on the cyclic strength and relative density of the material at Lake Amatitlan is presented in the study conducted by Seed et al., 1979. Direct test data on the form of the pore pressure response is not directly available and has to be assumed, however reliable analytical expressions have been proposed in the literature for this purpose. For example as noted earlier Chameau (1980) uses the following expression:

$$R_n = 1 - \left[\sin\frac{\pi}{2}(1-R_u)^{1/\beta} \right]^{2\alpha} \qquad (3.1)$$

The meaning of R_n, R_u, α and β is discussed in Section 2.1.3 . The values chosen for the shape parameters α and β are described with the presentation of the results of analysis.

3.2.2.2 Earthquake parameters

The seismoscope records of the tremor can only give information on the peak ground acceleration at the site. Information such as duration and dominant period of the motion must be deduced by other means. A study by Seed and Idriss (1969) relates magnitude and length of fault rupture. For earthquakes of magnitude greater or equal to 7 3/4 RM the fault break propagates along the fault at a velocity of about two miles per second. Considering the earthquake was assigned a magnitude of 7.5 and the reported fault rupture was about 140 miles, the duration of shaking was estimated as being somewhat less than 70 seconds. Duration of strong motion shaking can also be related the the Modified Mercalli Intensity (Trifunac and Brady, 1975). The writers give the following

values for duration of ground shaking for a Modified Mercalli Intensity of VI:

MMI VI: Mean Duration 30 seconds

Standard Deviation 16 seconds.

A duration of 50 seconds is chosen herein as a reasonable value for the duration of the earthquake.

The number of cycles in the earthquake is a function of the dominant period of the deposit. For a soft deposit such as the sand and pumice, relatively high natural periods can be expected. Accordingly a natural period ranging from 1 to 1.25 second is selected for the site. This choice along with the chosen duration of 50 seconds leads to a number of cycles ranging from 40 to 50. This number agrees with the average number of cycles observed in records of earthquakes of same magnitude.

No differentiation was made between earthquake loading parameters for Sites I and III since they are approximately equidistant from the epicenter .

3.2.3 Results

As mentioned previously the probabilistic evaluation of the development of pore pressures and strains was conducted for zones I and III. In the following analysis the duration of shaking will be taken as 50 seconds, the number of cycles as 40 to 50 and the PGA at 0.15 g. The parameters necessary in the probabilistic models were described in previous sections. For each site a table will present the values adopted for each parameter.

3.2.3.1 Zone I

Development of pore pressure

The results of the cyclic load tests in terms of the ratio $\sigma_{dp}/2\sigma_3'$ (Figure 3.5) can be converted to an equivalent loading condition in the field in terms of the ratio τ/σ_0' using the following expression proposed by Seed and Peacock, 1971:

$$\left(\frac{\tau}{\sigma_0'}\right)_{field} = C_r\left(\frac{\sigma_{dp}}{2\sigma_3'}\right)_{triaxial} \qquad (3.2)$$

where C_r is a coefficient dependent on the relative density of the soil. For the relative density found at Amatitlan, C_r was set as 0.57.

TABLE 3.2

Parameters for Zone I, Amatitlan

γ_t=90 pcf
Depth of Water Table D_w= 4 Feet
Number of Positive Zero Crossings = 40-50
α= 2.0 β= 1.05 PGA= 0.15 g SR=3.5 $\sigma_{1n\ 1}$=0.5

Depth	σ_0	σ_0'	r_d	r	r/σ_0'
15	1350	664	.97	56.1	.085
20	1800	802	.96	74.1	.092
25	2250	940	.95	91.6	.097
30	2700	1078	.92	106.5	.099
40	3600	1354	.87	134.2	.099
50	4500	1630	.75	144.6	.089

Liquefaction potential is computed deterministically at the depths shown in Table 3.2. The critical depth can be estimated by the value of the ratio τ/σ_0', the higher the ratio the greater the risk for liquefaction. For Zone I this critical depth is around 40 feet. Probabilistic analyses are performed at depths 25 to 50 feet to surround the most likely failure area. The results of the probabilistic analysis are presented in Figures 3.8 through 3.11 where the probability of exceeding a pore pressure ratio of 0.1, 0.5 and 1.0 are plotted versus the number of positive zero crossings for each depth. These results can be interpreted, for a specified depth, as follows; for depth 25 feet, after 20 cycles (positive zero crossings) of loading, the probability of exceeding pore pressure ratios of 0.1, 0.5 and 1.0 are 100%, 53%, and 36% respectively. After 70 cycles the probability of exceeding ratios of 0.1, 0.5 and 1.0 is 100%.

The probability of observing liquefaction, corresponding to a pore pressure ratio of one, can be evaluated at different depths throughout the deposit from the figures. Considering the likely range of cycles in the 1976 earthquake, (40 to 50), the following results are obtained :

Depth	Probability of Reaching Liquefaction
25′	88% to 97%
30′	91% to 98%
40′	92% to 99%
50′	58% to 78%

The very high probability of liquefaction at all depths in Zone I corroborates the behavior observed in the field, which indicated substantial evidences of liquefaction.

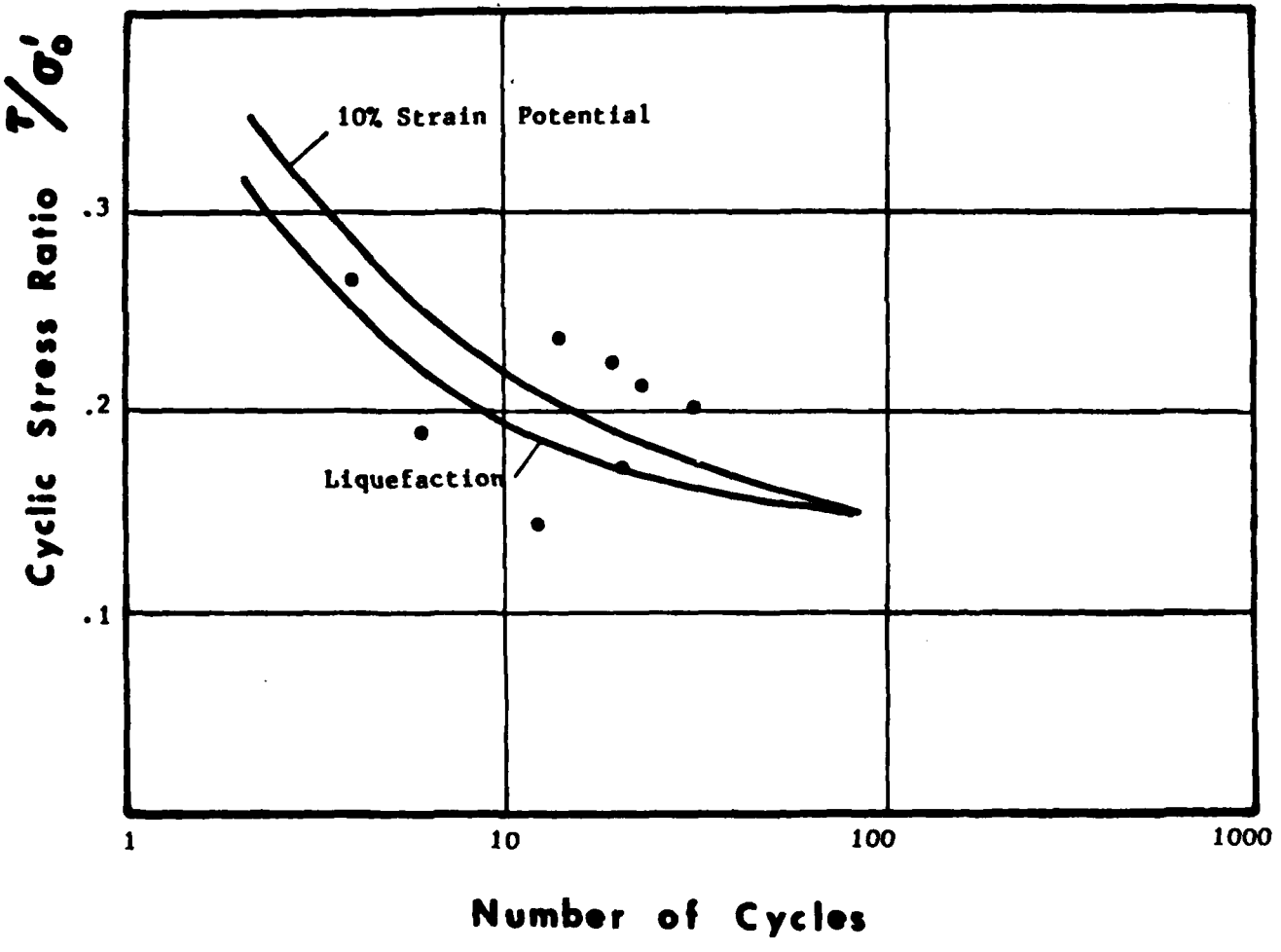

Figure 3.7: Cyclic Strength Curves Converted for Cyclic Shear

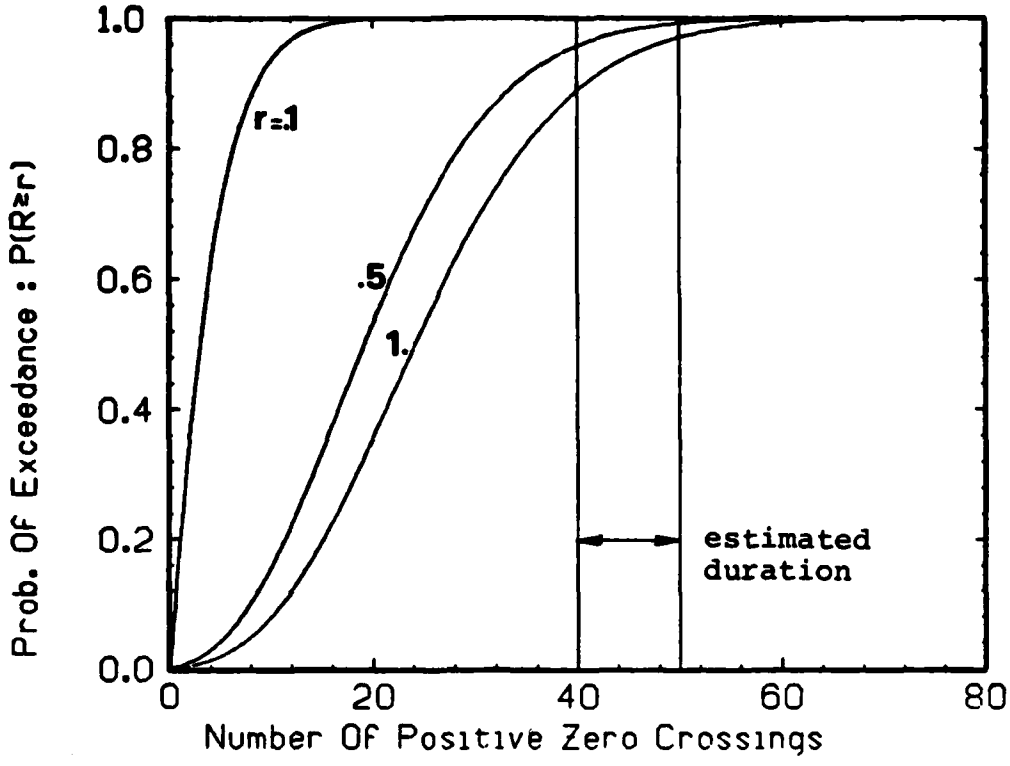

Figure 3.8: Prob. Dev. of Pore Pressures Amatitlan Zone I, D = 25 ft

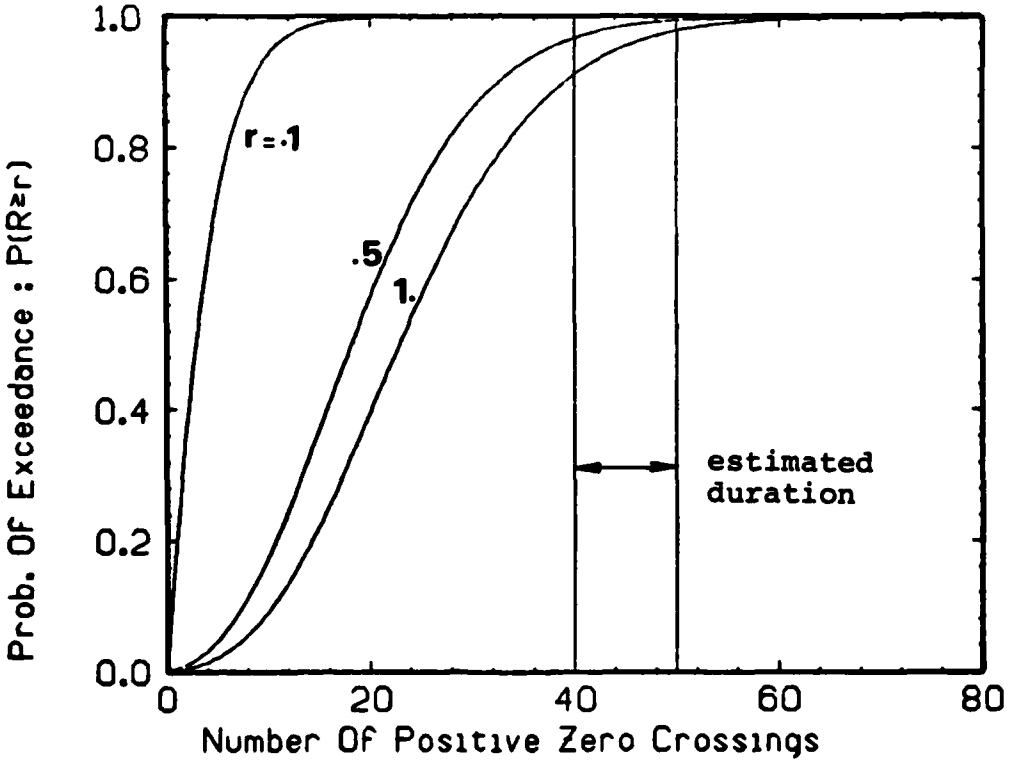

Figure 3.9: Prob. Dev. of Pore Pressures Amatitlan Zone I, D = 30 ft

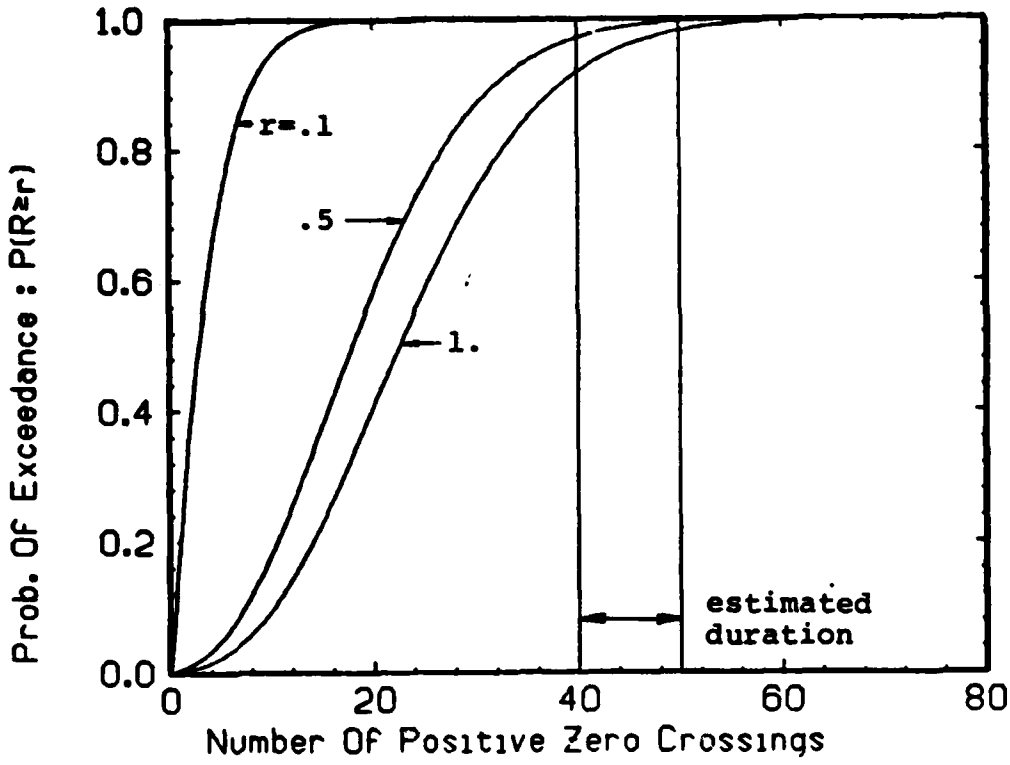

Figure 3.10. Prob. Dev. of Pore Pressures Amatitlan Zone I, D = 40 ft

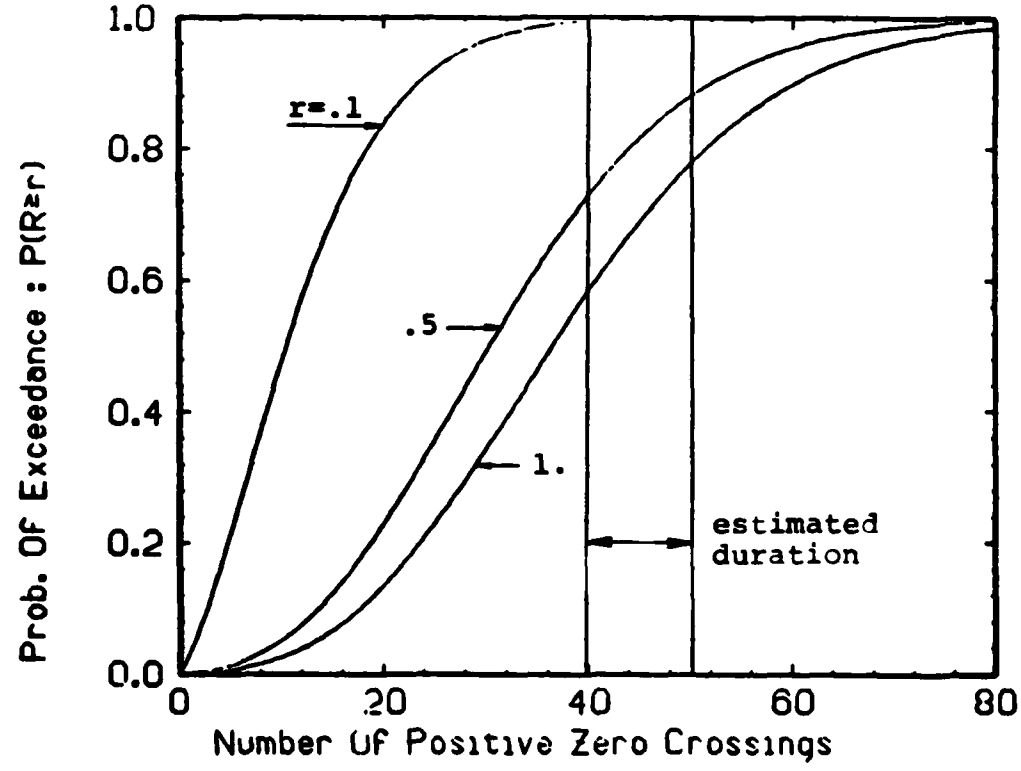

Figure 3.11: Prob. Dev. of Pore Pressures Amatitlan Zone I, D = 50 ft

Development of strains

The probabilistic development of strains is evaluated using the model presented in Chapter II, and the analysis will be performed at the calculated critical depth of 40 feet. A strain level of 10% is chosen as representative of severe damage to the ground. In order to evaluate the cyclic strength curve for a failure criterion of 10% strain, the following method is used. Results of cyclic triaxial or simple shear test on sands conducted for different failure criterion (5%, 10%, 15% strain) show that the curves tend to be proportional to each other. This is visible on Figure 3.12 from De Alba et al. (1975). Analysis of data published for other soils seems to show that the proportionality ratio needed to go from one level of strain to the other is constant for a given relative density. Cyclic strength curves for different strain criteria can hence be deduced from the knowledge of one initial curve. This fact was noted and used by Seed and his co-workers in their analysis of the slides of the San Fernando Dams (Seed et al., 1973). The cyclic strength curve representing the number of cycles necessary to reach 10% strain under a strain loading level is shown plotted on Figure 3.7. The probabilistic development of strain at site Zone I can be evaluated at depth 40' using the data in Table 3.2 and Figure 3.7. Probabilities of exceeding 10% strain after each positive zero crossing are shown on Figure 3.13. In the range of cycles of the earthquake the probability varies from 50% to 75% that a 10% ground strain will be reached.

It is interesting to compare the likelihood for pore pressure development to the likelihood for large strain potential. The

probability of reaching liquefaction is much higher than the probability of observing 10% strain, 92 to 99% versus 50 to 74%. The risk of development of large strain is still fairly high and the predicted behavior in Zone I agrees quite well with the observed behavior during the earthquake. At the La Playa resort located in site Zone I, important damage was reported; cracking, subsidence and eruption of sand boils. The results from the pore pressure and strain analyses can also be used to predict alternative response of the site. Assuming that an earthquake of similar level of acceleration but shorter duration (30 cycles) hits the area, there is a high probability it will generate high pore pressures but a relatively reduced probability for strains. Figures 3.10 and 3.13 show the probability of reaching liquefaction and 10% strains are about 75 and 25% respectively. These results illustrate the following two points:

1. Even if liquefaction is very likely to occur, as indicated by the pore pressures, the risk of high ground strains is often less, and hence there is less likelihood of damage to the site.

2. The duration of an event, in terms of number of positive zero crossings or number of cycles, has a strong influence on pore pressure and shear strain development.

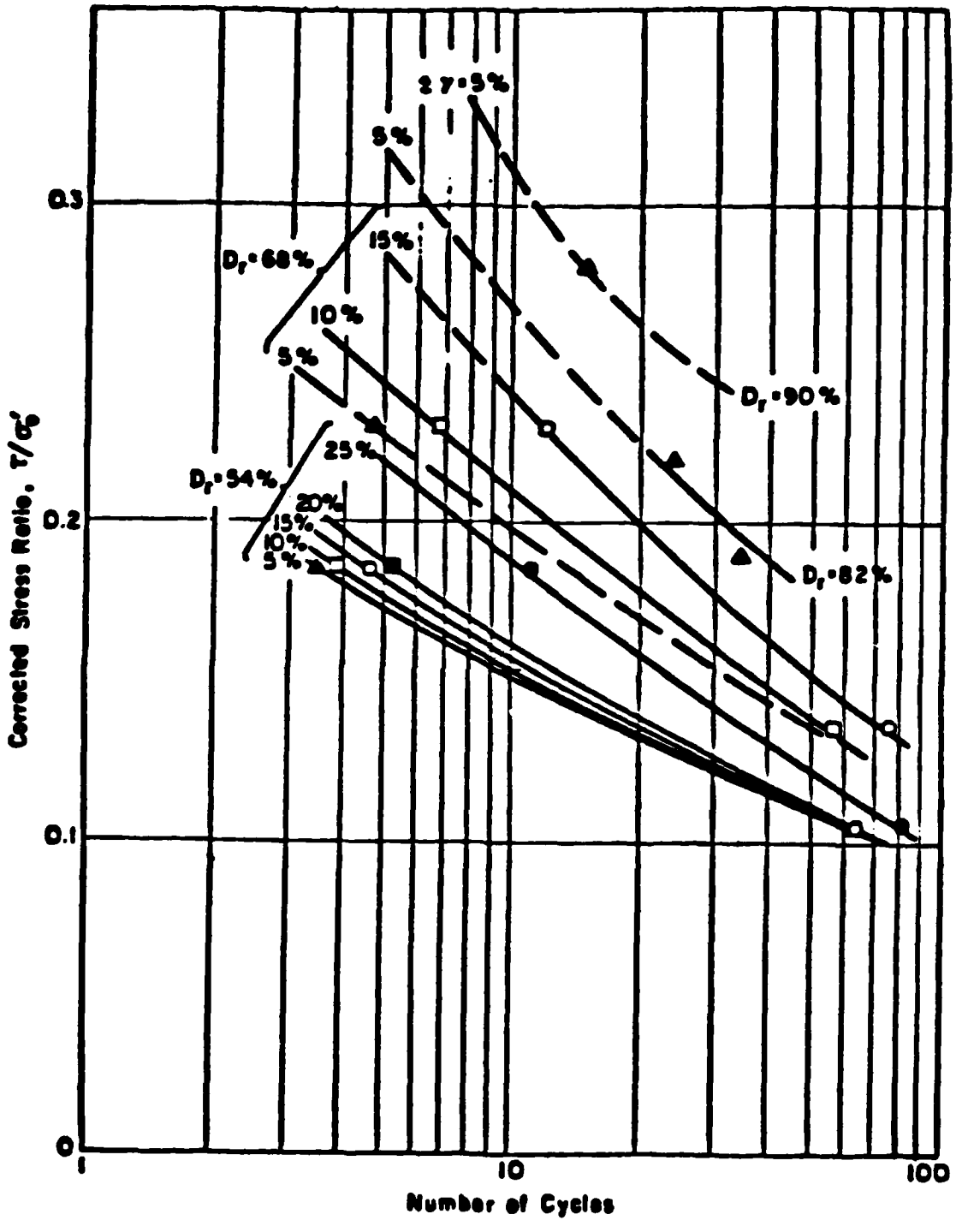

Figure 3.12: Cyclic Strength Curves for Strain Potential

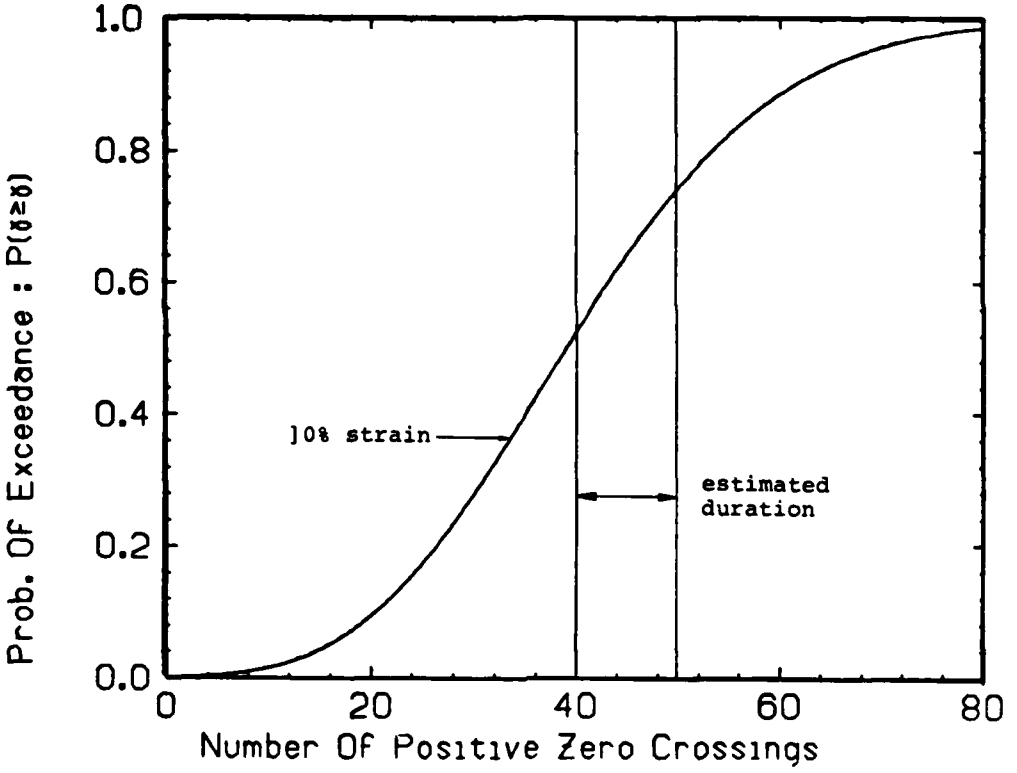

Figure 3.13: Prob. Dev. of Strain Potential, Amatitlan Zone I D=40 feet

TABLE 3.3

Parameters for Zone III, Amatitlan

γ_t=90 pcf for sand and γ_t=100 for clayey-silt
Depth of Water Table D_w= 10 Feet
Number of Positive Zero Crossings = 40-50
α= 1.9 β= 2.1 PGA= 0.15 g SR=3.5 $\sigma_{ln\ 1}$=0.5

Depth	σ_0	σ_0'	r_d	r	r /σ_0'
20	1920	1296	.96	79.0	.062
25	2370	1434	.092	96.5	.067
30	2820	1848	.92	111.2	.071
40	3720	1848	.87	138.7	.075
50	4620	2124	.75	148.5	.070

3.2.3.2 Zone III

Development of pore pressures

This location presented no evidence of liquefaction during the 1976 earthquake. The probabilistic development of pore pressure is evaluated using the parameters reported in Table 3.3 and the mean cyclic strength curve shown in Figure 3.7. Zone III is characterized by a deeper location of the water table (10 feet) and the presence of a 12 foot thick clayey silt layer (Figure 3.3) relative to Zone I. The results of the probabilistic analysis are presented in Figures 3.14 to 3.17 for depths of 30, 40, and 50 feet. At the end of the estimated numbers of cycles of loading in the earthquake the following probabilities of reaching liquefaction are obtained:

Depth	Probability of reaching liquefaction
25′	1-2%
30′	2-5%
40′	7-15%
50′	7-15%

Those probabilities are very low and agree quite well with the observed behavior in the field, where no evidence of liquefaction was reported.

Development of strains

It was observed in analyzing site Zone I that the probabilities of having strain of 10% are lower than the probabilities of reaching liquefaction. We may therefore assume, considering the low probability of reaching a stage of liquefaction at site Zone III that the probability of reaching 10% strain is very low. The analyses indeed show that the probability of reaching 10% strain at Zone III is on the order of zero.

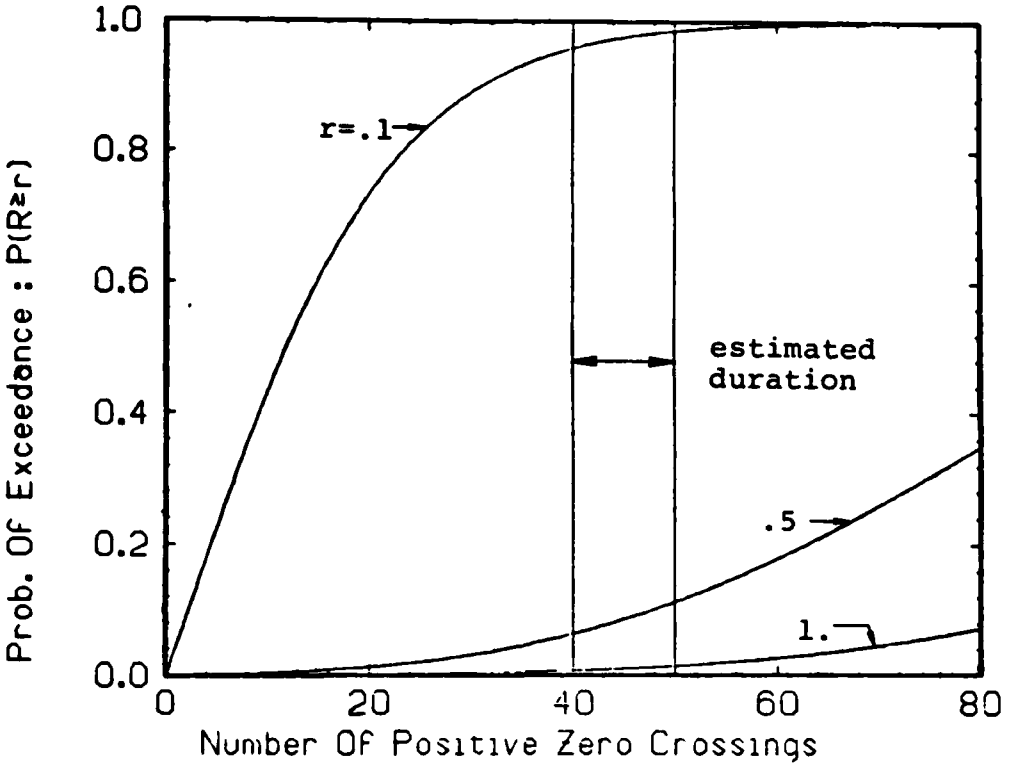

Figure 3.14: Prob. Dev. of Pore Pressures Amatitlan Zone III, D = 25 ft

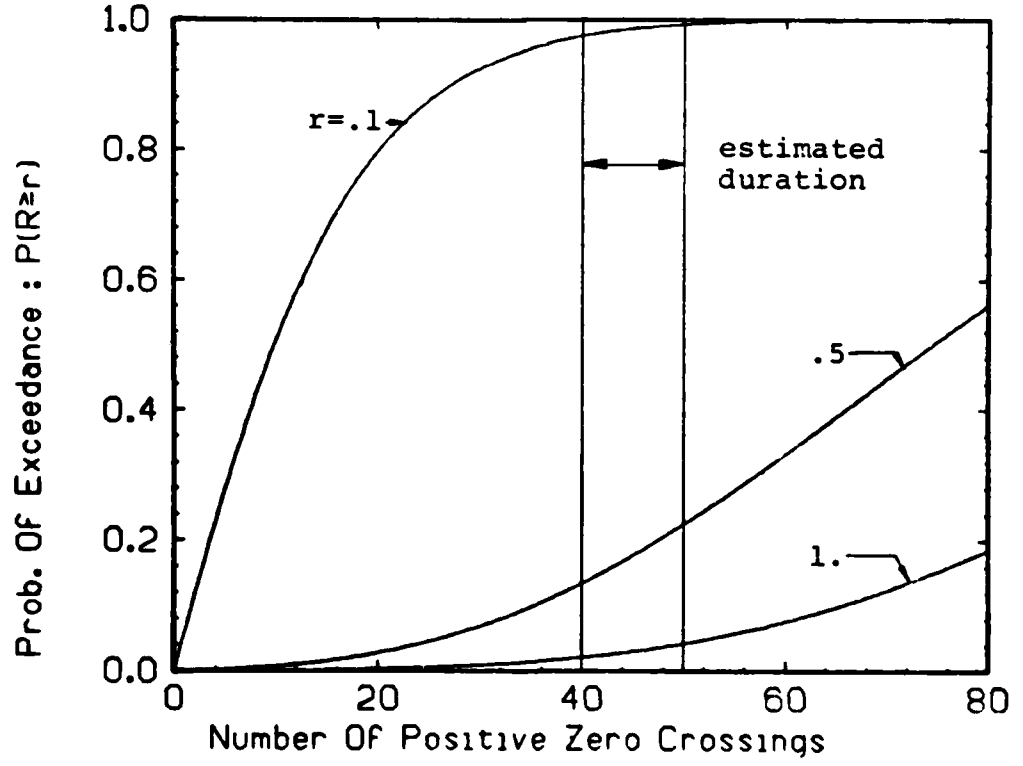

Figure 3.15: Prob. Dev. of Pore Pressures Amatitlan Zone III, D = 30 ft

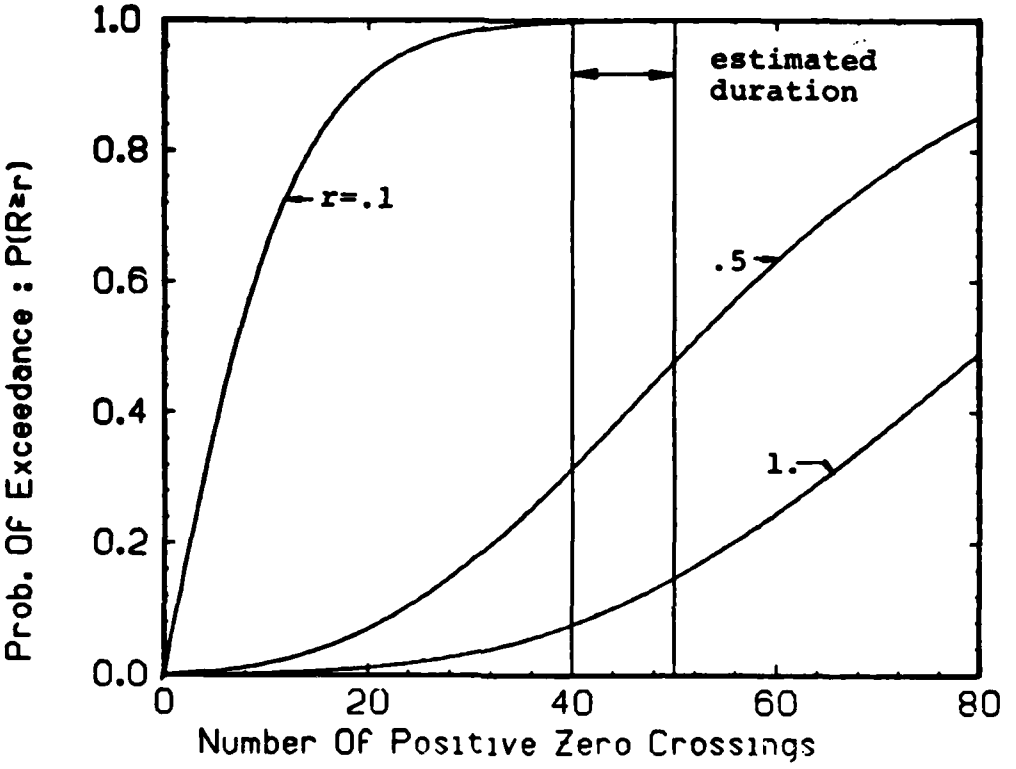

Figure 3.16: Prob. Dev. of Pore Pressures Amatitlan Zone III D=40 feet

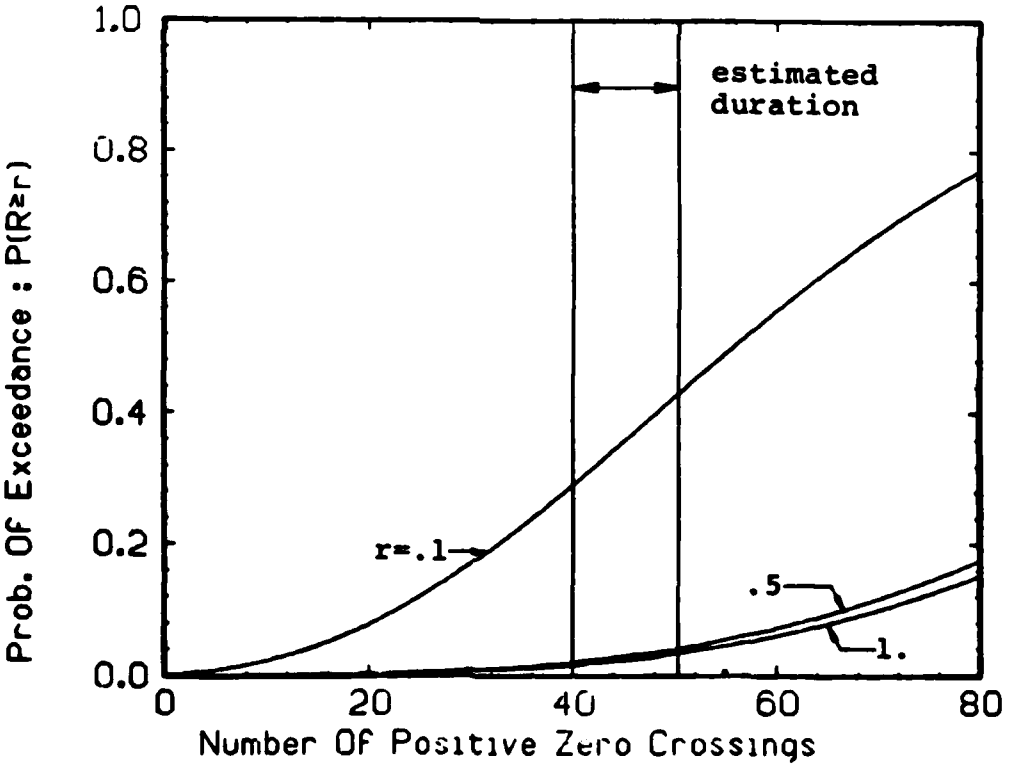

Figure 3.17: Prob. Dev. of Pore Pressures Amatitlan Zone III D=50 feet

3.2.4 Discussion

Comparison of the two sites

Figure 3.18 shows the probability curves for a pore pressure ratio of one occuring at a depth of 40 feet for Zone I and III at Lake Amatitlan. The difference in behavior is very striking, after 50 positive zero crossings the probability of observing initial liquefaction is in the order of 100% for Zone I and only in the order of 15% for Zone III. This shows the dramatic effect relative density can have on liquefaction potential. Only a longer lasting or stronger earthquake would eventually lead to liquefaction at Zone III.

Uncertainty of the cyclic strength curve

The uncertainty of the cyclic strength curve is incorporated in the probabilistic model by a lognormal distribution on the cyclic strength curve. The distribution is characterized by its standard deviation $\sigma_{ln\ 1}$ and in the preceeding analyses, $\sigma_{ln\ 1}$ was set at 0.5. This value was selected as a reasonable input based on previous statistical studies (Ferrito et al., 1979). The cyclic test results shown on Figure 3.5 are reported on Figure 3.19 and illustrate the large scatter of the data points around the best fit line. Assuming that the best fit line is the mean, the dispersion of the data points with respect to the mean can be evaluated. The standard deviation computed considering all the data points is $\sigma_{ln\ 1} = 1.104$. The farthest point from the best fit line (Point A) heavily biases the evaluation of the standard deviation. A calculation of $\sigma_{ln\ 1}$ omitting point A leads to $\sigma_{ln\ 1} = 0.734$. To illustrate the degree of this influence, the probabilistic development of pore pressure was reevaluated in Zone III at depth 40′ using $\sigma_{ln\ 1} =$

0.734. The result is shown on Figure 3.20 for a pore pressure ratio of 1.0. It is seen that the probability of reaching liquefaction in 40 to 50 cycles for the site considered increased by about 5% using 0.734 relative to the results obtained previously with 0.5. It can therefore be concluded that the use of $\sigma_{1n\ 1} = 0.5$, although slightly unconservative, is justified and gives reasonable results.

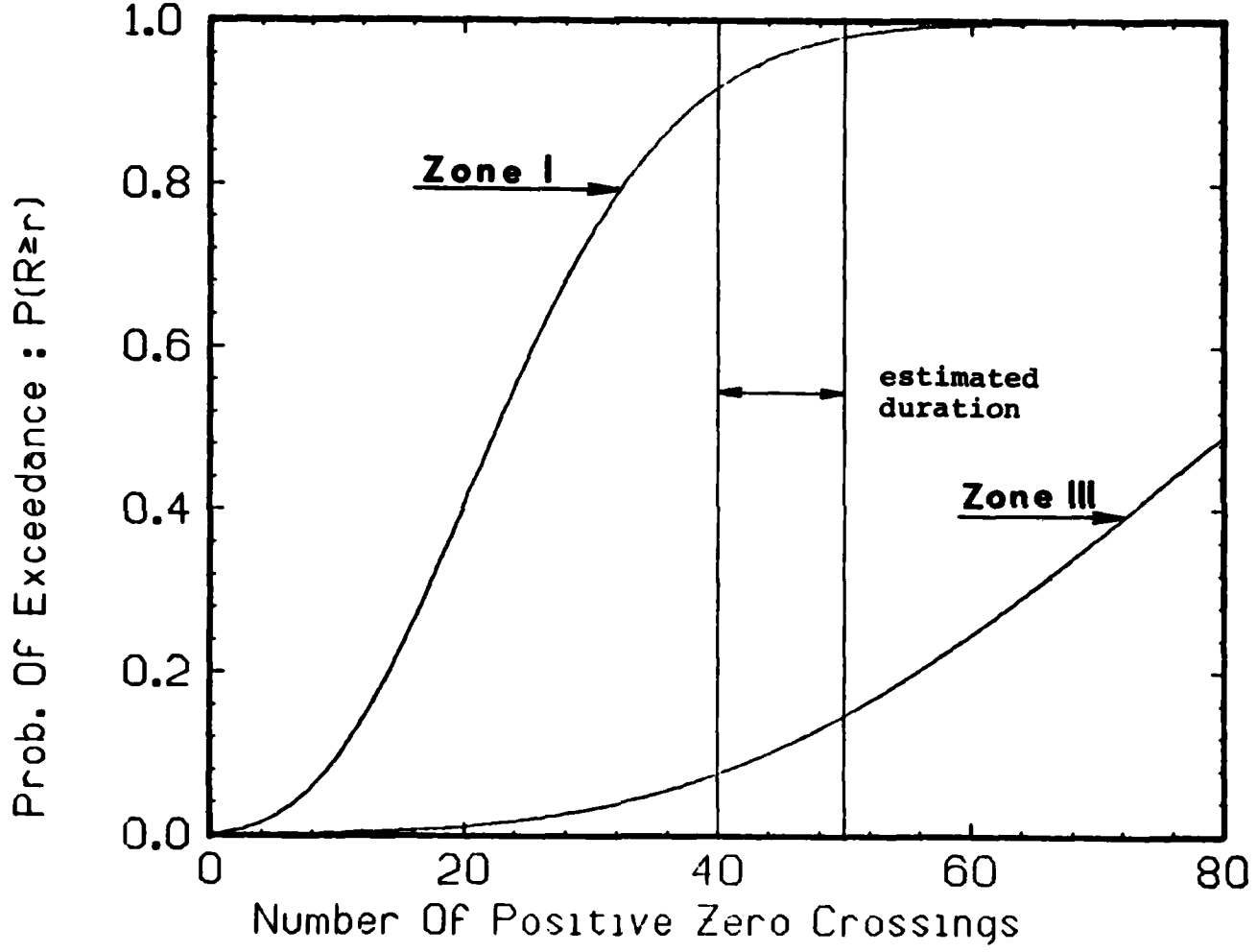

Figure 3.18: Comparison of Zone I and Zone III at Depth D = 40 ft

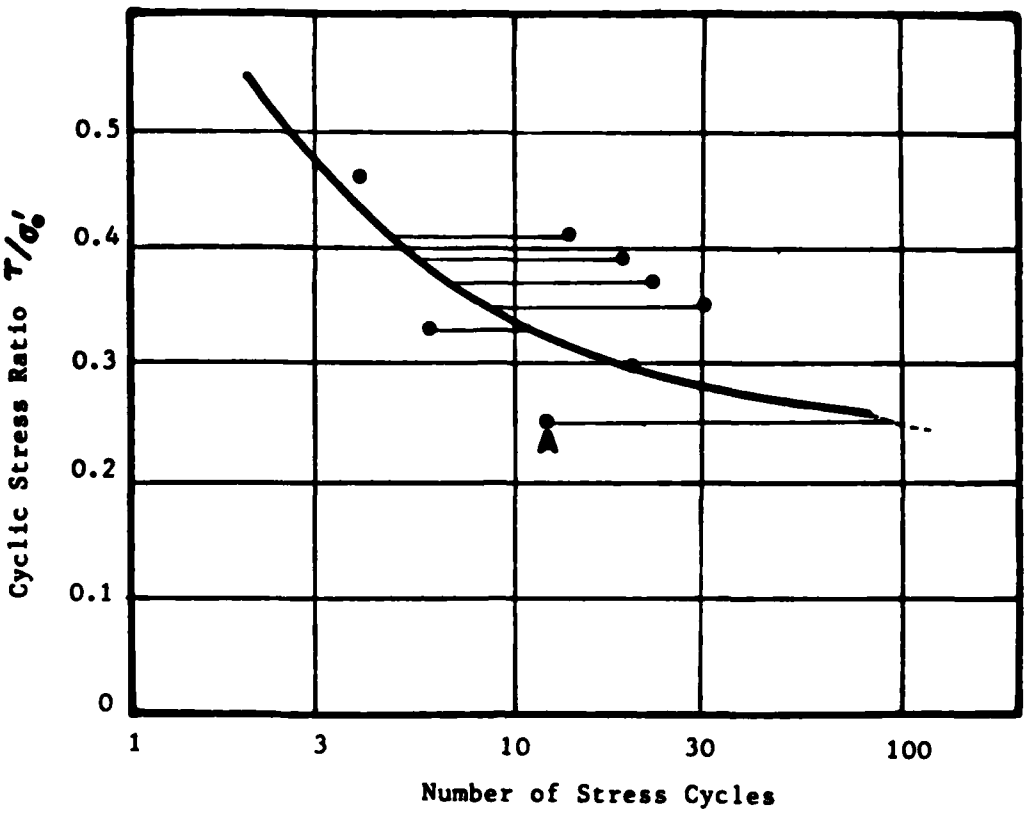

Figure 3.19: Dispersion of Data Point Around the Mean Cyclic Curve

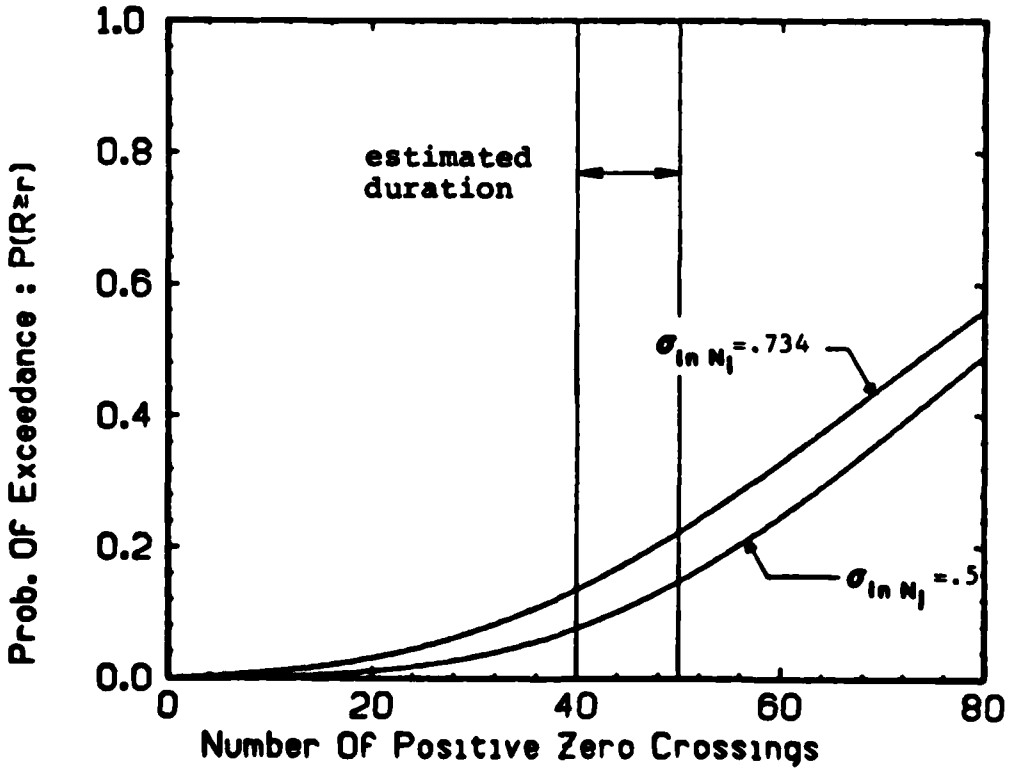

Figure 3.20: Effect of $\sigma_{\ln Nl}$ on the Prob. Dev. of Pore Pressures

3.3 IMPERIAL VALLEY, CALIFORNIA, 1979

On October 15, 1979 an earthquake registering 6.6 on the Richter Scale hit the Imperial Valley in Southern California. Damage was reported in the towns close to the Mexican border and many instances of soil liquefaction were observed.

3.3.1 The site and the earthquake

Liquefaction was observed at two sites near the towns of Brawley and El-Centro and they were selected by a team from the USGS for subsurface exploration (Bennett et al., 1981). The location of the sites is shown on Figure 3.21 . The one near Brawley will be referred to as the River Park Site (RP) and the one closer to El-Centro will be referred to as Heber Road Site (HR). Both showed strong evidence of liquefaction including sand boils and cracking of the ground , and formation of a lateral spread at the HR site.

3.3.1.1 The site

Bennett et al.(1981) described the geology of the area as follows :

The Imperial Valley occupies the northern part of the Salton Basin which is a northward extension of the crustal rifting that opened the Gulf of California. The basin is tectonically active as evidenced by movement on the Imperial and Brawley Faults. The basin ranges from 5 to 130 km in width and is about 200 km long. The central part of the basin contains the Salton Sea, 70 m below sea level, and it contains up to 6,100 m of Tertiary and Quaternary marine, continental and lacustrine sediment. Pleistocene and Holocene sediment (Holocene sediment is as

thick as 100 m in some areas) has been derived from two sources; (1) the Colorado Plateau, through the Colorado River and its distributaries which include the Alamo River, and (2) local hills and mountains bounding the basin. Sediment from bounding hills and mountains has carried into the basin through the New River system. The Holocene depositional history includes thick lacustrine deposits, channel-fill deposits, alluvial fans and eolian deposits.

Channel-fill deposits of the Alamo River form shoestring sand bodies within the lacustrine mud and deltaic sand facies. The channel deposits range from 3 to 20 m thick, and 65 to 300 m wide (Van De Kamp, 1973,). The Alamo and New Rivers contain distinctly different sediment because the rivers have different source areas. The Alamo, supplied by the Colorado River, contains red-brown, well-sorted fine sand and clay, whereas local sources supply the New River with yellow-white, medium to coarse, moderately sorted sand and pale green and tan clay. The juxtaposition of the channel, delta, and lacustrine deposits produces rapid changes in vertical and lateral profiles.

Between 300 and 1600 years ago natural flooding from the Colorado River filled the Imperial Valley and created Lake Cahuilla (Van De Kamp, 1973). Fine-grained muds deposited in Lake Cahuilla commonly interfinger with sand beds. Variations in lake level caused sand to prograde over the muds. The source of the muds can be identified from color. The brown-red muds originated from the Colorado River system, whereas pale green and tan muds originated from local valley margins.

Before agricultural modification, small lakes filled many depressions along river channels that meandered across the old lake bed. Sediment accumulated in these small lakes as deltas, similar to the modern deltas in the Salton Sea. The position of the deltas are controlled by: location of depressions, course of channels, and fluctuations in lake level. Van De Kamp reports that there probably are numerous small deltaic sequences in the southern part of the Imperial Valley.

One of these deltas, fed by a now abandoned channel, occurs west of the Alamo River between Holtville and the Mexican border. Archaeologic and stratigraphic evidence indicate that Lake Cahuilla covered this area 300 to 400 years ago (Sharp, in press). The delta is identified by topographic contour lines that show a lobe of higher ground (Youd and Wieczorek, in press) and by soil surveys (Strahorn and others, 1924) that indicate the lobe of high ground is composed of sandy soils (Figure 3.22). Aerial photography from 1937 shows one major remnant stream channel, outlined by levees and vegetative photolineaments, running down the axis of the delta. Since 1937 most of the channel features have been obliterated by land leveling and cultivation.

Liquefaction effects produced by the 1979 earthquake were concentrated within the delta and particularly in the naturally and artificially filled channel. A complete program of subsurface exploration, including cone penetration and standard penetration tests was performed at both HR and RP sites.

Heber Road Site

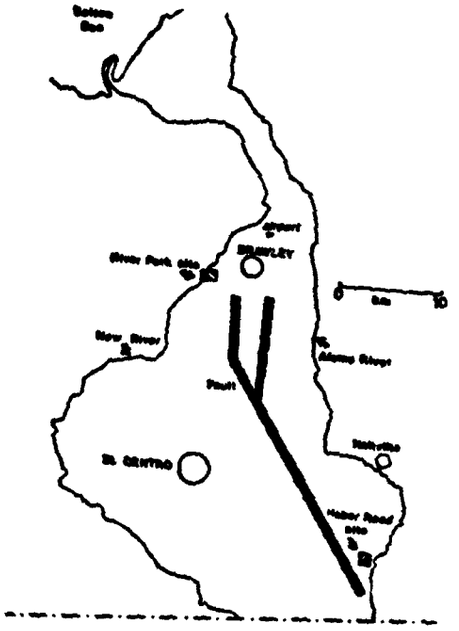

Figure 3.21: Liquefaction Sites in the Imperial Valley

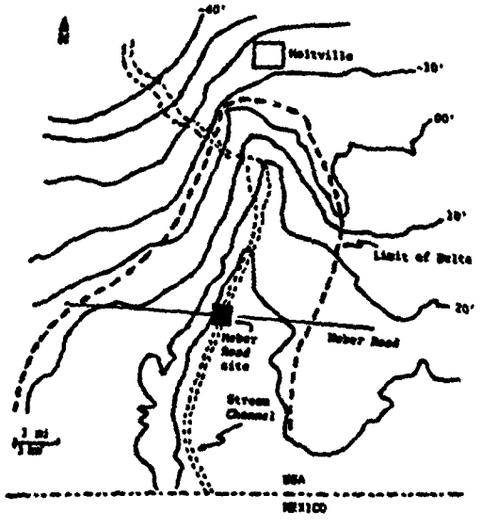

Figure 3.22: Heber Road Site

Heber Road crosses an old stream channel naturally and artificially filled, Figure 3.22. A total of 16 Cone Penetration Tests (CPT) and 17 Standard Penetration Tests (SPT) were conducted and from the results a soil profile of the HR Site can be inferred (Figure 3.23). The average characteristics of each stratum are summarized on Table 3.4. The upper 5 meters of the deposit , which are the most important for the liquefaction issue , consist of three different units of sand and silty soil.

1. Unit A1 is found on the west side of the channel. It is composed of dark brown, dense to very dense, very well sorted fine grained sand.

2. Unit A2 is found in the middle of the channel. It is composed of dark brown, very loose, moderately sorted silty sand and sand. The position of the unit in the channel and the fine grain size of this sediment and the abundance of fresh water gastropods indicate that the lower part of the unit is channel fill.

3. Unit A3 is found on the East side. The unit is composed of dark brown, medium dense, moderately sorted sand and silty sand.

Deposition of the three units in the upper part of the channel is related to the fluvial activity in the relict channel. The relationships between the three units and the channel indicate that they are of late Holocene age. Because unit A2 fills the channel it is probably younger than either unit A1 or A3.

River Park Site

The River Park was built on a flood plain of the New River and is therefore mainly composed of alluvial deposits. The results of the testing program are summarized in Figure 3.24 and Table 3.5. The deposit consists mainly of three units:

1. The upper unit, Unit A, consists of loose, brown sandy and clayey silts

2. The middle unit, Unit B, consists of very fine grained silty clay and clay

3. The lowermost unit, Unit C, is a generally dense well sorted fine sand.

The sand unit appears massive, the only subdivision seen was a color change from brown at the top to grayish brown at the bottom. The cone penetration tests show the upper part (45 cm) of the sand layer to be noticeably looser than the lower part. This lower density may have been caused by liquefaction in the 1979 and previous earthquakes (Bennett et al., 1981). An average density of 100 pcf (1.6 g/cm^3) was estimated for all the materials at both sites from the results of the in-situ tests.

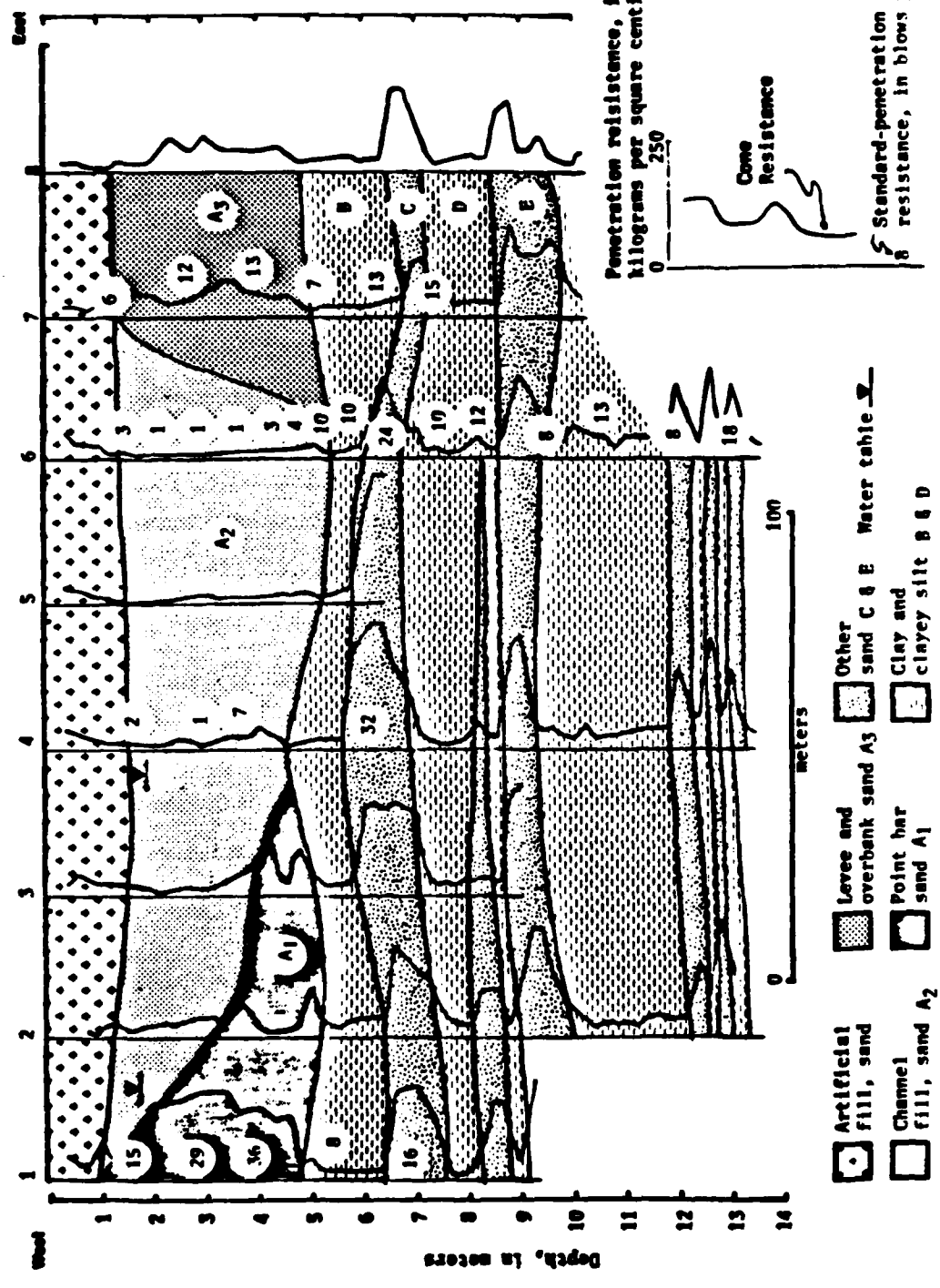

Figure 3.23: Profile of Sediments at Heber Road Site

TABLE 3.4

Characteristics of Sediments at HR Site

UNITS	$\bar{N}$	$\bar{q}_c$	$\bar{R}_f$	$\bar{D}_r$	approximate depth, in meters
Fill	5	22	3.0	52%	1.5
A_1- top * fine sand	12	75	3.40	80%	1.8
A_1- bottom * fine sand	31	160	2.87	119%	5
A_2- fine sand	4	20	2.76	23%	5
A_3- fine sand	11	49	2.46	69%	5
B- clay	8	22	3.36	-	6
C- fine sand	23	169	2.56	105%	7
D- clay	13	27	4.00	-	9
E- fine sand	26	138	2.53	88%	10
F- clayey silt	11	38	3.17	-	12

$\bar{N}$ = Average N, in blows per foot
$\bar{q}_c$ = Average cone resistance, in kg/cm^2
$\bar{R}_f$ = Average ratio, in percent
$\bar{D}_r$ = Average relative density, in per cent
Mechanical cone values converted to electrical cone values (Schmertmann, 1978a, p. 59)
Relative density was calculated from:

$$D_r = 1/2.91 * \ln(q_c/12.31 * \sigma_v'^{0.71}) * 100\%$$

σ_v' = effective vertical stress (from Schmertmann, 1978a, p. 40)

* The top part of unit A_1 is characterized by ripple bedding and medium dense sand. The bottom part of the unit is characterized by horizontal bedding and dense sand.

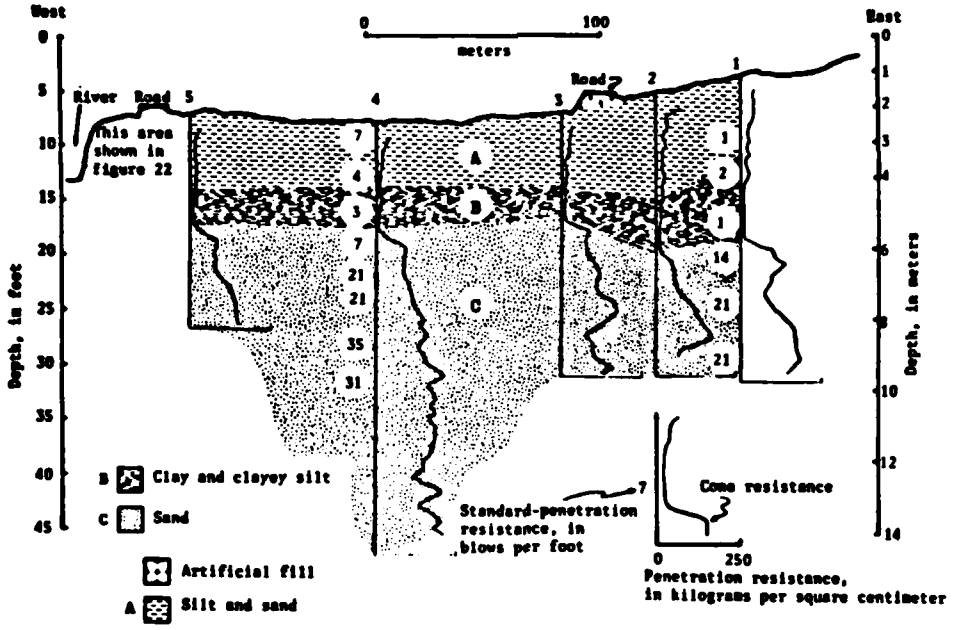

Figure 3.24: Profile of Sediments at River Park Site

TABLE 3.5

Characteristics of Sediments at RP Site

UNITS	$\bar{N}$	$\bar{q}_c$	$\bar{R}_f$	$\bar{D}_r$	approximate depth, in meters
Fill*	-	18	2.13	-	variable
A- clayey silt to silty sand	3	24	2.57	54%	2.0
B- clay to clayey silt	3	9	3.40	-	3.0
C top** fine to medium sand	7	69	2.28	80%	
C bottom** fine to medium sand	23	138	2.51	102%	
C all** fine to medium sand	21	117	2.41	99%	11.0

* Fill replaces units A and B in holes 6 and 9 on the slump

** The top 1-m of unit C is medium dense sand, whereas the bottom of the unit is dense sand

3.3.1.2 The earthquake

The October 15, 1979, Imperial Valley earthquake was caused by movement on the Imperial Fault. The epicenter was instrumentally located on the Imperial Fault approximately 25 km southeast of El Centro. About thirty strong motion records of the tremor are available from the USGS strong motion network in the Imperial Valley (Figure 3.25). The digitized and processed records are published by Brady et al. (1980) who give the following parameters for the main shock:

Epicenter: 32.63° N-115.33° W
Depth: 12 kms
Magnitude: ML = 6.6

The definition proposed by Page, Boore and Dietrich (1975) is used to evaluate the strong motion duration of the earthquake. The writers proposed to use an acceleration level of 0.05 g as a criterion to define strong motion. Observation of all the records from the thirty stations suggest a strong motion duration of about 12-18 seconds. The peak ground acceleration (PGA) at each site is determined using the records from the station closest to the site.

Heber Road Site

The site is located at about 7 km from the epicenter. The nearest recording station is Bonds Corner (Figure 3.25) where a PGA of 0.78 g was recorded. Allowing for attenuation, the PGA at the HR Site is estimated at 0.60 g. From the accelogram records published by Brady et al. (1980) the number of positive zero crossings is expected to be 16 to 22.

River Park Site

The closest recording station to RP is located at the Brawley Municipal Airport (Figure 3.25). From this record and records from neighboring stations, the PGA was estimated at 0.2 g and the number of cycles at 20 to 30.

The effects of the epicentral distance and the subsoil conditions can be seen in this particular example. Although only 20 miles (32 km) apart, the two sites experienced totally different loadings. These differences in loading and subsoil condition at the two site offer an interesting case for the probabilistic pore pressure and strain prediction models.

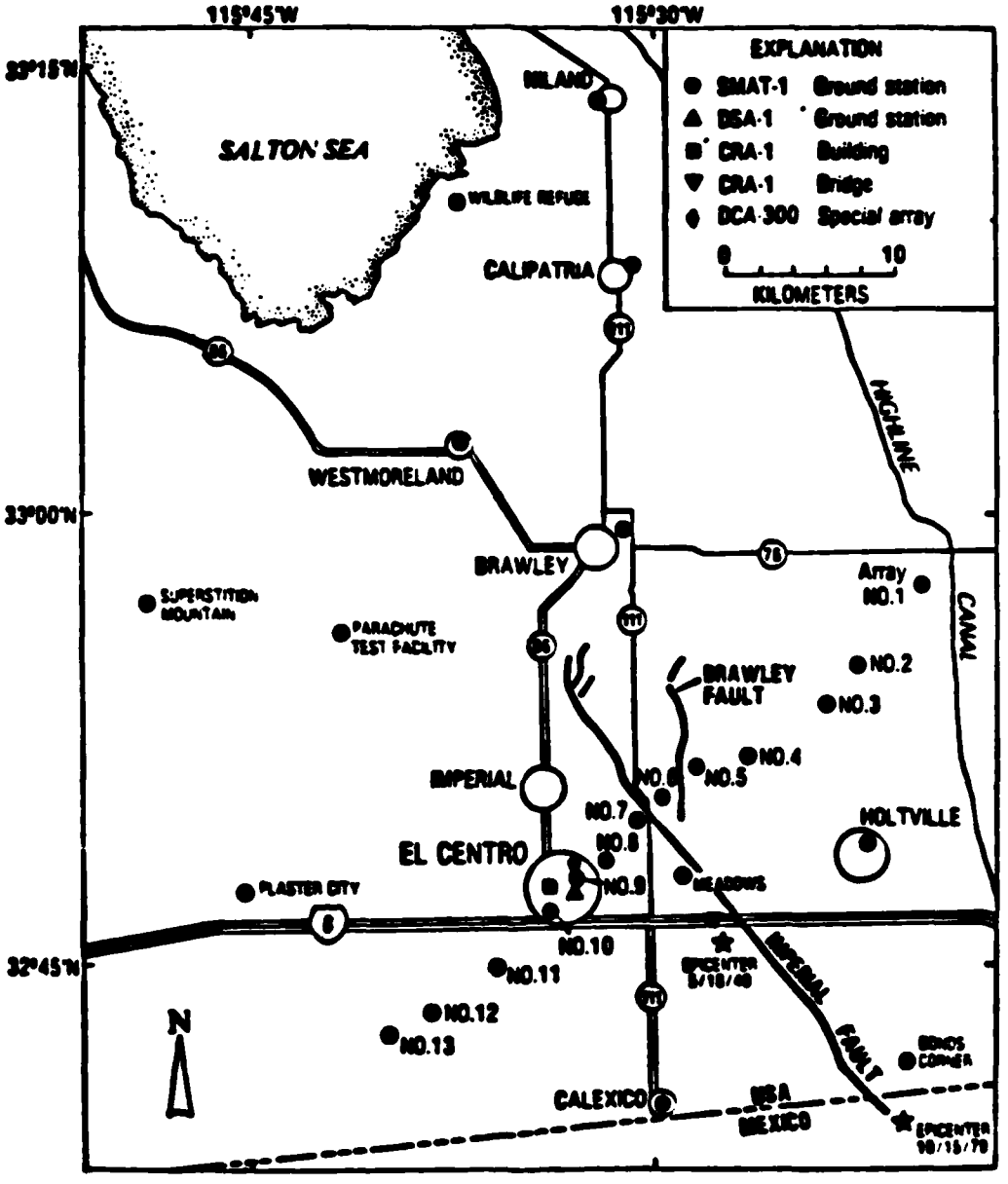

Figure 3.25: Strong Motion Instrument Network, Imperial Valley

3.3.2 Analysis

The soil strength and earthquake parameters necessary for analysis of the HR and RR sites are listed in Table 3.6. The last column in the table indicates whether the parameter is available from direct data or must be inferred from other literature.

TABLE 3.6

Parameters for the Imperial Valley

	PARAMETER	
Earthquake	PGA or RMS of Acceleration	yes
	Duration	yes
	Number of cycles	yes
Soil	Density	yes
	Cyclic strength curve	no
	Water table level	yes
	Pore pressure	no

3.3.2.1 Soil Parameters

In the model, the soil behavior is characterized by two sets of data: a cyclic strength curve and a pore pressure generation curve. Although no direct dynamic testing results are available on the materials available at either site, the data from the field investigation can give guidelines for the selection of reasonable dynamic strength parameters.

Heber Road Site

Detailed results from SPT and CPT show (Figure 3.23) that unit A2 is very loose whereas unit A1 is much denser. The cyclic strength curves for the materials at HR were selected from data presented by Clough and Chameau, (1979) on the San Francisco dune sands and data presented by De Alba et al., (1975) on Monterey Sand No. 0. The curves chosen are shown on Figure 3.26 for both pore pressure and strain potential.

River Park Site

From the soil profile shown in Figure 3.22 and the results from the CPT and SPT it may be assumed that the first few feet in unit C are the most likely to liquefy. The cyclic strength curve chosen for unit C at RP site is shown on Figure 3.26.

3.3.2.2 Loading Parameters

All the necessary information on the earthquake are available.

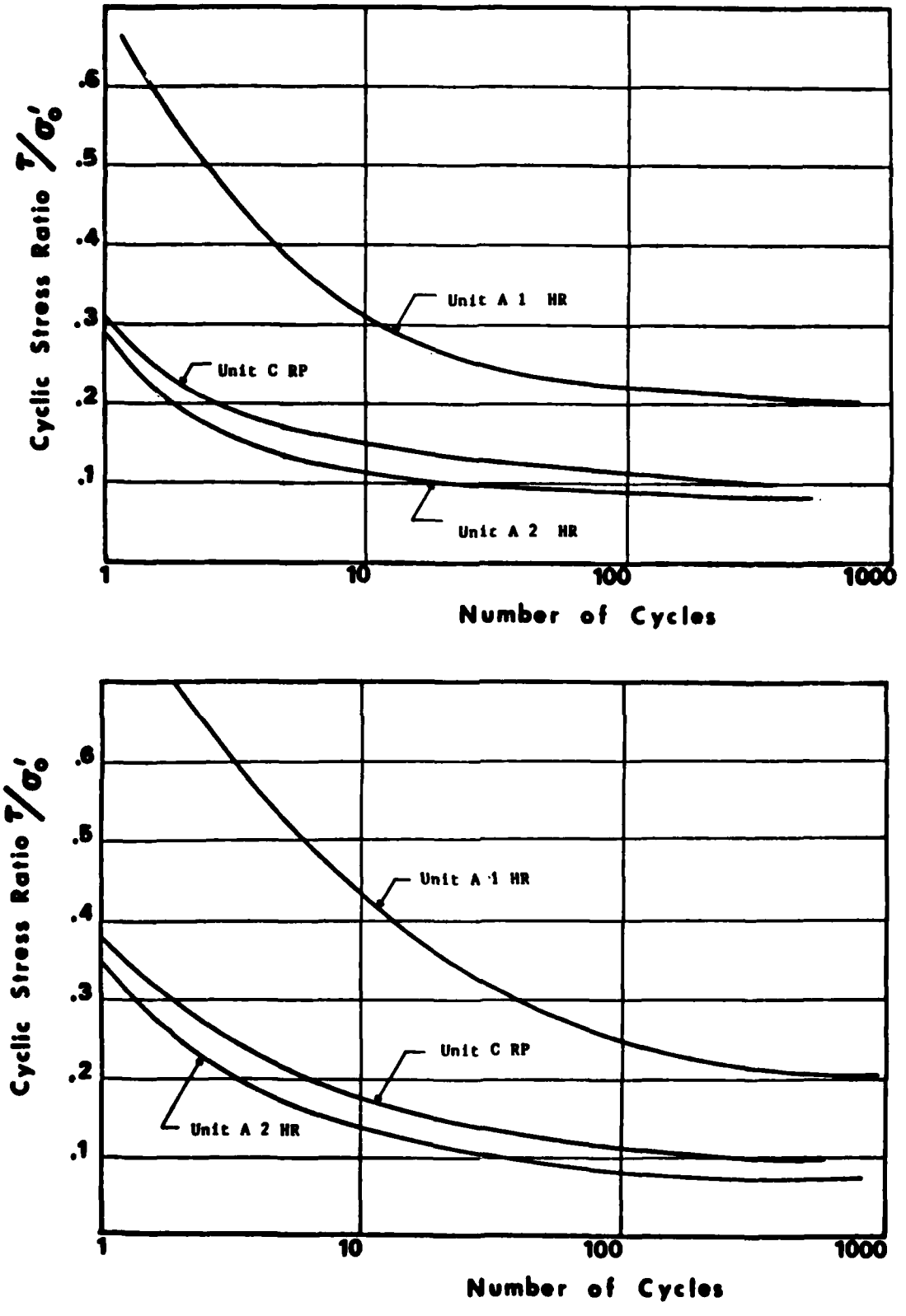

Figure 3.26: Cyclic Strength Curves for Sediments at HR and RP Sites

3.3.3 Results

Probabilistic evaluation of pore pressure and strain potential are conducted for both Heber Road and River Park sites.

3.3.3.1 Heber Road Site

Development of Pore Pressure

As noted there are three main sand deposits at the HR Site, Unit A1, A2, and A3. Unit A2 consists of very loose sand and Unit A1 is dense to very dense sand. They represent the extremes. We will assume Unit A3, composed of medium dense sand, to behave as an average between the two extremes. Analyses are conducted for units A1 and A2 using the data presented in Table 3.7 and the cyclic strength curves shown in Figure 3.26. In both cases analyses were applied to a depth of 13 feet (4 m) since this is near the bottom of the of the upper stratum and likely to represent the most critical area.

The results for unit A1 at HR are shown on Figure 3.27 where the probability of reaching pore pressure ratio of 0.1, 0.5, and 1.0 is plotted versus the number of positive zero crossings. The probability of reaching pore pressure ratio of 0.1, 0.5, and 1.0 after 10 positive zero crossing increases rapidly in unit A1; values of 95%, 55% and 43% are found respectively. The probabilities of reaching such pore pressure ratios in the range of positive zero crossings of the actual earthquake (16-22) are:

Pore pressure ratio	Probability of exceedance
0.1	100-100%
0.5	87-97%
1.0	79-95%

TABLE 3.7

Parameters for Heber Road Site

PGA= 0.60 g
Number of Positive Zero Crossings = 16-22
Depth of Water Table : 6.55 Feet
Depth of Interest : 13 Feet

Unit A1
γ_t = 115 pcf Very Dense Material D_r = 90%
Total Stress σ_0 = 1460 psf
Effective Stress σ_0' = 1051 psf
α = 1.1 β = 2.1

Unit A2
γ_t = 100 pcf Very Loose Material D_r = 23%
Total Stress σ_0 = 1310 psf
Effective Stress σ_0' = 903 psf
α = 1.2 β = 1.9

It is interesting that in spite of the high densities of the A1 soil, very high pore pressures are predicted to develop. This occurs because of the high level of loading (PGA =0.6 g). The results for unit A2 are shown on Figure 3.28, where it can be seen that due to the very loose density of this soil a very high loading leads to a probability of reaching a pore pressure ratio of one after only eight positive zero crossings. The high probabilities of reaching liquefaction at the HR site agree quite well with the actual behavior in the field where strong evidences of liquefaction were reported.

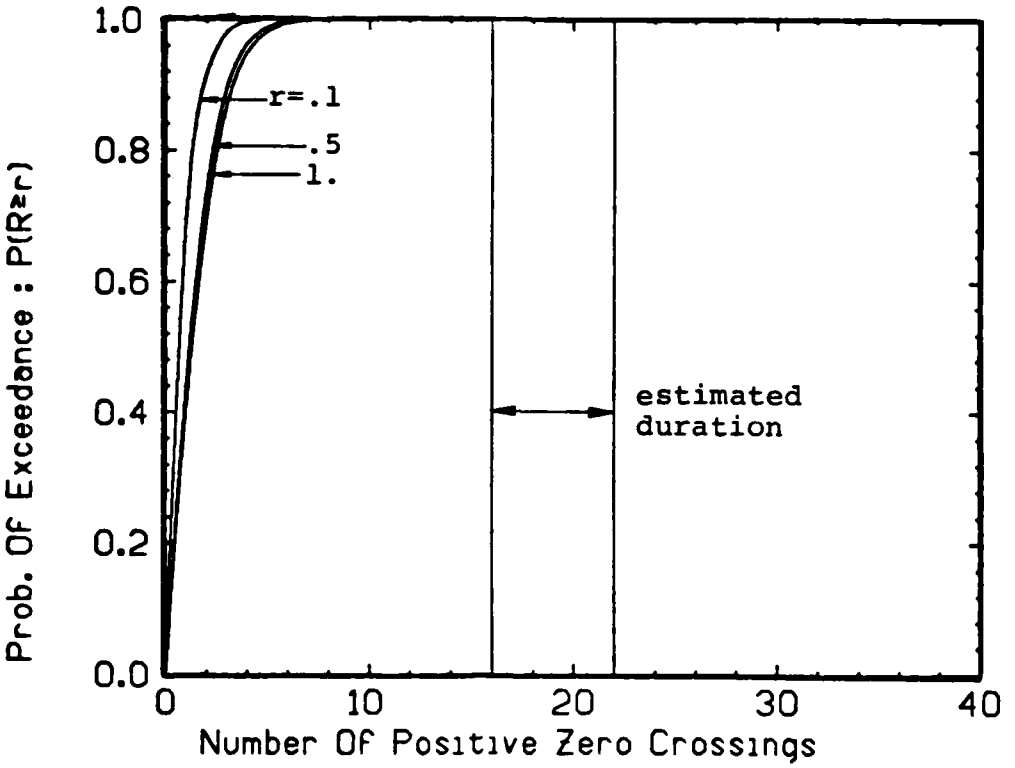

Figure 3.27: Prob. Dev. of Pore Pressures HR Site Unit A1

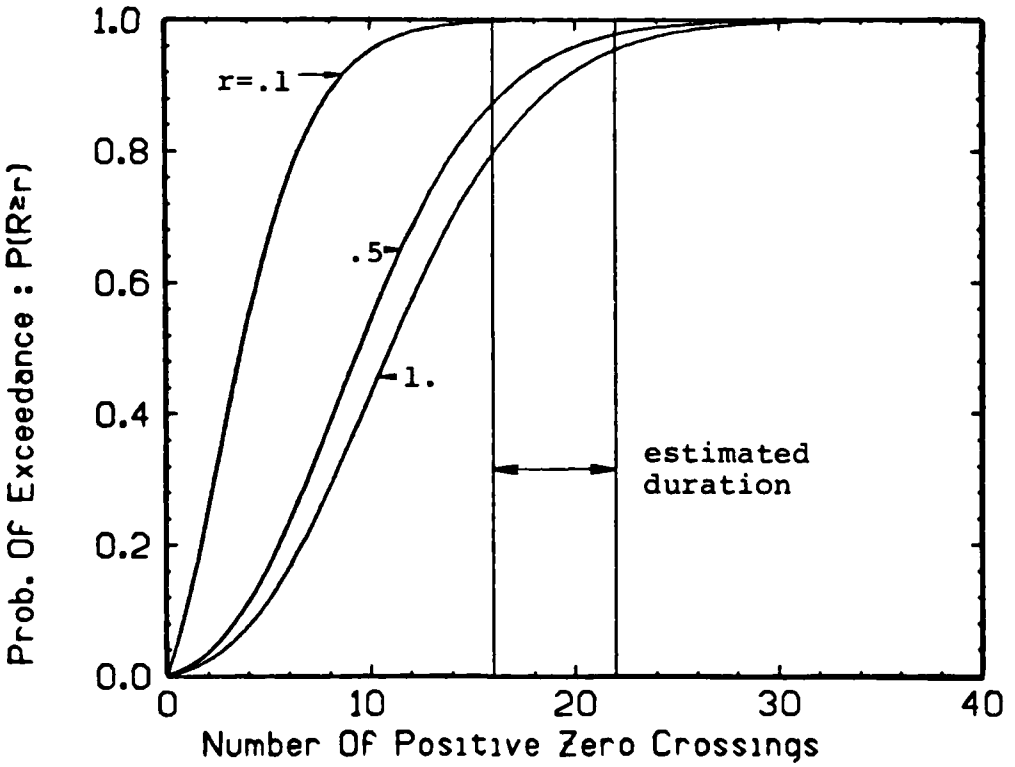

Figure 3.28: Prob. Dev. of Pore Pressures HR Site unit A2

Development of strains

Because no direct data are available the cyclic strength curve is derived as explained in Section 3.231. The curves developed for 10% strain are shown on Figure 3.26. Using these data and that in Table 3.7 , the probability curves shown in Figure 3.29 and 3.30 for units A1 and A2 are obtained. There is a large difference in predicted reponse ; the probability of reaching 10% strain ranges from 15 to 33% in unit A1 and is equal to one in Unit A2. Comparing these numbers to the probabilities of reaching liquefaction yields an interesting contrast :

	P [Strain ≥ 10%]	P [R ≥ 1]
Unit A1	15-33%	79-95%
Unit A2	100%	100%

Both units show an almost equal likelihood of developing high pore pressure but show a totally different behavior in terms of strains. The chances of observing important strains in Unit A1 are relatively small against a probability of 1 for unit A2. These differences are related to the different densities of the units and they are consistant with the actual behavior of the site during the 1979 earthquake. Figure 3.31 shows the location of the cracks and sand boils at the HR site. Unit A1 extends from the west up to Hole 3 and Unit A2 from Hole 3 to Hole 7 (Figure 3.31). Bennett et al. (1981) reported lateral spreading of the channel part of the deposit (Unit A2, Figure 3.23) which implies that most of the cracking and ground displacement occurred in unit A2.

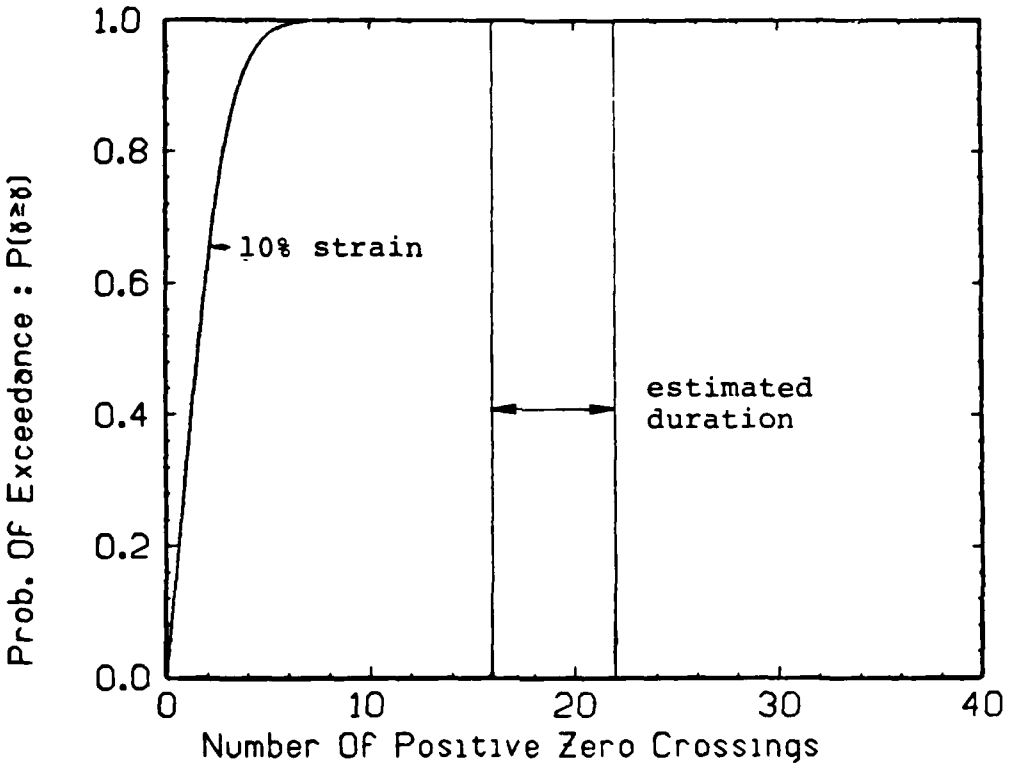

Figure 3.29: Prob. Dev. of Strain Potential HR Site Unit A1

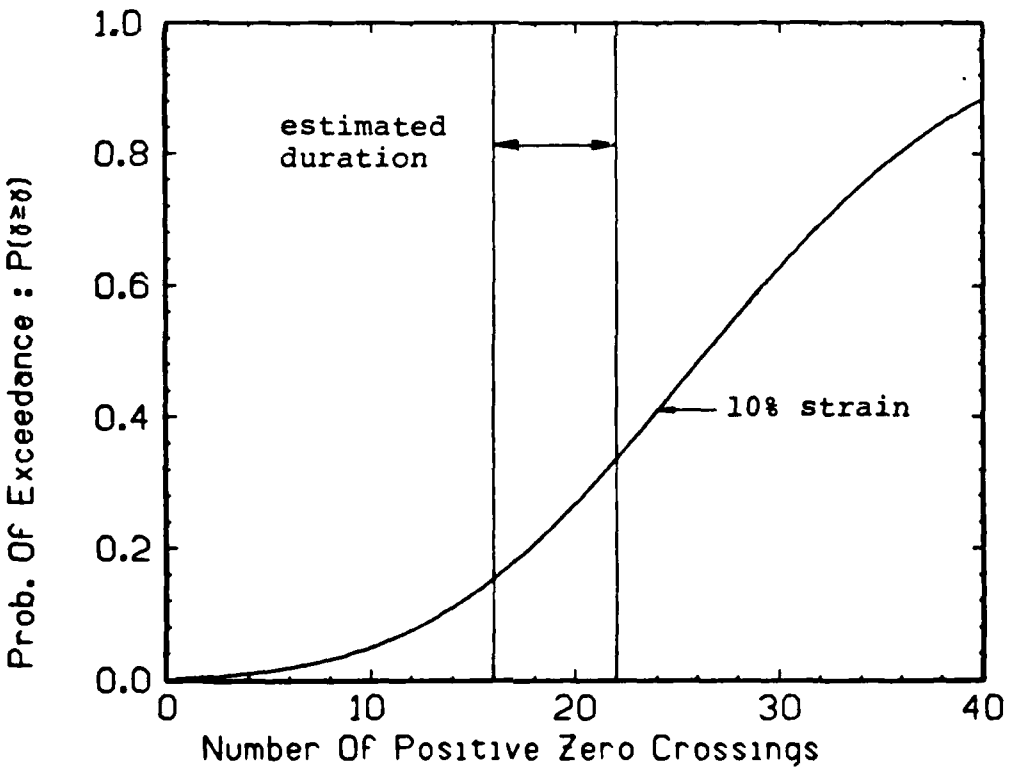

Figure 3.30: Prob. Dev. of Strain Potential HR Site unit A2

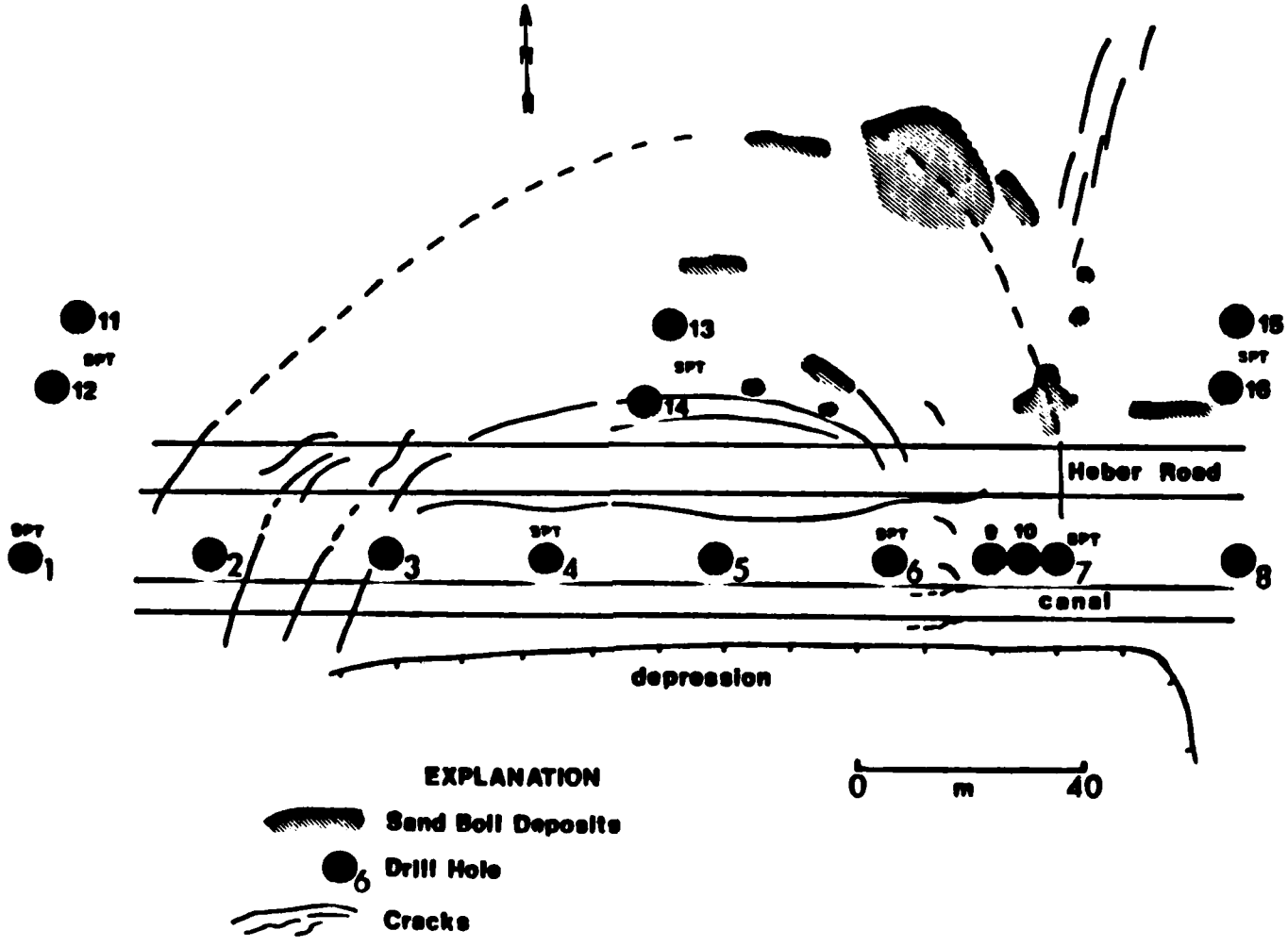

Figure 3.31: Location of SPT, CPT, and Sand Boils at HR Site

3.3.3.2 River Park Site

The critical depth for this site is located at the boundary between units B and C Figure 3.24 , because at that level (12 feet deep, 3.6 m) a weaker, looser layer of sand was reported. Note that due to the presence of a less pervious material (Unit B) capping a sand deposit (Unit C) it may well be expected to see liquefaction develop in Unit C at greater depth than 12 feet since pore pressure could build up without internal dissipation.

The probabilistic analysis is conducted at the depth of 12 feet (3.6 m) using the data shown on Table 3.8 and the cyclic strength curve shown on Figure 3.26. Figure 3.32 shows the probabilistic development of pore pressure at RP site, where it is observed that the probability of reaching liquefaction is almost 1 in the range of positive zero crossings of the earthquake.

TABLE 3.8

Parameters for River Park Site

PGA= 0.20 g
Number of Positive Zero Crossings = 20-30
Depth of Water Table : 2.0 Feet
Depth of Interest : 12 Feet

Unit C
γ_t = 100 pcf Medium Dense Material D_r = 50%
Total Stress σ_0 = 1200 psf
Effective Stress σ_0' = 576 psf
α = 1.1 β = 1.3

The probabilistic development of strain at RP site was evaluated using the parameters listed in Table 3.8 and the cyclic strength curve plotted in Figure 3.26. For the range of positive zero crossings of interest (20-30) the probability of reaching 10% strain varies from 80-97% (Figure 3.33), values very close to the probability of reaching liquefaction (98-100%). At the RP site large strain potential may be expected concurrently with the development of pore pressures. Thus the observation by Bennett, et al. (1981) of numerous sand boils is consistent with the model predictions.

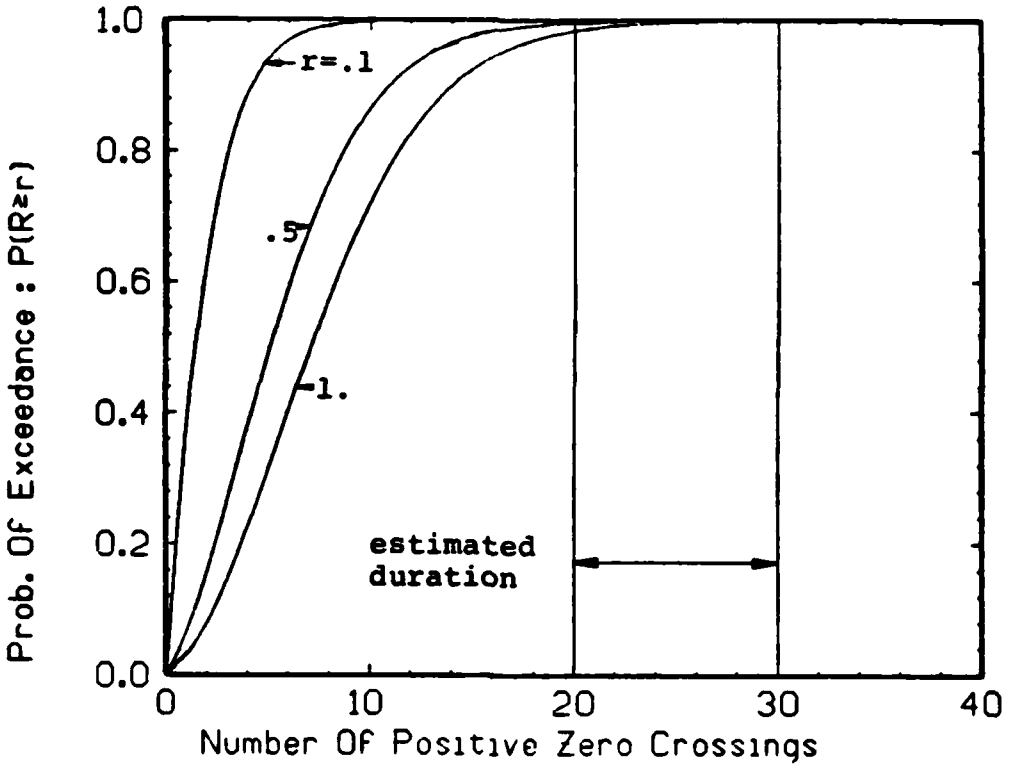

Figure 3.32: Prob. Dev. of Pore Pressures RP Site Unit C

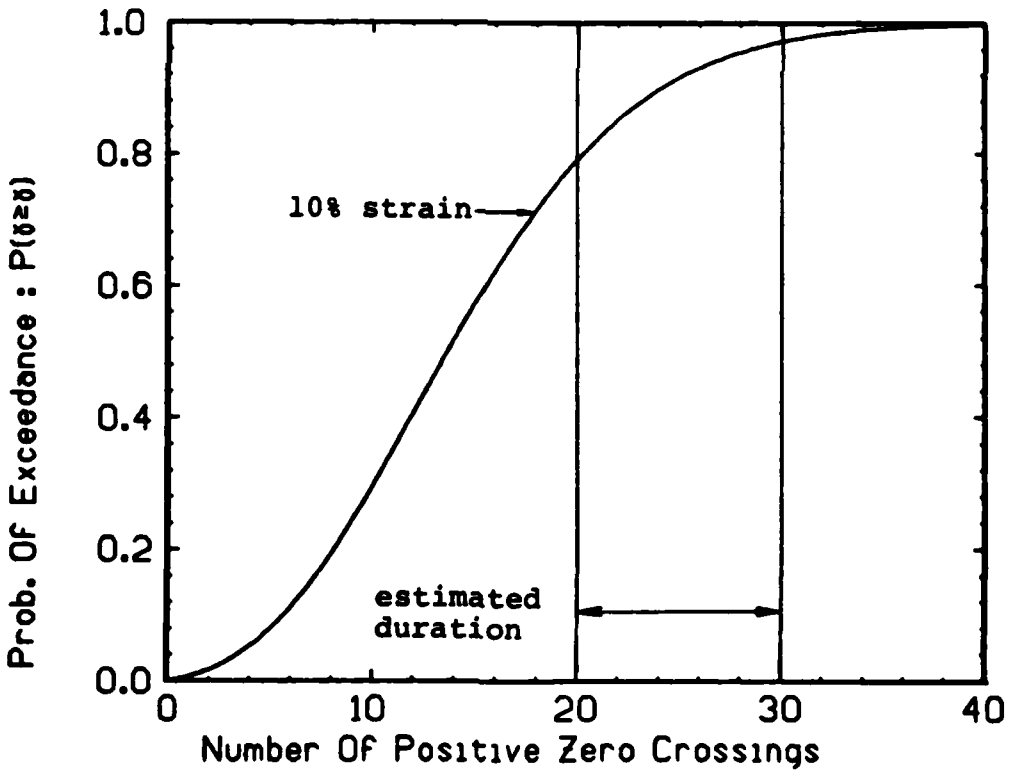

Figure 3.33: Prob. Dev. of Strain Potential RP Site unit C

3.3.4 Discussion

Comparison of sites

To better compare both units A1 and A2 at the Heber Road site the probability curves for initial liquefaction (Pore pressure ratio R=1.0) and large strain potential (10% strain chosen as criterion) are given in Figure 3.34. After 8 positive zero crossings the probabilities of reaching initial liquefaction and 10% strain potential equal one for unit A2 but are only equal to 0.3 and 0.05 for unit A1. If liquefaction did occur at that point in A2 it can be assumed that during the subsequent cycles (positive zero crossings) Unit A2 would tend to undergo large deformations which might evidence themselves as a lateral spread. Occurance of such large strain will change the drainage conditions and may allow high pore pressures to dissipate particularly in Unit A1. Although the probabilistic model yields a high likelihood of liquefaction for Unit A1 in the range of positive zero crossings of the earthquake high pore pressure may not develop if large movements in Unit A2 take place and alter the soil conditions. Figures 3.35 and 3.36 summarize the behavior of the two sites in terms of initial liquefaction and strain potential. For both sites the probabilities of reaching liquefaction are very high. The probabilities of reaching a 10% strain potential, on the other hand, show a wider range of values.

Effect of relative density on strain potential

The relative densities of the different units of soil at both HR and RP sites are available form the results of the field investigation (Bennett et al., 1981). It is possible for each site to relate relative density, probability of liquefaction and probability of large strain:

Site	D_r	P[R ≥ 1.0]	P[strain ≥ 10%]
Heber Road			
Unit A1	80-100%	78-95%	15-33%
Unit A2	23%	100%	100%
River Park	60%	98-100%	80-97%

For the very loose material, large strain will develop concurrently with high pore pressure. For denser soils liquefaction may be reached but with a reduced risk of observing large strains. In order to use the probabilistic models for engineering decision analysis it is necessary to look at both the pore pressure and the strain development potentials.

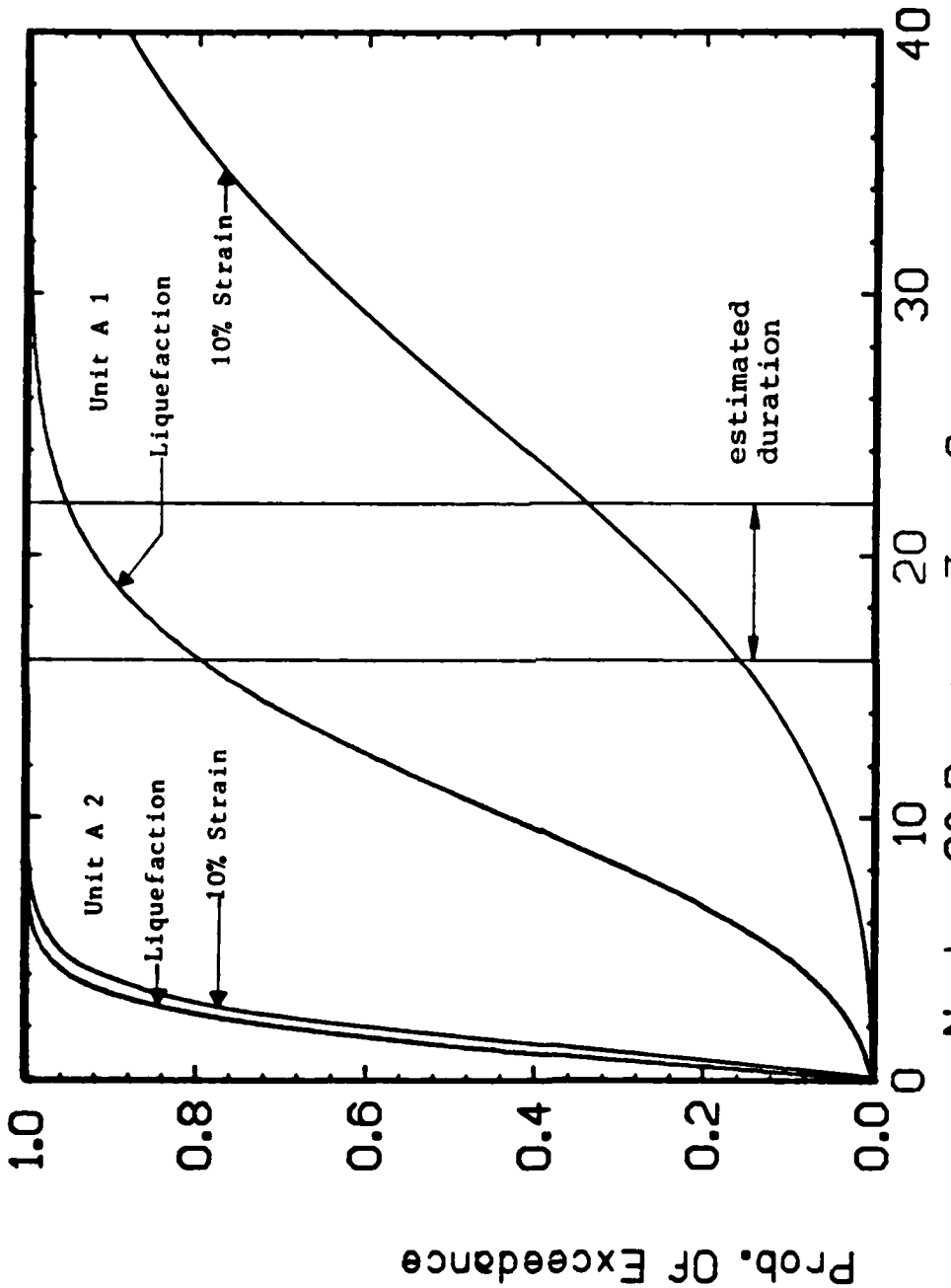

Figure 3.34: Comparison of Units A1 and A2 at HR Site

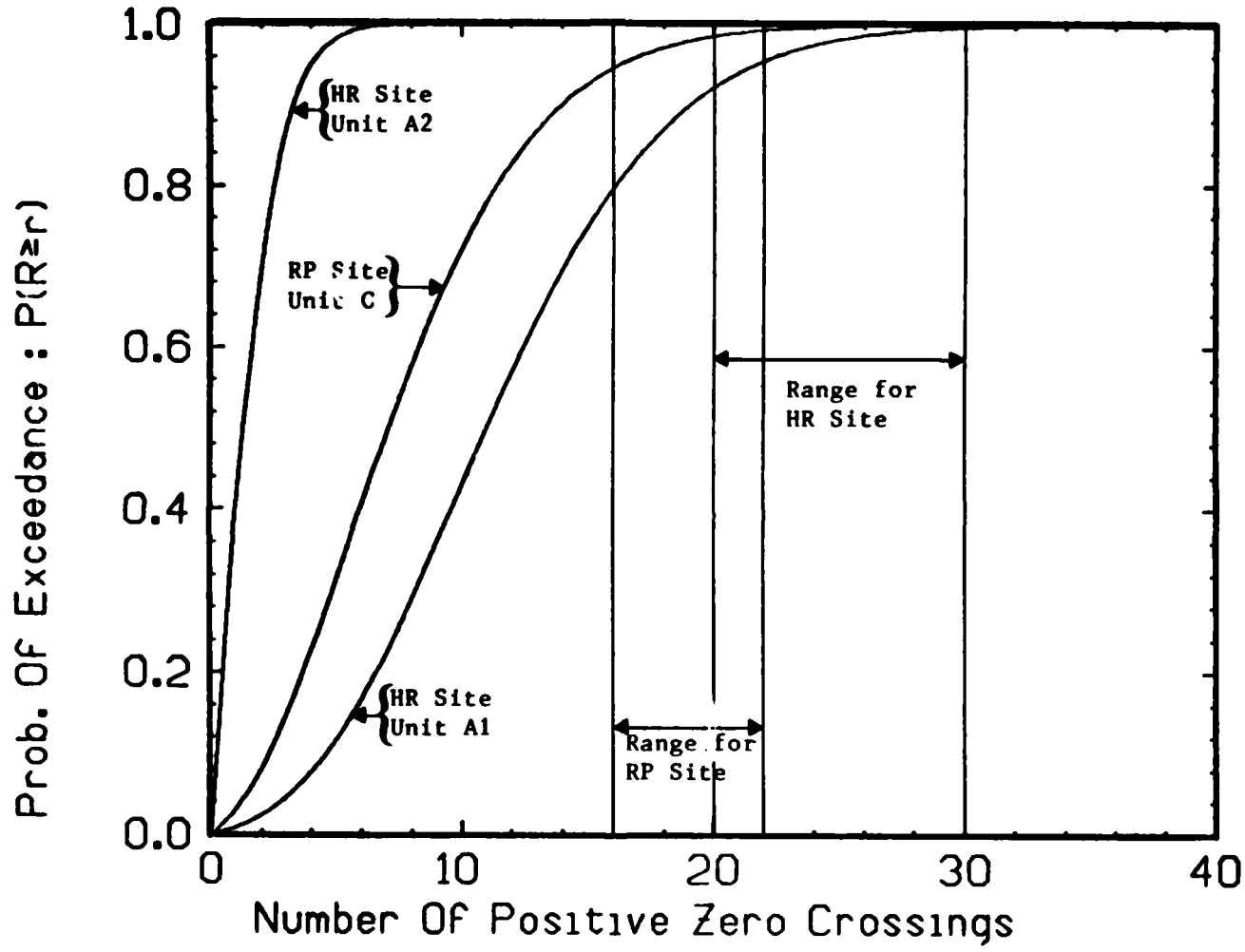

Figure 3.35: Comparison of HR and RP Sites, Pore Pressure r = 1

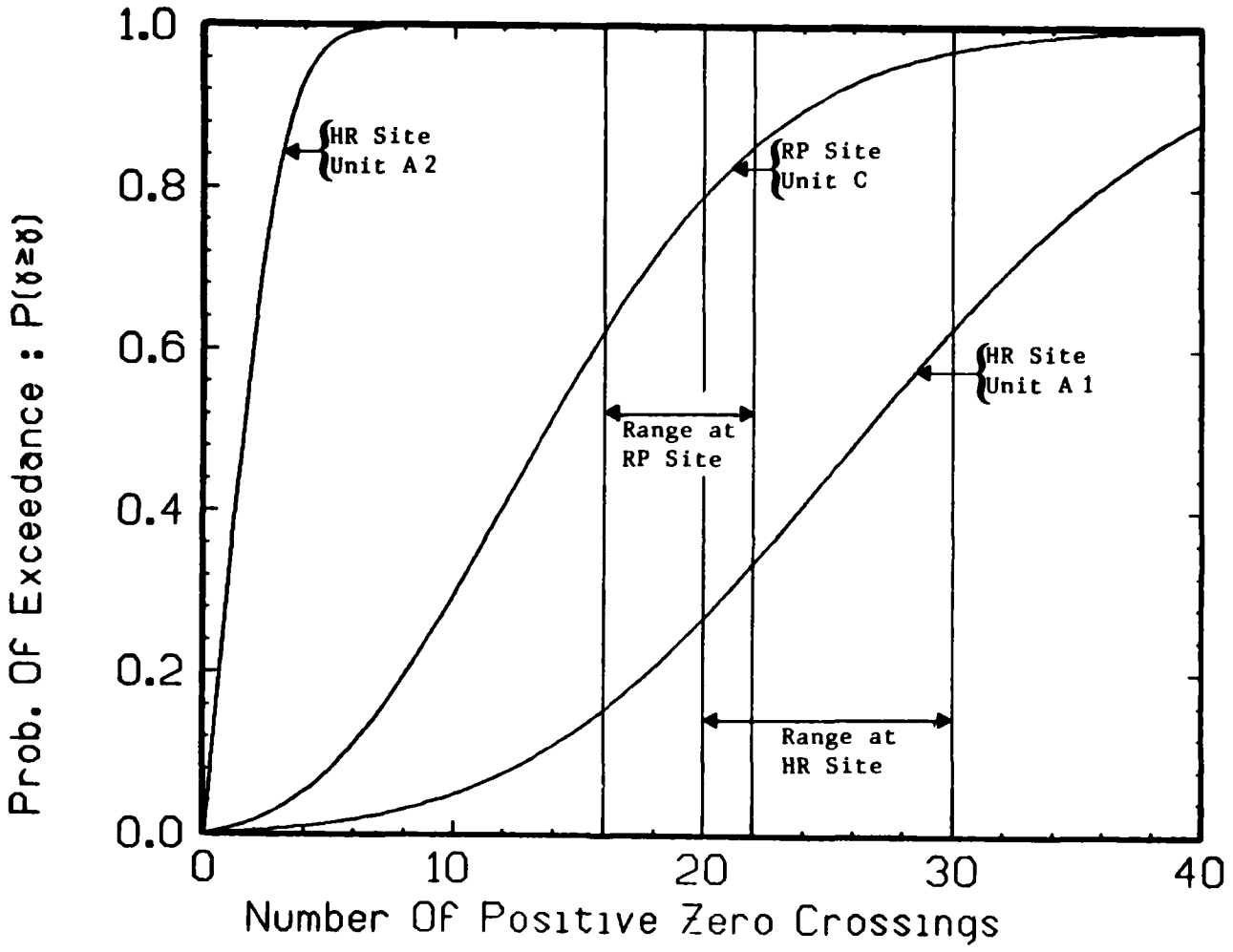

Figure 3.36: Comparison of HR and RP Sites, 10% Strain Potential

3.4 SAN FRANCISCO, CALIFORNIA

Studies conducted by Youd and House (1976) and Clough and Chameau (1979) attributed the ground failures that occurred along the waterfront during the 1906 San Francisco earthquake to liquefaction of the waterfront fill . In this case study, the behavior of the San Francisco waterfront fills are examined.

3.4.1 The site and the earthquakes

3.4.1.1 The site

The San Francisco Bay waterfront as we know it now was primarily created over the period 1850 to 1920 by a massive filling operation directed at shallow lagoons and coves along the shoreline of San Francisco, (Clough and Chameau, 1979). During the 1906 earthquake certain fill areas underwent large displacements whereas some others showed very little movements. In 1979 Clough and Chameau conducted a thorough investigation of two sites, one in the area that may have liquefied, the other in the area that showed very little displacement. Figure 3.37 shows the location of the two sites of interest:

1. Telegraph Hill site (TH site) located outside the large displacement zone

2. Yerba Buena Cove site (YBC site) inside the large displacement zone

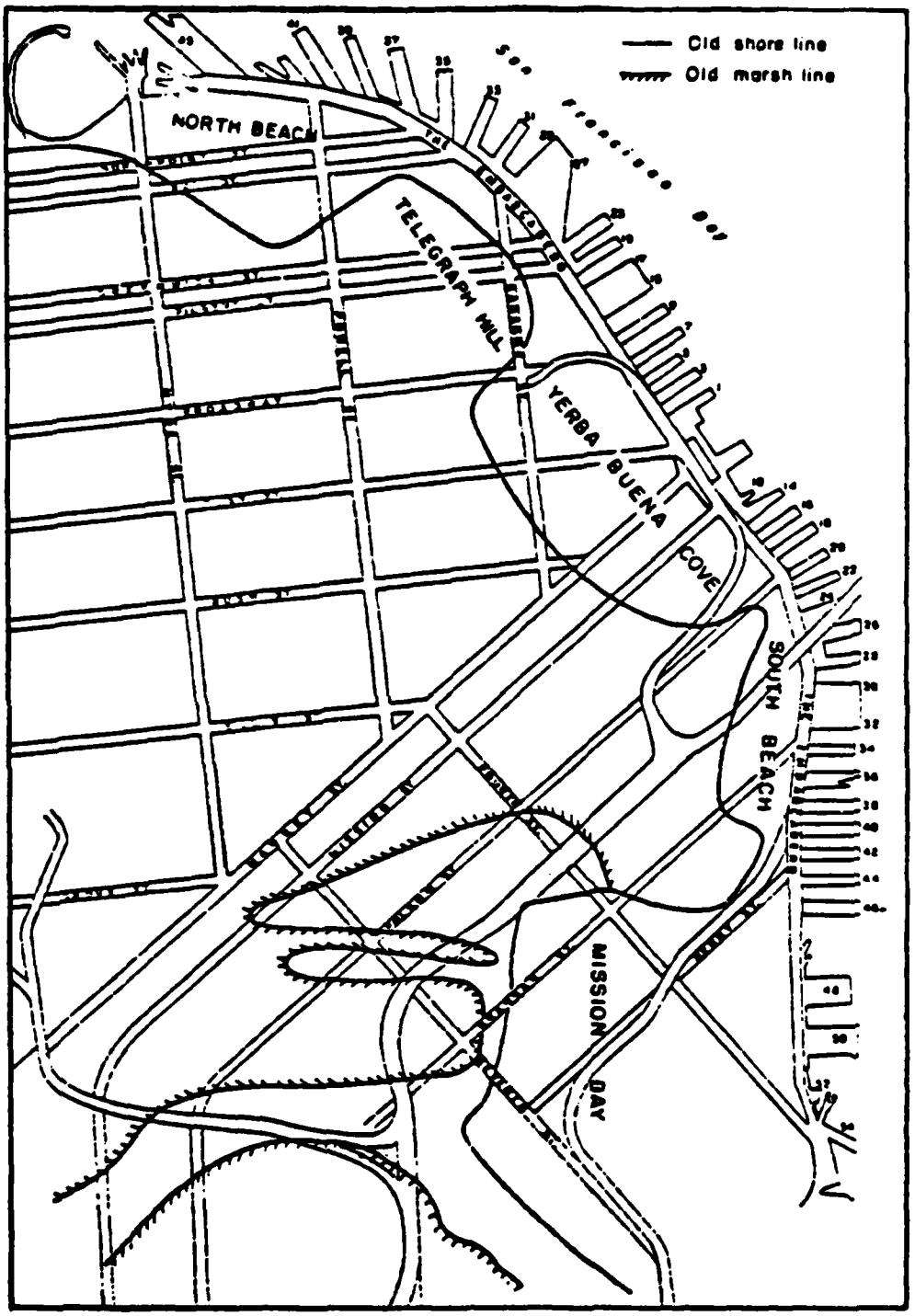

Figure 3.37: Location of San Francisco Sites

A complete history of the construction of the San Francisco waterfront is given by Clough and Chameau (1979) and will not be repeated. The fill consists primarily of dune sand and fragmented rocks from road cuts and quarries. The fill was dumped in place ; the subsoil beneath it depends on its location relative to the original shoreline. The further into the Bay the fill was placed, the more likely Bay Mud of increasing thickness is to be found underneath it. Close into the original shoreline, alluvial deposits of sands and clayey sands overlie Franciscan bedrock. In order to ascertain the nature of the fill, Clough and Chameau collected the results from some 50 borings made for the San Francisco Outfall Sewer project. From those borings the typical soil profile shown in Figure 3.38 was developed. A field and laboratory testing program was performed at both sites to evaluate the soil properties and the in situ densities were evaluated using CPT and SPT (Figure 3.39). The dune sand found in the fill is a uniform SP (Unified Soil Classification Procedure) sand, Figure 3.40. Cyclic triaxial tests were conducted on samples at different densities and the results are given on Figure 3.41.

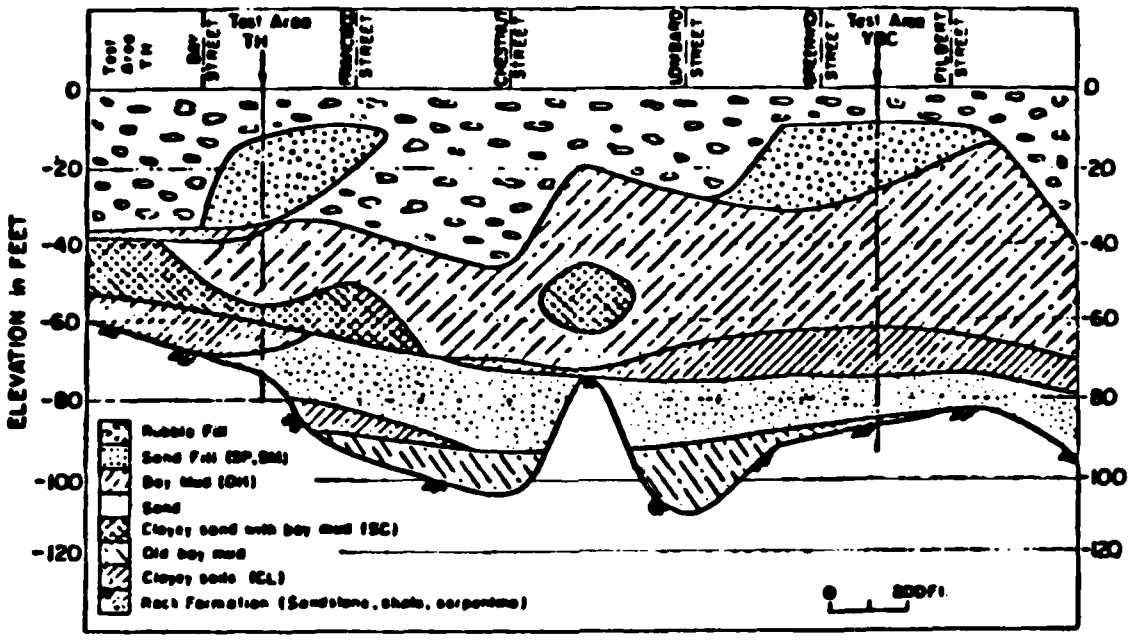

Figure 3.38: Typical Soil Profile Along the Embarcadero

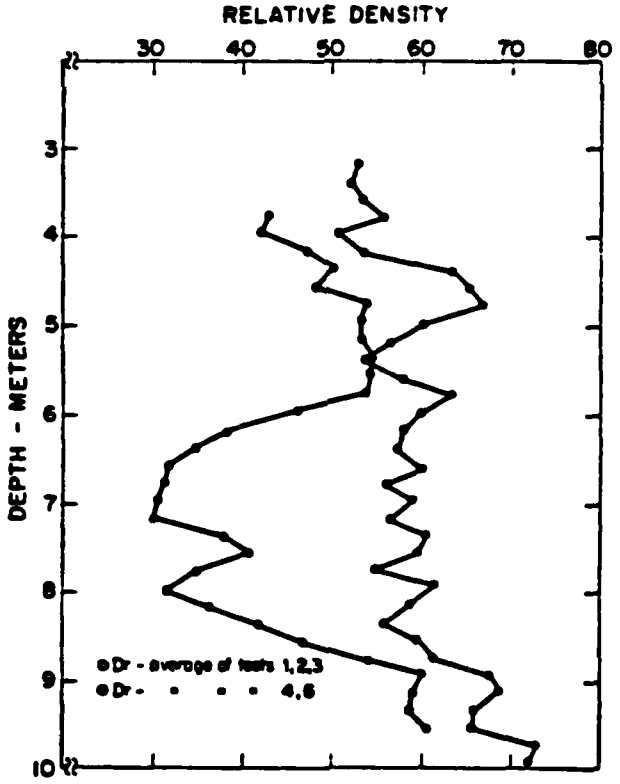

Figure 3.39: Relative Densities at TH and YBC Sites

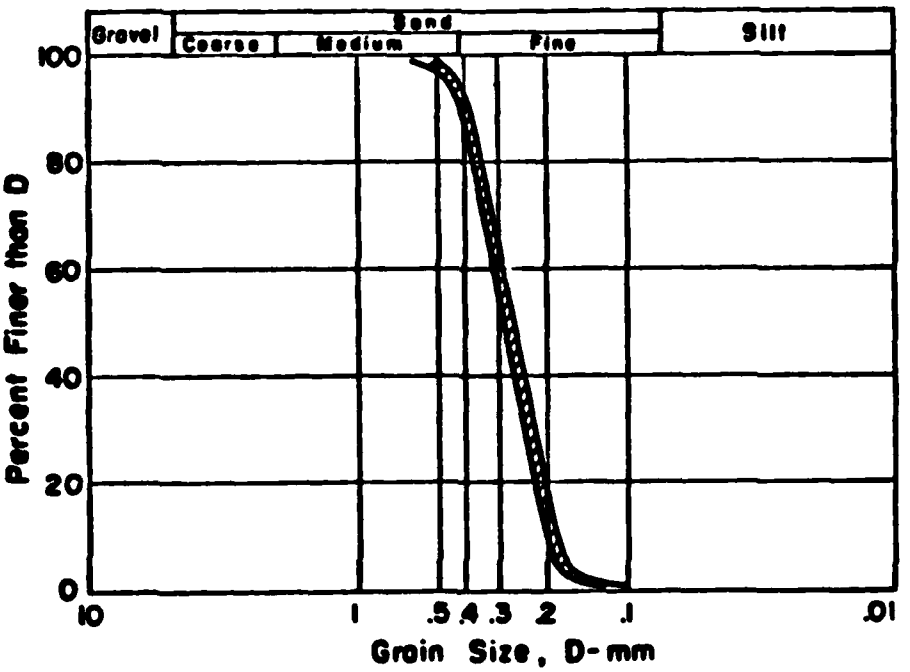

Figure 3.40: Range of Grain Size Distributions at TH and YBC Sites

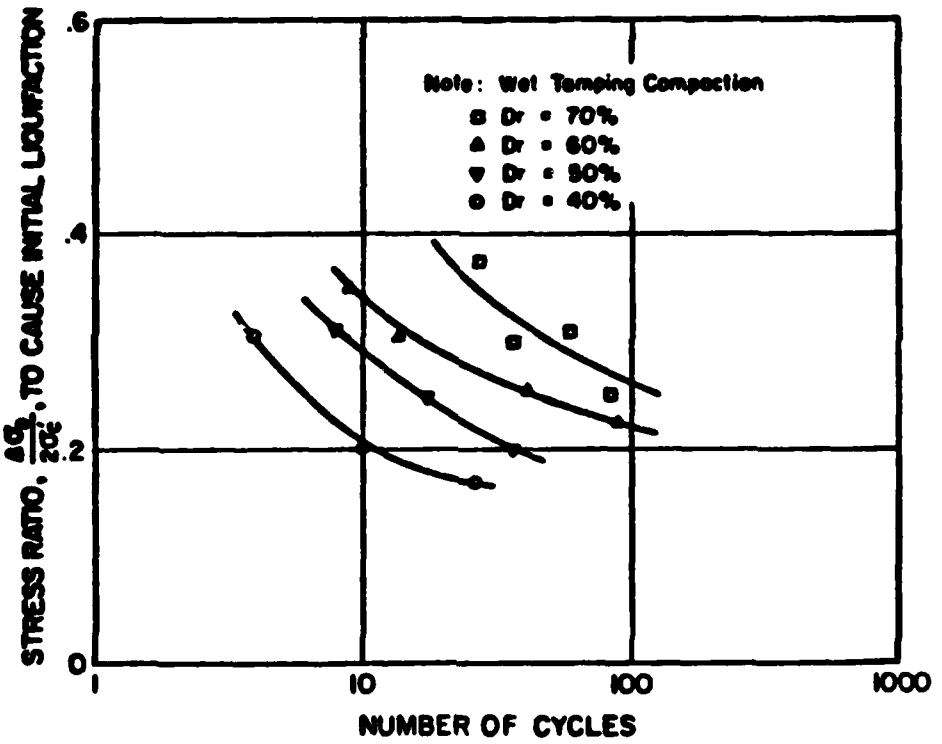

Figure 3.41: Cyclic Strength Curves for Dune Sand

3.4.1.2 The earthquakes

Two earthquakes will be selected for the present analyses , the 1906 San Francisco earthquake and the 1957 Daly City earthquake. The first one is the most severe tremor to hit the area in modern times and caused extensive damage while no damage due to waterfront fill displacement is known to have occured as a result of the second event.

There is no ground motion record of the 1906 earthquake, but based on consideration of damage, geological and geophysical conditions, past history and other recorded tremors researchers have developed a so-called synthetic acceierogram of the 1906 earthquake, (Seed and Idriss, 1969). There are records of the 1957 event and the characteristics of both earthquakes are summarized in Table 3.9.

TABLE 3.9

Characteristics of Earthquakes for San Fransisco Sites

Event	Richter Magnitude	PGA[1]	Number of Crossings
1906	8.25	0.30g	50-60
1957	5.30	0.1-0.14g	8-12

[1] At site of waterfront

3.4.2 Analysis and results for pore pressure

The probabilistic evaluation of pore pressure is conducted for both TH and YBC sites. Both earthquakes discussed previously are considered. Table 3.10 lists parameters that are needed to use the probabilistic model and their availability.

Soil Strength Parameters:

TABLE 3.10

Parameters for San Francisco

	PARAMETER	
Earthquake	PGA or RMS of acc.	Yes
	Duration	Yes
	number of Cycles	Yes
Soil	Density	Yes
	Cyclic Strength Curve	Yes
	Water table depth	Yes
	Pore Pressure Parameters	Yes

All the parameters needed are available but the pore pressure parameaters α and β . Their value will be chosen for each site as described in the following sections.

Earthquake Parameters:

As shown on Table 3.9 values of the necessary earthquake parameters are available for use in the probabilistic model.

3.4.2.1 Yerba Buena Cove Site

This site is known to have moved several feet horizontally and vertically in the 1906 earthquake. At that site the relative density of the dune sand was found to be relatively loose (D_r =30% to 40%), in a zone of a depth of about 25 feet (7.6m). The probabilistic analysis was conducted using the data presented in Table 3.11 and the cyclic strength curve shown in Figure 3.41. The depth for the analysis is taken at 25 feet (7.6 m) for both earthquakes. The results are shown on Figure 3.42

for the 5.3 Daly City earthquake and Figure 3.43 for the 8.25 San Francisco earthquake. The Daly City earthquake is predicted to yield very low probabilities of development of high pore pressures in the deposit, less than 5% for pore pressure ratios greater than 0.5. Even if the earthquake were to last longer with the same intensity (PGA=0.14g) it is predicted there is little chance for high pore pressure.

The 1906 earthquake on the other hand yields a very high probability of reaching high pore pressure. There is 100% chance of liquefaction after only 12 positive zero crossings and the earthquake apparently had 50-60 zero crossings.

The predicted pore pressures for the YBC site in the case of the two earthquakes are consistent with the facts that large problems occured there in the 1906 event, but nothing happened in the 1957 event.

TABLE 3.11

Parameters for YBC Site

Earthquakes

1906 San Francisco	PGA=0.3 g
	Richter Magnitude : 8.25
	Positive Zero Crossings : 50-60
1957 Daly City	PGA=0.14 g
	Richter Magnitude : 5.3
	Positive Zero Crossings : 12-16

Site Characteristics

γ_t = 120 pcf D_r = 40%
Depth of Interest : 25 Feet
Depth of Water Table : 10 Feet
Total Stress : σ_0 = 3000 psf
Effective Stress : σ_0' = 2064 psf
α = 1.5 β = 1.25

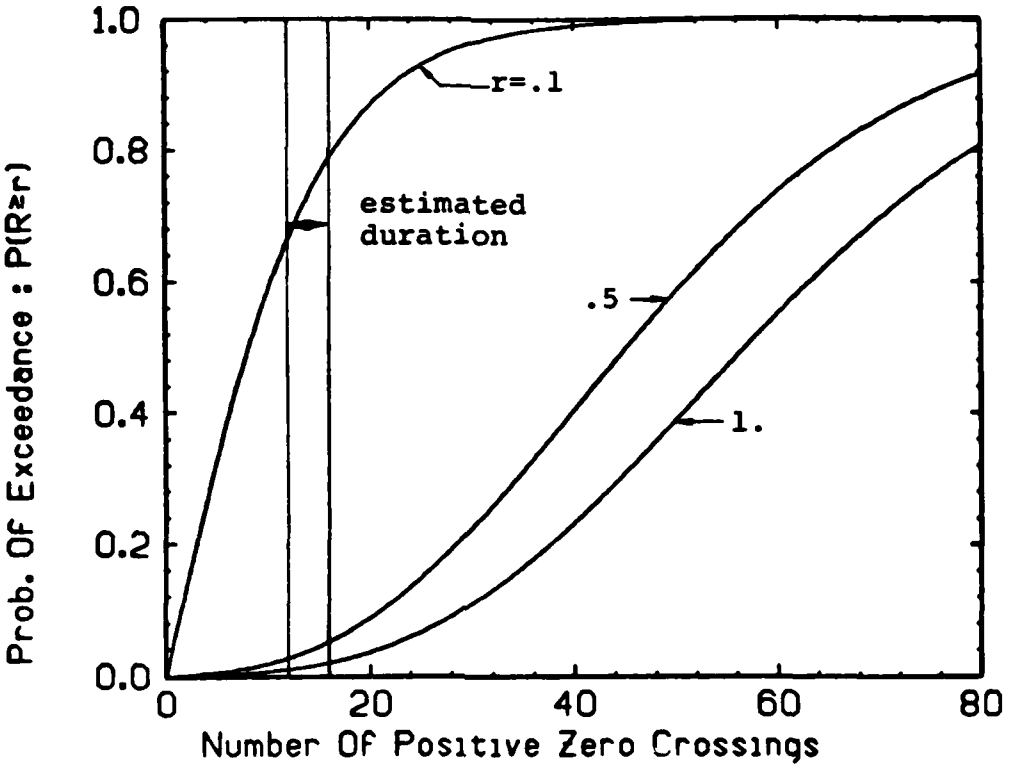

Figure 3.42: Prob. Dev. of Pore Pressures YBC Site, 1957 Event

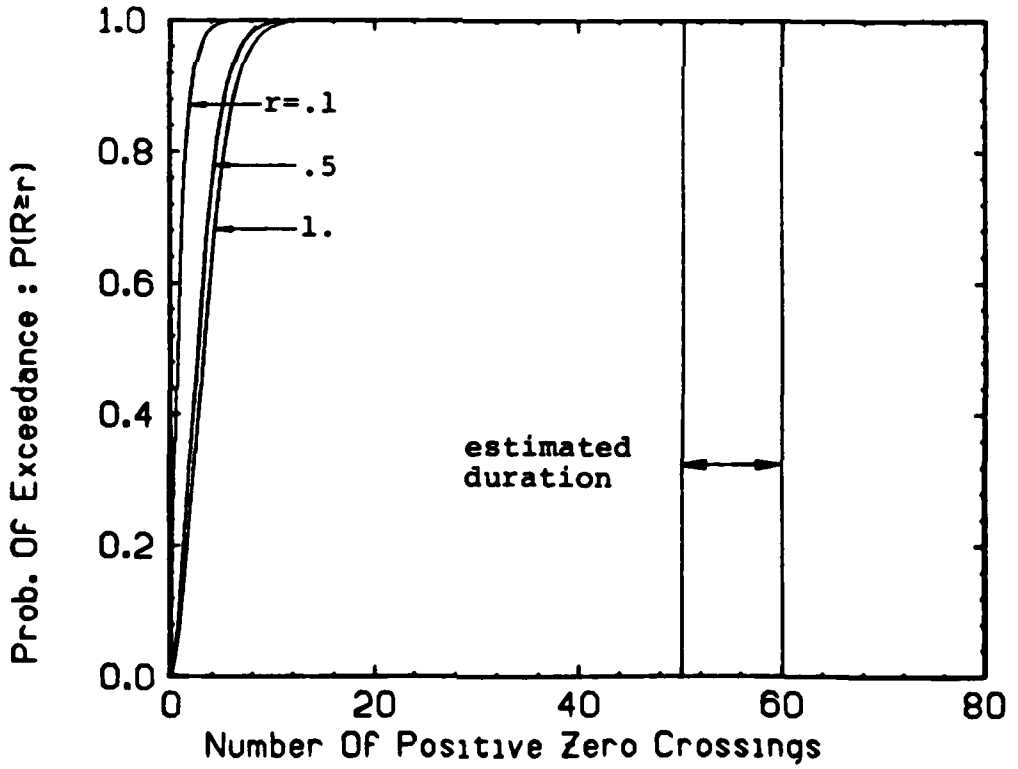

Figure 3.43: Prob. Dev. of Pore Pressures YBC Site, 1906 Event

3.4.2.2 Telegraph Hill Site

This site showed no evidence of significant liquefaction after either the 1906 or the 1957 earthquakes. Borings revealed the presence of pockets of dune sand at a relative density of 60%. The analysis is conducted using the data in Table 3.12 and the cyclic strength curve in Figure 3.41. Only the 1906 earthquake is considered since at the YBC site where the density of the material was looser (D_r = 40%) a very low probability of liquefaction was reached (20%) due to the 1957 earthquake. It can be concluded that a denser deposit such as exists at the TH site would exhibit an even stronger resistance to liquefaction in the 1957 event.

The result of the analysis is shown in Figure 3.44 as the plot of the probability of exceeding pore pressure ratio of 0.1, 0.5 and 1.0 versus the number of positive zero crossing for the 1906 earthquake. The probability of reaching liquefaction at the TH site in the range of positive zero crossings of the earthquake is equal to one. This level of pore pressure is high but before conclusions can be drawn in this case, the possible ground strain needs to be considered.

TABLE 3.12

Parameters for TH Site

Earthquakes

1906 San Francisco PGA=0.3 g
Richter Magnitude : 8.25
Positive Zero Crossings : 50-60

Site Characteristics

γ_t = 120 pcf D_r = 60%
Depth of Interest : 25 Feet
Depth of Water Table : 10 Feet
Total Stress : σ_0 = 3000 psf
Effective Stress : σ_0' = 2064 psf
α = 1.2 β = 1.7

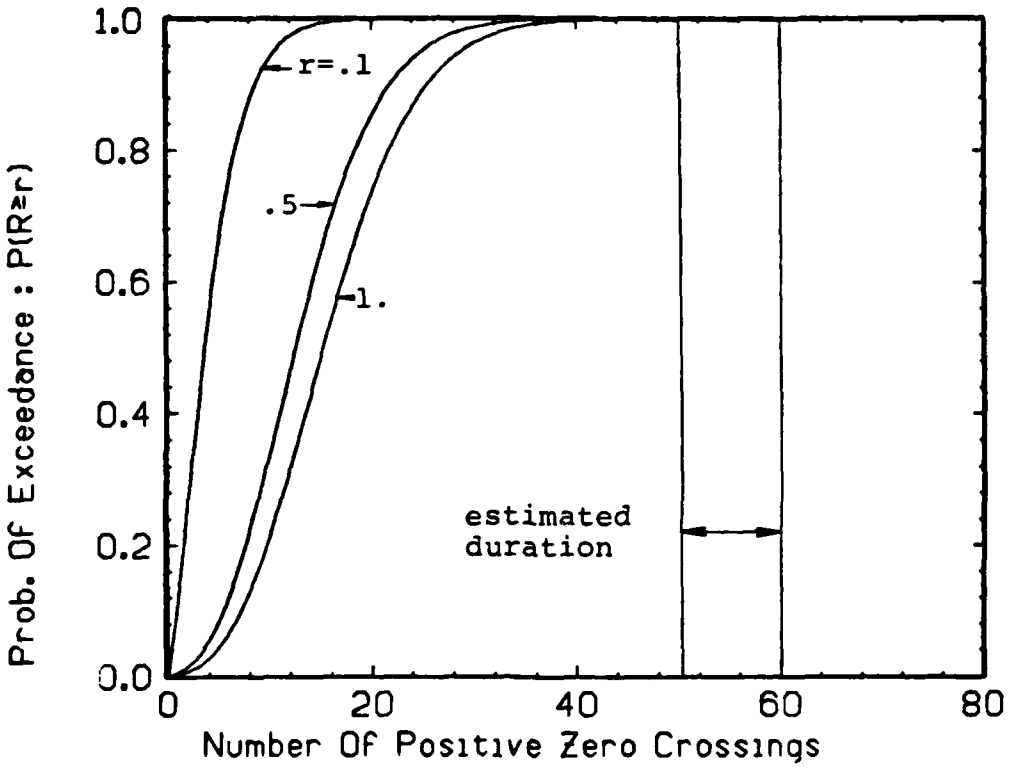

Figure 3.44: Prob. Dev. of Pore Pressures TH Site, 1906 Event

3.4.3 Analysis and results for strains

The probabilistic development of strain is evaluated at both the YBC and TH sites. For this work the results of Clough and Chameau (1979) for dynamic triaxial tests on the dune sands are used (Figure 3.45) along with the data presented in Tables 3.11 and 3.12.

3.4.3.1 Yerba Buena Cove

Studies of strain development at the Amatitlan and Imperial Valley sites have shown that there is usually a lower probability of reaching 10% strain than reaching liquefaction. Since the probability of reaching liquefaction during the 5.3 Magnitude earthquake at the YBC site is very low to begin with (less than 2%), the probability of reaching a 10% strain potential would be even lower. Thus the 5.3 magnitude earthquake is not considered further. The probability of reaching 10% strain at the YBC site is shown on Figure 3.46 for the 8.25 event, and we observe a probability of one of reaching 10% strain before the end of the shaking. The YBC site is reported to have experienced large movements during the 1906 earthquake which agrees with the high probability of large strain obtained.

3.4.3.2 Telegraph Hill Site

The analysis results in Figure 3.47 suggest that the probability of having large strain for the 1906 earthquake at the TH site is on the order of one, assuming the magnitude is 8.25. Since little displacement was observed here in 1906, there are two possible conclusions: one,

this method could yield incorrect results in this case, or two, the earthquake loading using a magnitude of 8.25, is too large. There is evidence for this latter case. A study by Jennings and Kanamori (1979) suggests that the 1906 earthquake may in the past have been attributed a larger magnitude than it should have. The writers based their study on the analysis of seismoscope records and propose to assign to the event a local magnitude ranging from ML=6.25 to ML=7.0 .

To investigate the effect of the possibility that the earthquake magnitude is less than 8.25, a second analysis is performed for an assumed magnitude of 7.5 with the following charcteristics :

Richter Magnitude RM=7.5
Peak Ground Acceleration PGA= 0.20 g
Number of Crossings = 40-50

The results of this analysis are reported on Figure 3.48 and provide a plausible explanation for the observed behavior. The analysis using the 7.5 RM event was also performed at the YBC site and the results are shown on Figure 3.49. Note that using the 7.5 RM earthquake also predicts the correct responses at the YBC site. On figure 3.50 the probability of reaching 10% strain at both YBC and TH site is shown. The probability is one at YBC and 0.03 at TH. These numbers agree very well with the reported 1906 behavior at both sites: large movements at YBC , little if any at TH.

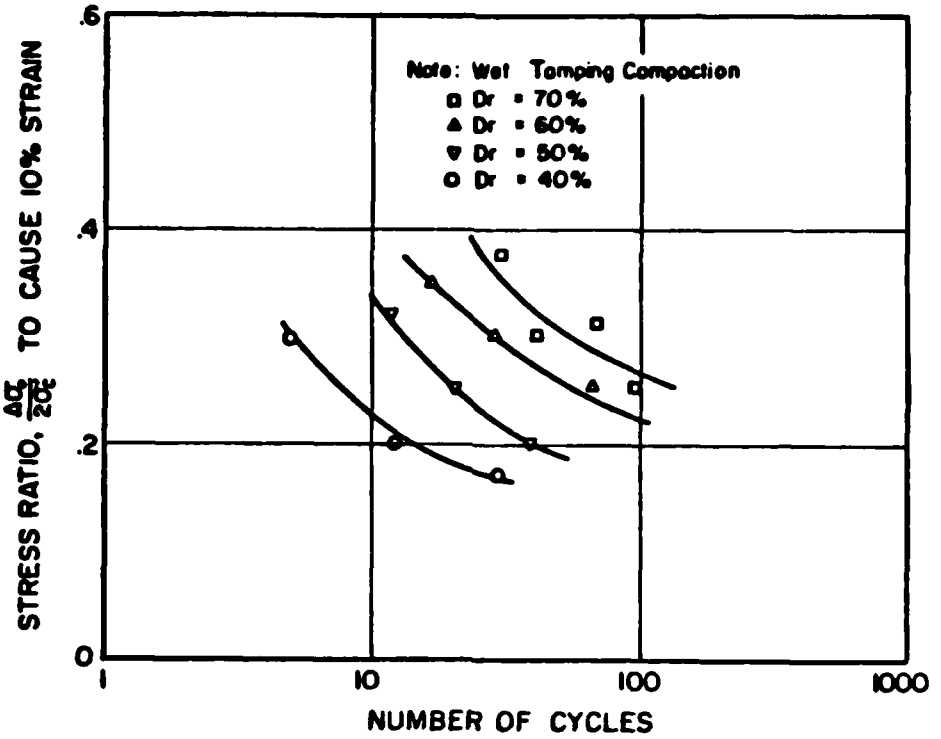

Figure 3.45: Cyclic Strength Curves 10 percent Strain, TH and YBC Sites

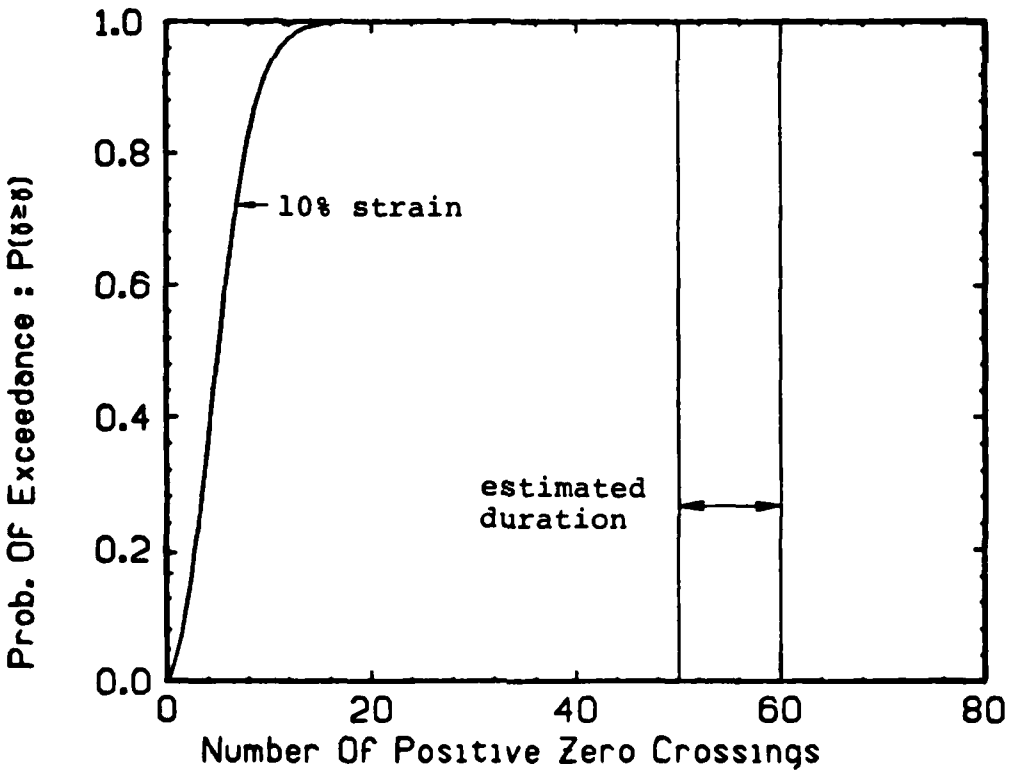

Figure 3.46: Prob. Dev. of Strain Potential, YBC Site, 1906 Event

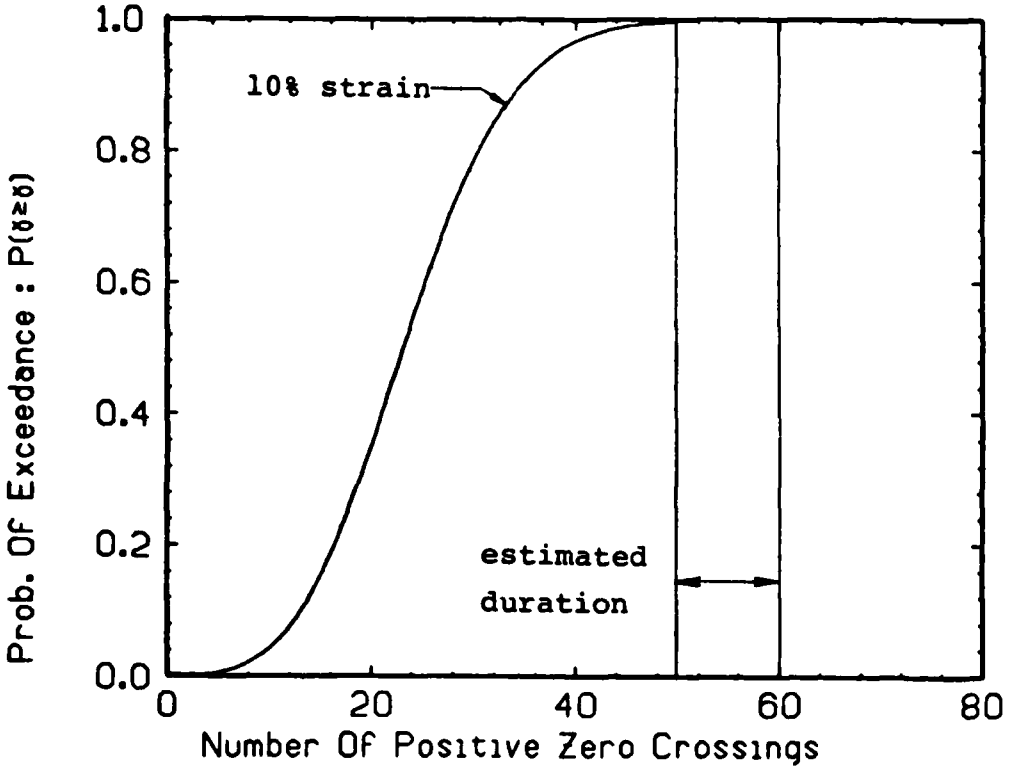

Figure 3.47: Prob. Dev. of Strain Potential ,TH Site, 1906 Event

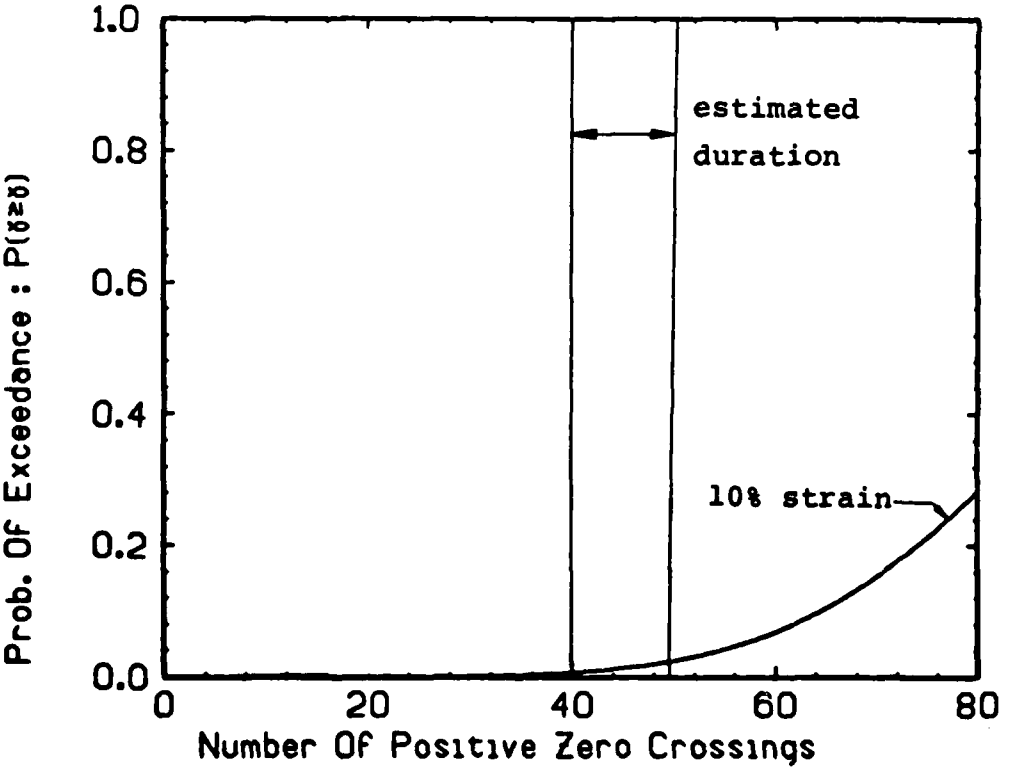

Figure 3.48: Prob. Dev. of Strain Potential ,TH Site, RM=7.5 Event

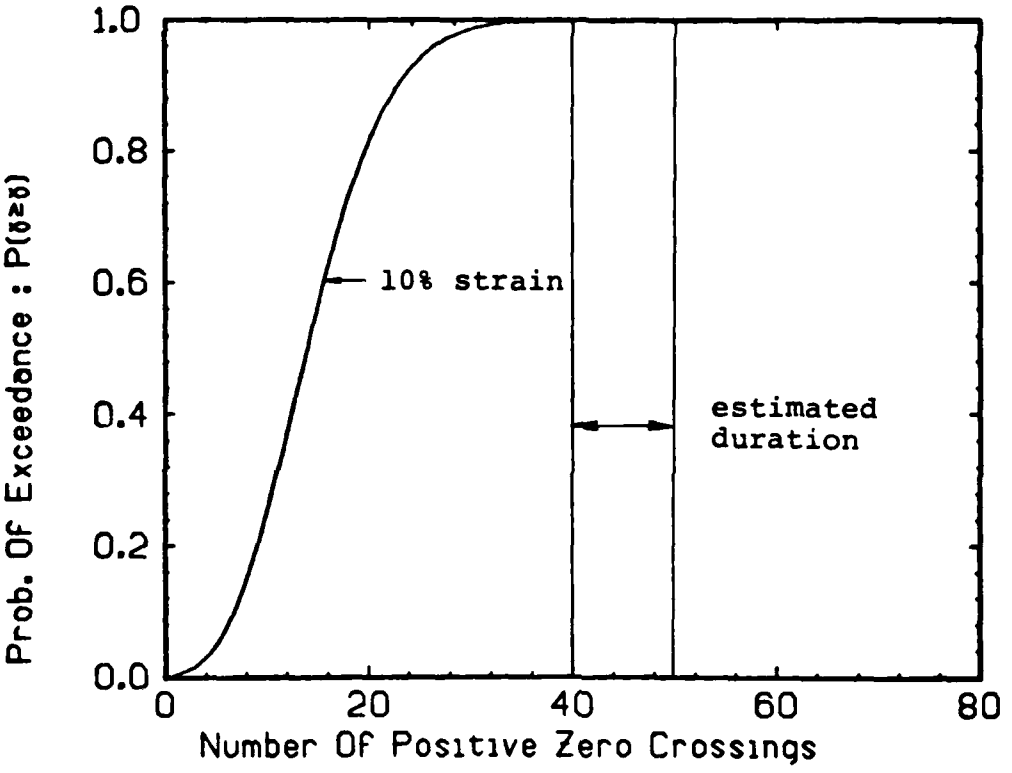

Figure 3.49: Prob. Dev. of Strain Potential ,YBC Site, RM=7.5 Event

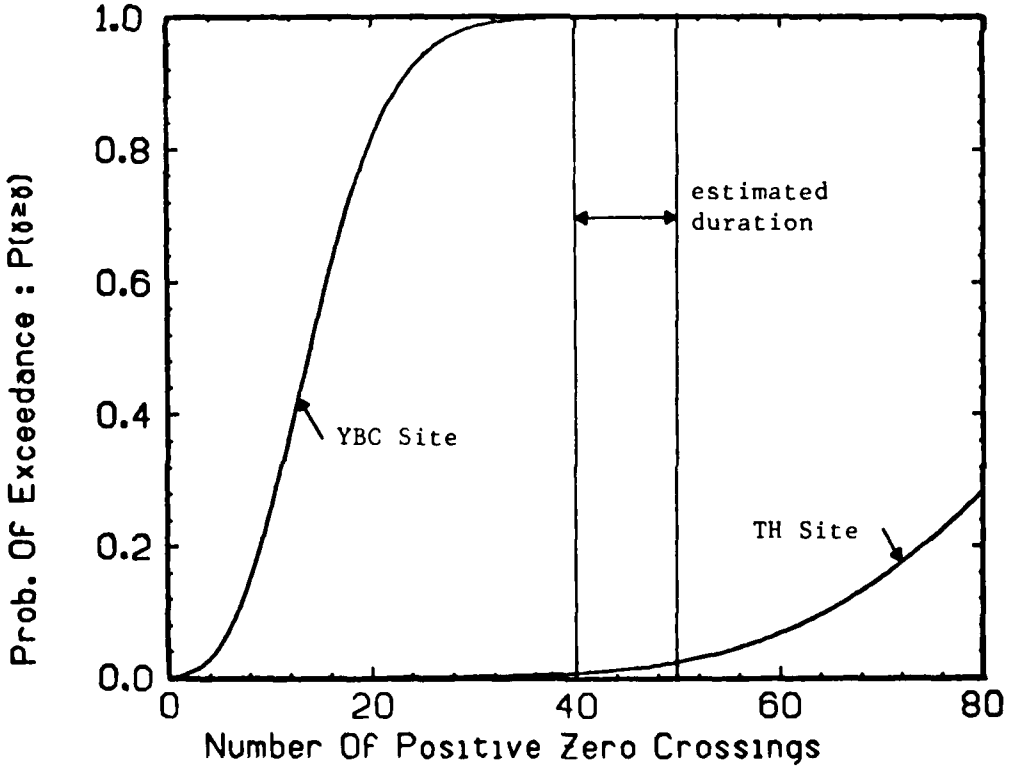

Figure 3.50: Comparison of TH & YBC Sites for RM=7.5 Event

3.5 SUMMARY

Three sites where liquefaction did and did not occur during earthquakes were examined using probabilistic pore pressure and strain development models. This study enabled us to test the validity of the models by comparing the predicted and observed behavior. A summary of the study is presented in Table 3.13. There is generally a good agreement between the predicted probabilistic behavior and the actual behavior at the sites during the earthquakes.

The models can therefore be used to anticipate future performance of sites that present a high potential for liquefaction in seismic areas. Such a study was performed for the San Francisco sites. The results can be used as input for engineering decision analysis. The TH site may be considered as more reliable in terms of high pore pressure related damage than the YBC site. Such conclusions may influence the choice of sites for economic development.

The next chapter in this report describes a comprehensive seismic hazard analysis which can be performed using these models and probabilistic information on the seismic environment. An application of this comprehensive analysis using the pore pressure model on a hypothetical site near San-Francisco is also presented.

TABLE 3.13

Summary of Study of Case Histories

LOCATION	YEAR	EARTHQUAKE			SOIL			
		RM	PGA, RMS	Duration # Cycles	Cyclic Curves	Relative Density	Pore Pressure Curves	Water Table Level
Amatitlan	1976	7.50	Yes	No	Yes	Yes	No	Yes
Imperial Valley	1979	6.60	Yes	Yes	No	Yes	No	Yes
San Francisco	1906	8.25	Yes	Yes	Yes	Yes	No	Yes
	1957	5.30	Yes	Yes	Yes	Yes	No	Yes

SITE		EARTHQUAKE				PROBABILITY in %		
LOCATION	D_r	RM	PGA	Duration sec	Number of Crossings	P[R>1.0]	P[γ>10%]	Observed Behavior
Amatitlan Zone 1	very loose	7.5	.15g	50	40-50	92-99	50-75	Numerous sand boils Large cracks, Lateral spread
Amatitlan Zone II	medium	7.5	.15g	50	40-50	7-15	$\simeq$0	Few small cracks
Imperial Valley								
Heber Road Unit A1	90%	6.6	.60g	18	16-22	79-95	15-33	Numerous sand boils Formation of a lateral spread
Heber Road Unit A2	23%	6.6	.60g	18	16-22	$\simeq$100	$\simeq$ 100	Large cracks
River Park	50%	6.6	.20g	18	20-30	98-100	80-97	Sand boils

SITE		EARTHQUAKE				PROBABILITY in %		
LOCATION	D_r	RM	PGA	Duration sec	Number of Crossings	P [R ≥ 1.0]	P[$\gamma \geq 10\%$]	Observed Behavior
San Francisco								
YBC Site	40%	5.3	.14g	20	12-16	2-4	≃0	No evidences
		8.25	.30g	70-80	50-60	≃100	≃100	Large ground displacement reported
		7.5	.20g	50-60	40-50	≃100	≃100	●
San Francisco								
TH site	60%	5.30	.14g	20	12-16	≃ 0	≃ 0	No evidences
		8.25	.30g	70-80	50-60	≃ 100	≃100	No ground movement reported
		7.50	.20g	50-60	40-50	8-20	2-4	●

●Theoretical Analysis

CHAPTER IV

SEISMIC HAZARD EVALUATION

4.0 SEISMIC HAZARD EVALUATION

In the results described in Chapter 3, the uncertainty in the soil resistance to cyclic loading is incorporated into an approach for evaluating effects of pore pressure development. However, the uncertainty in the earthquake loading could only be accommodated by explicitly considering different events. In this chapter, a preliminary solution is provided for the methodology to incorporate uncertainty in the earthquake loading into the question of pore pressure generation.

The overall methodology for performing seismic hazard assessments has been presented and discussed by several investigators (Cornell and Merz, 1975; McGuire, 1976; Mortgat, 1976). The seismic hazard is usually expressed in terms of peak ground acceleration, root mean square of acceleration or response spectrum. The seismic hazard methodology can be taken one step further to express the hazard in terms of a soil related parameter such as the level of pore pressure:

$$P(R > r) = \int_N \int_{n_a} P(R > r/r_a, N)\, f_{N/r_a}(r_a, N)\, f_{r_a}(f_a)\, dr_a\, dN \qquad (4.1)$$

where: $P(R > r)$ is the annual probability of exceedance of the pore pressure ratio r.

$P(R > r/r_a, N)$ is the probability that the pore pressure ratio R will be greater than or equal to r given the root mean square of acceleration r_a and the number of cycles (zero-cossings) N. This function is graphically represented by the probability curves presented in the previous chapters.

$f_{N/r_a}(N, r_a)$ is the conditional probability density function of the number of zero-crossings N given the root mean square r_a. $f_{r_a}(r_a)$ is the probability density function r_a which can be reduced from a root mean square versus return period graph. Such a graph is given in Figure 4.1.

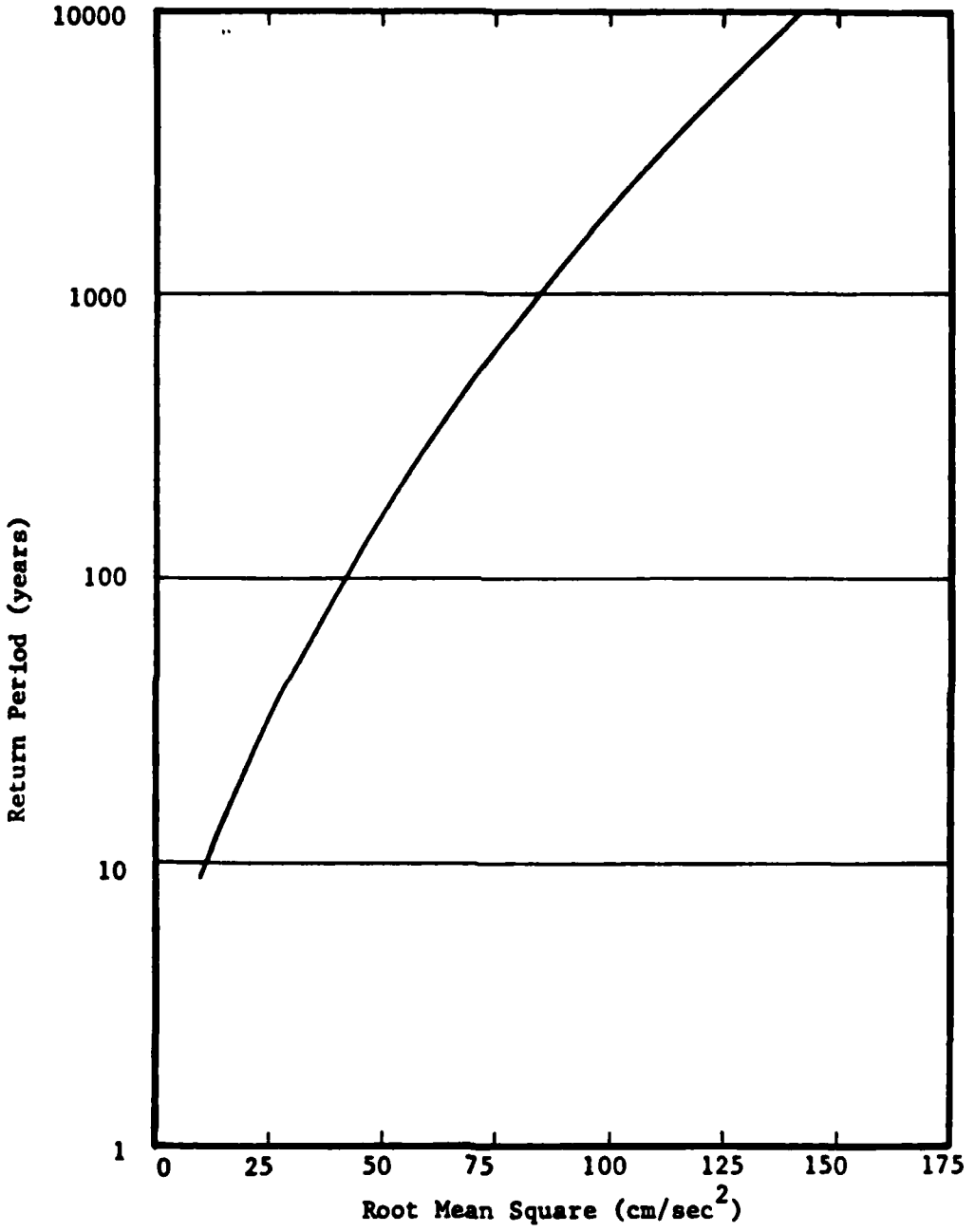

Figure 4.1: RMS Versus Return Period

The unknown term in Equation 4.1 is the conditional density function $f_{N/r_a}(r_a,N)$. Available studies and results to assess this relation are very sparse, and assumptions are necessary to define it. The simplest one is to consider r_a and N to be statistically independent. This approach was used by Mortgat (1980) and is substantiated by previous work on PGA and duration. With this assumption Equation 4.1 reduces to:

$$P(R > r) = \int_N \int_{r_a} P(R > r/r_a,N)\, f_{r_a}(r_a)\, dr_a\, dN \qquad (4.2)$$

where $f_N(N)$ is the probability density function of N, the number of zero-crossings. N can be assumed to be uniformly distributed between a minimum and maximum value. Based upon the limited data available the minimum and maximum values are about 50 and 250 to 350, respectively. Other distributions such as the Chi-square distribution can also be considered. Other potential assumptions are discussed by Chameau (1980). They include: (1) a weak dependence between N and r_a, where the range of N values slightly increases with r_a; (2) a global statistical relation between N, r_a and magnitude; and, (3) a weighted analysis of these assumptions where each assumption is given a subjective weight.

The results of a seismic hazard analysis for a site located close to San Francisco and having the characteristics of the hypothetical site with a relative density of 54% (previous chapter) are given in Figure 4.2. Two pore pressure ratios were considered in the analysis, 0.50 and 1.0. The probability of at least one occurrence of the ratio R = 1.0 is 0.61 for a 50 year time period and 0.84 for a 100 year time period. For the ratio R = 0.50, the probabilities of at least one exceedance are 0.75 and 0.96 for the same time periods, respectively. Such high numbers are to be expected for a site close to the San Andreas fault. Parametric studies were also performed to describe how the assumptions, seismic environment, and site resistance affect the hazard assessment at a given site. The results of such a study are given in Figure 4.3 where the probability of at least one occurrence of R = 1.0 is plotted as function of time period and relative density (same site as in Figure 4.2).

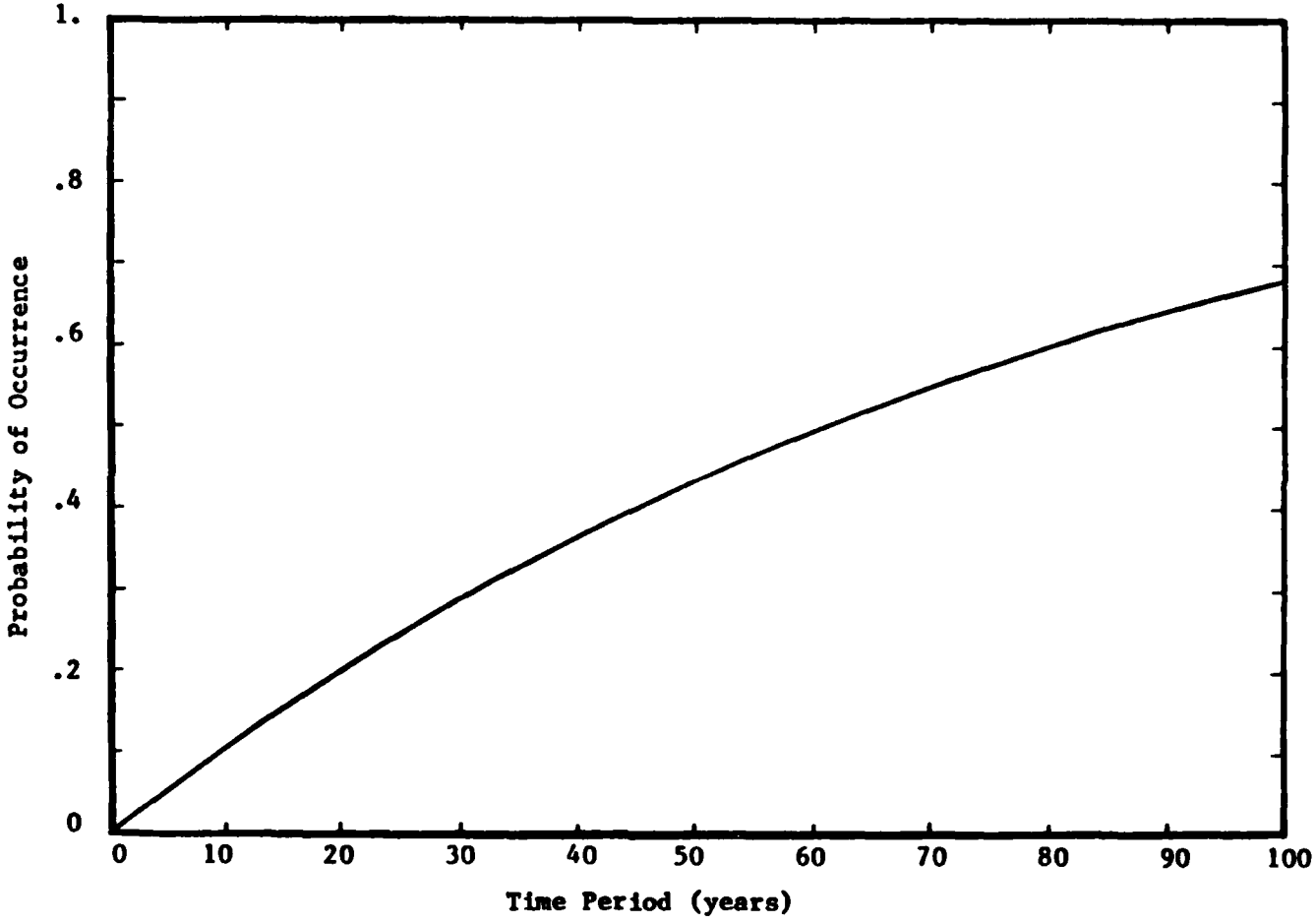

Figure 4.2: Seismic Hazard Evaluation for Hypothetical Site

CHAPTER V

SUMMARY

5.0 SUMMARY

Probabilistic pore pressure and shear strain potential models are applied to documented case histories of site behavior in seismic events. The results show that if the probabilistic design parameters are properly chosen the models can reasonably predict field performance. Of particular note is the ability of the shear strain model to differentiate between dense soil sites where the probability of initial liquefaction is high but the probability of damaging shear strains is low and looser sites where there is a high probability of potentially damaging shear strain accompanying the high probability of initial liquefaction. However, the potential value of these probabilistic models lies not in their predictive capabilities per se, since, in one form or another, other methods are available for this purpose. The intrinsinic advantage they posses is in providing predictive data in a framework which is useful for engineering decision making. The engineer is provided with a feel for the risks involved in his decision because the uncertainities inherent in this testing and analysis are considered.

BIBLIOGRAPHY

Benjamin, J. R., and Cornell, A. C., "Probability, Statistics and Decision for Civil Engineers," McGraw-Hill, 1970.

Bennett, M. J., Youd, T. L., Harp, E. L., and Wieczorek, G. F., "Subsurface Exploration of Liquefaction-Imperial Valley Earthquake, October 15, 1979. USGS, Open File Rept. 81-502.

Brady, A. G., Perez, Y., and Mork, P. N., "The Imperial Valley Earthquake of October 15, 1979. Digitization and Processing of Accelerograph Records." Seismic Engineering Data Rept., USGS Open File Rept. 80-703, April 1980.

Chameau, J. L., "Probabilistic and Hazard Analysis for Pore Pressure Increase in Soils Due to Seismic Loading," Ph.D. Dissertation, Stanford University, Stanford, Calif., October, 1980.

Clough, G. W., and Chameau, J. L., "A Study of the Behavior of the San Francisco Fills Under Seismic Loading," J. A. Blume Earthquake Engineering Center, Stanford University, Stanford, Calif., Rept. No. 35, February, 1979.

Cornell, C. A., and Merz, H. A., "A Seismic Risk Analysis of Boston," J. of the Structural Div., Am. Soc. Civil Eng., Vol 110, No. ST10, October 1975.

De Alba, P., Chan, C. K., and Seed, H. B., "Determination of Soil Liquefaction Characteristics by Large Scale Laboratory Testing," Rept. EERC 75-14, U. C. Berkeley, College of Engineering, Berkeley, Calif., 1975.

DeHerrera, M. A., "A Time Domain Analysis of Seismic Ground Motions Based on Geophysical Parameters," Ph.D. Dissertation, Stanford University, Stanford, Calif., July 1981.

Espinosa, E. F., Ed: "The Guatemalan Earthquake of February 4, 1976. A Preliminary Report." USGS Prof. Paper 1002, 1976.

Ferrito, J. M., Forrest, J. B., and Wu, C., "A Compilation of Cyclic Triaxial Liquefaction Test Data," Geotechnical Testing Journal, Vol 2, No. 2, June 1979.

Finn, Liam W. D., Lee, K. W., and Martin, G. R., "An Effective Stress Model for Liquefaction," J. of the Geotech. Eng. Div., Am. Soc. Civil Eng., Vol 103, No. GT6, June, 1977.

Hadk Hamou, T., "Probabilistic Evaluation of Damage Potential Due to Seismically Induced Pore Pressures," Ph.D. Dissertation, Stanford University, (In preparation), 1983.

Jenning, P. C., and Kanamori, H., "Determination of Local Magnitude ML from Seismoscope Record," Bull. of the Seismological Society of America, Vol 69, No. 4, p 1267-1788, August 1979.

Martin, G. R., Finn, W. D. Liam, and Seed, H. B., "Fundamentals of Liquefaction Under Cyclic Loading," J. of the Geotech. Eng. Div., Am. Soc. Civil Eng., Vol 101, No. GT5, May 1975.

Mortgat, C. P., and Shah, H. C., "A Bayesian Approach to Seismic Hazard Mapping; Development of Stable Parameters," J. A. Blume Earthquake Engineering Center, Report No. 28, Stanford, 1978.

Mortgat, C. P., "A Probabilistic Definition of Effective Acceleration," 2nd U. S. National Conference on Earthquake Engineering, Stanford University, August 1979.

Page, R. A., Boore, D. M., and Dietrich E. U., "Estimation of Bedrock Motions at the Ground Surface," Professional Paper No. 941-A, USGS.

Seed, H. B., and Idriss, I. M., "Rock Motion Accelerograms for High Magnitude Earthquakes," Report No. EERC 69-7, University of California - Berkeley, April 1969.

Seed, H. B., Idriss, I. M., Lee, K. L., and Makdisi, F. I., "Analysis of the Slides of the San Fernando Dams During the Earthquake of February 9, 1971," Report No. EERC 73-2, University of California - Berkeley, June 1973.

Seed, H. B., Arango, I., Chan, C. K., Gomez-Masco, A., and Ascoli, R. G., "Earthquake Induced Liquefaction near Lake Amatitlan - Guatemala," Report No. 79-27, University of California - Berkeley, 1979.

Stroiber, R. E., and Carr, M. H., "Quaternary Volcanic and Tectonic Segmentation of Central America," Bull. Volcanologique, Vol 37, No. 3, 1973.

Valera, J. E., and Donovan, N. C., "Soil Liquefaction Procedures, A Review," J. of the Geotech. Eng. Div., Am. Soc. Civil Eng., Vol 103, No. GT6, June 1977.

Van De Kamp, P. C., "Holocene Continental Sedimentation in the Salton Basin, California. A Reconnaissance," Bull. G.S.A., Vol 84, No. 3, 1973.

Vanmarck, E. H., "Structural Response to Earthquakes," Chap. 8, in: "Seismic Risk and Engineering Decision," Eds: Lornnitz, C. and Rosenblueth, F., Elsevier, 1976.

Youd, T. L., and Hoose, S. N., "Liquefaction During the 1906 Earthquake," J. of the Geotech. Eng. Div., Am. Soc. Civil Eng., Vol 102, No. GT5, May 1976.

Zsutty, T., and DeHerrera, M., 1979, "A Statistical Analysis of Accelerogram Peaks Based Upon the Exponential Distribution," Second U. S. National Conference on Earthquake Engineering, pp 733-742.

PROBABILISTIC SEISMIC AND GEOTECHNICAL EVALUATION AT A DAM SITE

by

Erik H. Vanmarcke

PROBABILISTIC SEISMIC AND GEOTECHNICAL EVALUATION AT A DAM SITE

By Erik H. Vanmarcke

PART I: INTRODUCTION

1. This report examines the use of probabilistic methods in dealing with the problem of potential earthquake-induced liquefaction of foundation soils at an example dam site located in the central United States, near the New Madrid earthquake zone. The example dam is assumed to be a 1-mile long rolled-filled embankment founded on a 100-ft deep deposit of interbedded alluvial gravels, sands, silts, and clays.

2. The study is seen as an opportunity to examine probabilistic concepts and procedures in the framework of an example engineering project. In this context, the main practical value of a probabilistic approach is that it permits more informed decision making about further data acquisition, additional engineering analysis, and if necessary, remedial action.

3. The specific aim of the study is to show how probabilistic procedures complement and help to reinterpret the results of deterministic (earthquake-induced) liquefaction analysis. The procedures focus on evaluating the impact of the different sources of variability (in the input parameters) on the uncertainty in performance predictions, and they permit results of the liquefaction analyses to be seen in the broader framework of assessment of earthquake-related dam failure risks.

4. A comprehensive probabilistic risk assessment under earthquake loading would involve at least these two steps: (a) evaluate the likelihood of occurrence of different levels of ground shaking at the dam site (seismic hazard analysis), and (b) evaluate the conditional probability of dam failure given the occurrence of an earthquake of given intensity at the site (conditional reliability analysis). Overall seismic safety assessment requires combining the information generated in these two steps. Although it is beyond the scope of this work, it is also advisable to evaluate and to try to balance seismic and non-seismic failure risks (e.g., hydrologic risk, piping) in decision making about remedial action at a dam site.

5. The present study is considerably more limited, seeking merely to extend and reinterpret preliminary analyses of liquefaction potential. In effect, we focus attention to step (b) mentioned above, focusing on the conditional reliability analysis given the occurrence of the design earthquake. The design ground motion at the example site is that which would be generated if the New Madrid earthquake were to recur. The degree of conservation in the choice of design earthquake (e.g., the implied mean return period) is not accounted for here. In any case, an overall (unconditional) seismic risk analysis, albeit most desirable, is judged to be beyond the scope of this study.

6. In what follows, we first review background information about the site stratigraphy and soil properties and about the results of deterministic liquefaction studies. The liquefaction potential assessment is then reevaluated from a probabilistic standpoint, and it is attempted to place the conventional analysis in the broader context of dam failure risk evaluation.

PART II: SITE STRATIGRAPHY AND SOIL PROPERTIES

7. Preliminary field investigation at the site consists of seven Standard Penetration Test (SPT) borings (spaced at approximately 1000-ft intervals), five undisturbed sampling borings and surface and subsurface geophysical measurements. These borings, all located downstream from the centerline of the dam, reveal a complex foundation stratigraphy in which gravels, sands, silts, and clays are interbedded. Soil classification data, undisturbed samples and SPT N values provide information about the presence of liquefiable materials and form the basis for the simplified liquefaction analyses.

8. A program of geophysical exploration provide estimates of shear-wave and compression-wave velocity profiles from refraction, downhole and crosshole test results in the vicinity of one station at the dam. At other boring locations, shear wave velocity profiles are predicted by means of empirical correlations with SPT N-values. Thus, shear-wave velocity zones are determined from the measured and empirically determined velocities and soil stratigraphy data available.

9. Information about local geology is of course also relevant to assessing the stratigraphy and especially the continuity of layers of liquefiable material in the foundation of the embankment. The deposits are expected to be continuous over a large area with no preferential direction if the deposits are predominantly lacustrine. If these are alluvial deposits, more continuity is expected in the direction of the flow of the river.

PART III: DETERMINISTIC SEISMIC LIQUEFACTION ANALYSIS

10. To assess liquefaction potential the two methods proposed by Seed and Idriss (1971) are followed. They yield predictions of the factor of safety $F = R/S$, where R = material resistance to liquefaction, and S = induced stress. Seed and Idriss (1981) state that: "The two methods involve the same basic approach and differ only in the manner in which the field liquefaction characteristics of the deposit are determined." In the first method, values for shear strength are obtained from cyclic tests on representative soil samples, while in the second (simplified) method they are estimated from empirical correlations with SPT N-values.

11. In both methods (as applied at this example site), earthquake-induced shear stresses were evaluated by means of the program SHAKE which does a one-dimensional (1-D) dynamic analysis using an earthquake accelerogram as input. The first step is a deconvolution of the surface motion through a soil profile presumably characterizing the recording site. This is followed by upward propagation of the computed bedrock motion through (i) the "free field" soil profile downstream (or upstream) of the dam, and (ii) the soil profile at the centerline of the dam. For these two locations, the initial horizontal shear stresses are zero, and the 1-D dynamic analysis predicts the earthquake-induced shear stresses fairly accurately in the foundation soils.

12. The output of the SHAKE analysis consists of shear stress histories at different depths in the profile. These are converted by the computer program EQCYCLE into sinusoidal motions with equivalent amplitude of shear stress so that the field stresses can be compared directly with the laboratory strengths for liquefaction potential assessment. A number of different analyses are carried out for different assumed pool levels (affecting water table elevation), and to investigate the effect of a protective berm on the downstream side of the dam.

13. At the locations of the seven SPT borings, safety factors were calculated by means of the simplified approach (with strengths based on individual N-values from each of these borings). Safety factors are computed at each depth for which an SPT N-value is given. This results in safety factor profiles at several locations along the axis of the embankment. In this deterministic approach, it is assumed that locations at which the factor

of safety against liquefaction (F) exceeds 1.25 are "safe" from earthquake-induced liquefaction. The hypothetical N-values corresponding to $F = 1$ and $F = 1.25$ are computed for direct comparison with field SPT measurements. The safety factors predicted by the two approaches (laboratory cyclic strength and SPT empirical correlations) both lead to the conclusion that for this example site, the depth range of concern ($F < 1.25$) lies between 20 ft and 60 ft.

PART IV: UNCERTAINTY IN "POINT" LIQUEFACTION POTENTIAL ASSESSMENT

14. In a probabilistic approach to the assessment of "point" liquefaction potential, the safety factor $F = R/S$ is seen as a random variable, i.e., the ratio of random resistance R to random induced stress S. Initial liquefaction will occur at locations where the stress exceeds the resistance, i.e., where the random safety factor F is below one. The event "$F < 1$" implies temporary and local loss of resistance to shearing. Of course, the dam is endangered only if such strength loss, indicated by $F < 1$, occurs over a sufficiently large volume to cause embankment sliding. (This latter question is addressed in a later section.)

15. Based on "first-order second-moment" analysis (assuming R and S to be statistically independent), the mean coefficient of variation (c.o.v.) of the safety factor F are, respectively:

$$m_F \cong m_R/m_S \tag{1}$$

$$V_F^2 \cong V_R^2 + V_S^2 \tag{2}$$

where m_R and m_S are the mean values and V_R and V_S the coefficients of variation of resistance and stress, respectively. If desired, probabilities of "initial liquefaction" can be estimated if a probability distribution is assumed for the safety factor F. (The most analytically convenient choice is the lognormal distribution.)

16. It is useful to express the random (equivalent, earthquake-induced) shear stress S in product form:

$$S = \bar{S}\, X_1\, X_2 \tag{3}$$

where $\bar{S}$ is the nominal shear stress, and X_1 and X_2 are statistically independent random factors. The factor X_1 represents a systematic error attributable to the choice of soil profiles for dynamic analysis (layer thicknesses, soil types and properties, water table elevation), to the method of one-dimensional analysis, and to possible biases in the acceleration history chosen as input to the SHAKE program. The factor X_2 is location-dependent and accounts for differences between the assumed profile and the actual

profile at different locations, and for the fact that earthquake ground motion is stochastic in space as well as in time. The product form implies the following approximations for the mean and the c.o.v. of S :

$$m_S = \bar{S}\, m_{X_1}\, m_{X_2} \tag{4}$$

$$V_S^2 \cong V_{X_1}^2 + V_{X_2}^2 \tag{5}$$

17. The random resistance R may be modeled in a similar way:

$$R = \bar{R}\, Y_1\, Y_2 \tag{6}$$

where $\bar{R}$ is the nominal (measured or predicted) strength, and Y_1 and Y_2 are independent random factors. The factor Y_1 accounts for measurement or estimation errors, both systematic and random. (The factor Y_1 could of course be split in order to isolate systematic and random error sources). The factor Y_2 is location-dependent and its variance is minimum at locations where the soil is actually samples and tested or where field measurements are made. Errors in soil classification may contribute to the variance of either or both factors. Again we may write:

$$m_R = \bar{R}\, m_{Y_1}\, m_{Y_2} \tag{7}$$

$$V_R^2 \cong V_{Y_1}^2 + V_{Y_2}^2 \tag{8}$$

18. This "propagation of variability" format permits quantification of technical uncertainties inherent in conventional liquefaction potential assessment. The mean values of the random error factors quantify different sources of bias (in laboratory tests, in measured or corrected SPT N-values, in their correlation with cyclic strength, due to systematic misclassification, etc.). Combining the equations involving the means yields:

$$m_F \cong m_R/m_S = (\bar{R}/\bar{S})\ (m_{Y_1}\, m_{Y_1}/m_{X_1}\, m_{X_2}) \tag{9}$$

19. If the nominal values S and R were not biased, F = R/S would become a genuine "best estimate" of the safety factor. This would imply that the four random factors (X_1, X_2, Y_1, Y_2) have unit mean values, leading to:

$$m_F \cong m_R/m_S = \bar{R}/\bar{S} \tag{10}$$

However, in this type of analysis there is a demonstrated tendency toward conservatism: accelerations and stresses are often overestimated while resistances are underestimated. In reference to the method based on cyclic shear strength determined from laboratory tests, Peck (1979) concluded that "(1) unless the cyclic loading tests used to evaluate liquefaction potential can be performed on absolutely undisturbed samples, which is manifestly impossible, the results will probably indicate too great a likelihood of liquefaction; and (2) in many instances the resistance to liquefaction may be appreciably, even spectacularly, greater than that determined on the basis of conventional cyclic laboratory tests on reconstituted or even 'undisturbed' samples if no allowances are made for various beneficial effects such as time, repeated small shearing forces, and stress history." Thus, the results of laboratory cyclic shear strength tests are conservatively biased estimators of the mean strength in the field. There are even more sources of random and systematic error in estimates of cyclic strength based on SPT N-values. Much relevant (quantitative) information is provided in a recent report by Kovacs et al. (1981).

20. The square of the coefficient of variation (c.o.v.) of the safety factor is approximately the sum of four contributions (from Equations 2, 5, and 8):

$$V_F^2 \cong V_{X_1}^2 + V_{X_2}^2 + V_{Y_1}^2 + V_{Y_2}^2 \tag{11}$$

The composite c.o.v. is a measure of confidence (or rather lack of confidence) in predicted safety factors. If the mean safety factor remains constant, smaller values of V_F imply smaller probabilities of "point" liquefaction. Whenever new data become available, a format of Bayesian analysis can be used to update mean values and reduce c.o.v.'s. In this context, the relative merit of alternative data acquisition strategies can be evaluated in terms of their impact on the composite c.o.v. of the factor of safety.

21. Tentative site-specific values for these coefficients at the example dam site are suggested in Table 1. Note that the c.o.v.'s of the random factors associated with the resistance are different for the two methods (laboratory versus field (SPT) based estimation of cyclic strength). If the mean safety factor is assumed to be predicted without bias by the deterministic analysis, knowledge of the c.o.v. of F suffices to obtain an approximation for the probability of initial liquefaction at different points (based on the lognormal distribution). These probabilities provide, in a sense, very crude upper bounds on the probability of earthquake-induced sliding (owing to liquefaction). This relationship is further discussed in the next section.

Table 1

Suggested Values for Coefficients of Variation

Coefficient of Variation	Borings Where Cross-hole Geotechnical Measurements Were Made	Other Borings	Other Locations Where There are no Borings*
V_{X_1}	0.1	0.1	0.1
V_{X_2}	0	0.1	0.1
V_{Y_1}	.15(.1)	.15(.1)	.15(.1)
V_{Y_2}	0.1	0.1	0.2
V_F	.206(.173)	.229(.2)	.29(.27)

* ("Other locations..." assumed to be to removed from SPT and undisturbed borings by lateral distances exceeding the correlation distance (20 to 50 ft).) (Values in parentheses refer to the method based on laboratory strength.)

22. It could be said that the probabilities of initial liquefaction are little more than "indicators" similar to conventional safety factors. Of course, their advantage is that they carry explicit information about sources of uncertainty. In particular, the format just presented allows quantification of the value of different kinds of new information in terms of reduction of variability.

23. The means of the random factors X_1, X_2, Y_1, and Y_2 should not all be set equal to one. Owing to the tendency toward conservatism, the (unbiased) mean safety factor may be as much as 1.5 to 2 times the conventional safety factor. It is easy to show that this will have a very beneficial impact on calculated probabilities of initial liquefaction.

24. Finally, it should be mentioned that it is possible to take an alternate, entirely empirical approach to evaluating the likelihood of liquefaction for level ground sites (see for example, Xie, 1979). It is directly based on information about actual cases of occurrence or non-occurrence of liquefaction, in function of pertinent site properties (average N-values) and ground motion characteristics (M.M. Intensity or peak acceleration). However, to the extent that the "strength-versus-blowcount" correlations are in fact calibrated to the same data base, the direct empirical approach is not expected to yield additional information or new insights.

PART V: RELATION TO PROBABILITY OF EARTHQUAKE-INDUCED DAM FAILURE

25. For the results of any probability analysis to be meaningful, it is essential to define clearly the events whose probability is sought. In the case at hand, the "failure" event is earthquake-induced liquefaction of foundation or embankment soils, leading to embankment deformation (sliding) large enough to cause overtopping, and followed by uncontrolled loss of the contents of the reservoir. The implied multi-step sequence leading to the failure event is depicted in Figure 1.

26. An important "weakest link" characteristic typifies the failure mechanism: earthquake-induced liquefaction and subsequent sliding can occur anywhere along the embankment axis, either on the upstream or on the downstream side, but the strength degradation caused by liquefaction must extend over a sufficiently large, more or less contiguous zone for embankment sliding to be possible.

27. If the soil properties are statistically homogeneous and the cross-section geometry is the same all along the embankment axis, one can show that the failure risk (for long embankments) is proportional to embankment length (Vanmarcke, 1977). More generally, the failure risk is approximately equal to the integral (over the total embankment length) of the mean failure rate per unit length measured along the axis. Since the dominant contribution to the integrated failure risk will come from the weakest zones along the axis, a simplified approach to the problem is to locate the weakest zone(s) and to insure that the corresponding mean failure rate(s) is (are) acceptably low.

28. One way to incorporate the concept of local spatial averaging or integration is to express the results of the liquefaction analyses in terms of the safety margin $M = R-S$ instead of the safety factor $F = R/S$; the error factors can then be modeled as additive rather than multiplicative, which makes them even more tractable. Of course, the events "$F < 1$" and "$M < 0$" are equivalent. The random safety margin M may be averaged over a potential sliding surface, and physically meaningful spatial averages of R , S , and M can in principle be obtained. This permits incorporating information about the presence of liquefiable materials (stratigraphy) and about the resistance of such materials in a consistent way into probabilistic embankment stability analysis.

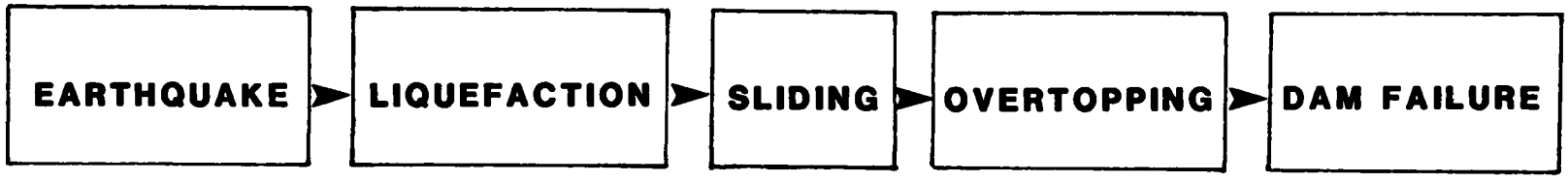

Figure 1. Sequence of events leading to loss of reservoir (failure)

29. The pool level of the example reservoir is assumed to be usually low, and the normal yearly variation in the amount of available freeboard is from 30 to 40 ft. At the maximum design pool, there is 15-ft of freeboard. Hence, under normal hydrologic conditions, very extensive sliding would have to occur for the embankment crest to drop below the pool level. A complete risk assessment evidently requires consideration of the likelihood of joint occurrence of floods (pool levels) and earthquakes.

PART VI: CONCLUDING COMMENTS

30. The advantages of a probability-based approach to seismic liquefaction studies are that: (a) it provides perspective on conventional liquefaction analysis by identifying it as only one in a sequence of steps comprising earthquake-induced failure risk assessment, (b) it yields information about the impact of uncertainty in the input parameters on the reliability of results of deterministic liquefaction analysis, and (c) it provides the basis for more informed decision making about further acquisition, analysis, and remedial action.

31. Ideally, the conditional reliability analysis (under a given level of earthquake shaking) should be repeated for different levels of ground motion. The resulting "fragility" curve could then be combined with the site "seismicity" curve (i.e., the output of a site-specific seismic hazard analysis) to yield estimates of the probability of earthquake-induced dam failure during a specified time period. Such a study is within the state-of-the-art.

REFERENCES

Kovacs, D. W., Salomone, L. A., and Yokel, F. Y., "Energy Measurement in the Standard Penetration Test," NBS Building Series 135, 1981.

Peck, R. B., "Liquefaction Potential: Science versus Practice," J. Geotechnical Engineering Division, ASCE, March 1979.

Seed, H. B. and Idriss, I. M., "Simplified Procedure for Evaluating Soil Liquefaction Potential," J. Soil Mechanics and Foundation Division, ASCE, Vol. 97, No. SM9, 1971.

Seed, H. B. and Idriss, I. M., "Evaluation of Liquefaction Potential of Sand Deposits Based on Observations of Performance in Previous Earthquakes," Presented at the St. Louis ASCE Convention, 1981.

Vanmarcke, E. H., "Reliability of Earth Slopes," J. Geotechnical Engineering Division, ASCE, November 1977.

Xie, Junfie, "Empirical Criteria of Sand Liquefaction," Proceedings Second U.S. National Conference on Earthquake Engineering, Stanford University, August 1979.

Table 1

Suggested Values for Coefficients of Variation

COEFFICIENT OF VARIATION	BORINGS WHERE CROSS-HOLE GEOPHYSICAL MEASUREMENTS WERE MADE	OTHER BORINGS	OTHER LOCATIONS* WHERE THERE ARE NO BORINGS
v_{X_1}	0.1	0.1	0.1
v_{X_2}	0	0.1	0.1
v_{Y_1}	0.15(0.1)	0.15(0.1)	0.15(0.1)
v_{Y_2}	0.1	0.1	0.2
v_F	0.206(0.173)	0.229(0.2)	0.29(0.27)

Note: Values in parentheses refer to the method based on laboratory strength.

* Other locations are assumed to be too removed from SPT and undisturbed borings by lateral distances exceeding the correlation distance (20 to 50 ft).

PROBABILISTIC SLOPE STABILITY METHODOLOGY

by

David S. Bowles
Loren R. Anderson
Ronald V. Canfield
and
Kevin D. Sharp

TABLE OF CONTENTS

AD-A136 497 PROCEEDINGS SEMINAR ON PROBABILISTIC METHODS IN GEOTECHNICAL ENGINEERING..(U) ARMY ENGINEER WATERWAYS EXPERIMENT STATION VICKSBURG MS GEOTE..

3/7

UNCLASSIFIED M E HYNES-GRIFFIN ET AL. SEP 83 F/G 8/13 NL

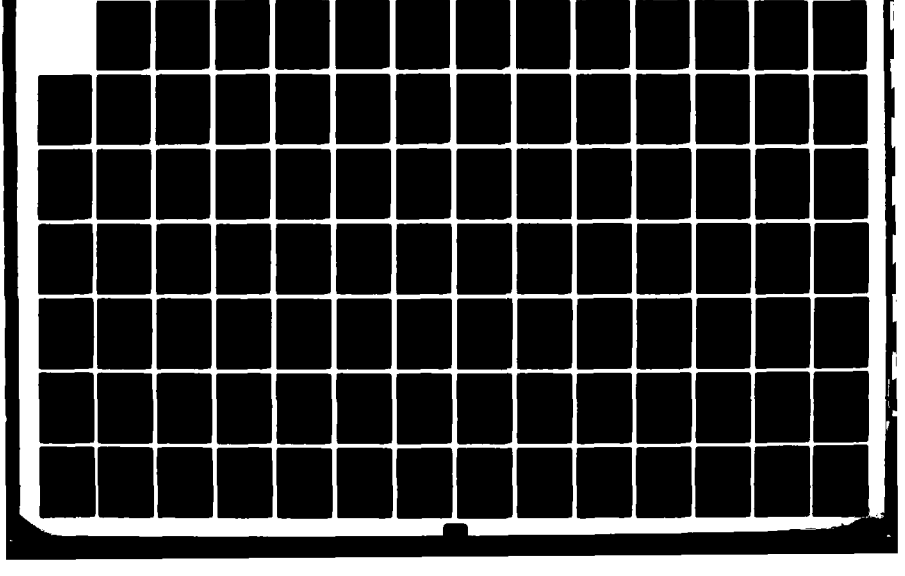

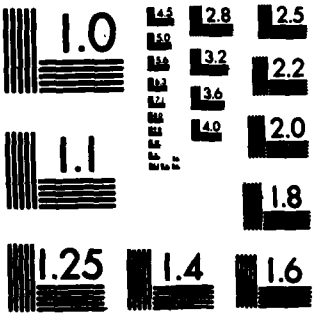

TABLE OF CONTENTS (cont'd.)

TABLE OF CONTENTS (cont'd.)

LIST OF TABLES

LIST OF FIGURES

1. EXECUTIVE SUMMARY

1.1 Introduction

A working methodology for probabilistic slope stability analysis is described in this report. The methodology was developed at Utah State University with funding from the U.S. Bureau of Mines. It is an extension of Vanmarcke's (1977) conceptual probabilistic slope stability model to effective stress analysis of zoned embankments. The necessary computer programs for the stability analysis and estimation of probabilistic parameters from field data are available and fully documented. Also procedures for conducting the necessary field investigations and laboratory testing are developed and have been applied to a case study performed on a tailings dam in Arizona. The methodology has been applied and evaluated by a firm of consulting engineers. In addition, training sessions have been provided to representatives of the U.S. Bureau of Reclamation and the U.S. Bureau of Mines. The U.S. Bureau of Mines is currently using the methodology in another case study. Additional case studies are needed to broaden the range of experience to both the evaluation of existing slopes and to the design of new slopes for a variety of materials and construction methods.

1.2 Probabilistic Slope Stability Analysis Method

The probabilistic slope stability analysis method is based on Mohr-Coulomb strength theory and the method of slices. The currently available version considers only a cylindrical failure surface although another version for considering non-circular failure surfaces is developed but still requires some verification. The method utilizes the usual input to a method of slices

analysis, plus the variance and autocorrelation (in three orthogonal directions) of shear strength for each zone of the embankment, to calculate a probability of failure of the embankment due to the spatial variability of shear strength. Embankment geometry and pore pressures are treated deterministically. The probability of failure is defined to be the probability that the factor of safety is less than unity. In conventional slope stability analysis, the critical case is determined to be the trial circle with the smallest safety factor, but in probabilistic analysis, the critical case is defined to be the trial circle with the highest probability of failure. The computer program for performing the probabilistic analysis is fully documented and easily used by engineers experienced with computer programs for the conventional slope stability analysis.

1.3 Field Program and Estimation of Probabilistic Parameters

In order to obtain sufficient data to estimate the variance and autocorrelation function of shear strength for each zone of an embankment, a more extensive field investigation program than is conventional would be required. However, conventional investigative procedures of drilling and sampling for laboratory testing would be prohibitively expensive on such a scale and thus in-situ testing procedures are attractive. Practical guidelines for planning and executing a field program suitable for estimating the necessary probabilistic parameters have been developed based on experience gained during the completed case study. In addition, methods for efficiently reducing field data were developed and documented by the USU team.

1.4 Case Study

The probabilistic slope stability methodology has been applied to the evaluation of the reliability of a tailings dam located in Arizona. This case

study provided the opportunity for a thorough testing of the methodology by the development team and also an independent evaluation by a consulting engineering firm.

Five conventional soil borings were made to define the embankment cross-section and 77 core penetrometer soundings were made to evaluate the necessary probabilistic parameters. The spacing and orientation of the soundings were carefully selected to minimize costs while providing adequate data.

Probabilistic slope stability analyses were performed for various positions of the phreatic surface. Thus, a probability of failure was calculated for each position of the phreatic surface. If monitoring were installed, operators of the dam could determine when the position of the phreatic surface was high enough to make the probability of failure unacceptable.

1.5 Evaluation of Existing Methodology

The probabilistic methodology comprises the field investigation and data reduction procedures, and the computer program for the probabilistic analysis and its use. An independent evaluation of the methodology by an engineering consulting firm concluded that the methodology has potential as a design tool.

An evaluation of the methodology by the Utah State University development team revealed the need for some technical refinement and an urgent need for additional case studies in order to generalize the applicability of the methodology to dams constructed from a variety of materials and using various construction methods. The technical refinements relate to the way in which autocorrelation or variance reduction is handled in the probabilistic analysis and the conversion of penetration resistance to shear strength and the interpretation of core penetrometer results.

1.6 Additional Case Studies and Development Work

Four objectives for the future work needed to further advance the methodology have been identified, as follows:

- To expand the range of experience in application of the probabilistic slope stability analysis methodology for both the evaluation of existing slopes and the design of new slopes.
- To generalize the existing practical guidelines and to continue technology transfer for engineers who are interested in applying the methodology.
- To improve certain details of the methodology including techniques for estimating and representing the spatial variability of soil properties affecting slope stability.
- To improve the interpretation of in situ testing procedure (i.e. electric cone penetrometer) results for describing the spatial variability of soil strength parameters.

Each of these objectives can be achieved through a set of carefully designed case studies. These case studies should be performed on existing slopes in the evaluation context and on slopes under construction in the design context which includes development of design values for variances and autocorrelograms for shear strength quality control programs to assume achievement of design values in the constructed embankment. Field work necessary for the case studies could be supplemented to include additional studies necessary to answer questions related to the technical refinements mentioned in Section 1.5.

1.7 Summary

In summary, the probabilistic slope stability methodology is already available in an operating form. It has been applied to one case study and is currently being applied to a second. Already-practicing geotechnical engineers have used the methodology and contributed to its development.

Remaining development work is primarily additional case studies to broaden the applicability of the methodology, especially in the design setting. Such case studies could also be conducted in cooperation with practicing engineers in government agencies or private firms.

2. INTRODUCTION

2.1 General

The safety of embankments depends on many factors including the correctness of design assumptions, the adequacy of quality control during construction, the level of inspection and maintenance, the skill of the operators where the embankment impounds water, and the occurrence of various natural phenomena such as floods, earthquakes, and landslides. A complete evaluation of all the factors contributing to embankment safety is very complex and procedures for developing and using this type of information in benefit/cost analyses are still in the formative stages. While progress is being made on the estimation of overall embankment reliability considering a broad range of factors, (Bowles, et al. 1978; Baecher, et al. 1979; Howell, 1981), much of the progress to date has been made in the area of probabilistic slope stability analysis.

Deterministic analysis has historically been the method of slope stability analysis. Conservative assumptions are used to simplify the concepts, mechanics, and mathematical models. Pessimistically selected engineering properties and an adequate safety factor are the ultimate insurance against uncertainties which may lead to a slope stability failure. This approach to handling the uncertainties does not include a quantification of the risks involved. Thus, there is no way of comparing the relative reliability level of alternative designs or determining what is an acceptably small level of risk.

In contrast, probabilistic modeling of slopes will provide a quantitative analysis of the uncertainties affecting the safety of a design or of an existing slope. The application of probabilistic modeling has been limited in the past; however, interest in its usefulness is becoming more widespread

among practicing engineers. Assessing the magnitude of the uncertainties gives the engineer a stronger basis to determine an appropriate safety level for an embankment. Risk/benefit analysis can be used to determine an acceptable reliability level.

There have been many contributions to probabilistic slope stability analysis (Wu and Kraft, 1970; Yucemen, 1973; Barboteu, 1972; A-Grivas, 1976; Harr, 1977; Morla-Catalàn and Cornell, 1976; Matsuo, 1976; Alonso, 1976; Veneziano, et al. 1977; Vanmarcke, 1977a, 1977b, 1980; Sharp, et al., 1981; and Anderson, et al. 1981). Among these, Vanmarcke (1977b, 1979) proposed a probabilistic slope stability model that considers the spatial variation in shear strength over the surface of a cylindrical failure mass.

Anderson, et al. (1981) at Utah State University developed a methodology for probabilistic slope stability analysis and applied it to a tailings embankment dam. This work included:

- Extending Vanmarcke's (1977) conceptual probabilistic slope stability model to accommodate an effective stress analysis of zoned embankments.
- Developing and documenting an interactive computer model to perform the probabilistic slope stability analysis.
- Developing a methodology for conducting a field and laboratory investigation to statistically characterize the embankment properties using the cone penetrometer.
- Developing and documenting an interactive computer program to compute the necessary probabilistic parameters from the cone penetrometer data obtained in the field investigation.
- Applying the methodology to a tailings embankment dam.

As part of the Utah State project, an evaluation of the probabilistic slope stability methodology was made by an engineering consulting firm and their findings are reported in Volume II of the final project report (Anderson, et al., 1981), and are summarized in this report.

2.2 Project Authorization

This report was prepared as part of a Survey of Probabilistic Methods in Soil and Rock Mechanics for the Waterways Experiment Station, U.S. Army Corps of Engineers, Vicksburg, Mississippi. The work of report preparation was authorized by Contract Purchase Order DACW39-82-M-4280 dated August 30, 1982.

2.3 Outline of Report

This report is divided into eight sections and an executive summary. Section 3 presents various kinds of uncertainties in slope stability analysis and methods for handling these in the probabilistic slope stability methodology. A description of the model for performing probabilistic slope stability analysis is presented in Section 4 and the field program to develop the necessary probabilistic parameters is described in Section 5. A case study which utilized the methodology is reviewed in Section 6. Section 7 contains evaluations of the methodology by an independent consultant and by the Utah State University development team. Section 8 outlines additional case studies and development work needed to generalize the applicability of the methodology. Finally, the relationship of the methodology to an integrated risk assessment framework which considers all likely causes of slope failure is discussed in Section 9.

3. UNCERTAINTIES IN SLOPE STABILITY ANALYSIS

3.1 General

Several sources of uncertainty are associated with assessing slope stability. These uncertainties include:

- Approximations in describing the geometry of the embankment.
- Errors in estimating pore pressures.
- Spatial variability in shear strength, and measurement and sampling errors in field measurements of shear strength.
- Inaccuracies in the mechanics of the deterministic slope stability model (model error).

Methods for handling each source of uncertainty in probabilistic slope stability analysis are presented in the following sections.

3.2 Embankment Geometry

The geometry of the embankment and the soil density are treated deterministically in the methodology presented by Anderson, et al. (1981). Alonso (1976) shows that probabilistic consideration of the density and geometry do not greatly influence embankment reliability because they occur in both the resisting moment and driving moment and their effects tend to cancel.

3.3 Pore Pressure

Uncertainty in the distribution of pore pressures can result from spatial variability and uncertainty in the permeability of the embankment soil, fluctuation in the phreatic surface due to variations in the reservoir level or variations in drawdown rates. At this time an efficient method to probabilistically characterize the spatial variability of pore pressure has not been developed. In research at Utah State University, Bergado (1982)

investigated pore pressure as a random variable for probabilistic slope stability analysis during steady state seepage. Pore pressure uncertainty was attributed to the spatial variability of permeability. A Monte Carlo technique was required to assess the probability of failure. This type of solution is generally expensive and not practical for routine applications.

Anderson, et al. (1981) treat pore pressure as a deterministic quantity. By computing the probability of failure for various positions of the piezometric surface, a critical location can be defined as the position of the piezometric surface that results in an unacceptable probability of failure. Pore pressures in the structure can then be monitored to determine the position of phreatic surface and compared with the pore pressures that would cause an unacceptable probability of failure. If a critical condition is approached, appropriate remedial action can be taken.

3.4 Spatial Variability of Soil Parameters

Vanmarcke (1977a) suggests three major sources of uncertainty in soil profile modeling for the purpose of describing spatial variation of soil parameters:

- natural heterogeneity
- limited information about subsurface conditions
- measurement errors

Natural heterogeneity refers to the actual spatial variation of the shear strength of the material and must be estimated to properly evaluate the probability of a slope failure. For constructed slopes, natural heterogeneity will be modified by construction methods. The accuracy of the spatial variation estimate depends on the extent of the subsurface investigation and the accuracy of the measurements (the second and third error sources listed above). Judgment must be exercised in planning the subsurface investigation in order to tradeoff between the number and location of soundings and the value of

obtaining the information. The scope of the required subsurface investigation for evaluating the spatial variation of shear strength is discussed in Section 5.0 of this report.

Even when using the best available techniques to sample and measure the soil parameters, measurement errors will be present and these could include a measurement bias. If an estimate of the bias can be made, the mean values of the soil parameters should be adjusted accordingly. When using an indirect method such as a cone penetrometer to evaluate shear strength, the uncertainty involved in making the conversion from the penetration resistance to shear strength will introduce an additional measurement error.

3.5 Model Error

Model error depends on the method of deterministic slope stability analysis and the assumptions that must be made to make the analysis statically determinant. Whitman and Bailey (1967) suggest that the plane strain safety factor computed by Bishop's simplified method may be in error by as much as 5 percent. It is generally accepted that all slope stability analysis methods make conservative assumptions. Thus the actual safety factor is greater than the analysis indicates. One of the difficulties in error analysis is in separating this bias from random error. The magnitude of the bias varies for each individual case, depending on the particular slope geometry, failure surface, soil conditions and pore pressure conditions. Thus this bias may be considered to be a random variable which can be described by a probability density function having positive skew, such as the beta distribution. Cornell (1971) has suggested that the variance of the safety factor can be written as a combination of the variance due to model error and the variance due to spatial variability of the resisting moment as follows:

$$\tilde{F}^2 = (V_F \bar{F}_e)^2 + \tilde{F}_s^2 \quad \ldots\ldots\ldots\ldots\ldots \quad (1)$$

in which

V_F = the coefficient of variation of the plane strain safety factor, $\bar{F}_e$ due to model error
$\tilde{F}_s^2$ = the variance of safety factor which includes the spatial variability of shear strength
$\tilde{F}^2$ = the total variance of the safety factor

4. PROBABILISTIC SLOPE STABILITY MODEL

4.1 General

The description of the probabilistic slope stability model begins with a presentation of the methods for calculating the mean and standard deviation of the safety factor. Following subsections discuss the representation of the spatial variation of shear strength by variance reduction and autocorrelation functions. The description concludes with the method for calculating the probability of failure and the influence of the width of the failure zone on that probability.

4.2 Mean of the Safety Factor

The probabilistic slope stability model presented by Vanmarke (1977b) and Anderson, et al. (1981), and briefly presented herein, considers a cylindrical failure surface as shown on Fig. 1. Based on the method of slices, the mean safety factor for the failure mass shown in Fig. 1 can be stated as

$$\bar{F}_b = \frac{\bar{M}_{r,b}}{M_{o,b}} = \frac{b\, r\, \Sigma\, (\bar{s}_i\, \Delta\ell_i) + R_e}{b\, \Sigma\, W_i a_i} \quad \ldots\ldots\ldots\ldots \quad (2)$$

in which

$\bar{M}_{r,b}$ = mean resisting moment
$M_{o,b}$ = overturning moment
b = length of failure mass
r = radius of cylindrical surface
R_e = resisting moment at ends of cylindrical mass
$\Delta\ell_i$ = base length of the i^{th} slice
$\bar{s}_i$ = mean shear strength of the soil at the base of the i^{th} slice
W_i = weight per unit wideth of the ith slice
a_i = perpendicular distance from the line of action of the W_i to the center of the failure arc

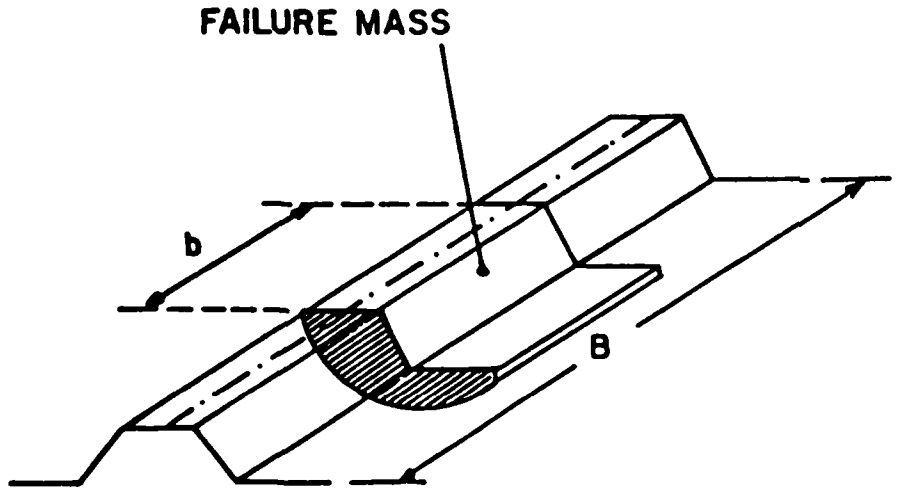

FIGURE 1a

Typical Cylindrical Failure Mass of an Earth Embankment (after Vanmarcke 1977b)

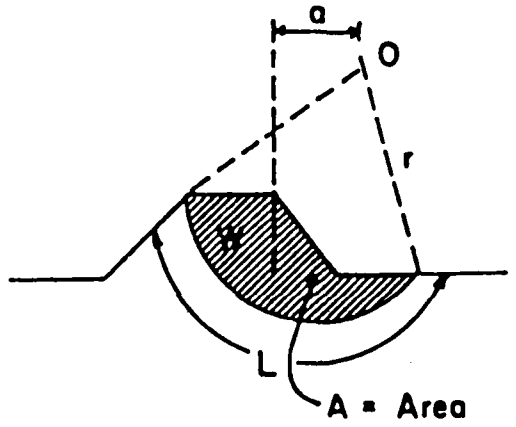

FIGURE 1b

Typical Cross-Section of Failure Mass (after Vanmarcke 1977b)

The mean shear strength at the base of each slice, as shown in Fig. 2, can be expressed in terms of the Mohr-Coulomb strength theory as

$$\bar{s}_i = \bar{c}_i + \sigma_i \overline{\tan \phi}_i \quad \ldots\ldots\ldots\ldots\ldots \quad (3)$$

in which

$\bar{c}_i$ = mean cohesion for the soil at the base of the i^{th} scale
σ_i = normal stress on the failure plane at the base of the i^{th} slice
$\overline{\tan\phi}_i$ = average coefficient of friction for the soil at the base of the i^{th} slice

The method of slices can be carried out either as an effective stress analysis or as a total stress analysis. Since pore pressures are treated deterministically in this model, the development will be in terms of total stress in the interests of simplicity.

For convenience define an average shear strength for each soil type along the failure plane as

$$\bar{s}_{bj} = \frac{\{\Sigma(s_i \, \Delta\ell_i)\}_j}{\{\Sigma \, \Delta\ell_i\}_j} = \frac{\{\Sigma(s_i \, \Delta\ell_i)\}_j}{L_j} \quad \ldots\ldots\ldots \quad (4)$$

in which

$\bar{s}_{bj}$ = mean shear strength of the j^{th} soil type averaged along the failure plane
L_j = length of the failure surface passing through the j^{th} soil type

Equation 2 can now be written as

$$\bar{F}_b = \frac{b \, r \, \Sigma \, \bar{s}_{bj} \, L_j + R_e}{b \, M_o} \quad \ldots\ldots\ldots\ldots \quad (5)$$

The average shear strength can also be expressed in terms of the Mohr-Coulomb strength theory as

$$\bar{s}_{bj} = \bar{c}_{bj} + (\sigma \overline{\tan \phi})_{bj} \quad \ldots\ldots\ldots\ldots \quad (6)$$

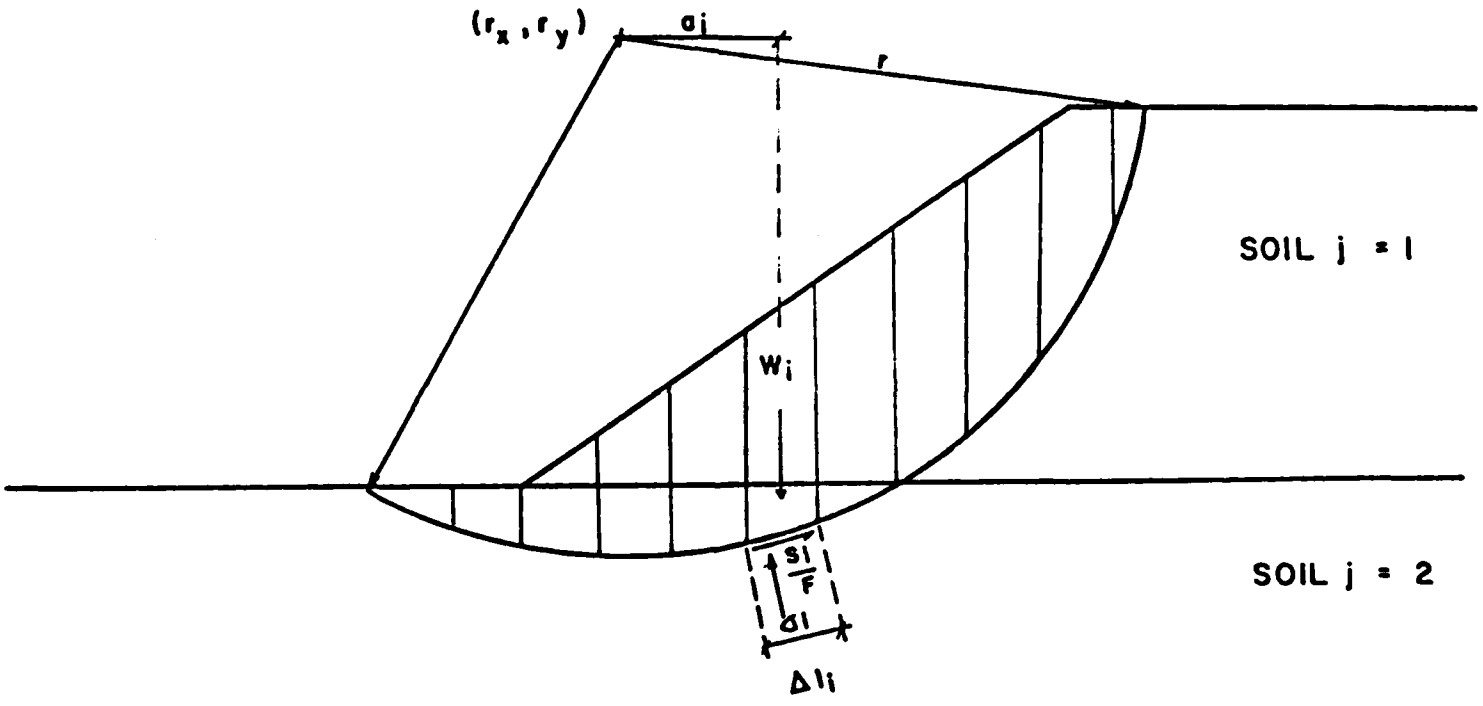

FIGURE 2

Slice Geometry in Method of Slices Analysis

in which

$\bar{c}_{bj}$ = mean cohesion of the j^{th} soil type averaged along the failure plane

$\overline{(\sigma \tan\phi)}_{bj}$ = mean frictional strength of the j^{th} soil type averaged along the failure plane

4.3 Standard Deviation of the Safety Factor

In calculating the standard deviation of the safety factor $\tilde{F}_b$ only the shear strength, with its components of cohesion and friction, is considered to be a random variable. The density, embankment geometry, and pore pressure are assumed to be deterministic. Furthermore, the variance of the resisting end moment, R_e, is neglected. Assuming the strength parameters of various soil types in an embankment to be statistically independent, the standard deviation of the safety factor can be expressed as

$$\tilde{F}_b = \frac{r \sqrt{\sum \tilde{s}_{bj}^{\,2} L_j^{\,2}}}{M_o} \quad \ldots\ldots\ldots\ldots\ldots (7)$$

An expression for the standard deviation of shear strength is dependent on whether or not the cohesion and friction strength components are statistically independent. Matsuo (1976) and Lumb (1974) have shown that the cohesion and friction components of shear strength have a slight negative correlation; that is there is a slight tendency to have smaller values of cohesion when the friction angle is larger. However, in this description it is conservatively assumed that the cohesion and friction are independent and therefore covariance terms can be omitted. Therefore, the standard deviation can be expressed as

$$\tilde{s}_{bj} = \{\tilde{c}_{bj}^{\,2} + (\sigma \widetilde{\tan} \phi)_{bj}^{2}\}^{1/2} \quad \ldots\ldots\ldots (8)$$

4.4 Spatial Variation of Shear Strength

Variations in strength occur naturally in a soil mass; however, the stability of an embankment dam is not affected by very small areas of weakness because these are compensated for by the strength of adjacent areas. Thus, local weaknesses tend to be "averaged out" when the strength of a larger area is considered, even though the point-to-point variation in the shear strength can be quite high. There may be several places in the soil mass where the strength is low or high but only for a short distance. If the average strength is calculated over an interval of length b which is moved along the axis of the embankment, this is referred to as the moving average of the point values of shear strength in soil j, s_j. The variance of this moving average is less than the variance of the point strength values. Consequently, the standard deviation of the averaged values, $\tilde{s}_{bj}$, is less than the standard deviation of the point values, $\tilde{s}_j$. As the averaging length Δb is increased, the standard deviation of the averaged shear strengths decreases. It is the value of the shear strength averaged over the failure surface and not the local weak or strong values which are important for determining the safety factor. It follows that it is the standard deviation associated with the average shear strength over the failure surface of length b and arc length L_j which is needed in Equation 6 and not the standard deviation of the point strength values.

Vanmarcke (1977b) showed that the standard deviation of shear strength, $\tilde{s}_{bj}$, averaged over the width of the failure mass b and arc length L_j is related to the point standard deviation, $\tilde{s}_j$, by variance reduction functions, as follows:

$$\tilde{s}_{bj} = \{\Gamma_{s,z}(b)\}_j \{\Gamma_{s,l}(L)\} \tilde{s}_j \quad \ldots\ldots\ldots\ldots (9)$$

in which

$\{\Gamma_{s,z}(b)\}_j$ = shear strength variance function along the embankment axis for the j^{th} soil type

$\{\Gamma_{s,l}(L)\}_j$ = shear strength variance function along the arc of the failure surface for the j^{th} soil type

For a soil with both cohesion and friction components, the variance and variance reduction functions must of course be stated in terms of cohesion and friction. The variance of the shear strength of the j^{th} soil can be expressed as follows:

$$\tilde{s}^2_{bj} = \{\Gamma_{c,z}(b)\}^2_j \{\Gamma_{c,\ell}(L)\}^2_j \tilde{c}^2_j + \{\Gamma_{\tan\phi,z}(b)\}^2_j \{\Gamma_{\tan\phi,\ell}(L)\}^2_j (\widetilde{\tan\phi})^2_j \quad . \quad . \quad . \quad (10)$$

Evaluation of the variance functions along the arc length is not convenient since spatial variance reduction functions are measured in terms of cartesian coordinates. This requires that the variance reduction functions in the x and y directions be tranformed to a reduction function along the failure arc. This transformation has been developed in Sharp, et al. (1981) and Anderson, et al. (1981).

As shown by Equation 10, an evaluation of the standard deviation of the safety factor (Equation 7) depends not only on the point standard deviation of the shear strength but also on the variance reduction functions for each component of shear strength.

4.5 Variance Reduction and Autocorrelation Functions

Equation 10 involves two variance reduction functions for each soil property. In this section only cohesion is considered, however, friction follows in the same manner and is developed in Anderson et al. (1981). These reduction functions are functions of the autocorrelation functions $\rho_x(\cdot)$, $\rho_y(\cdot)$ and $\rho_z(\cdot)$ and are derived in Anderson et al. (1981) as

$$\Gamma^2_{c,z}(b) = \frac{2}{b} \int_0^b \left(1 - \frac{z}{b}\right) \rho_z(z)dz \quad \ldots\ldots\ldots\ldots \quad (11)$$

and

$$\Gamma^2_{c,\ell}(L) = \frac{1}{(\theta_2 - \theta_1)^2} \int_{\theta_1}^{\theta_2} \int_{\theta_1}^{\theta_2} \rho_x(\Delta x)\rho_y(\Delta y)d\psi \; d\psi' \quad \ldots \quad (12)$$

in which

L = the failure arc length
$\Delta x = r|\cos\psi - \cos\psi'|$
$\Delta y = r|\sin\psi - \sin\psi'|$

It is seen that estimation of variance reductions requires estimation of the autocorrelation functions $\rho_x(\cdot)$, $\rho_y(\cdot)$ and $\rho_z(\cdot)$. The autocorrelation function in effect describes the rate of fluctuation of a spatially distributed random variable about its mean. If correlation remains high over a long distance, the rate of fluctuation is low and vice versa.

In the methodology presented by Anderson, et al. (1981), autocorrelation functions are used to describe variance reduction. The field methodology to estimate autocorrelation functions for soil materials is presented in Sectic : 5.

4.6 Description of Autocorrelation Functions

There are several ways in which the autocorrelation structure of the shear strength parameters may be described. Vanmarcke (1979) and Alonso and Krizek (1975) have suggested several functional forms for the autocorrelation structure. Autoregressive models may use a simple exponential decay function to describe the decrease in correlation with distance. The type of function and its coefficients are usually estimated from regression analysis curve fitting techniques. The autocorrelation function may also be a product of more than one random process and the resulting functional form may not

necessarily be a simple exponential decay. Thus, in order to accommodate any type of autocorrelation structure, an alternate way to describe the autocorrelation functions is to specify a series of sample estimates through confidence limits for autocorrelation values at various lag distances. This method can then be used to describe any type of function that may exist without the need for extensive effort in curve fitting. Additionally it allows a more versatile computer program which does not need extensive modification when the functional form of the fitted autocorrelogram is changed.

4.7 Probability of Failure

The probability of failure occurring along an assumed cylindrical failure surface such as that shown in Fig. 1 is defined as the probability of the safety factor being less than 1.0. The probability of the safety factor being less than 1.0 is graphically shown on Fig. 3 as the area under the probability density function of the safety factor where F_b is less than 1.0, written prob($F < 1.0$). This area can be computed from the mean and standard deviation of the safety factor for the assumed failure surface and for an assumed functional form of the probability density function. In the model, a Gaussian distribution is used for the safety factor and its use is justified by the Central Limit Theorem. The mean and standard deviation of the safety factor are calculated using Equations 4 and 6, respectively, which account for the spatial variability of shear strength and at this point do not take into account uncertainties from the other sources listed in Section 3.0.

In a probabilistic sense, the critical failure surface is defined as that surface with the largest value of prob($F < 1.0$) in contrast to the conventional analysis in which it is defined as the surface with the smallest safety factor. Because the spatial variation in shear strength is considered to be the critical failure surface based on a criterion of maximizing the

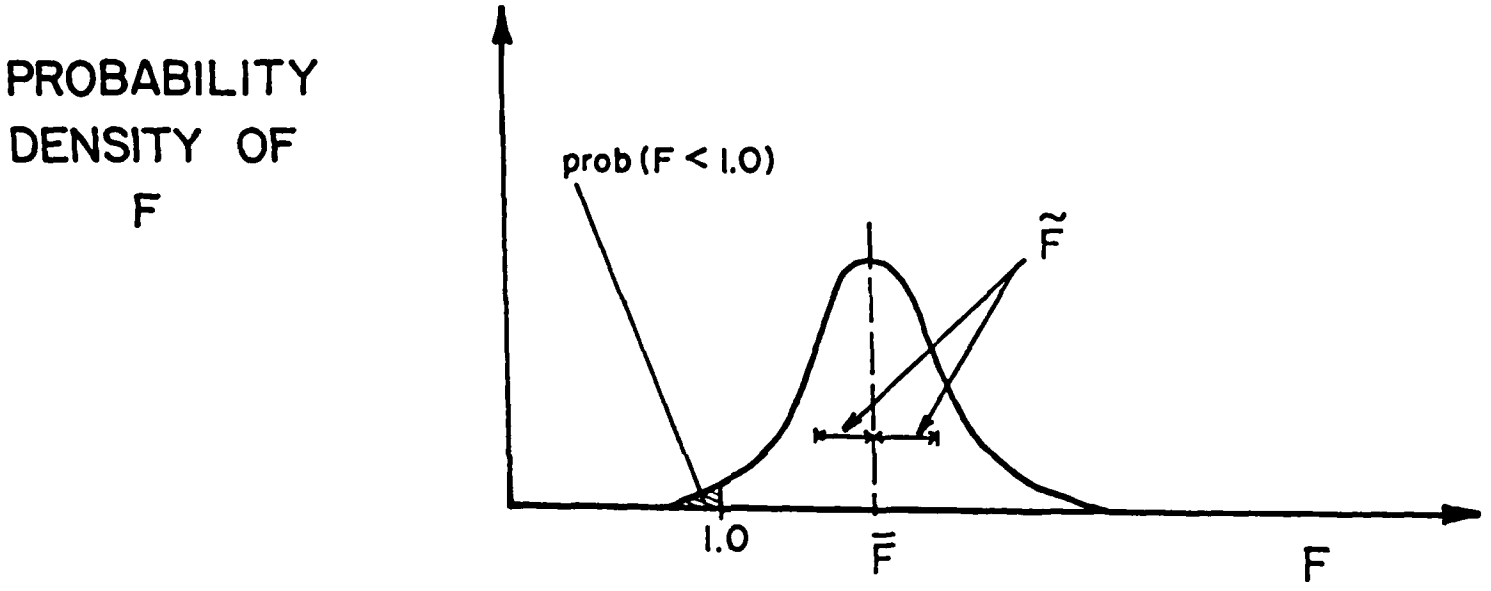

FIGURE 3
Probability Density of Safety Factor

probability of failure will not necessarily be the same surface as that based on minimizing the safety factor. The mean, point variance and variance reduction functions will all influence the location of the critical failure surface.

4.8 Failure Width

Unlike conventional slope stability analysis, the safety factor depends on the width, b, of the failure mass. Vanmarcke (1977b) shows that there is a critical width, b_c, and that it is a function of the end resistance, R_e, the mean resisting moment, $\bar{M}_r$, and the driving moment, M_o.

$$b_c = \frac{R_e}{M_r - M_o} \quad \ldots\ldots\ldots\ldots\ldots\ldots \quad (13)$$

This value, b_c, should be used to evaluate the mean and standard deviation of the safety factor, $\bar{F}_b$ and $\tilde{F}_b$. It is interesting to note that the critical width, b_c, is not a function of the variance properties.

For an embankment with an overall width, B, less than the critical width, b_c, the probability failure mass includes the entire embankment. However, when the overall embankment width exceeds the critical width, there are many possible locations of the critical width along the embankment. The probability of failure of the embankment increases as the total embankment width increases.

The documentation of an interactive slope stability computer model based on this theory is presented by Anderson, et al. (1981c).

5. FIELD PROGRAM TO DEVELOP PROBABILISTIC PARAMETERS

5.1 General

Performing a probabilistic slope stability analysis requires sufficient data to statistically characterize the soil properties for each soil zone within the embankment. The probabilistic soil properties include the mean and variance of the shear strength parameters, c and tan ϕ, and the autocorrelation function for each strength parameter in each coordinate direction. Conventional methods of performing subsurface investigations (drilling and sampling for laboratory testing) are not practical to economically develop the required probabilistic parameters. The electric cone penetrometer was used by the Utah State University team and appears to be an excellent way to develop the necessary data.

The electric cone penetrometer indirectly provides strength data at 0.125 foot depth intervals, and under ideal conditions up to 600 to 800 feet of soundings can be obtained per day in tailings material. The data are recorded on a strip chart recorder and can be simultaneously stored on a magnetic computer tape. By properly spacing the penetrometer soundings, the required parameters for a probabilistic slope stability analysis can be obtained. Since the cone penetrometer does not retrieve a sample, it is generally necessary to make several conventional soil borings to obtain samples for classifying the soil and for performing shear tests that can be used to calibrate the cone penetrometer.

This section discusses the use of the cone penetrometer to measure shear strength and also outlines the field investigation that is required to develop mean, variance and autocorrelation functions of the shear strength parameters.

5.2 Conversion of Cone Bearing to Strength

In order to perform the required statistical data analysis, cone penetrometer data must be converted to the appropriate strength parameters. Schmertmann (1977), Mitchell and Lunne (1977), Harr (1977), Dunn, et al. (1980) and Jones and Van Zyl (1981) discuss the conversion of cone penetrometer data to strength parameters. There are some questions in interpreting the cone penetration data because of uncertainty in the failure mechanism and the zone of influence of the cone as it advances through the stratified tailings deposits, and because of the influence of the water table on the response of the cone. Furthermore, there is some uncertainty in converting cone bearing resistance to strength parameters even when laboratory data are available for correlating cone bearing resistance and strength parameters. These uncertainties should be included in the probabilistic analysis. The methodology developed by Anderson, et al. (1981) accounts for these uncertainties in estimating the probabilistic parameters. The tailings embankment studied by Anderson, et al. (1981) was cohesionless and the cone bearing conversion considered only the frictional component (tan ϕ).

5.3 Mean and Point Variance

The estimates of the mean and variance of shear strength, $\hat{\bar{s}}$ and $\hat{\tilde{s}}^2$, must be representative of the soil type throughout the entire embankment. Thus, portions of the digitized records of representative penetrometer soundings should be pooled to compute a representative mean and variance. Portions of the records that are pooled must be from the same identifiable soil type and, in order to avoid unrepresentative results, soundings should not be concentrated in a small area of the embankment. Pooling can then be performed for each soil type identified in the embankment profile. Additionally, tests can

be performed on strength data obtained from each soil type to determine if each is statistically different in terms of mean and variance.

The documentation of a computer program for computing the mean and point variance of tan ϕ from cone penetrometer soundings is presented by Anderson, et al. (1981d).

5.4 Horizontal Autocorrelation

Horizontal autocorrelations may be estimated from the data derived by placing a series of soundings at constant spacing perpendicular to (x direction) and parallel with the embankment axis (z direction). The placement of the lines of soundings must be located such that the x and z autocorrelations can be determined for each soil type in the embankment section.

The x and z autocorrelograms can be computed by considering the values of shear strength along lines at constant elevation in the x and z directions, respectively. Estimates of autocorrelation functions can be improved by pooling autocorrelation estimates from successive elevations separated by a predetermined vertical distance. Documentation of a computer program for estimating horizontal autocorrelation functions from in situ strength measurements is presented by Anderson, et al. (1981d).

The layout of soundings for estimating horizontal autocorrelograms must be carefully selected. Since the autocorrelogram decays rapidly at short lag distances and more slowly with increasing lag distance, several different spacings should be used. Figure 4 shows a possible layout for developing a horizontal autocorrelogram. In Figure 4, the spacing between soundings was incremented by a factor of two for each overlapping set of soundings in order to make use of some soundings for computations at more than one lag distance. For instance, in the set of 7 soundings at 25 feet, 4 of the soundings can

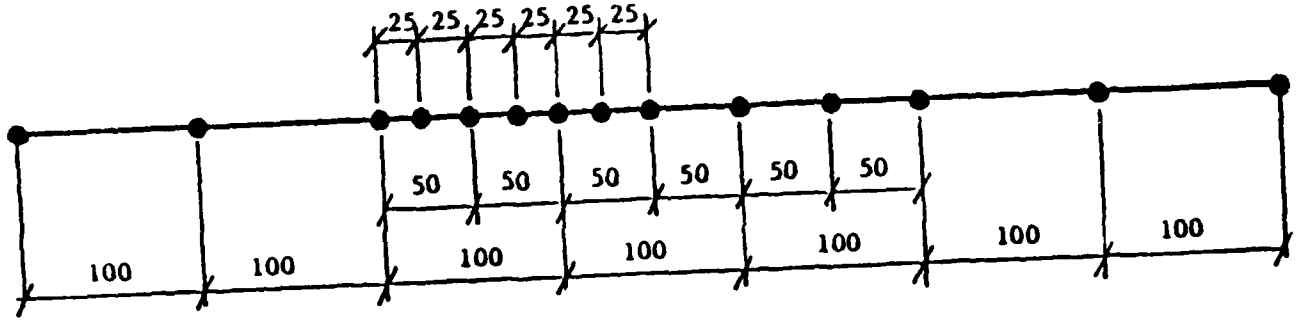

FIGURE 4

Example Cone Penetrometer Layout
for Determining Horizontal Autocorrelation

also be used at 50 feet and by placing 3 more soundings with a 50 foot spacing a set of 7 soundings at 50 foot spacing is obtained. Hence, starting out with a small spacing, doubling, and redoubling until a satisfactorily large spacing is obtained will increase the efficiency of the field program. It should be emphasized that the autocorrelation coefficients at both small and large lag distances are important, and thus a range of spacings is necessary to adequately estimate the entire autocorrelation function and optimize the field testing program.

Before using the autocorrelograms in the probabilistic slope stability analysis, they must be simplified by smoothing to account for estimation errors. The 95 percent confidence limits can be useful in simplifying the autocorrelogram obtained from field data. As mentioned previously, idealization of the autocorrelogram may be accomplished by specifying a series of best-fit linear segments through the autocorrelogram. These linear segments are selected to stay within the confidence limits. Figure 5 shows the results of horizontal autocorrelation analysis of a tailings dam including the 95 percent confidence limits in the z direction based on shear strengths obtained from cone penetrometer data. Figure 6 shows the smoothed autocorrelogram. The simplification is based on judgment and could vary depending on the individual involved. Although use of the piecewise linear functions has some theoretical limitations, exponential autocorrelograms do not closely represent the true autocorrelation either since it is the result of a composite random process. This is discussed further in a later section. At this time, it appears that piecewise linear autocorrelation functions provide an alternative method of modeling the spatial variability of the shear strength parameters for tailings dams.

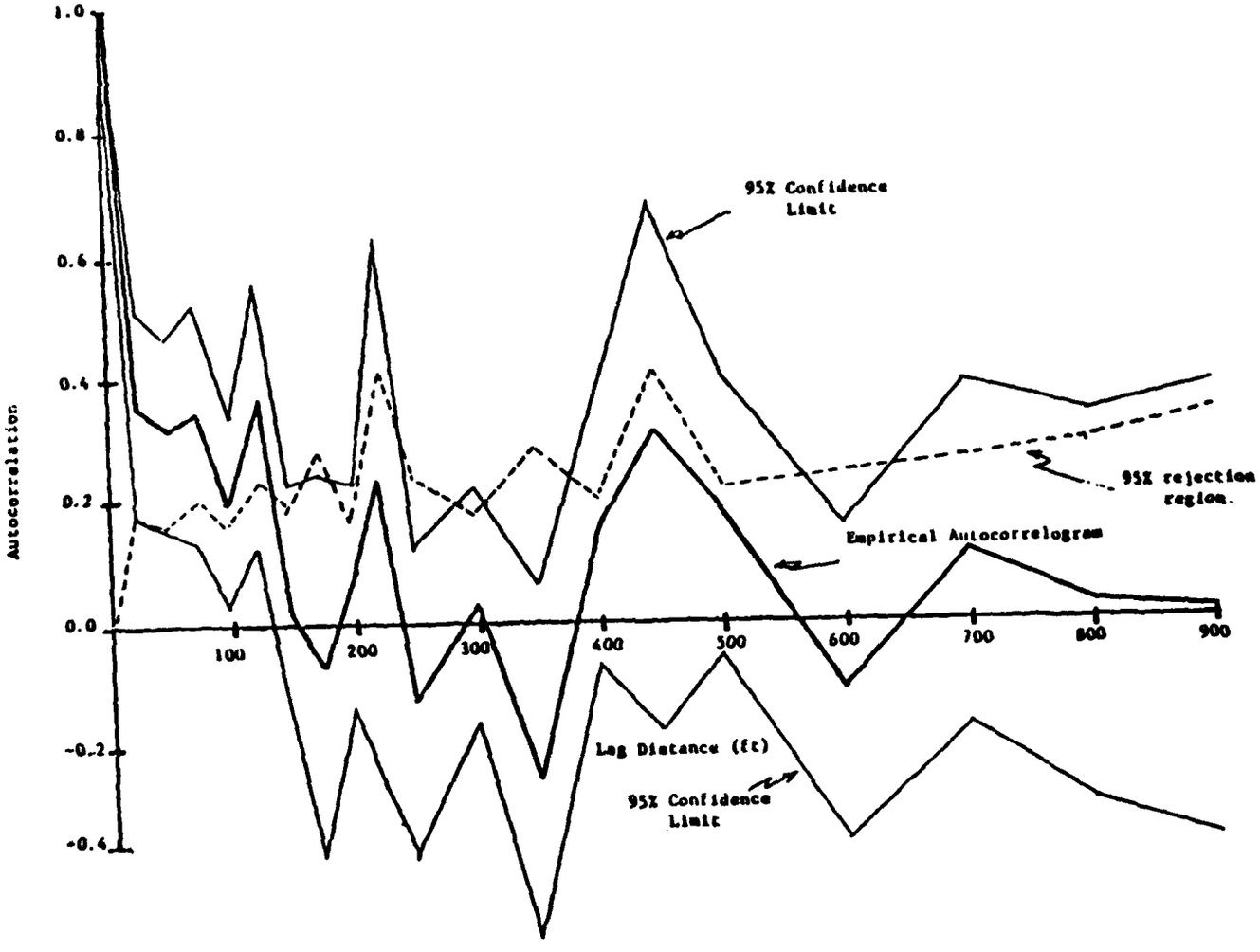

FIGURE 5

Horizontal Autocorrelogram Showing 95 Percent Confidence Intervals and 95 Percent Rejection Region

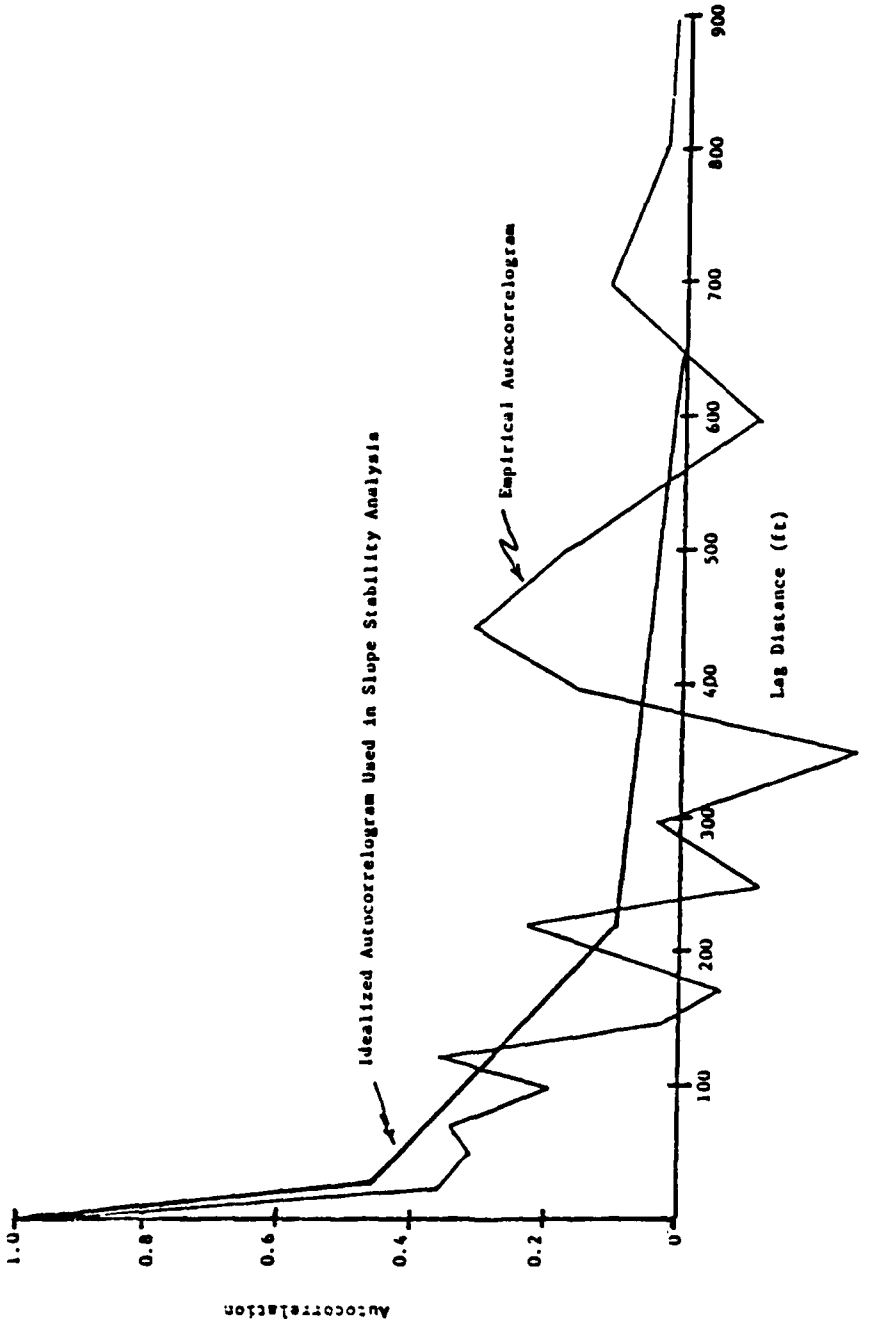

FIGURE 6
Idealization of Horizontal Autocorrelogram

5.5 Vertical Autocorrelation

Vertical autocorrelation is computed by considering the vertical series of point values of the shear strength. Pooling of vertical soundings can also be performed to improve the estimate and to get a vertical autocorrelation more representative of the entire embankment. Portions of the records that are used in pooling must be chosen so that they are representative of the soil type that is analyzed. When applied to the cone penetrometer, the top 5 to 10 feet should be avoided due to surface effects which make it unrepresentative. Additionally, the cone penetrometer record from the saturated material may not be representative of the in-situ shear strength because of excess pore pressure generation under constant cone penetration. Documentation of a computer program for computing vertical autocorrelations is also presented by Anderson et al. (1981d).

5.6 Trends

The analysis of the data should consider the effects of deterministic trends, such as an increase or decrease of the average value of tan ϕ with depth. If a deterministic trend is encountered in the data, de-trending should be performed before autocorrelation analysis is performed.

One difficulty that arises in ascertaining the presence of trends is that prolonged random fluctuations and deterministic trends may be difficult to distinguish, depending on the length of the record relative to the scale of a random fluctuation. Judgment must be exercised in analyzing the trends and in deciding whether to de-trend the data or not.

6. APPLICATION OF THE PROBABILISTIC SLOPE STABILITY MODEL

6.1 Description of Copper City Number 2 Tailings Dam

The probabilistic slope stability analysis presented in Anderson, et al. (1981) was conducted on Copper City No. 2 tailings embankment dam near Miami, Arizona. Due to the extreme topographic relief in the area of the tailings pond, the height of the embankment varies considerably. At the maximum section, the height of the embankment is approximately 330 feet. The embankment was constructed by the upstream method of construction. Tailings were transported to the pond through an 18 inch discharge pipe. The discharge pipe extended around the perimeter of the pond and spigots were spaced at 50 ft intervals. The discharge at any given time was limited to 500 foot segments along the perimeter. A typical section is shown in Figure 7.

6.2 Subsurface Investigation

The purpose of the subsurface investigation was to determine the embankment cross section and its associated soil properties. For use in the probabilistic slope stability model it was also necessary to describe the spatial variability of shear strength.

Five conventional soil borings to depths ranging from 50 to 214 feet and 77 cone penetrometer soundings to depths ranging from 40 to 221 feet were made at the locations shown on Figures 8 and 9.

The cone penetrometer soundings were made with an electric friction cone penetrometer. The penetrometer was advanced at a rate of 2 cm/sec. Continuous readings of the cone bearing resistance and friction resistance were recorded on a strip chart recorder. These data were later digitized at 0.125 foot intervals and stored on a magnetic tape.

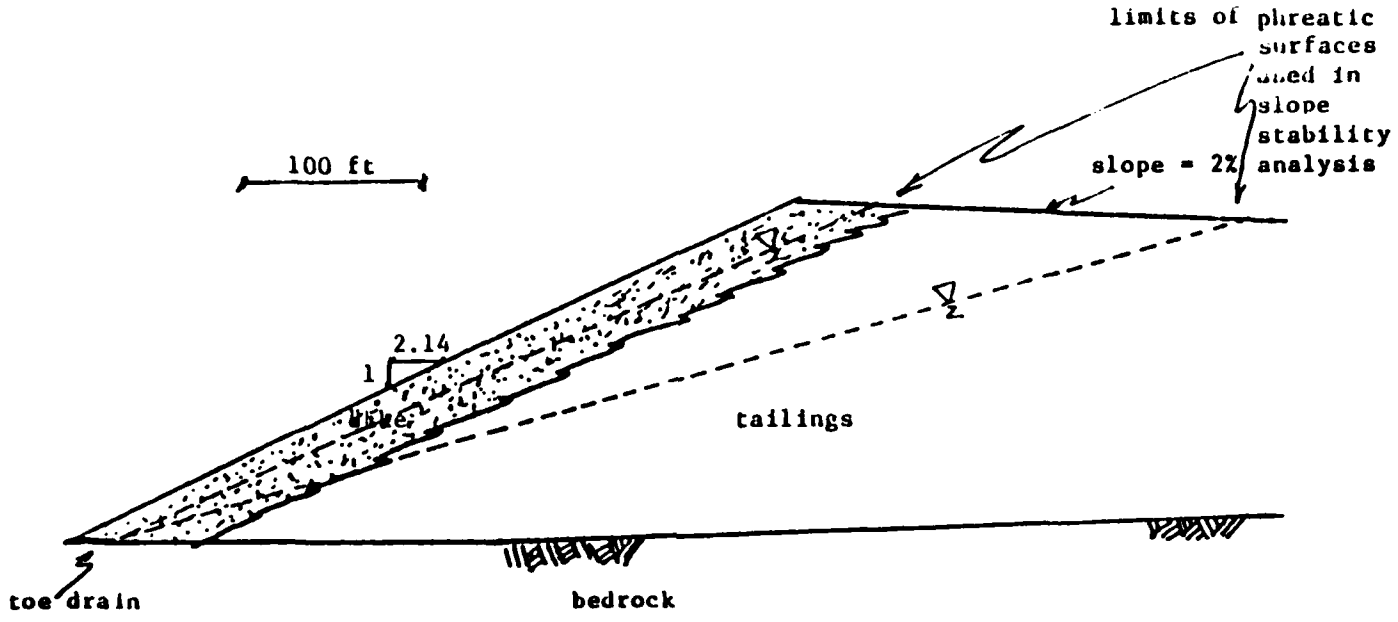

FIGURE 7

Typical Section Used in Stability Analysis, Copper City No. 2

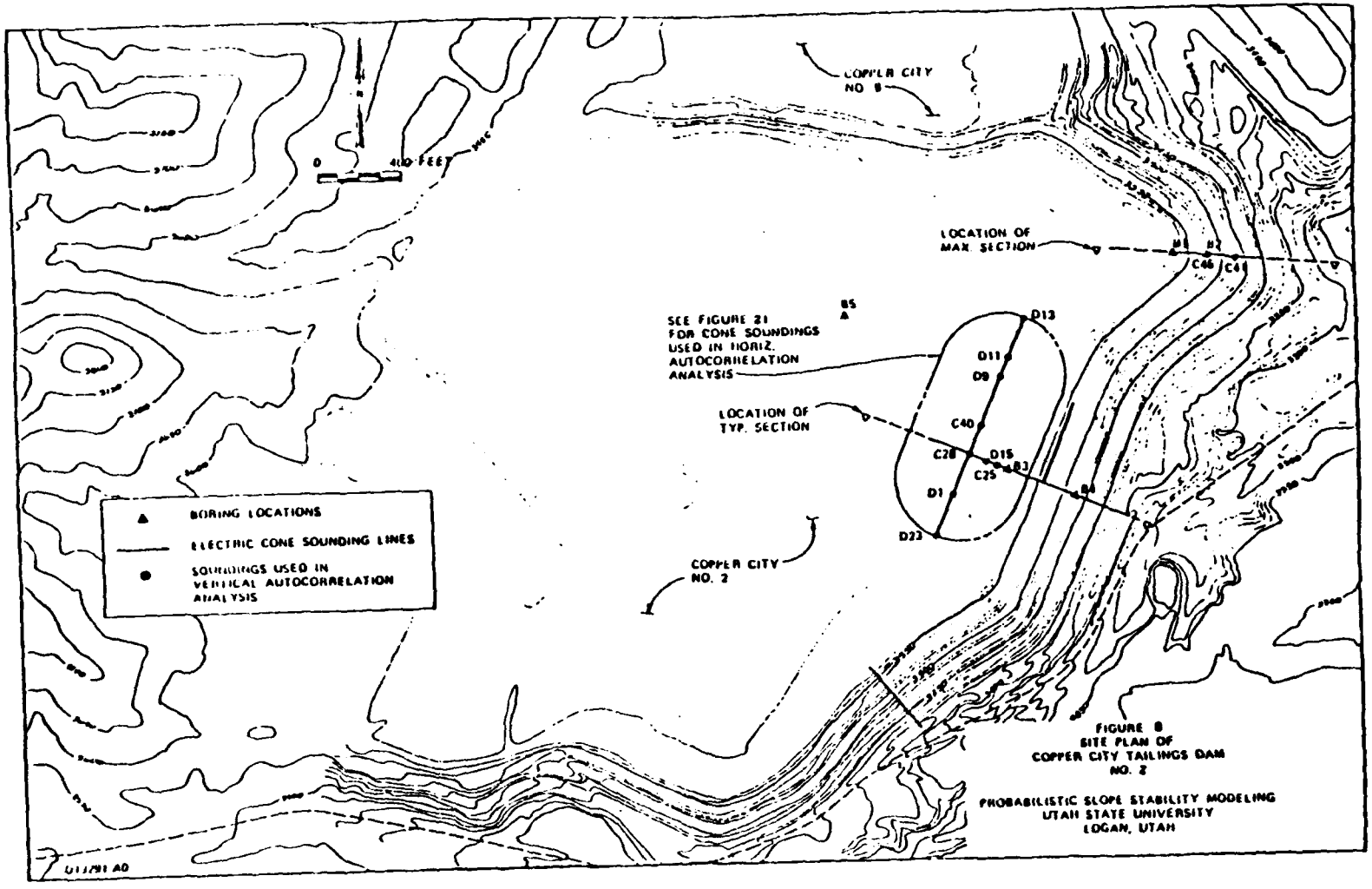

FIGURE 8

Site Plan of Copper City Tailings Dam No. 2

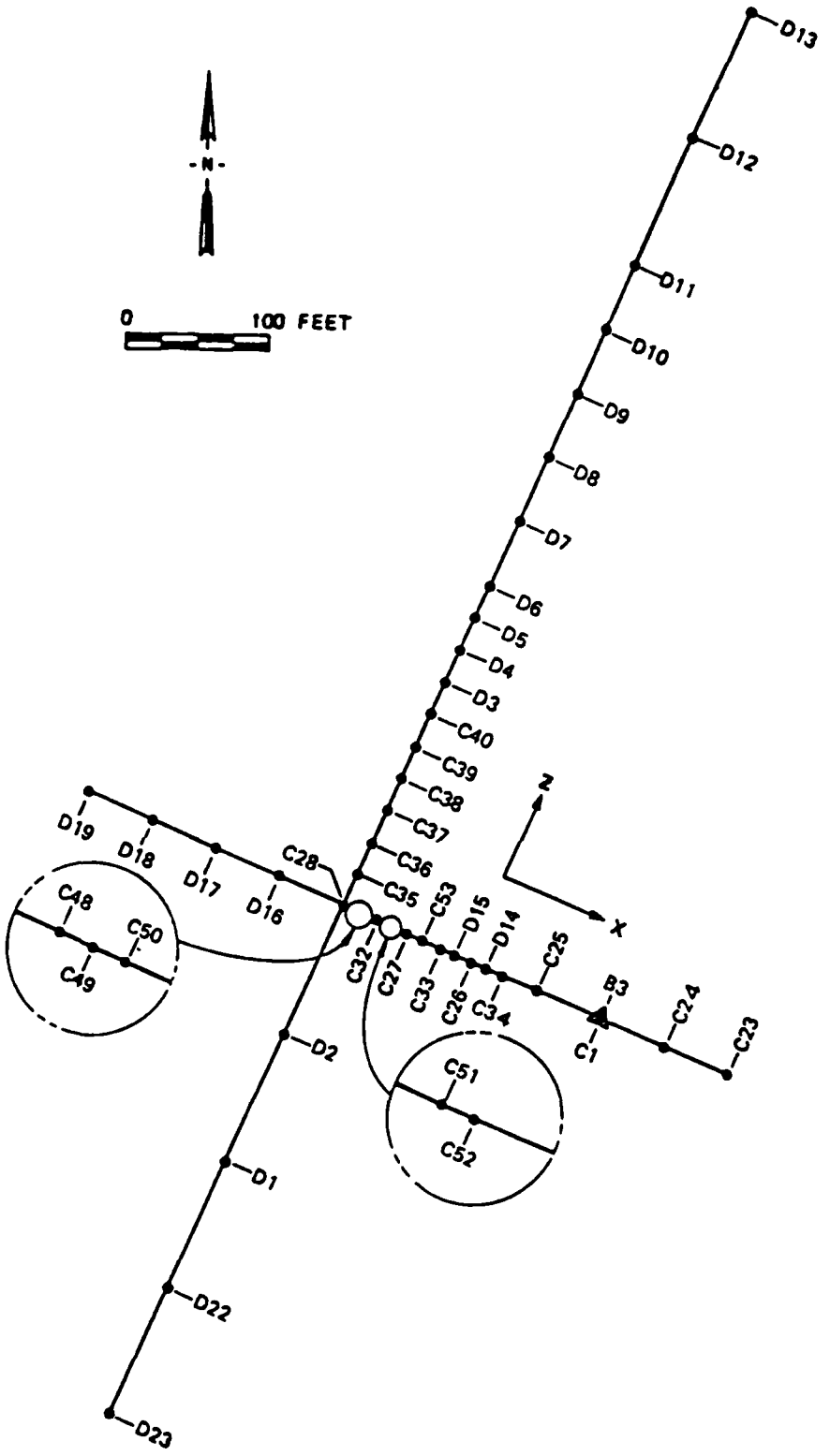

FIGURE 9

Cone Sounding Locations for
Horizontal Autocorrelation Analysis

The five soil borings and 15 of the cone penetrometer soundings were made to define the embankment cross section and to estimate the mean, point variance and the vertical autocorrelogram of shear strength. The remaining 62 cone penetrometer soundings were made to evaluate the horizontal autocorrelograms.

The soundings that were used to determine the autocorrelation relationships were located along the first bench and in the tailings pond area near to the dam crest. In order to obtain the autocorrelograms it was necessary to place the soundings at a constant spacing in the x and z directions. In each line, soundings placed at close spacings of 6.25 feet or 25 feet, were used to determine the initial decay of autocorrelation at short lags. Soundings were also spaced at large spacings of 50 or 100 feet, to determine the autocorrelation at intermediate to large lag distances.

In the x direction 22 soundings were made. Seven of the soundings were spaced at 6.25 feet, 11 at 12.5 feet, 7 at 25 feet and 11 at 50 feet. In the z direction, two lines of soundings were made. In the tailings pond area an additional 22 soundings were placed. The spacings were 11 at 25 feet, 11 at 50 feet and 12 at 100 feet. Along the first bench, 15 soundings were made with 13 spaced at 25 feet and 9 at 50 feet.

Grain size analysis tests were performed on all samples and direct shear tests were run on the Shelby tube samples. The tailings material was generally classified as a non-plastic silty fine sand. The percent passing the No. 200 sieve (0.075 mm) typically ranges from about 20 to 50 percent. The direct shear test results indicate that the material is in general cohesionless.

6.3 Analysis of Probabilistic Parameters

The cone penetrometer data were analyzed using three methods of cone bearing to friction angle conversion:

- Bearing Capacity Equation
- Schmertmann Equation
- USU Equation

The choice of method had a significant influence on the mean, variance and autocorrelation function of the strength parameter, tan ϕ. A comparison of the results from the three methods of cone bearing conversion indicates the need for using an accurate in situ procedure for evaluating shear strength. The USU Equation for converting cone bearing to tan ϕ was developed by regressing the results of direct shear tests on the cone penetration resistance. A standard error of conversion was evaluated and included in the probabilistic analysis. The strength values obtained from the USU equation were used in the probabilistic slope stability analysis. Special data pooling methods mentioned above and described in more detail by Anderson, et al. (1981) were developed and used to evaluate the mean, variance and autocorrelation functions for the embankment material.

6.4 Probability of Failure Analysis

The Copper City No. 2 tailings dam is currently inactive and the borings made to define the embankment section showed the phreatic surface to be at a great depth. If the tailings dam were reactivated, there would be a significant rise in the phreatic surface and much of the presently unsaturated tailings material would become saturated. The probabilistic analysis was, therefore, performed for seven different positions of the phreatic surface to develop a relationship between position of the phreatic surface and the

probability of failure. This allows identification of the position of the phreatic surface that would lead to an unacceptable probability of failure. A field program could then be set up to monitor the position of the phreatic surface if the dam were reactivated. The strength characteristics of the material were evaluated using the USU equation for cone bearing to friction angle conversion. It was assumed that the end bearing values of the penetrometer record were independent of the degree of saturation of the soil. Earthquake forces and the possibility of liquefaction of the tailings material were not considered.

The slope stability analysis was performed using a standard error of cone bearing to friction angle conversion of 2.1° on the shear strength variance, and a model error of 5 percent. The standard error of conversion was determined from the laboratory data that was used in developing the USU equation for converting cone bearing to friction angle under saturated conditions. The model error, 5 percent, was chosen based on work by Whitman and Bailey (1967). Although there are reports of the typical error in the slope stability methods, no precedent has been established for the appropriate model error to be used. Cornell (1971) uses magnitudes of model error ranging from 0.1 to 0.2 for illustrative purposes.

Table 1 shows the values of the mean, variance and autocorrelation estimates of tan ϕ that were used in the analysis. The autocorrelation function for the dike material in the x-direction was assumed to be the same as the tailings autocorrelation in the x direction.

Stability analyses were performed for various estimating positions of the phreatic surface. It was assumed that seepage control was provided by a 25 foot drain at the toe of the dam. Although the phreatic surfaces are known to be curved surfaces, they were assumed to be linear from the toe drain to the

TABLE 1

Probabilistic Parameters Used in Stability Analysis

Dike						Tailings					
x		y		z		x		y		z	
ρ	Lag (ft)	ρ	Lag (ft)	ρ	Lag (ft)	ρ	Lag (ft)	ρ	Lag (ft)	ρ	Lag (ft)
1	0	1	0	1	0	1	0	1	0	1	0
0.55	6	0.95	0.125	0.29	25	0.55	6	0.915	0.125	0.46	25
0.28	100	0.32	1.0	0	300	0.28	100	0.774	0.25	0.09	220
0.05	275	0.16	1.5	0	400	0.05	275	0.545	0.5	0	650
0	400	0.123	2			0	400	0.358	1	0	850
0	450	0.11	3			0	450	0.23	3.4		
		0	3.6					0.205	8		
		0	5.0					0.17	30		
								0	136		
								0	140		
$\bar{\phi} = 35.28°$						$\bar{\phi} = 33.60°$					
$(\widetilde{\tan \phi})^2 = 0.004863$						$(\widetilde{\tan \phi})^2 = 0.002921$					
$\gamma = 117$ pcf						$\gamma = 110$ pcf					

top of the dam merely to illustrate the effect of position of a phreatic surface on the probability of failure. The phreatic conditions were thus indicated by the distance from the dam crest to the ponded water.

For each phreatic condition, the critical surface was determined by the maximum probability of failure. Table 2 shows the results of the probabilistic analysis as a function of distance from the water surface to the dam crest. With the water surface at 100 feet from the crest, the probability of failure is 8.4×10^{-6}. The plane strain safety factor for this condition was 1.18, $\bar{F}_b$ for the critical failure width was 1.37, and $\tilde{F}_b$ was 0.0714. For this case, the plane strain safety factor was less than the typically accepted design value, yet the probability of failure was 8.4×10^{-6}.

In general, the computed failure probabilities were lower than expected and were significantly influenced by the model error. For this case study, the spatial variability of shear strength had a minor influence on probability of failure because the effects of variance reduction were large.

TABLE 2

Summary of Results, Copper City No. 2,
Data by USU Equation, 5 Percent Model Error

Distance of Water Surface From Crest (ft)	Probability of Failure
50	1.1×10^{-1}
60	1.8×10^{-2}
75	1.3×10^{-3}
100	8.4×10^{-6}
150	4.3×10^{-10}
200	3.2×10^{-13}
250	1.1×10^{-15}

7. EVALUATION OF PRESENT METHODOLOGY

7.1 General

The methodology for probabilistic slope stability analysis that was developed at Utah State University is more than a mathematical model. In addition to the theoretical model, computer programs for probabilistic slope stability analysis and statistical data analysis were developed, and a field investigation methodology for establishing the required probabilistic parameters were also developed. This evaluation is divided into two parts: an independent evaluation by a firm of consulting engineers, and a technical evaluation by the Utah State University development team.

7.2 Consultant's Evaluation

CH_2M Hill Consulting Engineers applied the methodology to the analysis of an existing tailings embankment dam as a means of testing the method. The practicing engineers who used the model had no previous training in probabilistic methods other than that obtained in a Master's-level graduate geotechnical engineering program. Approximately three days of instruction on the use of the model was given to these engineers by the model development team from Utah State University. The results of the consultant's study are presented as Volume II of Anderson, et al. (1981b). The conclusions reached by the consultants are reproduced below:

> The probabilistic slope stability model developed by Utah State University has been evaluated by CH_2M Hill regarding its present and potential application ability for design of tailings embankments by the engineering profession. Based on the foregoing analysis and redesign of Copper City No. 2 tailings dam using the model, we find the model to be a significant contribution to the engineering profession.

At this stage in model development, the ambiguities in the calculated probabilities of failure preclude their use for risk type analysis, or their use by people unfamiliar with slope stability analysis. However, the model provides insights into the influence of end effects, the effect of spatial variability on reducing variance, and the general probability of failure versus factor of safety relationship. These findings alone may warrant further research aimed at refining our understanding of conventional slope stability methods.

The present limitations to use of the model as a design tool are primarily due to lack of model refinement, lack of precedence and lack of knowledge. As with any unproven technique, the real applicability of the probabilistic slope stability model cannot be determined until it has been used systematically on a variety of embankments. Based on our limited application of the model to Copper City No. 2, we feel it holds possible promise as a design tool, and definite promise as a research tool for better understanding and use of conventional slope stability analysis and design methods.

7.3 Technical Evaluation

7.3.1 *Variance Reduction*

The probabilistic slope stability methodology appears to be straightforward and relatively easy for practicing engineers to understand and apply. There are still, however, some technical questions about the model that remain to be answered.

An important feature of the model is the inclusion of variance reduction in describing the spatial variability of the strength parameters. Although there is no question that variance reduction should be included, there is still some uncertainty as to how it should be computed. The model by Anderson et al. (1981) uses piecewise linear autocorrelation functions to evaluate the variance reduction functions. The autocorrelation functions are evaluated in the three coordinate directions and then transformed to be applied over the failure surface. The transformation assumes that autocorrelation functions over a surface area can be factored into their spatial components. This

assumption of spatial factorization is only valid when the autocorrelation functions are of the form given by Equations 14.

$$\rho_x(\Delta x) = \exp\{-(\frac{\Delta x}{k_x})^2\}$$

$$\rho_y(\Delta y) = \exp\{-(\frac{\Delta y}{k_y})^2\} \qquad \ldots\ldots\ldots \quad (14)$$

$$\rho_z(\Delta z) = \exp\{-(\frac{\Delta z}{k_z})^2\}$$

Previous studies have shown the particular function given by Equations 14 to be common for describing the autocorrelation properties of some geotechnical parameters. The values of k_x, k_y, and k_z determine the rate of decay of autocorrelation in each direction and must be determined for each soil type through field programs and data analysis techniques. Furthermore, the assumption of spatial factorability of the autocorrelation functions is valid when the functions are of the form given in Equations 14. The field investigation by Anderson, et al. (1981) showed that Equations 14 did not adequately describe the autocorrelation functions for tan ϕ. A better description used piecewise linear functions obtained by fitting data points to obtain an empirical autocorrelogram. Although the spatial factorization assumption is not valid, when the empirical autocorrelograms are used, the piecewise autocorrelogram appears to provide a more realistic description of the natural spatial variability than the functional forms of Equations 14.

Agterberg (1970) discusses the use of the exponential autocorrelation function in geology and resulting relationships in two and three dimensional random fields. In an isotropic random field having autocorrelation described by Equations 14, contours of equal autocorrelation in an x-y plane are

concentric circles. For the anisotropic case, the contours are ellipses. In a three dimensional field, equal autocorrelation contours are spheres and ellipsoids for the isotropic and anisotropic cases, respectively. However, when the autocorrelation functions are modeled by piecewise linear segments, the resulting contours of equal autocorrelation begin to deviate considerably from the spherical or ellipsoidal shape. The deviation is most severe in the autocorrelation range of 0.5 to 0.1 as reported by Sharp (1982). This effect is not conservative because of the assumption that the spherical/ellipsoidal contours are valid for piecewise linear segmented autocorrelograms and because the directional autocorrelation value is actually underestimated.

Additional field data are required to derive autocorrelation functions in any direction based on the piecewise autocorrelation functions obtained in the three coordinate directions. Once a method of obtaining "directional" autocorrelation functions has been obtained, the model can easily be modified. This information could be obtained from additional case studies.

7.3.2 Evaluation of Strength Parameters

Developing autocorrelation functions requires the evaluation of shear strength at many points in the three coordinate directions. At Copper City #2 tailings dam, Anderson et al. (1981) used an electric cone penetrometer to evaluate shear strength. Conventional soil borings and laboratory direct shear tests were used to correlate the cone penetrometer data with friction angle. A total of 77 cone penetrometer soundings and five soil borings were made to determine all of the statistical strength parameters.

Based on the case study at the Copper City #2 tailings dam, it is clear that the number of sampling points required to statistically evaluate strength parameters precludes the use of conventional soil borings to obtain samples

for laboratory testing as the primary method of obtaining strength data. The electric cone penetrometer appears to have the most promise for obtaining the required data. Data can be obtained rapidly and a nearly continuous record (0.125 ft intervals) of the soil profile can be obtained.

The major problem with using the cone penetrometer is that it does not measure shear strength directly. A conversion from penetration resistance to shear strength is required. There are several methods to convert penetration resistance to shear strength, but they produce different results. This leads to further uncertainty in slope stability evaluation. As mentioned earlier, Anderson et al. (1981) can account for measurement uncertainty in their methodology provided that the uncertainty can be quantified.

Therefore, it appears that additional work to improve in situ measurement of shear strength techniques, particularly with the cone penetrometer, will improve probabilistic assessment of slope stability.

7.3.3 Probabilistic Slope Stability Analysis as a Design Tool

To date, probabilistic slope stability analysis has been applied to existing embankments. In this mode, the probabilistic parameters must be evaluated from field and laboratory testing. When using probabilistic slope stability analysis as a design tool, the spatial variability of strength parameters of the in-place embankment material cannot be measured. Therefore, it will be necessary to establish standard autocorrelation functions and suggested values for variances of strength parameters that can be used for design purposes. Mean values of shear strength could be determined from conventional laboratory testing methods. These standard autocorrelation curves and variance values would need to be established for a variety of materials and construction techniques.

When using probabilistic slope stability analysis in a design mode, an important "follow up" activity is a good quality control program. The purpose of a quality control program is to assure that the design, including the design values of strength parameters that were used for analysis, is achieved during construction. A conventional quality control program for embankment construction involves, among other things, measuring the dry density and moisture content of the compacted embankment material. Certain density and moisture content requirements must be met to assure that the design strength parameters are achieved. Probabilistic slope stability analysis requires not only a design value for shear strength but a characterization of the spatial variability of shear strength. The quality control program during construction must, therefore, evaluate mean and variance of shear strength and the autocorrelation functions for each material. This can be done by making in-place density measurements during construction at specific locations along lines in the x and z directions. The autocorrelation functions in the y (vertical) direction can be established from measurements taken along vertical lines as construction proceeds. Assessment of the probability of slope failure can thereby be updated during the construction phase.

8. ADDITIONAL CASE STUDIES AND DEVELOPMENT WORK

8.1 Objectives

The current status of the probabilistic slope stability analysis methodology is that it is a working procedure which has already been applied to the evaluation of an existing tailings dam. The methodology is fully documented in terms of its theory, capabilities, and the completed case study. In addition, the methodology has been presented at training sessions to practicing geotechnical engineers from the U.S. Bureau of Mines, U.S. Bureau of Reclamation, and a consulting engineering firm. Several limitations of the methodology were described in Section 6.0. In particular there is a need for additional case studies so that guidelines for the application of the methodology can be generalized to the design of new slopes in addition to the evaluation of existing slopes.

Four specific objectives for future work have been identified, as follows:

- To expand the range of experience in application of the probabilistic slope stability analysis methodology for both the evaluation of existing slopes and the design of new slopes.
- To generalize the existing practical guidelines and to continue technology transfer for engineers who are interested in applying the methodology.
- To improve certain details of the methodology including techniques for estimating and representing the spatial variability of soil properties affecting slope stability.
- To improve the interpretation of in situ testing procedure (i.e. electric cone penetrometer) results for describing the spatial variability of soil strength parameters.

Each of these objectives for future work can be achieved through a set of carefully designed case studies. These case studies should be performed on both existing slopes under the evaluation setting and on slopes under

construction for the design setting. Additional work can be divided into five tasks described below. Field work should be designed to support both the case studies described in Sections 8.2 and 8.3 and the developmental tasks described in Sections 8.4 and 8.5. The existing application guidelines and technology transfer program should be generalized based upon experience gained in the new case studies. This latter task is described in Section 8.6.

8.2 Case Studies on Existing Slopes

The purpose of performing case studies on existing slopes would be twofold: first, to expand the range of experience with application of the methodology; and second, to provide data for refinement of the methodology as described in Section 8.4. Existing slopes would be selected to provide experience with a variety of soil types and in situ testing procedures, and a variety of construction methods.

The basic field program would be designed to provide estimates of the soil properties and their spatial variability as required for evaluation of slope stability using the methodology. It would therefore be based on past experience with the methodology and would be adapted to the selected sites. If timing of the case studies could be staggered to allow analysis of the results of one case study prior to the commencement of the next, then it would be possible to incorporate experience gained at previously completed sites into subsequent case study field programs. The basic field program would comprise in situ tests of soil strength properties at pre-selected spacings along orthogonal axes. A supplementary program of in situ tests along radials emanating from the same origin as the orthogonal axes would be needed to assist in evaluation of the adequacy of the method used for handling directional variance reduction.

Following the field program at each site, collected data would be reduced and analyzed to estimate parameters which describe the spatial variability of each soil type. The probabilistic slope stability analysis would then be performed and its results interpreted.

8.3 Case Studies on Slopes Under Construction

The purpose of performing case studies on slopes under construction is to develop experience with the methodology in a design setting. As described in Section 7.3.3, use of the methodology for design would require the availability and use of design values of variances and autocorrelation functions and then the application of a quality control program to monitor the achievement of satisfactory values of the mean, variance, and autocorrelation of strength parameters during construction. Selection of sites for these case studies should be based on soil types, construction method and stage and length of construction period. If case studies on slopes under construction could be timed to follow the completion of case studies on existing slopes, then the required design values of variances and autocorrelation functions could be developed based on the results of the case studies on existing slopes.

Using the design values, a probabilistic slope stability analysis would be performed on each structure. A quality control program would then be formulated and implemented on each structure. Because of the prolonged nature of major embankment construction, it is likely that field programs at different sites would need to be performed simultaneously, although it would be desirable to perform at least some sequentially on smaller embankments so that lessons learned on earlier case studies could be incorporated in later studies. The quality control program required for the methodology probably would be largely in addition to the normal quality control program required on

such structures. It would comprise in situ tests of soil strength parameters along two horizontal orthogonal axes which would be performed every lift or every other lift at locations that align vertically. Results from these tests would be aggregated and reviewed during the construction period. Also, slope stability would be reassessed using the probabilistic analysis to determine the effects of the updated distribution of shear strengths on the probability of failure.

8.4 Refinements to Methodology

Based on the results of the application of the probabilistic slope stability methodology to Copper City No. 7 tailings dam, two areas for further study of the basic methodology were identified:

- Relationship of "directional" autocorrelation functions to the autocorrelation functions in the three coordinate direction and the impact of this relationship on the computation of variance reduction functions in the model.
- Refinements in the model for use with non-circular failure surfaces.

As explained in Section 5.4, the effects of variance reduction were so small that the contribution of spatial variability of shear strength to the probability of failure was also very small. In other words, the variation of shear strength averaged over the failure surface was negligible. The evaluation of variance reduction was based on the assumption that the autocorrelation functions are factorable into their component parts as follows:

$$\rho_{s,\ell}(\cdot) = \rho_{s,x}(\cdot)\ \rho_{s,y}(\cdot) \quad \ldots\ldots\ldots\ldots\ (15)$$

However, since this factorability assumption is not valid for piecewise autocorrelation functions, the variance reduction functions may be too small and, hence, the variance reduction too severe.

In order to better represent the effects of variance reduction, the relationship of "directional" autocorrelation functions to the autocorrelation functions in the three orthodonal directions must be established from theoretical analysis and from further field testing on existing embankments and on embankments under construction. The procedure for establishing this relationship would be to determine autocorrelation functions in the x, y and z directions in a manner similar to that used for Copper City No. 2. Additional lines of soundings would then be added for the purpose of computing autocorrelation functions along radial axes emanating from the same origin as the x, y, and z axes. The relationship between the autocorrelation functions in the x and z directions and those in the radial direction (horizontal plane) could then be established. A similar procedure could be carried out for the x-y and z-y planes by evaluating autocorrelation functions along inclined planes.

After establishing an empirical or functional relationship between "directional" autocorrelation functions and those in the x, y, and z direction, the model may have to be revised appropriately. For example, additional covariance terms may be required in Equation 15.

The model that was applied to Copper City No. 2 tailings dam was based on evaluating slope stability along circular failure surfaces. A model using a non-circular failure surface was also developed but was not fully documented or tested. There are many cases where non-circular failure surfaces would be appropriate to consider and, therefore, an important refinement to the model would be to complete the non-circular failure surface feature.

8.5 Improvements to In Situ Strength Measurement

The determination of autocorrelograms requires the measurement of shear strength at many points. Conventional soil borings and laboratory tests on undisturbed samples are not a practical way to obtain the necessary data. The electric cone penetrometer was used at Copper City No. 2 and was found to be an efficient method. However, as pointed out in Section 5.2, there was uncertainty in converting the data from cone penetration resistance to friction angle. Various methods are available for this conversion and each yields different results.

It is clear that efficient in situ testing methods will be required for all types of probabilistic analysis. Although the cone penetrometer was used in the Copper City No. 2 study, there may be other methods that are more appropriate, especially for other soil types. For example, the vane shear test may be better for measuring the undrained strength of clay soils. Research should be continued to improve in situ testing methods that yield sufficient data for probabilistic analysis. All types of probabilistic geotechnical analysis will benefit from this type of research.

8.6 Generalization of Guidelines and Continuation of Technology Transfer

The Utah State University team which has developed and applied the probabilistic slope stability analysis methodology has prepared detailed documentation of their work and has participated in several technology transfer activities. The available documentation includes detailed descriptions of field program design and user manuals for data analysis and the probabilistic slope stability analysis computer programs. Technology transfer activities have included: training sessions in the use of the methodology for the U.S. Bureau of Mines, U.S. Bureau of Reclamation, and an

engineering consulting firm; presentation of the methodology at a U.S. Bureau of Mines Technology Transfer meeting; presentation of papers at professional meetings; preparation of papers for submission to technical journals; and cooperation with the U.S. Bureau of Mines and an engineering consulting firm in the future application of the methodology.

Experience developed in the case studies described in Sections 8.2 and 8.3 above should be used to generalize the existing guidelines to a wider range of soil types and construction methods. Also, attempts should be made to generalize design values of the variances and autocorrelation functions for shear strength parameters. Data on shear strength parameters could be assembled from testing laboratories, consultants, and government agencies to provide additional information on the variability of these parameters over different soil types and construction methods. However, the basic data for generalizing design autocorrelation functions are not available at this time.

The scope of the guidelines should include, but should not be limited to, the following:

- field program design for existing slopes
- quality control program design for new slopes
- interpretation of in situ test results
- estimation of statistical parameters from field test results
- design values of variances of autocorrelation functions of shear strength properties
- model setup and execution
- interpretation of model results in both the evaluation and design settings
- use of model results in evaluation and design settings
- descriptions of case studies

Technology transfer is an essential part of successfully making the probabilistic slope stability analysis methodology available to the geotechnical engineering profession and should continue during and after any additional case studies. Personnel from the U.S. Army Corps of Engineers or other agencies or private firms could assist in performing or be responsible for evaluating these case studies. An end product of the future studies described above should be a training manual for engineers interested in using the procedure. This manual should be designed to explain the theory and capabilities of the methodology to practicing engineers who have little or no background in probability and statistics. In addition, the already developed three-day training session in the methodology should be expanded to include the experience and guidelines developed from the additional case studies. Such a training session could be made available to groups of engineers interested in learning about the methodology.

9. RELATIONSHIP OF PROBABILISTIC SLOPE STABILITY ANALYSIS METHODOLOGY TO AN INTEGRATED RISK ASSESSMENT FRAMEWORK

Embankments and slopes fail due to many different causes, including floods, rapid drawdown, improper evaluation of soils properties, and earthquakes. Obviously, the probabilistic slope stability analysis methodology does not provide a means of considering the influence of all types of causative events on the probability of slope failure. It can, however, be used as part of an integrated framework for risk assessment of slopes or dams. At this time, such a framework has not been fully developed. Preliminary work to design an integrated risk assessment framework has been accomplished by Bowles, et al. (1978) and Howell (1979). The purpose of this brief section is to show that the probabilistic slope stability analysis methodology can be a useful tool for design and evaluation of slopes as part of an integrated risk assessment framework or independently of such a framework.

The role of the probabilistic slope stability methodology in the proposed framework is illustrated in Figure 10. This figure identifies situations in which the methodology can be used to estimate the conditional or transition probability that a particular type of event, such as inadequate quality control, will result in a response such as slope stability failure. Other techniques, some requiring mainly professional judgment, are needed to estimate transition probabilities represented by open boxes in Figure 10.

The end product of applying such an integrated risk assessment framework would be either a probability of a partial or complete failure or an expected value of damages (consequences) to the structure, adjacent property, or as a result of a loss of project revenues due to, for example, the discontinuation of irrigation water supply (Figure 11). If accurate methods of estimating the

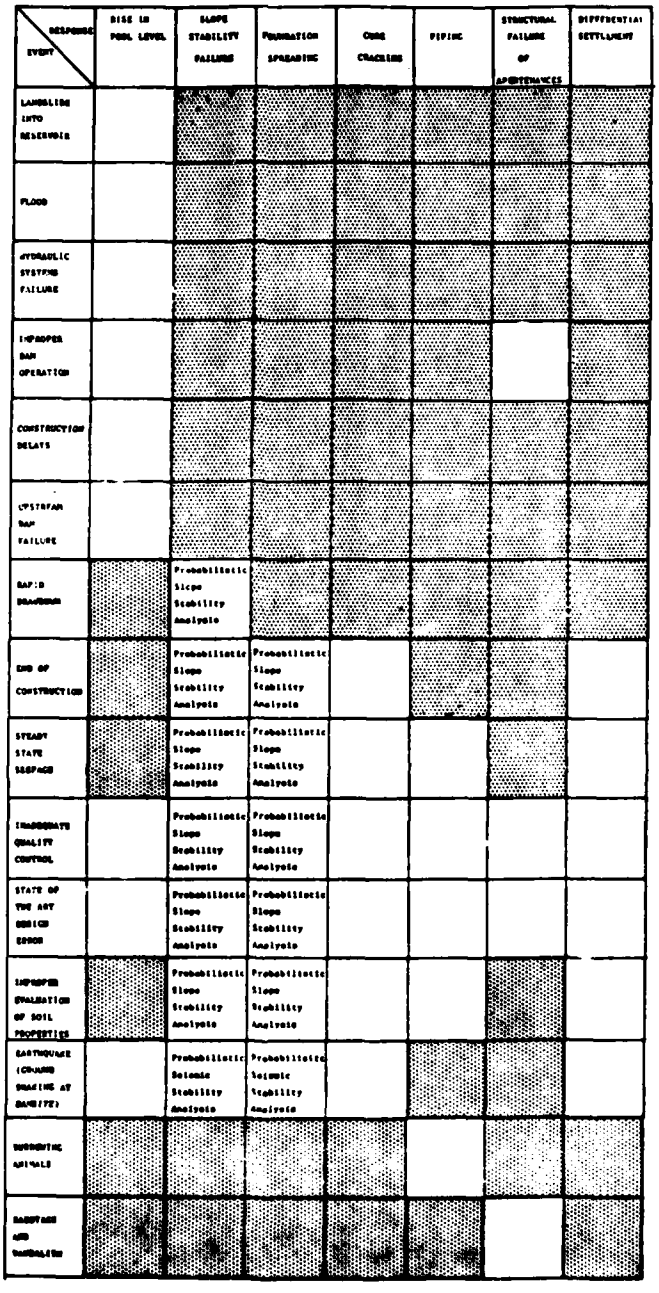

FIGURE 10

Situations in Which Probabilistic Slope Stability Analysis Could Be Used to Estimate Transition Probabilities of a Response Given the Occurrence of a Consecutive Event

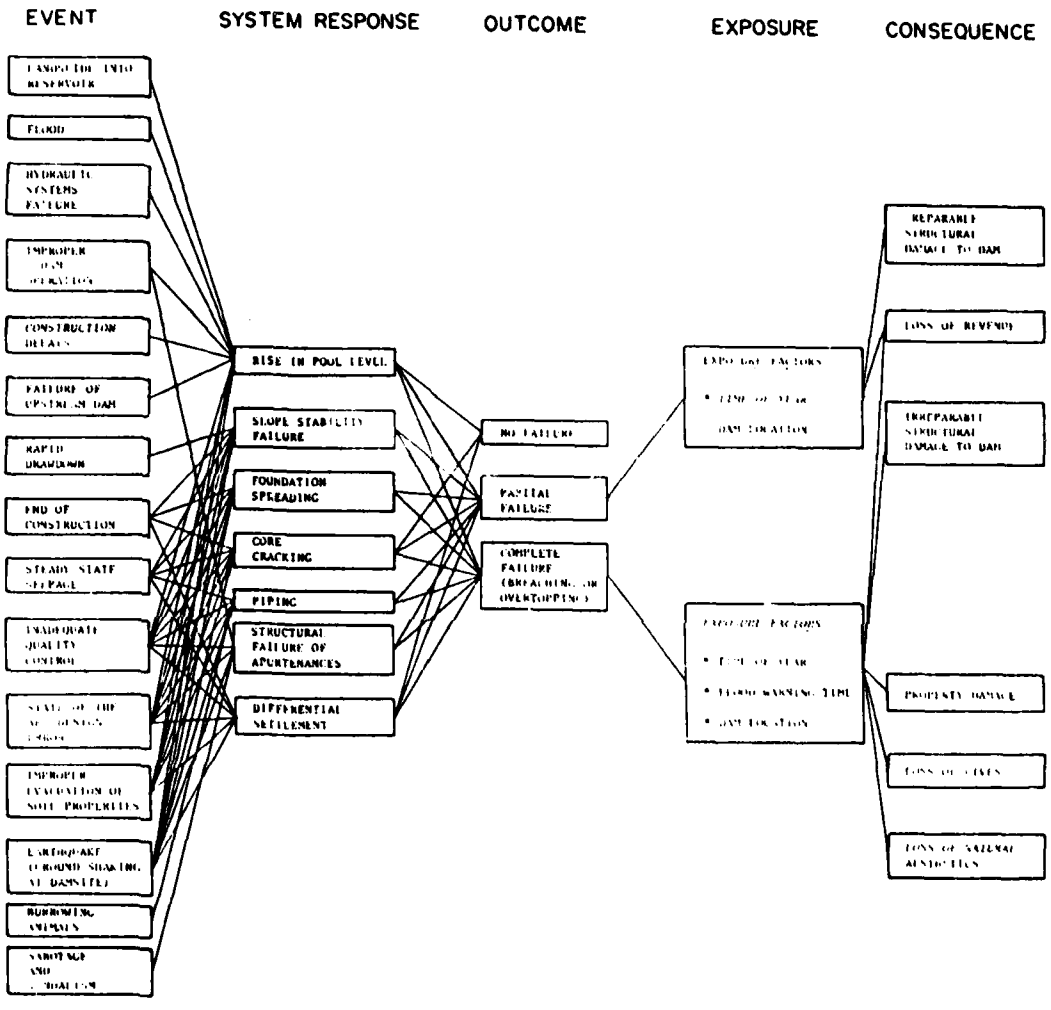

FIGURE 11

Event-System Response-Outcome-
Exposure-Consequence Diagram

various transition probabilities could be developed, then such estimates of damages could be used to make rational design decisions based upon some risk acceptability criterion (see Figure 12). This would be accomplished by trading off the additional costs of increased safety against its benefits derived in terms of reductions in the expected value of damages, as is done sometimes in highway design on mine pit slope stablity analysis. Such calculations could be introduced into a project benefit/cost analysis or could be considered separately.

Since the integrated framework is not currently available in working form, the methodology must be used independently and therefore, since only some failure mechanisms can be considered, it follows that the failure probabilities obtained from the methodology cannot be treated as absolute values which cover all likely failure mechanisms; rather they are only relative values representing the sensitivity of the failure probability to changes in such considerations as embankment cross-sectional geometry, materials selection, and even site selection or reservoir operating rules. By so doing, only the relative values or changes in the probability of failure can be utilized, rather than the absolute value, and therefore, benefit/cost tradeoffs cannot be made at this time.

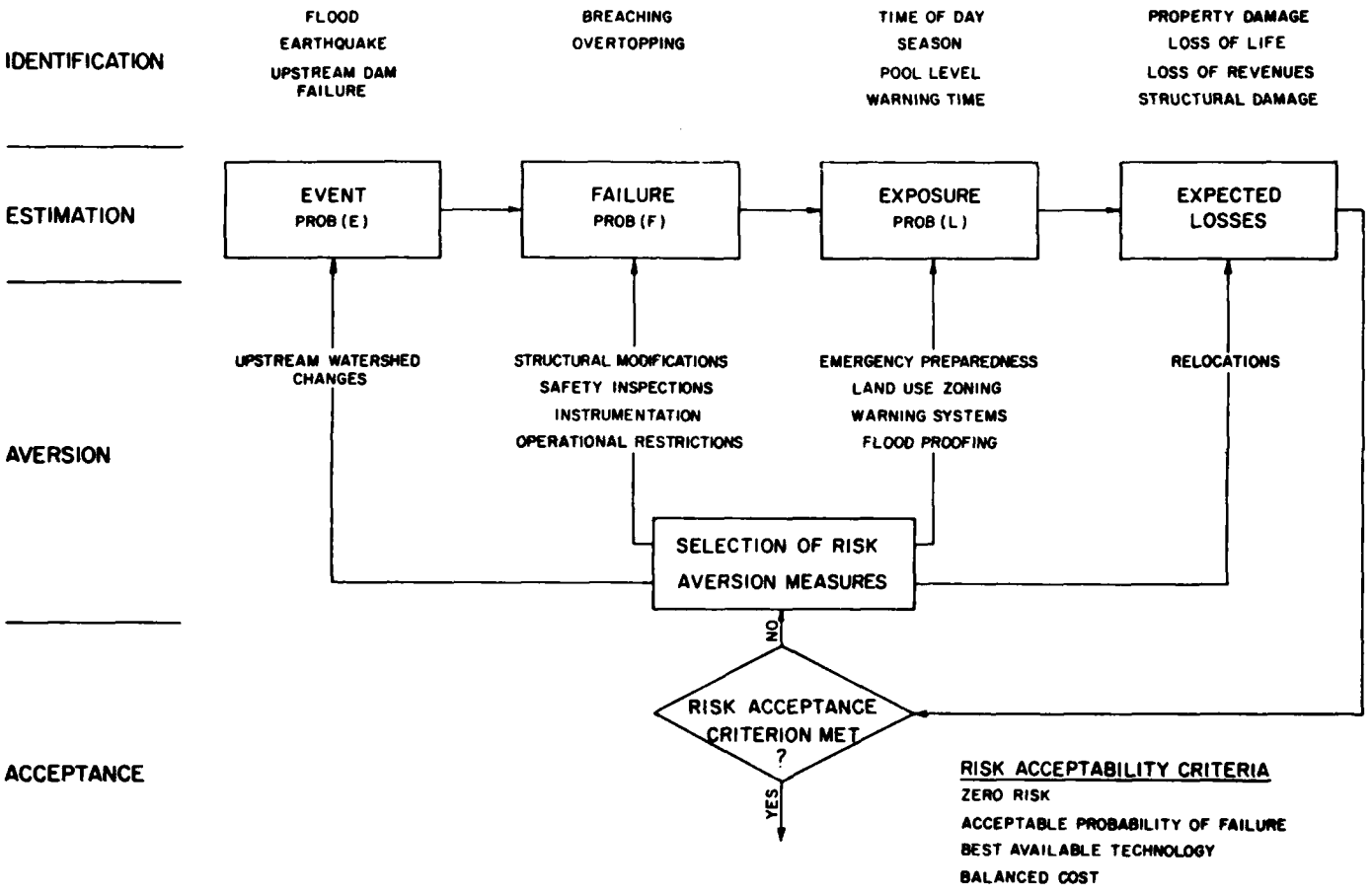

FIGURE 12

Risk-Based Method for Establishing Priorities for Alternative Dam Safety Improvements

REFERENCES

Agterberg, F. P. 1970. Autocorrelation functions in geology. Geostatistics, D. F. Merriam, ed. Plunem Press. pp. 113-141.

Alonso, E. E. 1976. Risk analysis of slopes and its application to slopes in Canadian sensitive clays. Geotechnique 26(3): 453-472.

Alonso, E. E., and R. J. Krizek, 1975. Stochastic formulation of soil properties. Proceedings, 2nd International Conference on Applications of Statistics and Probability in Soil and Structural Engineering, Aachen, W. Ger. pp. 9-32.

Anderson, L. R., D. S. Bowles, R. V. Canfield, and K. D. Sharp. 1981a. Probabilistic modeling of tailings embankment designs, volume I, model development and verification. Final report presented to the U.S. Bureau of Mines, Contract No. J0295029.

Anderson, L. R., D. S. Bowles, R. V. Canfield, and K. D. Sharp. 1981b. Probabilistic modeling of tailings embankment designs, volume II, model application and evaluation. Final report presented to the U.S. Bureau of Mines, Contract No. J0295029.

Anderson, L. R., D. S. Bowles, R. V. Canfield, and K. D. Sharp. 1981c. Probabilistic modeling of tailings embankment designs, volume III, user's manual for probabilistic slope stability computer program, PROBISH. Final report presented to the U.S. Bureau of Mines, Contract No. J0295029.

Anderson, L. R., D. S. Bowles, R. V. Canfield, and K. D. Sharp. 1981d. Probabilistic modeling of tailings embankment designs, volume IV, user's manual for cone penetrometer data analysis computer programs, HORZ and VERT. Final report presented to the U.S. Bureau of Mines, Contract No. J0295029.

Athanasiou-Grivas, D. S. 1976. Reliability of slopes of particulate materials. Thesis presented to Purdue University in partial fulfillment of the requirements for the degree of Doctor of Philosophy.

Baecher, G., M. Pate, and R. de Neufville. 1979. NED cost determination for probability of dam failure. Final Report, c/o Systems Analysis, Cambridge, Mass.

Barboteu, G. 1972. Reliability of earth slopes. Thesis presented to the Massachusetts Institute of Technology, at Cambridge Mass., in partial fulfillment of the requirements for the degree of Master of Science.

Bergado, Dennes. 1982. Probabilistic assessment of the safety of earth slopes using pore water pressure as a random variable. Dissertation submitted in partial fulfillment for the requirements of the degree of Doctor of Philosophy in Civil Engineering, Utah State University, Logan.

References (cont'd.)

Bowles, D. S., L. R. Anderson, and R. V. Canfield. 1978. A systems approach to risk analysis for an earth dam. International Symposium on Risk and Reliability in Water Resources, Waterloo, Ontario, Canada.

Cornell, C. A. 1971. First order uncertainty analysis of soils deformation and stability. Proceedings of the 1st International Conference on Applications of Statistics and Probability in Soil and Structural Engineering, held at Hong Kong. pp. 130-144.

Dunn, I. S., L. R. Anderson, and F. W. Kiefer. 1980. Fundamentals of geotechnical analysis. First ed., John Wiley & Sons, Inc., New York.

Harr, M. E. 1977. Mechanics of particulate media. First ed., McGraw-Hill Inc., USA.

Howell, Jon C. 1981. A framework for risk analysis of earth dams. Thesis submitted in partial fulfillment for the requirements of the degree of Master of Science in Civil Engineering, Utah State University.

Jones, G. A., and D. J. A. Van Zyl. 1981. The piezometer probe--a useful site investigation tool. Tenth International Conference on Soil Mechanics and Foundation Engineering, Stockholm, Sweden.

Lumb, P. 1974. Application of statistics in soil mechanics. Soil Mechanics-New Horizons, Butterworth and Co., London. pp. 44-111.

Matsuo, M. 1976. Reliability in embankment design. M.I.T. Department of Civil Engineering Research Report R 76-33, Massachusetts Institute of Technology, Cambridge, Mass.

Mitchell, J. K., and T. A. Lunne. 1977. Cone resistance as measure of sand strength. Journal of the Geotechnical Engineering Division, ASCE 104(GT7):995-1012. July.

Morla-Catalàn, J., and C. A. Cornell. 1976. Earth slope reliability by a level-crossing method. Journal of the Geotechnical Division, ASCE 102(GT6):591-604.

Schmertmann, J. H. 1977. Guidelines for cone penetration test performance and design. FHWA-TS-78-209, Federal Highway Administration Offices of Research and Development Implementation Division, Washington, D.C. February.

Sharp, K.D., 1982. Development of a Model for Probabilistic Slope Stability Analysis and Application to a Tailings Dam. Ph.D. Dissertation, Utah State University, Logan, Utah.

Sharp, K. D., L. R. Anderson, D. S. Bowles, and R. V. Canfield. 1981. Model for Assessing Slope Reliability. Transportation Research Record 809, pp. 70-78.

References (cont'd.)

Vanmarcke, E. H. 1977a. Probabilistic modeling of soil profiles. Journal of the Geotechnical Engineering Division, ASCE 103 (GT11):1127-1246.

Vanmarcke, E. H. 1977b. Earth slope reliability. Journal of the Geotechnical Engineering Division, ASCE 103(GT11): 1247-1268.

Vanmarcke, E. H. 1979. On the scale of fluctuation of random functions. M.I.T. Department of Civil Engineering, Research Report R79-17, Massachusetts Institute of Technology, Cambridge, Mass.

Whitman, R. V., and W. A. Bailey. 1967. Use of computers for slope stability analysis. Journal of Soil Mechanics and Foundations Division, ASCE 93(SM4):475-498.

Wu, T., and L. M. Kraft. 1970. Safety analysis of slopes. Journal of the Soil Mechanics and Foundation Division, ASCE 96(SM2):609-632.

Yucemen, M. S. 1973. A probabilistic study of safety and design of earth slopes. Thesis presented to University of Illinois at Urbana-Champaign, in partial fulfillment of the requirements for the degree of Doctor of Philosophy in Civil Engineering, Urbana, Illinois.

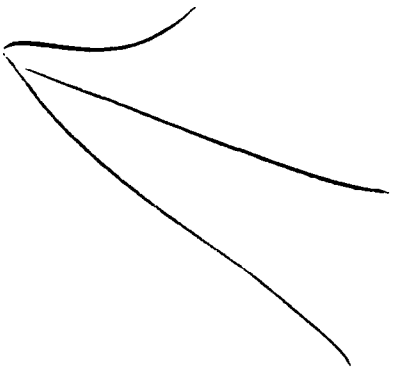

PROBABILITY OF LIQUEFACTION IN A 3-D SOIL DEPOSIT

by

Achintya Haldar

ABSTRACT

Historically, earthquake-induced liquefaction has caused an enormous amount of damage in terms of loss of human life, property damage, human suffering and environmental damage. A probabilistic three-dimensional liquefaction model is proposed here considering the damage aspect of the problem. Considerable uncertainty is expected in the estimation of several parameters in a liquefaction model. The estimation of in situ relative density is one of them. A new relationship, designated as the Haldar and Miller relationship, is proposed here between the Standard Penetration Test value and the in situ relative density. The in-situ shear resistance of a soil deposit is evaluated here by introducing a shear strength parameter R. Using large-scale shaking table test results, the relationship is corrected for the compliance effect, sample preparation methods, mean grain size, multidirectional shaking and some other secondary factors. There is also high uncertainty in the load parameters. Hence, the seismic activity of the region should be given serious attention in a liquefaction study. This probabilistic model is a first step toward developing a comprehensive decision analysis framework. Recommendations are also made here for future research work in the area of liquefaction.

TABLE OF CONTENTS

1. INTRODUCTION

The historical evidence of damage associated with earthquake-induced liquefaction is enormous in terms of loss of human life, property damage, human suffering and environmental damage. There are hundreds of recent cases of ground failure and damage to structures due to liquefaction during earthquakes in China, Japan, Yugoslavia, Chile, Central America and the United States. During the 1964 earthquake in Niigata, Japan, many structures settled several feet and suffered up to 80 degrees of tilting (Chameau, 1981; Haldar, 1976; Ohsaki, 1969, 1970; Seed and Idriss, 1971). The same year, in Valdez, Alaska, extensive flow slides washed entire sections of the waterfront into the sea. These events, more than anything else, generated a sensational amount of interest in the problem in the research communities, and a sense of urgency among practicing engineers. Due to the inherent complexities of the problem, research was conducted in many areas related to the liquefaction phenomenon (Annaki and Lee, 1977; Bazant and Krizek, 1976; Castro, 1975, 1977; Chameau, 1981; Christian and Swiger, 1975; DeAlba, Chan and Seed, 1975; Donovan, 1971; Drnevich, 1972; Faccioli, 1973; Fardis and Veneziano, 1979; Finn, Bransby, and Pickering, 1970; Finn, Lee, and Martin, 1977; Finn, Pickering and Bransby, 1969; Ghaboussi and Dikmen, 1978; Haldar, 1976, 1979, 1980, 1981a, 1981b; Haldar and Tang, 1979a, 1979b, 1981; Haldar and Miller, 1982a, 1982b, 1982c, 1982d, 1982e; Ishihara, Tatsouka, and Yasuda, 1975; Kishida, 1969; Ladd, 1977; Lee and Seed, 1967; Lee and Fitton, 1969; Liou, Streeter and Richart, 1977; Martin, Finn, and Seed, 1978;

Mori, Seed, and Chan, 1977; Mulilis, Seed, Chang, Mitchell, and Arulanandan, 1977; Ohsaki, 1970; Peacock and Seed, 1968; Pyke, Chan and Seed, 1974; Schmertmann, 1972; Seed, 1979; Seed and Idriss, 1967, 1971; Seed and Peacock, 1971; Seed, Pyke, and Martin, 1975; Silver and Park, 1976; Velera and Donovan, 1977; Whitman, 1971; Yegian and Whitman, 1976; Yegian and Vitelli, 1981; Yoshimi and Tokimatsu, 1977; Youd, 1977; Zienkiewicz, Chang, and Hinton, 1978). Several causes of liquefaction were identified. Numerous models with various degrees of complexity were also proposed. These will be discussed in detail in the literature review section. Researchers are investigating the causes of the problem, but the damage associated with liquefaction is another aspect which needs to be studied in great detail.

The onset of liquefaction in a deposit causes damage to a structure in terms of subsidence, settlement, relative settlement, tilting, etc. It is known that the estimation of liquefaction potential does not lead to the estimation of damage due to liquefaction. To estimate the damage during liquefaction, it is necessary to go one step beyond the evaluation of liquefaction potential. In spite of numerous studies on liquefaction, this area was overlooked in the past. It is clear that a volume of sand has to undergo a considerable amount of strain to produce a noticeable amount of damage at the referenced location. It is very important to identify this critical volume. Soil properties in this critical volume need to be modeled appropriately. Moreover, liquefaction does not always lead to damage and the initial deposit conditions affect the extent

of damage. Considering all this information, it is appropriate to develop a comprehensive liquefaction model considering damage as the design criterion.

This study will be limited to earthquake-induced liquefaction. "Cyclic Mobility" would be the most appropriate definition of the problem under consideration according to the most recent literature (Castro, 1975; Seed, 1979). However, the term "liquefaction" will be used in this report instead of "cyclic mobility" since the former is the most widely used by practicing engineers.

There is general agreement about the mechanism by which the onset of liquefaction occurs during an earthquake. The basic cause of liquefaction in a saturated cohesionless soil deposit during an earthquake is the buildup of pore water pressure due to the application of cyclic shear stresses induced by the ground motion. The cohesionless soil tends to become more compact while the soil structure rebounds to the extent necessary to keep the volume constant. This interplay of volume reduction and soil structure rebound determines the magnitude of the increase in pore water pressure. If sufficient pore water pressure is produced, the effective stress becomes zero and the deposit assumes the characteristics of a viscous liquid. This essentially leads to liquefaction.

The basic causes of liquefaction appear to be simple. However, it is a very complex problem. Quite a few factors influence the liquefaction potential evaluation. Moreover, each factor influences the evaluation to a different degree. For proper evaluation, information on soil properties affecting the liquefaction phenomenon

and earthquake loading needs to be available. The estimation of in situ soil parameters can be obtained by measuring them directly in the deposit, indirectly from empirical relationships, or by measuring them in the laboratory using so-called "undisturbed" samples. Considerable error can be incurred during these processes (Gibbs and Holtz, 1957; Haldar and Tang, 1979b; Marcuson and Bieganousky, 1977a; Martin, Finn, and Seed, 1978; Mulilis, Seed, Chang, Mitchell, and Arulanandan, 1977; Seed and Idriss, 1967; Tang and Ang, 1973; Tavenas, Ladd, and LaRochelle, 1972; Wu, 1974). The nonhomogeneity of the soil properties in the liquifiable volume has to be modeled in three dimensions. Long distance fluctuations and local variations in soil properties can only be modeled effectively using probability theory. Seismic loading is also unpredictable (Haldar, 1976). This necessitates the availability of a simple but efficient and practical probabilistic model to study the risk of damage associated with the liquefaction phenomenon. The purpose of this report is to develop such a model.

2. LITERATURE REVIEW

Numerous studies on cyclic testing, soil parameter definition, soil modeling and dynamic analysis, earthquake loadings, etc. were conducted in the past to study the liquefaction phenomenon. To effectively summarize all these studies, the currently available methods of liquefaction potential evaluation can be divided into the following major categories:

(1) Empirical methods based on observation of the performance of sand deposits in previous earthquakes (Castro, 1975; Kishida, 1969; Ohsaki, 1970; Whitman, 1971),

(2) Method based on evaluation of stress conditions in the field and laboratory determination of stress conditions causing liquefaction - the simplified method suggested by Seed and Idriss (1971),

(3) Analytical models (Bazant and Krizek, 1976; Finn, Lee, and Martin, 1977; Ghaboussi and Dikmen, 1978; Ishihara, Tatsuoka, and Yasuda, 1975; Liou, Streeter, and Richart, 1977) considering one-dimensional wave propagation theory, and horizontal layered soil excited vertically by the shear stresses, and

(4) Probabilistic methods (Chameau, 1978; Christian and Swiger, 1975; Donovan, 1971; Faccioli, 1973; Fardis and Veneziano, 1979; Haldar and Tang, 1979a; Yegian and Whitman, 1976).

All these studies helped to identify some of the important factors that affect liquefaction potential, such as relative density, mean grain size, initial confining pressure, intensity of ground shaking, duration of ground shaking, etc. Some other factors, whose influence on liquefaction potential evaluation may be significant when laboratory methods are used, have recently been identified. They include methods of preparation of test specimens (Ladd, 1977; Mulilis, Seed, Chang, Mitchell, and Arulanandan, 1977), size of specimens (Seed, 1979), sample disturbances (Mori, Seed, and Chan, 1977), effect of system compliance (DeAlba, Chan, and Seed, 1975; Martin, Finn, and Seed, 1978), soil fabric (grain and interparticle

contact orientations) (Ladd, 1977; Mulilis, Seed, Chang, Mitchell, and Arulanandan, 1977), period under sustained load, i.e., the age of the deposit (Ohsaki, 1969), previous strain history of the deposit (Finn, Bransby, and Pickering, 1970; Seed, Mori, and Chan, 1977), overconsolidation (Castro, 1975; Finn, Pickering, and Bransby, 1969; Seed and Peacock, 1971), multidirectional shaking (Pyke, Chan, and Seed, 1974; Seed, Pyke, and Martin, 1975), etc.

The limitations of the empirical methods are well understood in the engineering communities and will not be discussed further here. However, some of the analytical methods need some discussion. The results of these methods depend on the degree of simplification used in (i) the presentation of the stress-strain relationship, (ii) the pore pressure generation model, and (iii) the numerical integration methods used. The method proposed by Liou, Streeter and Richart (1977) is based on the theory of elasticity; however, the shear modulus is strain-dependent. Finn, Lee and Martin's (1977) model requires very good data on shear moduli and volume changes. Collection of this type of information is economically feasible only for very large projects. Little data is available on the parameters necessary for the endochronic model proposed by Bazant and Krizek (1976). The Stress Path model originally proposed by Ishihara, Tatsuoka and Yasuda (1975) and subsequently modified by Ghabousi and Dikmen (1978) has several limitations. In this sense, the simplified method suggested by Seed and Idriss (1971) has many desirable features.

However, it is very difficult to properly incorporate all the relevant information into the model. In view of the unpredictability of the earthquake loading, lack of information on the soil deposit, and the unavoidable errors in the modelling of the soil behavior and in the estimation of design parameters, a systematic probabilistic model has definite advantages over the so-called deterministic methods (Christian and Swiger, 1975; Fardis and Veneziano, 1979; Haldar, 1976; Yegian and Whitman, 1976).

The limitations of the currently available probabilistic methods need some mention here. They can be separated into two groups: methods based on the case histories of liquefaction available in the literature and methods relating laboratory experimental results and dynamic analysis of the deposit. Methods suggested by Christian and Swiger (1975) and Yegian and Whitman (1976) belong to the first group. The method suggested by Christian and Swiger is basically a multivariate statistical method called discriminant analysis. The authors even wrote in their paper that "Numerous assumptions are made in such analysis, including that the variates or parameters are normally distributed and that the variances and co-variances of individual cases (liquefaction and nonliquefaction) are the same as those for all cases taken together." Moreover, statistics of the two normal populations are estimated from sparse and unreliable data (Fardis and Veneziano, 1979). Estimation uncertainty is not considered at all. Yegian and Whitman (197(used historical data but avoided making the questionable assumption of the existence of two binormal populations with the same

covariance matrix. But they did not address many important factors that are presently thought to significantly affect liquefaction potential.

Methods relating laboratory experimental results and dynamic analysis were suggested by Donovan (1971), Faccioli (1973), Fardis and Veneziano (1979), Haldar and Tang (1979a), and Chameau (1981). Donovan assumed that the probability density function of the shear stress-time history envelope of an earthquake followed the Rayleigh distribution. The seismic activity of the region as well as the uncertainties in soil parameters affecting liquefaction were not considered. Faccioli applied one-dimensional amplification theory to find the probabilistic characteristics of the shear stress process, considering an earthquake as a stationary random process with a given power spectral density function. He did not consider uncertainties in soil parameters. Fardis and Veneziano considered an essentially one-dimensional mechanical model based on many assumptions (Seed, 1979; Youd, 1977). Chameau's (1981) model has limitations similar to those of Finn, Lee and Martin's model. Seed (1979) wrote "They do require, however, the determination of more material properties in order to make the analysis and some of them are vulnerable to testing errors or require further study before they are fully understood." Questions are frequently raised on the modeling of any future earthquake time history (from known spectra or any other way), damping characteristics of the deposit, finite element modeling, etc. Seed (1979) suggested a "more simplified approach seems to offer a more practical and less vulnerable

alternative at the present time." Haldar and Tang (1979a) used a relatively simple method commonly used by practicing engineers. It is the slightly modified simplified method suggested by Seed and Idriss (1971). This method considered the uncertainties in the soil deposit and the earthquake loading. All these methods will estimate the probability of liquefaction at a point in the deposit. Generally, the liquefaction risk is evaluated considering the weakest point in the deposit. In order to produce a noticeable amount of damage to a structure, a volume of sand has to undergo a considerable amount of strain. It is very important to identify this critical volume and to model the soil properties in this volume appropriately. Local variations as well as long-distance fluctuations of the soil properties in this liquefiable volume have to be modeled in three dimensions. These can only be modeled effectively using probability theory. A three-dimensional probabilistic model will be developed in the subsequent sections.

3. LIQUEFACTION PARAMETERS

The factors to be considered in the proposed method of liquefaction potential evaluation are numerous. For simplicity of discussion, these factors are divided into three groups: soil parameters; parameters related to laboratory test and sampling effects; and loading parameters. These parameters and their effects on liquefaction potential are described in the following sections.

3.1 Soil Parameters

The soil parameters characterize the type of soil and the physical state in which the soil exists. They can be identified as relative density, initial confining pressure, overconsolidation ratio, earth pressure coefficient at rest, mean grain size and gradation, drainage, angularity or particle shape, soil fabric, method of deposition, age of deposit and seismic history, degree of saturation, temperature and viscosity of pore water, etc.

Relative density, D_r, is one of the important parameters in a liquefaction potential evaluation. All field and laboratory investigations suggest that an increase in D_r results in an increase in the resistance to liquefaction.

From field and laboratory studies it has been found that the initial confining pressure, σ_o, on the soil element greatly affects the soil's resistance to liquefaction. The resistance to liquefaction will increase with an increase in the initial confining pressure.

The overconsolidation ratio, OCR, is the ratio of the preconsolidation pressure to the overburden pressure. An increase in the OCR will result in an increase in the liquefaction resistance of the soil. Overconsolidated soil deposits will not be considered in this study.

Earth pressure coefficient at rest, K_o, a measure of the lateral confining pressure on a soil element, has a significant effect on liquefaction resistance. An increase in K_o will result in an increase in the liquefaction resistance.

The type of soil greatly affects the liquefaction resistance of a soil deposit. For cohesionless soils, the soil type is perhaps most easily characterized by the grain size distribution. Among many parameters, the mean grain size, D_{50}, is generally considered to represent the soil type. The general ranges of D_{50} which will be critical to the liquefaction problem are between 0.02 mm and 0.6 mm (Lee and Fitton, 1969). Laboratory studies show that within this range of D_{50} sizes, vulnerability to liquefaction increases with decreasing D_{50} sizes for a given earthquake excitation. Soil deposits with a uniform gradation are considered to be the most liquefiable soils.

Drainage will dissipate excess pore water pressures during a cyclic load; therefore, the resistance to liquefaction is increased by drainage of the soil.

Much work needs to be done in the area of the effect of angularity or particle shape on the liquefaction resistance. However,

it seems reasonable that if the soil particles are more angular in shape, the soil structure will be more stable; hence, the soil will have a greater resistance to liquefaction.

The soil fabric or soil structure is characterized by the orientation and arrangement of the grains and interparticle contact planes. A change in the soil fabric will result in a change in the soil's resistance to liquefaction. Mulilis, et al. (1977), using triaxial tests have found that the distribution of the apparent long axes of sand grains apparently has no effect on liquefaction resistance, but samples that had a higher distribution of normals to interparticle contact planes parallel to the loading axis exhibited a greater resistance to liquefaction.

Through laboratory tests, it has been observed that the method in which the soil was deposited has a significant effect on liquefaction resistance. Ladd (1977) has found that samples prepared in a moist condition exhibited greater liquefaction resistance than samples prepared dry for the triaxial test; however, the method of densification had very little effect. On the other hand, Mulilis, et al. (1977) found that the method of densification does affect strength, and that samples densified by high frequency vibrations in the moist condition were strongest in their set of triaxial tests.

The age of the soil deposit has a significant effect on the cyclic strength of a soil. With time, cementation or welding of interparticle contact planes occurs, which strengthens the soil and increases its resistance to liquefaction.

The strength of a soil deposit is affected by its previous strain history. Finn, Bransby and Pickering (1970) have observed that static shear strains or cyclic shear strains below certain threshold values increase the strength of the soil, but strains larger than the threshold values will decrease strength. Mori, Seed and Chan (1977) subjected soil samples to a series of small shocks in order to simulate a prior seismic history, and found that the soil's resistance to liquefaction increased.

The soil will liquefy less readily during an earthquake if the soil conditions are less conducive to increases in excess pore water pressure; therefore, a reduction in the degree of saturation, S_o, will result in an increase in the cyclic strength of the soil.

The temperature and viscosity of pore water is expected to affect the cyclic strength of the soil, but the systematic effects resulting from these factors are not known clearly.

3.2 Parameters Related to Laboratory Test and Sampling Effects

Often laboratory tests are conducted using representative soil samples obtained from a deposit to evaluate the liquefaction potential of the deposit. The outcome of this type of evaluation will greatly depend on the quality of the sample used, the type of laboratory test and conditions of the test, etc. Some of the important parameters are quality of samples (i.e., undisturbed, disturbed or reconstituted samples), method of sample preparation, type of test, compliance effect, frequency and form of cyclic load used, etc.

Ideally, an undisturbed soil sample obtained from a deposit should be used in a laboratory investigation. Unfortunately, in the case of a liquefaction study, it is extremely difficult to collect undisturbed samples from a loose, saturated sand deposit. Mori, Seed and Chan (1977) have shown that even in the most carefully conducted undisturbed soil sampling, a small amount of sample disturbance still occurs. This disturbance is significant enough to change the relative density and destroy the effects due to cementation or long-term loading and seismic history. Often, disturbed or reconstituted samples are used for test specimens. These type of samples will fail to consider the effect of cementation, long-term loading or seismic history of the deposit, etc.

The effects of method of preparation of samples were discussed in the previous section.

Triaxial, simple shear, torsional shear, and large-scale shaking table tests are used in the laboratory to study the liquefaction potential. Strength as measured from the triaxial test can vary depending on the diameter of the sample and the state of stress concentrations at cap and base. Various reasons for stress concentration have been identified by Haldar (1976). Strength as measured from the simple shear device can vary depending on if smooth or rough platens are used, the magnitude of the seating load, development of complementary shear stresses and the preparation of the simple shear test specimens. Boundary effects and length-to-height ratios of soil samples can significantly affect results from large-scale shaking table tests.

The test specimens in the laboratory are enclosed by a rubber membrane. The penetration of the membrane in spaces between sand particles will produce compliance error. Test results from laboratory investigations are expected to have compliance error to some degree. Compliance in the testing apparatus causes a fictitious increase in the cyclic strength of the test specimen. It has been observed that large-scale shaking table tests give values for cyclic strength close to those which would be found in situ.

The frequency and form of cyclic load applied to a specimen in the laboratory may not have a significant effect on the liquefaction potential evaluation. The effect of the loading frequency on the shear strength of the sample has been investigated in several research programs (Lee and Fitton, 1969; Peacock and Seed, 1968). Peacock and Seed (1968) have shown that for an applied uniform cyclic shear stress with a frequency in the range from 1/6 to 4 cycles/sec, the frequency of the cyclic shear stress does not affect cyclic strength in simple shear tests. Yoshimi and Oh-Oka (1973) have found that for soil specimens tested in a ring torsion apparatus, the cyclic strength is independent of the frequency of the applied shear stress for frequencies in the range of 1 to 12 cycles/sec.

Tests have shown that the form of the applied shear stress history can have an effect on the cyclic strength of a soil. Yoshimi and Oh-Oka (1973) have found that soil specimens subjected to complete or partial shear stress reversals will undergo liquefaction, but will not liquefy if subjected to unreversed shear stress cycles. Ishihara and Yasuda (1975) found that the cyclic

strength of a soil is greater for shock type than vibration type random shear stress applications.

3.3 Loading Parameters

Earthquake-induced liquefaction is under consideration in this study. All parameters of earthquake loading related to the liquefaction problem need to be evaluated. They are earthquake acceleration, magnitude, duration of shaking, multi-directional shaking, stress reduction factor, etc.

A site's vulnerability to liquefaction during an earthquake increases as the intensity of ground shaking increases. The maximum ground surface acceleration, a_{max}, is a measure of the intensity of ground shaking. For a given intensity of ground shaking a_{max}, the site will liquefy only when the duration of ground shaking exceeds a certain value. If the load-time history of an earthquake is converted to an equivalent number of uniform stress cycles, N_{eq}, then the duration of the ground shaking can be represented by N_{eq}. Since the duration of the ground shaking depends on the magnitude of the earthquake, N_{eq} will also depend on the magnitude of the earthquake

Ordinarily a soil specimen is subjected to a cyclic shear stress in only one direction in the laboratory. However, ground motion induced by an earthquake is multi-directional. Laboratory tests have shown that the resistance of soil to liquefaction under multi-directional ground shaking is less than if the shaking was in one direction.

As a soil column deforms during earthquake excitation, the shear stress at a point depends on the depth of the point from the ground surface. A stress reduction factor, r_d, is introduced to account for this (Seed and Idriss, 1971). The maximum value of r_d is 1.0 at the ground surface. At other depths, the value of r_d is less than 1.0.

4. CONCEPT OF RANDOM VARIABLES

For the liquefaction problem, the shear resistance mobilized by a volume of soil, τ_R, represents the capacity of the system, and the shear stress generated during earthquake shaking, τ_A, represents the demand on the system. The safety or reliability of an engineering system is essentially the measure of its capacity to meet the demands. In the present study, liquefaction will occur when τ_R is less than τ_A. Unfortunately, these parameters are difficult to estimate. However, design decisions are often required to be made regardless of the state of completeness or quality of information available. Moreover, in view of the unavoidable errors in the modeling of soil behavior and of the unpredictability of the earthquake loading, τ_R and τ_A are intrinsically random. Therefore, a systematic probabilistic model of τ_R and τ_A is necessary. In the following sections, the probabilistic and statistical modeling techniques that are used in this study are presented very briefly. Haldar (1981b) discussed these procedures in detail elsewhere.

4.1 Modeling of Randomness

Randomness in a parameter such as τ_R means that more than one outcome is possible; in other words, the actual outcome is (to some degree) unpredictable. The possible outcomes are usually a range of measured or observed values; moreover, within this range certain values may occur more frequently than others. Mathematical representation of a random variable is thus a primary task in any probabilistic formulation.

The mathematical representation of a random variable can be described graphically in the form of a histogram or frequency diagram. For a more general representation of the randomness, the frequency diagram can be fitted to some theoretical probability density function $f_X(x)$. By integrating the probability density function thus obtained, a probability distribution function, $F_X(x)$ can be obtained. $F_X(x)$ is the probability that the random variable X will have a value less than or equal to x.

To describe the probability density function uniquely, some parameters of the distribution need to be estimated. The estimation of these parameters, which are called statistics, is itself a major part of the uncertainty analysis. These parameters or statistics need to be evaluated or estimated on the basis of a set of observed data obtained from the population. Among the most important statistical parameters are the mean value μ, which denotes the average or expected value of the random variable, and the standard deviation σ, which denotes the dispersion of a random variable with respect to the mean value. Another commonly used parameter is the variance, which is the square of the standard deviation. The mean value and the variance can also be interpreted as, respectively, the centroidal distance and the central moment of inertia of the density function. For most engineering problems, the absolute dispersion about the mean value may not be as important as the ratio of the degree of dispersion to the mean value. Hence, the coefficient of vatiation (COV) is often preferred. COV is the ratio of the standard deviation to the mean value.

Different methods for estimating these parameters are available;

among these are the method of moments and the method of maximum likelihood. Unless stated otherwise, the method of moments is used to estimate the parameters of a distribution in this report.

In general, to develop a probabilistic model the underlying distribution of a random variable as well as the statistics needs to be known. In practice the choice of the probability distribution may be dictated by mathematical convenience. In many cases, the functional form of the required probability distribution may not be easy to determine, or more than one distribution may fit the available data. Under certain circumstances, the basis or properties of the physical process may suggest the form of the required distribution. In some cases, the required probability distribution may be determined empirically based entirely on the available observed data.

4.2 Estimation of Uncertainties

The methods available to estimate the uncertainties in a single random variable, function of a single random variable, multiple random variables, etc., have been discussed by Ayyub and Haldar (1982) and Haldar (1981b) elsewhere. They will not be discussed here. However, the General Approximate method that is used in this study is described briefly in the following section.

4.2.1 General Approximate Method

In many engineering problems, the complete statistical description of a random variable may not be known. The information may be limited to the mean and variance of the random variables X_i's in Eq. 4.1. In this case, the approximate mean and variance of the function Y would be practically useful and can be estimated by the General Approximate method

as described hereafter.

Let Y be a function of several random variables, that is:

$$Y = g(X_1, X_2, \ldots, X_n) \tag{4.1}$$

then expanding the function $g(X_1, X_2, \ldots, X_n)$ in a Taylor series about the mean values $\mu_{X_1}, \mu_{X_2}, \ldots, \mu_{X_n}$, one would obtain

$$Y = g(\mu_{X_1}, \mu_{X_2}, \ldots, \mu_{X_n}) + \sum_{i=1}^{n} (X_i - \mu_{X_i}) \frac{\partial g}{\partial X_i} + \frac{1}{2} \sum_{i=1}^{n} \sum_{j=1}^{n} (X_i - \mu_{X_i})(X_j - \mu_{X_j}) \frac{\partial^2 g}{\partial X_i \partial X_j} + \ldots \tag{4.2}$$

where the derivatives are evaluated at the mean values of X_i's.

Truncating the series at the linear terms, the first-order approximate mean and variance of Y can be obtained as

$$E(Y) \simeq g(\mu_{X_1}, \mu_{X_2}, \ldots, \mu_{X_n}) \tag{4.3}$$

which indicates that the mean of the function is approximately equal to the function of the means; and

$$\mathrm{Var}(Y) \simeq \sum_{i=1}^{n} E_i^2 \, \mathrm{Var}(X_i) + \sum_{i}^{n} \sum_{\neq j}^{n} E_i \, E_j \, \mathrm{COV}(X_i, X_j) \tag{4.4}$$

where E_i and E_j are constants and are the values of the partial derivatives $\partial g/\partial X_i$ and $\partial g/\partial X_j$, respectively, evaluated at the mean values. If X_i and X_j are statistically independent, for all i and j, Eq. 4.4 reduces to

$$\mathrm{Var}(Y) \simeq \sum_{i=1}^{n} E_i^2 \, \mathrm{Var}(X_i) \tag{4.5}$$

This approximate mean and variance may also be improved by including the higher order terms of the Taylor series expansion of $g(X_1, X_2, \ldots, X_n)$. If X_i and X_j are statistically independent, the second-order mean of Y would be

$$E(Y) \simeq g(\mu_{X_1}, \mu_{X_2}, \ldots, \mu_{X_n}) + \frac{1}{2} \sum_{i=1}^{n} \left(\frac{\partial^2 g}{\partial X_i^2}\right) \mathrm{Var}(X_i) \tag{4.6}$$

In many engineering problems, second-order mean and first-order variance would improve the accuracy of the estimation. Although the method is approximate, the method is very powerful and will be used in this study.

4.3 Regression Analysis

The regression analysis technique is used extensively in this report. Therefore, it is desirable to address some of the critical elements of a regression analysis.

When dealing with two or more variables, the functional relation between the variables is often of interest. However, if the variables are random, there will be no unique relationship between the variables. Thus, a probabilistic relationship between variables is necessary and can be developed using regression analysis techniques.

The functional relationship between the response or dependent variable and the regressor or independent variables can be developed using a scatter diagram (Montgomery and Peck, 1982). The unknown regression coefficients can be estimated by the method of least squares satisfying all the basic assumptions of regression analysis. The basic assumptions can be summarized as:

1. The true relationship between the dependent and independent variables or their transformations is linear, or at least may well be approximated by a straight line.

2. The error term ϵ has a zero mean. ϵ is a random variable representing the differences between the observed and the predicted values of the dependent variable.
3. The error term ϵ has a constant variance σ^2.
4. The errors are uncorrelated, and
5. The errors are normally distributed.

Assumptions 4 and 5 imply that the errors are independent random variables. Standard summary statistics, in particular the r^2 and $\hat{\sigma}^2$ values, and residual analysis can be used to determine how well the regression model satisfies the aforementioned assumptions. This will be discussed briefly in the following sections.

4.3.1 r^2-Value - Coefficient of Determination

The total variability (S_x) in the observations of a dependent variable X in a regression analysis has two components: the amount of variability in the observations $\{X_i\}$ accounted for by the regression line (SS_R) and the residual variation left unexplained by the regression line (SS_E). The total variability of X can be written as:

$$S_X = SS_R + SS_E \tag{4.7}$$

SS_R, generally known as the regression sum of squares, can be calculated as

$$SS_R = \sum_{i=1}^{n} (\hat{X}_i - \bar{x})^2 \tag{4.8}$$

in which n is the total number of observations, $\hat{X}_i$ is the predicted value of X for a given set of independent variables obtained from the

regression model and $\bar{x}$ is the mean value of X. SS_E, generally known as the error sum of squares, can be estimated as

$$SS_E = \sum_{i=1}^{n} (x_i - \hat{x}_i)^2 \tag{4.9}$$

in which x_i is the i-th observation. All other parameters were defined earlier.

The quantity r^2 is defined as

$$r^2 = \frac{SS_R}{S_X} = 1 - \frac{SS_E}{S_X} \tag{4.10}$$

Since S_X is a measure of the variability in X without considering the effect of the regressor variable Y, and SS_E is a measure of the variability in X after Y has been considered, then the r^2-value refers to the proportion of variation in X explained by the independent variables. Thus, $0 \leq r^2 \leq 1$, and when r^2 is close to 1 it implies that most of the variability in X is explained by the regression model.

4.3.2 Mean Square Error $\hat{\sigma}^2$

The unbiased mean square error, which is also sometimes called the residual mean square, can be estimated as

$$\hat{\sigma}^2 = \frac{SS_E}{n-2} \tag{4.11}$$

All the parameters have been described earlier. As can be seen from Eq. 4.9, when the error in the prediction is small, $\hat{\sigma}$ will be small. A smaller value of $\hat{\sigma}^2$ is always desirable.

5. PROBABILISTIC LIQUEFACTION MODEL

A three-dimensional probabilistic liquefaction model will be developed in several stages. They are described in the following sections.

5.1 Point Predictive Model for τ_R and τ_A

Seed and Idriss (1971) suggested a simplified deterministic procedure to evaluate the liquefaction potential of a site. It has some advantages as well as some shortcomings (Haldar and Miller, 1982a). Keeping its basic simplicity, this method is extended here in a probabilistic sense.

As discussed earlier, during earthquake shaking the average intensity of shear stress that will act at a point in a saturated sand deposit is τ_A. The shear resistance mobilized by the deposit is represented by τ_R. The equivalent uniform shear stress, τ_A, can be estimated as

$$\tau_A = S_L \, r_d \, \frac{\gamma_s h}{g} \, a_{max} \tag{5.1}$$

in which S_L = a factor to convert the maximum shear stress intensity to an equivalent uniform stress intensity that will act on a soil deposit for N_{eq} number of cycles during an earthquake; r_d = the stress reduction coefficient to consider the flexibility of the soil column under consideration; γ_s = the saturated unit weight of the soil; h = the depth of the soil element from the ground surface; g = the acceleration due to gravity; and a_{max} = the maximum ground acceleration.

τ_A as calculated by Eq. 5.1 will act on the soil element for a number of significant stress cycles, N_{eq}. The value of N_{eq} depends on the duration of ground shaking, and thus on the magnitude of the earthquake. The relationship of N_{eq} and earthquake magnitude will be discussed in more detail later.

The shear resistance of the soil element, τ_R, that will be mobilized to resist the applied shear stress can be evaluated from the shear strength parameter R. R can be defined as

$$R = \frac{R}{\sigma'_m D_r} \tag{5.2}$$

in which σ'_m = the average effective normal stress and D_r = the relativ density. The parameter R was introduced by Haldar and Miller (1982a). σ'_m can be estimated as

$$\sigma'_m = \frac{\sigma'_1 + \sigma'_2 + \sigma'_3}{3} \tag{5.3}$$

in which σ'_1, σ'_2, and σ'_3 = the effective stresses in three directions at a point in the deposit. Eq. 5.3 can be simplified as

$$\sigma'_m = \frac{1 + 2 K_o}{3} \sigma'_v \tag{5.4}$$

in which K_o = the coefficient of earth pressure at rest and σ'_v = the effective vertical stress at a point. The in situ value for R can be inferred from laboratory test results if the value for R measured in the laboratory is modified by a corrective factor, C_r, i.e.

$$R_{field} = C_r \cdot R_{Lab} \tag{5.5}$$

Replacing R_{field} by Eq. 5.2, the in situ shear resistance, τ_R, at a particular point in a deposit can be estimated from laboratory test results by the following expression:

$$\tau_R = C_r \, R_{Lab} \, \sigma'_m \, D_r \tag{5.6}$$

σ'_m and D_r values need to be estimated in the in situ conditions. Liquefaction will occur when τ_A is greater than τ_R.

5.2 Probabilistic Liquefaction Model

To develop a probabilistic model, the probabilistic characteristics of all the parameters in Eqs. 5.1 and 5.6 need to be evaluated. Assuming that the mean value and COV of each parameter are known, the following statistics of τ_A can be obtained assuming statistical independence between parameters in Eq. 5.1.

$$\mu_{\tau_A} = S_L \, \mu_{r_d} \, \mu_{\gamma s} \cdot h \, \frac{\mu_{a_{max}}}{g} \tag{5.7}$$

$$\Omega^2_{\tau_A} = \Omega^2_{r_d} + \Omega^2_{\gamma_S} + \Omega^2_{a_{max}} \tag{5.8}$$

The values of g, S_L and h are assumed to be known.

Because of the various simplifying assumptions and empirical approximations, the model represented by Eq. 5.6 is only an estimate of the in situ shear resistance of the soil mass. A corrective factor, N_{τ_R}, can be introduced such that

$$\tau_R = N_{\tau_R} \, \hat{\tau}_R \tag{5.9}$$

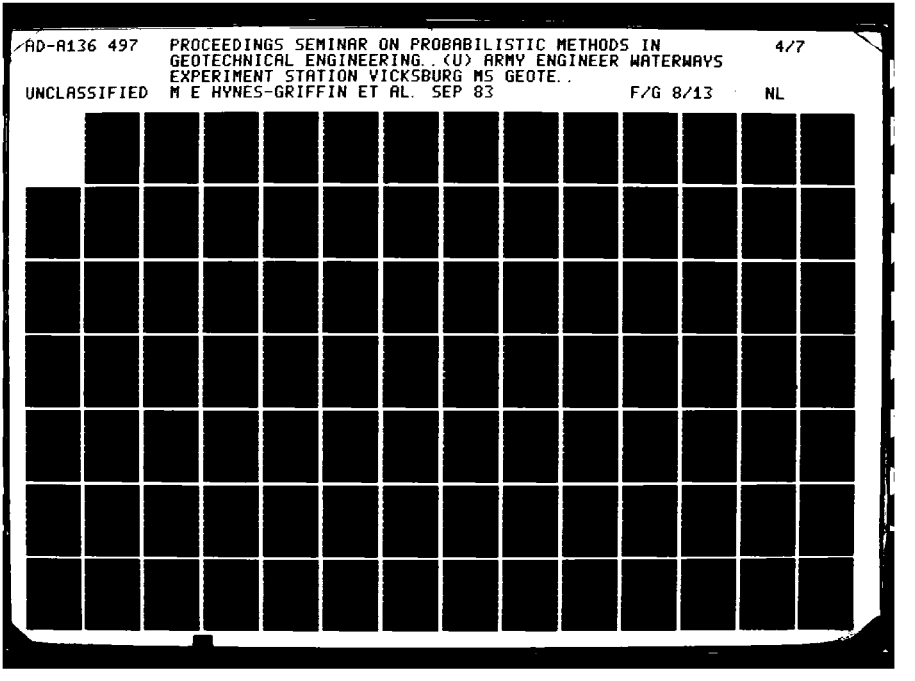
AD-A136 497
PROCEEDINGS SEMINAR ON PROBABILISTIC METHODS IN GEOTECHNICAL ENGINEERING..(U) ARMY ENGINEER WATERWAYS EXPERIMENT STATION VICKSBURG MS GEOTE..
4/7
UNCLASSIFIED
M E HYNES-GRIFFIN ET AL. SEP 83
F/G 8/13
NL

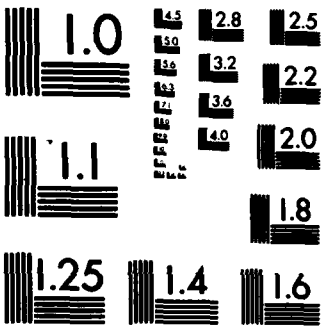

where $\hat{\tau}_R$ is the predictive model of τ_R defined by Eq. 5.6. Using first-order approximate analysis, the mean and COV of τ_R become

$$\mu_{\tau_R} = \mu_{N_{\tau_R}} \cdot \mu_{C_r} \cdot \mu_R \cdot \mu_{\sigma'_m} \cdot \mu_{D_r} \tag{5.10}$$

and

$$\Omega^2_{\tau_R} = \Omega^2_{N_{\tau_R}} + \Omega^2_{C_r} + \Omega^2_R + \Omega^2_{\sigma'_m} + \Omega^2_{D_r} \tag{5.11}$$

assuming N_{τ_R}, C_r, R, σ'_m and D_r are uncorrelated random variables.

Since τ_A and τ_R are individually random variables, the event $\{\tau_R \leq \tau_A\}$ is uncertain. Hence, the risk of liquefaction failure can be defined by the probability

$$p_f = p(\tau_R \leq \tau_A) \tag{5.12}$$

or

$$p_f = \int_o^\infty \int_o^{t_A} f_{\tau_R, \tau_A}(t_R, t_A)\, dt_R\, dt_A \tag{5.13}$$

where $f_{\tau_R, \tau_A}(t_R, t_A)$ is the joint density function of τ_R and τ_A. Haldar (1976) noted that τ_R and τ_A can be considered as statistically independent random variables for all practical purposes. Thus, Eq. 5.13 reduces to

$$p_f = \int_o^\infty \int_o^{t_A} f_{\tau_R}(t_R)\, f_{\tau_A}(t_A)\, dt_R\, dt_A \tag{5.14}$$

There is not sufficient data available to justify or ascertain a particular density function for τ_A or τ_R. However, reliability analysis is useful in a comparative rather than in an absolute sense. Hence, a prescribed density function for Eq. 5.14 would provide a consistent relative measure of risk. For the present reliability analysis, the primary objective is the systematic assessment of uncertainties associated with the liquefaction phenomenon and the development of a consistent basis by which design alternatives can be compared.

In this study, for the sake of simplicity, lognormal distributions are prescribed for τ_A and τ_R in estimating the probability of liquefaction. Therefore, it can be shown that for lognormal variates, Eq. 5.14 reduces to

$$p_f = 1 - \Phi\left(\frac{\ln\left[\frac{\mu_{\tau_R}}{\mu_{\tau_A}}\sqrt{\frac{1+\Omega_{\tau_A}^2}{1+\Omega_{\tau_R}^2}}\right]}{\sqrt{\ln\left[(1+\Omega_{\tau_R}^2)\ (1+\Omega_{\tau_A}^2)\right]}}\right) \tag{5.15}$$

where $\Phi(\ )$ is the standard normal cumulative distribution function.

It can be seen from Eq. 5.15 that the risk depends not only on the ratio of μ_{τ_R} to μ_{τ_A}, but also on the uncertainties in τ_R and τ_A, an aspect of the problem completely neglected by a deterministic approach.

5.3 Three-Dimensional Probabilistic Liquefaction Model

Soil deposits typically exhibit local variations about their average properties or about major trends (horizontally and vertically). Moreover, a sufficient volume of sand has to undergo a considerable amount of strain in order to produce a noticeable amount of damage at the referenced location. Thus, evaluation of the risk of liquefaction at just a point in the soil deposit may not be appropriate. The local random fluctuations in the soil properties affecting the liquefaction potential in the liquifiable volume must be considered. These random fluctuations of soil properties can be incorporated into the point reliability model developed in the previous section.

τ_A and τ_R represented by Eqs. 5.1 and 5.6, respectively, need to be estimated over a volume Δv. The spatial average of τ_R can be represented as

$$\tau_{R_{\Delta v}} = \frac{1}{\Delta v} \int_{\Delta x} \int_{\Delta y} \int_{\Delta z} \tau_R (x, y, z)\, dx\, dy\, dz \qquad (5.16)$$

in which $\tau_{R_{\Delta v}}$ = the spatial average over the volume Δv, $\Delta v = \Delta x \cdot \Delta y \cdot \Delta z$, and Δx, Δy, Δz are the lengths of the soil volume in the x, y and z directions, respectively. The spatial average of τ_A, denoted by $\tau_{A_{\Delta v}}$ can be evaluated in the same way.

The statistics of $\tau_{R_{\Delta v}}$ in terms of mean, variance and COV should be available to be used in a probabilistic model. They can be evaluated by using the following procedures. For simplicity of discussion, consider a soil property given by the random variable u(z). For the

liquefaction problem the soil property could be the relative density of the deposit. The local variations of u(z) can be expressed with the help of two parameters as shown in Fig. 5.1. It can be expressed as the point standard deviation σ_u of the soil properties and the scale of fluctuation θ_u, which measures the distance within which the soil property u(z) shows relatively strong correlation or persistence from point to point. The quantity θ_u is closely related to the average distance between intersections (crossings) of u(z) and the mean $\bar{u}$; small values of θ_u imply rapid fluctuations about the average, while large values of θ_u suggest that a slowly varying component is superimposed on the average value $\bar{u}$.

The scale of fluctuation, θ_u, can also provide a host of practical information; for example, to avoid wasteful redundancy in information gathering, sampling distances should be chosen in such a way that they are large in comparison with θ_u. On the other hand, when a soil property is being determined by two different tests, the locations of pairs of samples should be well within the correlation distance for maximum effectiveness.

The scale of fluctuation θ_u can be estimated in two ways. A procedure is described by Vanmarcke (1977) when observations of soil properties are available at equidistant intervals. This approach uses the concept of coefficient of correlation between values of u at two points. When points are located at very small intervals, the coefficient of correlation will be close to 1, and it usually decays as the distance increases. For an assumed theoretical correlation

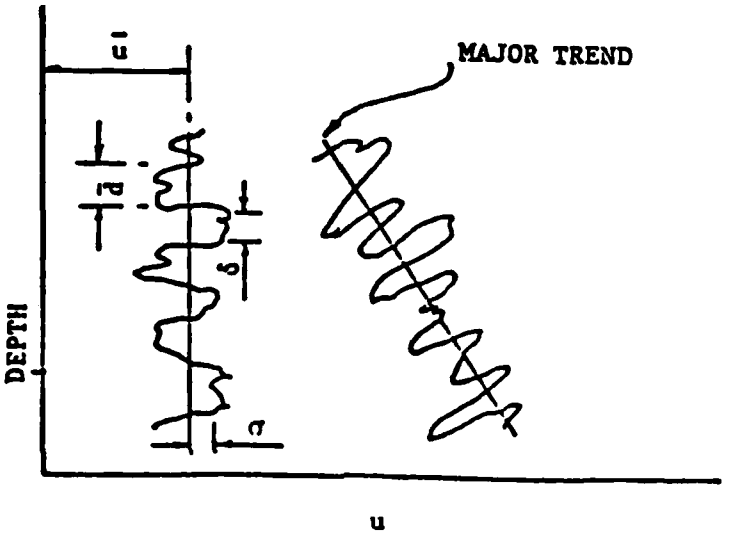

Fig. 5.1 Main Descriptors of the Local Random Fluctuations of the Soil Property, u

function model, the scale of fluctuation θ_u can be estimated. The other method can be used to estimate θ_u if a reasonably complete record of u(z) is available. It is based on the approximate relationship between the scale of fluctuation, θ_u, and the average distance, $\bar{d}$, between the intersections of the fluctuating property, u(z), and its mean $\bar{u}$. The average distance between mean crossings is approximately (Vanmarcke, 1977)

$$\bar{d} \simeq \frac{\pi}{2} \theta_u \simeq 1.25\, \theta_u \tag{5.17}$$

The details of these two methods will not be discussed here but can be found elsewhere (Vanmarcke, 1977, 1979).

A deposit could have three different scales of fluctuation in the three directions. The scales of fluctuation will be used to estimate the statistics of spatially averaged soil properties.

For a statistically homogeneous soil deposit the point mean $\bar{u}$ and variance Var(u) of a random variable can be evaluated as

$$\bar{u} = \frac{1}{N} \sum_{i=1}^{N} u_i \tag{5.18}$$

and

$$\text{Var}\,(U) = \frac{1}{(N-1)} \sum_{i=1}^{N} (u_i - \bar{u})^2 \tag{5.19}$$

in which N = the total number of observations.

The spatial mean, $\bar{u}_{\Delta v}$, and the spatial variance, $\text{Var}(u_{\Delta v})$, can be shown to be

$$\bar{u}_{\Delta v} = \bar{u} \tag{5.20}$$

and

$$\mathrm{Var}(u_{\Delta v}) = \Gamma_u^2 \ (\Delta v)\ \mathrm{Var}(u) \tag{5.21}$$

in which $\Gamma_u^2\ (\Delta v)$ is called the variance function. It describes the decay of the variance of the spatial average as the averaging dimensions increase. If the correlation structure of u(x, y, x) is separable, then Eq. 5.21 reduces to

$$\mathrm{Var}(u_{\Delta v}) = \Gamma_u^2\ (\Delta x)\ \Gamma_u^2\ (\Delta y)\ \Gamma_u^2\ (\Delta z)\ \mathrm{Var}(u) \tag{5.22}$$

in which $\Gamma_u^2\ (\Delta x)$, $\Gamma_u^2\ (\Delta y)$, and $\Gamma_u^2\ (\Delta z)$ are the variance functions in the X, Y, and Z directions, respectively.

The variance function can be calculated from the information on the scale of fluctuation in a given direction. For all practical purposes, the variance function in the X direction can be estimated as

$$\begin{aligned} \Gamma_u^2(\Delta x) &= 1.0; \ \Delta x \le \theta_{u_x} \\ &= \frac{\theta_{u_x}}{\Delta x}; \ \Delta x > \theta_{u_x} \end{aligned} \tag{5.23}$$

in which θ_{u_x} is the scale of fluctuation of u in the X direction. The variance functions in the other two directions can be estimated similarly from the knowledge of the corresponding scale of fluctuation.

The concept discussed here can be applied to Eq. 5.16 to estimate the statistics of $\tau_{R_{\Delta v}}$. Since τ_R is a function of R, σ_m', and D_r, $\tau_{R_{\Delta v}}$ is also a function of these variables. Each variable can be

treated separately similar to Eqs. 5.18 through 5.23, and all the required statistics can be estimated. Using first-order approximate analysis, the mean value of $\tau_{R_{\Delta v}}$ can be shown to be

$$\tau_{R_{\Delta v}} \simeq \bar{R} \cdot \bar{\sigma}'_m \cdot D_r \tag{5.20}$$

The spatial variability is expected to be much greater for D_r than for the other parameters in Eq. 5.6. For practical considerations and mathematical simplicity, only the spatial variability of D_r is considered here, although the spatial variability of other parameters can be considered similarly. Using first-order approximation analysis and assuming statistical independence among the parameters, the spatial variance of τ_R over the volume Δv becomes

$$\mathrm{Var}\left(\tau_{R_{\Delta v}}\right) = \bar{\tau}^2_{R_{\Delta v}} \left[\Omega^2_R + \Omega^2_{\sigma'_m} + \Gamma^2_{D_{r_x}}(\Delta x) \cdot \Gamma^2_{D_{r_y}}(\Delta y) \cdot \Gamma^2_{D_{r_z}}(\Delta z) \cdot \Omega^2_{D_r}\right] \tag{5.25}$$

in which Ω represents the point coefficient of variation (COV). The variance function of D_r in the X, Y, and Z directions can be estimated using Eq. 5.23 from the information on the scale of fluctuation in the three directions.

In a similar manner, the spatial mean and variance of $\tau_{A_{\Delta V}}$ can be estimated.

It can be shown that

$$\tau_{A_{\Delta v}} \simeq S_L \cdot \bar{r}_d \cdot \gamma_s \cdot h \cdot \frac{\bar{a}_{max}}{g} \tag{5.26}$$

and

$$\mathrm{Var}\left(\tau_{A_{\Delta v}}\right) \simeq \bar{\tau}^2_{A_{\Delta v}} \left[\Omega^2_{r_d} + \Omega^2_{\gamma_s} + \Omega^2_{a_{max}}\right] \tag{5.27}$$

In Eqs. 5.26 and 5.27, the parameters S_L, h, and g are assumed to be constant. Also, in Eq. 5.27 the spatial variability of a_{max} and r_d can be considered negligible. The spatial variability of γ_s is not considered here directly; however it is considered indirectly in the spatial variability of D_r.

The probability that the soil volume Δv will liquefy is given by the probability of the event $\tau_{R_{\Delta v}} \leq \tau_{A_{\Delta v}}$. Since the statistics of $\tau_{A_{\Delta v}}$ and $\tau_{R_{\Delta v}}$ cannot be adequately defined beyond the first two moments, for simplicity lognormal distributions can be prescribed for $\tau_{A_{\Delta v}}$ and $\tau_{R_{\Delta v}}$ in estimating the probability of liquefaction. The probability of liquefaction is thus given by

$$P_{f_{\Delta v}} = 1 - \Phi\left(\frac{\ln\left[\dfrac{\mu_{\tau_{R_{\Delta v}}}}{\mu_{\tau_{A_{\Delta v}}}} \sqrt{\dfrac{1+\Omega^2_{\tau_{A_{\Delta v}}}}{1+\Omega^2_{\tau_{R_{\Delta v}}}}}\right]}{\sqrt{\ln\left[\left(1+\Omega^2_{\tau_{R_{\Delta v}}}\right)\left(1+\Omega^2_{\tau_{A_{\Delta v}}}\right)\right]}}\right) \tag{5.28}$$

where $\Phi(\ )$ is the standard normal cumulative distribution function.

Equation 5.28 can be used to estimate the risk of liquefaction in a volume of sand when both the maximum ground acceleration and the earthquake magnitude at a site are known. Basically, Eq. 5.28 can be used to investigate past case studies.

The procedures described in the previous section would be inadequate if a site has to be designed for future earthquakes where a_{max} and N_{eq} or M are unknown. The risk of liquefaction can still be estimated if the uncertainties in these parameters are incorporated into the model. Using the theorem of total probability, the probability of liquefaction of a soil volume can be calculated as

$$P_f = \int_{(n_{eq})_o}^{(n_{eq})_u} \int_0^{a_{max}} (P_{f_{\Delta v}} \mid a_{max}, n_{eq}) \, f_{A_{max}}(a_{max}) \, f_{N_{eq}}(n_{eq}) \, da_{max} \, dn_{eq} \qquad (5.29)$$

in which $f_{A_{max}}(a_{max})$ and $f_{N_{eq}}(n_{eq})$ are the density functions of A_{max} and N_{eq}, respectively. $(n_{eq})_u$ and $(n_{eq})_o$ are the values of N_{eq} corresponding to the upper and lower bound magnitudes of the earthquakes. The conditional probability, $(P_{f_{\Delta v}} \mid a_{max}, n_{eq})$, can be estimated using Eq. 5.28.

Eqs. 5.28 and 5.29 can be evaluated only when the uncertainty associated with all the parameters is quantified. As mentioned earlier, a considerable amount of uncertainty is expected in the estimation of several parameters in a liquefaction model. Among them, the in situ cyclic shear strength, in situ relative density and the design earthquake acceleration are the most important. They are discussed in the following sections.

6. UNCERTAINTY ANALYSIS

All parameters used in the three-dimensional probabilistic model are random variables. The major sources of uncertainties affecting these parameters are evaluated in this section.

6.1 Uncertainty of Resistance Parameters

6.1.1 Relative Density

The relative density of sand is an important parameter in a liquefaction study. However, due to the error-prone definition of the relative density (Haldar and Tang, 1979; Haldar and Miller, 1982a), significant error can be incurred with the present methods of determining in situ relative density. In situ relative density can be estimated in two ways: (1) direct method and (2) indirect method.

Using the direct method, Haldar and Tang (1979b) showed the mean and COV of the relative density D_r to be

$$\bar{D}_r \cong \frac{\bar{\gamma}_{max}}{\bar{\gamma}} \frac{\bar{\gamma} - \bar{\gamma}_{min}}{\bar{\gamma}_{max} - \bar{\gamma}_{min}} \tag{6.1}$$

$$\text{and } \Omega^2_{D_r} \cong E_1^2 \Omega^2_{\gamma_{max}} + \left[\frac{(E_1 + 1)(1 - \bar{D}_r)}{\bar{D}_r}\right]^2 \cdot \Omega^2_{\gamma_{min}} + \left[\frac{E_1 + 1}{\bar{D}_r} - 1\right]^2 \cdot \Omega^2_{\gamma}$$

$$= E_1^2\Omega^2_{\gamma_{max}} + E_2^2\Omega^2_{\gamma_{min}} + E_3^2\Omega_{\gamma}^2 \tag{6.2}$$

in which $E_1 = \bar{\gamma}_{min}/(\bar{\gamma}_{max} - \bar{\gamma}_{min})$; and γ, γ_{max}, and γ_{min} are assumed to be mutually independent. The coefficients E_1, E_2, and E_3 could be interpreted as the amplification factors for the uncertainties in each of these densities, respectively. The uncertainty in γ is amplified more than that in γ_{max} or γ_{min}. These densities are generally

evaluated with the ASTM D 2049-69 method. Tavenas, et al. (1972) estimated that the COVs of γ_{min} and γ_{max} are 0.018 and 0.023, respectively, based on 62 tests. Moreover, they suggested that the intralaboratory (reproducibility) error is approximately one-third of the interlaboratory error. Thus, the combined uncertainties, $\Omega_{\gamma_{min}}$ and $\Omega_{\gamma_{max}}$, may be estimated as 0.019 and 0.025, respectively.

The uncertainties associated with the existing procedures for estimating the in situ density of sands under the water table were discussed in great detail by Haldar (1976) and Haldar and Tang (1979b). It was noted that the in situ density generally cannot be estimated within $\pm$ 2 pcf with present techniques.

Considering all the aforementioned uncertainties, Haldar and Tang (1979b) observed that the uncertainties in D_r in terms of COV could be of the order of 0.11 to 0.36. This uncertainty is not negligible.

In many practical cases, information on in situ γ values may not be available, at least in the initial stage of the project. Thus, a reliable indirect method to estimate the relative density is a necessity from a practical point of view.

The Standard Penetration Test (SPT) values are routinely used to estimate relative density indirectly. Haldar and Miller (1982a) summarized several relationships available between the relative density and SPT-values. The most commonly used relationships are Gibbs and Holtz's equation (1957), Bazaraa's equations (1967), and the Waterways Experiment Station (WES) equation (Marcuson and Bieganousky, 1977a, 1977b). The merits and demerits of each of these equations

have been discussed by Haldar and Miller (1982a, 1982e). The WES equation is based on reliable information. However, it is based on non-standard procedures (freefall of the hammer was obtained by trip hammer mechanism). Moreover, it has never been calibrated to predict in situ relative density.

Haldar and Miller (1982a), using WES test results, proposed a new relationship between SPT values and D_r values. They estimated the relative density by first calculating the in place dry density Γ from a Γ vs. SPT relationship. Their results can be summarized as follows:

$$E(\Gamma \mid N=n,\ \Gamma_{max} = \gamma_{max},\ \Gamma_{min} = \gamma_{min}, \textstyle\sum_v{}' = \sigma_v') = \frac{5.50116 + n^{1/2} + 0.32280\ \gamma_{min} - 0.06053\ (\gamma_{max} - \gamma_{min})}{0.36243 + 0.00278\ \sigma_v'} \tag{6.3}$$

and

$$\mathrm{Var}\ (\Gamma \mid N = n,\ \Gamma_{max} = \gamma_{max},\ \Gamma_{min} = \gamma_{min}, \textstyle\sum_v{}' = \sigma_v') = \frac{0.183}{(0.36245 + 0.00278\sigma_v')^2} \tag{6.4}$$

In the proposed liquefaction model, the mean and COV of the relative density need to be known. They can be estimated at this stage in the following way:

$$E(D_r \mid N = n,\ \Gamma_{max} = \gamma_{max},\ \Gamma_{min} = \gamma_{min}, \textstyle\sum_v{}' = \sigma_v') = \frac{\gamma_{max}}{E(\Gamma)} \times \frac{\left[E(\Gamma) - \gamma_{min}\right]}{\left[\gamma_{max} - \gamma_{min}\right]} \tag{6.5}$$

and

$$\delta^2_{D_r} = E_3^2 \ \Omega_\gamma^2 \tag{6.6}$$

where

$$E_3 = \left(\frac{\left[\frac{\gamma_{min}}{(\gamma_{max} - \gamma_{min})} + 1 \right]}{E(D_r)} \right)^{-1} \tag{6.7}$$

$E(\Gamma)$, Ω_γ, and $E(D_r)$ can be calculated by using Eqs. 6.3, 6.4, and 6.5, respectively. Eq. 6.5 can be used to estimate the relative density indirectly in the laboratory.

Eq. 6.5 needs to be calibrated to estimate in situ relative density. In the WES study, the standard penetration test was conducted with a hydraulically driven trip hammer; in the field, however, the hammer is raised and lowered by a rope and cathead system. Tokimatsu and Yoshimi (1981) have shown that, on the average, the SPT value measured by the rope and cathead system may be greater by 2.7 blows than that measured by the trip hammer, particularly when SPT values are greater than 10 blows. In light of this observation, Eq. 6.5 or in essence Eq. 6.3 needs to be modified. It is proposed here that the value of N in Eq. 6.3 should be modified in the following way:

$$N = N_{th} = N_{rc}; \ N \leq 10 \tag{6.8}$$

and

$$N = N_{th} = N_{rc} - 2.7; \ N > 10 \tag{6.9}$$

where N_{th} is the SPT value as measured by the trip hammer system, and N_{rc} is the SPT value as measured in the field with a rope and cathead system.

Considering the values of D_r actually measured in the field versus the values of D_r predicted from Eq. 6.5, Haldar and Miller (1982e) estimated the total COV of the in situ relative density as

$$\Omega^2_{D_r} = \delta^2_{D_r} + \Delta^2_{D_r} \tag{6.10}$$

in which δ_{D_r} can be calculated using Eq. 6.6 and $\Delta^2_{D_r}$ can be shown to be

$$\Delta^2_{D_r} = 0.95393 - 1.62679\ \bar{D}_r + 0.85357\ \bar{D}_r^{\,2} \tag{6.11}$$

Eq. 6.5 can be used to estimate the mean relative density. All the presently available methods used to estimate the in situ relative density indirectly are shown in Figure 6.1. The predictability of the Haldar and Miller relationship is much better than the other available methods.

6.1.2 Shear Strength Parameter

The shear strength parameter R can be estimated in two stages: (1) developing a laboratory model using laboratory test results, and (2) calibrating this laboratory model to consider the in situ field conditions. Since the large-scale shaking table tests reproduce in situ conditions very closely (Haldar and Miller, 1982b), only test results obtained from the large-scale shaking table tests are considered for developing the shear resistance model. Also, in this study, the

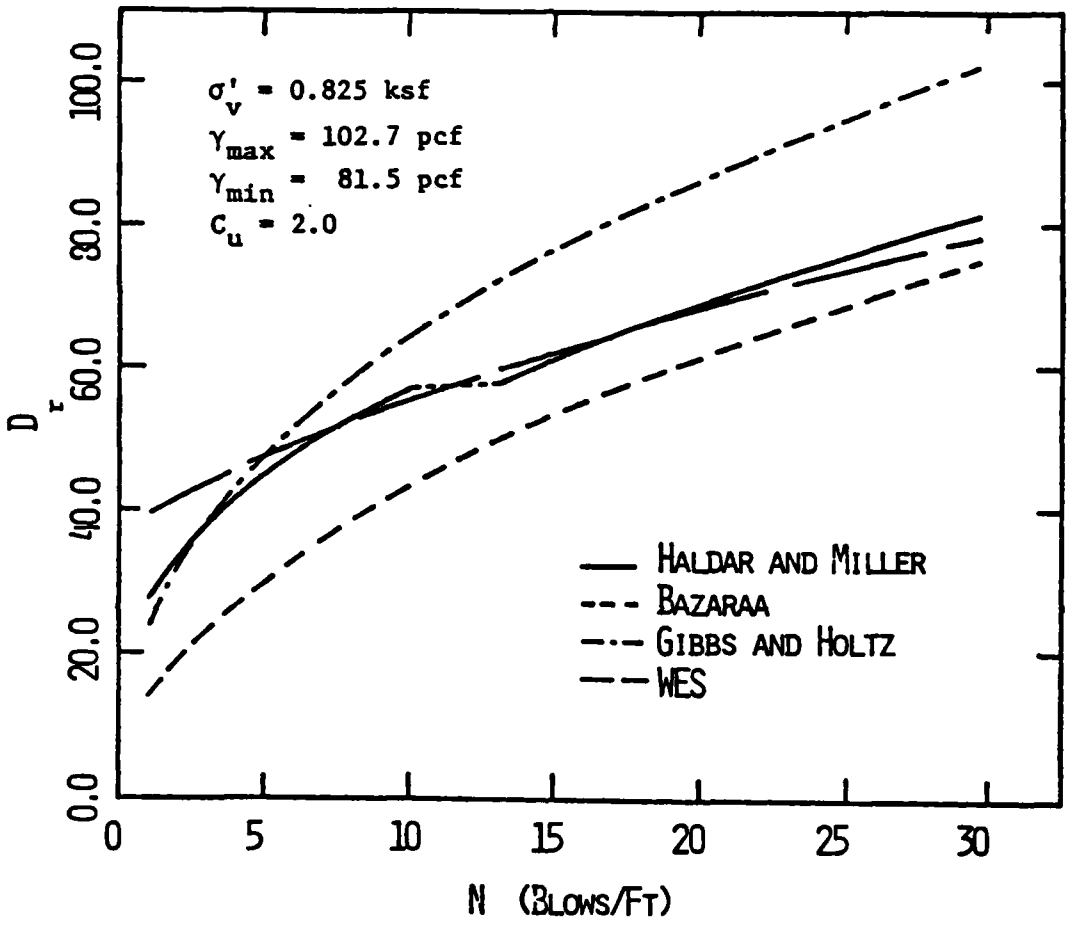

Fig. 6.1 Comparison of D_r -N Relationships

model to estimate the R parameter is developed considering the initial liquefaction failure criterion.

Haldar and Miller (1982a) proposed a model to estimate the shear strength parameter in the laboratory. They developed the model considering the effect of system compliance, sample preparation, mean grain size, multidirectional earthquake shaking, and secondary factors including the frequency of the uniform cyclic load, shape of the uniform cyclic load, grain size distribution, grain shape, etc. Considering the effects of all these factors, the mean and variance of the estimater of R, $\hat{R}$, can be shown to be

$$E(\hat{R} \mid N_{eq}, D_{50}) = 0.9 \times \left(0.7309 - 0.08778 \text{ Ln } (n_{eq})\right) \times \left(0.750 + 1.01\, d_{50} - 0.878 \cdot d_{50}^{2}\right) \; ; \quad (6.12)$$

$$2 \leq N_{eq} \leq 63, \; 0.06 \leq D_{50} \leq 0.6,$$

and

$$\text{Var } (\hat{R} \mid N_{eq}, D_{50}) = 0.000610 + (0.10^2 + 0.152^2) \times E(\hat{R} \mid N_{eq}, D_{50})^2 \quad (6.13)$$

Haldar and Miller (1982a) noted that the laboratory model (Eq. 6.12) does not consider the site-specific characteristics, e.g., cementation, age, seismic history of the deposit, etc. However, it is very difficult to make a general statement on the effect of these factors on the shear strength parameter for all deposits. In most cases, they increase the shear resistance of the deposit. In the absence of any direct information on the site-specific characteristics,

the laboratory model is expected to give a very conservative estimate of the in situ shear strength parameter in most cases. Moreover, the effect of some of the aforementioned parameters will be considered indirectly in the SPT value obtained from the site. However, the site-specific characteristics do increase the level of uncertainty in the estimation of the R parameter. A COV of 0.10 is considered here for the site-specific characteristics.

It has been assumed so far that N_{eq}, the number of earthquake-induced uniform stress cycles, is known. However, as will be discussed in Section 6.2.2 a considerable amount of uncertainty is expected in the estimation of N_{eq} (Eq. 6.24).

Thus, considering the effects of all major factors, the mean in situ shear resistance parameter, R, of a deposit can be estimated as

$$E(R|N_{eq}, D_{50}) = E(\hat{R}|N_{eq}, D_{50}) \tag{6.14}$$

and

$$Var(R|N_{eq}, D_{50}) = 0.000610 + 0.0431 \times E(\hat{R}|N_{eq}, D_{50})^2 + 0.0077 \times \Omega^2_{(N_{eq}|M)} \tag{6.15}$$

where $E(\hat{R}|N_{eq}, D_{50})$ can be estimated from Eq. 6.12, and $\Omega_{(N_{eq}|M)}$ can be estimated from Eq. 6.24.

6.1.3 Mean Effective Overburden Pressure

Eq. 5.4 can be used to estimate the mean effective overburden pressure, σ'_m. The mean and variance of σ'_m can be shown to be

$$\bar{\sigma}'_m = \frac{1 + 2K_o}{3} \bar{\sigma}'_v \tag{6.16}$$

and

$$\mathrm{Var}(\sigma'_m) = \left(\frac{1 + 2K_o}{3}\right)^2 \cdot \mathrm{Var}(\sigma'_v) \tag{6.17}$$

K_o is assumed to be a constant in Eqs. 6.16 and 6.17. The mean and variance of the effective overburden pressure, σ'_v, can be estimated as

$$\bar{\sigma}'_v = \bar{\gamma}_s h - \gamma_W (h - \bar{h}_{WT}) \tag{6.18}$$

and

$$\mathrm{Var}(\sigma'_v) = \mathrm{Var}\ (\gamma_s)\ h^2 + \mathrm{Var}(h_{WT})\ \gamma_W^2. \tag{6.19}$$

in which h = depth being considered; γ_s = the saturated unit weight weight of the soil deposit; γ_W = the unit weight of water; and h_{WT} = the depth of the water table from the ground surface. For this study, h and γ_W are assumed to be known, and Ω_{γ_s} and $\Omega_{h_{WT}}$ are considered to be 0.01 and 0.20, respectively (Haldar and Miller, 1982a).

6.2 Uncertainty of Load Parameters

For a liquefaction study, the magnitude and duration of the future earthquake, as well as the maximum ground acceleration at a particular site within a specified time period, need to be estimated. In the following sections, models and procedures for estimating the earthquake loading parameters are described.

6.2.1 Earthquake Magnitude

The objective of this section is to formulate a procedure for obtaining the probability distribution of the annual maximum earthquake magnitude. The distribution of magnitude M is needed to determine the distribution of the equivalent number of stress cycles N_{eq}.

The probability distribution of the annual largest magnitude $F_{M_{max}}(m)$ can be estimated as (Haldar, 1976):

$$F_{M_{max}}(m) = \sum_{n=0}^{\infty} \frac{e^{-\nu}(\nu)^n}{n!} [F_M(m)]^n \qquad (6.20)$$

$$= \exp(-\nu e^{-\beta m}); \; m \geq 0$$

in which ν = the mean occurrence rate of earthquakes in a region; n = the number of occurrences with magnitude m or greater; and β = the slope of the earthquake magnitude recurrence line (Derkiureghian and Ang, 1977). Assuming earthquakes with magnitudes smaller than m_o have no engineering importance, and that from a practical point of view the magnitude cannot exceed an upper bound magnitude m_u, the density function of M_{max} can be shown to be (Haldar, 1976):

$$f_{M_{max}}(m) = C \cdot \frac{dF_{M_{max}}(m)}{dm}$$

$$= C \cdot [\exp(-\nu e^{-\beta m})] \times [\nu \beta e^{-\beta m}];$$

$$m_o \leq m \leq m_u \qquad (6.21)$$

$$= 0 \text{ elsewhere}$$

where

$$C = \frac{1}{\exp(-\nu e^{-\beta m_u}) - \exp(-\nu e^{-\beta m_o})} \tag{6.22}$$

6.2.2 Number of Equivalent Significant Cycles in Strong Motion Earthquake, N_{eq}

An earthquake loading pattern is extremely irregular. The use of the actual earthquake loading in the laboratory may not be practical in many cases for the following reasons:

(i) The exact shear stress-time history of a future earthquake at a particular site is unknown.

(ii) Assuming a given time history of earthquake acceleration, the induced shear stress-time history may vary from site to site.

(iii) Even if a shear stress-time history is assumed, it is very difficult and expensive to duplicate this loading on a soil specimen in the laboratory.

Moreover, in the past a considerable number of laboratory investigations were carried out under uniform cyclic loading conditions to predict the in situ soil behavior under any dynamic loading, including earthquake loading conditions. The past research results can be utilized properly only when a successful correlation between the two loading conditions can be found.

The underlying principles of converting the irregular-patterned earthquake motions to the equivalent number of uniform cycles N_{eq} were well explained by Lee and Chan (1972). According to Lee and Chan,

"N_{eq} refers to that number of uniform cycles of stress intensity τ_{av}, which if applied to an element of soil in the field or a sample of the same soil in the laboratory, would have the same effect in terms of the soil strength or deformation as if the actual train of irregular cyclic shear stresses were applied." This concept of N_{eq} is essentially based on Miner's damage rule. In an earthquake engineering problem, it may be convenient to base N_{eq} calculations on acceleration rather than on stress-time histories because of the direct proportionality between acceleration, force and stress.

When the uniform cycles of stress intensity concept was used in solving problems related to earthquake excitation, some implicit assumptions were made. They include (i) the ground motion is uniform at all sites in the same general area; (ii) the stress-time history at the depth of interest is directly proportional to the acceleration recorded at or near the ground surface; and (iii) for all soils, the laboratory liquefaction test data results can be represented by a single normalized curve relating stress ratio or stress level S_L to the number of cycles causing liquefaction.

These assumptions have been studied extensively by Annaki and Lee (1977), Lee and Chan (1972) and Haldar and Tang (1981). They will not be repeated here. However, some questions need to be addressed in converting earthquake motions to uniform cyclic motion. They are: (i) would the value of N_{eq} be sensitive to the shape of the soil strength curve?, (ii) what stress level S_L should be used?, (iii) how would N_{eq} vary with the magnitude of the earthquake?, and (iv) if past

earthquake records are used to find a relationship between N_{eq} and the earthquake magnitude, which one or both of the two horizontal records should be considered?

Haldar and Tang (1981) studied the problem in great detail. They concluded that if the stress level S_L is chosen to be 75% of the maximum stress, the uncertainty in the soil strength curve would not have a significant effect on the N_{eq} versus M relationship. They also found that N_{eq} could be estimated adequately by considering the component of excitation containing the peak acceleration. They proposed an N_{eq} versus M relationship as:

$$E(N_{eq}|M=m) = 106.08-36.42m + 3.312\ m^2$$

$$5.0 \leq M \leq 8.25 \qquad (6.23)$$

and the corresponding $Var(N_{eq}|M) = 29.05$. When M is less than 5.0, N_{eq} is assumed to be 6.0 cycles. Considering a COV of 0.05 to represent any prediction error associated with the form of Eq. 6.23, the uncertainty in N_{eq} in terms of COV can be shown to be (Haldar and Tang, 1981):

$$\Omega_{N_{eq}|M=m} = \sqrt{0.05^2 + \frac{29.05}{[E(N_{eq}\,|\,M=m)]^2}} \qquad (6.24)$$

Combining Eqs. 6.21 and 6.23, the density function of N_{eq} can be found to be (Haldar and Miller, 1982a):

$$f_{N_{eq}}(n_{eq}) = C\left[\exp\left\{-\nu \exp\left[-\beta\left(5.5 + \frac{1}{2}\sqrt{1.21\ln n_{eq} - 7.20}\right)\right]\right\}\right]$$

$$\times \left[\nu\beta \exp\left\{-\beta\left(5.5 + \frac{1}{2}\sqrt{1.21\ln n_{eq} - 7.20}\right)\right\}\right]$$

$$\times \left[\frac{1.21}{4}(1.21\ln n_{eq} - 7.20)^{-\frac{1}{2}}\right]; \; n_{eq} \geq 6.0 \qquad (6.25)$$

6.2.3 Maximum Acceleration

The maximum acceleration a_{max} at a particular site may be estimated by identifying all potential sources of earthquakes in the vicinity of the site. Consideration should be given to the earthquake magnitude, the distance of each source of earthquakes from the site, the direction of fault slip, if any, and the attenuation equation applicable for the region under consideration. The objective of this section is to determine the maximum acceleration a_{max} such that the probability of exceeding this intensity at the site is within a specified limit.

Several researchers (Cornell, 1968; Derkiureghian and Ang, 1977) have studied this problem. Analytical models were proposed by Cornell (1968) and by DerKiureghian and Ang (1977), considering different types of sources (i.e., fault lines, areal sources, and point sources), each having the magnitude distribution and activity rate assessed based on statistical data. They also used an attenuation equation to relate site intensity to magnitude and focal distance. Cornell's model does not consider that tectonic earthquakes are caused by the sudden release of built-up elastic strain in the earth's crust and

originate as slips along geologic faults. He assumed that the energy released during an earthquake is concentrated at a point. DerKiureghian and Ang's model instead assumed that the slip length for a large earthquake may be several hundred kilometers, and the greatest contribution to the intensity at the site might be caused by the slip that was closest to the site. Since DerKiureghian and Ang's model (line source model) is more general, and Cornell's model (point source model) is a special case of the line source model, the former is chosen for this reliability study.

A typical result from this study would be acceleration in terms of return period or annual probability of exceedence of the given acceleration as shown in Fig. 6.2. For simplicity of discussion, the relationship shown in Fig. 6.2 for the San Francisco Bay area can be expressed mathematically as

$$\ln[P(A_{max} > a_{max})] = - 0.12202 - 18.013a_{max} + 24.291a_{max}^2 - 13.703a_{max}^3 \quad (6.26)$$

Using Eq. 6.26 and normalizing the relationship so that the area under the density curve of A_{max} is unity, the density function of A_{max} for the San Francisco Bay area can be expressed as

$$f_{A_{max}}(a_{max}) = [\exp(0.12202)]\,[\exp(- 0.12202 - 18.013a_{max} + 24.291a_{max}^2 - 13.703a_{max}^3)]\,[+ 18.013 - 48.582a_{max} + 41.109a_{max}^2] \quad (6.27)$$

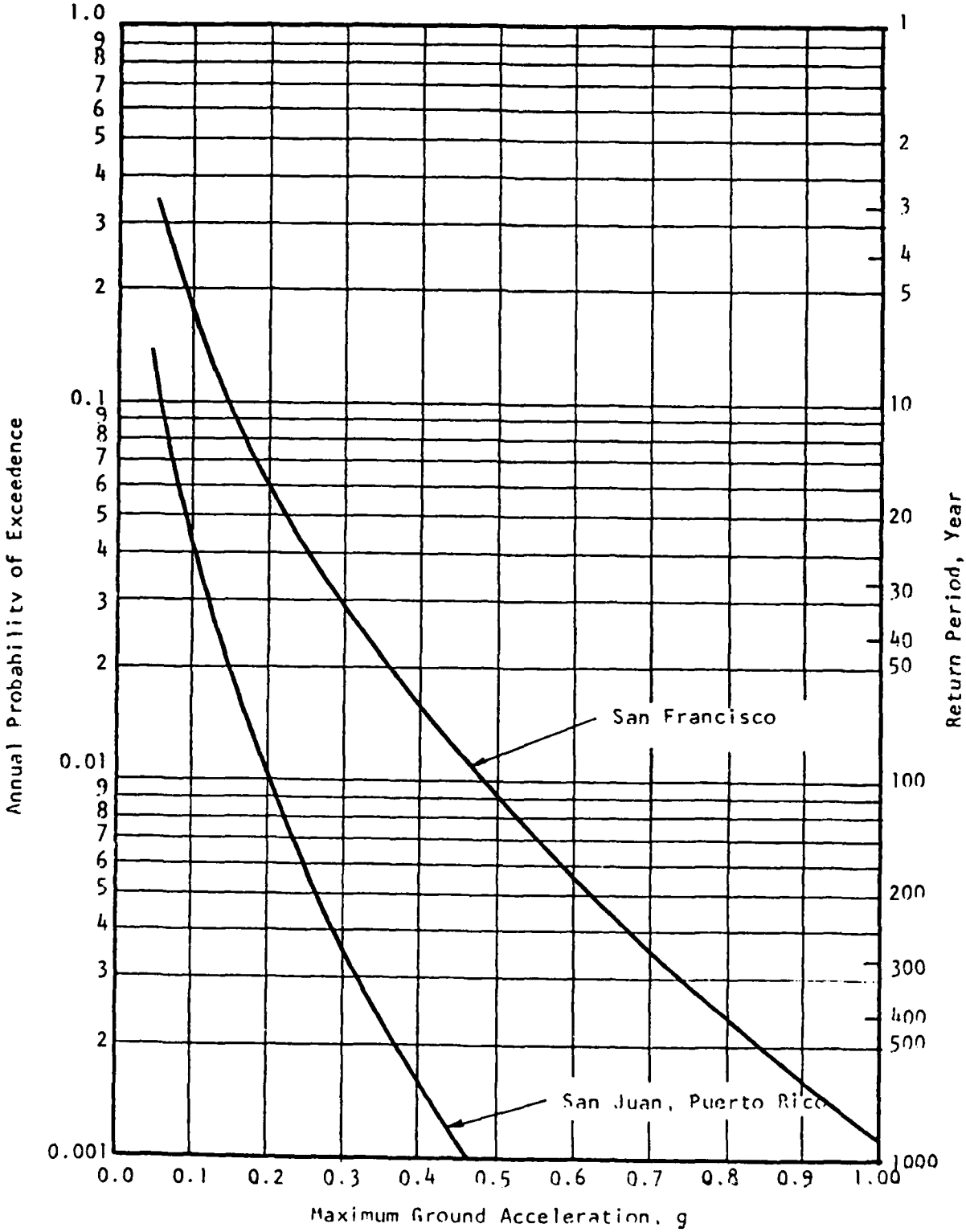

Fig. 6.2 Estimated Risks for Maximum Ground Acceleration for San Francisco and San Juan, Puerto Rico

6.2.4 Stress Reduction Coefficient r_d

Seed and Idriss (1971) reported a range of values of r_d, calculated for a wide variety of earthquake motions and soil conditions. The average curve can be mathematically represented by the following equation:

$$\mu_{r_d} = 10^{-4} (9995.7 - 22.857h + 0.707h^2 - 0.025h^3) \quad (6.28)$$

in which h = the depth under consideration in feet. The standard deviation of r_d can be shown to be (Haldar, 1976):

$$\sigma_{r_d} = \exp(\frac{h-84}{14.5}) \quad (6.29)$$

7. DESIGN EXAMPLE

A three-dimensional probabilistic liquefaction model is developed in Section 5. The uncertainty associated with each parameter in the proposed model is quantified in Section 6. The stage is now set to explain the model with the help of an example.

A site in Niigata, Japan which liquefied during the 1964 earthquake is considered here. This site is selected because all the relevant information was identified by Haldar (1976).

The site experienced 0.16 g maximum ground acceleration and the magnitude of the earthquake was 7.5. The SPT-value of 6 was measured at the critical depth 20 ft. The depth of the water table was 3 ft. from the ground surface. The saturated unit weight and the mean grain size, D_{50}, were considered to be 120 pcf and 0.26 mm, respectively (Haldar, 1976). The maximum and minimum dry densities of the deposit are considered to be 102.7 pcf and 81.5 pcf, respectively from indirect information. The scales of fluctuation, Θ_x, Θ_y, and Θ_z cannot be estimated from the site. The scales of fluctuation in the two horizontal directions are assumed to be the same. Θ_x, Θ_y, and Θ_z are considered to be 120 ft., 120 ft., and 7 ft., respectively. The volume of the liquefied sand is assumed to be 200 ft. x 200 ft. x 5 ft. The COV of γ_s and h_{WT} can be taken as 0.01 and 0.20, respectively.

For this site, the risk of liquefaction will be estimated using three different assumptions: (i) M and a_{max} are known, (ii) M is known but a_{max} is estimated, and (iii) M and a_{max} are both unknown.

7.1 M and a_{max} are known.

This is a tool to study past case histories where both M and a_{max} are known. In this case Eq. 5.28 needs to be evaluated to estimate the risk of liquefaction. The mean and COV of $\tau_{R_{\Delta v}}$ and $\tau_{A_{\Delta v}}$ can be shown to be

$$\mu_{\tau_{R_{\Delta v}}} = 0.1493 \text{ ksf}$$

$$\mu_{\tau_{A_{\Delta v}}} = 0.2771 \text{ ksf}$$

$$\Omega_{\tau_{R_{\Delta v}}} = 0.348$$

$$\Omega_{\tau A_{\Delta v}} = 0.016$$

Using Eq. 5.28, the probability of liquefaction can be estimated as

$$p_f = 1.0 - \Phi \left[\frac{\text{Ln} \left(\frac{0.1493}{0.2771} \sqrt{\frac{1 + 0.000259}{1 + 0.12078}} \right)}{\sqrt{\text{Ln} \left[(1 + 0.12078)\ (1 + 0.000259) \right]}} \right]$$

$$= 1.0 - \Phi\ (-2.00) = \phi\ (2.00)$$

$$= 0.9770$$

If the probability of liquefaction at a point instead of a volume needs to be considered, then all parameters except the COV of τ_R will be the same. In this case

$$\Omega^2_{\tau_R} = 0.475$$

Again, using Eq. 5.28, the probability of liquefaction can be estimated as 0.944.

7.2 M known, a_{max} Estimated

The assumption that both M and a_{max} are known at a particular site may not be justifiable in many cases. Even if the information on earthquake magnitude is available, unless a_{max} is measured at the site, it is unknown for all practical purposes. This is discussed in section 6.2.3. It can be shown that the logarithm of the ratio ℓn(a_{max} measured at the site/a_{max} estimated from the attentuation equation) is normally distributed. Considering the uncertainty in the attentuation equation and the slip length equation, the standard deviation of the logarithm of the above ratio could be between 0.573 and 0.894 (Haldar, 1976). Thus, the COV of a_{max} estimated from an attenuation equation could be between 0.62 and 1.11. When a_{max} is estimated, the minimum value of COV of a_{max} may be taken as 0.60, assuming that the most applicable attenuation equation is used for the site. The methodology developed in Section 7.1 could be used in this case, except that in the calculation of Ω_{τ_A}, $\Omega_{a_{max}} = 0.60$ has to be added. If the uncertainty in a_{max} is added in the example given in Section 7.1, then

$$\Omega_{\tau_A} = 0.000259 + 0.6^2 = 0.360259$$

Thus, when a_{max} is estimated, the revised probability of failure for the given volume of sand will be

$$p_f = 1.0 - \Phi \left[\frac{\text{Ln}\left(\frac{0.1493}{0.2771}\sqrt{\frac{1 + 0.360259}{1 + 0.12078}}\right)}{\sqrt{\text{Ln}\left[(1 + 0.12078)\ (1 + 0.360259)\right]}} \right]$$

$$= 1.0 - \Phi\ (-0.80) = \Phi\ (0.80)$$

$$= 0.78555$$

7.3 Both M and a_{max} are Unknown

Eq. 5.29 needs to be used in this case. This procedure should be followed to design a site against liquefaction for future earthquakes.

A hypothetical site with site characteristics similar to that considered in Section 7.0 is considered in the San Francisco Bay area. For the site, the probability of liquefaction for different SPT-values are shown in Fig. 7.1. The figure clearly indicates that the probability of liquefaction decreases as the SPT-values increase.

In addition to the San Francisco site, two other sites are considered. One is a site in San Juan, Puerto Rico which has the same soil conditions as the site in San Francisco. The other is a site designed against liquefaction. In Fig. 7.1 the annual probabilities of liquefaction for both of these sites are plotted versus SPT-values for various soil volumes. Fig. 7.1 shows that the site in San Juan has a smaller annual risk of liquefaction than the site with the

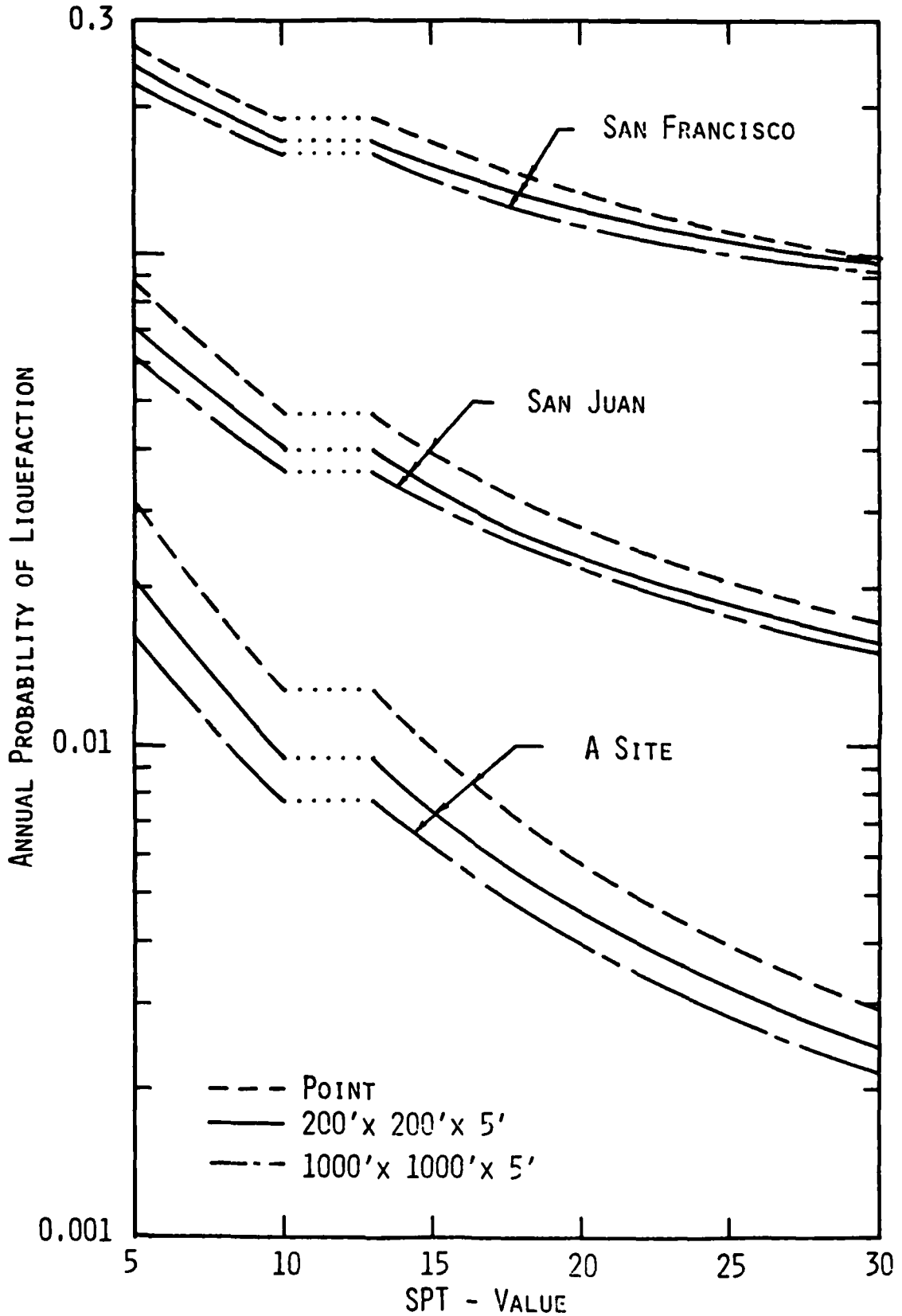

Fig. 7.1 Estimated Annual Probability of Liquefaction

same soil conditions in San Francisco. This result is due to the different seismicities of the two areas. Furthermore, for all three sites, Fig. 7.1 shows that the annual risk of liquefaction decreases with larger liquefiable volumes. The effect of the size of the liquefiable volume of sand on the annual risk of liquefaction is considerable for sites with a small annual risk of liquefaction (such as the site designed against liquefaction).

8. CONCLUSION

There is considerable uncertainty in the estimation of parameters related to earthquake-induced liquefaction. Thus, it is essential that any deterministic evaluation of liquefaction potential be complemented by a probabilistic evaluation. The main advantage of a probabilistic method over a deterministic method is that it can be modeled in three dimensions. Consequently, the damage associated with earthquake-induced liquefaction, which is the most important thing to a practical engineer, can be evaluated. A simple but efficient and practical probabilistic model is proposed here to obtain such information. In general, the three-dimensional probabilistic model would give a smaller risk of liquefaction compared to the point probabilistic model.

To estimate the resisting shear stress that will be mobilized in a deposit during earthquake shaking, considerable attention should be given to estimating the in situ relative density and shear strength parameter. Haldar and Miller's proposed relationship should be used to estimate the in situ relative density indirectly from the SPT-value. The relationship proposed here to estimate the in situ cyclic shear strength considering the effects of compliance, mean grain size, sample preparation, multidirectional shaking, and other secondary factors, is expected to be quite reliable. However, further research is necessary to evaluate the effect of secondary factors on the shear strength parameter.

In the evaluation of the liquefaction potential of a site, it is found that the uncertainties in the load parameters could be higher

than those in the resistance parameters. Hence, the seismic activity of the region should be given serious attention in a liquefaction study.

The proposed probabilistic model provides information on the relative risk of liquefaction between various design alternatives. This information will be valuable to designers in selecting the appropriate design alternative.

8.1 Recommendation for Future Work

A three-dimensional working probabilistic model is proposed here. However, more research is necessary to study the three-dimensional characteristics of all the important parameters. This includes the development of an appropriate sampling strategy so that three-dimensional soil properties can be obtained.

The model developed here considers the damage aspect of the problem. However, the model needs to be refined by relating damage to some performance criteria in terms of settlement, differential settlement, tilting, etc.

The site-specific characteristics also need further study. This area has not yet been explored properly.

The ultimate objective of a risk-based design is to develop a decision analysis framework considering the technical, economic, and political aspects of a project. A comprehensive study is needed in this area.

9. REFERENCES

Annaki, M., and Lee, K. L. (1977), "Equivalent Uniform Cycle Concept for Soil Dynamics," Journal of the Geotechnical Engineering Division, ASCE, Vol. 103, No. GT6, Proc. Paper 12991, pp. 549-564.

Ayyub, B. M., and Haldar, A. (1982), "Practical Structural Reliability Techniques," Journal of the Structural Engineering Division, ASCE, (under review).

Bazant, Z. P., and Krizek, R. J. (1976), "Endochronic Constitutive Law for Liquefaction of Sand," Journal of the Engineering Mechanics Division, ASCE, Vol. 102, No. EM2.

Bazaraa, A.R.S.S. (1967), "Use of the Standard Penetration Test for Estimating Settlements of Shallow Foundations on Sand," thesis presented to the University of Illinois at Urbana, Illinois, in partial fulfillment of the requirements for the degree of Doctor of Philosophy.

Castro, G. (1975), "Liquefaction and Cyclic Mobility of Saturated Sands," Journal of the Geotechnical Engineering Division, ASCE, Vol. 101, No. GT6, Proc. Paper 11388.

Castro, G., and Poulos, S. J. (1977), "Factors Affecting Liquefaction and Cyclic Mobility," Journal of the Geotechnical Engineering Division, ASCE, Vol. 103, No. GT6, Proc. Paper 12994, pp. 501-516.

Chameau, J. L. (1981), "Probabilistic and Hazard Analysis for Pore Pressure Increase in Soils Due to Seismic Loading," Report No. 51, Department of Civil Engineering, Stanford University, Stanford, Calif.

Christian, J. T. and Swiger, W. F. (1975), "Statistics of Liquefaction and SPT Results," Journal of the Geotechnical Engineering Division, ASCE, Vol. 101, No. GT11, Proc. Paper 11701, pp. 1135-1150.

Cornell, C. A. (1968), "Engineering Seismic Risk Analysis," Bulletin of Seismological Society of America, Vol. 58, No. 5, pp. 1583-1606.

DeAlba, P., Chan, C. K., and Seed, H. B. (1975), "Determination of Soil Liquefaction Characteristics by Large-Scale Laboratory Tests," Earthquake Engineering Research Center Report. No. EERC 75-14, University of California, Berkeley.

Derkiureghian, A., and Ang, A. H-S. (1977), "Fault-Rupture Model for Seismic Risk Analysis," Bulletin of Seismological Society of America, Vol. 67, No. 4, pp. 1173-1194.

Donovan, N. C. (1971), "A Stochastic Approach to the Seismic Liquefaction Problem," Proceedings, Conference on Statistics and Probability in Soil and Structural Engineering, Hong Kong, pp. 513-535.

Drnevich, V. P. (1972), "Undrained Cyclic Shear of Saturated Sand," Journal of the Soil Mechanics and Foundations Division, ASCE, Vol. 98, No. SM8, Proc. Paper 9134, pp. 807-825.

Faccioli, E. (1973), "A Stochastic Model for Predicting Seismic Failure in a Soil Deposit," Earthquake Engineering and Structural Dynamics, Vol. 1, pp. 293-307.

Fardis, M. N., and Veneziano, D. (1979), "Probabilistic Liquefaction of Sands During Earthquakes," Report No. R79-14, Massachusetts Institute of Technology, Cambridge, Mass.

Finn, W. D. L., Bransby, P. L. and Pickering, D. J. (1970), "Effect of Strain History on Liquefaction of Sands," Journal of the Soil Mechanics and Foundations Division, ASCE, Vol. 96, No. SM6, Proc. Paper 7670, pp. 1917-1934.

Finn, W. D. L., Lee, K. W. and Martin, G. R. (1977), "An Effective Stress Model for Liquefaction," Journal of the Geotechnical Engineering Division, ASCE, Vol. 103, No. GT6, Proc. Paper 13008, pp. 517-533.

Finn, W. D. L., Pickering, D. J. and Bransby, P. L. (1969), "Sand Liquefaction in Triaxial and Simple Shear Tests," Soil Mechanics Research Report Series No. 11, University of British Columbia, Vancouver, Canada.

Ghaboussi, J., and Dikmen, U. S. (1978), "Liquefaction Analysis of Horizontally Layered Sands," Journal of the Geotechnical Engineering Division, ASCE, Vol. 104, No. GT3.

Gibbs, H. J. and Holtz, W. G. (1957), "Research of Determining the Density of Sand by Spoon Penetration Test," Proceedings, Fourth International Conference on Soil Mechanics and Foundations Engineering, Vol. 1, pp. 35-39.

Haldar, A. (1976), "Probabilistic Evaluation of Liquefaction of Sand Under Earthquake Motions," thesis presented to the University of Illinois at Urbana, Ill., in partial fulfillment of the requirements for the degree of Doctor of Philosophy.

Haldar, A. (1979), "Decision Analysis in Liquefaction Study," Preprint 3785, ASCE Fall Convention, Atlanta.

Haldar, A. (1980), "Liquefaction Study - A Decision Analysis Framework," Journal of the Geotechnical Engineering Division, ASCE, Vol. 106, No. GT12, Proc. Paper 15925, pp. 1297-1312.

Haldar, A. (1981a), "Uniform Cycles in Earthquakes: A Statistical Study," Proceedings, International Conference on Recent Advances in Geotechnical Earthquake Engineering and Soil Dynamics, St. Louis, Missouri, Vol. 1, pp. 195-198.

Haldar, A. (1981b), "Statistical and Probabilistic Methods in Geomechanics," NATO - Advanced Study Institute, Lisbon, Portgugal.

Haldar, A., and Miller, F. J. (1982a), "Research Initiation - Probabilistic Evaluation of Damage Potential in Earthquake-Induced Liquefaction in a 3-D Soil Deposit," Report No. SCEGIT-101-82, School of Civil Engineering, Georgia Institute of Technology, Atlanta, March 1982.

Haldar, A., and Miller, F. J. (1982b), "Factors in Laboratory Evaluation of Cyclic Strength," ASCE Spring Convention of 1982, Las Vegas.

Haldar, A., and Miller, F. J. (1982c), "Probabilistic Evaluation of Liquefaction in a 3-D Soil Deposit," International Conference on Soil Dynamics and Earthquake Engineering, Southampton, U.K.

Haldar, A., and Miller, F. J. (1982d), "Probabilistic Evaluation of Cyclic Strength of Sand," Journal of the Geotechnical Engineering Division, ASCE (under review).

Haldar, A., and Miller, F. J. (1982e), "Indirect Estimation of Relative Density - A New Approach," Specialty Conference, Geotechnical Practice in Offshore Engineering, University of Texas, Austin, April 27-29, 1983 (under review).

Haldar, A., and Tang, W. H. (1979a), "Probabilistic Evaluation of Liquefaction Potential," Journal of the Geotechnical Engineering Division, ASCE, Vol. 105, No. GT2, Proc. Paper 14374, pp. 145-163.

Haldar, A., and Tang, W. H. (1979b), "Uncertainty Analysis of Relative Density," Journal of the Geotechnical Engineering Division, ASCE, Vol. 105, No. GT7, Proc. Paper 14665, pp. 899-904.

Haldar, A., and Tang, W. H. (1981), "Statistical Study of Uniform Cycles in Earthquake Motions," Journal of the Geotechnical Engineering Division, ASCE, Vol. 107, No. GT5, Proc. Paper 16239, pp. 577-589.

Ishihara, K., Tatsuoka, F., and Yasuda, S. (1975), "Undrained Deformation and Liquefaction of Sand Under Cyclic Stresses," Soils and Foundations, Vol. 15, No. 1.

Ishihara, K., and Yasuda, S. (1975), "Sand Liquefaction in Hollow Cylinder Torsion Under Irregular Excitation," Soils and Foundations, Vol. 15, No. 1.

Kishida, H. (1969), "Characteristics of Liquefied Sands During Mino-Owari, Tohnankai, and Fukui Earthquake," Soils and Foundations, Vol. IX, No. 1, pp. 76-92.

Ladd, R. S. (1977), "Specimen Preparation and Cyclic Stability of Sands," Journal of the Geotechnical Engineering Division, ASCE, Vol. 103, No. GT6, Proc. Paper 13014, pp. 535-547.

Lee, K. L., and Seed, H. B. (1967), "Cyclic Stress Conditions Causing Liquefaction of Sand," Journal of the Soil Mechanics and Foundations Division, ASCE, Vol. 93, No. SM1, Proc. Paper 5058, pp. 47-70.

Lee, K. L., and Fitton, J. A. (1969), "Factors Affecting the Cyclic Loading Strengths of Soil," Vibration Effects of Earthquakes on Soils and Foundation, STP 450, American Society for Testing and Materials, pp. 71-95.

Lee, K. L., and Chan, K. (1972), "Number of Equivalent Significant Cycles in Strong Motion Earthquakes," Proceedings, International Conference on Microzonation, Seattle, Washington.

Liou, C. P., Streeter, V. L., and Richart, F. E., Jr. (1977), "Numerical Model for Liquefaction," Journal of the Geotechnical Engineering Division, ASCE, Vol. 103, No. GT6, Proc. Paper 12998, pp. 589-606.

Marcuson, W. F. and Bieganousky, W. A. (1977a), "Laboratory Standard Penetration Tests on Fine Sands," Journal of the Geotechnical Engineering Division, ASCE, Vol. 103, No. GT6, Proc. Paper 12987, pp. 565-588.

Marcuson, W. F. and Bieganousky, W. A. (1977b), "SPT and Relative Density in Coarse Sands," Journal of the Geotechnical Engineering Division, ASCE, Vol. 103, No. GT11, Proc. Paper 13350, pp. 1295-1309.

Martin, G. R., Finn, W. D. L. and Seed, H. B. (1978), "Effects of System Compliance on Liquefaction Tests," Journal of the Geotechnical Engineering Division, ASCE, Vol. 104, No. GT4, Proc. Paper 13667, pp. 463-479.

Montgomery, D. C., and Peck, E. A. (1982), Introduction to Linear Regression Analysis, John Wiley & Sons, New York.

Mori, K., Seed, H. B., and Chan, C. K. (1977), "Influence of Sample Disturbance on Sand Response to Cyclic Loading," Report No. EERC 77-03, Earthquake Engineering Research Center, University of California, Berkeley, CA.

Mulilis, J. P., Seed, H. B., Chang, C. K., Mitchell, J. K., and Arulanandan, K. (1977), "Effects of Sample Preparation on Sand Liquefaction," Journal of the Geotechnical Engineering Division, ASCE, Vol. 103, No. GT2, Proc. Paper 12760, pp. 91-108.

Ohsaki, Y. (1969), "The Effects of Local Soil Conditions Upon Earthquake Damage," Proceedings, Seventh International Conference on Soil Mechanics and Foundation Engineering, Mexico City, Mexico.

Ohsaki, Y. (1970), "Effects of Sand Compaction on Liquefaction During the Tokachioki Earthquake," Soils and Foundations, Vol. 10, No. 2, pp. 112-128.

Peacock, W. H., and Seed, H. B. (1968), "Sand Liquefaction Under Cyclic Loading Simple Shear Conditions," Journal of the Soil Mechanics and Foundation Division, ASCE, Vol. 94, No. SM3, Proc. Paper 5957, pp. 689-708.

Pyke, R. M., Chan, C. K., and Seed, H. B. (1974), "Settlement and Liquefaction of Sands Under Multi-Directional Shaking," Report No. EERC 74-2, Earthquake Engineering Research Center, University of California, Berkeley, Calif.

Schmertmann, J. H. (1972), Discussion on "Simplified Procedure for Evaluating Soil Liquefaction Potential," Journal of the Soil Mechanics and Foundations Division, ASCE, Vol. 98, No. SM4, Proc. Paper 8371, pp. 430-433.

Seed, H. B. (1979), "Soil Liquefaction and Cyclic Mobility Evaluation for Level Ground During Earthquakes," Journal of the Geotechnical Engineering Division, ASCE, Vol. 105, No. GT2, Proc. Paper 14380, pp. 201-255.

Seed, H. B., and Idriss, I. M. (1967), "Soil Liquefaction in the Niigata Earthquake," Journal of the Soil Mechanics and Foundations Division, ASCE, Vol. 93, No. SM3, Proc. Paper 5233, pp. 83-108.

Seed, H. B., and Idriss, I. M. (1971), "Simplified Procedure for Evaluating Soil Liquefaction Potential," Journal of the Soil Mechanics and Foundations Division, ASCE, Vol. 97, No. SM9, Proc. Paper 8371, pp. 1249-1273.

Seed, H. B., Mori, K., and Chan, C. K. (1977), "Influence of Seismic History on Liquefaction of Sands," Journal of the Geotechnical Engineering Division, ASCE, Vol. 103, No. GT4, Proc. Paper 12841, pp. 246-270.

Seed, H. B., and Peacock, W. H. (1971), "Test Procedures for Measuring Soil Liquefaction Characteristics," Journal of the Soil Mechanics and Foundations Division, ASCE, Vol. 97, No. SM8, Proc. Paper 8330, pp. 1099-1119.

Seed, H. B., Pyke, R., and Martin, G. R. (1975), "Analysis of the Effect of Multi-directional Shaking on the Liquefaction Characteristics of Sands," Report No. EERC 75-41, Earthquake Engineering Research Center, University of California, Berkeley, Calif.

Silver, M. L., and Park, T. K. (1976), "Liquefaction Potential Evaluation from Cyclic Strain-Controlled Properties Tests on Sands," Soils and Foundations, Vol. 16, No. 3, pp. 51-65.

Tang, W. H., and Ang, A. H-S. (1973), "Modeling Analysis and Updating of Uncertainties," Preprint No. 2016, ASCE National Structural Engineering Meeting, San Francisco.

Tavenas, F. A., Ladd, R. S., and LaRochelle, P. (1972), "The Accuracy of Relative Density Measurements: Results of a Comparative Test Program," Relative Density Involving Cohesionless Soils, STP 523, American Society for Testing and Materials, pp. 18-60.

Tokimatsu, K., and Yoshimi, Y. (1981), "Field Correlation of Soil Liquefaction with SPT and Grain Size," Proceedings, International Conference on Recent Advances in Geotechnical Earthquake Engineering and Soil Dynamics, St. Louis, Mo., Vol. I, pp. 203-208.

Valera, J. E., and Donovan, N. C. (1977), "Soil Liquefaction Procedures - A Review," Journal of the Geotechnical Engineering Division, ASCE, Vol. 103, No. GT6, Proc. Paper 12996, pp. 607-625.

Vanmarcke, E. H. (1977), "Probabilistic Modeling of Soil Profiles," Journal of the Geotechnical Engineering Division, ASCE, Vol. 103, No. GT11, Proc. Paper 13364, pp. 1227-1246.

Vanmarcke, E. H. (1979), "On the Scale of Fluctuation of Random Functions," Research Report No. R79-19, M.I.T., Department of Civil Engineering.

Whitman, R. V. (1971), "Resistance to Soil Liquefaction and Settlement," Soils and Foundations, Vol. 11, No. 4, pp. 59-68.

Wu, T. H. (1974), "Uncertainty, Safety, and Decision in Soil Engineering," Journal of the Geotechnical Engineering Division, ASCE, Vol. 100, No. GT3, Proc. Paper 10434, pp. 324-348.

Yegian, M. K., and Whitman, R. V. (1976), "Risk Analysis for Earthquake-Induced Ground Failure by Liquefaction," M.I.T., Seismic Design Decision Analysis Report No. 26.

Yegian, M. K., and Vitelli, B. M. (1981), "Probabilistic Analysis for Liquefaction," Report No. CE-81-1, Department of Civil Engineering, Northeastern University, Boston, Mass.

Yoshimi, Y., and Oh-Oka, H. (1973), "A Ring Torsion Apparatus for Simple Shear Tests," Proceedings, Eighth International Conference on Soil Mechanics and Foundation Engineering, Vol. 1.2, Moscow, pp. 501-506.

Yoshimi, Y., and Tokimatsu, K. (1977), "Settlement of Buildings on Saturated Sand During Earthquakes," Soils and Foundations, Vol. 17, No. 1, pp. 23-38.

Youd, T. L. (1977), Discussion on "Seismic Response and Liquefaction of Sands," by Finn, W. D. L., Byrne, P. M., and Martin G. R., Journal of the Geotechnical Engineering Division, ASCE, Vol. 103, No. GT7, Proc. Paper 13025, pp. 827-829.

Zienkiewicz, O. C., Chang, C. T., and Hinton, E. (1978), "Non-linear Seismic Response and Liquefaction," International Journal for Numerical and Analytical Method in Geomechanics, Vol. 2.

PROBABILISTIC DESIGN OF FLOOD LEVEES

by

Dimitri A. Grivas

An approximate solution to the correct problem (even if it is not clearly defined) is infinitely better than an exact solution to the wrong problem (which may be precisely defined).

CONTENTS

LIST OF TABLES

LIST OF FIGURES

LIST OF SYMBOLS

B = Length of horizontal section of creep line

C = Capacity (resistance) of levee against failure

C_W = Weighted creep ratio

c = Cohesion

D = Demand (forces or moments that tend to cause failure)

$E[\ ]$ = Expected value of the quantity in brackets

FS = Factor of safety

$f(\ )$ = Probability density function of the variable in parenthesis

H = Height of levee

H_c = Critical height of levee

h_{cr} = Hydraulic head

L = Length of creep line

N_S = Stability number

P_f = Probability of failure

p_i = Mass density function

SM = Safety margin

T = Length of vertical section of creep line

u = Standardized normal variate

β = Angle of levee slope

β_1 = Coefficient of skewness

γ = Unit weight

ρ = Correlation coefficient

σ = Standard deviation

Φ_u = Cumulative distribution of standardized normal variate

ABSTRACT

A probabilistic procedure is presented that can be used for the design of new flood levees as well as the assessment of the safety of levee systems that are already in operation. The various steps involved in the procedure are briefly outlined, with emphasis placed in the identification and description of possible failure modes, and the determination of the corresponding values of the probability of failure. The latter is achieved with the aid of an approximate method based on "point estimates" of the statistical moments of the levee failure functions (safety margins).

The developed procedure is illustrated in two examples and the obtained results are presented and discussed. Example I involves the determination of the probability of failure of a given levee in slope (both upstream and downstream) sliding and piping. The likelihood for the occurrence of the latter is found under the assumption that the levee material is strong enough to allow the mechanism of piping ("roofing") to develop. Example II involves the selection of a levee cross-section and type of fill for a desired value of the probability of failure (P_f), and the determination of the corresponding value of the conventional factor of safety (FS). This is achieved by developing a relationship (in the form of nomographs) between P_f and FS for a range of values for the levee geometry.

Finally, it should be noted that the present study represents only a first attempt towards a probability-based analysis and design of flood levees. As attention is focused mainly on the development of the probabilistic procedure, the failure models utilized in the illustrative

examples are, of necessity, among the simplest available. It is, therefore, recommended that additional work be undertaken for the incorporation of the details of the failure mechanism(s) of levees and the development of a thorough methodology on the subject.

1. INTRODUCTION

Flood levees are small dams usually built along the shores of a river in order to protect adjoining lands and man-made facilities from storm floods or higher tides. Levees are also used to regulate water or ice flow for agricultural and other land development purposes, and to protect sea-front facilities.

There are three distinct characteristics that make levees different from other types of earth dams, namely: (a) they are in operation only during the flooding season and, consequently, their inner slopes (on the river side) are submerged for a limited time (days or weeks) over the period of one year; (b) their location is selected to satisfy the need for flood control without consideration of the foundation conditions; and (c) the material of which they are made is obtained from nearby borrow pits and is commonly characterized by high plasticity, the presence of very fine particles, and a wide scatter in the values of its properties.

Thus, the randomness around the loads (floods), foundation conditions that commonly involve very soft and unstable ground, and the generally low quality of the construction material introduce a considerable amount of uncertainty in the design of flood levees.

In accordance with conventional practice, the selection of a cross-section for levees is made on the basis of the least favorable material used for their fill, while their construction is pursued solely on the basis of minimum cost. For example, flood levees built in the Mississippi Valley are often uncompacted with low slopes, as this design has been traditionally considered less expensive than the one with compacted fill and steeper slopes. In Fig. 1 are shown representative cross-sections of levees found in the lower Mississippi Valley[3], the inner and outer slopes

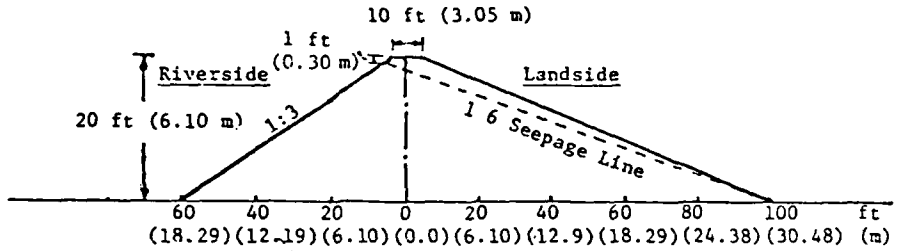

(a) Case A: 75% Clay

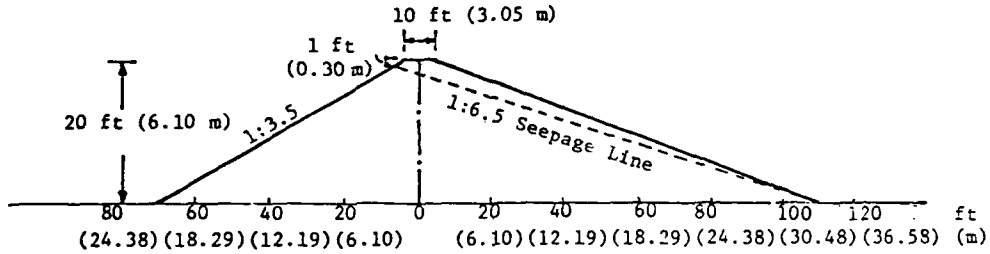

(b) Case B: Less than 75% Sand or Clay

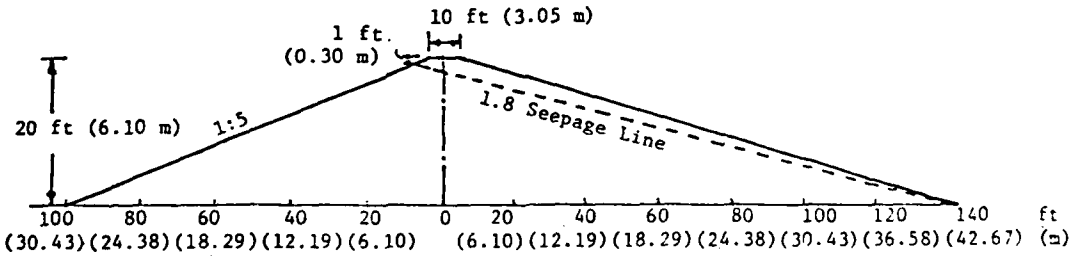

(c) Case C: More than 75% Sand

FIGURE 1 TYPICAL CROSS-SECTION OF FLOOD LEVEES IN LOWER MISSISSIPPI VALLEY

of which are at least equal to 1:3 and 1:6, respectively. It can be seen that, as the percentage of fine material within the fill increases, the values of the slope decrease.

In Fig. 2 are shown examples of levee cross-sections used along important rivers in European countries[8]. They are designed as homogeneous media made of clayey sand or sandy gravel with a considerable portion of loamy material, and can have simple slopes or include berms of various widths.

The recent increase, however, in the value of land and property, particularly in industrialized areas, has dictated the need for economic solutions to the design of flood levee systems; i.e., the development of design procedures that will provide steeper slopes at an adequate safety level. It is the objective of this study to explore uncertainties associated with the geotechnical aspect of the problem and to present a probabilistic procedure that will be useful for both the assessment of the safety of existing levees and the design of new levee systems.

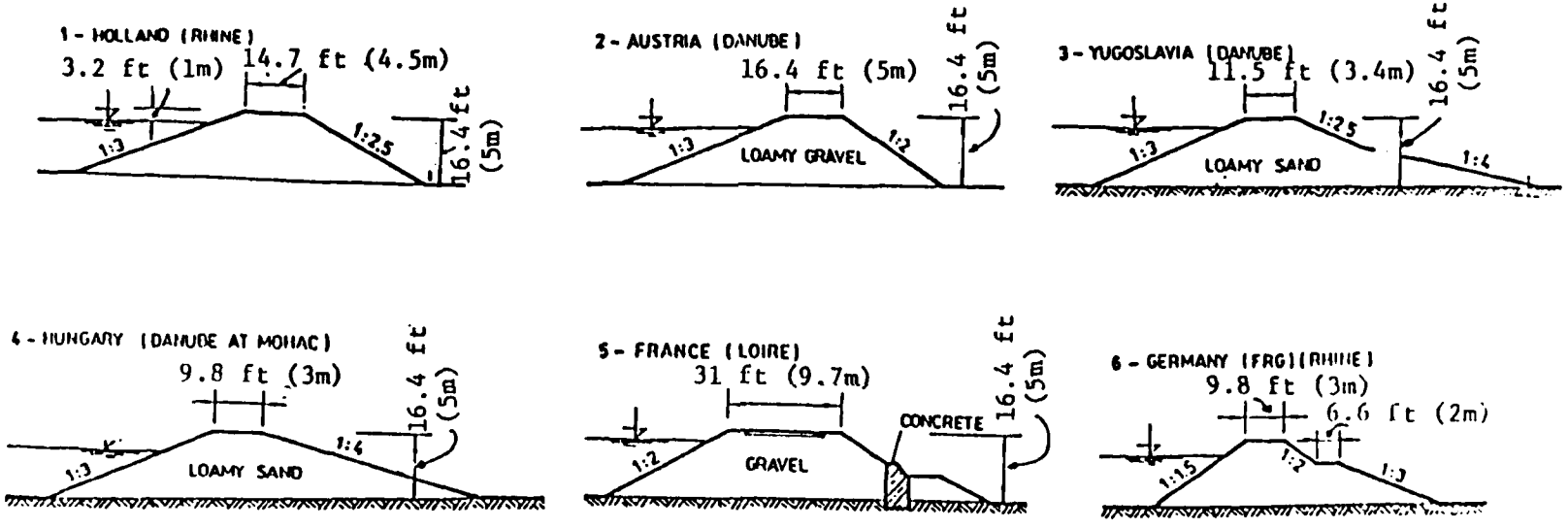

FIGURE 2. EXAMPLES OF LEVEE CROSS-SECTIONS USED IN EUROPE (after [8])

2. PROBABILISTIC DESIGN

2.1 The Design Procedure

In Fig. 3 is shown schematically the procedure for the probabilistic design of a flood levee and the selection of an optimal cross-section. It consists of three main stages, namely: (a) identification of the possible modes of failure and determination of the capacity and demand for each mode; (b) determination of the probability of failure for each mode individually and in combination through a system reliability analysis; and (c) a cost-risk analysis that enables the selection of an optimal cross-section.

For given operating conditions, the ultimate decision on the acceptance of a certain cross-section is based on a cost-risk analysis that accounts for the various uncertainties that affect the design of flood levees. These uncertainties can be classified into hydrological (e.g., maximum flood expected during the lifetime of the facility), hydraulic (e.g., overtopping of levee), geotechnical (e.g., variability of soil parameters), economic (e.g., land value and interest rates), and social (e.g., determination of fair insurance premium, proper allocation of damage awards, etc.).

In many regions where a system of levees is required for flood control, different cross-sections may be used for different segments of the levee system. For example, the main levee system in the lower Mississippi River, that includes about 2,200 miles (3,540 km) of levees[3], consists of various segments of levees with an average height of about 30 ft (9.14 m). In such cases, the procedure illustrated in Fig. 3 may be used for the

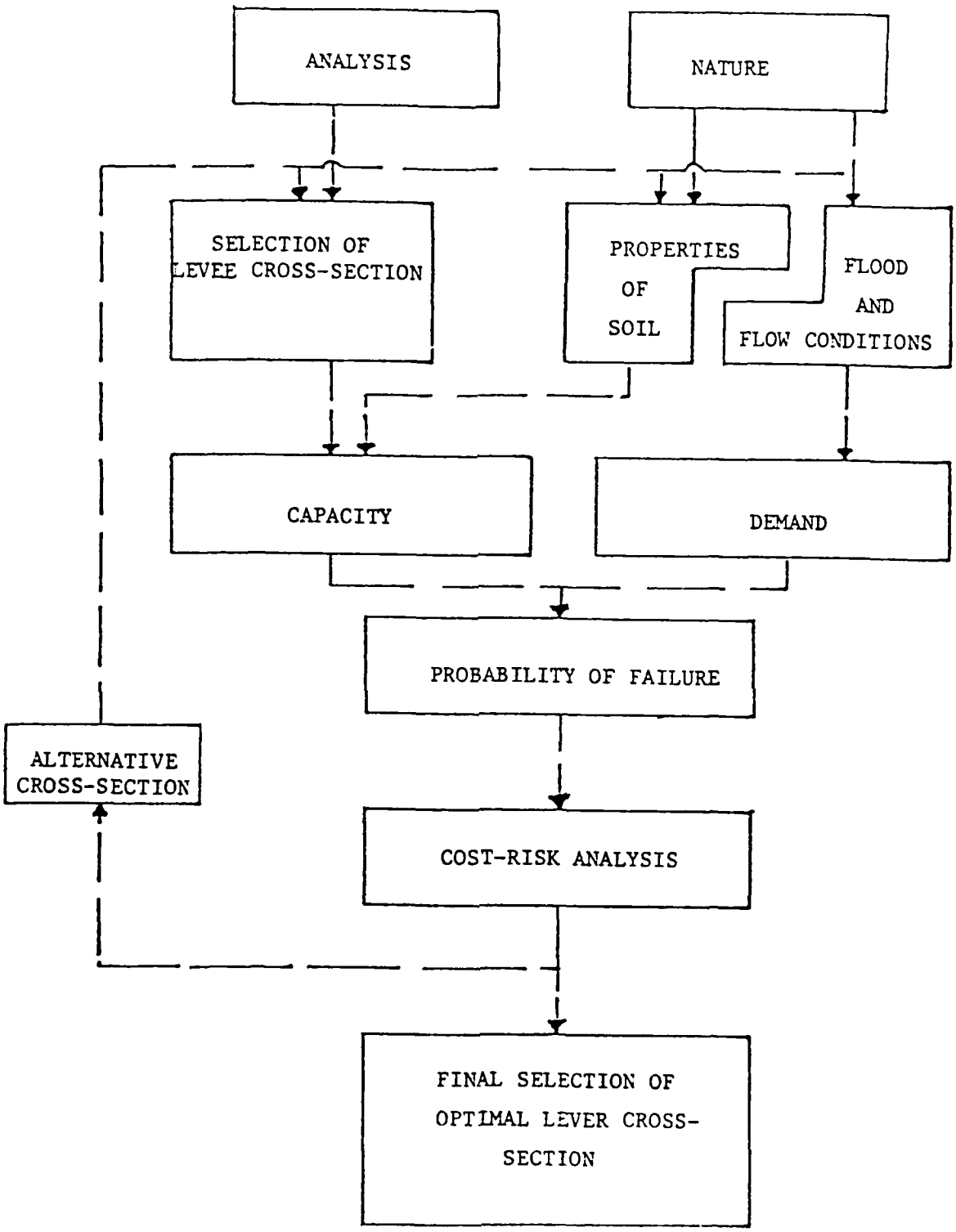

FIGURE 3 ILLUSTRATION OF THE PROBABILISTIC DESIGN PROCEDURE FOR FLOOD LEVEES

selection of a cross-section of each levee segment separately.

2.2 Possible Modes of Failure

Bogárdi and Zoltán[1] have identified four possible modes of failure for flood levees: (a) through wind wave action (causing scour that reduces the levee strength), (b) overtopping (when the elevation of the flood waters exceeds that of the levee), (c) sliding of the levee inner and/or outer slope, and (d) subsoil failure (e.g., due to piping). The factors which influence the reliability of each of these modes have been examined by Tung and Mays[11].

From a geotechnical point of view, levees must be designed to perform successfully under two distinct loading conditions: (a) without flood water, during and after construction, and (b) with flood water, during operation of the facility. In the first case, potential failure modes of a levee are those usually considered for common embankments. In the second case, the inner slope of a levee is submerged and additional failure modes caused by the presence or flow of the flood water must be examined.

The specific modes of failure that must be considered in an analysis of the safety of levee systems are as follows:

(a) Local or base sliding of inner or outer slope.

The low quality of construction material makes levees prone to local sliding, particularly when the material used is loam (i.e., mixture of moist clay, sand, and silt). A similar low quality of the foundation soil may cause base slope failure along a surface passing through the levee foundation.

(b) Excessive settlement.

As the foundation material is commonly loose, uncompacted soil, it undergoes settlement after the application of the loading (levee fill and flood water). Possible consequences of excessive settlement are reduced

free board (that may cause overtopping) and development of cracks (resulting from differential settlement) that may in turn cause piping.

(c) Piping.

This may occur to levees that are made of, or placed on, material strong enough to allow the mechanism of piping (roofing) to occur. It may be due to (a) scour or subsurface erosion by the water that starts downstream and proceeds to the inner slope along the base of the levee, and (b) the sudden rise of soil located near the downstream toe (heaving). Failure in piping due to subsurface erosion is accelerated if the levee has previously suffered extensive cracking due to settlement or shrinkage. In this case, the flow of the water can enlarge the cracks to cause piping.

(d) Sliding of the entire levee along the horizontal direction.

This mode of failure may be caused by the hydrostatic pressure of the flood water and can occur along the levee base or any horizontal surface between the base and the levee crest.

(e) Liquefaction, which may cause failure to levees made of, or placed on, loose sands.

Finally, available experience with the performance of flood levees indicates that the two most often occurring modes of failure are overtopping of the structure (hydraulic failure) and sliding of the downstream (outer) slope (geotechnical failure).

2.3 Probability of Failure

In general, both the capacity (available resistance) C and the demand (forces or moments that cause failure) D of any mode of failure of a levee system exhibit some degree of randomness. This may be attributed mainly to the random variation of the material properties of the fill and foundation soil as well as to the randomness associated with the applied loads (e.g.,

floods). The difference between capacity C and demand D, called the safety margin SM (SM = C-D), is also a random variable.

Failure of the levee in any of the possible modes will occur when the capacity C along this mode is exceeded by the demand D; i.e.,

$$\text{Failure} = [C < D] \tag{1}$$

The probability of the occurrence of this event is equal to the probability of failure P_f, or

$$P_f = P[C < D] = P[SM < 0] \tag{2}$$

If f(SM) denotes the probability density function of the safety margin SM, P_f may be determined as

$$P_f = \int_{-\infty}^{0} f(SM)\, d(SM) = F(0) \tag{3}$$

in which F(0) is the cumulative distribution of SM evaluated at zero.

For example, in the case where SM is represented by the normal distribution, f(SM) is equal to

$$f(SM) = \frac{1}{\sqrt{2\pi}\,\sigma_{SM}} \exp\left[-\left(\frac{SM-\overline{SM}}{\sigma_{SM}}\right)^2\right], \qquad -\infty < SM < \infty \tag{4}$$

where $\overline{SM}$ and σ_{SM} are the mean value and standard deviation of SM, respectively. In this case, the probability of failure P_f becomes

$$P_f = \Phi_u\left(-\frac{\overline{SM}}{\sigma_{SM}}\right) \tag{5}$$

in which Φ_u is the cumulative distribution of the standardized normal variate u defined as $u = (SM-\overline{SM})/\sigma_{SM}$.

2.4 Statistical Values of Safety Margin: The Point-Estimate Method

The statistical values (e.g., mean value, variance, etc.) of the safety margin SM may be estimated from the statistical values of the soil properties with the aid of the "point estimate method". This method, presented for the first time by Rosenblueth[9], is based on simple point estimations of a function of one or more (independent or correlated) random variables.

2.4.1 Case of One Random Variable

In the simplest case when the safety margin is a function of only one soil parameter (random variable) x, denoted as y(x), the method involves a replacement of the continuous distribution f(x) of x by a mass density function $p_i(x_i)$. This is defined at specified discrete locations x_i. Therefore, function y(x) is also defined at discrete locations $y_i = y(x_i)$ and has a mass density function $p_i(y_i)$. The discrete distribution $p_i(x)$ is subject to the following constraints:

$$0 < p_i < 1$$

$$\sum_{i=1}^{N} p_i = 1 \qquad (6)$$

where N is the number of points used in the discrete approximation of f(x).

Points x_i and the associated probabilities p_i are determined by letting the moments of the discrete distribution become equal to those of the original distribution. For a two point approximation (N = 2) of

x, denoted as x_- and x_+, with mass densities p_- and p_+, respectively, one has

$$\begin{aligned} p_- + p_+ &= 1 \\ p_-x_- + p_+x_+ &= \bar{x} \\ p_-(\bar{x}-x_-)^2 + p_+(x_+-\bar{x})^2 &= \sigma_x^2 \\ p_-(\bar{x}-x_-)^3 + p_+(x_+-\bar{x})^3 &= \beta_1 \sigma_x^3 \end{aligned} \tag{7}$$

in which $\bar{x}$, σ_x, and β_1 are the mean value, standard deviation, and coefficient of skewness of the variate x, respectively.

The solution of Eqns. (7) provides the following expressions for p_-, p_+, x_- and x_+:

$$\begin{aligned} p_- &= 1 - p_+ \\ p_+ &= \frac{1}{2}\left\{1 \pm \left[1 - \frac{1}{1 + \beta_1^2/4}\right]^{1/2}\right\} \\ x_- &= \bar{x} - \sigma_x(p_-/p_+)^{1/2} \\ x_+ &= \bar{x} + \sigma_x(p_-/p_+)^{1/2} \end{aligned} \tag{8}$$

The sign preceeding the radical in the above expression for p_+ is opposite to that of β_1.

In the special case where x has a symmetric distribution ($\beta_1 = 0$), Eqns. (8) are reduced to

$$\begin{aligned} p_- &= p_+ = \frac{1}{2} \\ x_- &= \bar{x} - \sigma_x \\ x_+ &= \bar{x} + \sigma_x \end{aligned} \tag{9}$$

The n-th order statistical moment $E[y^n]$ of function $y(x)$ is equal to

$$E[y^n] = p_+ y_+^n + p_- y_-^n \tag{10}$$

in which $y_+ = y(x_+)$ and $y_- = y(x_-)$.

For n = 1, Eqn. (10) provides the mean value $E[y] = \bar{y}$ of y and for n = 2 its second moment; i.e.,

$$\begin{aligned} &(n = 1) \quad E[y] = \bar{y} = p_+ y_+ + p_- y_- \\ &(n = 2) \quad E[y^2] = p_+ y_+^2 + p_- y_-^2 \end{aligned} \tag{11}$$

The variance σ_y^2 of y is found from Eqns. (11) as:

$$\sigma_y^2 = E[y^2] - (E[y])^2 \tag{12}$$

2.4.2 Case of Two Random Variables

Let y be a function of two correlated, approximately symmetric random variables x_1 and x_2, i.e., $y = y(x_1, x_2)$, concentrated at points $x_{1_+} = \bar{x}_1 + \sigma_{x_1}$, $x_{1_-} = \bar{x}_1 - \sigma_{x_1}$ and $x_{2_+} = \bar{x}_2 + \sigma_{x_2}$, $x_{2_-} = \bar{x}_2 - \sigma_{x_2}$, respectively. The n-th statistical moment $E[y^n]$ of $y = y(x_1, x_2)$ is equal to

$$E[y^n] = p_{++} y_{++}^n + p_{+-} y_{+-}^n + p_{-+} y_{-+}^n + p_{--} y_{--}^n \tag{13}$$

in which $y_{++} = y(x_{1+}, x_{2+})$, $y_{+-} = y(x_{1+}, x_{2-})$, $y_{-+} = y(x_{1-}, x_{2+})$, $y_{--} = y(x_{1-}, x_{2-})$ and

$$p_{++} = p_{--} = \frac{1+\rho}{4}$$

$$p_{+-} = p_{-+} = \frac{1-\rho}{4} \tag{14}$$

where ρ is the correlation coefficient between x_1 and x_2. In the case where x_1 and x_2 are independent ($\rho = 0$), Eqns. (14) are reduced to $p_{++} = p_{+-} = p_{-+} = p_{--} = \frac{1}{4}$.

For $n = 1$, Eqn. (13) provides the mean value $E[y] = \bar{y}$ of y and for $n = 2$ its second moment. The variance σ_y^2 of y can be found using Eqn. (12).

3. ILLUSTRATIVE EXAMPLE I: PROBABILITY OF FAILURE OF A LEVEE IN SLOPE SLIDING AND PIPING

3.1 Statement of the Problem

The safety of the levee shown schematically in Fig. 4 is investigated with regard to (a) the stability of its inner and outer slopes, and (b) piping, when the inner slope is submerged in flood water. The levee has a height equal to 20 ft (6.10 m) and its inner and outer slopes are equal to 1:3 ($\beta' = 18°$) and 1:6 ($\beta'' = 9°$), respectively.

The unit weight of the soil has a mean value equal to $\bar{\gamma} = 100$ pcf (15.7 kN/m^3), a standard deviation of $\sigma_\gamma = 10$ pcf (1.57 kN/m^3), and a coefficient of variation of ten percent ($V_\gamma = 10\%$). The strength of the fill and foundation soil, determined in a series of conventional tests under undrained conditions, has a mean value equal to $\bar{c} = 400$ psf (19.15 kN/m^2), a standard deviation of $\sigma_c = 100$ psf (4.79 kN/m^2), and a coefficient of variation of twenty five percent ($V_c = 25\%$).

3.2 Probability of Failure in Sliding

The stability of each slope is examined with the aid of stability charts[10] and for three possible sliding (circular) surfaces: one, passing through the midpoint of the slope; another, passing through its toe; and a third, passing anywhere through the slope itself. The capacity of each slope is taken to be equal to the critical height H_c which is expressed as a function of the material parameters c (cohesion) and γ (unit weight), while the demand is given as the available height H. The expression for the safety margin is then equal to

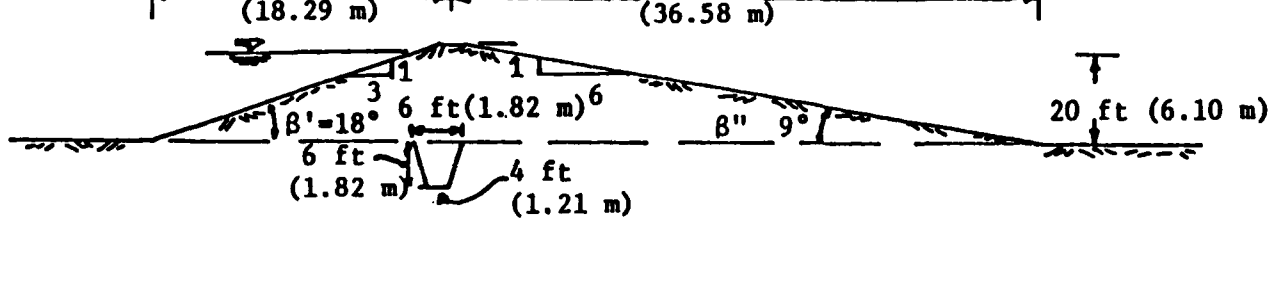

FIGURE 4 CROSS-SECTION OF THE LEVEE USED IN ILLUSTRATIVE EXAMPLE I

$$SM = H_c - H = N_S \frac{c}{\gamma} - H \qquad (15)$$

in which N_S is the stability number. For the inner slope, the values of N_S are[10]: $N_S = 5.52$, for midpoint circle, $N_S = 7.10$, for toe circle, and $N_S = 10.0$, for slope circles; while for the outer slope, $N_S = 5.52$, for midpoint circle, and $N_S = 11.5$, for both toe and slope circles.

The mean value and second moment of the safety margin SM are found using Eqn. (13), while the variance is found from Eqn. (12). Under the assumption that SM follows a normal distribution, the probability of failure for each case examined is found with the aid of Eqn. (5).

The obtained values of the probability of failure as well as those of the factor of safety are listed in Table 1.

3.3 Probability of Failure in Piping

The likelihood for piping of the levee shown in Fig. 4 is evaluated under the assumption that (a) the material is strong enough to allow the mechanism of piping (roofing) to develop, and (b) piping is caused by erosion along the surface of contact between the fill and the foundation soil. In this case, the capacity of the levee in piping may be expressed as the length of the line of creep (i.e., the path followed by water particles) required so that the average hydraulic gradient is smaller than a certain critical value. Using the expression for the weighted creep ratio[10], given as

$$C_W = \frac{\frac{1}{3} B + T}{h_{cr}} \qquad (16)$$

in which B is the length of the horizontal section of the line of creep, T is the sum of all vertical sections of same line, and h_{cr} is the

Table 1. Probability of Failure and Factor of Safety for the Various Failure Modes Considered in Illustrative Example I

FAILURE MODE	FACTOR OF SAFETY	PROBABILITY OF FAILURE
Local Failure of Inner Slope:		
along midpoint circle	1.12	3.5×10^{-1}
along toe circle	1.44	1.4×10^{-1}
along slope circle	2.00	3.6×10^{-2}
Local Failure of Outer Slope:		
along midpoint circle	1.12	3.6×10^{-1}
along toe circle	2.34	2.0×10^{-2}
along slope circle	2.34	2.0×10^{-2}
Piping	2.10	10^{-1}

hydraulic head, one has that the available value for B is equal to

$$B = 3C_W h_{cr} - 3T \tag{17}$$

If L denotes the actual length of the line of creep, the expression for the safety margin in piping becomes

$$SM = B - L = 3C_W h_{cr} - 3T - L \tag{18}$$

It is assumed that the variation of SM is due to the uncertainty in the value of the weighted creep ratio C_W, the hydraulic head h_{cr}, and the actual length L of the flow path. For fine sand or silt, the mean value of C_W is given as $\bar{C}_W = 8.5$[10]. The employed values for the standard deviation and coefficient of variation of C_W and the statistical values for h_{cr} and L are listed in Table 2, while, from Fig. 4, it is seen that T = 22 ft (3.66 m). Under the assumption that SM follows a normal distribution, the probability of failure in piping is found to be equal to 10^{-1} ($P_f = 10^{-1}$).

In summary, from Table 1 it is seen that for the conditions considered in this example, the highest probability of failure corresponds to a local failure of the downstream slope along a midpoint circle ($P_f = 3.6 \times 10^{-1}$).

Table 2. Statistical Values of Variables Entering the Expression for the Safety Margin in Piping

Parameter	Mean Value	Standard Deviation	Coefficient of Variation
Weighted creep ratio, C_w	8.5	3.4	40%
Hydraulic head, h_{cr}	15 ft (4.57 m)	1 ft (0.30 m)	7%
Length of creep line, L	180 ft (54.86 m)	40 ft (12.19 m)	22%

4. ILLUSTRATIVE EXAMPLE II: SELECTION OF A LEVEE CROSS-SECTION

In this example, the selection is examined of values for the height H and angle β of a levee slope (Fig. 5) at a specified level of safety. Two types of construction material are contemplated, denoted as Type A and Type B. The values of the soil parameters (random variables) c (cohesion) and γ (unit weight) are determined for each soil type in a series of tests and the results are presented in Table 3.

The expression for the factor of safety FS of the slope under the critical undrained ("$\phi = 0$") condition is equal to[10]

$$FS = \frac{N_S \, c}{\gamma \, H} \tag{19}$$

in which N_S is the stability number. The mean value and standard deviation of FS are determined with the aid of Eqn. (13) and the probability of failure P_f for both pair of values of height H and slope angle β is determined as the probability with which FS receives values smaller than, or at most, equal to unity; i.e.,

$$P_f = P[FS \leq 1] \tag{20}$$

The probability distribution for FS is taken to be normal, a model known[4] to provide somewhat higher values for P_f than other types of distribution (e.g., lognormal, beta, etc.).

A general relationship between FS and P_f for any slope angle β and height H is shown in Figs. 6 and 7, for soil Types A and B, respectively. These two figures can be used for the determination of the factor of safety FS and the corresponding value of the probability of failure P_f of the levee slope for given values of height H and angle β. And vice

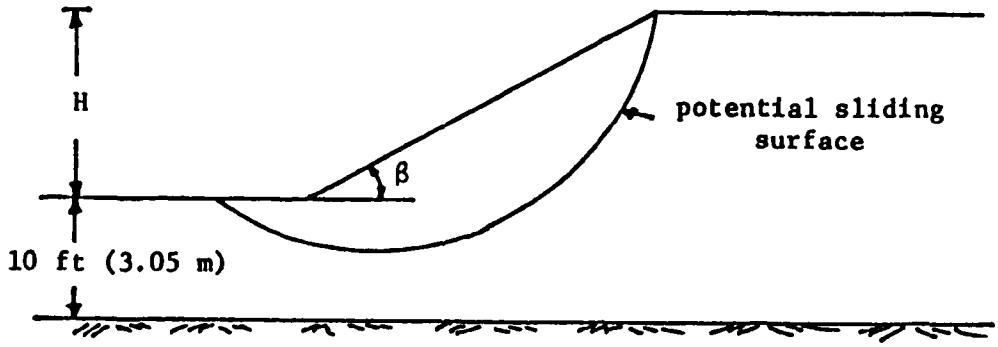

FIGURE 5 GEOMETRY OF LEVEE SLOPE USED IN ILLUSTRATIVE EXAMPLE II

Table 3. Statistical Values of the Material Parameters for Two Soil Types Used in Example II

Soil Type	Soil Parameter	Statistical Values		
		Mean Value	Standard Deviation	Coefficient of Variation
A	cohesion, c	500 psf (23.94 kN/m^2)	75 psf (3.59 kN/m^2	15%
	unit weight, γ	100 pcf (15.7 kN/m^3)	10 pcf (1.57 kN/m^2)	10%
B	cohesion, c	250 psf (11.97 kN/m^2)	75 psf (3.59 kN/m^2)	30%
	unit weight, γ	100 psf (15.7 kN/m^3)	15 pcf (2.35 kN/m^3)	15%

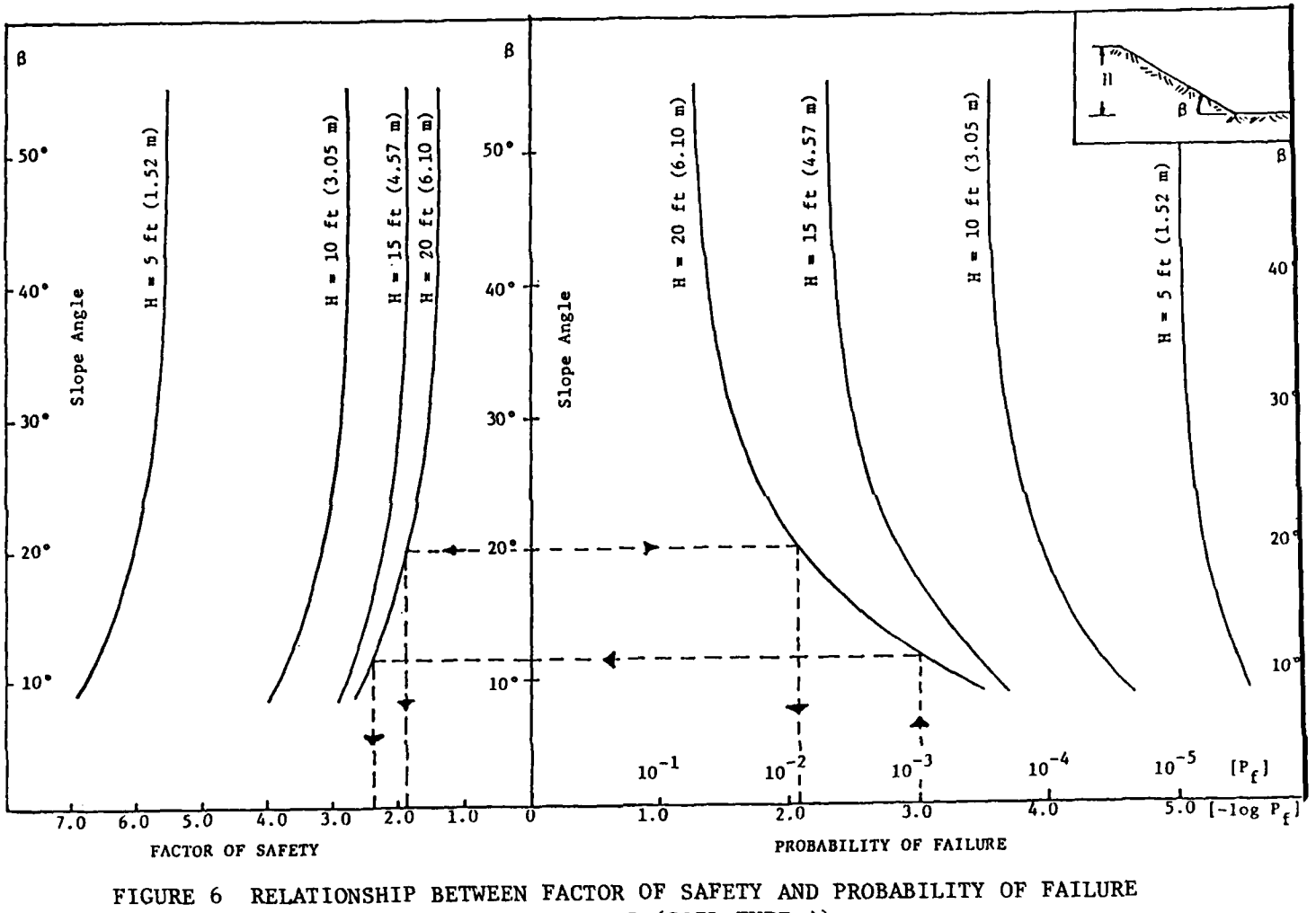

FIGURE 6 RELATIONSHIP BETWEEN FACTOR OF SAFETY AND PROBABILITY OF FAILURE FOR VARIOUS SLOPE GEOMETRIES (SOIL TYPE A)

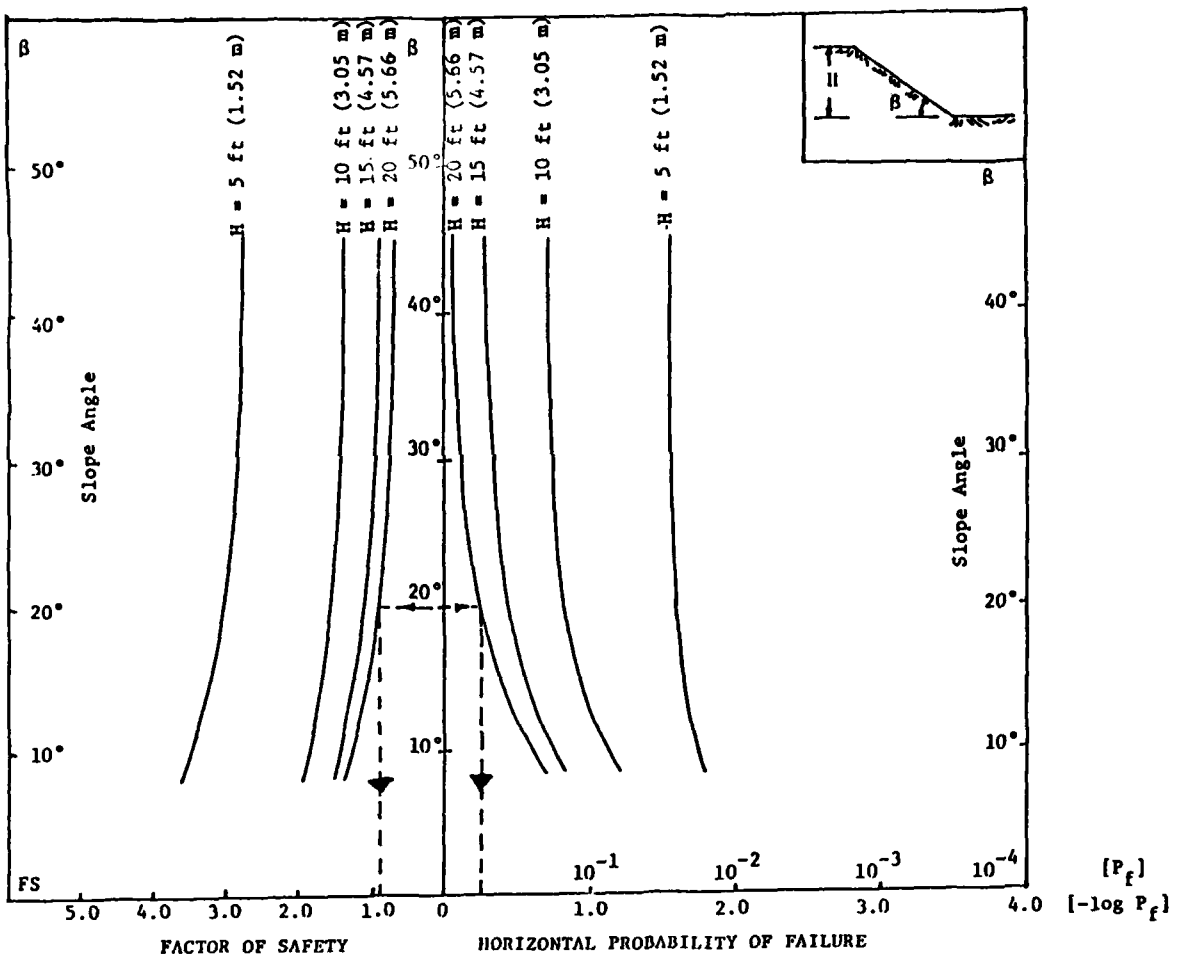

FIGURE 7 RELATIONSHIP BETWEEN FACTOR OF SAFETY AND PROBABILITY OF FAILURE FOR VARIOUS SLOPE GEOMETRIES (SOIL TYPE B)

versa, for a given value of P_f (or FS), Figs. 6 and 7 can be used to select values for H and β, and also to determine the corresponding value for FS (or P_f).

For example, for a levee slope of soil Type A, with height h = 20 ft (6.10 m) and angle $\beta = 20°$, from Fig. 6 one has that the probability of failure is equal to $P_f = 8.9 \times 10^{-3}$ ($-\log P_f = 2.05$) and the corresponding value of the factor of safety is FS = 1.9. If the same levee was comprised of soil Type B, the corresponding values for the two safety measures (Fig. 7) would be equal to $P_f = 0.60$ and FS = 0.93, respectively.

As another example of the use of Fig. 6 or 7 one may consider the selection of a value for slope β for the case where the desirable value for the probability of failure P_f of a levee slope having a height H = 20 ft (6.10 m) and which is made of soil Type A is, say, 10^{-3}. From Fig. 6, one has that for $P_f = 10^{-3}$ and H = 20 ft (6.10 m), the value for β is 12° and the corresponding value for FS is 2.4.

5. REFERENCES

1. Bogárdi, I. and Zoltán, M., "Determination of the Degree of Protectection Offered by Flood Levees and the Economic Improvement Thereof", Department of Flood Control and River Training, National Water Authority, Budapest, Hungary, 1968.

2. Coates, D.R., "Geomorphology and Engineering", John Wiley and Sons, Inc., 1976.

3. "Construction Plans and Methods for Flood Control on the Lower Mississippi River and Similar Streams", Manual of Engineering Practice, No. 12, American Society of Civil Engineers, June, 1935, p. 65.

4. Grivas, D.A., "How Reliable Are Present Methods of Slope Failure Prediction?", Tenth International Conference on Soil Mechanics and Foundation Engineering, Stockholm, Sweden, June, 1981, Vol. 3, pp. 427-430.

5. Grivas, D.A. and Harrop-Williams, K., "Joint Distribution of the Components of Soil Strength", Proceedings 3rd International Conference on Applications of Statistics and Probability in Soil and Structural Engineering, Sydney, Australia, 1979, pp. 189-197.

6. Lumb, P., "Variability of National Soils", Canadian Geotechnical Journal, Vol. 7, No. 3, pp. 225-242.

7. McGuffey, V., Iori, J., Kyfor, Z. and Grivas, D., "Statistical Geotechnical Properties of Lockport Clay", Transportation Research Board No. 809, National Academy of Science, 1981, pp. 54-60.

8. Peter, P., "Canal and River Levees", Developments in Geotechnical Engineering, Vol. 29, Elsevier Scientific Publishing Co., New York, 1982.

9. Rosenblueth, E., "Point Estimates for Probability Moments", Proceedings of National Academy of Science, Vol. 72, No. 10, March, 1975, pp. 3812-3814.

10. Terzaghi, K. and Peck, R.B., "Soil Mechanics in Engineering Practice", John Wiley and Sons, Inc., NY, 1967.

11. Tung, Y-K. and Mays, L.W., "Optimal Risk-Based Design of Flood Levee Systems", Water Resources Research, Vol. 17, No. 4, August, 1981, pp. 843-852.

12. Wood, E., "An Analysis of Flood Levee Reliability", Water Resources Research, Vol. 13, No. 3, June, 1977, pp. 665-671.

6. SUMMARY

A probabilistic procedure was presented that can be used for both the design of new levees and the assessment of the safety of levees already in operation. The various stages involved in the procedure were outlined, with emphasis placed in the description of failure modes and the determination of the probability of failure.

The procedure was applied to two illustrative examples: one, involving the determination of the probability of failure of a given levee in slope sliding and piping; and, another, involving the selection of a levee cross-section and type of fill for desired levels of reliability. The latter was achieved by developing a relationship between the conventional facotr of safety and the probability of failure (in the form of nomographs) for a range of values of the levee geometry.

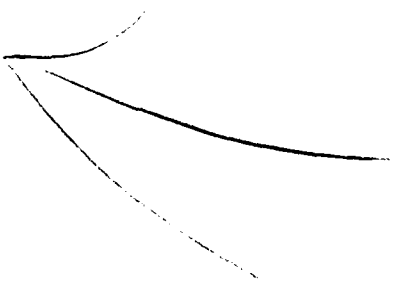

ROCK MECHANICS PROGRAM

PROBABILISTIC AND STATISTICAL METHODS FOR DETERMINING ROCK MASS DEFORMABILITY BENEATH FOUNDATIONS: AN OVERVIEW

by

Charles W. Schwartz

CONTENTS

PROBABILISTIC AND STATISTICAL METHODS FOR DETERMINING ROCK MASS DEFORMABILITY BENEATH FOUNDATIONS: AN OVERVIEW

by

Dr. Charles W. Schwartz
Department of Civil Engineering
University of Maryland

1. INTRODUCTION

Rock mass deformability, the measure of the level of movement within a rock mass due to a given applied loading, is a property of fundamental importance to the rock engineer. The designs for most major structures on or in rock depend to some extent on the movements within the underlying or surrounding geologic formations. Large dams, and especially large concrete arch dams, are perhaps the most obvious examples. High foundation and abutment pressures can induce differential settlements of the rock surface which in turn may induce high stresses in the thin and relatively rigid concrete arch.* Foundations for tall buildings and long-span bridges exhibit similar problems. Support design for underground openings may also require knowledge of rock mass deformability (Einstein and Schwartz, 1979).

Field instrumentation and monitoring, a technology that pervades nearly all of rock engineering, is another area in which quantitative estimates of rock mass deformability are essential if full benefits from the measurements are to be derived. Extensometers, inclinometers, and convergence devices measure <u>deformations</u> only. However, if the rock mass deformability is known, then it is possible to infer changes in <u>stresses</u> from the measured movements.

---

* A common rule of thumb for concrete arch dams in that if $E_m > E_c/4$ then the foundation stiffness will have little influence on the stresses in the arch; if $E_m < E_c/4$ the foundation will have considerable effect; and if $E_m < E_c/16$ the foundation will dominate the arch design (E_m = rock mass modulus, and E_c = concrete modulus).

The combination of displacements and stresses may greatly improve the engineer's ability to interpret the measured performance and to verify his design assumptions.

Lastly, numerical analysis methods like finite elements require specification of the rock mass deformability properties as part of the input data. Even in cases in which only stresses are desired, the analysis results may be dependent on the rock mass deformability (e.g., the stress distributions around an opening in a nonhomogeneous rock mass).

Unfortunately, although the engineering importance of rock mass deformability is clear, the means for determining it accurately are not. As in nearly all rock engineering phenomena, rock mass deformability will be a function not only of the intact rock properties but also of the properties and geometry of the discontinuity systems. The consideration of all of the relevant variables in any sort of theoretical framework is exceedingly difficult. Consequently, most attempts at quantifying rock mass deformability have entailed either direct in situ testing or empirical correlations with rock quality indices. A few idealized theoretical models have also been proposed.

To complicate matters further, there will not in general be a single value for most of the parameters -- e.g., joint spacing, orientation, stiffness -- influencing the deformability of a given rock mass, but rather some distribution of values. The problem thus seems well-suited to the application of statistical and probabilistic methods. Some beginning attempts have been made to apply these techniques.

2. SCOPE OF THIS REPORT

The purpose of statistical and probabilistic methods in rock engineering is to provide information -- albeit sometimes very crude -- regarding the level of uncertainty in our knowledge of rock mass behavior. This

uncertainty will in general be due to a combination of factors: spatial variability, statistical uncertainty, measurement bias errors, and modeling uncertainty (Baecher, 1981). Usually it is impossible to define the contribution of each of these component factors and thus only the aggregate or total uncertainty can be estimated.

In broadest terms, statistical and probabilistic methods for rock mass deformability range from simple statistical measures (e.g. mode, mean, variance) of in situ test data to trend analyses using regression techniques (e.g. correlations of rock mass modulus with rock quality indices) to full-blown Monte Carlo-type computer simulations that model each individual joint beneath a foundation. For the purposes of the present discussion, it is convenient to group these various techniques into two categories: descriptive methods and predictive methods (Figure 2.1). Descriptive methods use a more precise specification of measured conditions as they exist -- for example, the mean and variance of measured RQD across a site. Predictive methods use theory and analysis to extrapolate from basic or fundamental data in order to provide new information -- for example, the expected value of foundation settlement based on RQD data filtered through some appropriate model. For engineering purposes, predictive methods are generally the more valuable of the two.

It is worth noting here that in one sense the determination of rock mass deformability is just one part of the more general problems of site exploration and site characterization. In these problems, one is trying to answer the questions "How does one sample (core, map, test, etc.) to get the 'best' estimate of the rock mass deformability (or some other property)?" and "How does one 'best' describe the properties of the entire subsurface region based on this information obtained from discrete samples, i.e. points?" The problems

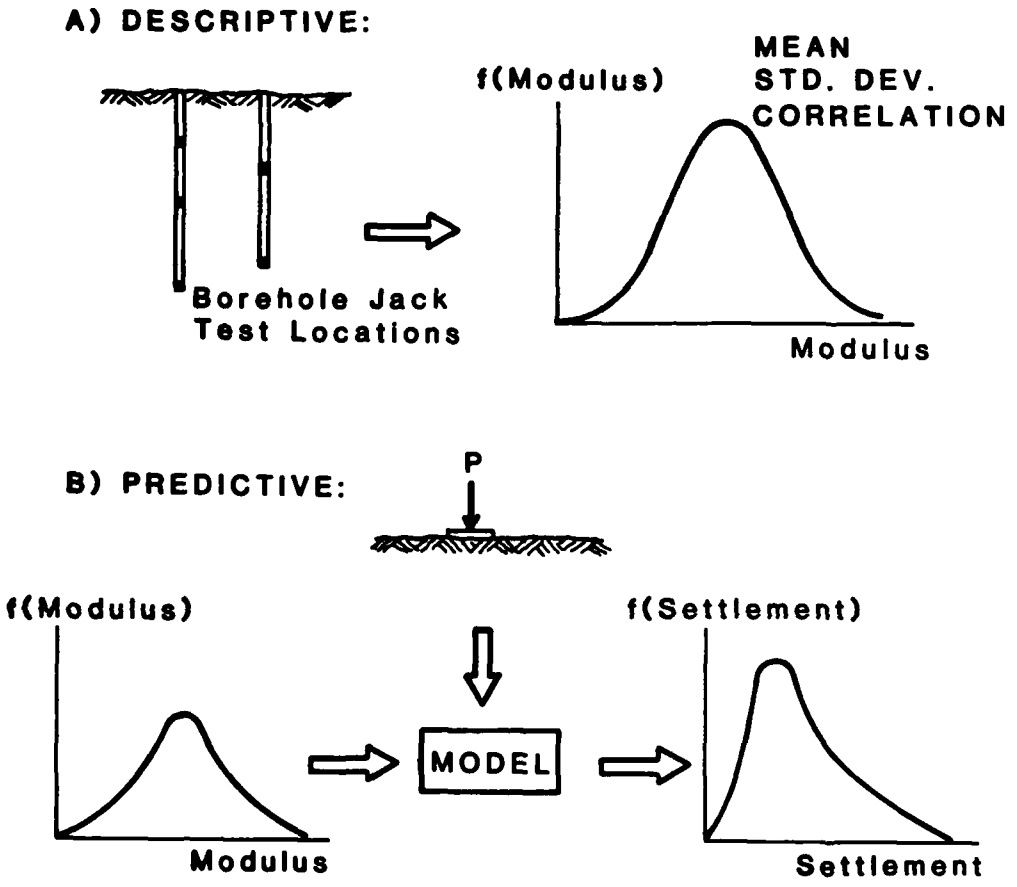

Figure 2.1 Descriptive versus Predictive Statistical/ Probabilistic Methods

of site exploration and site characterization have in recent years been the subjects of much probabilistic and statistical modeling. Good summaries of this work can be found in Dowding (1979).

The present report will ignore these larger questions of site exploration and characterization and concentrate instead on the more restrictive problem of determining rock mass deformability at a point given some set of quantitive parameters for the rock at that point. Emphasis will be on predictive methods and on those descriptive methods that provide insight into the fundamental mechanisms underlying the rock mass behavior. The focus of the discussion will be the rock foundation problem. Methods that deal with rock deformability for other types of problems will also be mentioned if they provide additional insight.

3. EXISTING METHODS FOR DETERMINING ROCK MASS DEFORMABILITY

A review of existing deterministic methods for establishing rock mass deformability is needed to provide a proper context for the more specific assessment of the probabilistic and statistical techniques. The wide range of these existing methods can be grouped into four categories, as described in the following subsections.

3.1 In Situ Testing

The oldest and most straightforward method for determining rock mass deformability is to measure it directly in the field. Many imaginative testing techniques have been proposed over the years; standard rock engineering references (e.g. Obert and Duvall, 1967; Stagg and Zienkiewicz, 1968; and, more recently, Goodman, 1980) describe these well. The most successful and widely used in situ testing methods are categorized in Table 3.1.

Elastic theory with all of its limitations is generally used to interpret

TABLE 3.1 In Situ Testing Methods for Rock Deformability

Tests in Underground Galleries	- Axial Jacking (Plate Loading) - Radial Jacking (Loading of a Circumferential Ring) - Pressure Tunnel Tests - Excavation-Induced Stress Relief
Borehole Methods	- Dilatometer - Pressuremeter - Goodman Jack
Surface Methods	- Plate Loading - Flat Jack Tests
Geophysical Methods	- Acoustic Velocity - "Petite Séismique"

TABLE 3.2 Factors Influencing Rock Mass Quality

Intact Rock Properties	- Type - Strength - Stiffness - Anisotropy
Discontinuity Properties	- Strength and Stiffness (will be functions of roughness, wall strength, aperture, filling) - Number of Sets - Spacing/Frequency (often correlated with RQD) - Orientation - Persistence
General Conditions	- In Situ Stresses - Groundwater

the data from these testing methods. An equivalent elastic modulus is back-figured from the measured response of the rock.

Although in situ tests can provide accurate and direct data on the rock mass deformability, they do have some drawbacks: (a) they are expensive, especially as the loaded rock volume and the applied stress level increase, (b) they are time consuming, and (c) their results are site specific -- i.e., a new test is required for each new location. While these drawbacks may not be too severe for large and expensive projects (e.g. large dams), clearly it would be better and cheaper if the engineer could estimate the rock mass deformability given some other more fundamental and easily measured rock parameters. Empirical methods provide one means for accomplishing this.

3.2 Empirical Correlations with Rock Quality Indices

The assumption underlying this approach is that rock mass properties are strongly related to some quantitative index of rock mass quality. The problem, of course, is defining the correct quality index to use. Ideally, the rock quality index for rock mass deformability should combine the effects of all relevant rock parameters; a sampling of these are summarized in Table 3.2. As many of these parameters are difficult to measure or quantify individually (e.g., roughness, persistence), it is clear that combining them into a comprehensive rock quality index is not an easy task. Consequently, most existing rock mass classification systems rely upon only some subset of parameters, presumably the most important.

Much of the development of rock mass classification systems and quality indices has been oriented toward underground construction problems. Steiner and Einstein (1980) provide a very thorough review of historical and current empirical design methods for rock tunnels and caverns. A more general discussion of the state-of-the-art for all types of rock classification is given

by Bieniawski (1980).

Although there is an extensive literature on rock mass quality indices for underground construction problems, there are only a few correlations existing for rock mass deformability. A relationship between the equivalent elastic modulus for a rock mass (E_m) and the intensity of jointing was originally established by Deere et al. (1967) in their widely-cited work at Dworshak Dam. Using standard uniaxial compression tests, they measured the elastic modulus, E_{lab}, for small intact samples at the site and compared it to the in situ elastic modulus, E_m, backfigured from plate loading tests. This comparison was repeated for 24 locations at the site, and the ratio E_m/E_{lab} was then plotted as a function of the RQD value at each location. The observations from Deere et al.'s original study were subsequently supplemented with other field data by Coon and Merritt (1970), producing the composite relationship between E_m/E_{lab} and RQD illustrated in Figure 3.1.

Deere et al. (and later, Coon and Merritt) also tried to establish a relationship between modulus ratio and seismic velocity ratios. However, the scatter in the data was much greater than for the correlation between modulus ratio and RQD.

Despite the apparently good correlation between rock mass deformability and RQD shown in Figure 3.1, the relationship must be viewed with some caution for three reasons. First, nearly all of the field data came from fair to excellent quality rock masses (RQD > 60%). For poorer quality rock masses, -- for which deformability is often particularly important -- the relationship between modulus ratio and RQD is unclear, as is indicated by Coon and Merritt's question marks in Figure 3.1.* Second, only two rock parameters are treated

* The modulus ratio vs. acoustic velocity ratio data suggest that the modulus ratio reaches a constant value of approximately 0.15 for RQD less than about 60%.

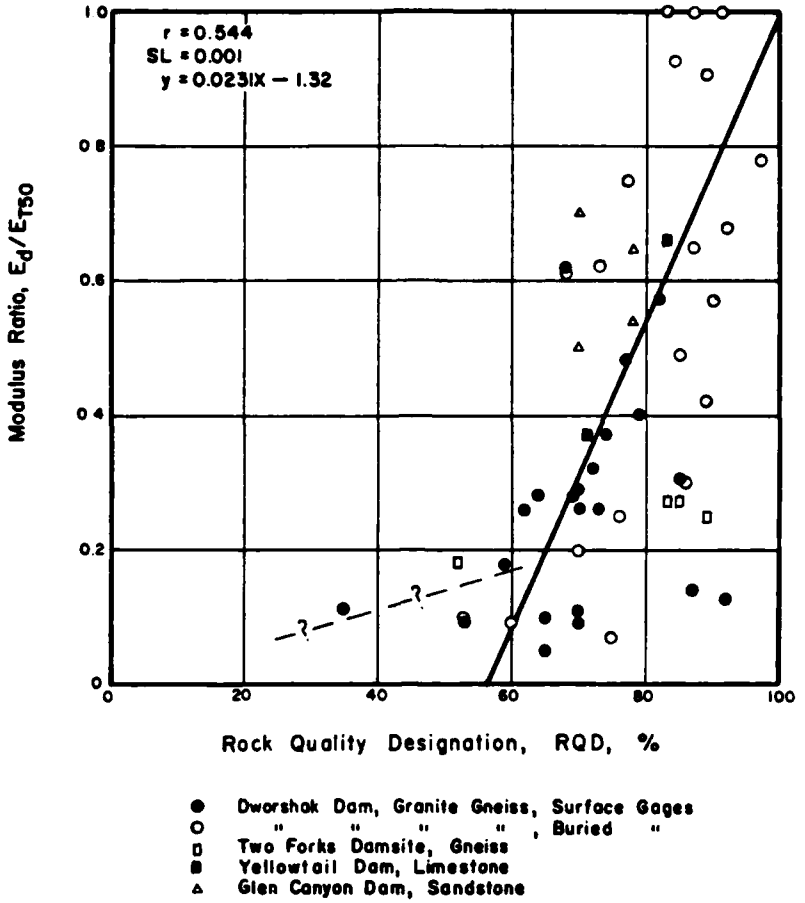

Figure 3.1 Coon and Merritt's (1970) Correlation Between RQD and Modulus Ratio

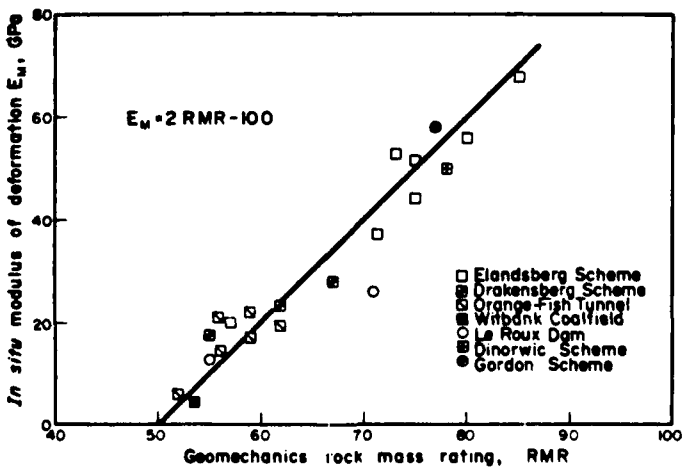

Figure 3.2 Bieniawski's (1978) Correlation Between RMR and Rock Mass Modulus

in the correlations: E_{lab}, which is a measure of the intact rock stiffness, and RQD, which, although influenced by the intact rock strength and joint orientation, is primarily a measure of discontinuity spacing (see, for example, the work by Priest and Hudson, 1976). Third, in statistical terms the regression is not very strong; the coefficient of determination, r^2, is only 0.30 -- in other words, the "best fit" trend line explains only 30% of the observed variation in modulus ratio.

Bieniawski (1978) has avoided the limitations of the RQD-based correlation by developing a multiparameter rock quality index, his Geomechanics Classification System's Rock Mass Rating (RMR) value, which is a weighted function of the intact rock compressive strength, RQD, discontinuity spacing and condition (roughness, aperture, persistence, and filling), groundwater conditions, and joint orientations. Using data from seven large projects, Bieniawski correlates RMR directly with the rock mass modulus measured in situ. The strength of this correlation is attested to by the data in Figure 3.2.

As with Coon and Merritt's correlations, Bieniawski's equations are valid only for fair to very good quality rock masses (RMR > 50). Within this range, the multi-parameter RMR is a much better index for E_m than is RQD, at least for the field data considered. However, neither method is of much assistance to the rock engineer interested in the deformability of poor quality rock; for that, he must still test in situ or (perhaps) look for guidance to the theories described in the next section.

3.3 Theoretical Models

The methods described under this heading are best subdivided into two categories: (a) "mechanistic" approaches, and (b) equivalent continuum models based on composite material theory. There is some overlapping between these categories.

3.3.1 "Mechanistic" Approaches

These methods are all based upon the following set of assumtions: (a) a volume of the rock mass containing a representative sample of discontinuities and intact rock blocks can be isolated -- i.e. the rock mass is statistically homogeneous and the discontinuity spacing is small; (b) the discontinuities are all fully persistent; and (c) the representative volume of rock is subjected to a uniform state of stress -- i.e. the stresses across the discontinuities are equal to the stresses within the intact rock. Given these assumptions, the deformations of the discontinuities and the intact rock can be derived independently, given the applied stress level and the stiffnesses (usually assumed elastic) of the discontinuities and intact rock. Once the total deformation of the rock mass, which is simply the sum of the deformations of the discontinuities and the intact rock blocks, is known, the equivalent continuum stiffness moduli of the rock mass can be derived.

Salamon (1968) has applied this mechanistic approach to the case of a stratified rock mass (which can be reduced to the problem of a rock mass with one set of parallel, fully persistent joints). Assuming that all strata are parallel, homogeneous, transversely isotropic, and elastic with varying properties and thicknesses, Salamon derives equations for the elastic constants for the equivalent transversely isotropic elastic continuum.

Following reasoning similar to Salamon's, Morland (1974a, 1974b) has formulated a more general model which can treat two or more (in theory) joint sets as well as frictional slip along individual joints. Interlocking of adjacent rock blocks is explicitly neglected. Gerrard (1982a, 1982b) has extended this theory to the case of orthorhombic elastic properties.

Kulhawy (1978) has developed a simple geomechanical model for the case of a rock mass transected by three orthogonal joint sets (see Figure 3.3).

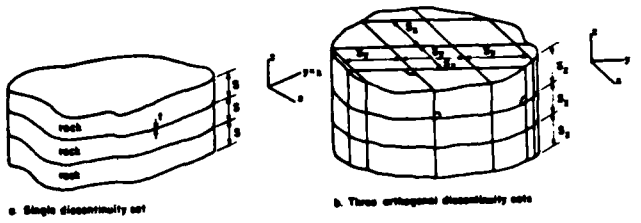

Figure 3.3 Kulhawy's (1978) Mechanistic Model for Rock Mass Deformability

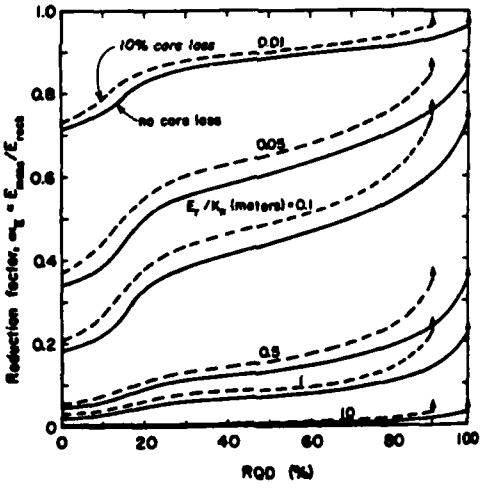

Figure 3.4 Results from Kulhawy's (1978) Model

The joints in each set are assumed to be parallel with known mean spacing and normal and shear stiffnesses; the intact rock is assumed to be homogeneous, isotropic, and elastic. Interlocking effects between intersecting joints are ignored. The rock mass is modeled as an homogeneous, orthotropic, elastic equivalent continuum; Kulhawy provides expressions for the elastic constants in each coordinate direction:

$$E_i = \frac{1}{\frac{1}{E_r} + \frac{1}{S_i K_{ni}}} \tag{3.1}$$

$$G_{ij} = \frac{1}{\frac{1}{G_r} + \frac{1}{S_i K_{si}} + \frac{1}{S_j K_{sj}}} \tag{3.2}$$

$$\nu_{ij} = \nu_{ik} = \nu_r \frac{E_i}{E_r} \tag{3.3}$$

in which E_r, G_r, ν_r = elastic constants for the intact rock, S = joint mean spacing, K_n and K_s = joint normal and shear stresses, and i = x, y, z (with j = y, z, x and k = z, x, y). K_{ni} denotes the normal stiffness for joints perpendicular to the i-coordinate direction, etc.

Recognizing that RQD rather than spacing is the joint intensity parameter most commonly measured from borings, Kulhawy proposes a mechanistic model relating mean joint spacing to RQD. Having related RQD to mean spacing, Kulhawy then uses his geomechanical model is express rock mass stiffness (defined in terms of the modulus ratio E_m/E_r) as a function of RQD, as shown in Figure 3.4. The modulus ratio is also dependent upon the ratio of intact rock modulus to joint normal stiffness (E_r/K_n). The curve for E_r/K_n = 0.5 meters approximately matches the field data from Coon and Merritt's (1970)

study (see Figure 3.1)

All of the above models are based on several restrictive assumptions. For example, they require that the discontinuities be parallel in each set. Dershowitz et al. (1979) relax this assumption by considering a uniformly stressed cylindrical volume of rock in which the joints within a set are subparallel (as will be described in a later section, the joints are actually probabilistically oriented according to a Fisher distribution). Interlocking at intersecting joints is still neglected. Their model, which qualitatively reproduces many trends observed empirically, produces some new and interesting conclusions. For example, variation of the dip angle about the mean has a strong influence an E_m/E_r for joint sets with a high mean dip (relative to the direction of applied stress).

Two serious restrictions in all of the "mechanistic" models are: (a) the discontinuities are all fully persistent, and (b) there are no interactions between intersecting discontinuities. Without these assumptions, the determination of the stresses, and therefore the strains, in the discontinuities and the intact rock becomes considerably more complex. For the opposite extreme of nonpersistent and nonintersecting joints, though, these stresses and strains can be derived using composite material theory.

3.3.2 Composite Material Models

These models are all based either directly or indirectly on the composite material theory formulated by Hill (1963, 1965) and others. The fundamental postulate of the theory is as follows: if the boundary tractions (stresses) are macroscopically uniform -- i.e., deviation from the mean are small relative to the mean, then the average stress in a composite material should be related to the average strain through the effective

elastic moduli. Thus, if one can, through simple geometric or theoretic considerations, determine these average stresses and strains, then the unknown effective moduli can be backfigured.

The problem, of course, is determining the average stresses and strains in the material. In a heterogeneous, composite material the stresses and strains in the component phases will be functions of the applied loads, the geometry of the phases, and the relative stiffnesses of the phases. Singh (1973), in one of the more widely cited applications of this theory to the jointed rock problem, assumes that the joints are all aligned in orthogonal patterns. The joints need not be continuous; one of the cases Singh considers consists of a set of continuous parallel joints intersected by a second staggered orthogonal set. For this assumed geometry, Singh expresses the average stress in the joints as equal to the average stresses in the intact rock multiplied by a stress concentration factor. Knowing this factor, the volumetric percentages of the joint phases, and the compliances of the intact rock and joints, it is possible to derive an expression for the effective compliance of the composite rock mass.

Unfortunately, in order to evaluate the stress concentration factor Singh must resort to a finite element analysis of a particular joint configuration under a particular idealized loading. Thus, although Singh's method can in theory be applied to any arbitrary rock mass, the analysis effort required to determine the stress concentration factor may be nearly as great as the effort to perform a regular finite element analysis for the actual problem at hand.

Another approach toward determining the average stresses and strains in a rock mass is to assume that the joints are isolated, ellipsoidal, elastic inclusions in an infinite, elastic intact rock body with uniform

free-field stresses. The stresses and strains in the inclusions can be derived from classical elasticity theory (Eshelby, 1957). These techniques, often called "self-consistent methods", have been reviewed recently in a thorough paper by Cleary et al. (1980). The assumption that the ellipsoidal inclusions are completely isolated can be relaxed somewhat; Cleary et al. discuss several approximate methods for dealing with the interactions between proximate but nonintersecting inclusions. Intersecting inclusions (e.g., joints) cannot be treated in the theory.

Many researchers have used the self-consistent methods as the starting point for investigations into the constitutive behavior of heterogeneous geological materials. In addition to the original studies on polycrystalline minerals (Hill, 1965; Beran and Molyneux, 1966), the theoretical behavior of rock containing pores (Walsh, 1980) and microfractures (Budiansky and O'Connell, 1976; Kachanov, 1980) with varying degrees of statistical disorder (Kroner, 1980) has been investigated.

Although the equivalent continuum models are useful tools for studying the deformability of many types of composite materials, they suffer several limitations when applied to the jointed rock mass problem: (a) the behavior of the intact rock and joint phases must be assumed linear and elastic, (b) the joints cannot intersect (although this restriction has been relaxed by Singh, but only at some expense of theoretical elegance and computational practicality), and (c) the stress fields must be macroscopically uniform -- i.e., the average stress gradient must be negligibly small. Of course, in real rock masses none of these limitations is even closely satisfied, at least for problems with any engineering significance -- e.g., foundations, underground openings. The errors in the model when the last of these limitations is violated, for example, are illustrated by a set of analyses performed by Singh (1973). He considered the problem of a footing on a rock

mass transacted by one set of horizontal, parallel joints. The rock displacements beneath the foundation were analyzed two ways: (a) an anisotropic continuum finite element analysis using elastic moduli calculated from Singh's equivalent continuum model, and (b) a discontinuum finite element analysis that modeled the intact rock and joints as discrete features. The results from the Singh's analyses are given in Figure 3.5. Directly under the footing, where the stress gradients are the highest, the equivalent continuum model predicts vertical displacements two to three times those predicted by the discrete joint analysis. Hungr and Coates (1978) noted this same trend in their equivalent continuum analyses. Clearly, this magnitude of error limits the usefulness of the theories.

3.4 Numerical Models

3.4.1 Finite Element Methods

As alluded to in the last section, an alternative approach toward determining the deformability of a discontinuous rock mass is to perform some type of numerical analysis that treats the intact rock and joints as discrete features. Finite element methods have, in the past, been the most popular. In fact, since very few analytical solutions exist for the stresses and displacements within anisotropic continua, the equivalent continuum models described in the preceding sections would generally be used only to determine the material properties for the rock mass; these properties would then be used as input for a finite element stress analysis.

In order to treat rock discontinuities as discrete features, some type of joint finite element is required. Goodman et al. (1968) presented an early formulation in which the joints were assumed to be linearly elastic-plastic, with failure governed by a no-tension Mohr-Coulomb criterion. This

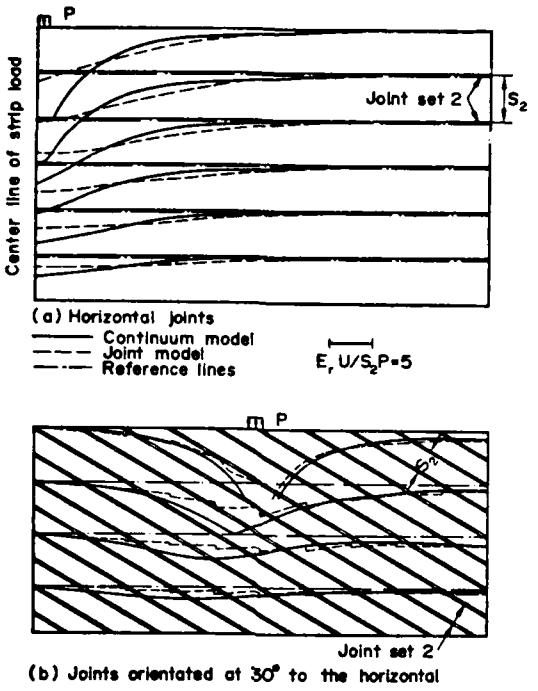

Figure 3.5 Singh's (1973) Results for the Rock Movements Below a Surface Foundation. (Vertical Deflections Computed by Finite Element Analysis, Using a Joint Model and an Anisotropic Continuum Model. Joint Shear Stiffness is One-Tenth of Joint Normal Stiffness)

AD-A136 497 PROCEEDINGS SEMINAR ON PROBABILISTIC METHODS IN GEOTECHNICAL ENGINEERING. (U) ARMY ENGINEER WATERWAYS EXPERIMENT STATION VICKSBURG MS GEOTE.. 5/7

UNCLASSIFIED M E HYNES-GRIFFIN ET AL. SEP 83 F/G 8/13 NL

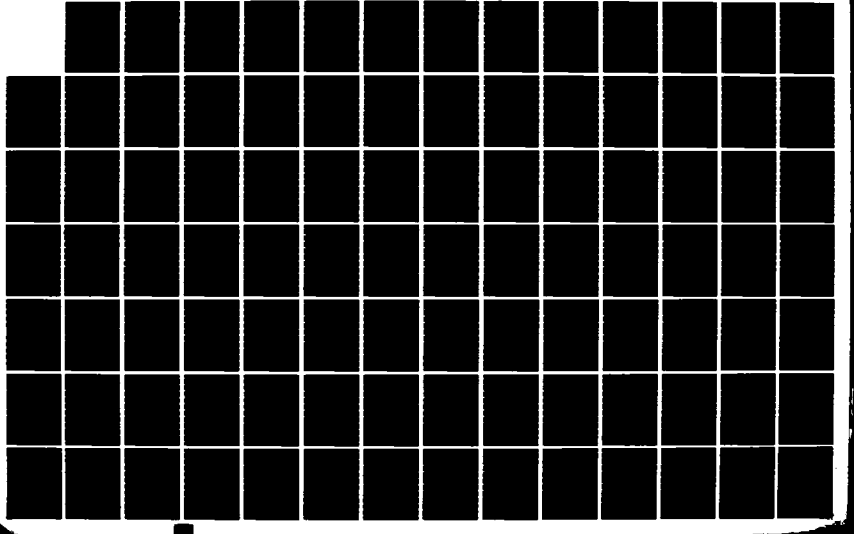

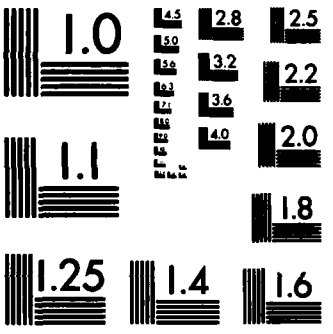

MICROCOPY RESOLUTION TEST CHART
NATIONAL BUREAU OF STANDARDS-1963-A

element was later refined to include the effects of nonlinear joint stiffness and dilatancy (Goodman and DuBois, 1972; Goodman, 1976). Joint elements are now readily available in several large-scale finite element programs such as the U.S. Bureau of Mines' BMINES code (Agbabian Associates, 1980), which was specifically developed for analytical modeling of rock-structure interaction problems.

3.4.2 Boundary Element Methods

A newer and potentially more powerful technique for the numerical analysis of rock mechanics problems is the boundary element method (see for example, Brebbia and Walker, 1978; Brady and Bray, 1978; Brady, 1979a, 1979b; and others). In the boundary element method, only the boundaries of the problem are discretized -- i.e., broken up into elements -- for the numerical approximation. In a discontinuous rock mass, these boundaries consist of the geometrical boundaries (e.g., the ground surface or the wall of a tunnel) and the discontinuities (joints)). This is in contrast to the finite element method, in which the entire region enclosed by (and including) the boundaries must be discretized.

Although the boundary element method is a powerful numerical technique, it is not without its limitations. The method is based in essence on influence functions for stresses and displacements in an infinite region. Therefore, one must be able to find what is termed the "elementary solution" for these influence functions. These solutions are readily available for the case of linearly elastic material behavior (see Brebbia and Walker, 1978, for example). Viscoelasticity (Crawford and Curran, 1979) and classical plasticity (Banerjee and Mustoe, 1978) can also be treated, although with more difficulty. Fortunately, in the jointed rock mass problem most of the

nonlinear behavior is concentrated in the joints. Compared with the joints, the intervening intact rock blocks can be treated as being linearly elastic without sacrificing much accuracy in the analysis. Joint slip, separation, creep, and other types of nonlinear behavior can easily be incorporated into a boundary element analysis (see Crouch, 1976a, 1976b; Crawford and Curran, 1979).

Although numerical methods can in principle be applied to any rock mass deformability problem, they are not necessarily the ideal approach. Like in situ testing, numerical analyses are project-specific, time consuming, and expensive (especially finite element analyses). Numerical methods by themselves are not comprehensive theoretical models for the behavior of rock masses, but are merely analysis techniques. Nevertheless, numerical methods can be used in parametric studies to determine the relationships between rock mass deformability and the underlying geological parameters.

4. PROBABILISTIC AND STATISTICAL METHODS FOR DETERMINING ROCK MASS DEFORMABILITY

As outlined in the preceding section, the existing techniques for determining and/or predicting the deformability of rock masses in situ are numerous and varied in approach. One of the few traits common to all of these techniques is that they are almost exclusively deterministic in nature. Nevertheless, efforts have been made recently to include some of the probabilistic and statistical aspects of the problem. Much of this development has been of a theoretical and academic nature, although the reasons for this are not clear. The complexity of the problem makes the development of even a comprehensive deterministic model difficult. Moreover, there is a reluctance to use even the deterministic models in practice, a reluctance that is only intensified (in some quarters) when a probabilistic component

is added. Considering the accuracy and applicability of most of these methods, this reluctance is somewhat justified at present. This topic will be discussed further in Section 5.

The discussion of probabilistic and statistical methods will be organized along lines similar to those in the preceding section. Each category of methods will be considered in turn. The current probabilistic and statistical content of the various methods will be highlighted, with comments as appropriate regarding possible fruitful means for enhancing this content.

4.1 In Situ Methods

There has been very little application of statistical or probabilistic techniques to in situ testing. Even purely descriptive statistical methods for representing test results have been bypassed. However, this is in large part due to the special nature of in situ deformability testing in rock. When measuring geometric parameters such as joint spacing, trace length, and orientation in the field, it is relatively easy to derive information such as the mean, standard deviation, and distributional forms. Each joint survey may consist of samples of hundreds or thousands of joints. When measuring in situ deformability, however, the high cost of most tests means that one or at most a few sample points are measured. There are simply insufficient data for deriving any truly useful statistical measures.

This problem of limited sample size is alleviated somewhat when borehole methods are used to measure in situ deformability. These tests are relatively inexpensive and can therefore be economically performed at many location over the site. However, borehole methods suffer from other problems such as the size effect (Heuze, 1980) that may distort the results. Since these distortions tend to affect magnitudes rather than trends, though, borehole tests

can still be useful for estimating parameters for autocorrelation or semi-variogram representations of spatial variability.

There is a need for more but simple statistical interpretation of the results from in situ deformability tests. Rock mass deformability is widely acknowledged to be a highly variable quantity. However, there are not really any quantitative "rules-of-thumb" for the magnitude of this variability. More published tabulations of means and ranges or coefficients of variation for rock mass deformability at selected sites would be of practical value.

4.2 Empirical Correlations with Rock Quality Indices

The empirical correlation methods as a group are related to the model-building and regression techniques found in many other disciplines such as econometrics. These methods are statistical in the sense that the sampled data is assumed to exhibit a random error or "scatter" about some trend. Regression theory provides algorithms for selecting this trend to minimize the error.

The empirical correlations for rock mass deformability are derived using techniques ranging from simple curve fitting by eye to the more formal least squares regression methods. However, even in these more formal approaches, it is rare to find statistical data given regarding the power of the correlation (beyond the occasional r^2 value). This is unfortunate, especially in view of the trend toward more sophisticated multiparameter correlations.

Because of their wide usage as a substitute for expensive in situ testing, the further development of empirical correlations for rock mass deformability will continue. These correlations will be based on increasingly sophisticated rock quality indices, and they should accordingly be

developed using increasingly sophisticated statistical regression techniques. These techniques, borrowed from other disciplines, can be used to consider such factors as model identification and specification, the relative explanatory power of the independent variables, and the level of confidence (in a statistical sense) in the predictions.

As an example of the benefits that could be derived from the application of more rigorous statistical techniques, consider the empirical correlation between rock mass modulus and Rock Mass Rating (RMR) described in Section 3.2. The RMR value is a weighted function of six variables: intact rock strength, joint spacing, RQD, joint condition, joint orientation, and groundwater conditions. A more detailed statistical testing of the correlation might well find that certain variables are insignificant (e.g., the groundwater variable, at least for near-surface foundation problems), that other variables are correlated (e.g., joint spacing and RQD or joint condition, joint orientation, and RQD), that variables are missing from the correlation, and that the weighting of the variables should be modified (i.e., specially tailored to the rock deformability problem). The practical benefits from these findings extend beyond an improvement of the correlation for rock mass modulus. Improvements and economies in field exploration would also be achieved, since the engineer would no longer spend money to measure insignificant parameters (e.g., the groundwater) or all of the variables that are strongly correlated (only one would need to be measured -- e.g., RQD or joint spacing, but not both).

A concomitant need in this area is for more field data. More well-documented case studies of rock mass deformability testing need to be published, and the data from these cases need to be incorporated in the empirical correlations to improve their strength. Much of this information

may already reside in project files in engineering offices; these data need to be made more widely available.

4.3 Theoretical Models

As one might expect, these are the methods in which probabilistic techniques can be considered most explicitly. Although the simplifying idealizations underlying the theoretical treatments may often reduce their suitability for use in practice, these methods are nonetheless valuable for studying the fundamental mechanisms underlying rock mass deformability and for drawing qualitative conclusions.

4.3.1 "Mechanistic" Approaches

Some probabilistic concepts have been incorporated in even the simplest mechanistic theories. For example, Kulhawy's (1978) model needs as input quantities the mean joint spacing for the three orthogonal joint sets (see Section 3.3). Since RQD rather than mean spacing is usually measured from drill cores, Kulhawy proposed a simple, deterministic method for relating mean spacing to RQD. Goodman and Smith (1980) improved on this technique by using a random number generator on a small programmable calculator to generate spacing (and RQD) for randomly located joints along a line. They calculated a range of RQD values for each mean joint spacing; if one ran enough simulations one could develop the complete distribution for RQD as a function of spacing.

In probabilistic terms, Goodman and Smith's method is simply a numerical simulation of a Poisson process for joint locations along a line. This stochastic process produces an exponential distribution for joint spacing, a distributional form that has been repeatedly observed in the field for joint sets (e.g., Baecher, Lanney, and Einstein, 1977). A theoretical

relationship between RQD and true joint frequency* for joints with exponentially distributed spacings was derived by Priest and Hudson (1976):

$$RQD = 100e^{-0.1\lambda}(0.1\lambda + 1.0) \qquad (4)$$

in which λ is the mean true joint frequency (joints per meter). This relationship can be inverted to give the spacing vs. RQD relation needed in Kulhawy's model. The results from Kulhawy's model after incorporating this change are shown in Figure 4.1. The principal effect is to increase the modulus reduction factor in the high RQD range, bringing it more in line with the field data points.

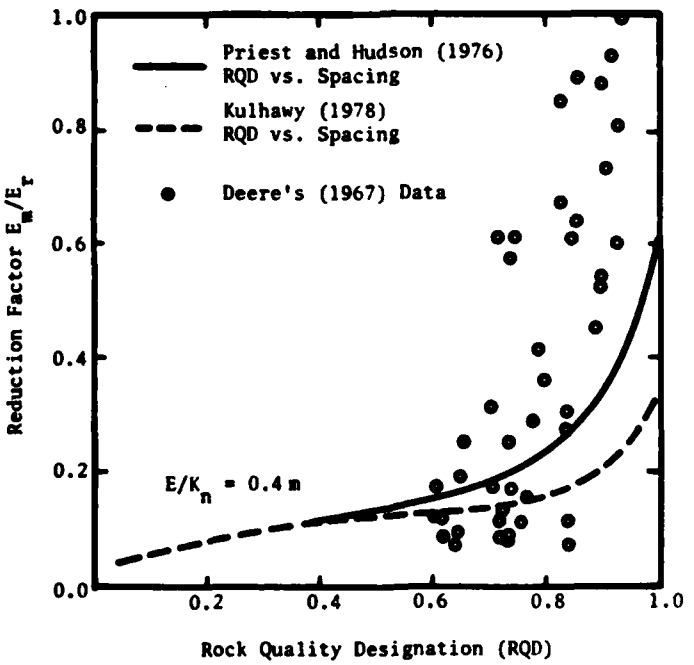

Figure 4.1 Kulhawy's (1978) Model Modified to Incorporate Priest and Hudson's (1976) RQD vs. Spacing Relationship

* True joint frequency is the inverse of true joint spacing, the perpendicular distance between parallel joints; Dershowitz (1979) presents a modified version of Priest and Hudson's work in terms of apparent frequency.

Of course, joint spacing is not the only factor in Kulhawy's model that exhibits natural variability. Other factors such as E_r, G_r, K_{ni}, and K_{si} should also be treated as random variables. This has been considered by Madhav and Rama Krishna (1980), who performed a second moment analysis of the rock foundation settlement problem using Kulhawy's model for the rock constitutive behavior. They also analyzed a second, similar model of their own devising. Their results are expressed as the probability that the foundation settlement will exceed some specified design value; their assumptions are that the foundation settlement is either normally or log-normally distributed (the assumption of a distributional form is necessary to extract probabilities from the second moment analysis, which gives only mean and variances). Based on some limited parametric studies, Madhav and Rama Krishna concluded that the variability in each parameter contributes significantly to the uncertainty in the settlement predictions as long as the variability in the other parameters is not excessive -- e.g., coefficients of variation less than 0.6. If any one parameter is highly variable, then the variability in the other parameters has only a slight effect on the overall settlement uncertainty. Put into practical terms, this implies that if, for example, the intact rock modulus E_r is highly variable,there is little benefit from measuring the joint normal stiffness K_n with much precision.

The influence of variable joint orientation on rock mass deformability has been investigated by Dershowitz et al. (1979). Their model is similar to Kulhawy's but the joints are no longer assumed parallel (interactions at intersecting joints are ignored, however). Joint spacing and orientation are treated as random variables; spacing

is assumed exponentially distributed and orientation, Fisher distributed. As shown in Figure 4.2, this model demonstrates that the inclusion of orientation variability leads to rock mass deformability values that are significantly different from those predicted by deterministic models, particularly when the joints have a high mean dip angle. Uncertainty in both spacing and orientation produces the relationship between the expected value of E_m/E_r and expected value of RQD shown in Figure 4.3. Although many assumptions were made regarding input parameters, the comparison between the model predictions and Deere's empirical data in Figure 4.3 indicate that the model is at least qualitatively correct.

Based on their deterministic and probabilistic parametric studies, Dershowitz et al. were able to draw several intriguing conclusions. First, rock mass deformability is extremely sensitive to joint geometry; joint stiffness has a major but secondary effect. This is of some practical significance, because it is relatively easy to determine joint geometry (at least joint spacing and orientation) while quite difficult to determine joint stiffness. Second, for cases of low dispersion of joint orientation about the mean, RQD appears to be a reasonable index for deformability. For cases with high orientation dispersion, RQD is "sufficient only as a first approximation, since different combinations of spacing and orientation lead to the same RQD but different deformabilities." Third, higher quality rock masses with high RQD tend to have larger variances in E_m/E_r than poorer quality rock. In other words, poor quality rock masses, which in practice are usually the cases for which rock mass deformability is an important issue, will tend to have lower but more certain modulus values than will high quality rock.

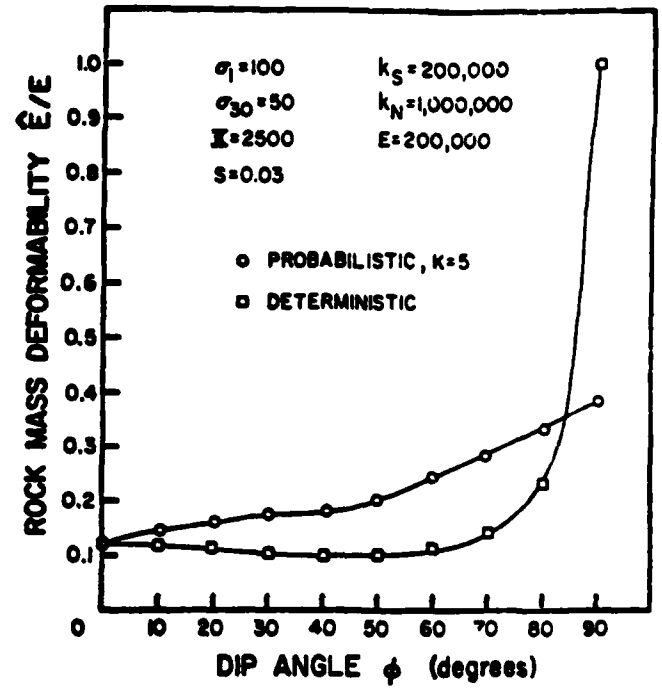

Figure 4.2 Comparison of Deterministic and Probabilistic Rock Mass Deformability Models (Dershowitz, 1979)

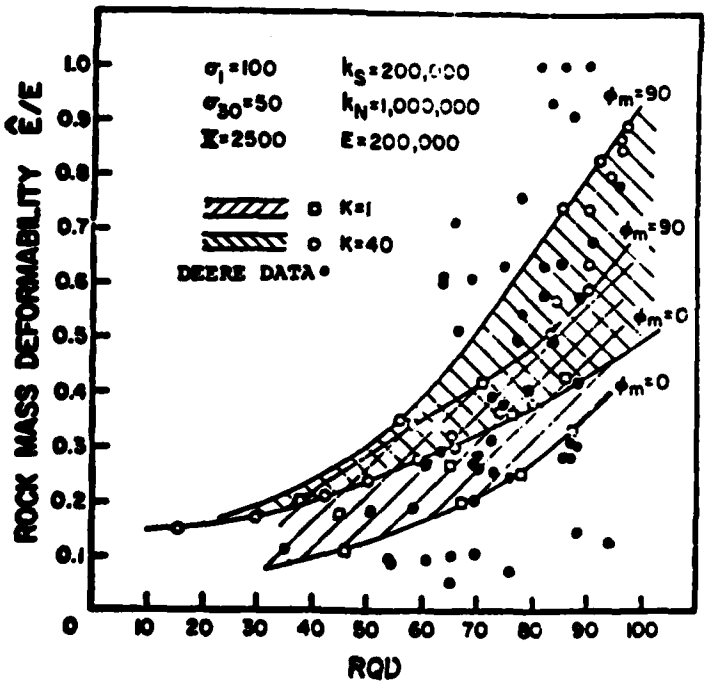

Figure 4.3 Rock Mass Deformability vs. RQD, Considering Joint Spacing and Orientation Variability (Dershowitz, 1979)

4.3.2 Composite Material Models

As mentioned in Section 3.3, the basic assumption in the class of composite material models known as the "self-consistent" methods is that one phase of the composite -- e.g., the pore phase in an intact rock -- can be represented as a distribution of nonintersecting elastic inclusions in an elastic matrix. Effective elastic moduli can then be derived in terms of the elastic moduli of the inclusions and the matrix.

The earliest self-consistent theories all assumed that the elastic moduli of the constituent phases were deterministically uniform (see, e.g., Cleary et al., 1980). This requirement can be relaxed slightly by assuming the moduli in each phase are only statistically uniform -- i.e., the moduli have a spatially invariant mean but a random spatial variation about this mean. Effective elastic moduli for this case were developed by Beran and Molyneux (1966) and Kroner (1967). Kroner later extended this theory to consider spatial correlation of the elastic moduli, a condition he calls "graded disorder" (Kroner, 1980). By considering graded disorder with appropriate direction-dependent correlation functions, it is possible to model anisotropic as well as isotropic materials.

The main advantage of both the mechanistic and the composite material theoretical approaches to the rock mass deformability problem is that once enough idealizations have been clearly identified the ensuing analysis can be "rigorous". The main disadvantage, of course, is that the process of idealization tends to divorce the analysis from reality. The resulting errors can only be evaluated by comparing results from simple theories to those from more complex theories and ultimately to measured data from the field. To date, these comparisons have not been close. Deterministic equivalent continuum representations based on the mechanistic and some of the composite material models can significantly overestimate the

deformability of the rock mass (Singh's 1973 results were mentioned previously in Section 3.3). Comparisons between predictions from the theoretical models and measurements from the field are nearly nonexistent.*

More studies need to be conducted to determine the applicability of these simple theoretical models to the rock mass deformability problem. It is quite possible that over certain ranges of the parameters -- e.g., joint spacing, stiffness, etc. -- the theoretical models may be sufficiently accurate for engineering purposes. However, these ranges still need to be defined. And, there are the twin needs for more comparisons with field data and more field data for making these comparisons.

4.4 Numerical Models

In a stochastic setting, numerical methods are useful for performing Monte Carlo-type simulations of the behavior of the rock mass. The power of these simulations is limited only by one's knowledge of the detailed constitutive behavior of the rock and joints and by the capacity of one's computer. In even very simple simulations, though, it is possible to relax many of the extreme idealizations required by the theoretical models.

The simplest simulations, originally developed for foundations on soil, treat the subsurface as a series of layers with the elastic properties of each layer treated as random variables (Resendiz and Herrera, 1970; Hilldale, 1971). Since each layer is assumed homogeneous in the horizontal as well as vertical directions, only total settlements can be predicted. Baecher and Ingra (1981) generalize on this using two-

* Predictions from the self-consistent composite material models agree well with measured values of bulk modulus for polycrystalline intact rock specimens. However, the applicability of these models to the rock mass problem has not been demonstrated.

dimensional finite element techniques, enabling the study of both vertical and horizontal spatial variability on the total and differential settlements of the foundation. The elastic properties of the individual finite elements are treated here as spatially correlated random variables. The results for differential settlements, in particular, show the significant influence of the "randomness in the finite element stress field and [the] mechanistic dependence on commonly shared random variables," two phenomena that cannot be studied using one-dimensional finite layer models. Overall, the two-dimensional simulations predict settlement uncertainties lower than those from the one-dimensional models.

Finite element simulations have also been applied to underground opening problems (Su, Wang, and Stefanko, 1970; Fug, Haimson, and LaPointe, 1979). These studies, which treat the individual element elastic properties as uncorrelated random variables, generally indicate that the spatial variability in the stress field caused by the material variability tends to reduce the magnitude of the maximum stresses at the wall of the cavity. Maximum displacements also are reduced, implying that the effective rock mass modulus in the spatially variable case is higher that in the corresponding homogeneous (deterministic) analysis.

LaPointe (1981) emphasizes the need to include spatial correlation of the random variables in the simulation if any valid conclusions are to be drawn. His studies, which actually deal with rock mass stability rather than deformability, show that uncorrelated analyses (i.e., most conventional Monte Carlo simulations) may be unconservative (in terms of stability). For the foundation problem, Baecher and Ingra (1981) demonstrate that the expected differential settlement increases to a peak and then decreases as the degree of spatial correlation increases. As would

be expected, increasing spatial correlation also increases the uncertainty in the total settlement predictions.

Simulations employing boundary element techniques have not been attempted to date. Nevertheless, these techniques have much potential. As an example of one simulation scheme, a stochastic joint geometry generator could be used to "sprinkle" joints into an elastic half space beneath a foundation (Figure 4.4). These joints could be automatically discretized with boundary elements and used to perform one analysis cycle in the simulation.

In summary, numerical simulations are an appealing approach for gaining insight into the probabilistic rock mass deformability problem. The studies that have been performed to date are few and rudimentary, however. More investigations are needed, but special effort must be devoted to drawing practical conclusions from their results.

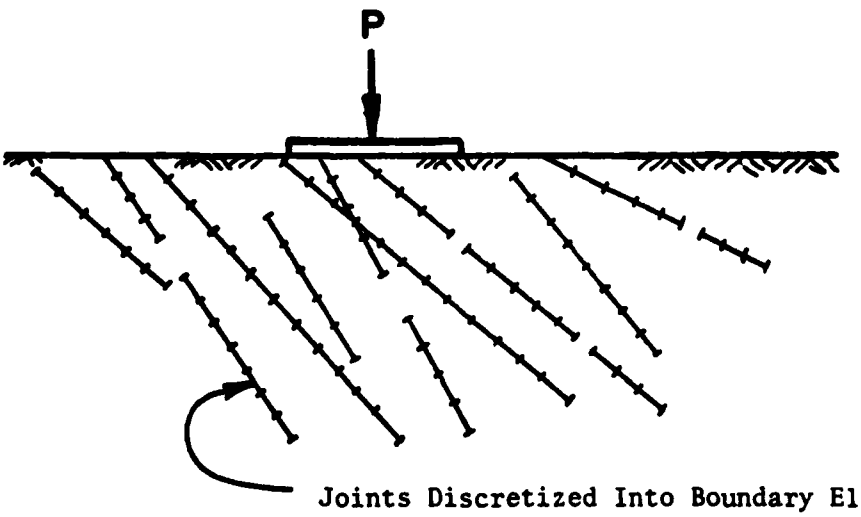

Figure 4.4 Scheme for Simulating Rock Mass Deformability Using Boundary Elements

5. CURRENT STATUS OF PROBABILISTIC METHODS

To put it bluntly, the application of statistical and probabilistic techniques to the characterization of rock mass deformability is still in its infancy; these techniques have not been, nor are they yet ready to be, much used in practical engineering analysis and design. Rock mass deformability is an extremely difficult property to assess precisely. Even the interpretation of direct in situ measurements is by no means a straightforward process. Given that rock mass behavior is so complex and poorly understood and that projects for which rock mass deformability is important are usually major and expensive, it is unsurprising that practicing engineers are inclined toward conservatism and empirical methods rooted in the sparse field evidence that is available.

Nevertheless, there is a strong need for improved rock mass modeling, and especially for statistical and probabilistic modeling, in rock engineering. The most distinguishing characteristics of rock masses are variability and uncertainty. Thus, sufficient in situ testing to completely define by direct measurement the nature of the rock mass is expensive and time consuming. Even if this could be accomplished, the incorporation of a highly variable set of measurement data into a quantitative deterministic analysis is problematic at best and may, in fact, produce serious misleading conclusions. The potential savings resulting from more informative models for deformability are quite large, if for no other reason than that the projects to which they would be applied are usually very costly.

The need for better models for rock mass deformability is not limited to pre-construction analysis and design. During site exploration, correct interpretation of most in situ stress tests requires

precise knowledge of the rock's deformability. In situ instrumentation used during construction monitoring -- e.g., extensometers, inclinometers, and convergence measurements -- would provide more robust information if rock deformability values were available to convert measured displacements to induced stress changes.

Improvements are needed over the entire range of methods used for characterizing rock mass deformability. More insitu test data should be interpreted using simple descriptive statistics. Empirical correlations between rock mass modulus and rock quality indices should be refined using more statistically sophisticated techniques. Lastly, better stochastic theoretical and analytical models should be developed to provide further insight into the underlying mechanisms and variables in the problem.

These improvements in stochastic methods can produce practical results in rock engineering. Consider the progress made in rock slope stability: probability-based risk analyses are increasingly accepted and used by engineers in charge of large open pit mines. Similar trends can be expected in other rock engineering problems, including deformability.

6. RECOMMENDATIONS FOR RESEARCH

The danger in addressing a problem like rock mass deformability is that, since so much progress needs to be made, too many research recommendations are made with too little ordering of priorities. Accordingly, the emphasis here will be on those topics which have a clear present need for further study and which must be investigated before any future progress can be made.

For some perspective on research needs, one can look to the recommendations in the recent report by the National Academy of Sciences (NAS),

"Rock Mechanics Research Requirements for Resource Recovery, Construction, and Earthquake Hazard Reduction" (1981). The need for improved characterization of rock mass properties, including rock mass deformability, is noted pervasively through the report. Of the eight major research areas identified, three deal either directly or indirectly with deformability: (1) the development of improved methods for determining in situ stresses, (2) the development of methods for detecting and analyzing discontinuities and for determining their effects on the mechanical properties of rock masses, and (3) the resolution of the disparities that exist between laboratory and field test results, of the effect of scale on rock properties, and of methods for in situ measurement.

The need for increased utilization of stochastic methods for a wide range of rock problems is repeatedly noted in the NAS report. This is perhaps best illustrated by a series of quotations:

> "[There is a need to] develop numerical techniques for estimating rock-mass response to static and dynamic loads, within a probabilistic framework. The probabilistic approach is necessary because the data sampled represent a small fraction of the parent population of the rock mass properties." (pg. 13)

> "The wide disparity between the sample population and the actual target population containing rock-mass properties will make a deterministic functional relationship all but impossible to define uniquely. For this reason, probabilistic techniques that incorporate the spatial and statistical uncertainties that inevitably enter into rock design, such as stochastic models in which rock properties are assumed to be spatially variable and uncertain, should be developed and utilized more fully." (pg. 113)

> "It should be noted that numerical or physical modeling is an important approach for scaling measured quantities to in situ conditions." (pg. 117)

Recommendations for further research on rock mass deformability can be summarized in two categories. The first consists of general recommendations that also apply to other areas in rock engineering:

- *Additional in situ testing, and the statistical interpretation of the test results.* Properly interpreted field test results provide the necessary data base for the determination of both the nature and degree of variability and uncertainty in the rock mass properties. These data also provide a benchmark for the validation of predictive analytical models.

- *Increased monitoring of prototype projects, and reinterpretation of measured data from previous projects.* Properly interpreted, these data can provide the same types of information as the results from in situ tests.

- *Improved modeling of rock mass behavior.* Analytical models should reflect the stochastic nature of the rock mass. Deterministic models are also useful, both in their own right and because they often serve as the basis for probabilistic models. Both analytical and physical modeling permit the investigation of the fundamentals of rock mass behavior under controlled conditions.

The second category of recommendations consists of suggestions more specific to the rock mass deformability problem:

- *Better statistical interpretation of field deformability data.* Typical values for simple measures of variability such as means, variances, coefficient of variation, and spatial correlation are needed. Unfortunately, the sample data base for these measures is limited at present. However, more studies like those currently being conducted at the Colorado School of Mines (El Raaba, et al., 1982) should alleviate this problem.

- *Re-examination of existing empirical correlations in statistical terms.* These correlations generally give the mean trend of rock mass modulus as a function of rock quality. Statistical methods can also be applied to assess the suitability of the formulation for the rock quality index, the strength of the correlation, the uncertainty in the predictions, etc.

- *Evaluation of existing models.* These models need to be more fully compared against each other and against field data to determine their appropriateness and range of applicability.

- *Development and improvement of formal probabilistic models.* The value of these models has already been described above. Improved models for rock mass geometrical properties (i.e., jointing patterns) are needed as well as models for rock mass mechanical behavior.

- *Increased use of numerical simulations.* Parametric simulation studies provide comparisons for other probabilistic models. Furthermore, they can incorporate effects (such as spatial correlation) not easily included in the simple theories.

In all of this research, emphasis should be placed on extracting conclusions of practical engineering value. Many of these research areas will also provide knowledge of a more scientific nature regarding the basic behavior of rock masses. This too has much long-term value. Nonetheless, the ultimate product of rock engineering is constructed facilities; engineering research should be focused accordingly.

REFERENCES

_____ (1981), "Rock Mechanics Research Requirements for Resource Recovery, Construction, and Earthquake Hazards Reduction," National Academy of Sciences, Washington, D.C.

Agbabian Associates (1980), "User's Guide for BMINES -- A Computer Program for Analytical Modeling of Rock/Structure Interaction," Draft Version, November.

Baecher, G.B. (1981), "Uncertainties in Geotechnical Engineering," Lecture Notes, Short Course on Statistical and Probabilistic Methods in Rock Engineering, Massachusetts Institute of Technology, June.

Baecher, G.B., N.A. Lanney, and H.H. Einstein (1977), "Statistical Description of Rock Properties and Sampling," 18th USSRM (U.S. Symposium on Rock Mechanics), Colorado School of Mines.

Baecher, G.B. and T.S. Ingra (1981), "Stochastic FEM in Settlement Predictions," Journal of the Geotechnical Engineering Division, ASCE, Vol. 107, No. GT4, April, pp. 449-463.

Banerjee, P.K., & Mustoe, G.G. (1978), "The Boundary Element Method for Two-Dimensional Problems of Elastoplasticity," Recent Advances in Boundary Element Methods, C.A. Brebbia (Ed.), Pentech Press LTD., London, pp. 283-300.

Beran, M.J. and J. Molyneux (1966), "Use of Classical Variational Principles to Determine Bounds for the Effective Bulk Modulus in Heterogeneous Media," Quarterly of Applied Mathematics, Vol. 24, pp. 107-118.

Bieniawski, Z.T. (1978), "Determining Rock Mass Deformability: Experience from Case Histories," IJRMMS, Vol. 15, pp. 237-242.

Bieniawski, Z.T. (1980), "Rock Classifications -- State of the Art and Prospects for Standardization," presented at the annual meeting of the Transportation Research Board, Washington, D.C., January.

Brady, B.H.G. (1979a), "Boundary Element Method of Stress Analysis for Non-Homogeneous Media and Complete Plane Strain," Proceedings, 20th U.S. Symposium on Rock Mechanics, Austin, Texas, pp. 243-250.

Brady, B.H. (1979b), "A Direct Formulation of the Boundary Element Method of Stress Analysis for Complete Plane Strain," Int. J. Rock Mech. Min. Sci. & Geomech. Abstr., Vol. 16, No. 4, August, pp. 235-244.

Brady, B.H., and Bray, J.W. (1978), "The Boundary Element Method for Determining Stresses and Displacements Around Long Openings in a Triaxial Stress Field," Int. J. Rock Mech. Min. Sci. & Geomech. Abstr., Vol. 15, No. 1, February, pp. 21-28.

Brebbia, C.A., & Walker, S. (1978), "Introduction to Boundary Element Methods," Recent Advances in Boundary Element Methods, C.A. Brebbia (Ed.), Pentech Press Ltd., London, pp. 1-43.

Budiansky, B. and R.J. O'Connell (1976), "Elastic Moduli of a Cracked Solid," J. Solids & Structures, Vol. 12, pp. 81-97.

Cleary, M.P., I.W. Chen, and S.M. Lee (1980), "Self Consistent Techniques for Heterogeneous Media," JEMD (Journal of the Engineering Mechanics Division), ASCE, Vol. 106, No. EM5, October, pp. 861-887.

Coon, R.F. and A.H. Merritt (1970), "Predicting In Situ Modulus of Deformation Using Rock Quality Indices," Determination of the In Situ Modulus of Deformation of Rock, ASTM STP 477, pp. 154-173.

Crawford, A.M. and J.H. Curran (1979), "A Displacement Discontinuity Approach to Modelling the Creep Behavior of Rock and Its Discontinuities," Report 79-09, Department of Civil Engineering, University of Toronto, Toronto, Canada.

Crouch, S.L. (1976a), Analysis of Stresses and Displacements Around Underground Excavations: An Application of the Displacement Discontinuity Method, Report Prepared for National Science Foundation, Research Applied to National Needs, Washington, D.C., November (NTIS #PB-267 109).

Crouch, S.L. (1976b), "Solution of Plane Elasticity Problems by the Displacement Discontinuity Method: I. Infinite Body Solution; II. Semi-Infinite Body Solution," Int. J. Num. Meth. Eng., Vol. 10, pp. 301-343.

Deere, D.U., A.J. Hendron, Jr., F.D. Patton, and E.J. Cording (1967), "Design of Surface and Near-Surface Construction in Rock," Proceedings, 8th U.S. Symposium on Rock Mechanics, Minneapolis, Minn., pp. 237-303.

Dershowitz, W.S. (1979), "Rock Mass Deformability: A Probabilistic Approach," Master of Science Thesis, Massachusetts Institute of Technology.

Dershowitz, W., Baecher, G., and Einstein, H. (1979), "Prediction of Rock Mass Deformability," Proceedings, 4th International Congress on Rock Mechanics, ISRM, Montreux, Switzerland, Vol. I, pp. 605-611.

Dowding, C.H. (e.d.)(1979), Site Characterization and Exploration, National Science Foundation Workshop, Northwestern University (Available through ASCE).

Einstein, H.H. and C.W. Schwartz (1979), "Simplified Analysis for Tunnel Supports," Journal of the Geotechnical Engineering Division, ASCE, Vol. 105, No. GT4, April, pp. 499-518.

Eshelby, J.D. (1957), "The Determination of the Elastic Field of an Ellipsoidal Inclusion and Related Problems," Proceedings of the Royal Society of London, Series A, pp. 376-396.

El Rabaa, A.W.M.A., W.A. Hustrulid, and W.F. Ubbes (1982), "Spatial Distribution of Deformation Moduli Around the CSM/ONWI Room, Edgar Mine, Idaho Springs, Colorado," Proceedings, 23rd U.S. Symposium on Rock Mechanics, Berkeley, California.

Fug, G. - F., B.C. Haimson, and P.R. LaPointe (1979), "Annular Rock Caverns for Energy Storage Under Fourier Expandable Stress Fields," Proceedings, 3rd Inst. Conf. on Numerical Methods in Geomechanics, Aachen, West Germany, pp. 627-638.

Gerrard, C.M. (1982a), "Equivalent Elastic Moduli of a Rock Mass Consisting of Orthorhombic Layers," Int. J. Rock Mech. Min. Sci., Vol. 19, No. 1, February, pp. 9-14.

Gerrard, C.M. (1982b), "Elastic Models of Rock Masses Having One, Two, and Three Sets of Joints," Int. J. Rock Mech. Min. Sci., Vol. 19, No. 1, February, pp. 15-23.

Goodman, R.E. (1976), Methods of Geological Engineering in Discontinuous Rock, West Publishing Co., St. Paul, Minn.

Goodman, R.E. (1980), Introduction to Rock Mechanics, John Wiley and Sons, New York.

Goodman, R.E. and J. DuBois (1972), "Duplication of Dilatancy in Analysis of Jointed Rocks," JSMFED (Journal of the Soil Mechanics and Foundation Engineering Division), ASCE, Vol. 98, p. 399.

Goodman, R.E., R.L. Taylor, and T.L. Brekke (1968), "A Model for the Mechanics of Jointed Rock," JSMFED (Journal of the Soil Mechanics and Foundation Engineering Journal) ASCE, V. 94, No. SM3, pp. 637-659.

Goodman, R.E. and H.R. Smith (1980), "RQD and Fracture Spacing," Technical Note, Journal of the Geotechnical Engineering Division, ASCE, V. 106, N. GT2, February, pp. 191-193.

Heuze, F.E. (1980), "Scale Effects in the Determination of Rock Mass Strength and Deformability," Rock Mechanics, Vol. 12, Nov. 3, March, pp. 167-192.

Hill, R. (1965), "Elastic Properties of Reinforced Solids: Some Theoretical Principles," J. Mech. Phys. Solids, Vol. 11, pp. 357-372.

Hill, R. (1965), "A Self-Consistent Mechanics of Composite Materials," J. Mech. Phys. Solids, Vol. 13, pp. 213-222.

Hilldale, C. (1971), "A Probabilistic Approach to Estimating Differential Settlement of Footings on Sand," Master of Science Thesis, Massachusetts Institute of Technology.

Hungr, O. and D.F. Coates (1978), "Deformability of Joints and Its Relation to Rock Foundation Settlements," Canadian Geotechnical Journal, Vol. 15, pp. 239-249.

Kroner, E. (1967), "Elastic Moduli of Perfectly Disordered Composite Materials," J. of the Mech. Phys. Solids, Vol. 15, pp. 319-329.

Kroner, E. (1980), "Graded and Perfect Disorder in Random Media Elasticity," Journal of the Engineering Mechanics Division, ASCE, Vol. 106, No. EM5, October, pp. 889-914.

Kulhawy, F.H. (1978), "Geomechanical Model for Rock Foundation Settlement," Journal of the Geotechnical Engineering Division, ASCE, Vol. 104, No. GT2, April, pp. 211-227.

LaPointe, P.R. (1981), "Improved Numerical Modeling Through Geostatistical Characterization," Proceedings, 22nd U.S. Symp. Rock Mech., MIT, pp. 386-391.

Madhav, M.R. and K.S. Rama Krishna (1980), "A Probabilistic Analysis of Settlement of Foundations on Rock," Structural Foundations on Rock, P.J.N. Pells, ed., A.A. Balkema, Rotterdam, Vol. 1, pp. 173-180.

Morland, L.W. (1974a), "Elastic Response of Regularly Jointed Mediums," Geophysical Journal, Vol. 37, pp. 435-446.

Morland, L.W. (1974b), "Continuum Model of Regularly Jointed Mediums," Journal of Geophysical Research, Vol. 79, pp. 357-362.

Obert, L. and W.I. Duvall (1967), Rock Mechanics and the Design of Structures in Rock, John Wiley and Sons, Inc., New York.

Priest, S.D. and J.A. Hudson (1976), "Discontinuity Spacings in Rock," Int. J. Rock Mech. Min. Sci., Vol. 13, pp. 135-148.

Resendiz, D. and I. Herrera (1970), "A Probabilistic Formulation of Settlement Controlled Design," Proceedings of the Seventh International Conference on Soil Mechanics and Foundation Engineering, Mexico City.

Salamon, M.D.G. (1968), "Elastic Moduli of a Stratified Rock Mass," IJRMMS (Int. J. Rock Mech. Min. Sci.), Vol. 5, pp. 519-527.

Singh, B. (1973), "Continuum Characterization of Jointed Rock Masses, Part I -- The Constitutive Equations. Part II -- Significance of Low Shear Modulus," Int. J. Rock Mech. Min. Sci. & Geomech. Abstr., Vol. 10, No. 4, pp. 311-350.

Stagg, K.G. and O.C. Zienkiewicz (ed.)(1968), Rock Mechanics in Engineering Practice, John Wiley and Sons Inc., New York.

Steiner, W. and H.H. Einstein (1980), "Improved Design of Tunnel Supports: Volume 5 -- Empirical Methods in Rock Tunneling, Review and Recommendations," Report No. UMTA-MA-06-0100-80-8, Urban Mass Transit Administration, Washington, D.C.

Su, Y.L., Y.J. Wang and R. Stefanko (1970) "Finite Element Analysis of Underground Stresses Utilizing Stochastically Simulated Material Properties," Proc. 11th USRMS, Berkeley, pp. 253-266.

Walsh, J.B. (1980), "Static Deformation of Rock," Journal of the Engineering Mechanics Division, ASCE, Vol. 106, No. EM5, October, pp. 1005-1019.

SIMPLE STATISTICAL METHODOLOGY FOR EVALUATING ROCK MECHANICS EXPLORATION DATA

by

Gregory B. Baecher

SIMPLE STATISTICAL METHODOLOGY FOR EVALUATING ROCK MECHANICS EXPLORATION DATA

Gregory B. Baecher

ABSTRACT

Advances in rock mechanics instrumentation and in situ testing in recent years have not been paralleled by concurrent advances in systematic procedures for designing site characterization programs and analyzing data. First-order second-moment methods for describing rock mechanics data and expressing the uncertainties of parameter estimates provide a practical and inexpensive vehicle for both improving the efficiency of exploration programs and for developing quantified, defensible estimates of engineering parameters. These methods are based on simplified approximations to the relationships among data and estimates, and use means, variances and covariances to describe uncertainties. The foundation for a simplified sampling theory for in situ testing is developed.

TABLE OF CONTENTS

1. INTRODUCTION

This report intends to lay the groundwork for a simplified approach to the design and interpretation of in situ testing programs for rock engineering. The goal of this simplified approach is to provide a scientific basis for allocating testing and instrumentation, and a systematic procedure for interpreting field observations. No claim is made that the approach addresses all of the subtleties of site characterization. The aim is rather a practical tool that can be used and understood. The methods proposed here require little familiarity with probability theory or statistics. They deal only with the averages, variances, and covariances of uncertain parameters, and lead to mathematically simple relations among sources of error or uncertainty, and estimates of engineering parameters. The purpose of a more scientific treatment of site characterization and data analysis is not that it might lead to probabilistic design and risk analysis, but only that it might improve traditional practice.

This report is organized in four subsequent sections. The first places the present work within the larger frame of reference of site exploration and characterzation. The second briefly summarizes the mathematical background upon which later developments rest. The third presents a procedure for identifying probable errors in estimates of rock mass

properties or profiles. The fourth develops a simplified sampling theory by which testing programs might be designed. Finally, conclusions are drawn on how one should prodeed from the foundation already developed.

2. SITE CHARACTERIZATION AND EXPLORATION

Site characterization in rock engineering involves uncertainties of many types. Rock masses vary from one location to another, the procedures used to measure engineering properties introduce both random and systematic errors, and the low density of exploration measurements across a site makes the likelihood of discovering geological details low. Furthermore, the essential geologic concept of a site, upon which most inferences of zonation and structure rest, is never based on logical deduction from measurements and observations, but is arrived at intuitively and by analogy. All these uncertainties are well recognized by the practicing profession, and design strategies have arisen over the course of time to deal with them.

In recent years interest has developed in attempts to make exploration and site characterization more "scientific." This interest would appear to be driven by at least three developments: an increased availability of new testing apparatus and electronic instrumentation, improved analytical ability in soil and rock mechanics, particularly numerical modeling, and by increased regulatory concern, particularly in dam safety, nuclear plant construction, and waste storage. One result of this increased interest and ability has been a proliferation of new testing devices, which now provide more

data than ever before--more perhaps than can reasonably be put to use with traditional data analysis procedures. Another result, especially in the sister discipline of soil engineering, is a rapid increase in the use of in situ measurements.

The need to process increased numbers of data and to provide "scientific," defensible engineering properties for design leads naturally to the consideration of statistical techniques. These techniques aim at

1) drawing the strongest inferences possible from a given set of data,

2) establishing the confidence that can reasonably be placed in parameter estimates, and

3) allowing exploration programs to be efficiently designed.

These techniques are quite distinct from so-called probabilistic design or risk analysis. They focus on data analysis and parameter estimation, and their results are just as useful for traditional deterministic design as for reliability modeling. Brief surveys of the use of statistical methods in site characterization are given in Baecher (1978, 1982). Statistical techniques, like other tools at the engineer's disposal, are based on simplifications of reality, that is, they are models. They are useful only to the extent that they provide insight and lead to conclusions that were not

otherwise obvious. Statistical techniques cannot solve all the problems of site characterization, and it would be foolish to pretend that they could.

As a first approximation, the principal tasks of site characterization can be thought of as:

> Developing a geological concept (reconnaissance).

> Delineating geometry, boundary conditions, and zonation (mapping).

> Establishing engineering properties for analysis (testing).

> Identifying potentially difficult conditions (search and screening).

To one extent or another each of these enterprises can be aided by statistical methodology. In the present discussion, however, only the third is considered. The intent here is to develop a simple model for engineering property data, and to use that model as the basis for statistical procedures to analyze in situ data and to design testing programs.

3. SECOND-MOMENT ALGEBRA

This section summarizes certain mathematical background to the development of simplified sampling theory for in situ testing.

3.1 Second-Moment Description of Uncertainty

A simple and convenient description of variability or uncertainty in a parameter estimate is the mean and variance. Given a set of data

$$X = \{x_1, \ldots, x_n\} \quad , \tag{3.1}$$

the mean is defined as

$$E(x) = (1/n) \Sigma x_i \quad , \tag{3.2}$$

also called the "expectation" of x. The variance is defined as

$$V(x) = (1/n) \Sigma \{x_i - E(x)\}^2 \quad , \tag{3.3}$$

$$= E(\{x_i - E(x)\}^2) \quad . \tag{3.4}$$

Occasionally, the variance is calculated using the denominator (n-1) rather than n, in light of certain desirable statistical properties of that formula. The square root of the variance,

or standard deviation,

$$S(x) = V^{\frac{1}{2}}(x) \quad , \tag{3.5}$$

is also sometimes useful, as it has more intuitive meaning than does the variance and also as it allows direct comparisons with the mean.

The mean describes the location of the mass of data along the x-axis, and is analogous to the center of gravity of the data. Similarly, the variance describes the dispersion of the data about the mean, and is analogous to the moment of inertia of the mass of data about the mean. Thus, the mean and variance are said to be the first two moments of the variability or uncertainty. For paired data (x_i,y_i) the cross product moment,

$$C(x,y) = E(\{x_i - E(x)\} \{y_i - E(y)\}) \quad , \tag{3.6}$$

or covariance, describes the degree of association between values of x and y. The familiar correlation coefficient is found by normalizing the covariance with respect to the standard deviations of x and y,

$$r_{x,y} = \frac{C(x,y)}{S(x)S(y)} \tag{3.7}$$

For linearly related variables x,y the correlation coefficient approaches plus or minus one, depending on the slope of the

relation. For unassociated (i.e., independent) variables the correlation coefficient approaches zero.

3.2 Functions of Uncertain Variables and Vectors

Given a scalar function of a vector of uncertain variables $\underline{x} = \{x_1, \ldots, x_n\}$,

$$y = g(x) \quad , \tag{3.8}$$

the moments of y can be calculated from the moments of x by introducing a linearizing approximation. Expanding $g(x)$ in a Taylor's series about E(x) and truncating to the first two (i.e., linear) terms,

$$y \doteq g(E(X)) + \frac{dg}{dx} (X - E(X)) \quad . \tag{3.9}$$

Taking the expectations of both sides,

$$E(y) \doteq g(E(X)) \quad , \tag{3.10}$$

and expanding the square to calculate the variance

$$V(y) \doteq \Sigma \Sigma \frac{dg}{dx_i} \frac{dg}{dx_j} C(x_i, x_j) \quad . \tag{3.11}$$

When the components of X are mutually independent, this expression reduces to the familiar

$$V(y) \triangleq \Sigma \left(\frac{dg}{dx_i}\right)^2 V(x_i) \quad . \tag{3.12}$$

That is, the variance of some derived variable can be calculated approximately from the variances of the input parameters and the derivative of the derived parameters with respect to the input parameters. Since these expressions are based on first order relations and treat only second moments, they are sometimes referred to as a first-order second-moment (FOSM) algebra.

For vector $Y=\{y_1, \ldots, y_n\}$ the corresponding relations become,

$$E(Y) \triangleq g(E(X)) \quad , \tag{3.13}$$

and

$$\underline{\underline{\Sigma}}_Y \triangleq \underline{\underline{D}}^t \underline{\underline{\Sigma}}_X \underline{\underline{D}} \tag{3.14}$$

in which

$$\underline{\underline{\Sigma}}_Y = \{ C(y_i,y_j) \}_{m\times m} \tag{3.15}$$

$$\underline{\underline{\Sigma}}_X = \{ C(x_i,x_j) \}_{n\times n} \tag{3.16}$$

are the covariance matrices of Y and X, and D is the matrix of partial derivatives of the elements of Y with respect to the elements of X. All of the derivations and sampling theory

results of later sections are based on these simple FOSM relations.

3.3 Implicit Functions

Frequently, the functional relations among uncertain variables are expressed as a set of implicit equations rather than as direct functions. For example, the calculation of planar stress changes from borehole deformation measurements is one such case. In these cases a modifiction of the FOSM algebra above is necessary.

Given a vector Y of uncertain quantities expressed implicitly by the set of differentiable equations

$$\begin{aligned} f_1(X,Y) &= 0 \\ &\cdots \\ &\cdots \\ f_m(X,Y) &= 0 \end{aligned} \tag{3.17}$$

where the X are known quantities, the expected values of the Y's can be calculated to a first approximation by substituting the expected values of X into the set of equations and solving as in the deterministic case.

The covariance matrix of the Y's, as shown by Ditlevsen (1981), can be calculated as

$$\underline{\underline{\Sigma}}_Y \doteq \underline{\underline{B}}^{-1} \underline{\underline{A}} \, \underline{\underline{\Sigma}}_X \, \underline{\underline{A}}^t \, \underline{\underline{B}}^{t^{-1}} \tag{3.18}$$

in which A is the mxn matrix whose ij-th element is the derivative of the i-th equation with respect to j-th element of X, and B is the mxm matrix whose ij-th element is the derivative of the i-th equation with respect to the j-th element of Y, with all derivatives evaluated at the means of X and Y.

4. PROFILE ESTIMATION

For engineering purposes, parameter estimates are typically summarized in a design profile, describing the variation of mean (i.e., best estimate) properties vertically or horizontally in the rock mass, and having envelopes about the mean describing uncertainty in the estimate. As a first approximation this uncertainty includes three parts: One due to spatial variation, one due to bias and one due to statistical estimation error. The envelopes do not however include random measurement error (noise), because this error partially averages over the number of measurements made. Thus, noise affects profile uncertainty only to the extent that it inflates statistical estimation error or that it is confused with spatial variation. This section develops a procedure for evaluating uncertainty envelopes about the mean profile using a composition of variances.

The scatter observed in in situ measurements (Fig. 4.1) principally reflects two things: actual variation of engineering properties from one spot to another, and random pertubations introduced by the procedures or instruments of measurement. The latter is said to be random measurement error or noise,

$$\text{Data scatter} = \begin{matrix}\text{Spatial variation} \\ + \\ \text{Measurement noise}\end{matrix} \qquad (4.1)$$

For purposes of estimation, random measurement error is considered just as likely to increase measured values as to decrease them, and on the average to cancel out. Systematic errors of measurement, or biases, affect each measurement in the same way. Thus, they either increase or decrease every measurement by the same magnitude--although that magnitude and its direction may be uncertain--and therefore they do not appear as a component of data scatter (Fig. 4.2).

4.1 Random Measurement Error

The spatial part of the data scatter is precisely that which the exploration program intends to characterize, while the noise part is spurious. Thus, it is important to separate the contributions of these two components of scatter. However, since spatial variability and measurement error combine in producing data scatter, they can not be simply separated by inspection. Some indirect procedure must be used. At least three methods can be thought of. The first is replicate measurement on the same or similar materials, the second is multiple profiling with different instruments, and the third is analyzing the structure of spatial variability. Since

replicate measurement is often impossible in geotechnical investigation, and since multiple profiling confuses noise with biases, the third method is often the least expensive and most practical. In a sense, analyzing the structure of spatial variation exploits the "signature" contained in data scatter which distinguishes spatial variation from noise.

The spatial structure of data scatter about a mean trend is conveniently summarized by an autocovariance function, or equivalently a variogram. Adopting the simple model,

$$z(t) = x(t) + e(t) \quad , \tag{4.2}$$

$$V\{z(t)\} = V\{x(t)\} + V\{e(t)\} \quad , \tag{4.3}$$

in which z(t) is the measurement at point t in the rock mass, x(t) is the actual geotechnical property at t, and e(t) is a corrupting measurement noise, the autocovariance function of z(t) is defined as

$$C_z(r) = E\{\big(z(t) - E(z)\big)\cdot\big(z(t+r) - E(z)\big)\} \tag{4.4}$$

in which E(z) is the mean or mean trend of z(t). This is simply the cross product moment of Eqn. 3.6, expressed as a function of separation distance and location. Assuming stationarity, homogeneity of the rock mass in a statistical sense, $C_z(r)$ simply expresses the covariance of the observations as a function of their separation alone.

Typically, $C_z(t)$ is anisotropic, depending importantly on geology, stress history and rock mass fracturing (i.e., jointing). Similar autocovariance funtions can be defined for x(t) and e(t), and these can be shown algebraically to be related to $C_z(r)$ by

$$C_z(r) = C_x(r) + C_e(r) \quad . \tag{4.5}$$

This leads to an important and useful result. $C_x(r)$ has some form, that takes on the value V(x) at r=0 and then decays somehow to zero as r becomes larger (e.g., as suggested by Fig. 4.3a). As e(t) is presumably independent from one measurement to another--i.e., it is assumed to be "noise"--$C_e(r)$ must be a spike of height V(e) at r=0, and zero elsewhere (Fig. 4.3b). Thus, $C_z(r)$ should look something like Fig. 4.3c, and extrapolation of the observed $C_z(r)$ back to r=0 should allow an estimate of V(e) to be made (Fig. 4.3d). This procedure does not distinguish between real errors caused by the instruments or procedures of measurement, and very fine scale geological variability. However, for most engineering purposes this distinction is arbitrary. Fig. 4.4 shows empirical data for joints.

4.2 Error on The Mean

In addition to data scatter, which is associated with variation about the mean trend, two systematic errors affect the estimation of the mean trend itself. Combining, the total

variance in an estimated profile becomes

$$V\{\hat{x}(t)\} = \begin{matrix}\text{Variance about mean}\\ + \\ \text{Variance of mean}\end{matrix} \tag{4.6}$$

in which "^" signifies an estimate. First, the measurement procedure may introduce a systematic but uncertain bias, B,

$$z(t) = B\,x(t) + e(t) \quad , \tag{4.7}$$

$$E\{z(t)\} = E(B)\,E\{x(t)\} \quad , \tag{4.8}$$

$$V\{z(t)\} = B^2\,V\{x(t)\} + V\{e(t)\} \quad , \tag{4.9}$$

in which V{B} reflects the uncertainty of the bias, typically back calculated from prototype performance. Second, the total number of measurements is limited, thus statistical fluctuations introduce estimation errors. Rearranging terms and removing measurement noise to yield the error in the profile estimate

$$V\{x(t)\} = R\,V\{x(t)\} + V(B)\,E^2(z) + E^2(B)\,V\{E(x)\} \tag{4.10}$$

in which R is a scale factor, V{x(t)} is the spatial variance of the data, V(B) is the variance of the measurement bias, and

$V\{E(x)\}$ is the statistical estimation error in the mean trend. For n widely spaced measurements,

$$V\{E(x)\} \doteq \frac{V\{x(t)\} + V\{e(t)\}}{n} \quad . \tag{4.11}$$

For closely spaced measurements,

$$V\{E(x)\} \doteq \frac{(\underline{1}\ \underline{\underline{\Sigma}}_x\ \underline{1}^t) + V\{e(t)\}}{n} \quad , \tag{4.12}$$

in which

$$\underline{1} = \{1, \ldots, 1\}_n \quad , \tag{4.13}$$

and $\underline{\underline{\Sigma}}_x$ is the covariance matrix of the x(t).

Based on Eqns. 4.4 and 4.6, a mean profile and standard deviation envelopes are easily constructed. Note, however, that the standard deviation envelopes, which express uncertainy in the enginering parameters for analysis, are a function of mode of behavior and scale. This dependency is summarized in the factor R. For example, circular shear instability as in a copper porphyry slope depends on total

resistance over a surface of sliding. Thus, spatial variation in part averages out. Therefore, for small instabilities R approaches 1, but as the scale increases R diminishes. Similarly, for wedge slope failures in a jointed crystalline rock instability depends on the least favorably oriented joints, thus spatial variation exacerbates uncertainty. For small slopes R is about 1.0, but for large slopes R increases well above 1.0 as the chance of encountering that one adverse block increases.

4.3 A Priori Estimates of Measurement Error

This section considers random and systematic (i.e., bias) measurement error, and direct, a priori (i.e., prior to sampling) approaches to their evaluation.

4.3.1 DIRECT CALCULATIONS OF RANDOM MEASUREMENT ERROR

A lower bound on random measurement error can be obtained prior to data collection, or at the time of instrument design, by identifying possible sources of measurement imprecision and calculating their aggregate effect using FOSM algebra. This technique is widely used in other branches of experimental science--where it is typically called error propagation. analysis--but it is somewhat less useful in soil and rock testing where much of the apparent noise is introduced by specimen disturbance, differences between test and prototype conditions, and fine scale geological structure. In this

latter case the technique is principally useful in instrument design and in the identification of important sources of istrument imprecision. A simplified example illustrates the procedure.

The multiple position borehole extensometer (MPBX) is simply a device composed of a set of metal rods, typically about 4 in number, which can be used to measure relative displacements along a borehole between a set of anchors and the boring collar. Each rod is fixed to an anchor at some position along the borehole, and the position of the opposite end of the rod is precisely monitored with a linear displacement transformer or dial gage to detect movements. The measurements of displacement made with the MPBX are subject to a number of possible errors. Among others these include various read-out errors (e.g., voltage ratios), calibration constants and drift, thermal expansion or contraction of the rods (as, e.g., in the case of radioactive waste repositories where temperatures may attain 200 degrees C), interpolation errors in estimating temperature profiles along the rods, movements of the anchor relative to the borehole wall (e.g., due to creep, seating irregularities, etc.), and several others.

As a first-approximation, the displacement between anchor and collar is commonly calculated from a formula of the form

$$d = K_1(V_o/V_i) - a\,(T_2-T_1) \quad , \tag{4.14}$$

in which d is displacement, K_1 is a calibration constant for the LVDT, V_o/V_i is the output:input voltage ratio, a is the coefficient of linear thermal expansion of the rod material, (T_2-T_1) is the change in average rod temperature between installation and testing.

$$V(d) \doteq (V_o/V_i)^2 V(K_1) + K_1^2 V(V_o/V_i) + (T_2-T_1)^2 V(a) + a^2 V(T_2-T_1) \quad . \tag{4.15}$$

The variance of K_1 depends on testing and empirical verification of the slope of the displacement:voltage relation for the electronic equipment under service conditions and environmental stresses. The variance of V_o/V_i depends on the manufacturers specifications and the care of the field personnel. The variance of a depends on empirical verification, and may be a function of geometry and scale. Finally, the variance of (T_2-T_1) depends on the instrumentation for measuring temperature changes, their number, and the algorithm used for interpolating temperatures along the rod between measurements. Fig. 4.5 shows the results of such calculations for a specific waste repository site, indicating the relative influence of the various contributions.

4.3.2 SYSTEMATIC (BIAS) MEASUREMENT ERROR

Systematic error in field measurements are known to be common in rock testing. These include scale effects, errors

due to theories of rock behavior, model uncertainty in engineering predictions, differences between test and prototype conditions, and a number of other things. Indeed, much of the rock mechanics literature is devoted to correlations of test results with engineering parameters back-calculated from observations on prototype structures. In many cases there is little statistics can offer in dealing with systematic errors. Such errors in general can only be evaluated by professional judgement, or by comparison with prototype performance. In both cases, the estimates of bias that result confound many sources of error, including the models used to back-calculate from field observations, presumed boundary and initial conditions, definitions of engineering variables, and the like. Therefore it is usually difficult to transfer to new cases. Statistical estimation techniques for inferring systematic errors from data are well known, and discussed in many texts on introductory statistics (e.g., Benjamin and Cornell, 1971).

TABLE 4.1 -- VARIANCE COMPONENTS FOR CLUSTER SAMPLING

variance component	degrees of freedom	variance
within clusters	n(m-1)	Vw
among clusters	n-1	Va
total	nm-1	$\frac{(N-1)Vb + N(M-1)Vw}{NM - 1}$

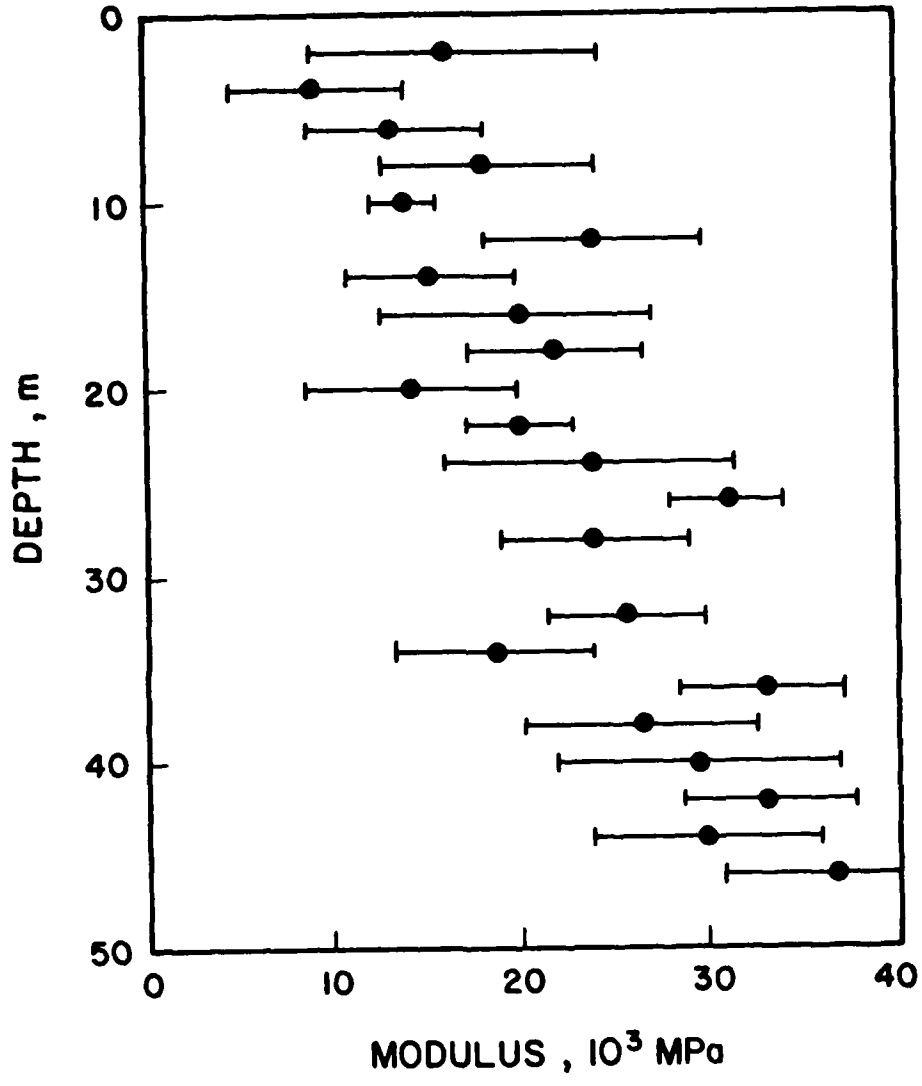

Figure 4.1 -- Scatter of borehole jacking moduli from in situ measurements. Circle shows averages at depth intervals; lines show plus,minus one standard deviation.

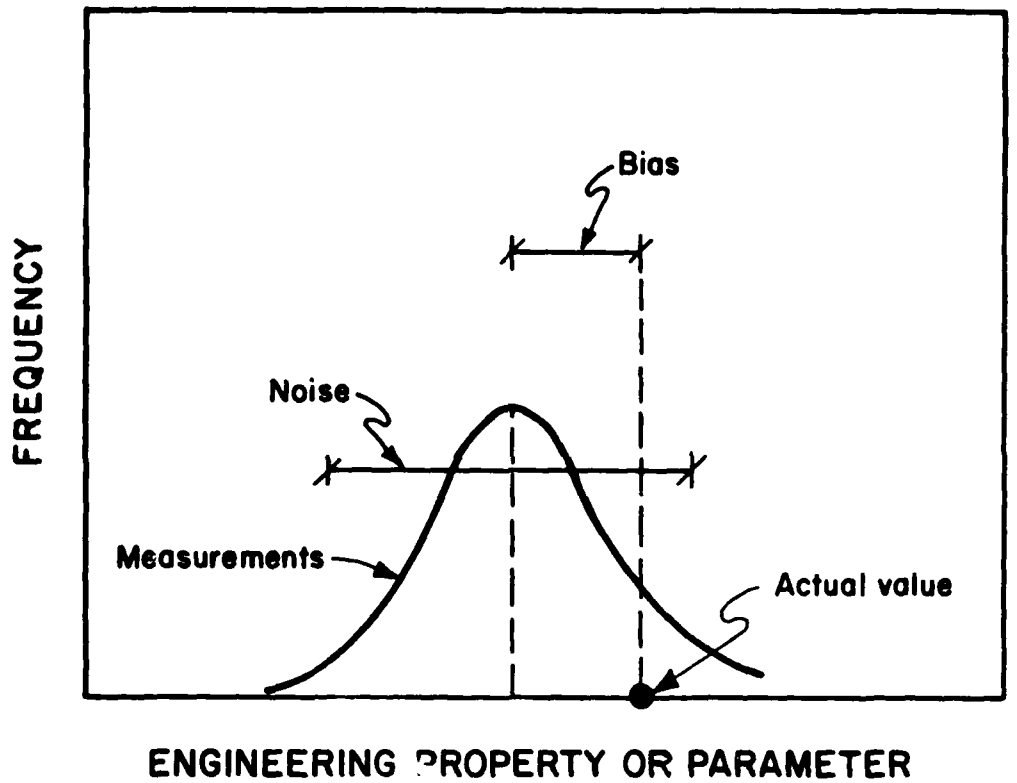

Figure 4.2 -- Distinction between noise and bias measurement errors.

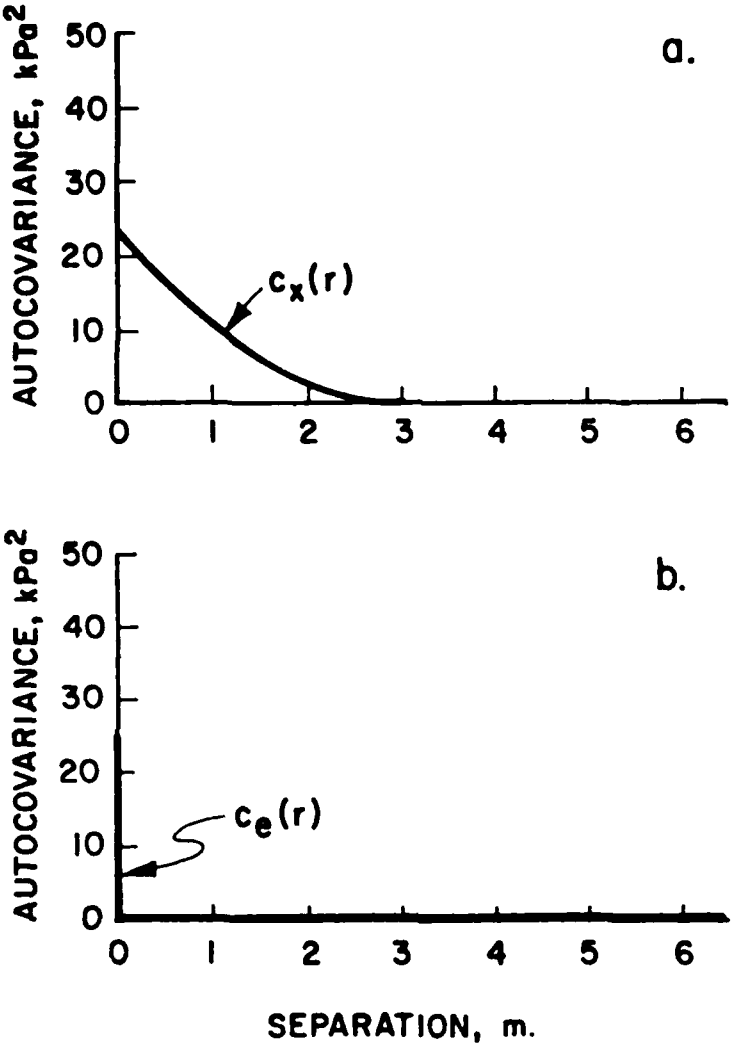

Figure 4.3 -- Composition of sample autocovariance function: a) spatial variable, b) measurement noise, c) spatial variable + noise, and d) inference from field measurements.

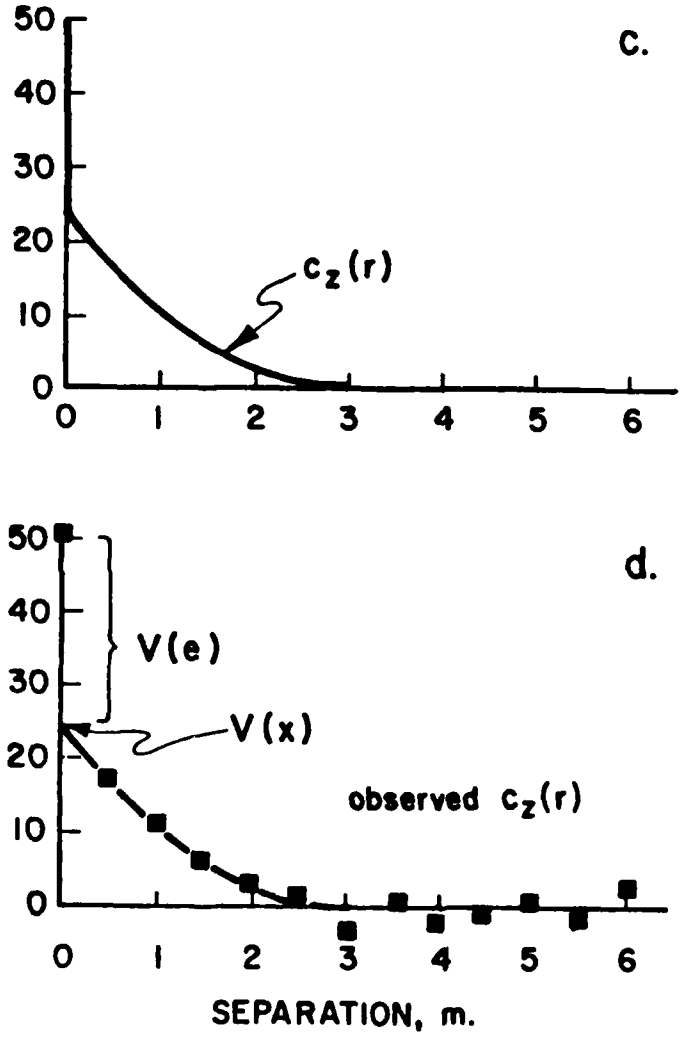

Figure 4.3 (Continued).

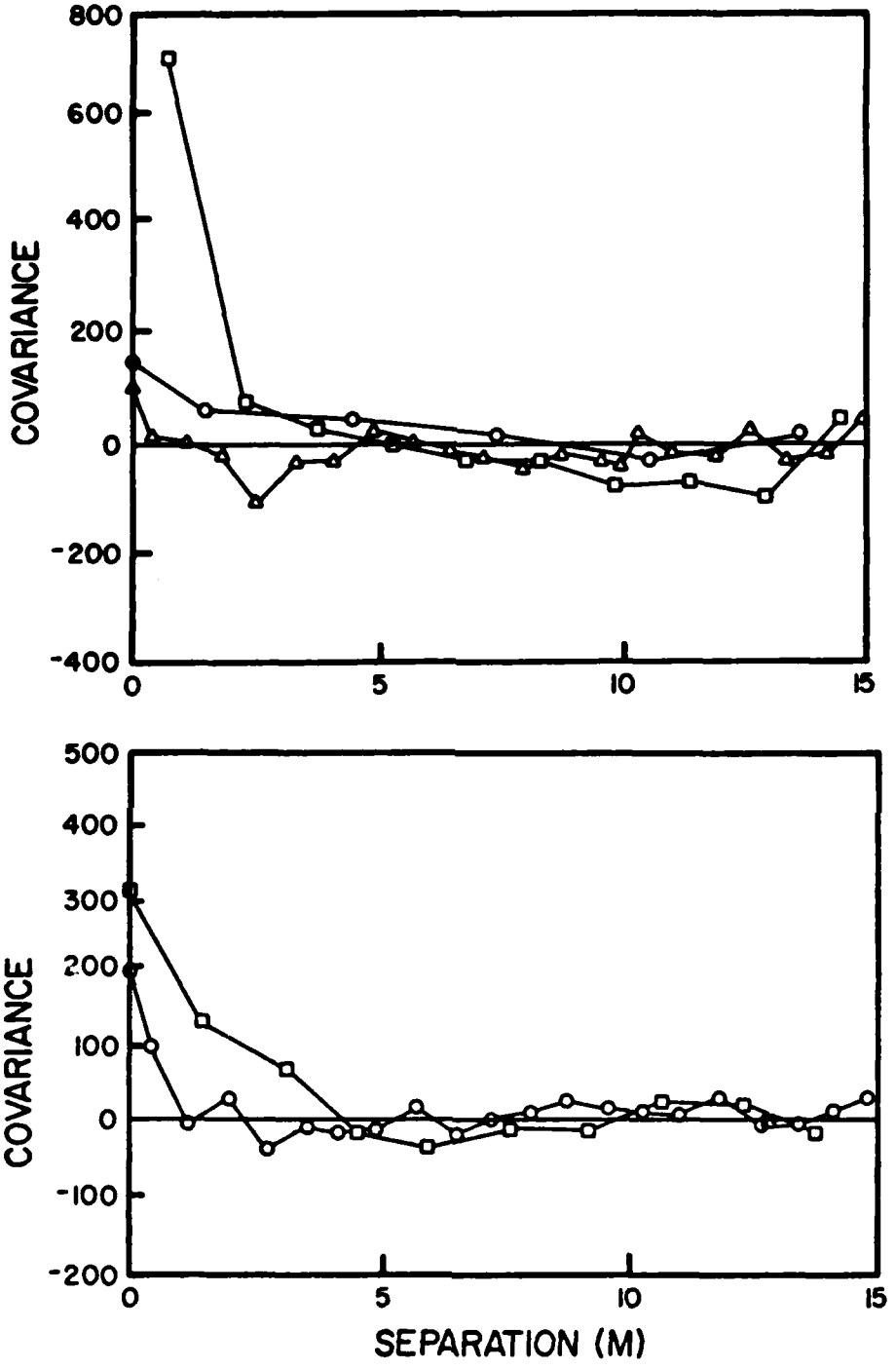

Figure 4.4 -- Empirical autocovariance functions for joint strike (top) and dip (bottom).

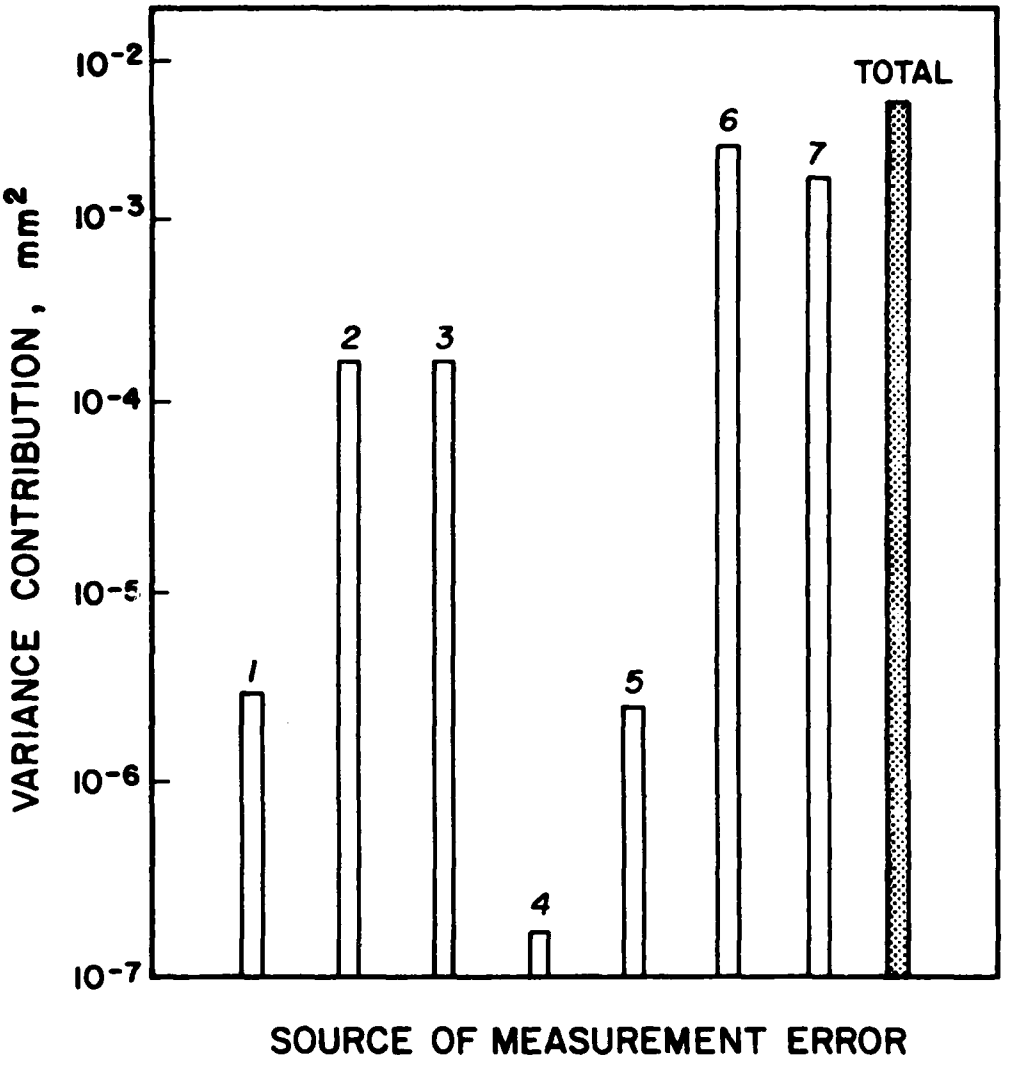

Figure 4.5 -- Variance contributions to measurement error of multiposition borehole extensometer (work done in conjuction with Brian Dorwat and William Deloff of Soil and Rock Instrumentation, Inc.): 1) calibration, 2) thermal expansion of instrument, 3) numerical approximation, 4) thermal expansion of stainless steel, 5) temperature base, 6) expansion of rods, 7) temperature of rods.

5. SAMPLING THEORY

5.1. Fundamentals of Sampling Theory

All inferences on site characterization are made from limited numbers and types of observations, that is from samples. The word "sample" here is used to mean the set of measurements made at the site or on site materials. The more restrictive term "specimen" is used in referring to the physical pieces of soil or rock on which the measurements are made. In the past, little attention has been given to problems of how to obtain a good sample of site materials or conditions, and how to draw sound conclusions from the results. The design of sampling programs has been based primarily on intuition and professional concensus. These have served us well, particularly when dealing with fairly uniform sites or conditions; but greater efficiency is possible, and the study of techniques that ensure trustworthy samples becomes particularly important when sites and conditions become less uniform.

This chapter contains an account of the application of basic principles of scientific sampling to in situ testing in rock mechanics, and to some extent in geotechnical engineering generally. The fundamental ideas are founded on widely accepted concepts of sampling theory; the actual procedures discussed, however, are tailored to the special needs of

geotechnical engineering. Thus, they differ from those found in standard sampling theory texts.

The question might reasonably be asked, why we now need scientific sampling in rock engineering when intuition and concensus have served us well for so long? The reason is threefold:

> First, more data are now collected in site characterization than was heretofore the case, and the trend accelerates as newer in situ devices are developed. The trend is especially advanced in soil mechanics, and is increasingly apparent in rock mechanics. Data analysis by inspection is simply becoming less possible as time goes by.

> Second, while increasing amounts of data are being collected in order to satisfy public and regulatory concern for facility safety and to insure cost effective engineering design, at the same time, pressure is being exerted to insure that exploration programs are efficient, accurate, and completed on schedule.

> Third, again due to public and regulatory concern, inferences of engineering properties drawn from site characterization programs must be technically defensible. For better or worse, the engineer's professional judgement about site conditions, if not based on cogent technical argument, is being more and more questioned in licensing hearings and legal actions.

5.1.1 POPULATIONS

Sampling in rock engineering is undertaken to gather information about specific rock units, and in so doing to characterize the engineering properties of a site for the purposes of analysis and design. These specific rock units might be called the "target population," in that they are the objects of the sampling effort. In statistical terminology, a "population" is simply any aggregate of values. The population from which the sample itself is taken might be called the "sampled population," and ideally should be the same as the target population. However, this is not always practical. For example, in a site exploration program to characterize tunneling conditions at depth the only part of the rock mass accessable for testing might be surface outcrops or shallow excavations. Thus, the sampled population might only overlap the target population, or it might merely be of similar character to the target population (Fig. 5.1). A sample--that is, a finite set of observations--is taken from the sampled population, and from the properties of the sample the properties of the sampled population are inferred.

The inference of properties of the sampled population from those of the sample is the principal task of scientific (i.e., statistical) sampling theory. This theory provides a quantitative basis for establishing both the accuracy and the precision of such inferences. However, sampling theory does not deal with the

question of inferring properties of the target population from those of the sampled population: That is a question of geology, not statistics.

5.1.2 PROBABILITY SAMPLES

In order for quantitative conclusions to be drawn from the results of sampling, the sampling plan must meet three conditions,

1). Each element within the sampled population must have a non-zero probability of being chosen for the sample.

2). The relative probabilities of each element with the sampled population being chosen for the sample must be known (but need not be equal).

3). The method for computing estimates from the sample must be stated, lead to a unique estimate for any specific sample, and weight observations of elements in the sample in inverse proportion to their relative probabilities of being chosen.

If the sampling plan meets these conditions, it is said to be a "probability sampling plan," and sampling theory can be developed for it.

This is not the only way samples can be chosen, of course. For example, the sample can be restricted to easily accessable elements, as when the orientations of only the more exposed or weathered joints on an outcrop are included in a joint survey. Similarly, the sample may be chosen haphazardly, as when borings are placed at the discretion of the field staff. A sample may

also be chosen purposefully, as when "typical" sections of an adit are chosen for load testing (this is sometimes called a "purposive sample"). All of these sampling plans are used in geotechnical exploration, but they preclude the application of sampling theory because they are not statistically representative--that is, because they do not satisfy the requirements of probability sampling plans. They each introduce unknown biases, and thus neither the accuracy nor the precision of estimates made from them can be established scientifically.

5.2 Random Sampling

In section 4 the variance of the first-order estimate of an engineering property or profile was shown to be expressable as a sum of three terms (Eq. 4.8)

$$V(\text{estimate}) = \begin{matrix} V(\text{spatial}) \\ + \; V(\text{bias}) \\ + \; V(\text{statistical}) \end{matrix} \quad . \tag{5.1}$$

This section addresses the question of how numbers and allocations of tests affects this estimation variance.

5.2.1 MODEL OF TEST PRECISION

The precision of a test procedure is reflected in V(e), the variance of the measurement noise term, as discussed in section 4. As a first approximation, one might presume the cost of testing

and test precision to be related, more expensive tests having greater precision than less expensive tests and hence the reason for their use. A simple but reasonable model of this relationship might be that precision is proportional to the unit cost of testing,

$$V(e) = K_e / c \tag{5.2}$$

in which K_e is a constant and c is the unit cost per test. This model has been suggested by Schmertmann (1982), and is supported by certain preliminary data taken from the literature (Fig. 5.2). More complex models could be used if found to be empirically justified, but would not significantly alter the present development. The simple model of Eqn. 5.2 is intuitively appealing in that the rms measurement error (i.e., S(e)) displays diminishing marginal reductions as test cost increases.

5.2.2 OPTIMAL NUMBERS OF TESTS

From section 4 the error in estimating a property or profile, neglecting measurement bias, is approximately

$$V(\hat{x}) = V(x) + \frac{V(x) + V(e)}{n} \tag{5.3}$$

in which n is the number of tests. Substituting Eqn. 5.2 into the above,

$$V(\hat{x}) = V(x) + \frac{V(x) + K_e/c}{n} \tag{5.4}$$

If only one test type is used then the total cost is,

$$C = c_o + n\,c \tag{5.5}$$

in which c_o is a mobilization cost. Thus, neglecting mobilization cost (or presuming it to be roughly the same for different types of tests) the number of tests of unit cost c that can be performed is

$$n = C/c \tag{5.6}$$

Substituting into Eqn. 5.4,

$$V(\hat{x}) = V(x) + \frac{V(x) + K_e/c}{C/c} \tag{5.7}$$

and rearranging terms,

$$V(\hat{x}) = V(x)\ (1 + c/C) + K_e/C \tag{5.8}$$

This is plotted in Fig. 5.3. Clearly, for this model the increased number of inexpensive tests more than compensates for lower test precision. Inexpensive, imprecise tests lead to lower estimate error than do expensive, precise tests.

Changing the model of test precision in Eqn. 5.2 does little to change the qualitative conclusion that large numbers of

inexpensive tests lead to more precise estimates than do small numbers of expensive tests, as long as bias is ignored. For example, an obvious alternative to the precision model of Eqn. 5.2 is that the root mean square error (rms) be inversely proportional to cost,

$$S(e) = K_e/c \quad . \tag{5.9}$$

This again leads to an optimal unit test cost which is independent of C, but unlike Eqn. 5.8 it also leads to an unique optimal test precision. Substituting Eqn. 5.9 into Eqn. 5.3 and setting the derivative with respect to c equal to zero, the optimal unit cost is,

$$c^* = K_e/S(e) \quad . \tag{5.10}$$

The test type leading to the most precise estimate under a fixed exploration budget is that whose noise equals the spatial variability of the property being estimated. This is clearly an imprecise test.

5.2.3 MULTIPLE TYPES OF TESTS

Data from different types of tests, having different precisions but no bias, are sometimes combined to form a simple estimator of the mean

$$E(\hat{x}) = \frac{\Sigma z_i + \Sigma y_i}{m + n} \quad , \tag{5.11}$$

(5.11)

in which $\{z_1, \ldots, z_n\}$ and $\{y_1, \ldots, y_m\}$ are the data having variances $V(z) = V(x)+V(e_z)$ and $V(y) = V(x)+V(e_y)$. The error in $\hat{x}$ using this estimator can be found from Eqn. 4.11 to be

$$V(\hat{x}) = V(x) + \frac{V(x)}{m+n} + \frac{n}{(m+n)^2} V(e_z) + \frac{m}{(m+n)^2} V(e_y) \quad . \tag{5.12}$$

Using the fact that the variances of z and y are different, a better estimator than the above can be obtained by weighting the mean of the z's and the mean of the y's differently. Specifically, the estimator

$$\hat{E}(x) = w\,E(z) + (1-w)\,E(y) \quad , \tag{5.13}$$

can be defined, in which w is a weighting factor between 0 and 1 which can be set so as to minimize the error of $\hat{E}(x)$. Again using Eqn. 2.11, the variance of E(x) about the true mean m is found to be

$$\begin{aligned} V\{\hat{E}(x)\} &= E\{(E(x)-E(x))^2\} \\ &= w^2\,V(z)/n + (1-w)^2\,V(y)/m \quad . \end{aligned} \tag{5.14}$$

Setting the derivative w.r.t. w equal to zero, the optimal weight w* is found to be

$$\frac{w^*}{(1-w^*)} = \frac{n}{m}\,\frac{V(x) + V(e_z)}{V(x) + V(e_y)} \quad . \tag{5.15}$$

That is, the weight ratio minimizing the error of $\hat{E}(x)$ is

proportional to the ratio of the respective numbers of tests, and inversely proportional to the ratio of the respective data scatters. The derivation of Eqn. 5.15 pressumes that the individual test results are independent of one another.

For more than 2 types of test Eqn. 5.13 becomes

$$\hat{E}(x) = \Sigma\, w_i\, E(z_i) \quad , \tag{5.16}$$

and the optimal weights are (Baecher, 1981)

$$\underline{w}^* = \begin{pmatrix} \underline{\underline{\Sigma}} & \underline{1}^t \\ \underline{1} & \lambda \end{pmatrix}^{-1} \begin{pmatrix} \underline{0} \\ 1 \end{pmatrix} \tag{5.17}$$

in which $\underline{\underline{\Sigma}}$ is the covariance matrix of the $E(z_i)$, $\underline{1}$ is a vector of 1's, and λ is a Lagrange multiplier (dummy dariable). For mutually independent test results, $\underline{\underline{\Sigma}}$ is a diagonal matrix with elements $V(x_i)/n$.

5.2.4 ERROR IN THE SPECIFICATION OF THE STANDARD ERROR

The results of preceeding sections for estimation errors require knowledge--or at least an estimate--of the spatial variance of x and the test precision V(e). Since neither of these is generally known prior to testing, they must be estimated from test data. This has two implications. First, in order to plan a test program something must be known or assumed about the

engineering property and test procedure; and second, even after testing the calculation of estimate precision is subject to error. This section considers the magnitude of that error and the number of tests required to specify standard errors of sampling plans.

An estimate of the variance of the data scatter V(z) from sample data z_1 , ... , z_n is taken from the sample variance

$$S^2(z) = \frac{1}{n-1} \sum (z_i - E(z))^2 \quad , \tag{5.18}$$

in which the term (n-1) rather than n ensures that the estimator is unbiased, and leads to somewhat simpler mathematical results. The sampling variance of $S^2(z)$ is approximately

$$V(S^2) = \frac{2\ V^2(z)}{n-1} \quad , \tag{5.19}$$

which means that the standard error is approximately proportional to the reciprocal of root n. Thus, the imprecision in estimates of the variance of the mean,

$$\hat{V}(\hat{E}(x)) = S^2(z)/n \quad , \tag{5.20}$$

can be found from Eqn. 2.11 to be*

$$V\{\hat{V}(\hat{E}(x))\} \pm \frac{2\ V^2(z)}{n^2(n-1)} \quad . \tag{5.21}$$

In practice there are three ways of making advance estimates of population variances: (1) Taking a sample in two stages, from

the first of which an estimate of V(z) is made and used to choose a sample size for the second stage, (2) by comparison with other sites or properties, and (3) by guesswork.

5.2.5 ON DRAWING CONCLUSIONS FROM ONE TEST

It is not uncommon in rock mechanics for estimates of engineering properties to be made from a limited number of tests, often just one. Quite clearly, using traditional sampling theory the confidence bounds on that estimate are infinitly wide, because from only one datum two parameters must be estimated, a mean and a variance. Even with two or three tests the confidence bounds are too wide to be operationally useful. Yet, much of rock engineering practice is based on these severely restricted samples. Given such uncertainty, how can any structure be built in rock? The answer is twofold. On the one hand, much of civil construction is designed very conservatively. On the other hand, collateral information on rock mass properties is usually available.

Collateral information is information in addition to that contained in the test data themselves. It consists primarily of two types, some prior estimate of reasonable or usual engineering parameters (e.g., mineral friction angles on unweathered surfaces are almost always between 30 and 40 degrees), and some prior estimate of the variance of the data scatter. Having these two pieces of information the test data are used either to confirm the

original estimate or to make a new estimate having simply the prior estimate of variance.

In principle, collateral information may be explicitly included in statistical calculations, but this requires a quantification of so-called prior probabilities on the parameter estimate. Usually the collateral information is qualitative or based on experience, and thus quantificaion requires an assessment of subjective probabilities which some people are reluctant to include in engineering analysis.

It is of interest to note that the formulae of preceeding sections allow collateral estimates of V(x) and V(e) to be included in the statistical formulations, and do not require that these variances be based on sample data. For example, an estimate of V(x) could be based on experience at other sites, and an estimate of V(e) could be based on analytical calculations as described in Section 4.3. Clearly, error may be introduced by using such estimates rather than those based directly on in situ data. On the other hand, ignoring collateral data may mean that the entire statistical analysis fails to take account of engineering reality, and therefore fails to be relevant to project needs.

5.2.6 MODEL OF TEST BIAS

In deriving Eqn. 5.7 no account was taken of test bias. However, bias in addition to precision is related to test cost.

More expensive tests not only have less measurement error than inexpensive tests, they are generally also are more accurate.

Bias introduces systematic error in an estimate but the magnitude--and sometimes the direction--of this error is seldom known with certainty. Thus, bias is typically characterized by a mean describing its expected value and by a variance describing its uncertainty. The mean will be of little concern, for bias can be corrected as long as its magnitude and direction are known. The variance, however, introduces an additional component of estimation error.

As before, a simple model relating the uncertainty of test bias to test cost might be taken to be,

$$V(B) = K_b/c \tag{5.22}$$

in which K_b is a constant. Unlike measurement imprecision, the uncertainty of bias error is not diminished by repeated testing. The bias is presumably the same for each test (otherwise, with no loss of generality, it could be treated as imprecision), but its value is unknown. Thus, from above the estimate error is

$$V(\hat{x}) = V(x) + \frac{V(x) + K_e/c}{C/c} + K_b/c \quad . \tag{5.23}$$

Bias complicates the simple picture of Fig. 5.3, as shown in Fig. 5.4. For limited exploration programs (i.e., small C) inexpensive tests may still lead to less overall estimate error than do

expensive tests; however, for extensive programs this may be reversed.

5.2.7 OPTIMAL MIXES OF TESTS

In any truely extensive exploration program a mix of test types is used. A few expensive tests are made (e.g., pressure tunnels or large surface loadings) and cheaper tests (e.g., index tests such as borehole jacking) are calibrated to them. Then a large number of the cheaper tests may be performed across the site to characterize rock mass variability. In this way advantage is taken both of the precision and lower bias of the expensive tests, and of the large numbers of cheap tests. The question now is how to best allocate a fixed budget among different types of tests?

In calibrating an inexpensive test to a more expensive one, uncertainty in the bias of the former is reduced up to the uncertainty in the bias of the latter. That is, the calibration of the less expensive test against the more expensive test is determined, but the calibration of the more expensive test against reality is still uncertain. Thus, the uncertainty in the bias of the less expensive test, say type 2, is reduced in accordance with the uncertainty in the bias of the more expensive test, say type 1, and in accordance with the number of calibrating tests of type 1 performed:

$$V(B_2) = V(B_1) + V(e_1)/n \quad . \tag{5.24}$$

Since the 'real' rock mass properties are unknown even for the expensive tests, the uncertainty in bias cannot be reduced below $V(B_1)$; and since there may be noise even in the expensive test, the uncertainty in the calibration of index test to expensive test depends on $V(e_1)$ (if the number of index tests made in conjunction with each calibrating test is itself small, then $V(B_2)$ would be increased by the amount $V(e_2)/n_2$.

Combining $V(B_2)$ with Eqn. 5.3 leads to

$$V\{\hat{E}(x)\} = V(x) + \{\frac{V(x) + K_e/c_2}{n_2}\} E^2(B) + \{V(B_1) + V(e_1)/n_1\} E^2(x) \quad (5.25)$$

in which E(B) and E(x) are the means of B and x, respectively. Setting the derivatives with respect to n_1 and n_2 equal to zero gives the optimal ratio of tests

$$n_1/n_2 = \frac{E(B)}{E(x)} \{\frac{V(x) + K_e/c_2}{K_e/c_1}\}^{\frac{1}{2}} \quad (5.26)$$

subject to the constraint

$$C = c_1 n_1 + c_2 n_2 \quad . \quad (5.27)$$

This provides a straightforward way of identifying efficient strategies of testing, based on simple measures of test performance and cost.

5.3 On deciding upon sample sizes

The discussion throughout this section has focused on the relation between numbers of tests and the accuracy and precision with which engineering profiles can be established. The normative question of how may tests "should" be performed has been purposely ignored. The reason for doing so is straightforward: The answer to the question depends on economics and possibly legal matters, but not statistics. In essence the question is not, "how many tests should be performed," but rather, "how accurately and precisely must engineering properties be established, and what will the consequences of marginal improvements to that knowledge be?"

As most engineers know, the most difficult part of answering such questions is how to identify specific consequences of improvements in estimates of engineering properties, and how to place values on those consequences. In essence the question is one of decision analysis, and outside the scope of the present report. However, a simple approach to the decision (i.e., optimization) problem within a second-moment context can be formulated, once consequences are identified, and if one is willing to explicitly place values on the acceptability of risk.

From a decision theory point of view, the choice of numbers of tests can be formulated as a set of decision alternatives (i.e., the numbers or mix of tests and consequently the accuracy and precision with which the engineering properties are

established), a set of outcomes and their conditional probabilities (i.e., facility performance and the mean and variance of performance as a function of accuracy and precision of the engineering properties), and a quantified value function specified over the outcomes (e.g., a utility function). Under very general conditions (Raiffa and Schlaifer, 1964), the best decision option can be shown to be that which maximizes the expectation of the value function of the consequences (or of some one-to-one transformation of the function, as e.g., utility). Thus, the best option is that which maximizes,

$$E\{u(y)\} = \int u(y)\, f(y|n)\, dy \quad , \tag{5.28}$$

in which X is the engineering property(ies), and u(X) is the utility function assessed over X. Since f(X) is a function of n, the number of tests, the expected utility can be maximized over n to find the "best" number of tests.

For any distribution of uncertainty about the value of X, some specific known value of X can always be found whose utility equals Eu(X). This value of X is said to be the "certainty equivalent;" it is the value which, if known to obtain, would be judged just as desirable as the current uncertainty about X. Let this certainty equivalent be X_{ce}. Thus,

$$u(X_{ce}) = E\{u(x)\} \quad . \tag{5.29}$$

Expanding both sides of this relation as Taylor series

$$u\{E(X)\} - \dot{u}\{E(X)\}\ \{E(X)-X_{ce}\}$$

$$= u\{E(X)\} - \frac{1}{2}\ \ddot{u}\{E(X)\}\ V(X) \quad , \tag{5.30}$$

in which $\dot{u}$, $\ddot{u}$ are the first and second derivatives of u(X) with respect to X. Upon rearrangement,

$$X_{ce} = E(x) - \frac{1}{2}\ R\ V(x) \quad . \tag{5.31}$$

in which R, the so-called risk reduction factor, is

$$R = -\dot{u}(X)/\ddot{u}(X) \quad . \tag{5.32}$$

Since maximizing X_{ce} is equivalent to maximizing Eu(X), the best number of tests (or mix, etc.) can be directly found once an estimate of the risk aversion factor is made. This approach uses only second-moment information on the engineering property X, and the equivalent of second-moment information on the value or utility function, i.e., R. Discussion of utility function assessment is to be found in Keeney and Raiffa (1976).

5.4 Sampling for Spatial Variability

The main thrust of this section has been the development of sampling plans for establishing engineering properties in presumably homogeneous zones within a rock mass. However, site characterization programs also face problems of establishing trends or changes of engineering properties across a site. Sampling strateges to estimate trends is a major area of work in the statistical literature and also a difficult one (see, e.g., Federov, 1972), and can only be touched upon here in summary.

Clearly, there is nothing "random" about the engineering properties of a rock mass. In principle, with sufficiently many measurements the spatial variability of geological formations could be established up to the measurement error in the instruments used. However, it is sometimes convenient for engineering purposes to divide the actual spatial variability into two parts: A deterministic trend in space, and a residual fluctuation about that trend. The trend is estimated using various techniques, such as regression analysis or interpolation, and the residual is modelled using the mathematics of random process theory. This is not to say that the residual fluctuations are assumed to be random, they are not. It simply happpens that the mathematics of random process theory can, without loss of generality, also be used to model

spatial variation. These mathematics can therefore be used to quantify interpolation errors and to perform related tasks.

The question of sampling for spatial variability resolves to two tasks: Establishing the trend component of variability, and establishing the structure of the residuals off that trend.

5.4.1 ESTIMATING TRENDS WITH FIXED SAMPLING PLANS

This section briefly considers three standard sampling plans for estimating spatial trends or zonation: Stratified, cluster, and systematic sampling. Each uses a different strategy for allocating measurements and each carries benefits in certain applications.

5.4.1.1 STRATIFIED RANDOM SAMPLING

In stratified sampling the entire population is divided into units or strata which are treated as internally homogeneous, but possibly varying from one to another. While "strata" is common usage in the statistical literature, "units"is used here to avoid confusion with the geological meaning of "strata." Each unit is sampled according to a plan which may vary among units. In stratified random sampling the entire population of size (or extent) N is separated into k non-overlapping units of individual size N_i such that

$$N_1 + N_2 + \ldots + N_k = N \qquad (5.33)$$

From each unit a random sample of size n_i is taken, leading to a total sample size of

$$n_1 + n_2 + \ldots + n_k = n \tag{5.34}$$

The principal reasons for using stratified sampling over simple random sampling are, that (1) geological conditions vary across a site, (2) desired estimate precisions may vary from one unit to another, (3) testing problems and procedures may differ among units, (4) contracting or administrative procedures may favor separations among units, and (5) overall precisions may be improved for a fixed total exploration cost.

The precisions with which unit properties can be estimated follow directly from the results of Section 5.2 with n_i replacing n, and unit means and variances replacing global means and variances. The variance of the total data scatter, although seldom of interest to rock mechanics, is simply the sum of the weighted unit variances plus the variance among unit means,

$$V(z) = \frac{n_i\, V(z_i) + \ldots + n_k\, V(z_k)}{n} + V(m_z) \tag{5.35}$$

in which $V(m_z)$ is the variance among unit means $m_{z_1}, \ldots m_{z_k}$.

Presuming that a constant estimate precision is desired across the entire rock mass and that the total exploration budget is fixed at C, then numbers of tests should be allocated

to units proportional to $V(z_i) = V(x_i) + V(e_i)$, subject to the constraint $C = n_1c_1 + \ldots + n_kc_k$. Thus, the allocations are proportional to

$$n_i \propto \left(\frac{V(x_i) + V(e_i)}{c_i} \right)^{\frac{1}{2}} \tag{5.36}$$

To minimize the precision of an estimate of the mean across all units (i.e., the site mean)--which might be of interest, say, in sampling borrow materials--numbers of tests should be set in proportion to

$$n_i \propto N_i \left(\frac{V(x_i) + V(e_i)}{c_i} \right)^{\frac{1}{2}} \tag{5.37}$$

as unit size affects the site mean.

Stratified sampling provides more precise estimates of rock mass profiles than does simple random sampling when the units composing the rock mass vary widely in size, the units have dissimilar variances, and when the geometry of the units is well defined. Because variance among the means $V(m_z)$ is removed from influencing estimate precision, greater efficiency is obtained from the overall exploration effort. Considerations of different types or mixes of tests within each unit are similar to those discussed in Section 5.2.

5.4.1.2 CLUSTER SAMPLING

In cluster sampling individual sampling elements or clusters are selected and random samples taken from each. One such plan is to locate initial tests at various places about a site, and then to place a fixed number of additional tests in the vacinity of each. Cluster plans are very common in joint surveys, where mobilization costs are much larger than individual measurements. They are also common in phased sampling, where a mix of test types is used and correlated to one another. Cluster plans are particularly useful in the analysis of spatial variance, as they profile data at different levels of spatial separation.

In single staged cluster sampling n clusters are chosen with m tests being made in each. Thus, the total number of tests is nm. The variance structure within the resulting data scatter is conveniently summarized as in Table 4.1.

For clusters of equal size the overall mean of the sample

$$m_z = (1/m) \sum_{}^{n} \sum_{}^{m} z_{ij} \quad , \tag{5.38}$$

has sampling variance

$$V(m_z) = \frac{V_a}{n} + \frac{V_b}{nm} \quad . \tag{5.39}$$

Adopting a simple cost model comprising a mobilization cost for

each cluster and a unit test cost within clusters,

$$C = c_1 n + c_2 mn \tag{5.40}$$

an optimal sampling plan can be found that minimizes V for a fixed C, or minimizes C for a fixed V.

5.4.1.3 SYSTEMATIC SAMPLING

Systematic sampling plans, which specify testing at a regular interval or on some regular pattern (e.g., grid boring) are common in geotechnical engineering. The advantages of such plans are that they are easy to design and administer, little time is lost in locating test positions, and at first glance they seem to provide better coverage of a site than do other plans. From a statistical point of view this last advantage is at times fallacious, however systematic sampling in many cases leads to higher probabilities of detecting inhomogeneities in a rock mass than do other plans (Baecher, 1979).

5.4.2 SAMPLING FOR RESIDUAL VARIATIONS

The principal sampling problem in establishing the structure of residual variations off a mean trend is the estimation of autocovariance functions. This problem, often of more importance in soils than in rock testing, is statistically difficult and not widely worked on. For these reasons it is considered outside the scope of the present document, however,

a discussion of the precision of the common moment estimator of autocorrelation can be found in Baecher (1982).

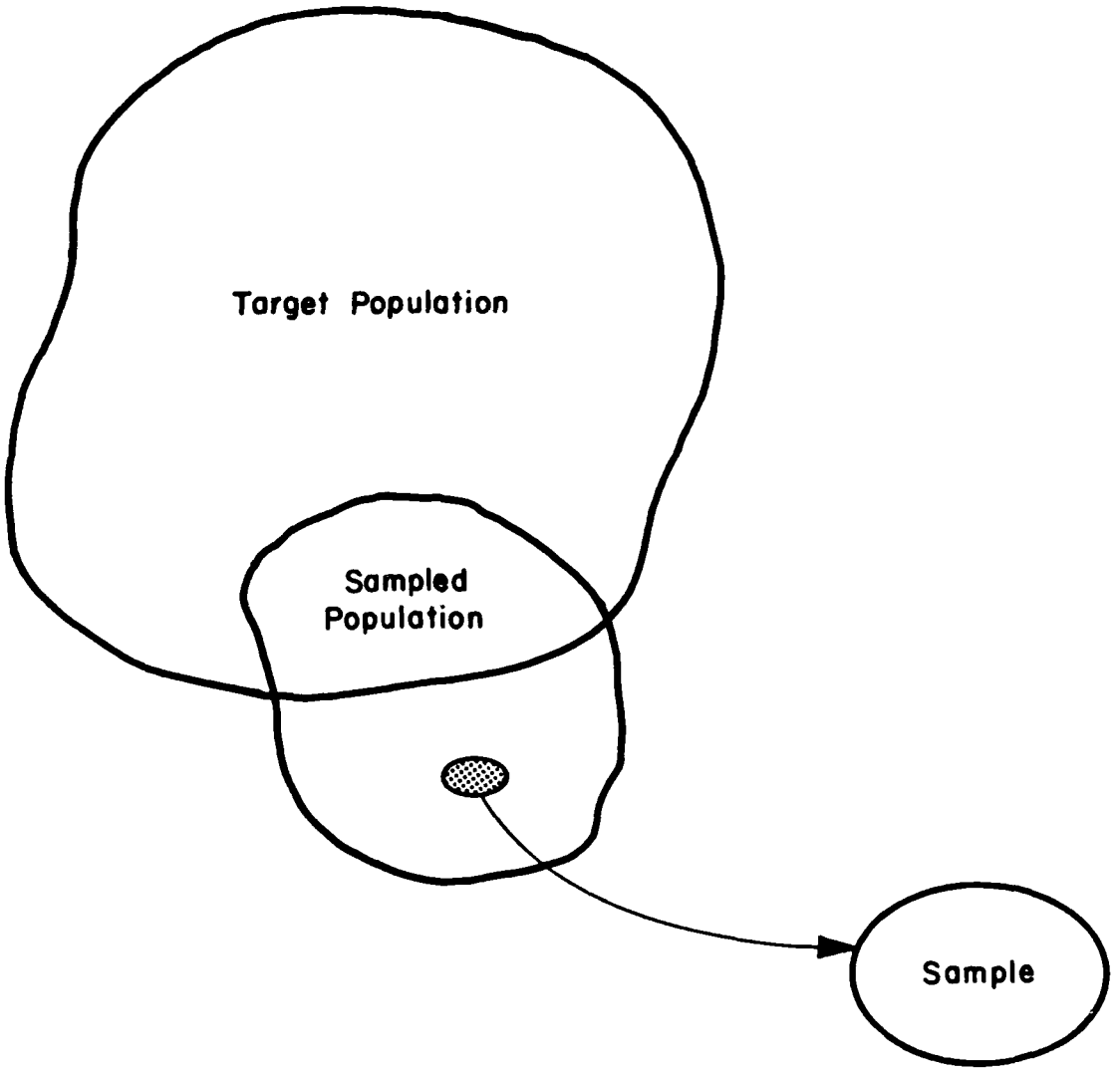

Figure 5.1 -- Populations of interest to sampling and inference.

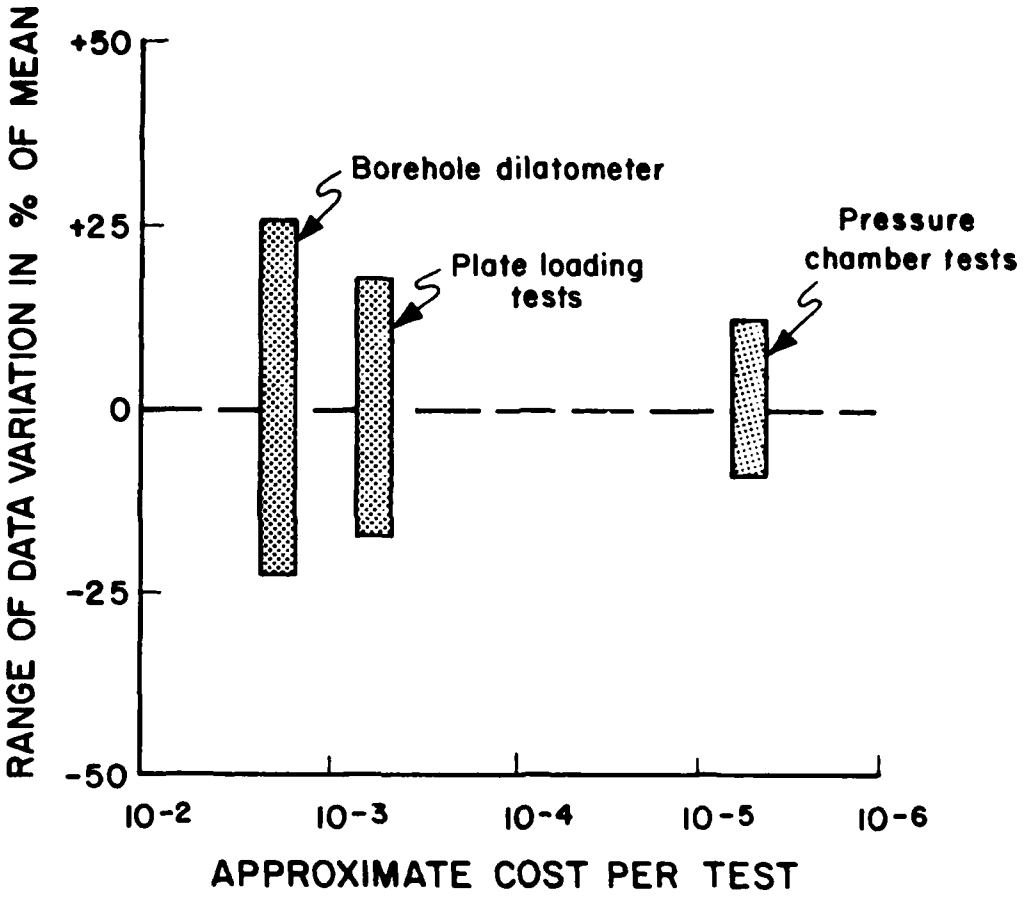

Figure 5.2 -- Typical precisions (i.e., data scatter) and costs of insitu tests for rock mass deformation properties, from various sources.

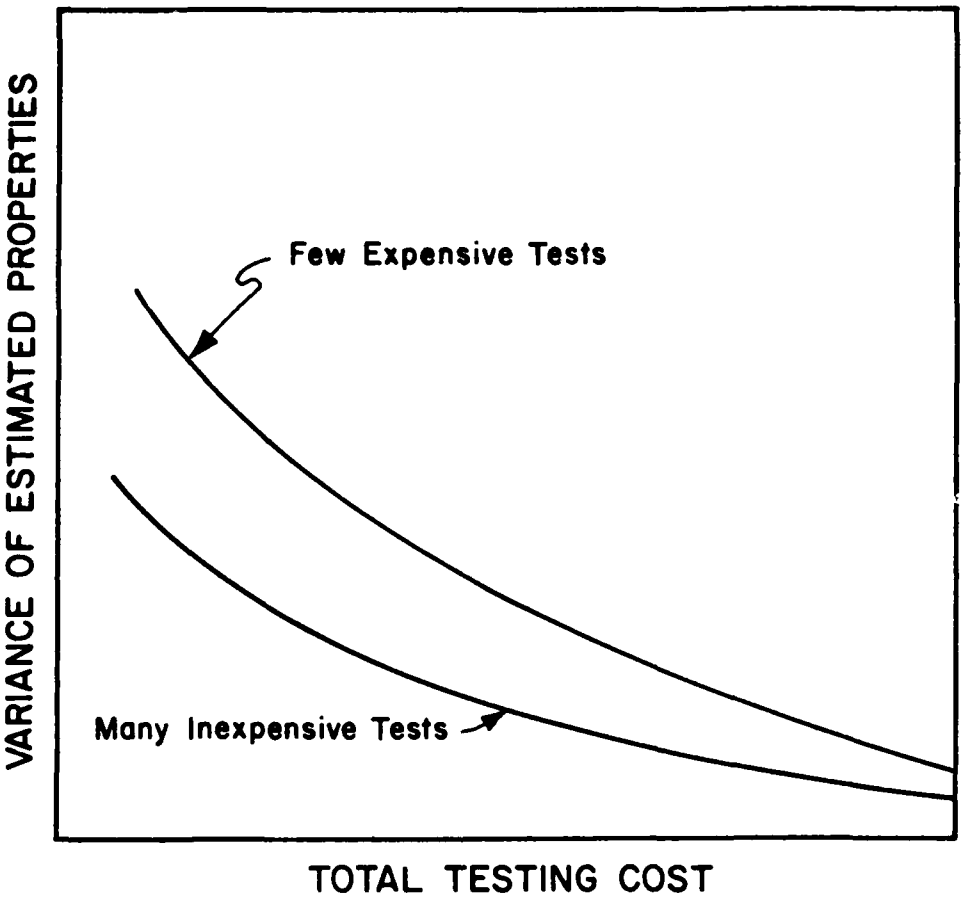

Figure 5.3 -- Relation of estimate variance to the total cost of measurement, comparing expensive tests with inexpensive tests. Bias error excluded.

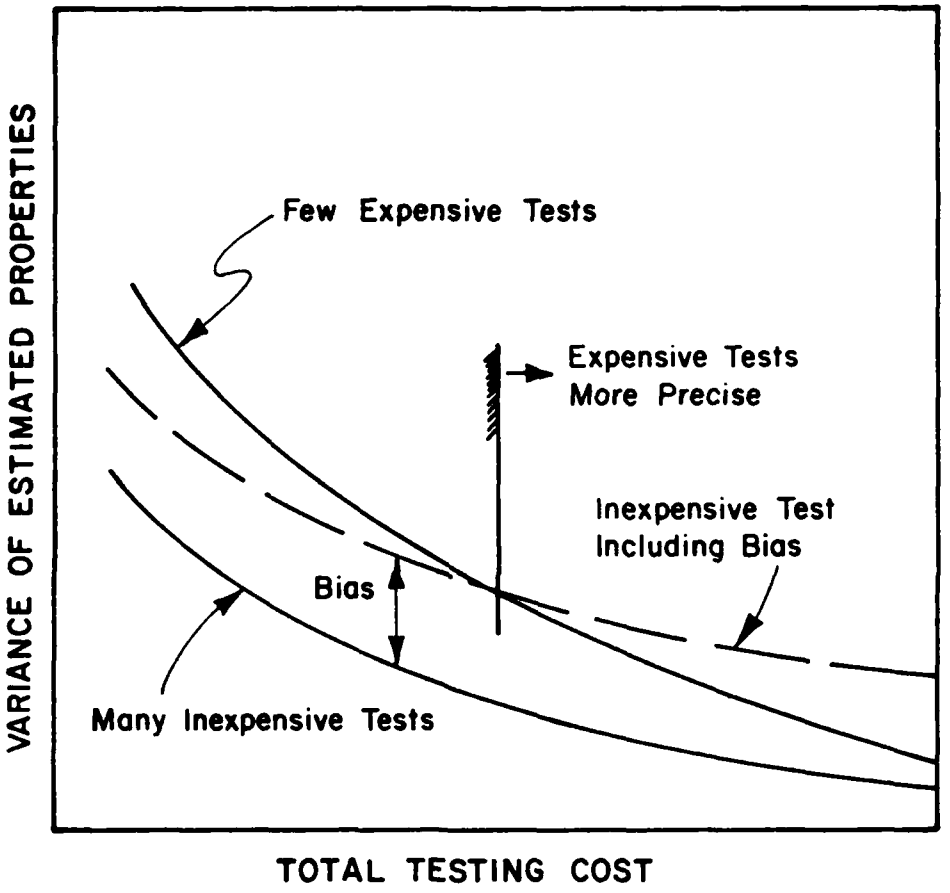

Figure 5.4 -- Comparison of estimate variances including measurement bias.

6. CONCLUSIONS

An attempt has been made in this document to lay the groundwork for a "scientific" approach to sampling and parameter estimation for rock mass characterization. This approach has nothing directly to do with so-called probabilistic design, although the development of statistically based site characterization procedures is a neccessary precursor to that design philosophy. The groundwork presented here does not constitute a complete theory, and many further developments are required before a set of practical tools results. However, a limited set of tools is now available, and would appear to offer a potentially useful addition to current practice. These tools are based on simple mathematics, require essentially no background in statistical theory, do not introduce esoteric probabilistic assumptions, and address practical problems. Basically, they represent technology that has proven useful for several decades in other branches of engineering and applied science, even in related geosciences such as agronomy.

A pragmatic approach to the design and analysis of in situ testing programs can be based on simple descriptions of data scatter and estimation uncertainties through means, variances, and covariances. This approach provides two important capabilities. First, it allows the sources of data scatter and uncertainty to be separated and evaluated independently, and an informed measure of estimate uncertainty to be established.

Second, it allows investments in in situ testing to be efficiently allocated, such that the error in engineering estimates is minimized. These capabilities can be enjoyed with no change in current practice either of field testing or design, and at negligible cost.

The latter sections of this document have demonstrated that simplified sampling theory techniques for rock testing show promise, and that for certain problems useful techniques can be readily developed. However, the work reported here is only a small step. An extensive and well developed technology is available, and significant advances in geotechnical practice can be realized merely by its transfer. This technology is useful not only in the design and interpretation of site characterization programs, but also in the important area of designing instrumentation and monitoring networks for assessing the safety of waste repositories, dams, and other facilities subject to regulatory control.

REFERENCES

Baecher, G.B. (1982). "Statistical methods in site characterization," Proceedings of the Engineering Foundation Conference on Updating Subsurface Exploration and Testing for Engineering Purposes, Santa Barbara.

Baecher, G.B. (1979). "Search in geotechnical exploration," Proceedings, Third International Conference on Applications of Statistics and Probability to Soil and Structural Engineering, Aachen.

Baecher, G.B. (1978). "Analyzing exploration strategies," in C.H. Dowding (Ed.), Site Exploration and Characterization. ASCE/NSF.

Benjamin, J, and C.A. Cornell (1971). Probability, Statistics, and Decision for Civil Engineers. McGraw-Hill Book Company, NY.

Ditlevsen, O. (1981). Uncertainty Modeling, with Applications to Multidimensional Civil Engineering Systems. McGraw-Hill International Book Company, NY.

Cochran, W.G. (1963). Sampling Techniques (2nd Ed.). John Wiley and Sons, New York.

Federov, V.V. (1972). Theory of Optimal Experiments. Academic Press, NY.

Keeney, R.L. and H. Raiffa (1976). Decisions with Multiple Objectives. John Wiley and Sons, NY.

Raiffa, H. and R. Schlaifer (1961). Applied Statistical Decision Theory. Division of Research, Graduate School of Business Administration, Harvard University, Boston.

Schmertmann, J. (1982). Remarks before the Engineering Foundation Conference on Updating Subsurface Exploration and Testing for Engineering Purposes, Santa Barbara.

NOTES TO TEXT

Section 4:

The ideas and suggestions of William Beloff and Brian Dorwat of Soil and Rock Instrumentation, a division of Goldberg Zoino Associates of Newton Upper Falls, MA, on this section are gratefully acknowledged.

Section 5:

The sampling variance of the estimate S^2 of the population variance

$$V(S^2) = 2V^2/(n-1) \quad ,$$

is based on a normality assumption. In fact, if the population is non-normal, the sampling varinace may be either larger or smaller, although empirically it usually is larger (Cochran, 1963). Fisher (1932, see Cochran, p. 43) has shown that the sampling variance for any infinite population is,

$$V(S^2) = 2V^2/(n-1) + K_4/n \quad ,$$

in which K_4 is Fisher's fourth cumulant,

$$K_4 = E(zi-m_z)^4 - 3V^2 \quad .$$

For a normal pdf, $K_4=0$; for other pdf's it may be either positive or negative. Expressed in Fisher's measure of kurtosis

$$G_2 = K_4/v^2 \quad ,$$

the sampling variance becomes,

$$V(S^2) = \frac{2\,V^2}{n-1}\left(1 + \frac{n-1}{2n}\,G_2\right) \quad .$$

Note, the second factor is almost independent of n, so the inflation remains high even for large samples. Cochran reports values of G_2 as high as 6, thus, inflations of as much as 4.

SYMBOL LIST

$\underline{\underline{A}}$	derivative matrix for implicit functions.
a	calibration constant.
B, B_1, B_2	bias error.
$\underline{\underline{B}}$	derivative matrix for implicit functions.
C, c, c*	total exploration cost, unit cost, optimal unit cost.
$\underline{\underline{D}}$	derivative matrix for vector-vector function.
d	calibration constant.
e, e_x, e_y, e_z	random measurement error general, and in specific measurements.
e(t)	random measurement error as a function of location.
$f_i(X,Y)$	function of the variables X and Y.
g(x)	function of the variable x.
K_1	instrument calibration function.
K_e	constant of proportionality for random measurement error.
K_b	constant of proportionality for bias measurement error.
n, m	number or sample sizes.
R	reduction factor for spatial variability.
r	distance index for autocovariance function, scalar or vector.
$r_{x,y}$	(sample) correlation coefficient.
T_1, T_2	temperatures at times 1 and 2.
u(y)	utility function at y
Va, Vb	within and between cluster variances.
V_o, V_i	initial and later voltages.
w, w*	weight and optimal weight
X, x, x_i	soil or rock property
Y, y, y_i	soil or rock property
Z, z, z_i	measurement of soil or rock property
x(t), y(t), z(t)	soil or rock properties or measurements as functions of location.

$f(\cdot\|\cdot)$	conditional probability density function.
$C(\cdot)$	covariance.
$C_x(r)$	autocovariance function of x (or z, e, etc.).
$E(\cdot)$	expectation.
$S(\cdot)$	standard deviation.
$V(\cdot)$	variance.
λ	Lagrange multiplier.
$\underline{\underline{\Sigma}}_x$, $\underline{\underline{\Sigma}}_y$	covariance matrices of x, y.
$\hat{}$	estimate.
$\cdot$	first derivative.
$\ddot{}$	second derivative.

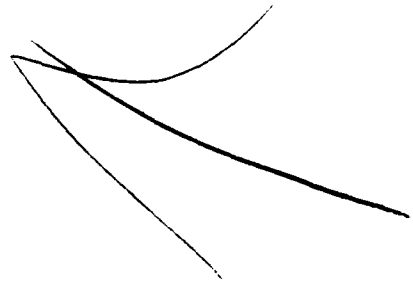

NEW DEVELOPMENTS IN STATISTICAL TECHNIQUES FOR ANALYZING ROCK SLOPE STABILITY

by

Stanley M. Miller

ACKNOWLEDGEMENTS

A considerable portion of this report represents a summary of Ph.D. dissertation research conducted by the author in 1981 and 1982 at the University of Wyoming. The research was funded by Climax Molybdenum Co., a subsidiary of AMAX Inc., of Golden, Colorado. The author is grateful to Climax, and especially to W. White and D. Stewart of the Geology Department for their energetic help and support.

Sincere appreciation is also extended to Dr. L.E. Borgman, the dissertation advisor, for his encouragement, guidance, and expert advice throughout the research period.

TABLE OF CONTENTS

Chapter Page

CHAPTER 1

INTRODUCTION

1.1 The Need for Probabilistic Techniques

Natural variabilities in rock mass properties and measurement uncertainties associated with their estimation imply the probabilistic nature of geologic parameters that are required for the engineering design of rock slopes. A deterministic slope design based on the average values of input parameters does not take into account statistical variabilities and may provide misleading results. In fact, some deterministic stability analyses can lead to a supposedly conservative design that actually has a substantial probability of failure (Hoeg and Murarka, 1974).

In addition, many current economic evaluations of open pit mines include risk analyses that require input from a probabilistic slope stability analysis (Kim and Wolff, 1978). Such an analysis can only be conducted if the natural variabilities and measurement uncertainties of the input parameters have been statistically quantified and described. Typical random variables that must be described are the geometrical characteristics of structural discontinuities (orientation, spacing, length, and waviness) and the shear strengths of the discontinuities.

The most common discontinuities in rock are fractures. The general term "fracture" includes both joints (along which there has been no displacement) and faults (along which there has been displacement).

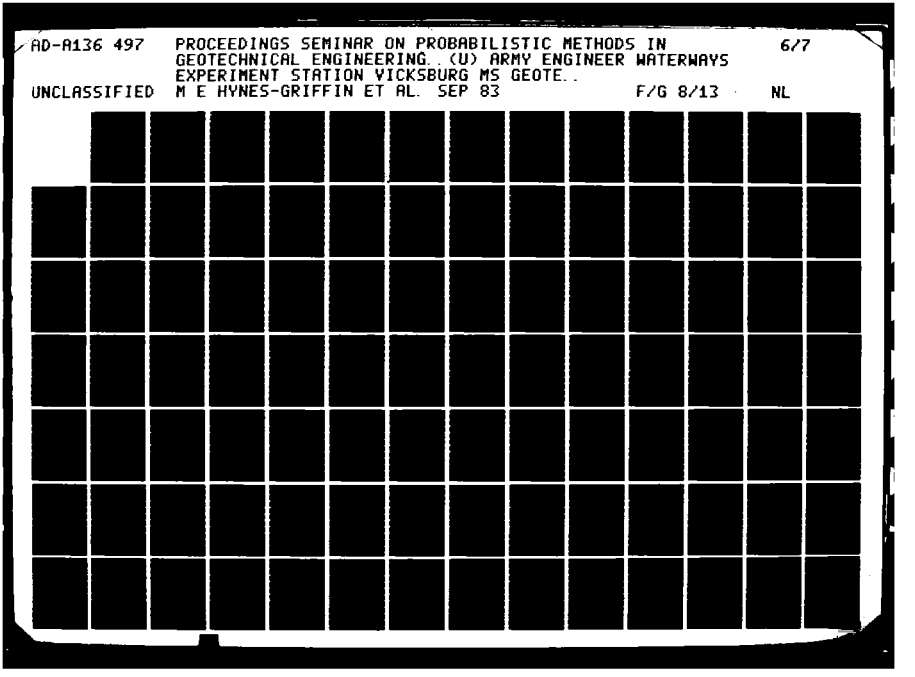
AD-A136 497 PROCEEDINGS SEMINAR ON PROBABILISTIC METHODS IN GEOTECHNICAL ENGINEERING. (U) ARMY ENGINEER WATERWAYS EXPERIMENT STATION VICKSBURG MS GEOTE..
6/7
UNCLASSIFIED M E HYNES-GRIFFIN ET AL. SEP 83
F/G 8/13
NL

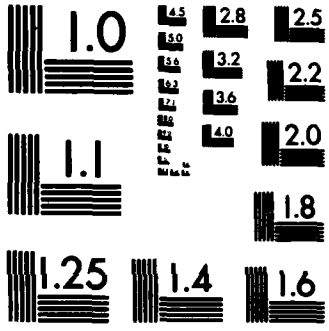

Statistical distributions of fracture characteristics can be estimated from mapping data. The shear strength along fractures can be estimated by laboratory direct shear tests of rock specimens that contain natural fractures.

1.2 Probabilistic Slope Design Procedures in Current Use

The techniques discussed in this report are primarily intended for application to the engineering design of open pit mine slopes. Because slope angles have a significant economic impact on any open pit mining operation, reliable stability analyses and slope design procedures are essential for the overall mine planning program. The techniques are also applicable to more conventional civil engineering projects, such as the stability of road cuts or other manmade cuts in a fractured rock mass.

A slope design project should begin with a thorough evaluation of regional and local geology. Major rock units and structural features are identified in the study area. Spot mapping techniques are then used to collect detailed information about fracture characteristics and about bedding or foliation if they are present. Lower-hemisphere Schmidt plots are constructed to display the fracture orientations obtained at each mapping site. Visual comparisons of the plots usually allow for the identification of structural domain boundaries. A structural domain represents an area characterized by a distinct rock unit or by a distinct pattern of fracture orientations.

The proposed shape of the pit and the locations of structural do-

mains are used to select design sectors, each of which has a distinct slope face strike in a specified structural domain. Potential slope failure modes in a design sector are identified by evaluating how the fracture orientations mapped in the particular structural domain interact with the slope face orientation. Lower-hemisphere Schmidt projections that display poles to fractures are helpful for predicting potential failure modes (Hoek and Bray, 1977, p. 57).

Fracture sets that comprise potential failure modes are often called design sets because they tend to be critical to the slope design. Fracture mapping data are used to estimate the statistical distributions of pertinent characteristics in the design sets. Usually, the distributions of dip and dip direction in a design set are normally distributed, and the distributions of spacing, length, and waviness are exponentially distributed (waviness is the angle between the average dip and the minimum dip observed in a mappable structure).

Shear strengths along the fractures can be estimated by laboratory direct shear tests of rock specimens that contain natural fractures. Test results are presented as a plot of shear strength as a function of applied normal stress. Least-squares regression procedures are applied to the data to estimate the statistical distribution of shear strength at any given normal stress.

After the above input parameters have been statistically described, probabilistic stability analyses can be conducted for those failure modes identified in the given design sector. Monte Carlo simulations are used to repeatedly sample input values from the distributions and

calculate a number of possible safety factors. The probability of sliding is the area under the safety factor distribution where the values are less than one or the simple percentage of simulated safety factors that are less than one.

Experience with probabilistic slope stability studies during the past several years has indicated that the critical parameter for stability in most cases is the fracture length. Major geologic structures like faults or contacts usually have lengths great enough to affect overall pit slope stability, and they should be analyzed individually in the slope design project. However, the lengths of smaller, more numerous fractures (those mapped in outcrops and statistically treated) are commonly less than 10 m and, therefore, do not affect overall slope stability. The exception, of course, is the step path failure mode which has a nearly continuous failure surface defined by fractures from two or more design sets. If a step path failure mode does not occur in a design sector, or if the simulated step path heights are quite short, then a significant impact on overall slope instability is not expected.

On the other hand, fracture lengths are great enough to affect bench stability because benches are typically 12 to 20 m high. Bench geometry and, thus, bench stability has a direct influence on the overall slope angle that can be attained. Consequently, mapped fracture data should be used to analyze bench stability in a probabilistic manner, and the results should guide in the selection of overall slope angles.

1.3 New Probabilistic Methods

The main purpose of this W.E.S.-funded project was to describe and summarize five recently developed statistical methods for analyzing rock slope stability. Two of the methods deal with the statistical analysis of geologic data. One is a statistical procedure for analyzing structural data to assist in the delineation of structural domains. A simple chi-squared test procedure based on a contingency table analysis of Schmidt plots was investigated and shown to be a useful tool for identifying domain boundaries. The other method is a statistical regression analysis that estimates the probability distributions of the shear strength along structural discontinuities of the same character. Results of laboratory direct shear tests of similar specimens are essential input for such an estimation. A weighted, nonlinear regression analysis based on a modified power curve model was developed to estimate the expected value (mean) of the shear strength and the variance of the expected shear strength at a given applied normal stress for a specified rock type or discontinuity type.

Another new statistical technique is the use of spectral analysis procedures to simulate spatially correlated fracture set characteristics. Such procedures have been developed to simulate normally distributed and exponentially distributed fracture data. The simulated data have the proper mean and variance, as well as the appropriate spatial correlations as defined by the imposed covariance function. This covariance function is derived from the variogram function estimated for the actual data.

One of the major new probabilistic developments in slope design is a Fourier analysis for estimating the probability of sliding for several common failure modes. Plane shear, step path, and tetrahedral wedge failure modes have been analyzed to date. The Fourier methods are based on the principle that the sum of independent probability densities in space domain is analogous to the product of their Fourier transforms (characteristic functions) in frequency domain. Thus, the probability density function of the safety factor can be directly estimated by discrete Fourier procedures, provided that the safety factor can be expressed as the sum of independent random variables. The probability of sliding is the area under the safety factor distribution where values of the safety factor are less than one. The computational procedures are highly efficient because they take advantage of the fast Fourier transform algorithm. This high efficiency is not associated with Monte Carlo simulation techniques that estimate probability of sliding. In addition, the Fourier methods estimate the true safety factor distribution, whereas Monte Carlo methods provide only simulations, or realizations, of the true safety factor distribution.

Another new development is a probabilistic analysis for evaluating bench stability that incorporates the analytical procedures discussed above. The bench analysis in a given design sector consists of simulating spatially correlated fracture properties and then analyzing the stability of all the resulting potential failure modes. The probabilities of stability are accumulated over several bench simulations to provide the probabilities of stability for back-failure cells on top

of the bench. The cell probabilities are then accumulated to produce the probabilities of retaining various bench widths. Because bench stability (and thus, bench geometry) affects the geometry of the overall slope, results from the bench analysis are used to generate slope design charts that display probabilistic parameters useful for selecting an overall slope angle.

CHAPTER 2

A STATISTICAL METHOD TO HELP DELINEATE STRUCTURAL DOMAINS

2.1 Introduction

A structural domain is commonly defined as an area characterized by a distinct pattern of structure orientations, where the structures include mappable features like fractures, bedding planes, and foliations. The identification of domain boundaries is essential to rock engineering investigations because geologic and hydrologic properties vary from one domain to another. Obvious domain boundaries correspond to lithologic contacts caused by depositional environment, intrusion, or fault displacement. However, structural domain boundaries are not restricted only to lithologic contacts, but may occur within the same rock unit. Statistical procedures are often needed to help identify these less obvious domain boundaries.

Mapped fracture orientations are plotted on lower-hemisphere projections that display poles to fractures. Schmidt plots are usually preferred because they are equal-area projections and allow for the contouring of pole densities. The data from one mapping site in the study area are plotted on one Schmidt plot, which typically displays at least 150 fracture orientations. Structural domain boundaries within a given rock unit often can be determined by visually comparing the plots that represent fracture orientation samples from various mapping

sites.

Fracture patterns consist of several preferred orientations that appear as clusters of poles on a Schmidt plot (Figure 2.1). Each cluster represents a fracture set, and the spatial relationships of clusters on a plot allow for meaningful visual comparisons with other plots. The blind zone shown in Figure 2.1 corresponds to the orientation of the mapped outcrop where fractures that parallel the outcrop are sampled to a lesser degree than those with strikes more perpendicular to the outcrop (Terzaghi, 1965). When visually evaluating two or more plots, geologic experience and judgement are the basis for determining if the plots are alike and, thus, represent samples from the same structural domain.

However, when fracture orientations appear more dispersed on the plots (Figure 2.2), visual comparisons are not appropriate for determining whether the samples were obtained from the same structural domain (that is, from the same structural population). A quantitative, statistical method is needed to evaluate the plots and provide guidance in identifying the locations of domain boundaries.

2.2 Contingency Table Analysis of Schmidt Plots

A multinomial chi-squared test can be used as such a statistical tool. In fact, it provides a way to evaluate one's confidence in claiming that the sampled structural populations are homogeneous, or alike. The procedure is based on the analysis of a contingency table that contains frequencies of fracture poles that occur in corresponding,

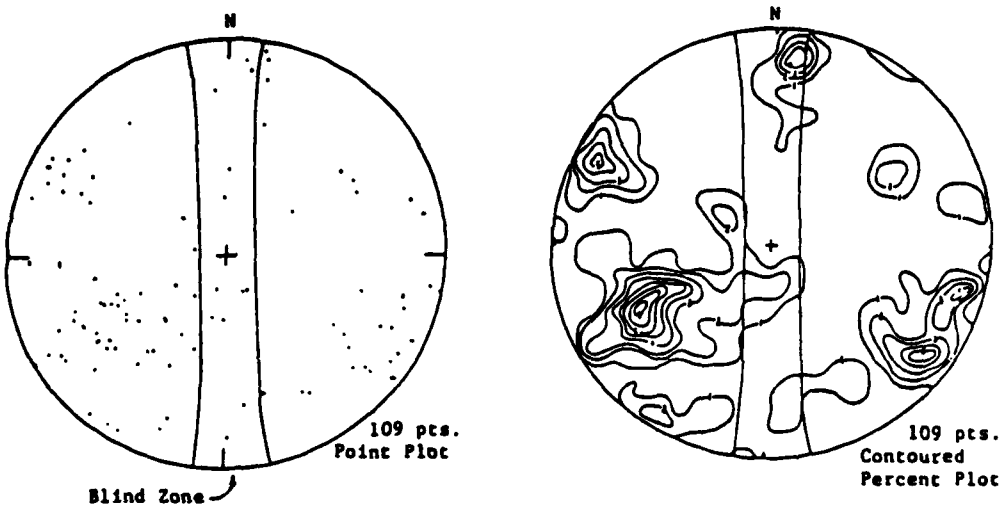

Figure 2.1. Example of Clustered Fracture Orientations on a Lower-Hemisphere Schmidt Plot

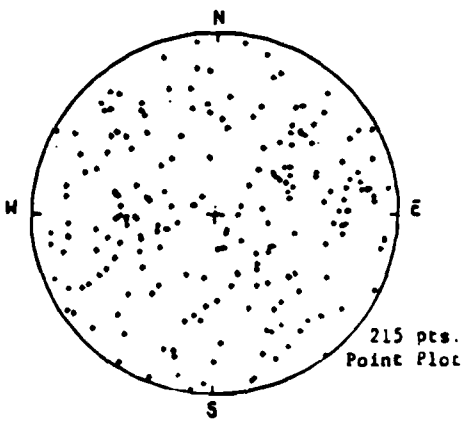

Figure 2.2. Example of Dispersed Fracture Orientations on a Lower-Hemisphere Schmidt Plot

equal-area patches on the Schmidt plots being compared.

Application of contingency table analysis to Schmidt plots which represent samples of structural populations requires that the plots be divided into cells, or classification categories. A reasonable approach is to divide the lower hemisphere into patches that have equal surface areas on the hemisphere. Each patch is then considered a cell in the contingency table and its entry in the table is the number of fracture poles that occur in that patch.

A simple procedure for determining these equal-area patches on the Schmidt plots is given by Miller (1982a). Example networks of equal-area patches are shown in Figure 2.3. The 38-patch scheme incorporates split patches to provide a more reasonable treatment of steeply dipping fracture sets (so-called "split sets"). To help minimize potential bias when comparing several Schmidt plots, the selected network should contain patches that are nearly equidimensional.

Table 2.1 represents a contingency table for analyzing Schmidt plots. Samples from r structural populations are listed down the rows in terms of the plots. Each sample is classified into c categories, or patches. The frequency, or number, of observed fracture poles in the ij cell is given by f_{ij}. To test the null hypothesis that the structural populations are homogeneous (alike), the following statistic is calculated:

$$\chi^2 = \sum_{i=1}^{r} \sum_{j=1}^{c} \frac{(f_{ij} - e_{ij})^2}{e_{ij}} \qquad (2.1)$$

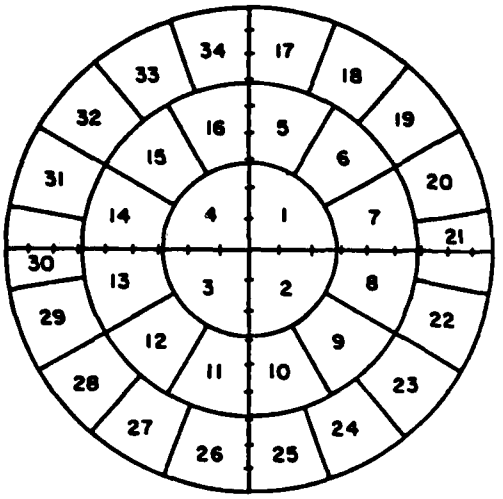

A. 34 Patches

Dip Band	No. of Patches	Max. Dip, θ (deg.)
1	4	28.1
2	12	59.0
3	18	90.0

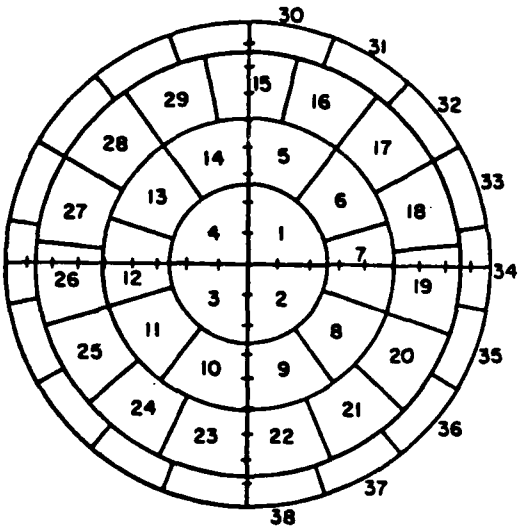

B. 38 Patches

Dip Band	No. of Patches	Max. Dip, θ (deg.)
1	4	26.5
2	10	50.8
3	15	76.3
4	9	90.0

Figure 2.3. Example Networks of Equal-Area Patches on Lower-Hemisphere Schmidt Projections (from Miller, 1982a)

where: r = total number of Schmidt plots (samples),

c = total number of patches in each plot,

f_{ij} = observed frequency of fracture poles in the ij cell,

e_{ij} = expected frequency of fracture poles in the ij cell.

Table 2.1. Contingency Table for Schmidt Plots

Rows	Patch 1	Patch 2	Patch 3 . . .	Patch c	Row Total
Schmidt Plot 1	f_{11}	f_{12}	f_{13} . . .	f_{1c}	R_1
Schmidt Plot 2	f_{21}	f_{22}	f_{23} . . .	f_{2c}	R_2
Schmidt Plot 3	f_{31}	f_{32}	f_{33} . . .	f_{3c}	R_3
.	.	.	.	.	.
.	.	.	.	.	.
.	.	.	.	.	.
Schmidt Plot r	f_{r1}	f_{r2}	f_{r3} . . .	f_{rc}	R_r
Column Totals	C_1	C_2	C_3 . . .	C_c	N

The expected frequency in the ij cell is given by the following expression:

$$e_{ij} = \frac{R_i C_j}{N} \qquad (2.2)$$

where: R_i = total observed number in the i-th row,

C_j = total observed number in the j-th column,

N = total number of observations.

If the null hypothesis is true, then the above statistic is chi-squared distributed with (r-1)(c-1) degrees of freedom, and its value does not exceed that of a chi-squared variate evaluated at a specified significance level, α. The usual test procedure consists of selecting a value of α, and then calculating the value of χ^2 from the contingency table. The null hypothesis is rejected if this calculated value exceeds the known tabulated value of χ^2 with (r-1)(c-1) degrees of freedom at the specified α value. Consequently, if the contingency table produces a large χ^2 value, then the sampled populations are probably not the same. The α value is the area under a chi-squared distribution to the right of its associated χ^2 value and is also the probability of rejecting the null hypothesis when it is actually true. An erroneous rejection with an associated high cost (say, in terms of lost dollars or manpower) would dictate that a small α value be specified.

Rather than selecting a particular significance level for comparing Schmidt plots, it is often desirable from a geologic standpoint to use the calculated χ^2 value from the contingency table to compute its corresponding right-tailed area, α. This computed α value is not really a level of significance, but rather a measure of one's confidence in

accepting the null hypothesis. The right-tailed area provides a quantitative and standardized measure of comparison among different contingency table analyses. In other words, it allows the investigator to have greater (or lesser) confidence in accepting the null hypothesis for one set of Schmidt plots than for another set. A numerical procedure for estimating the right-tailed area under a chi-squared distribution with more than 30 degrees of freedom is given in the Handbook of Mathematical Functions (Abramowitz and Stegun, 1965, p. 941, 932).

Another standardized index that may be useful in contingency table analyses of Schmidt plots is the calculated χ^2 value divided by the appropriate degrees of freedom. Clearly, the larger the value of this index, the greater the difficulty in accepting that the Schmidt plots in a given table were obtained from homogeneous structural populations. However, usage of the right-tailed area, α, is preferred because its concept is well known in statistical literature and its value has some real significance in that it equals a percentage of area under a chi-squared distribution.

Careful selection of the number and size of patches on the Schmidt plots is critical because the multinomial chi-squared test is valid only when the expected frequencies are sufficiently large. The commonly accepted general rule is that the test should be used only when none of the cell expectations is less than five. However, Cochran (1954, p. 420) suggested that if relatively few expectations are less than five (say, in one-fifth or fewer of the cells), then a minimum expectation of one is allowable in calculating χ^2 from the contingency table. Baker and

Lee (1975) indicated that simulation studies and theoretical investigations have shown that even more liberal rules are appropriate for contingency tables with more than one degree of freedom. For example, Lancaster (1969, p. 175) suggested that a third of the cells may have expectations less than five, as long as no expectations are less than one. An even more lenient rule was given by Chapman and Schaufele (1970) whereby any expected frequency could be small, but never less than one.

Lancaster's criterion is currently preferred for most contingency table analyses of Schmidt plots. A reasonably sized mapping sample of fracture orientations contains at least 150 observations (Call and others, 1976), and if the displayed poles are fairly dispersed, then Lancaster's criterion is met in most cases. In contrast, the more strict criterion of Cochran is met in only a majority of cases while the more relaxed criterion of Chapman and Schaufele is met in practically all cases. Because the common sample size ranges from 150 to 250 observations, the example patch networks shown in Figure 2.3 usually suffice for contingency table analyses. Larger samples would require more patches. A larger number of patches is also required when the Schmidt plots display mapping blind zones because those patches in the blind zones are not used in calculating the χ^2 value. Each unused patch causes a loss of one degree of freedom, so usually a net with more than 50 patches is recommended to assure that at least 30 degrees of freedom are obtained.

Therefore, the investigator should select the number of equal-area

patches on the Schmidt plots so as to have as many as possible, but not at the expense of causing most of the expected cell frequencies to be less than five. By neglecting the effect of blind zones and assuming that the fracture orientations are random, the following expression yields the approximate number of required patches:

$$N_p \cong N/5r \tag{2.3}$$

where: N_p = number of equal-area patches on Schmidt plots,

N = total number of observations in all plots,

r = total number of Schmidt plots (samples).

2.3 Contingency Table Analysis When Expectations are Small

When the contingency table used to compare Schmidt plots has small expectations in a number of cells and Lancaster's criterion cannot be met, the analytical procedure must be modified slightly. According to Cochran (1954, p. 420) the calculated χ^2 tends to be normally distributed when it has more than 30 degrees of freedom; but when calculated from a contingency table with many small expectations, its mean and variance are different from those of the tabulated χ^2 variate. Consequently, the right-tailed area based on the standard chi-squared distribution will not be correct.

If the true mean and variance of the calculated statistic are known, then the correct right-tailed area can be determined from the approximately normal distribution of the statistic by using a table of the

normal distribution function. Expressions for the true mean and variance of χ^2 when cell expectations are small have been derived by Haldane (1939) and are given below:

Mean

$$E(\chi^2) = \frac{(r-1)(c-1)N}{N-1} \tag{2.4}$$

Variance

$$\mathrm{Var}(\chi^2) = \frac{N}{(N-1)(N-2)(N-3)} \left\{ \frac{AN^3 + BN^2 - (D+G)N - H}{N-1} - (KC+LR)N^2 + (MC+QR)N + RC(N+1)N^2 \right\} \tag{2.5}$$

where:

$A = 2(r-1)(c-1)$

$B = r^2c^2 + 2r + 2c - 4$

$D = 2rc(r-1)(c-1)$

$G = 2(r+c)(r+c-2)$

$H = rc(r-2)(c-2)$

$K = r^2 + 2r - 2$

$L = c^2 + 2c - 2$

$M = r(r-2)$

$Q = c(c-2)$

$R = \sum_{i=1}^{r} \frac{1}{R_i}$

$C = \sum_{j=1}^{c} \frac{1}{C_j}$

2.4 Example Problem

To illustrate how the contingency table analysis can be used to delineate structural domains, the three Schmidt plots shown in Figure 2.4 were compared in pairs. The approximate number of equal-area patches needed is calculated by using equation (2.3):

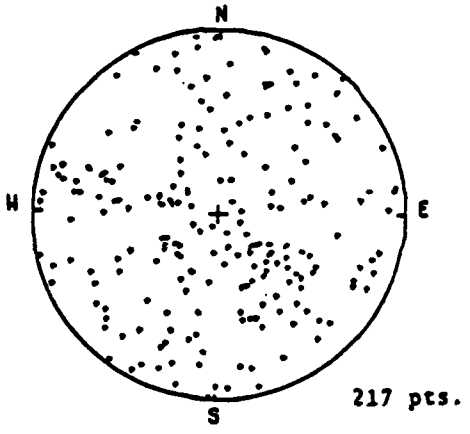

Plot No. 2

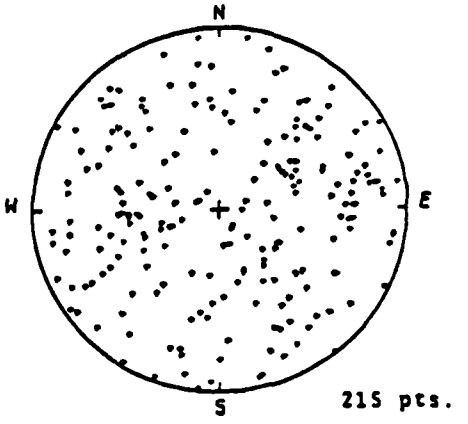

Plot No. 1

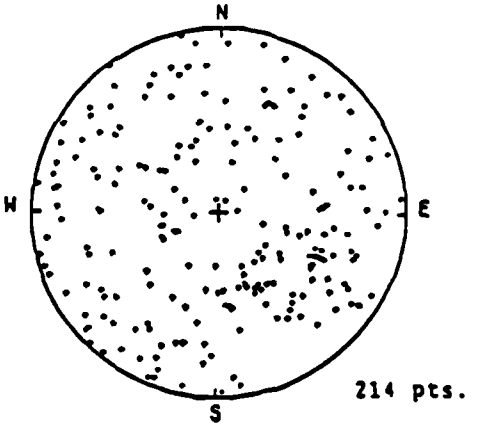

Plot No. 3

Figure 2.4. Lower-Hemisphere Schmidt Plots for Example Problem

$$N_p \approx N/5r = 420/5(2) = 43.$$

There is not an abundance of high-angle fractures displayed in any of the plots, so the 34-patch net was chosen instead of the 38-patch net of Figure 2.3.

To help minimize the subjective nature of the patch orientations, each pair of Schmidt plots was analyzed 18 times as the patch network was rotated through 180 degrees by 10-degree increments. Results from the contingency table analyses are summarized in Table 2.2 and indicate that plots 2 and 3 represent samples from the same structural domain, while plot 1 represents a sample from a different domain. Therefore, a domain boundary likely is present between mapping sites 1 and 2, and between sites 1 and 3.

Variation in the 18 calculated α values for a given comparison indicates that the fracture poles are not distributed in a truly random fashion on the plots. It may also be caused by natural variation and measurement uncertainty, which often produce an undesirable misalignment of clusters, even when they represent the same fracture set in Schmidt plots obtained from the same structural domain. A process of smoothing or filtering the fracture poles on the plots would probably help to minimize the variation in α, but such a procedure has not been developed or investigated to date.

This example and other experiences with the contingency table analysis indicate there is not a definite α value which specifies whether or not the Schmidt plots were obtained from the same structural population. However, the desired α value is usually between 0.10 and 0.20

Table 2.2 Summary of Contingency Table Analysis for Example Schmidt Plots Rotated Through 18 Orientations (10-degree increments through 180 degrees).

Schmidt Plots	Calculated χ^2 Value Divided by Degrees of Freedom			Right-Tailed Area (α)		
	Min.	Avg.	Max.	Min.	Avg.	Max.
1 and 2	1.5167	1.6512	1.7866	0.0037	0.0125	0.0289
1 and 3	1.2896	1.5660	1.8296	0.0026	0.0351	0.1230
2 and 3	0.9743	1.0994	1.2828	0.1278	0.3327	0.5072

for most situations. The major advantage of calculating α when comparing Schmidt plots is that a standard scale is provided for measuring one's confidence in claiming that the sampled structural populations are alike.

2.5 Summary

Contingency table analysis, based on a multinomial chi-squared statistic, is a useful tool for comparing Schmidt plots and evaluating the alikeness of sampled structural populations. The method is intended for plots that display dispersed fracture orientations where the lack of well defined clusters makes visual comparisons difficult and oftentimes useless. There is no limit to the number of plots used in the contingency table, although the usual number is from two to four. The necessary mathematical calculations can be easily programmed on a desktop computer.

The most notable benefit of using this statistical method is that it provides a quantitative, standard scale for measuring one's confidence

in claiming that the sampled structural domains are alike. One disadvantage is that the selection of a network of equal-area patches on the lower-hemisphere projection is almost completely arbitrary. However, even though different patch networks may provide different numerical results, the final conclusions will likely be the same. As with all statistical tools, the application of the method and the interpretation of results should be guided by experience and sound judgment.

One of the major applications of the contingency table analysis has been in comparing Schmidt plots of surface data with those of subsurface data. By evaluating Schmidt plots of oriented-core data from various segments of a drill hole, the method can provide an indication as to the subsurface extent of a structural domain that is exposed in surface outcrops. In this way, domains in the study area can be delineated to allow for intelligent planning of further data collection and of a sound program for the engineering design of proposed rock slopes.

CHAPTER 3

NONLINEAR REGRESSION ANALYSIS FOR ESTIMATING ROCK SHEAR STRENGTH

3.1 Introduction

For slopes cut in discontinuous rock, failures commonly occur along structural weaknesses such as faults, joints, bedding planes, and foliations. In soil or weak rock materials that lack discontinuities or significant substance strength, failures commonly occur as shear planes through intact substance. Therefore, estimation of the shear strength along potential failure surfaces is necessary for the engineering analysis of rock slope stability.

Shear strength is usually evaluated in the laboratory by direct shear testing of rock specimens collected at the project site. The typical direct shear test is performed on two blocks of rock separated by a discontinuity such as a fracture. Irregularly shaped blocks are trimmed so as to fit the shear box on the testing machine. A load is applied to the blocks perpendicular to the fracture, and the shear load required to displace the blocks relative to each other is monitored (Figure 3.1). Fault gouge or soft rock specimens are tested in a similar fashion, except that a single block of material is sheared through its intact substance.

The laboratory test curves for a given specimen are used to calculate the associated normal and shear stresses. Results of the direct

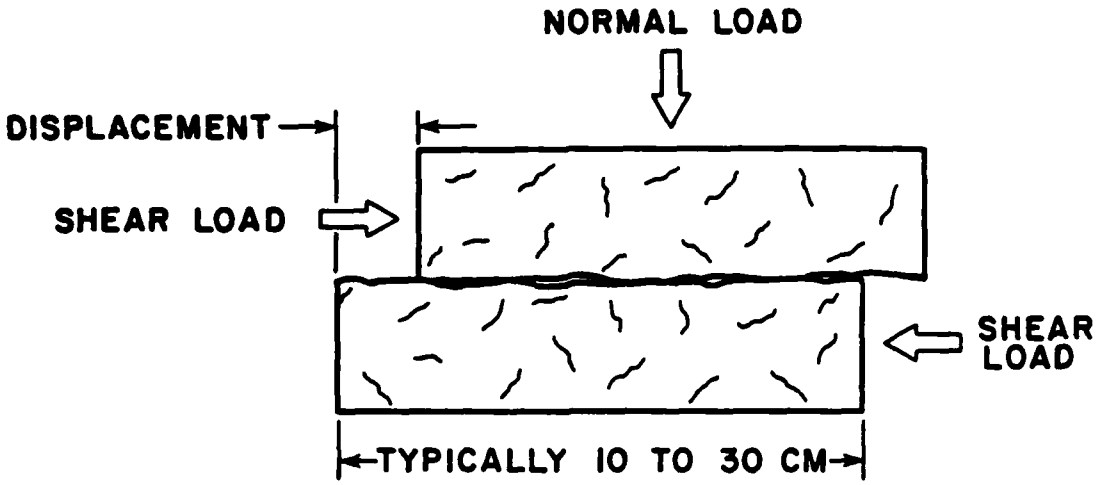

A. Loading Diagram for Direct Shear Test

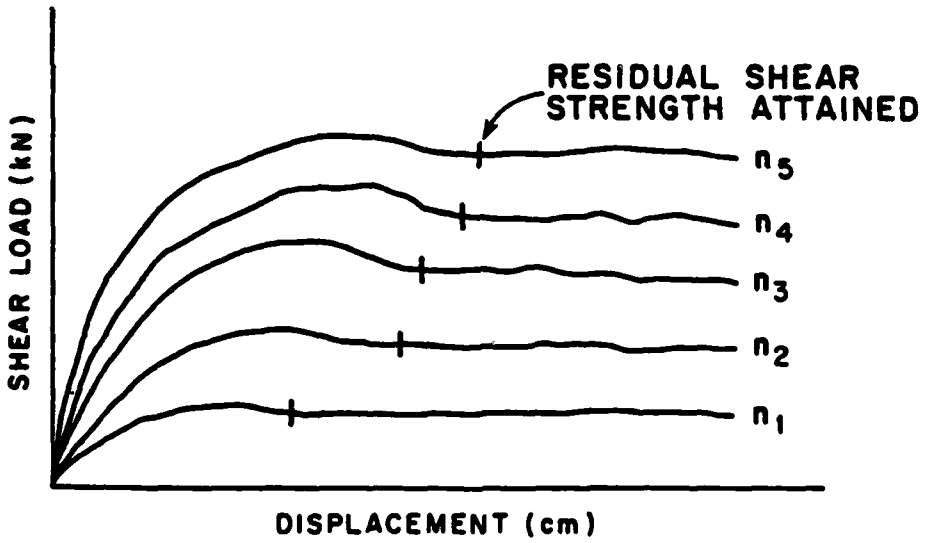

B. Laboratory Test Curves for Five Normal Loads

Figure 3.1. Direct Shear Loading Diagram and Laboratory Test Curves

shear testing are then displayed as a graph with the normal stress plotted as the independent variable (Figure 3.2). Statistical regression models can be applied to the test results and used to describe the mean and variance of the shear strength at a given normal stress. Details for fitting a linear regression model and a power, or geometric, regression model to the shear strength data are given by Miller (1981). A more general regression model proposed by Jaeger (1971) is given in the following form:

$$\tau = a\sigma_n^b + c \tag{3.1}$$

where: σ_n = applied normal stress,

τ = predicted shear strength,

a, b, c = regression parameters.

This modified power curve model readily degenerates to the linear model if b equals one or to the power model if c equals zero. For the linear model, the parameter a is the coefficient of friction and the parameter c is the cohesion.

3.2 Nonlinear Regression for a Single Specimen

Laboratory direct shear testing of one rock specimen usually involves four to six normal loads. Having no more than six data points to regress, the modified power curve model of equation (3.1) with three unknown parameters can not be confidently applied in a nonlinear regression sense because there are insufficient degrees of freedom.

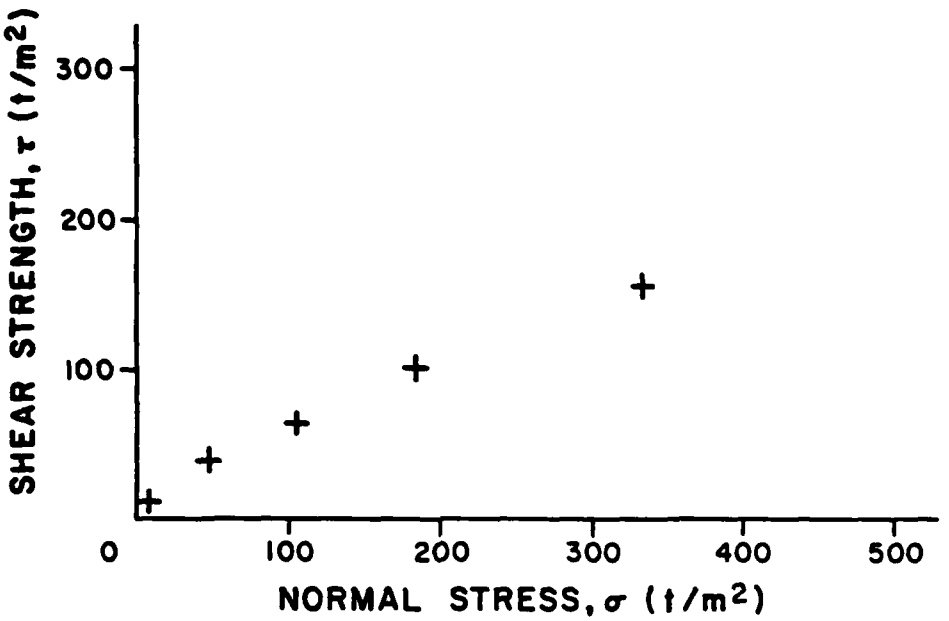

A. Test Results for a Specimen with Low Shear Strength

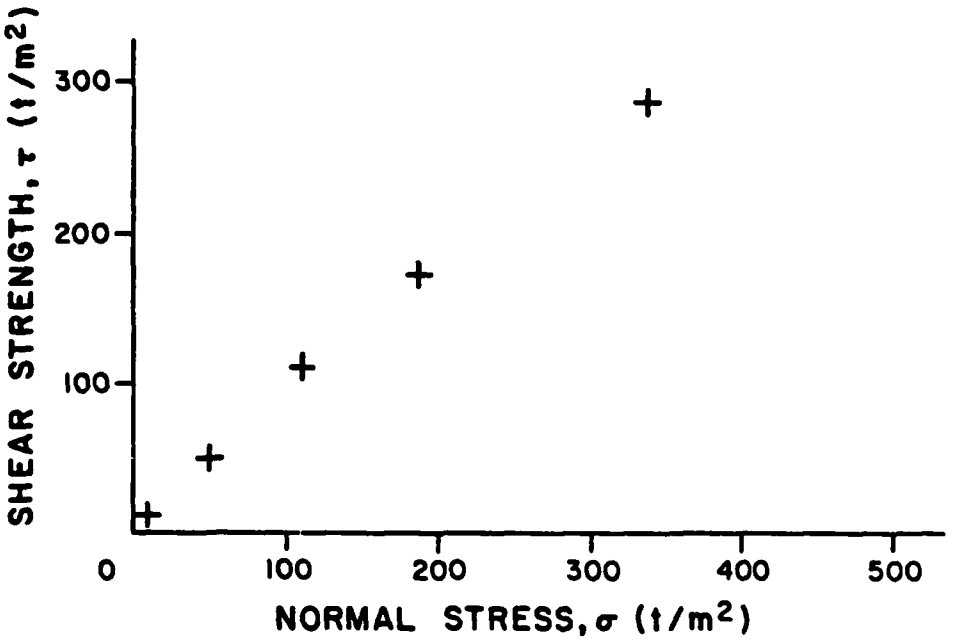

B. Test Results for a Specimen with High Shear Strength

Figure 3.2. Examples of Direct Shear Test Results

For this regression model, the degrees of freedom equal N-3, where N is the number of data points. Empirical studies have shown that at least 12 degrees of freedom are desired when a linearization method is used in this nonlinear regression model (refer to section 3.3).

The modified power curve model could be fit to the data by making a logarithmic transformation to a linear system and then applying linear regression techniques. However, this procedure minimizes the mean squared error of the estimate for the logarithms of the data values, not for the data values themselves. Although it may suffice for a few data points, the transformation method does not truly minimize the mean squared error of the estimate for many data points or for dispersed data points.

A numeric approximation technique can be used to obtain a modified power curve fit that minimizes the mean squared error of the estimate of the dependent variable, which in this case is the shear strength. For notation convenience, equation (3.1) is rewritten in the form:

$$y = ax^b + c \tag{3.2}$$

where: x = applied normal stress,

y = predicted shear strength at the applied normal stress,

a, b, c = best estimators of regression parameters.

The expected squared error of the estimated shear strength is given by:

$$s_e^2 = \frac{1}{N-3} \sum_{n=1}^{N} \left(y_n - ax_n^b - c \right)^2 \tag{3.3}$$

where: s_e^2 = expected squared error of estimated shear strength,

x_n = normal stress of the n-th data point,

y_n = shear strength of the n-th data point,

N = number of data points.

After expanding the square and implementing some algebra, equation (3.3) can be expressed in the form:

$$s_e^2 = \frac{1}{N-3}\left(c^2 + \sum_n y_n^2 + a^2\sum_n x_n^{2b} + 2ac\sum_n x_n^b - 2c\sum_n y_n - 2a\sum_n y_n x_n^b\right) \qquad (3.4)$$

To determine the regression parameters that minimize s_e^2, the partial derivatives with respect to a, b, and c are set equal to zero, and then an iterative procedure based on Newton's method of approximation is used to solve for parameter b (Miller, 1982b). The estimated value of b is then used to calculate parameters a and c. The computational procedures can be easily programmed on a desk-top computer.

For a single test specimen, the least-squares estimate of the mean shear strength curve is now defined by using the estimates of a, b, and c in equation (3.1). The squared error of the estimate is calculated by using equation (3.3). The so-called standard error of estimate (s_e) is the square root of the squared error of the estimate. Figure 3.3 illustrates the least-squares regression curves for the shear strength data presented in Figure 3.2.

3.3 Weighted, Nonlinear Regression for Several Like Specimens

A probabilistic stability analysis is rarely based on the results

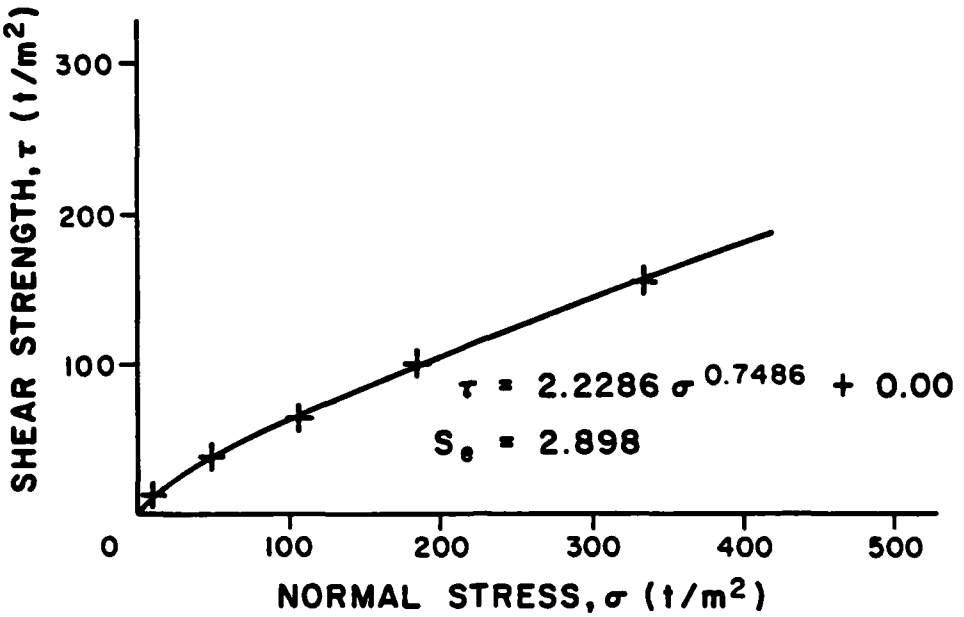

A. Regression Curve for Specimen with Low Shear Strength

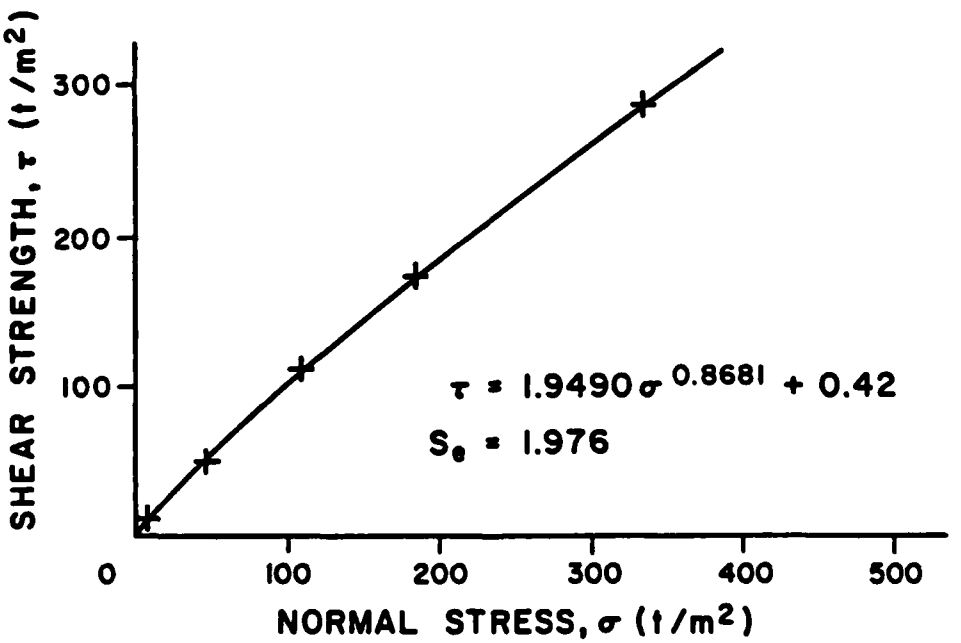

B. Regression Curve for Specimen with High Shear Strength

Figure 3.3. Modified Power Regression Curves for Shear Strength Data Illustrated in Figure 3.2.

of a single direct shear test. Typically four or more specimens of a given rock type or fracture type are tested in order to provide a reasonable estimate of the predicted shear strength. The process of grouping data points from all like specimens on a single graph and then fitting a regression curve produces a very small variance in the mean shear strength, regardless of thedispersion in the raw data points. This effect is caused by the increased number of data points, which provides a better estimate of the overall mean shear strength. This reduced variation that results from obtaining more data points is misleading, because the actual variability within the rock mass does not depend on the number of normal stresses applied to test specimens. The incorrect statistical assumption is that the individual data points are independent samples, when, in reality, the specimens themselves represent independent samples.

Therefore, the combination of test data from several like specimens should be analyzed in a manner different from that used for a single specimen. Data points for a single specimen estimate the distribution of shear strengths for that particular specimen. Strength estimates from a given specimen should be combined with those of other like specimens to determine the distribution of shear strengths for the population defined by rock type or fracture type. In essence, several regression curves must be combined to produce a regression curve representative of the population. Some of the sample curves will be better estimators of the population curve than others. Therefore, a weighted regression scheme is desirable for combining the regression curves of several like specimens.

A linearization method discussed by Draper and Smith (1981) often can be applied to nonlinear regression problems. As indicated at the beginning of section 3.2, this method usually requires that at least 12 degrees of freedom be available from the data set. This implies that test results from at least three specimens with five data points each are required to estimate three regressions parameters.

The modified power curve regression model given by equation (3.2) is linearized by approximating the power term by a Maclaurin series. Consider the following regression model:

$$y = ax^{b_o} x^{(b-b_o)} + c + \varepsilon \tag{3.5}$$

where: x = applied normal stress,

y = predicted shear strength,

a, b, c = best estimators of regression parameters,

b_o = guess, or estimate of parameter b,

ε = random error.

Let $u = b - b_o$ and then approximate x^u by a Maclaurin series expansion:

$$f(u) = x^u = f(0) + u f'(0) + \frac{u^2}{2!} f''(0) + \frac{u^3}{3!} f'''(0) + \ldots$$

$$x^u = 1 + u \ln x + \frac{u^2}{2} (\ln x)^2 + \frac{u^3}{6} (\ln x)^3 + \ldots \tag{3.6}$$

Thus, the linearized version of equation (3.5) can be written in the form:

$$y = ax^{b_o} + a(b-b_o)x^{b_o} \ln x + \frac{a(b-b_o)^2}{2} x^{b_o}(\ln x)^2$$

$$+ \frac{a(b-b_o)^3}{6} x^{b_o}(\ln x)^3 + \ldots + c + \varepsilon \qquad (3.7)$$

Experience with this particular regression model has shown that only the first two terms in the series expansion are needed to provide quite good estimates of the regression parameters. The inclusion of additional terms often results in a curve with unreasonable flucuations and poor overall estimation of the expected shear strength. A suitable approximation of equation (3.7) can thus be written in the following matrix form:

$$\underline{Y} \approx \begin{bmatrix} x_1^{b_o} & x_1^{b_o} \ln x_1 & 1 \\ x_2^{b_o} & x_2^{b_o} \ln x_2 & 1 \\ \cdot & \cdot & \cdot \\ \cdot & \cdot & \cdot \\ \cdot & \cdot & \cdot \\ x_n^{b_o} & x_n^{b_o} \ln x_n & 1 \end{bmatrix} \begin{pmatrix} \beta_1 \\ \beta_2 \\ \beta_3 \end{pmatrix} + \underline{\varepsilon} \qquad (3.8)$$

where: $\underline{Y}$ = vector of shear strenths for n data points,

x_n = normal stress of n-th data point,

b_o = guess, or estimate, of parameter b,

β_1 = parameter a,

β_2 = $a(b-b_o)$,

β_3 = parameter c,

$\underline{\varepsilon}$ = vector of random errors.

For combining the test results of like specimens, let J be the number of specimens and I_j be the number of data points for the j-th specimen. Equation (3.8) can be rewritten in shorthand form:

$$\underline{Y}_j = X_j \underline{\beta} + \underline{\varepsilon}_j \qquad (3.9)$$

where: $\underline{Y}_j$ = vector of shear strength values for the j-th specimen,

X_j = large X matrix for the j-th specimen,

$\underline{\beta}$ = vector of regression parameters,

$\underline{\varepsilon}_j$ = vector of random errors for the j-th specimen.

To incorporate the weighting of specimens, a weighted least-squares criterion is applied wherein the estimated vector of regression parameter solutions is given by:

$$\hat{\beta} = (X'WX)^{-1}(X'WY) \qquad (3.10)$$

where: $$(X'WX) = \sum_{j=1}^{J} X_j' W_j X_j \qquad (3.10i)$$

$$(X'WY) = \sum_{j=1}^{J} X_j' W_j Y_j \qquad (3.10ii)$$

Diagonal elements in a given W_j matrix are equal to the inverse of the standard error from the regression of the j-th specimen (s_{e_j}). The assumption here is that greater confidence can be placed in the reliability of a regression curve with a smaller standard error of estimate. The matrices that are derived from the testing data of the j-th specimen are given below:

$$X_j = \begin{pmatrix} x_{1j}^{b_o} & x_{1j}^{b_o} \ln x_{1j} & 1 \\ x_{2j}^{b_o} & x_{2j}^{b_o} \ln x_{2j} & 1 \\ \vdots & \vdots & \vdots \\ x_{I_jJ}^{b_o} & x_{I_jJ}^{b_o} \ln x_{I_jJ} & 1 \end{pmatrix} \qquad (3.11)$$

$$Y_j = \begin{pmatrix} y_{1j} \\ y_{2j} \\ \vdots \\ y_{I_jJ} \end{pmatrix} \qquad (3.12)$$

$$W_j = \begin{bmatrix} w_j & 0 & 0 & 0 \\ 0 & w_j & 0 & 0 \\ 0 & 0 & w_j & 0 \\ 0 & 0 & 0 & \ddots \\ & & & w_j \end{bmatrix} = \begin{bmatrix} 1/s_{e_j} & 0 & 0 & 0 \\ 0 & 1/s_{e_j} & 0 & 0 \\ 0 & 0 & 1/s_{e_j} & 0 \\ 0 & 0 & 0 & \ddots \\ & & & 1/s_{e_j} \end{bmatrix} \qquad (3.13)$$

where W_j is a $(I_j \times I_j)$ matrix.

Equation (3.10) can be solved provided that $(X'WX)$ has an inverse, regardless of whether or not the I_j values are equal. The $(X'WX)$ matrix will always be a (3 x 3) matrix, and the $(X'WY)$ matrix will always be a (3 x 1) matrix. This can be shown as follows:

$$(X_j'W_jX_j) : (3 \times I_j)(I_j \times I_j)(I_j \times 3) = (3 \times 3) \quad ,$$

$$(X_j'W_jY_j) : (3 \times I_j)(I_j \times I_j)(I_j \times 1) = (3 \times 1) \quad .$$

The following steps summarize computational procedures for finding the modified power regression curve that best describes the mean shear strength for a given rock type or fracture type. The steps can be easily programmed on a desk-top sized or larger computer.

1. Initial estimates of a, b, and c are obtained by applying Newton's method of approximation to a number (usually 30 to 50) of artificial data points. Each of these points has a regularly incremented normal stress value (x_o) between zero and the maximum normal stress

tested and has a shear strength value equal to the mean of the values predicted at x_o by the regression curves of the individual samples.

2. The first guess, b_o, equals the b from Step 1, and the X_j and Y_j matrices are formed according to equations (3.11) and (3.12) from the raw data points of each specimen.
3. The W_j weight matrices are formed according to equation (3.13) by using the standard error of estimate from the regression curve of each specimen. To weight each specimen equally the W_j matrices are set equal to identity matrices.
4. The $(X_j'W_jX_j)$ and $(X_j'W_jY_j)$ products are summed according to equations (3.10i) and (3.10ii) to produce the respective overall $(X'WX)$ and $(X'WY)$ matrices.
5. The $(X'WX)$ matrix is inverted and the solution vector $\hat{\beta}$ is determined by using equation (3.10).
6. The new estimate of b is determined by the following expression:

$$b = \frac{\hat{\beta}_2}{a} + b_o = \frac{\hat{\beta}_2}{\hat{\beta}_1} + b_o \qquad (3.14)$$

7. The new guess, b_o, equals this value of b, and steps 2 through 6 are repeated until the difference between b_o and b is negligible (say, less than 0.0001).
8. Parameters a and c for the overall regression curve are respectively equal to $\hat{\beta}_1$ and $\hat{\beta}_3$ as predicted by the final iteration.
9. The regression curve for the rock type is further improved by

repeating the weighted least-squares regression with new standard errors, computed as follows:

$$s_{e_j} = \sqrt{\frac{1}{I_j - 3} \sum_{n=1}^{I_j} (y_n - ax_n^b - c)^2} \qquad (3.15)$$

where: I_j = number of data points for the j-th specimen,

x_n = normal stress of the n-th data point,

y_n = shear stress of the n-th data point,

a, b, c = regression parameters for the rock type as determined in steps 7 and 8.

This new standard error of estimate represents how well the raw test data from the j-th specimen predict the regression curve for the rock type.

Step 9 is repeated until the b values of consecutive iterations are nearly equal. Usually, three to six iterations are required to produce the final estimates of a, b, and c for the weighted, least-squares regression curve that describes the expected shear strength of a particular set of like specimens. Thus, for a specified rock type or fracture type, the estimated mean shear strength $\hat{y}_o$ that corresponds to a given normal stress x_o is given by the following equation:

$$\hat{y}_o = ax_o^b + c \qquad (3.16)$$

3.4 Estimation of the Variance of Expected Shear Strength

More information than the expected shear strength is needed for probabilistic stability analyses. The variance and distribution of shear strength at a given normal stress x_o are also required. For the nonlinear, modified power regression model an assumption of normality for the random errors, and thus the expected shear strengths, is not appropriate because negative values of shear strength would be possible at very low normal stresses. The probability distribution of expected shear strengths is expected to favor a gamma or lognormal type of distribution. A gamma distribution has been assumed in this current research because it allows the predicted shear strengths to always be positive and also approximates a normal distribution when its coefficient of variation is less than 0.10 (Andrew, 1981). The coefficient of variation equals the standard deviation divided by the mean.

The expected squared error of the estimate s_e^2 is commonly used to estimate the variance σ^2 of the random errors in the regression analysis (Miller and Freund, 1977, p. 297). Therefore, the covariance matrix of errors for the j-th specimen is defined as:

$$\text{Cov } \underset{\sim}{\varepsilon}_j = C_j = \sigma_j^2 I = s_{e_j}^2 I \qquad (3.17)$$

where I is an identity matrix.

At a given normal stress x_o let Δ be the difference between the predicted mean shear strength $\hat{y}_o$ and the expected value of y_o given by $\underset{\sim}{x}_o'\beta$. That is,

$$\Delta = \hat{\underline{y}}_o - \underline{x}_o'\beta = \underline{x}_o'\hat{\beta} - \underline{x}_o'\beta$$

$$\Delta = \underline{x}_o'(\hat{\beta} - \beta) \tag{3.18}$$

The following expression for $\hat{\beta}$ can be derived from equation (3.10):

$$\hat{\beta} = \beta + (X'WX)^{-1} X'W\varepsilon \tag{3.19}$$

This expression for $\hat{\beta}$ is substituted into equation (3.18) to give the following equation:

$$\Delta = \underline{x}_o' (X'WX)^{-1} X'W\varepsilon .$$

The variance of $\hat{y}_o$ can now be derived as follows:

$$\text{Var}(\hat{y}_o) = E(\Delta^2)$$

$$\text{Var}(\hat{y}_o) = E\left[\underline{x}_o' \left[(X'WX)^{-1} X'W \right] \varepsilon\varepsilon' \left[W'X(X'WX)^{-1} \right] \underline{x}_o \right]$$

$$\text{Var}(\hat{y}_o) = \underline{x}_o' \left[(X'WX)^{-1} X'W \right] E(\varepsilon\varepsilon') \left[W'X(X'WX)^{-1} \right] \underline{x}_o \tag{3.20}$$

But $E(\varepsilon\varepsilon')$ equals C, the overall covariance matrix which is expressed as follows:

$$C = \begin{bmatrix} [C_1] & & & 0 \\ & [C_2] & & \\ & & \ddots & \\ 0 & & & [C_J] \end{bmatrix} \tag{3.21}$$

where C_j is the covariance matrix of the regression for the j-th specimen as given by equation (3.17). The overall weight matrix W is related to C in the following manner:

$$W = C^{-\frac{1}{2}} \tag{3.22}$$

because a specified diagonal element in W is $1/s_{e_j}$ and the corresponding element in C is $s^2_{e_j}$. Therefore, equation (3.20) can be rewritten as follows:

$$\text{Var}(\hat{y}_o) = \underline{x}_o' \left[(X'WX)^{-1} X' \right] WCW' \left[X(X'WX)^{-1} \right] \underline{x}_o$$

$$\text{Var}(\hat{y}_o) = \underline{x}_o' (X'WX)^{-1} X' (C^{-\frac{1}{2}} \; C \; C^{-\frac{1}{2}}) X (X'WX)^{-1} \underline{x}_o$$

$$\text{Var}(\hat{y}_o) = \underline{x}_o' (X'WX)^{-1} X' \; I \; X (X'WX)^{-1} \underline{x}_o$$

$$\text{Var}(\hat{y}_o) = \underline{x}_o' (X'WX)^{-1} X' \; X \; (X'WX)^{-1} \underline{x}_o \tag{3.23}$$

where:
$$X'WX = \sum_{j=1}^{J} X_j' W_j X_j \tag{3.23i}$$

$$X'X = \sum_{j=1}^{J} X_j' X_j \tag{3.23ii}$$

$$\underline{x}_o = \begin{pmatrix} x_o^b \\ x_o^b \ell n \; x_o \\ 1 \end{pmatrix} \tag{3.23iii}$$

Equation (3.23) is an expression for the variance of the expected shear strength predicted by the weighted, nonlinear regression model at any given normal stress x_o. Recall that the estimated mean shear

strength at x_o is found by using equation (3.16). The following steps summarize necessary computational procedures for calculating the distribution parameters of the expected shear strength at normal stress x_o.

1. During the computational iterations described in step 9 of section 3.3, the matrix $X'X$ should be formed according to equation (3.23ii) as well as the matrix $X'WX$ which is formed according to equation (3.23i).
2. After the final iteration the $X'WX$ matrix is inverted and saved in a convenient form (stored in a computer file) along with the final $X'X$ matrix.
3. For a specified value of normal stress x_o, the expected shear strength y_o is calculated by using equation (3.16).
4. The vector $\underline{x}_o$ is formed according to equation (3.23iii).
5. Equation (3.23) is then used to calculate the variance of the expected shear strength at normal stress $\underline{x}_o$.
6. By having stored the (3 x 3) matrices described in step 2, steps 3 through 5 can be easily applied to any specified normal stress value.

The gamma probability density function (p.d.f.) of the predicted mean shear strength is now defined at any given normal stress for the particular rock type or fracture type being analyzed. An example graph of a weighted, nonlinear regression curve that describes the shear strength of a group of four like specimens is shown in Figure 3.4. The dashed curves represent a one-standard-deviation belt about the mean curve.

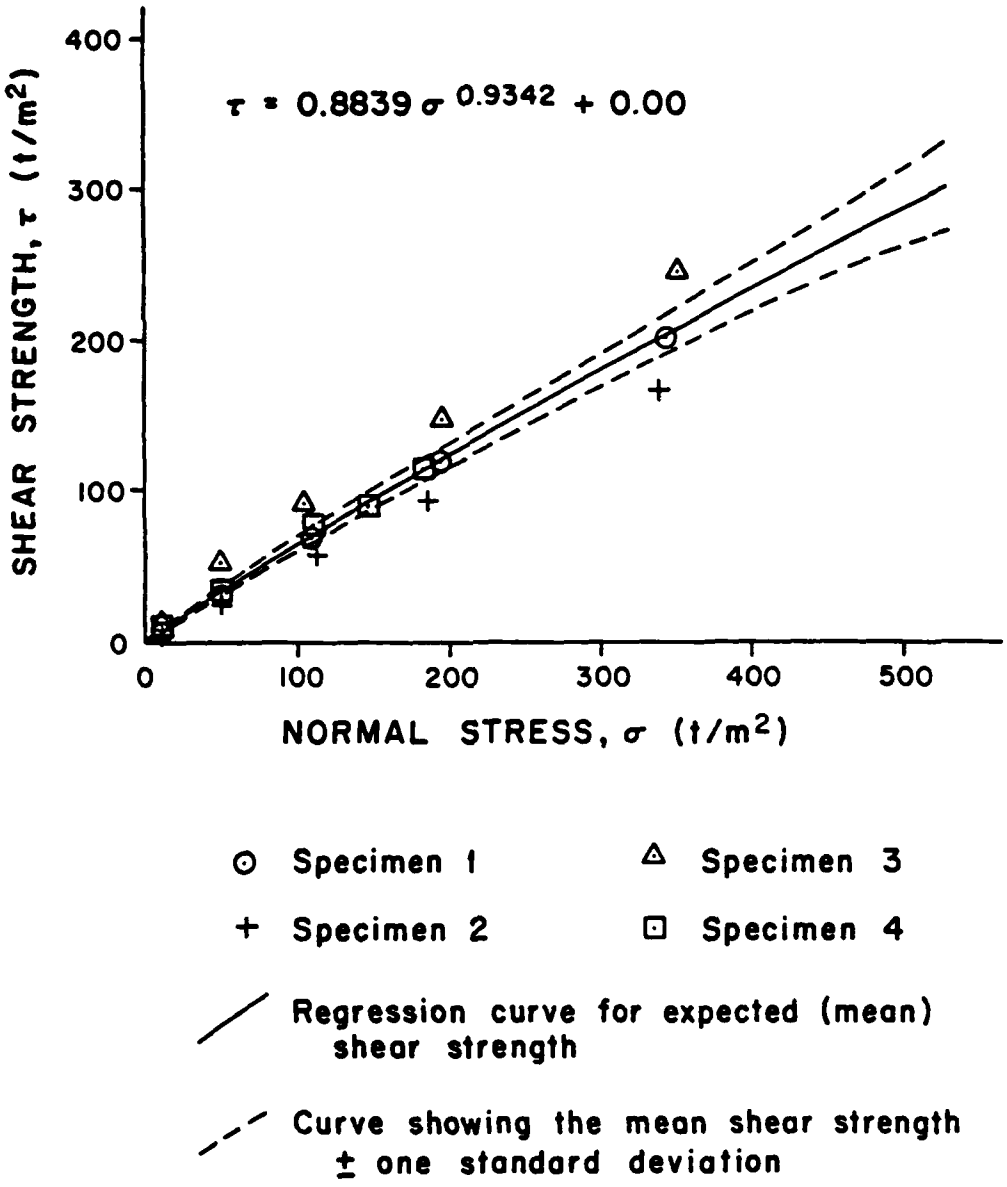

Figure 3.4. Example of a Weighted Nonlinear Regression Curve that Describes the Shear Strength of Four Like Specimens

3.5 Summary

Probabilistic stability analyses require a statistical description of the rock shear strength, especially the shear strength along weak structural features or discontinuities. Laboratory direct shear testing of natural discontinuities provides a data set that represents the relationship between the applied normal stress and the resulting shear strength. A nonlinear, least-squares regression analysis based on a modified power curve model can be applied to the shear data of individual test specimens. This analysis uses Newton's approximation method to iteratively solve for the regression parameters.

A weighted, nonlinear regression analysis has been developed to estimate the shear strength regression parameters for a group of like specimens. Linearization techniques and iterative calculations incorporate the regression parameters and standard errors of estimate from individual specimens to predict the overall regression curve that best describes the expected shear strength as a function of normal stress. The variance of the predicted shear strength at a specified normal stress can also be determined.

The statistical distribution of shear strength at a given normal stress is assumed to be a gamma p.d.f. with parameters defined by the predicted mean and variance of the shear strength. Therefore, for any specified normal stress, the p.d.f. of the shear strength of a particular rock type or fracture type can be estimated from laboratory direct shear testing and subsequent nonlinear regression analyses.

CHAPTER 4

SIMULATION OF SPATIALLY CORRELATED FRACTURE SET CHARACTERISTICS

4.1 Introduction

Fracture set characteristics such as orientation, spacing, length, and waviness tend to be spatially correlated like many other geologic variables. By using mapped fracture data, the spatial correlation of any characteristic in a fracture set can be analyzed by geostatistical methods and expressed in the form of a variogram function (Miller, 1979; La Pointe, 1980). Simulations of fracture data for probabilistic slope stability studies should include the measured spatial relationships.

Current fracture simulation procedures are based on Monte Carlo techniques that use random sampling of the probability distributions of fracture set characteristics (Marek and Savely, 1978; Call and Nicholas, 1978). These techniques are plagued by two major disadvantages. They are not capable of incorporating known spatial correlations, and they often require excessive amounts of computer time.

Spectral analysis procedures that take advantage of the computational speed of the fast Fourier transform (FFT) algorithm provide an efficient way to simulate spatially correlated fracture set characteristics. Such a simulated series of data values has the desired mean, variance, and variogram function.

4.2 Background Information

Within a particular fracture set, the random process represented by the mapped fracture data is assumed to be covariance stationary. That is, the covariance function of a specified characteristic depends only on lag (separation distance between sample locations) and not on sample location. Also, the p.d.f. of a specified characteristic does not vary within the fracture set, inferring that the data have a constant mean and variance.

If trends in mean or variance are observed, then the data can be normed by subtracting the local mean and then dividing by the local standard deviation. The normed data are practically always stationary or approximately stationary, and can be used to estimate the needed covariance function or variogram function (Borgman, 1981).

The relationship between the variogram and covariance functions can be expressed in the following equation (Journel, 1974):

$$C(h) = C(0) - \gamma(h)$$

or

$$C(h) = \sigma^2 - \gamma(h) \qquad (4.1)$$

where: h = lag, or separation distance between sample locations,

$C(h)$ = value of the covariance function at lag h,

$\gamma(h)$ = value of the variogram function at lag h,

σ^2 = variance of data.

Consequently, the covariance function needed for the simulation is de-

termined from the estimated variogram of the fracture property of interest. This variogram is generated along the mean vector of the fracture set, and should be referenced to fracture number rather than to distance (Miller, 1979).

Spectral analysis is based on the principal of Fourier transforms (Blackman and Tukey, 1958; Jenkins and Watts, 1968; Bremermann, 1965). The so-called spectral density of a random process is the Fourier transform of the covariance function. In discrete form the spectral density is defined as follows:

$$S_m = \Delta h \sum_{n=0}^{N-1} C_n \, e^{-i2\pi mn/N} \qquad (4.2)$$

where: S_m = the m-th digitized value of the spectral density,

C_n = the n-th digitized value of the covariance function,

Δh = digitization interval for the C_n values,

N = number of digitized values of the covariance function.

Because a covariance function is real-valued and symmetrical about lag zero, its corresponding spectral density is real-valued and symmetrical about frequency zero (Borgman, 1973a, p. 4.1). A digital estimate of the spectral density can be readily obtained by applying the FFT to the digitized covariance function. For covariance functions of fracture set characteristics referenced to fracture sequence number, the digitization interval Δh is equal to one.

The FFT consists of programmable mathematical procedures that compute the finite Fourier transform at extremely high speed on a digital

computer (Cooley and Tukey, 1965). Computational efficiency of the FFT is particularly dramatic for very long sequences of digitized data. Consequently, it has led to a substantial computer revolution in Fourier analysis. Important applications of the FFT to Fourier problems are discussed by Cooley and others (1967).

If the digitization interval Δh equals one, then the length of record, or period T, of the digitized covariance function is given by:

$$T = N\Delta h = N \quad , \tag{4.3}$$

and the corresponding frequency increment Δf of the discrete spectral density is given by:

$$\Delta f = 1/T = 1/N \quad . \tag{4.4}$$

Correlated, stationary data in the space domain are traded for uncorrelated, non-stationary Fourier coefficents in the frequency domain (Taheri, 1980). However, the variance of each coefficient is defined by the spectral density which is derived from the covariance function estimated from the data set. Therefore, the essence of simulating correlated fracture set data by spectral procedures is actually a frequency-domain simulation of uncorrelated Fourier coefficients that are assigned proper variance according to the estimated spectral density. These coefficients are then reverse Fourier transformed to provide a simulated set of fracture data values that have the desired covariance function.

4.3 Simulation of Normally Distributed Data

Spectral analysis procedures for simulating spatially correlated, normally distributed data in two dimensions are presented by Taheri (1980). The simulation of normally distributed fracture set characteristics is a simpler one-dimensional problem and, therefore, is somewhat easier.

Spatial relationships of a particular fracture set characteristic usually can be described by a spherical variogram model (Miller, 1979). Therefore, simulation techniques presented in this chapter are based on the spherical model which is expressed in the form:

$$\gamma(h) = a^2 + (\sigma^2 - a^2)\left[1.5(h/h_r) - 0.5(h/h_r)^3\right] \qquad (4.5)$$

where: h = lag, or separation distance between sample locations,

$\gamma(h)$ = value of variogram function at lag h,

σ^2 = variance of sample data,

a^2 = nugget value,

h_r = range of influence.

Figure 4.1 illustrates a typical spherical variogram model and its associated covariance function, which have the relationship defined by equation (4.1). However, for the spherical variogram, equation (4.1) is not mathematically consistent because:

$$\lim_{h \to 0} C(h) = \sigma^2 - a^2 \quad .$$

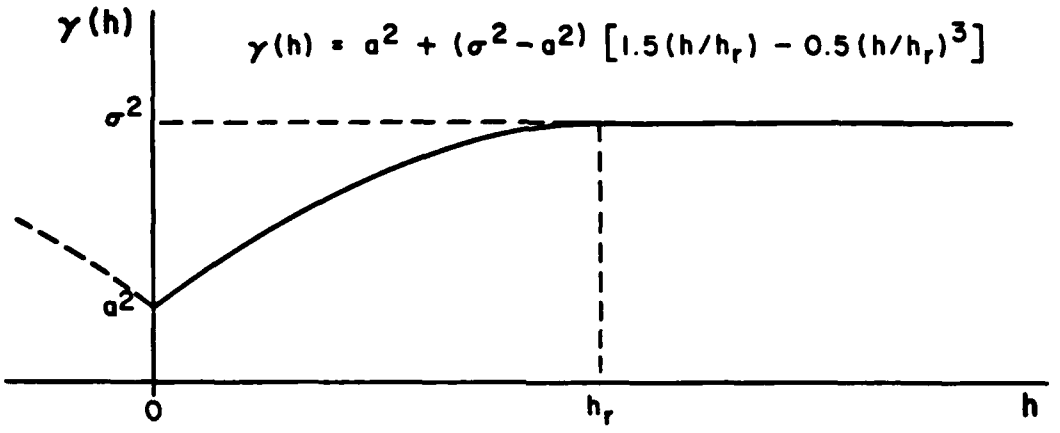

A. Spherical Variogram

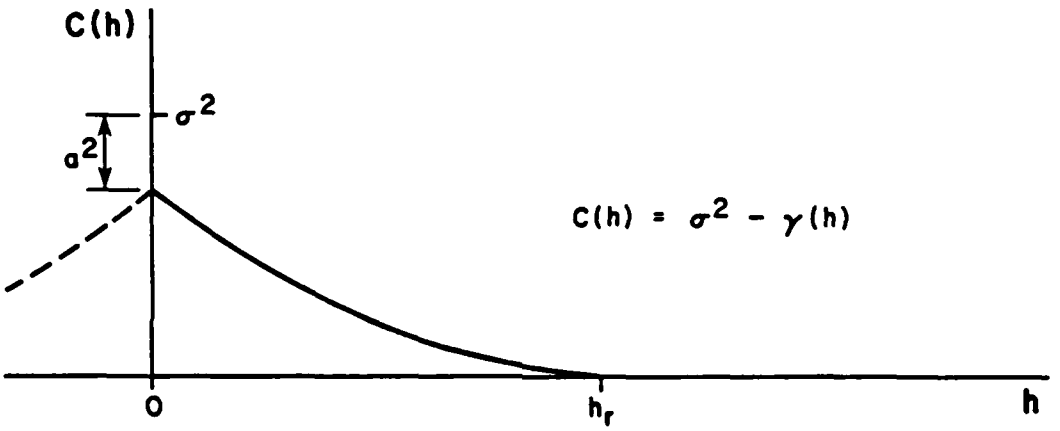

B. Covariance Function Corresponding to Spherical Variogram

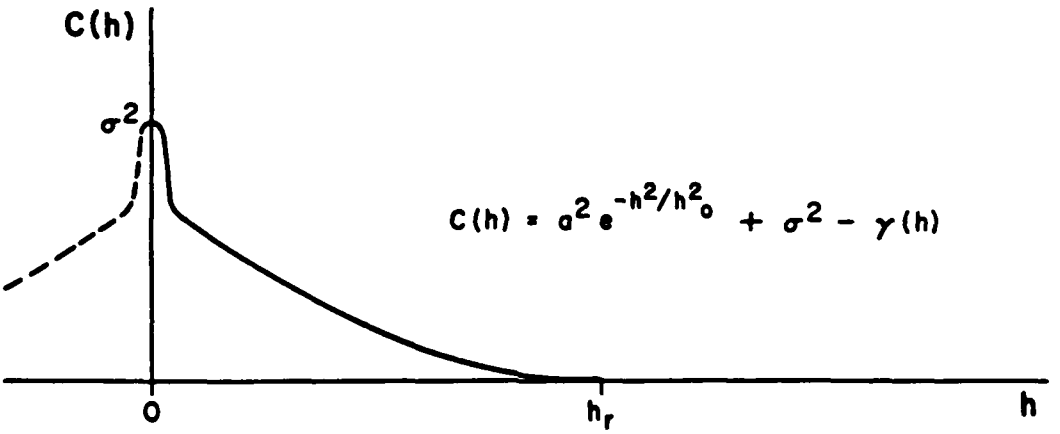

C. Modified Covariance Function

Figure 4.1. Typical Spherical Variogram and Associated Covariance Functions

The limit should equal σ^2 for consistency. Therefore, equation (4.1) should be modified to the following form:

$$C(h) = a^2 e^{-h^2/h_o^2} + \sigma^2 - \gamma(h) \qquad (4.6)$$

where h_o is much less than the smallest h value. This equation is mathematically consistent, as seen by evaluating the following limit:

$$\lim_{h \to 0} C(h) = a^2 + \sigma^2 - a^2 = \sigma^2 \quad . \qquad (4.7)$$

The spherical variogram model estimated for a fracture set characteristic is used to produce its associated covariance function according to equation (4.6). This covariance function is then digitized at N increments of width Δh equal to one. It is then fast Fourier transformed to produce S_m (spectral density) values at frequency increments of widths Δf equal to 1/N.

The next step in the simulation process is the simulation of uncorrelated Fourier coefficients that are assigned proper variance according to the discrete spectral density obtained from the estimated variogram function. First, a series of N independent, psuedo-random, normally distributed numbers with mean zero and variance one are generated. Mathematical procedures for accomplishing this task with a computer are discussed by Borgman (1982). Second, the real and imaginary parts of the Fourier coefficients A_m for m = 0, 1, 2, . . . N/2 are assigned the proper variances, which are given below (Borgman, 1973b):

If $A_m = U_m - iV_m$, then:

$$\text{Var}(U_m) = \begin{cases} TS_m , & \text{if } m = 0 \text{ or } m = N/2 \\ TS_m/2 , & \text{otherwise} \end{cases} \tag{4.8}$$

$$\text{Var}(V_m) = \begin{cases} 0 , & \text{if } m = 0 \text{ or } m = N/2 \\ TS_m/2 , & \text{otherwise} \end{cases} \tag{4.9}$$

Thus, the simulated Fourier coefficients are:

$$U_m = Z \sqrt{\text{Var}(U_m)} \tag{4.10}$$

$$V_m = Z' \sqrt{\text{Var}(V_m)} \tag{4.11}$$

where Z and Z′ are two independent, normally distributed (0,1) numbers. Values of the remaining coefficients for $N/2 < m \leq N$ are assigned according to conjugate symmetries that are described by Borgman (1973b). These symmetries are summarized below:

$$\left.\begin{aligned} U_m &= U_{N-m} \\ V_m &= -V_{N-m} \\ V_0 &= V_{N/2} = 0 \end{aligned}\right\} \tag{4.12}$$

The series of simulated Fourier coefficients are then reverse Fourier transformed by FFT to produce a spatially correlated series of normally distributed data values with mean zero and variance equal to the variance of the original data. The mean of the original data is then added to each value in the series to produce a spatially correlated set of fracture data that has the proper mean, variance, and covariance function. Example simulation results for normally distributed fracture set characteristics are shown in Figure 4.2.

4.4 Simulation of Exponentially Distributed Data

Spectral analysis procedures for simulating spatially correlated exponential data are also needed because fracture set characteristics like spacing, length, and waviness typically tend to be exponentially distributed. The simulation procedures take advantage of the statistical property that an exponential distribution is actually a chi-squared distribution with two degrees of freedom.

If X and Y are independent normally distributed $(0, \sigma^2)$ random variables, then the sum of their squares yields a chi-squared distributed variable with two degrees of freedom. That is,

$$Z = X^2 + Y^2 \quad , \tag{4.13}$$

and Z is exponentially distributed. The mean and variance of Z can be derived in terms of the variance of X and Y (Miller, 1982b) and are given below:

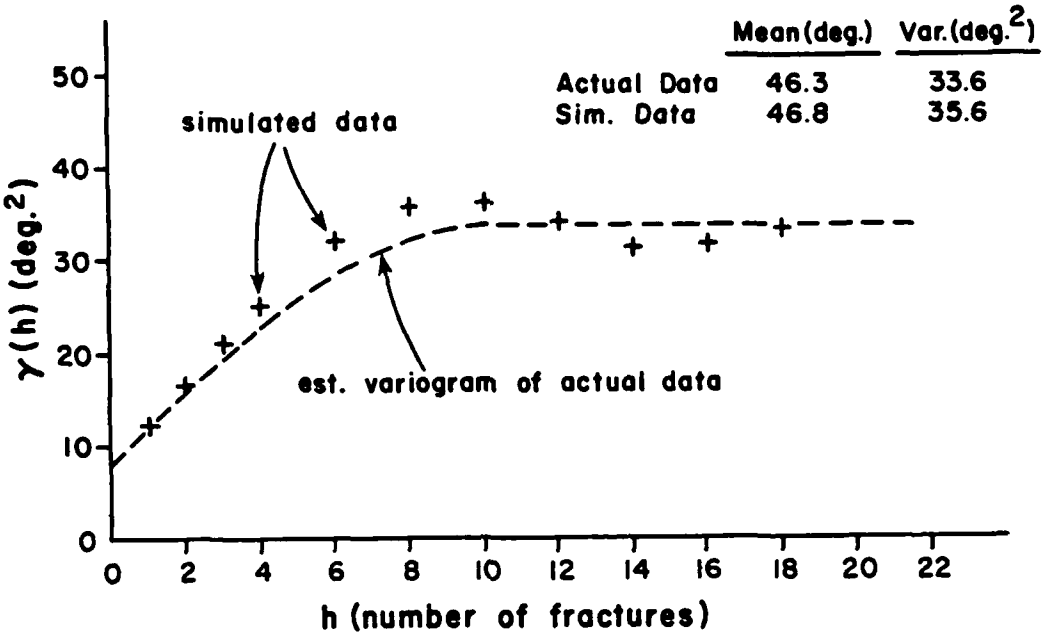

A. Results of an Example Simulation of Fracture Dips

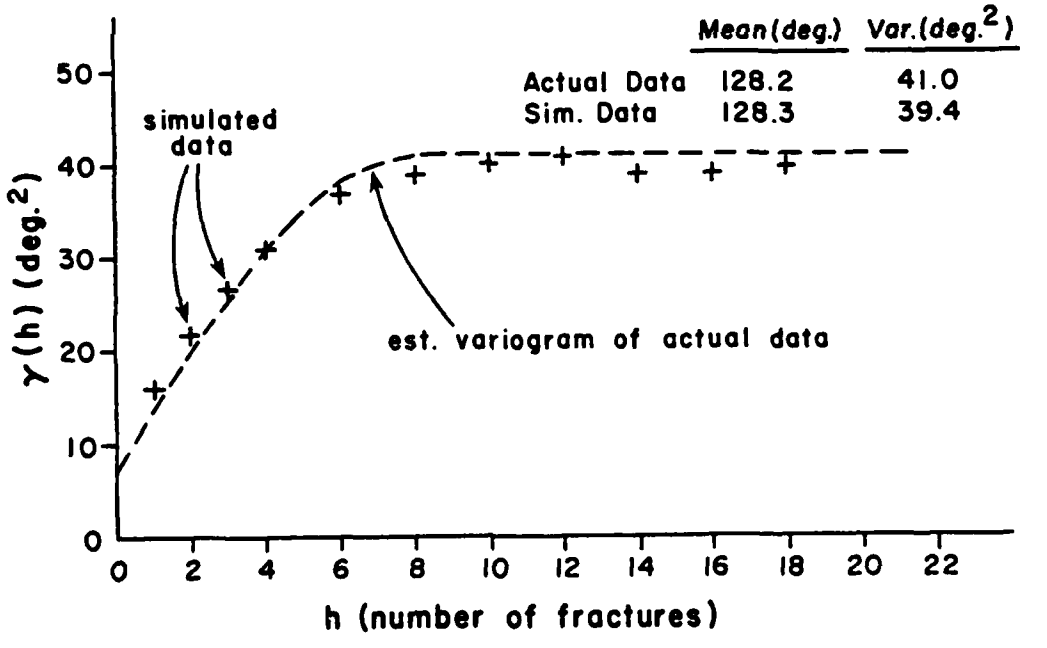

B. Results of an Example Simulation of Fracture Set Dip Directions

Figure 4.2. Results of Example Simulations of 256 Spatially Correlated, Normally Distributed Fracture Set Data

Mean of Z

$$\mu_Z = 2\sigma^2 \tag{4.14}$$

Variance of Z

$$\text{Var}(Z) = 4\sigma^4 \tag{4.15}$$

The derived results shown in equations (4.14) and (4.15) indicate that the variance equals the mean squared, an expected result because Z is exponentially distributed.

The covariance function of the random process responsible for the distribution of Z can also be derived (Miller, 1982b).

Covariance Function for Z

$$C_Z(h) = 4C^2(h) \tag{4.16}$$

where: h = lag, or separation distance between sample locations,

C(h) = value of the covariance function for X or Y at lag h,

$C_Z(h)$ = value of the covariance function for Z at lag h.

The estimated covariance function for the exponential variable Z can be obtained from the variogram function estimated from the actual fracture data (refer to equation (4.6)). The covariance function of either X or Y is then given by:

$$C(h) = \sqrt{\frac{C_Z(h)}{4}} \tag{4.17}$$

Recall that the variance of either X or Y (from equation (4.14)) is

given by:

$$\sigma^2 = \frac{\mu_Z}{2} \tag{4.18}$$

Procedures for a spectral-type simulation of exponentially distributed fracture set characteristics can now be summarized. The first step in the simulation of N exponential Z values is to generate two sets of independent, normally distributed (0, 1) numbers. Using the procedures of section 4.3, N values of correlated X values and N values of correlated Y values are simulated where X and Y are independent, and both have mean zero, variance given by equation (4.18), and covariance function given by equation (4.17). The desired N values of Z are then determined according to the following expression:

$$Z_i = X_i^2 + Y_i^2 \tag{4.19}$$

where i ranges from one to N. The simulated Z values will have the correct mean and covariance function. Example simulation results for exponentially distributed fracture set characteristics are presented in Figure 4.3.

4.5 Summary

Spatially correlated fracture set characteristics can be efficiently simulated by spectral a .lysis procedures that take advantage of the computational speed of the FFT. The covariance function needed for the simulation is obtained from the variogram function estimated from the actual data. This variogram is generated along the mean vector of the

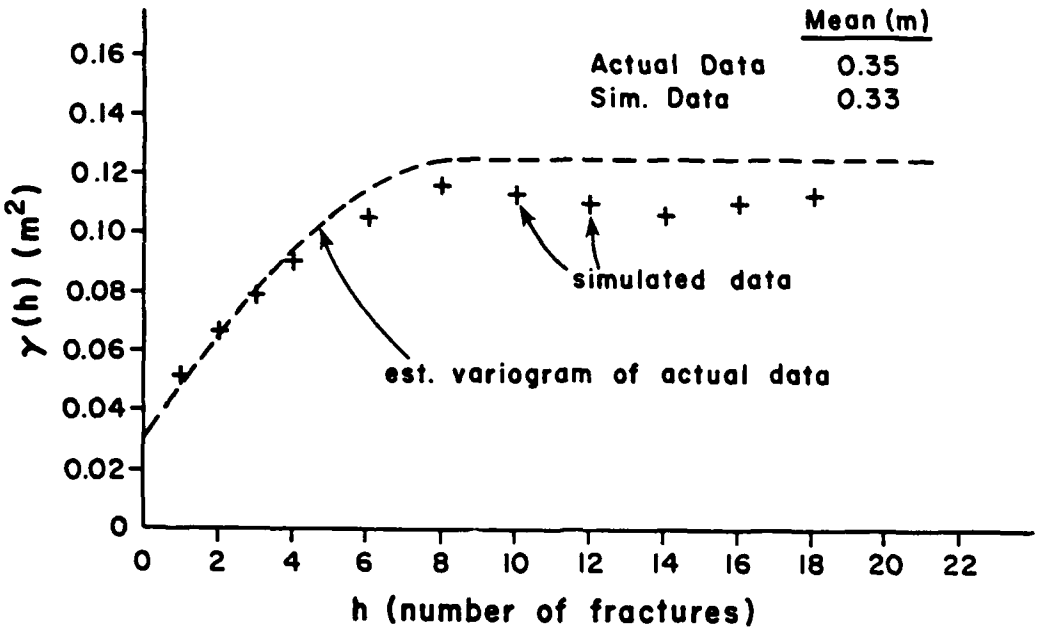

A. Results of an Example Simulation of Fracture Set Spacings

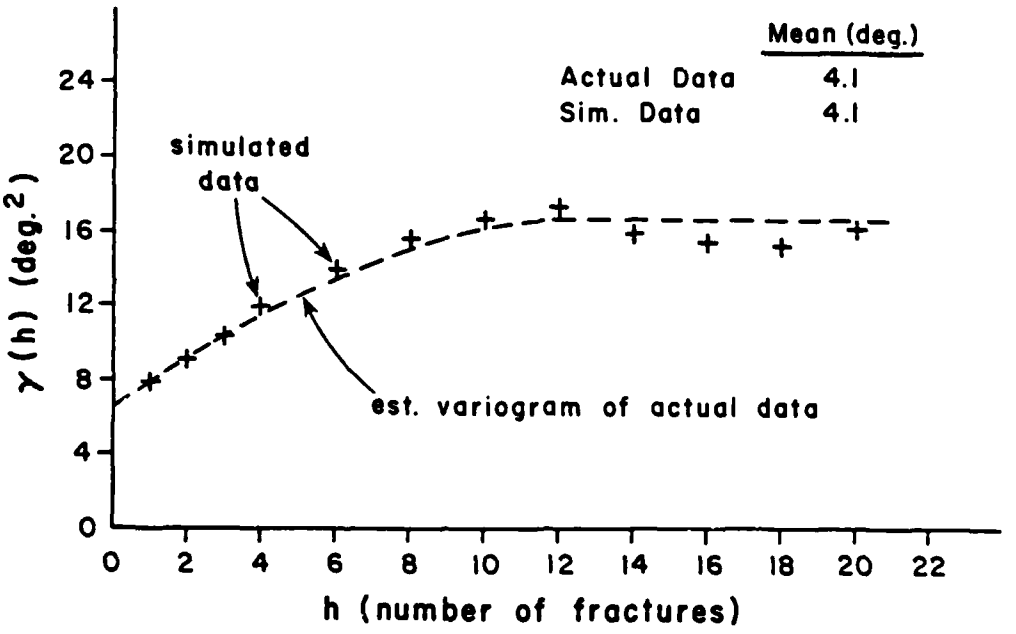

B. Results of an Example Simulation of Fracture Set Waviness Angles

Figure 4.3. Results of Example Simulations of 256 Spatially Correlated, Exponentially Distributed Fracture Set Data

fracture set and is referenced to fracture number rather than to distance.

Whether the characteristics are normally distributed or exponentially distributed, the simulation method essentially involves generating nonstationary, uncorrelated Fourier coefficients that are assigned proper variance according to the spectral density, which is the Fourier transform of the desired covariance function. These coefficients are then reverse Fourier transformed by FFT to produce a series of simulated fracture set data that has the proper variance and covariance function. For normally distributed data, the desired mean must be added to the initially simulated data because they have a mean of zero. For exponentially distributed data, no correction is needed because the variance equals the mean squared.

CHAPTER 5

FOURIER ANALYSIS FOR ESTIMATING THE PROBABILITY OF SLIDING

5.1 Introduction

The probability of sliding for various failure modes is usually estimated by Monte Carlo simulation techniques. These procedures rely on repeated sampling of the statistical distributions of input parameters to calculate a distribution of safety factors (Marek and Savely, 1978). The probability of sliding is defined as the area under this simulated distribution where values of the safety factor are less than one. Unfortunately, a Monte Carlo simulation provides only one possible realization of the true probability density function (p.d.f.) of the safety factor. Consequently, a large number of sampling iterations (typically over a thousand) are often required to provide a reliable estimate of the probability of sliding, making the associated computational time and costs objectionable, and sometimes prohibitive. Therefore, fewer iterations are used, resulting in a poorer estimate of the probability of sliding due to an increase in its sampling variance (Mihram, 1972, Chap. 4).

Fourier analysis procedures can be used to estimate the true p.d.f. of the safety factor. They are based on the principle that the sum of two or more independent density functions can be expressed as the convolution of the functions with each other (Feller, 1966, p. 7). In

other words, the sum of independent densities in the space domain is analogous to the product of their Fourier transforms (characteristic functions) in the frequency domain. Therefore, discrete Fourier techniques that use the computational speed of the FFT provide an efficient means to estimate the safety factor p.d.f. provided that the safety factor can be expressed as the sum of independent random variables.

5.2 Analysis of the Plane Shear Failure Mode

The plane shear failure mode in fractured rock slopes is characterized by a potential failure mass capable of sliding along a semi-planar discontinuty that dips flatter than the slope angle ("daylighting" criterion). The mode is kinematically viable if the average strike is parallel or nearly parallel to that of the slope face (Hoek and Bray, 1977, p. 150). In addition, the assumption is made in a two-dimensional plane shear analysis that the potential sliding mass is laterally unconstrained ("side-release" assumption).

5.2.1 Safety Factor Equation

For the typical plane shear geometry shown in Figure 5.1, a two-dimensional stability analysis can be developed that includes the effect of the waviness of the sliding surface. Recall that waviness is defined as the angle between the average and flattest dips observed in a mappable geologic structure (Call and others, 1976).

The safety factor, a random variable denoted by S, is the ratio of resisting force to driving force and can be expressed in the following algebraic form:

$$S = R_f / D_f \tag{5.1}$$

$$S = \frac{\tau L + W\cos(\alpha)\ \tan(R)}{W\sin(\alpha)} \tag{5.2}$$

$$S = \frac{2L\sin(\delta)}{h^2\ \sin(\delta - \alpha)} \left(\frac{\tau}{\gamma}\right) + \cot(\alpha)\ \tan(R) \tag{5.3}$$

where: L = length of sliding surface,

W = weight of potential failure mass,

h = height of potential failure mass,

δ = average dip of slope face,

α = average dip of sliding surface,

γ = estimated rock density,

τ = estimated shear strength of sliding surface,

R = estimated waviness of sliding surface.

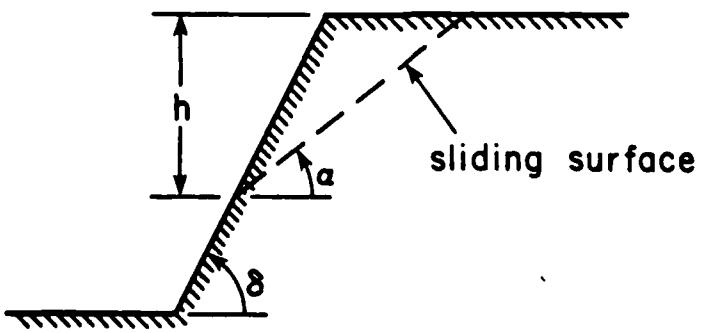

Figure 5.1. Typical Plane Shear Failure Mode in a Rock Slope

For a specified slope geometry and sliding surface, the parameters δ, α, h, and L are fixed. However, the shear strength and waviness are random variables whose probability distributions must be estimated by laboratory testing and structure mapping, respectively. The rock density can also be treated as a random variable (usually considered as being normally distributed), although in most cases it has such a small coefficient of variation that it is assumed to be constant. For example, typical mean density values for crystalline rock range from 2.40 to 2.96 g/cm^3 (150 to 185 pcf), while typical standard deviations range from 0.032 to 0.192 g/cm^3 (2 to 12 pcf). These values result in coefficients of variation that are less than 0.08, indicating that rock density can typically be treated as a constant.

5.2.2 Characterization of Random Variables

The probability distribution of shear strength is a function of the applied normal stress. Laboratory direct shear tests of natural fracture surfaces or fault gouge provide plots of shear strength as a function of normal stress. After several specimens of the same rock type have been tested, a weighted least-squares regression procedure can be used to provide estimates of the mean and variance of shear strength for the given rock type at specified normal stress values as shown in section 3.4. The p.d.f. of the shear strength is assumed to be a gamma probability density (refer to section 3.4) and is defined as:

$$f_\tau(t) = \begin{cases} \dfrac{e^{-t/\beta}\, t^{\alpha-1}}{\beta^{\alpha}\,\Gamma(\alpha)} & , \text{for } t > 0 \\ 0 & , \text{for } t \leq 0 \end{cases} \tag{5.4}$$

where: $\alpha = \mu_\tau^2/\sigma_\tau^2$,

$\beta = \sigma_\tau^2/\mu_\tau$,

$\Gamma(\alpha)$ = value of complete gamma function with argument α,

μ_τ = mean shear strength at the given normal stress,

σ_τ^2 = variance of shear strength at the given normal stress.

Copious fracture mapping data indicate that waviness tends to be exponentially distributed (Call and others, 1976; Savely, 1980). Therefore, the p.d.f. of waviness is given in the following form:

$$f_R(r) = \begin{cases} \dfrac{e^{-r/\mu_R}}{\mu_R} & , \text{for } r \geq 0 \\ 0 & , \text{for } r < 0 \end{cases} \tag{5.5}$$

where: r = waviness of sliding surface,

μ_R = mean waviness.

To determine the p.d.f. of the safety factor by Fourier procedures, equation (5.3) is expressed in the form:

$$S = AU + BV, \tag{5.6}$$

where A and B are constants, and U and V are random variables. For the general case in which rock density is considered a random variable, A and B are defined as:

$$A = \frac{2L \sin(\delta)}{h^2 \sin(\delta - \alpha)} \tag{5.7}$$

$$B = \cot(\alpha). \tag{5.8}$$

The new random variable U is the ratio of shear strength to rock density, and V is the tangent of the waviness. That is, $U = \tau/\gamma$ and $V = \tan(R)$.

The effective normal stress σ must also be considered a variable, because it depends on the rock density (and thus, the weight) according to:

$$\sigma = \frac{W \cos(\alpha)}{L} - \frac{p}{L} \tag{5.9}$$

where p equals the uplift force caused by pore pressures in the slope. The value of p is determined by multiplying the saturated volume of the potential failure mass times the unit weight of water (1.0 g/cm^3). If the piezometric ground water surface does not intersect the plane shear structure, then p equals zero. Equation (5.9) can be rewritten in the following form:

$$\sigma = D\gamma - C \tag{5.10}$$

where:

$$D = \frac{h \cos(\alpha) \sin(\delta - \alpha)}{2 \sin(\delta)} \tag{5.10i}$$

$$C = \frac{p \sin(\alpha)}{h} \tag{5.10ii}$$

By assuming that γ is normally distributed, then σ is normally distributed with mean and variance given by:

$$\text{Mean}(\sigma) = D\left[\text{Mean}(\gamma)\right] - C \tag{5.11}$$

$$\text{Var}(\sigma) = D^2\left[\text{Var}(\gamma)\right] \quad . \tag{5.12}$$

The cumulative distribution function of the random variable U is expressed as:

$$F_U(u) = P(U \leq u) = P\left[\frac{\tau D}{\sigma+C} \leq u\right]$$

$$F_U(u) = P\left[\tau \leq \frac{u(\sigma+C)}{D}\right] \quad , \text{ for } \sigma + C > 0,\ D > 0 \tag{5.13}$$

Equation (5.13) can be expressed in the following integral form:

$$F_U(u) = \int_0^{\infty} \int_0^{u(x+C)/D} f_{\sigma,\tau}(x,y)\, dy\, dx$$

$$F_U(u) = \int_0^{\infty} f_{\sigma}(x) \left[\int_0^{u(x+C)/D} f_{\tau|\sigma=x}(y)\, dy\right] dx \tag{5.14}$$

The p.d.f. of U is determined by differentiating the cumulative distribution (given by equation (5.14)) with respect to u. This differentiation leads to the following result:

$$f_U(u) = \int_0^{\infty} f_{\sigma}(x) \left[\frac{x+C}{D}\right] f_{\tau|\sigma=x}\left[\frac{u(x+C)}{D}\right] dx \tag{5.15}$$

The p.d.f. of variable V is determined by incorporating a simple variable change. If v is set equal to tan(r), then r = arctan(v). After the change in variable is made and the Jacobian included, equation (5.5) is modified as follows:

$$f_V(v) = f_R(r) = f_R(\arctan(v)) \left| \frac{\partial r}{\partial v} \right|$$

$$= f_R(\arctan(v)) \left(\frac{1}{1 + v^2} \right)$$

$$f_V(v) = \begin{cases} \dfrac{e^{(-\arctan(v)/\mu_R)}}{\mu_R(1 + v^2)} & , \text{ for } v \geq 0 \\ 0 & , \text{ for } v < 0 \end{cases} \qquad (5.16)$$

In summary, the probability density functions of random variables U and V are respectively described by equations (5.15) and (5.16) for the general case. Much simplification results when the rock density γ is treated as a constant. If γ is assumed constant then it is included in the constant A as part of the denominator (equation (5.7)). Consequently, the random variable U has the same distribution as that of τ, and its gamma p.d.f. is given by equation (5.4). The p.d.f. of V does not change and is the same as that given for the general case (equation (5.16)).

5.2.3 Discrete Fourier Analysis

The safety factor as expressed in equation (5.6) has a p.d.f. equal to the reverse Fourier transform of the product of the Fourier transforms (characteristic functions) of AU and BV. This relationship can be presented in the following notation:

$$f_S(s) = F^{-}\left[F^{+}\left[f_{AU}(Au) \right] \cdot F^{+}\left[f_{BV}(Bv) \right] \right] \qquad (5.17)$$

The FFT algorithm can be used to solve for a discretized version of the safety factor p.d.f. according to equation (5.17). The p.d.f.'s of AU and BV are digitized at N increments of width Δx and then transformed by FFT to produce two sets of complex Fourier coefficients that have the same Δf increments ($\Delta f = 1/N\,\Delta x$). At each frequency determined by Δf, the complex coefficients are multiplied together to produce a new set of coefficients, which is then reversed transformed to produce a real-valued, discretized approximation of the safety factor p.d.f. This p.d.f. must be shifted to the right by an amount equal to the minimum value of AU as defined at the extreme left tail of the p.d.f. of AU.

For the typical case where rock density is treated as a constant, the safety factor is expected to be approximately gamma distributed, especially when the mean waviness of the sliding surface is small (less than 10 degrees). For small values of the waviness, the value of v is approximately equal to r, making the distribution of BV approximately exponential (refer to equation (5.16)). In addition, the shear strength

τ is assumed to be gamma distributed. Thus, the safety factor should be approximately gamma distributed as shown by the example in Figure 5.2. This result has been confirmed by Fourier analyses of plane shear stability for various slope geometries, sliding surfaces, and rock types.

There are aliasing effects in the Fourier analysis due to the transformation of the BV p.d.f., which is approximately exponential. However, the effects are negligible when the input p.d.f.'s are properly digitized and when the number of digitization increments is at least 2048 for the base-2 FFT (Miller, 1982b).

5.3 Analysis of the Step Path Failure Mode

The availability of a single surface of sliding such as that required for plane shear failure is comparatively rare in slopes cut in discontinuous rock. Any single fracture usually lacks the required continuous length for failure, whereas a more complex failure path comprised of multiple fractures is much more likely to provide the continuous path needed for sliding. From a two-dimensional standpoint, according to Jaeger (1971) the most likely situation in practice is that two conjugate fracture sets form a stepped geometry. Both sets strike parallel or nearly parallel to the strike of the slope, and sliding occurs on the flatter dipping set. Figure 5.3 illustrates typical step path geometries in a fractured rock slope.

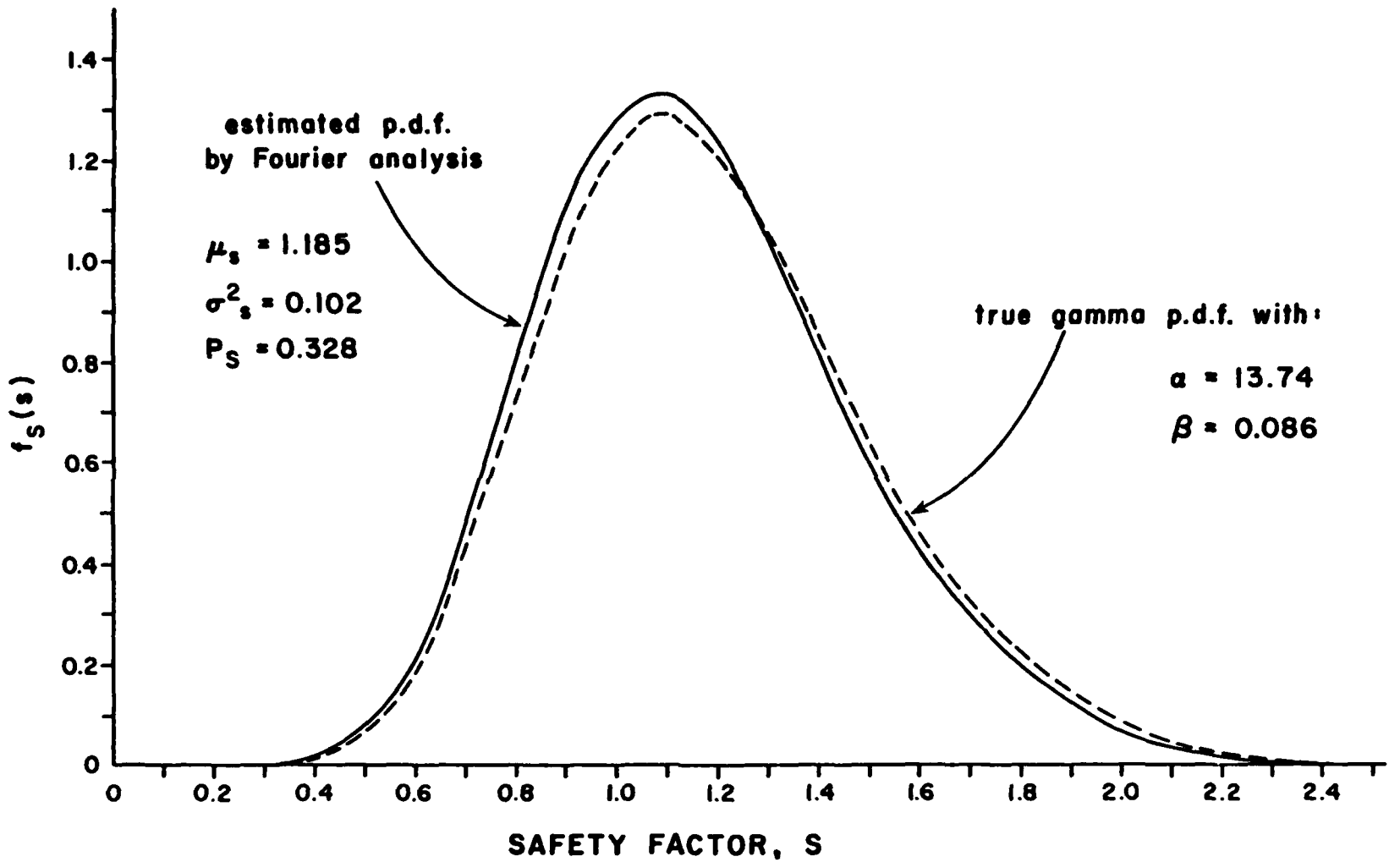

Figure 5.2. Example Comparison of a True Gamma P.D.F. with a Plane Shear Safety Factor P.D.F. Estimated by Fourier Analysis (h = 15 m, α = 35°, δ = 65°, dry slope)

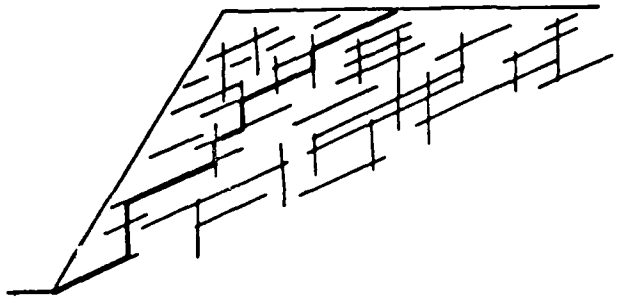

A. Continuous Step Path

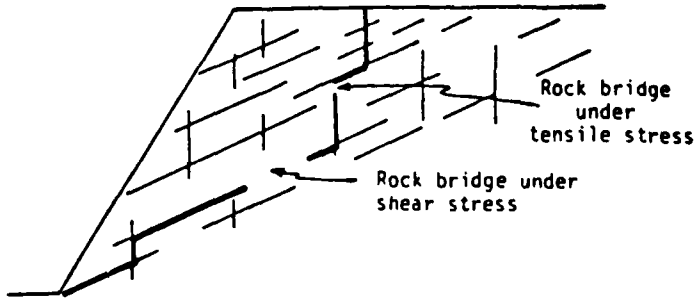

B. Discontinuous Step Path with Intact Rock Bridges

Figure 5.3. Examples of Step Path Geometries in a Rock Slope (from Call and Nicholas, 1978).

5.3.1 Prediction of Step Path Geometry

A probabilistic analysis for predicting the minimum-resistance step path failure geometry has been presented by Call and Nicholas (1978). They consider the master joint set to be gently dipping (usually 20 to 50 degrees) and the cross joint set to be steeply dipping (usually 50 to 90 degrees). The path with least resistance is assumed to be the one with continuously intersecting master joints and cross joints (Figure 5.3A). Intact rock bridges may occur if fracture lengths are short in comparison to fracture spacings (Figure 5.3B). Additional assumptions made for the minimum-resistance step path model are also given by the authors.

Computational procedures for predicting the step path geometry are outlined by the same authors. However, their simulations of fracture set characteristics are based on Monte Carlo techniques which do not take into account the spatial correlations of the characteristics. To incorporate the spatial correlations, a FORTRAN computer code obtained from the authors has been modified to include the fracture simulation procedures given in Chapter 4. Consequently, more realistic predictions of the step path geometry can now be obtained.

5.3.2 Safety Factor Equation

For the typical step path geometry shown in Figure 5.4, a two-dimensional stability analysis can be developed that includes the effects of waviness of the master joints and the effects of intact tensile

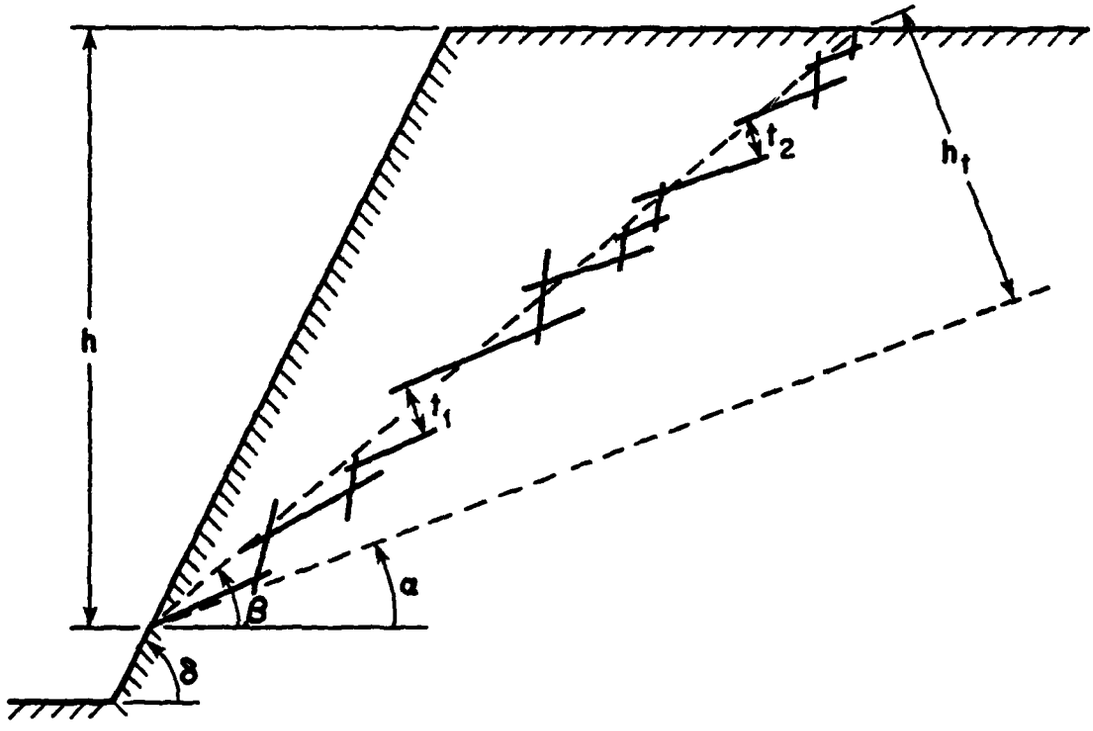

h = step path height

β = step path angle

α = average dip of master joints used in the path

t_1, t_2 = length of tensile rock bridges

Fraction of Tensile Intact Rock = $(t_1 + t_2)/h_t$

Figure 5.4. Descriptive Parameters for a Discontinuous Step Path with Tensile Rock Bridges

rock bridges. The probabilistic analysis is fundamentally based on the deterministic work of Jaeger (1971) except that it is more general and allows for the incorporation of statistical variability and uncertainty.

The safety factor, a random variable denoted by S, is the ratio of resisting force to sliding force and can be expressed in the following algebraic form:

$$S = \frac{\tau L + W \cos(\alpha_m) \tan(R) + T_s L}{W \sin(\alpha_m)} \tag{5.18}$$

$$S = \frac{L}{W \sin(\alpha_m)} (\tau) + \cot(\alpha_m) \tan(R) + \frac{L}{W \sin(\alpha_m)} (T_s) \tag{5.19}$$

where: L = length of sliding,

$$L = \frac{h \sin(\alpha_c - \beta)}{\sin(\beta) \sin(\alpha_c - \alpha_m)} \tag{5.20}$$

W = weight of potential failure mass,

$$W = \frac{\gamma h^2 \sin(\delta - \beta)}{2 \sin(\delta) \sin(\beta)} \tag{5.21}$$

h = height of step path,

δ = average dip of slope face,

α_m = average dip of master joint set,

α_c = average dip of cross joint set,

γ = mean rock density,

τ = estimated shear strength of master joint set,

R = estimated waviness of master joint set,

T_s = estimated tensile strength of rock bridges

= (Fraction of Intact Rock) (h_t) $(T_o)/L$

= $T(h_t)/L$,

h_t = perpendicular height of step path (refer to Figure 6.2),

T_o = estimated tensile strength of rock substance,

T = (Fraction of Intact Rock)$\cdot(T_o)$

$$T_s = \frac{T \sin(\beta - \alpha_m) \sin(\alpha_c - \alpha_m)}{\sin(\alpha_c - \beta)} \tag{5.22}$$

Using equations (5.20), (5.21), and (5.22), the safety factor equation can be rewritten as follows:

$$S = A\tau + B \tan(r) + GT \tag{5.23}$$

where: $$A = \frac{2 \sin(\delta) \sin(\alpha_c - \beta)}{\gamma h \sin(\alpha_m) \sin(\alpha_c - \alpha_m) \sin(\delta - \beta)} \tag{5.23i}$$

$$B = \cot(\alpha_m) \tag{5.23ii}$$

$$G = \frac{2 \sin(\delta) \sin(\beta - \alpha_m)}{\gamma h \sin(\alpha_m) \sin(\delta - \beta)} \tag{5.23iii}$$

For the analysis of a specified slope geometry and step path, the random variables are the shear strength (τ), the waviness (R), and the

tensile strength available to the intact rock bridges (T). Because of the various assumptions and uncertainties in the step path analysis, the variability of the rock density has only a negligible affect on the outcome, especially when its coefficient of variation is small (refer to section 5.2.1). Therefore, the mean of the rock density is used, and it is assumed to be constant.

5.3.3 Characterization of Random Variables

Equation (5.23) provides the basis for estimating the safety factor p.d.f. by Fourier analysis procedures. For convenience of notation the equation can be rewritten in the following form:

$$S = AU + BV + GT, \tag{5.24}$$

where A, B, and G are constants as defined above, and U, V, and T are random variables. The variable U equals the shear strength τ, and its p.d.f. is given by equation (5.4). When water pressures affect the stability of the step path geometry, the effective normal stress as defined by equation (5.10) must be used to determine the p.d.f. of the shear strength. The random variable V equals the tangent of the waviness angle R, and its p.d.f is defined by equation (5.16).

As stated in section 5.3.2, the random variable T equals the fraction of tensile intact rock times the estimated tensile strength of the rock substance (T_o). The statistical distribution of T_o is determined by rock tensile tests in the laboratory (usually Brazilian disk tension tests). To have units consistent with those elsewhere in the analysis,

the test results are expressed in metric tons per square meter (t/m^2). Tensile strength test data are typically normally distributed, so the random variable T is assumed to be normally distributed as indicated below:

$$f_T(t) = \frac{e^{-\frac{1}{2}((x - \mu_T)/\sigma_T)^2}}{\sqrt{2\pi}\ \sigma_T} \quad , \text{ for } -\infty < t < \infty \qquad (5.25)$$

where: μ_T = mean of T

= (Fraction Intact Rock) μ_{T_o}

σ_T^2 = variance of T

= (Fraction Intact Rock)^2 $\sigma_{T_o}^2$.

5.3.4 Discrete Fourier Analysis

The safety factor as expressed in equation (5.24) has a p.d.f. equal to the reverse Fourier transform of the product of the Fourier transforms (characteristic functions) of the p.d.f.'s of AU, BV, and GT. This relationship can be presented in the following notation:

$$f_S(s) = F^- \left[F^+ \left[f_{AU}(Au) \right] \cdot F^+ \left[f_{BV}(Bv) \right] \cdot F^+ \left[f_{GT}(Gt) \right] \right] \qquad (5.26)$$

Procedures for estimating the probability of step path sliding by discrete Fourier analysis are similar to those given for the plane shear failure mode (refer to section 5.2.3). The major difference is that

three sets of complex Fourier coefficients must be multiplied together according to equation (5.26). Also, the safety factor p.d.f. is shifted to the right by an amount equal to the sum of the minimum value of AU and the minimum value of GT as defined at the extreme left tails of their respective probability densities.

Typically the safety factor is approximately gamma distributed, because it represents the combination of a gamma variable, a nearly exponential variable, and a normal variable. Figure 5.5 shows an example comparison of an estimated safety factor p.d.f. with the true gamma p.d.f. predicted by the mean and variance of the safety factor.

Aliasing effects are noticeable (but negligible) in the Fourier analysis of step path stability, mainly due to the exponential character of BV (refer to section 5.2.3). Discrete Fourier transforms of the p.d.f.'s of AU and GT cause little or no aliasing because of their gamma and normal distributional forms.

5.4 Analysis of Tetrahedral Wedge Failure Modes

Stability evaluations of plane shear and step path failure modes consist of two-dimensional analyses in which the geologic structures of sliding are assumed to strike parallel or nearly parallel to the slope face. When two structures upon which sliding can occur strike across the slope crest, then a tetrahedral wedge can be formed where sliding occurs along the line of intersection of the two structures. Three-dimensional vectorial methods have been developed to analyze the stability of simple, rigid-block wedges (Wittke, 1965; Goodman and

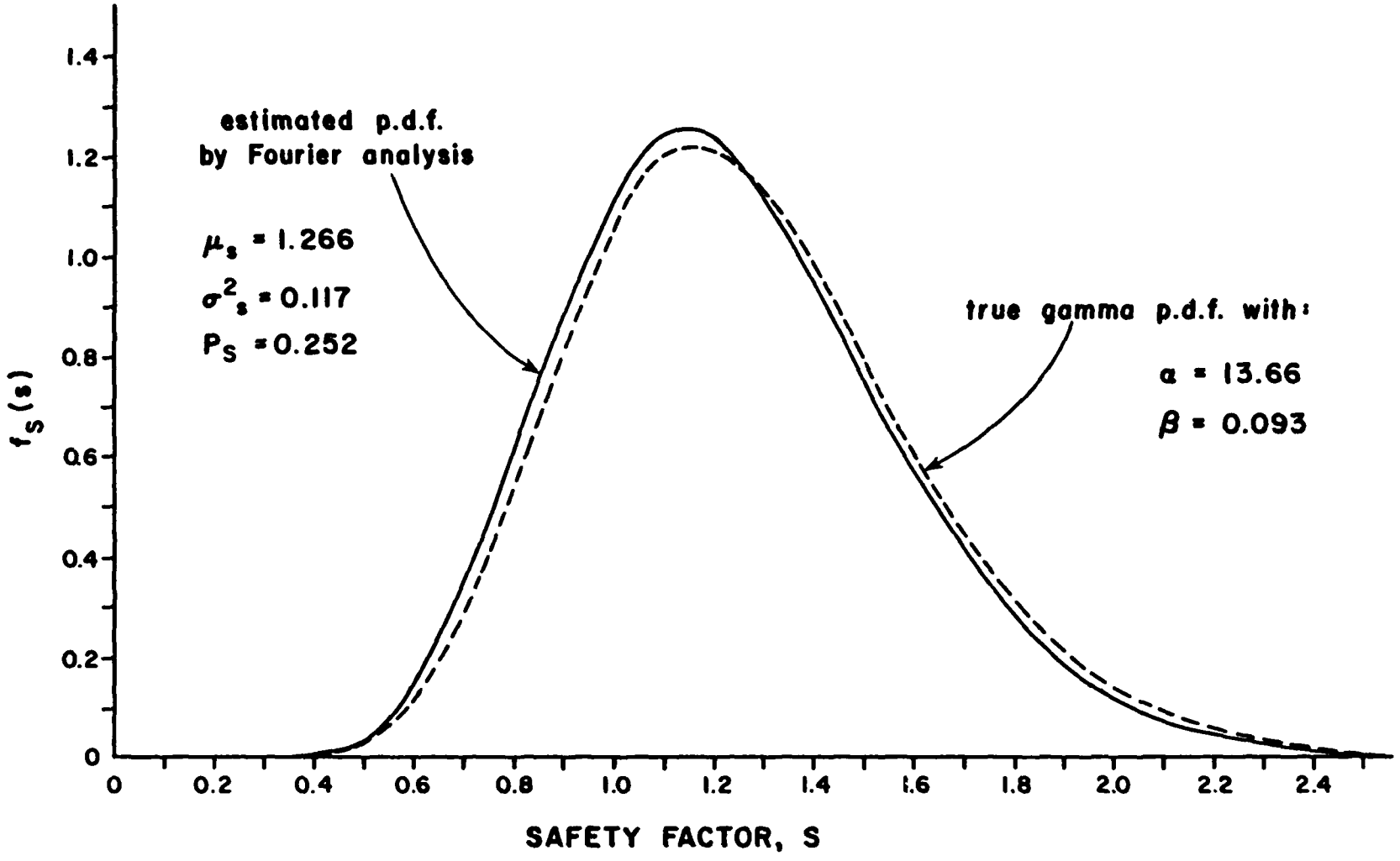

Figure 5.5. Example Comparison of a True Gamma P.D.F. with a Step Path Safety Factor P.D.F. Estimated by Fourier Analysis (h = 15 m, α_m = 34°, α_c = 82°, β = 42°, F.I.R. = .02, dry slope)

Taylor, 1967). Vectorial methods are preferred over stereographic-projection analyses (John, 1968; Londe and others, 1970; Goodman, 1976) for computer programming and calculation efficiency and, thus, have been used in developing a Fourier analysis for estimating the probability of wedge sliding.

A typical three-dimensional wedge failure geometry is illustrated in Figure 5.6. In order for a wedge to slide, it must first be kinematically viable. That is, the geometry must be such that movement can occur. To satisfy such a criterion the line of intersection must be inclined in the same general direction as the dip direction of the slope face and it must be daylighted by the slope. For some geometries sliding may occur on only one plane rather than on both planes along the line intersection, and the stability analysis becomes similar to that of a plane shear geometry (Goodman, 1976, p. 248). A simple, rigid-block stability analysis of kinematically viable wedges is amenable to probabilistic and Fourier techniques.

A Fourier analysis similar to that described for the plane shear failure mode can be used to estimate the p.d.f. of the safety factor for tetrahedral wedge failure modes. The probabilistic analysis relies on vector algebra to determine the geometry and kinematic viability of a given wedge and to calculate its volume and associated loads. Waviness angles of the two intersecting structures are not considered in the simple, rigid-block analysis. Fourier procedures are applicable to estimating the probability of sliding provided that the safety factor can be expressed as the sum of independent random variables.

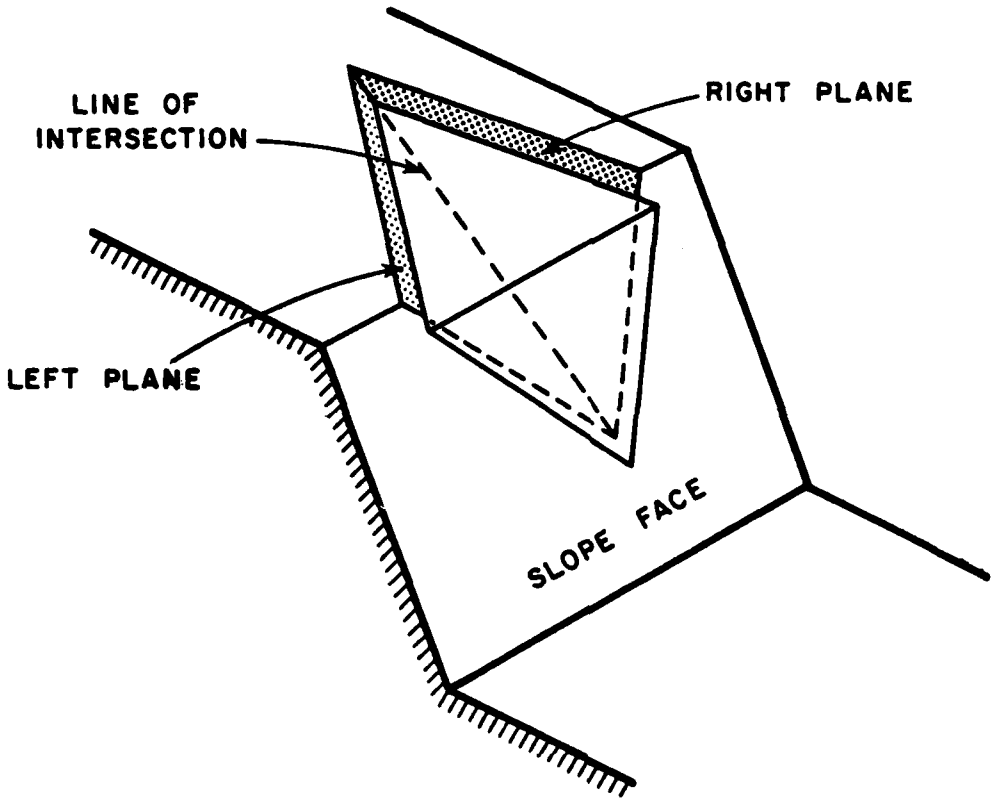

Figure 5.6. Typical Tetrahedral Wedge Failure Mode in a Rock Slope

5.4.1 Safety Factor Equation

For the typical three-dimensional wedge geometry shown in Figure 5.6, the probability of sliding can be estimated by determining the p.d.f. of the safety factor. As a random variable denoted by S, the safety factor equals the resisting force divided by the driving force and can be expressed in the following algebraic form:

$$S = \frac{A_L \tau_L + A_R \tau_R}{D_F}$$

$$S = \left(\frac{A_L}{D_F}\right) \tau_L + \left(\frac{A_R}{D_F}\right) \tau_R \qquad (5.27)$$

where: A_L = contact area of the left plane,

A_R = contact area of the right plane,

D_F = driving force of the wedge,

τ_L = estimated shear strength of the left plane,

τ_R = estimated shear strength of the right plane.

In the analysis of a specified slope geometry and wedge, the random variables are the two shear strengths, τ_L and τ_R. The areas of the two sides of the wedge are determined by the orientations of the structures, the slope geometry, and the wedge height. The driving force is a function of the weight of the wedge (which depends on the volume and the rock density) and the orientations of the structures (which determine the plunge of the intersection). The rock density is assumed to be constant for the same reasons as those given for the step path analysis (refer to section 5.3.2).

5.4.2 Characterization of Random Variables

Equation (5.27) provides the basis for estimating the safety factor p.d.f. by Fourier analysis procedures. For convenience of notation the equation can be rewritten in the following form:

$$S = AU + BV \tag{5.28}$$

where: $A = A_L/D_F$, (5.28i)

$B = A_R/D_F$, (5.28ii)

$U = \tau_R$,

$V = \tau_L$.

Both of the random variables U and V are equal to shear strengths and, therefore, have gamma probability density functions defined by equation (5.4).

For the special case of a symmetrical wedge with equal normal stresses on the left and right planes, then U and V are equal, provided that their shear strength regression models are identical. Consequently, the safety factor can be expressed as:

$$S = (A + B)U \quad , \tag{5.29}$$

and its p.d.f. is determined directly by multiplying U times the sum of the constants A and B. Thus, Fourier procedures are not needed for this special case of a symmetrical wedge, because the safety factor has a gamma p.d.f. derived directly from the p.d.f. of the shear strength. Unfortunately, this situation occurs only rarely in the field, and discrete Fourier procedures are still required for a general analysis of wedge stability.

5.4.3 Discrete Fourier Analysis

The safety factor as expressed in equation (5.28) has a p.d.f.

equal to the reverse Fourier transform of the product of the Fourier transforms (characteristic functions) of the p.d.f.'s of AU and BV. This relationship can be expressed in the following notation:

$$f_S(s) = F^- \left[F^+ \left[f_{AU}(Au) \right] \cdot F^+ \left[f_{BV}(Bv) \right] \right] \qquad (5.30)$$

which is the same as that given in equation (5.17) except for the random variable BV.

Even though the safety factor is the linear combination of two independent gamma distributed random variables, it is not necessarily gamma distributed. The sum of independent gamma variables is gamma distributed only when their β parameters are the same (Fisz, 1963, p. 151-154). However, the safety factor in a wedge analysis is expected to be approximately gamma distributed (as shown by the example in Figure 5.7) and may be approximately normal if the shear strength distributions have small coefficients of variation.

Procedures for estimating the probability of wedge sliding by discrete Fourier analysis are the same as those given for the plane shear failure mode (refer to section 5.2.3). The only exceptions are that BV is gamma distributed for the wedge analysis and the shift of the safety factor to the right corresponds to the sum of the minimum values of AU and BV.

It is not necessary to FFT a gamma p.d.f. to determine its characteristic function, because the function is explicitly defined as follows (Fisz, 1963, p. 151):

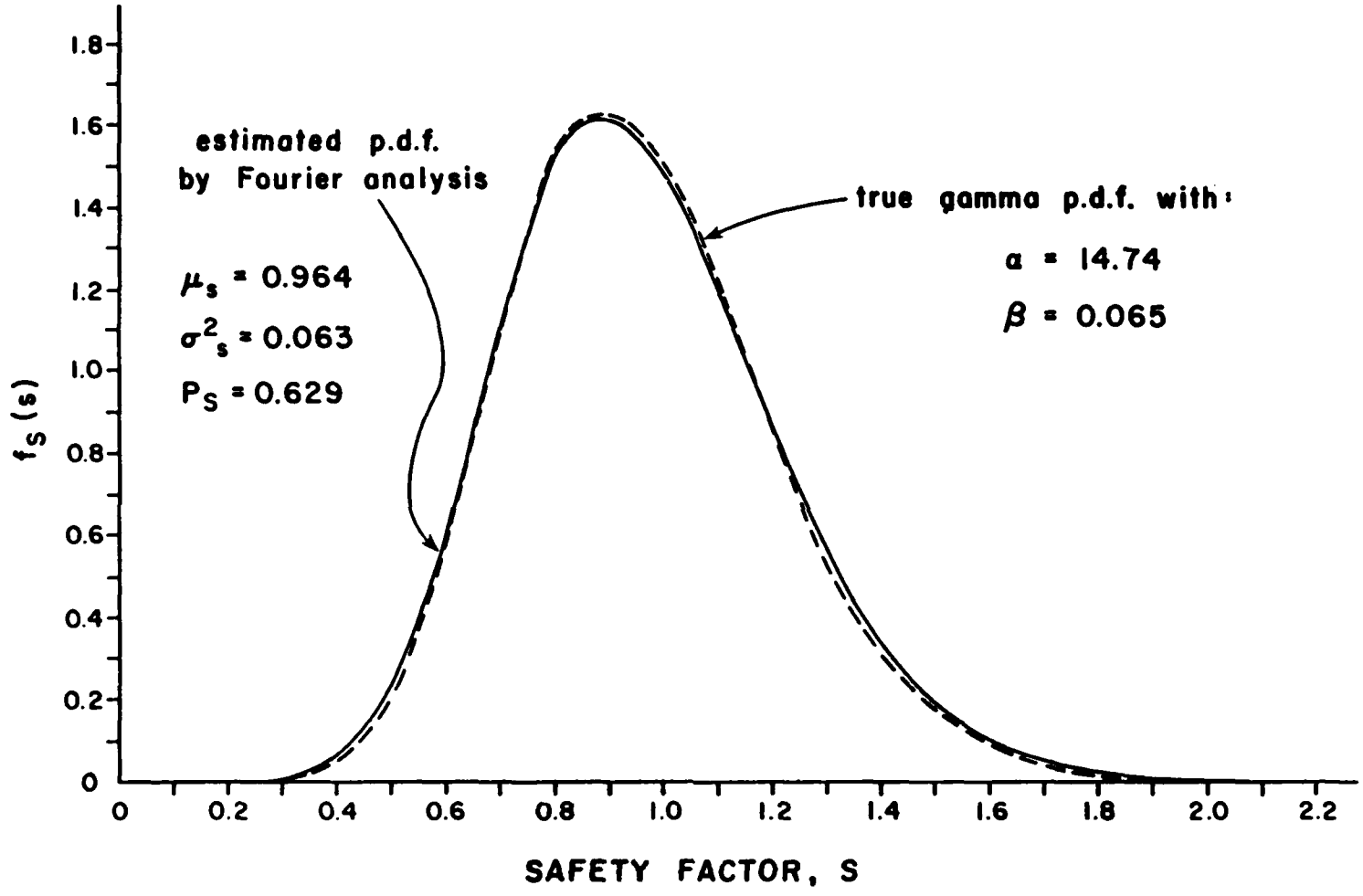

Figure 5.7. Example Comparison of a True Gamma P.D.F. with a Wedge Safety Factor P.D.F. Estimated by Fourier Analysis (h = 15 m, δ = 65°, int. plunge = 46.2°)

$$\phi(2\pi f) = \frac{1}{(1 - i2\pi f\beta)^{\alpha}} \qquad (5.31)$$

where: $\phi(2\pi f)$ = complex value of the characteristic function at frequency $2\pi f$,

α, β = parameters of the gamma p.d.f.

Consequently, the two sets of complex Fourier coefficients that are multiplied in frequency domain can be obtained directly by using equation (5.31) with frequency values defined by $\Delta f = 1/N\,\Delta x$. However, Fourier transformations of the two gamma p.d.f.'s cause no aliasing even when N is as small as 512, so the FFT method is still highly efficient and accurate, and may be preferred over the direct characteristic function method.

5.5 Summary

A Fourier analysis method can be used to estimate the probability of sliding for any failure mode that has a safety factor expressed as the sum of independent random variables. This method is based on the convolution principle whereby the sum of independent probability density functions in space domain is analogous to the product of the Fourier transforms of the functions in frequency domain.

Therefore, by expressing the safety factor as a sum of independent variables, its true p.d.f. is estimated by discrete Fourier procedures that take advantage of the computational speed of the fast Fourier transform (FFT) algorithm. This estimate is an improvement over a simulated realization of the p.d.f. produced by Monte Carlo techniques

that are often prone to excessive amounts of computer time and computational instability.

If the shear strength is assumed to be gamma distributed, and the waviness is assumed to be exponentially distributed, then the calculated safety factor distribution is approximated by a gamma p.d.f. This result has been confirmed for plane shears, step paths, and tetrahedral wedges in various rock types and for various slope geometries. The probability of sliding, which is needed for probabilistic slope stability analyses, is equal to the area under the estimated safety factor p.d.f. where values of the safety factor are less than one.

CHAPTER 6

PROBABILISTIC ANALYSIS OF BENCH STABILITY

6.1 Introduction

As indicated in section 1.2 most of the fractures mapped in a study area lack sufficient length to individually cause a failure in slopes higher than one or two benches. Due to mining operational constraints or equipment capabilities, bench heights typically range from 12 to 20 meters. When longer, more continuous structures are observed they should be treated individually in the slope stability analysis.

A probabilistic analysis of bench stability should include the variabilities in fracture set properties and the occurrences of multiple failure modes. To be of value in the engineering design, output from the analysis would include the probabilities of retaining various bench widths after failures occur. Except for step paths, failures are much more likely to occur near the crest, because the fracture lengths required for failure are shorter and, thus, have higher probabilities of occurrence near the crest.

6.2 Bench Stability Analysis

A hybrid analysis of bench stability has been developed that

is a combination of probability theory and simulation. It uses the fracture simulation techniques of Chapter 4 to generate potential failure modes in the bench and then applies probability calculations to predict bench stability. The probabilities of stability for back-failure cells on top of the bench are determined, and a graph is then constructed to illustrate the relationships between bench face angles and the probabilities of retaining various bench widths.

6.2.1 Plane Shear Contribution

A typical plane shear fracture set in a bench is illustrated in Figure 6.1. Back-failure distance is defined as the horizontal distance from the original bench crest back to the point where a given plane shear structure intersects the top of the bench.

Stability of a potential plane shear failure mass is realized in one of two ways:

1. the plane shear structure is not long enough,
2. the plane shear structure is long enough, but sliding does not occur.

Therefore, the probability of stability can be expressed as follows:

P(stability) = P(fracture not long enough) + P(fracture long enough and no sliding occurs)

$$P_{stab.} = (1 - P_L) + P_L(1 - P_S) \qquad (6.1)$$

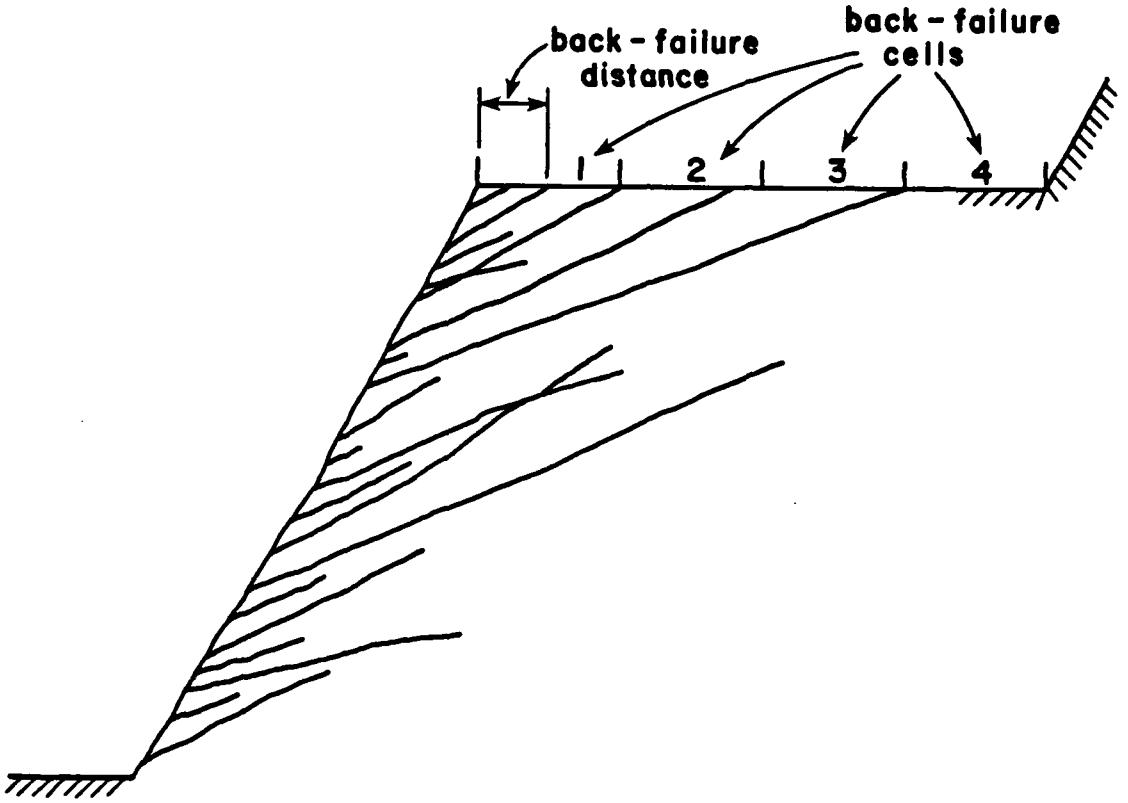

Figure 6.1. Multiple Plane Shear Failure Modes and Associated Back-Failure Cells in a Bench

where: P_L = probability that fracture is long enough,

P_S = probability of sliding along the fracture.

The probability that the fracture length is equal to or greater than the required length for failure is given by:

$$P_L = e^{-L_r/\mu_L} \tag{6.2}$$

where: P_L = probability that the fracture is the required length or longer,

L_r = required length for failure,

μ_L = mean fracture length in the plane shear fracture set.

By simulating realizations of benches that contain the plane shear fracture set, the probability of stability for any given back-failure cell (shown in Figure 6.1) can be determined.

Let: s_i = i-th bench simulation,

N_T = total number of bench simulations,

N = number of bench simulations that have one or more fractures in the given back-failure cell,

J_i = number of fractures in the given back-failure cell for the i-th bench simulation.

Then, the probability of stability in a given cell is given by:

$$P(\text{stab. in cell}) = \sum_{i=1}^{N_T} P(\text{stab.} \mid s_i \text{ with } J_i \text{ fractures in cell}) \cdot P(s_i \text{ with } J_i \text{ fractures in cell})$$

$$P(\text{stab. in cell}) = \sum_{i=1}^{N_T} \Big(P(\text{stab.} \mid s_i \text{ with no fractures in cell}) \cdot P(s_i \text{ with no fractures in cell}) + P(\text{stab.} \mid s_i \text{ with one or more fractures in cell}) \cdot P(s_i \text{ with one or more fractures in cell}) \Big)$$

$$P(\text{stab. in cell}) = 1.0 \left(\frac{N_T - N}{N_T} \right) + \frac{N}{N_T} \left(\frac{1}{N} \right) \sum_{i=1}^{N} P(\text{stab.} \mid s_i \text{ with one or more fractures in cell}) \tag{6.3}$$

$$P(\text{stab. in cell}) = \frac{N_T - N}{N_T} + \frac{1}{N_T} \sum_{i=1}^{N} \left\{ \prod_{i=1}^{J_i} \Big(P(\text{stab. of fracture } j \mid s_i) \Big) \right\} \tag{6.4}$$

$$P(\text{stab. in cell}) = \frac{N_T - N}{N_T} + \frac{1}{N_T} \sum_{i=1}^{N} \left\{ \prod_{j=1}^{J_i} \Big((1 - P_{L_j}) \mid s_i + P_{L_j} (1 - P_{S_j}) \mid s_i \Big) \right\} \tag{6.5}$$

The probability of retaining a specified bench width is the joint probability that stability occurs in each back-failure cell contained in the bench width. This relationship can be expressed in the following form:

$$P(\text{stab. of bench width with } N_c \text{ cells}) = \prod_{i=1}^{N_c} P(\text{stab. in cell}_i) \qquad (6.6)$$

The bench simulation procedure begins by generating required spatially correlated fracture set characteristics using the techniques described in Chapter 4. The characteristics are assumed to be independent of each other. That is, properties like dip direction and dip are not significantly correlated in a given fracture set (Miller, 1979, p. 28-29). Probabilities of length and sliding are computed for each daylighted fracture. Probabilities of stability are then calculated and the bench simulation repeated. After the desired number of simulations have been completed, the bench width reliabilities can be calculated. The complete process is then repeated for several different bench face angles (and different bench heights, if desired).

After analyzing benches with various face angles, a bench stability graph can be produced that displays the probabilistic results (Figure 6.2). The information shown on this graph, which is based on plane shear failure modes, can be combined with that for other possible failure modes to help select an overall slope angle in the particular design sector or to assist in mine planning.

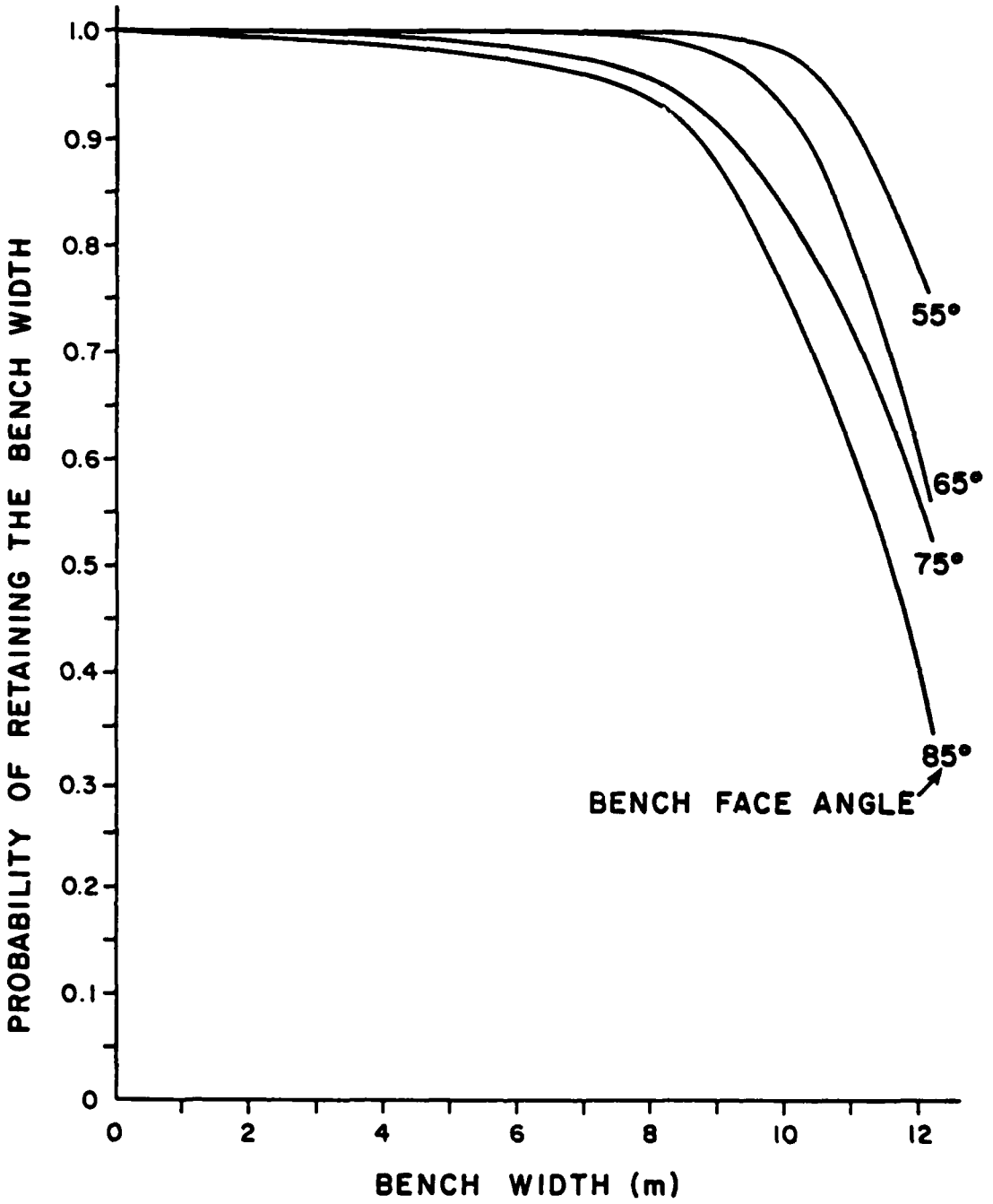

Figure 6.2. Example Bench Stability Graph for Plane Shear Failure Modes

6.2.2 Step Path Contribution

Step path failure geometries typically have lower probabilities of stability than plane shear geometries of similar scale, because step paths are assumed to have continuous lengths except for intact tensile rock bridges. Experience has shown that for benches (12 to 20 m high) cut in typical crystalline rock (tensile strength of 500 to 2,000 t/m^2) the probability of sliding is nearly zero when the fraction of intact rock exceeds approximately 0.08. Therefore, unless the intact rock exceeds approximately 8 percent, step path geometries usually are much less stable than comparable plane shear geometries.

Failures are much more likely to occur near the bench crest, because the required step path heights are shorter and, thus, the fractions of intact rock are smaller. Figure 6.3 illustrates a typical bench with multiple step path geometries.

The bench stability analysis provides the same type of output as that for plane shears. That is, the probabilities of retaining specified bench widths are computed. The probability of length for step paths is assumed to equal one because they are considered continuous. Consequently, equation (6.1) should be modified for step path failure modes to the following form:

$$P_{stab.} = 1 - P_S \tag{6.7}$$

where P_S is the probability of step path sliding. The probability of stability for a given back-failure cell is computed from equation (6.5)

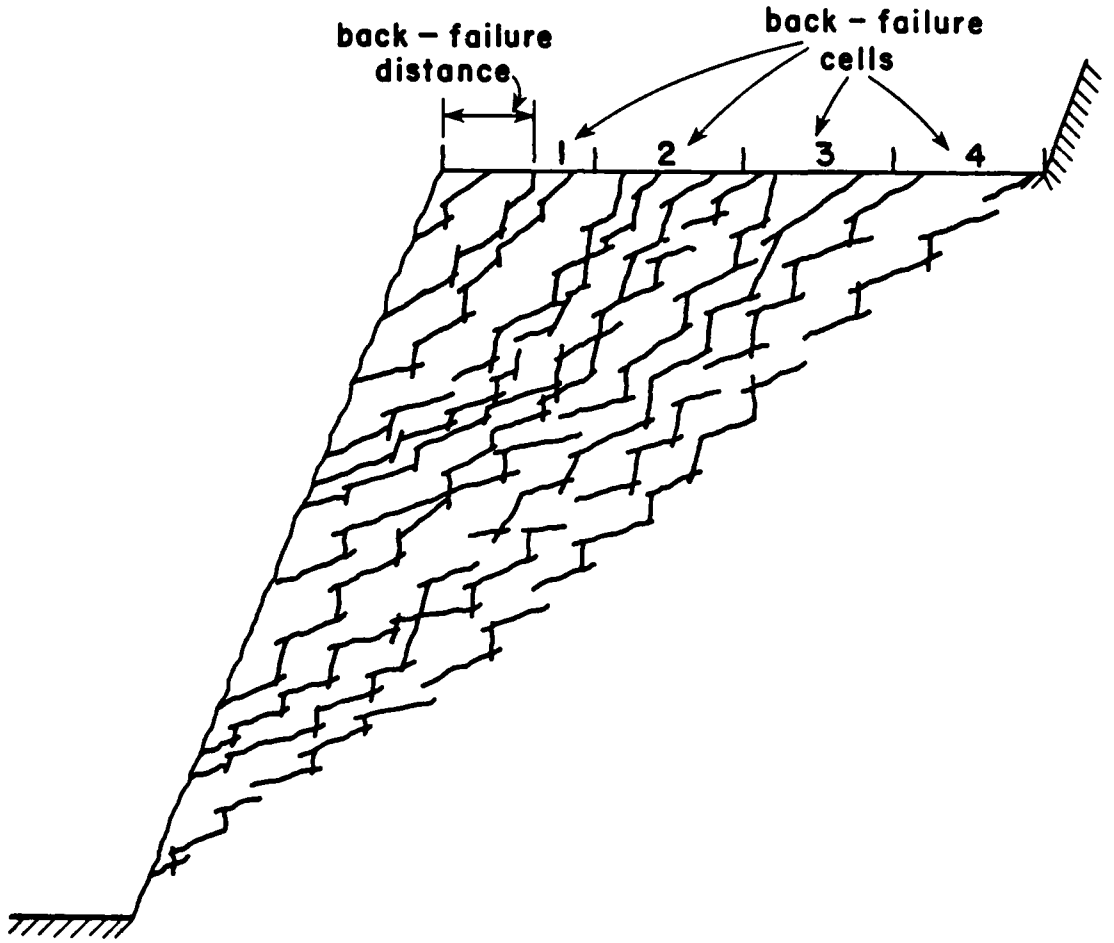

Figure 6.3. Multiple Step Path Failure Modes and Associated Back-Failure Cells in a Bench

except that the P_{L_j} term is set equal to one. The probabilities of retaining specified bench widths are then given by equation (6.6).

A step path analysis of bench stability commonly requires more simulations than a comparable plane shear analysis (which usually requires 6 to 12 bench simulations; Miller, 1982b). The final selection of N_T (the total number of bench simulations) is usually based on projected computer costs and on engineering judgment.

After analyzing benches with various face angles, a graph can be produced that displays the probabilistic results (Figure 6.4). This graphical information is then combined with that for other failure modes that occur in the particular design sector.

6.2.3 Tetrahedral Wedge Contribution

A probabilistic analysis of bench stability based on wedge failure modes should include the variabilities in properties of the two fracture sets that form multiple wedges in the bench. Wedge failures are much more likely to occur near the crest, because lengths of the fractures that form intersections long enough to allow failure are shorter and, thus, have higher probabilities of occurrence. This problem of required length for failure is more severe for wedges than for plane shears, because the probability that the intersection is long enough to allow failure is the joint probability that the two fractures are long enough. The fracture traces shown in Figure 6.1 can be viewed as wedge intersections. From this viewpoint back-failure

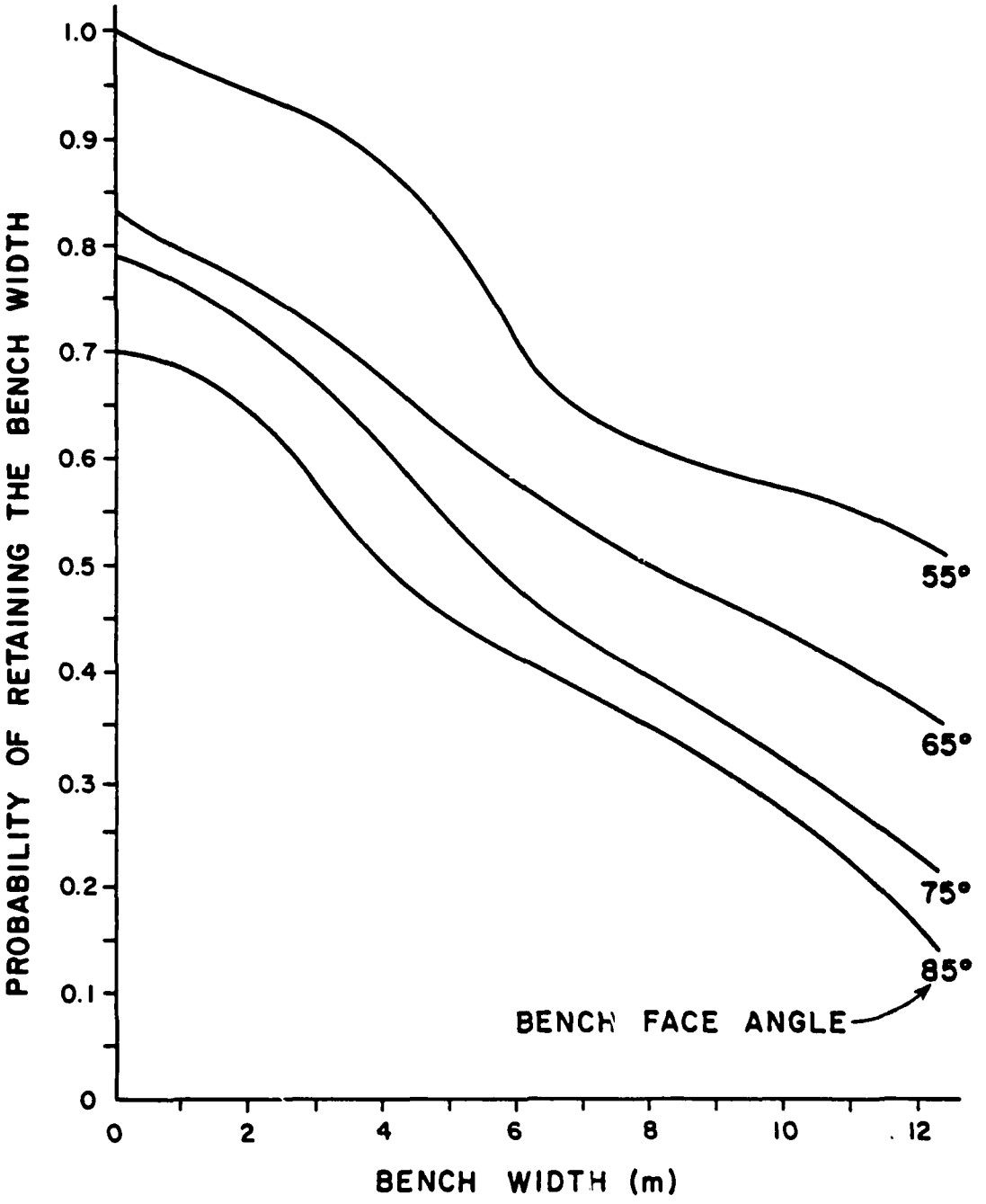

Figure 6.4. Example Bench Stability Graph for Step Path Failure Modes

distance is defined as the horizontal distance from the original bench crest back to the point where the intersection line of the wedge intersects the top of the bench.

Stability of a potential tetrahedral wedge failure mass is realized in one of two ways:

1. the wedge intersection is not long enough,
2. the wedge intersection is long enough, but sliding does not occur.

Therefore, the probability of stability for a given wedge can be expressed by equation (6.1) where P_L is the joint probability that both fractures are long enough. This joint probability is given by:

$$P_L = e^{-L_r/\mu_{Ll}} e^{-L_r/\mu_{Lr}} \tag{6.8}$$

where: P_L = probability that the wedge intersection is the required length or longer,

L_r = required length for failure,

μ_{Ll} = mean fracture length in the left fracture set,

μ_{Lr} = mean fracture length in the right fracture set.

The probability of stability for a given back-failure cell is computed from equation (6.5), and the probabilities of retaining specified bench widths are given by equation (6.6). The three-dimensional character of wedge geometries requires that a standard length along the bench face be specified to define an area for probability accumulations. An arbitrary, but rational, decision is to set this length

AD-A136 497 PROCEEDINGS SEMINAR ON PROBABILISTIC METHODS IN GEOTECHNICAL ENGINEERING. (U) ARMY ENGINEER WATERWAYS EXPERIMENT STATION VICKSBURG MS GEOTE.. 7/7

UNCLASSIFIED M E HYNES-GRIFFIN ET AL. SEP 83 F/G 8/13 NL

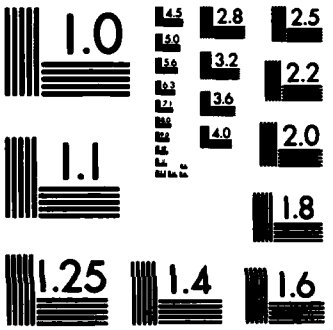

equal to the bench height, allowing for square "units" that can be analyzed along the bench face (Figure 6.5). Typically, if more than 50 to 60 viable wedges are simulated along each simulation line in the bench face, then only three or four bench simulations are needed (Miller, 1982b). A larger number of simulations is required if fewer viable wedges are present.

After analyzing benches with various face angles, a bench stability graph for wedges can be produced (Figure 6.6). This graph shows that, like plane shear instability, wedge instability is much greater near the crest compared to greater back-failure distances.

6.3 Bench Stability Graphs

The probabilistic results shown on the bench stability graphs for individual failure modes are combined to produce a final overall bench stability graph for each design sector in the open pit. The probability of retaining a specified bench width is the joint probability that the width will be retained for all failure modes present. Therefore, the probability values for the failure modes are multiplied together at given bench widths to produce a final bench stability graph. The information from Figures 6.2, 6.4, and 6.6 has been combined to produce an example of such a graph (Figure 6.7).

A comparison of Figures 6.4 and 6.7 indicates the strong influence that step path failures have an overall bench instability because of their continuous or nearly continuous lengths. The stability of plane shear and wedge failure modes is enhanced by their usually low prob-

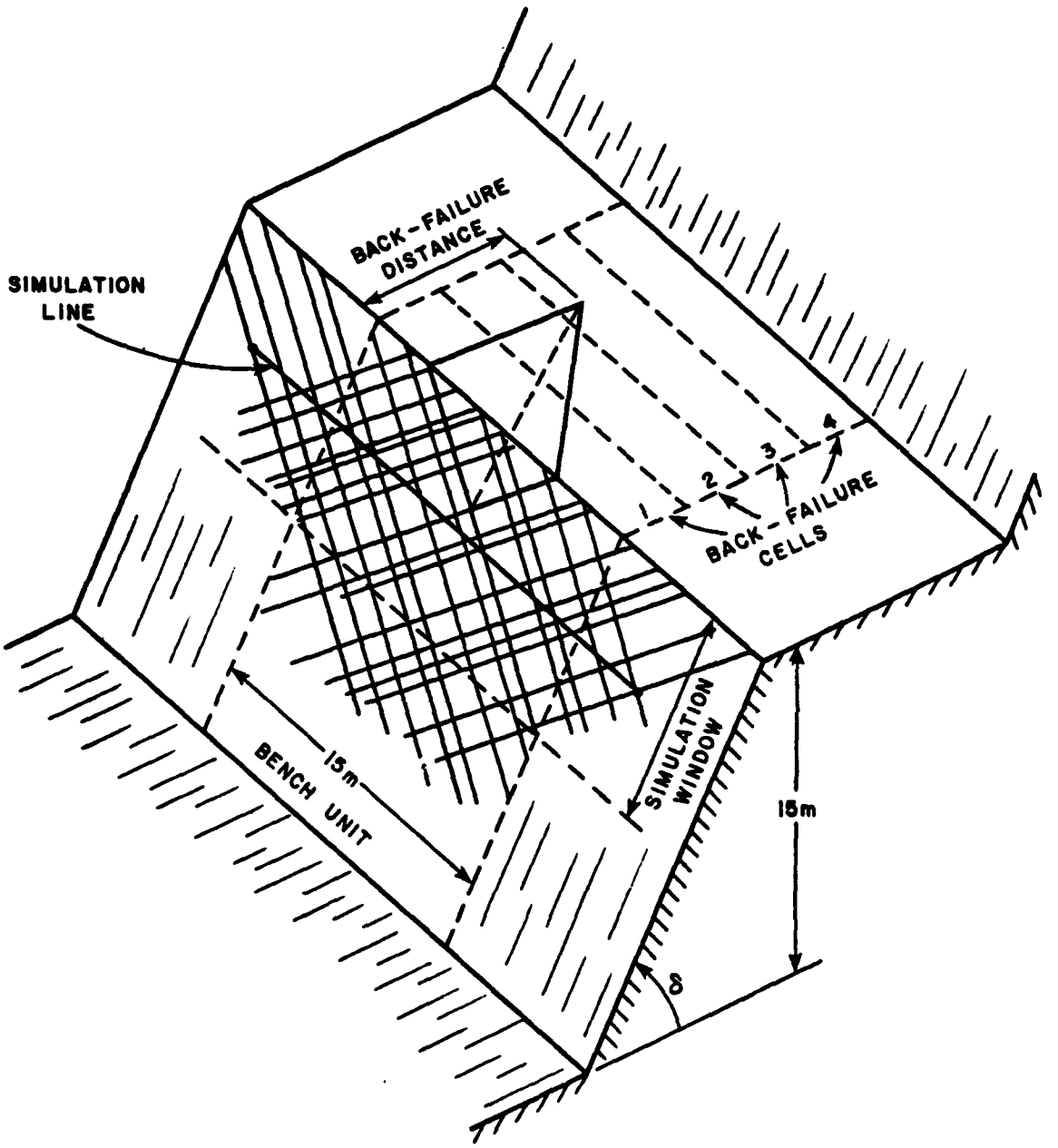

Figure 6.5. Example of Simulated Wedge Intersections and Associated Back-Failure Cells in a Bench Unit

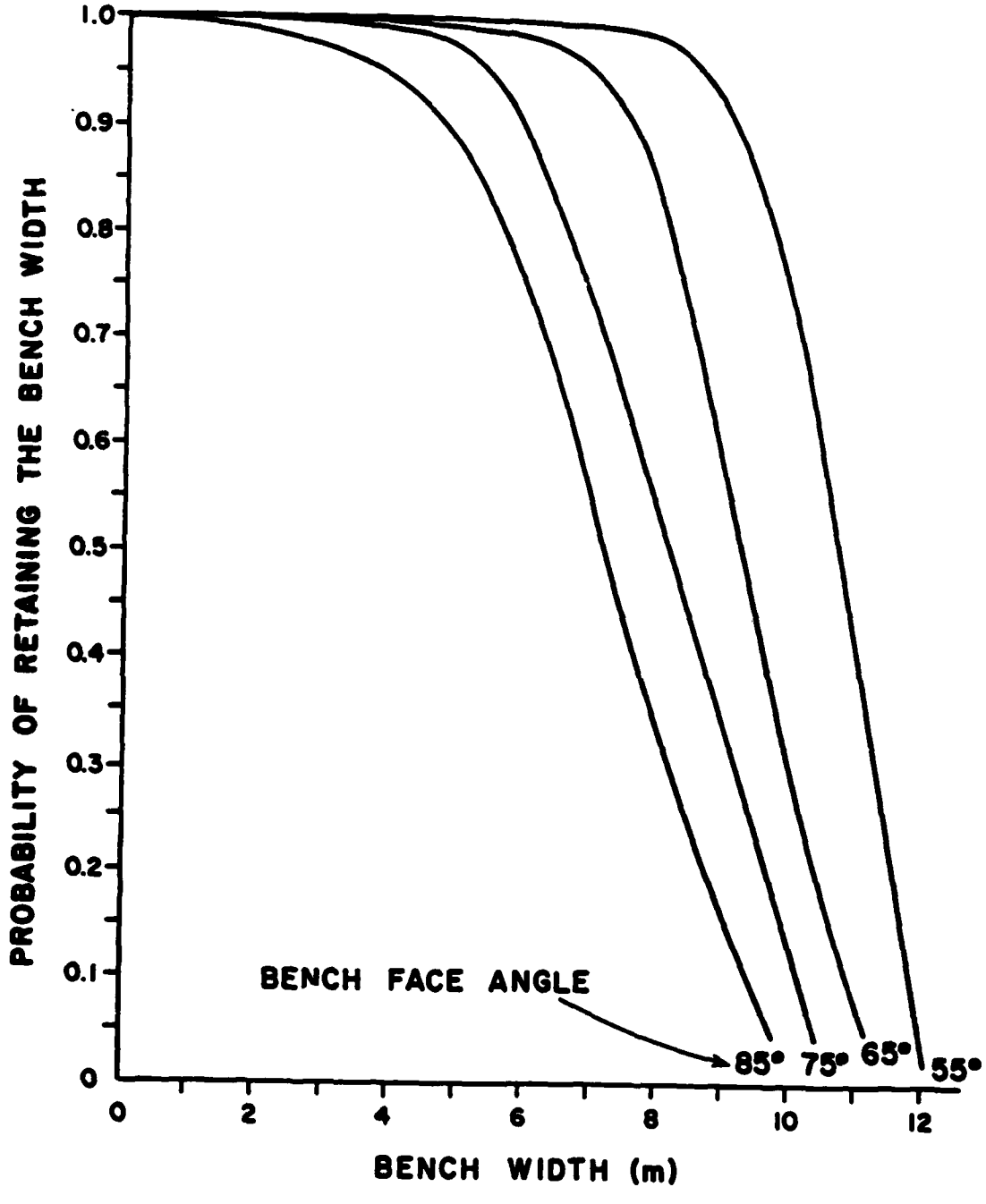

Figure 6.6. Example Bench Stability Graph for Tetrahedral Wedge Failure Modes

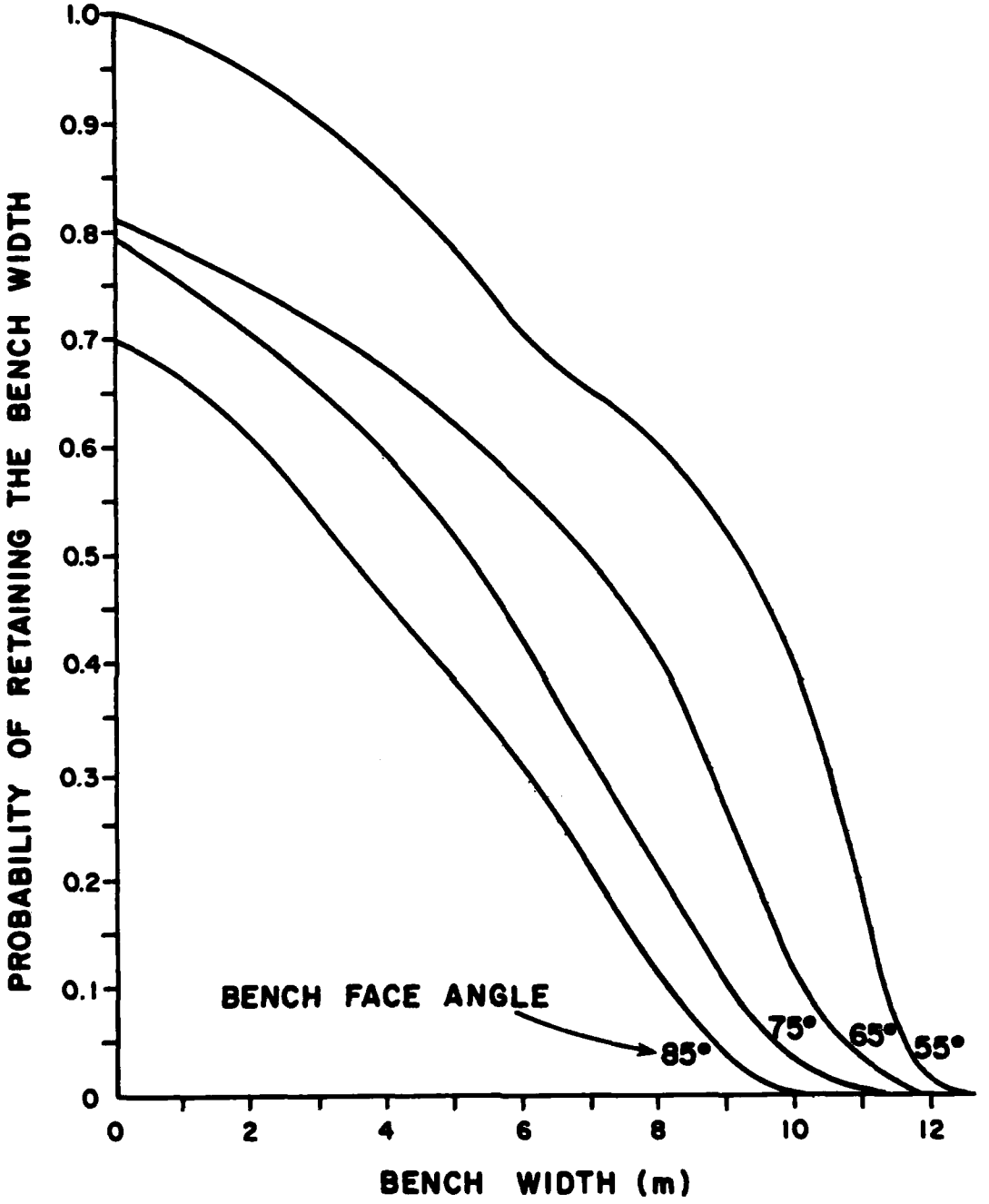

Figure 6.7. Example of Final Bench Stability Graph

abilities of having structures long enough to allow failures that break back very far from the initial bench crest. Therefore, much instability near the crest is expected, and instability farther back from the crest tends to be caused by step paths.

Physical inferences of the probability of retaining a specified bench width are illustrated by the following example. Consider a situation where the probability of retaining a bench width of 5 m is calculated to be 0.70. This infers that 70 percent of the bench length (or of the square bench units if wedge failure modes are present) in the design sector is expected to have a retained width of a least 5 m after all possible failures occur. Each of the remaining 30 percent of the bench units is expected to have at least one back-failure that causes the retained width to be less than 5 m.

6.4 Application of Bench Analysis Results to Overall Slope Design

Results of a probabilistic bench analysis that are displayed in a bench stability graph can be used to determine bench design parameters and help select an overall slope angle. Bench geometry has a direct influence on the overall slope angle. Therefore, the information from a bench stability graph can be combined with the geometrical relationships shown in Figure 6.8 to produce slope stability charts that depict the relationships among bench face angle, overall slope angle, and the probabilities of retaining various bench widths. Examples of slope stability charts that can be produced from Figure 6.7 are shown in Figure 6.9. They can be used to determine overall slope

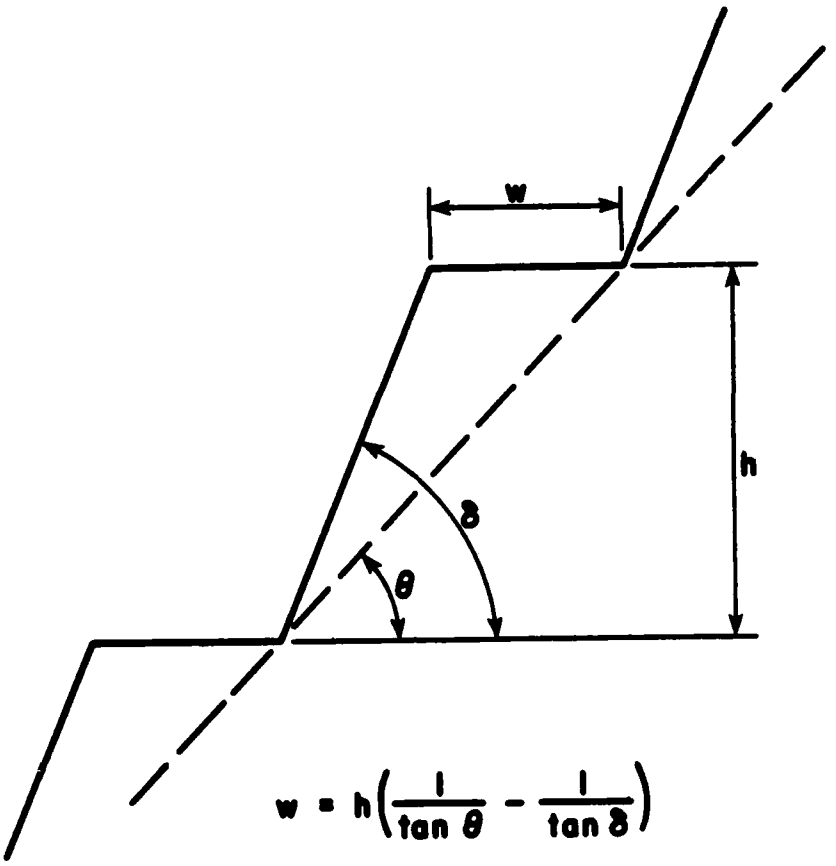

$$w = h\left(\frac{1}{\tan\theta} - \frac{1}{\tan\delta}\right)$$

θ = Overall slope angle
δ = Bench face angle
h = Bench height
w = Bench width

Figure 6.8. Relationship Between Bench Geometry and Overall Slope Angle

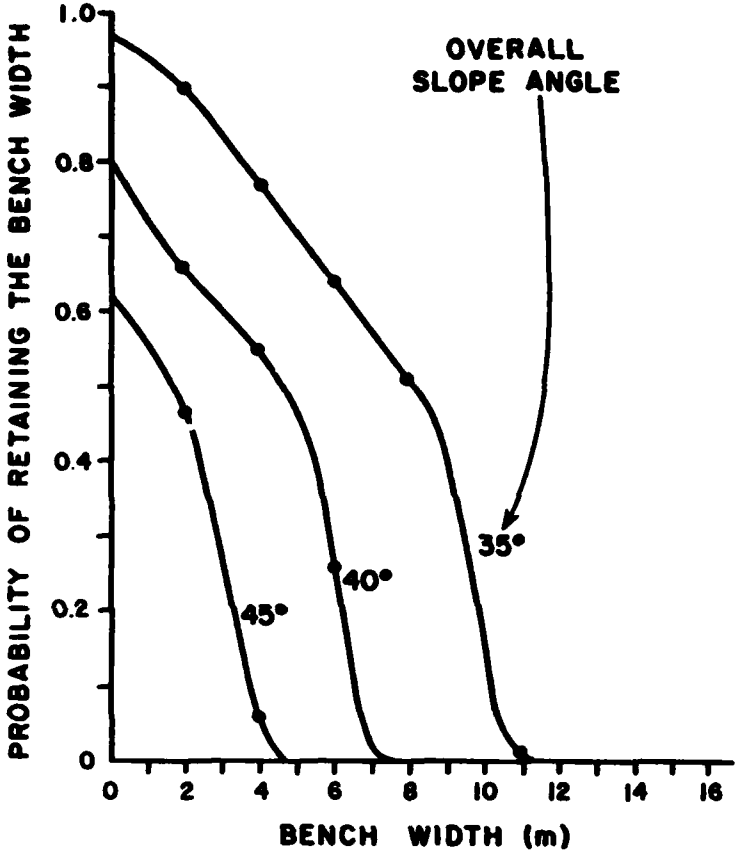

A. For Bench Face Angle of 55°

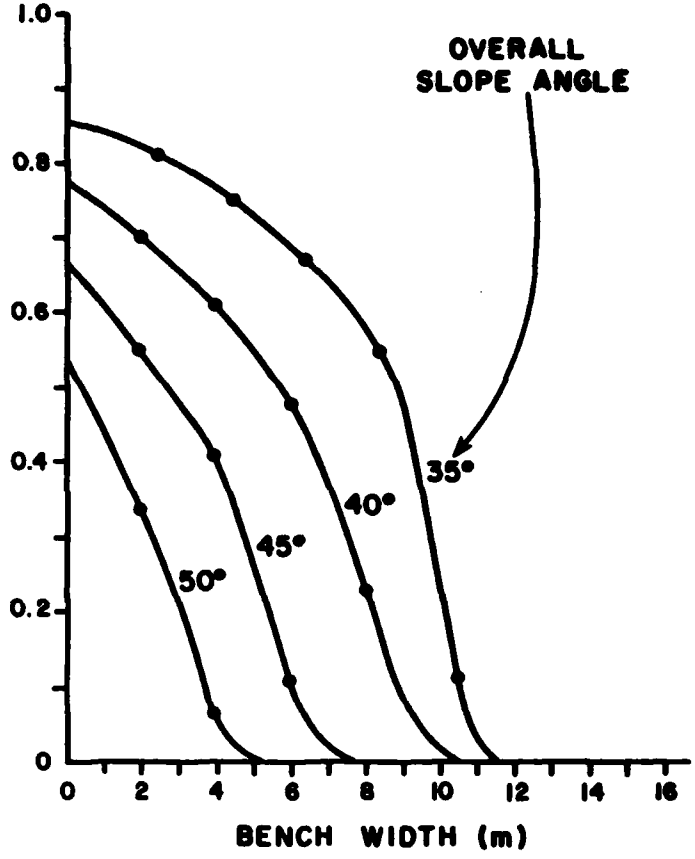

B. For Bench Face Angle of 65°

Figure 6.9. Examples of Slope Design Charts Based on Bench Stability

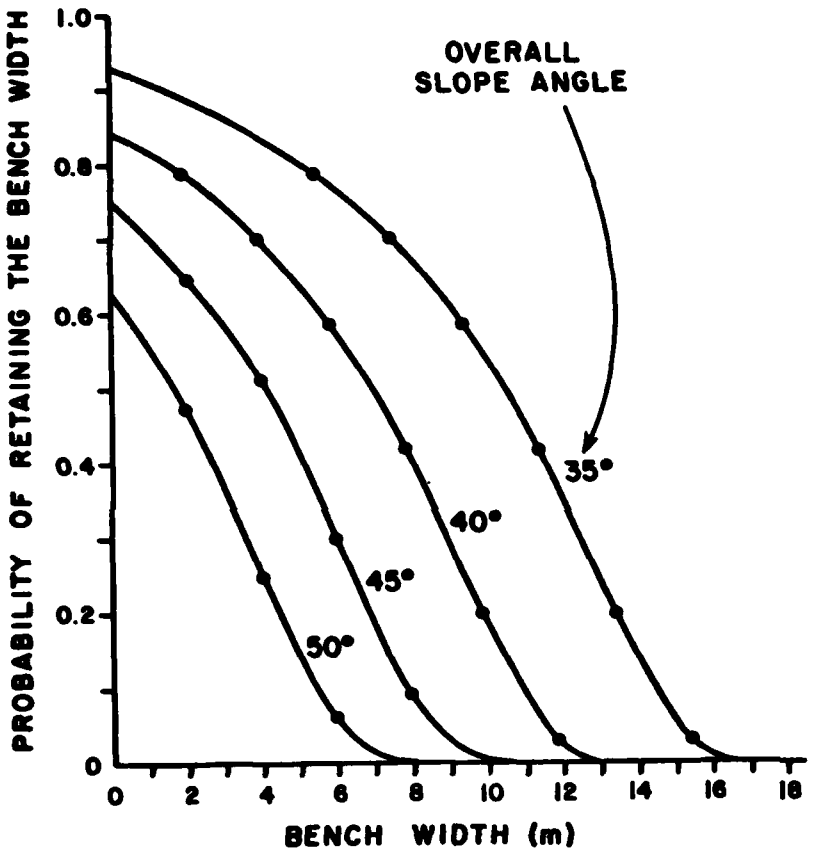

C. For Bench Face Angle of 75°

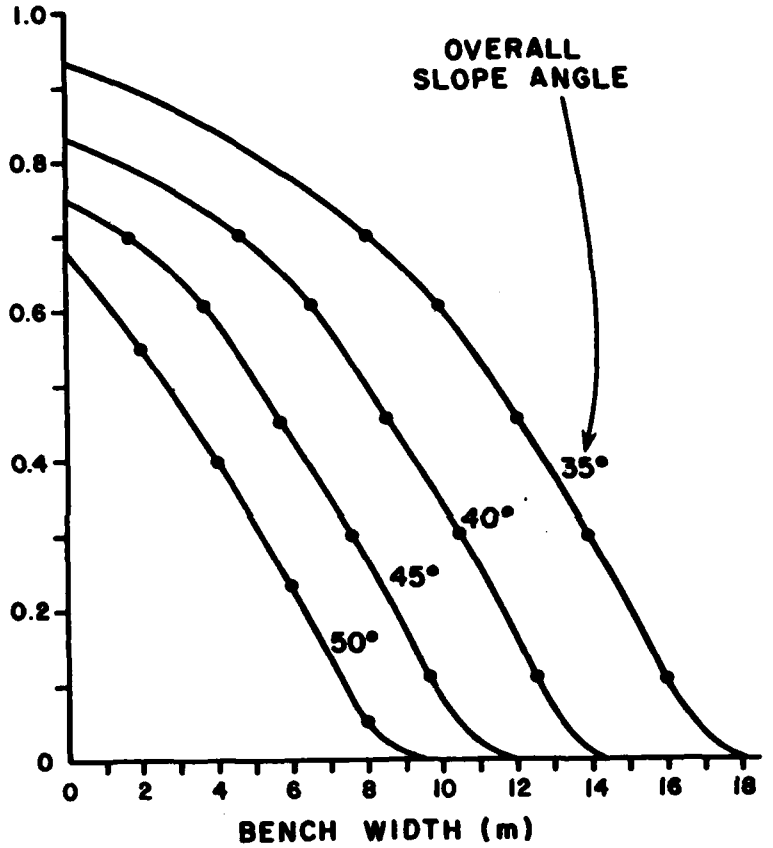

D. For Bench Face Angle of 85°

Figure 6.9 (Continued). Examples of Slope Design Charts Based on Bench Stability

angles when the probability of retaining a certain bench width is specified.

Failure of the total bench width will have a significant influence on overall slope stability because multiple bench failures are likely when benches are undercut by excessive failure of underlying benches. Therefore, the probability that the back-failure distance is less than the design (original) bench width should also be considered in the selection of an overall slope angle. This probability is the same as the probability of retaining a bench width of zero.

Another parameter that may be useful in the overall slope design is the median retained bench width, which can be considered the best estimate of the width after failures occur. Half of the bench length (or half of the bench units if wedge failure modes are present) is expected to have a retained bench width less than the median width, which corresponds to a 0.50 probability of retaining the bench width as shown in the slope design charts.

The bench stability analyses are based on the assumption that no significant bench backbreak occurs due to blasting. At most mining properties there is a complex trade-off relationship between achieving adequate fragmentation and suitable bench stability. This relationship is often geologically controlled and varies from one structural domain to another. Combinations of buffer and long-delay blasting techniques are usually recommended to produce minimal bench damage and provide acceptable fragmentation at a reasonable cost.

6.5 Summary

A probabilistic analysis of bench stability based on plane shear, step path, and tetrahedral wedge failure modes has been developed. It incorporates the variabilities and spatial correlations of fracture set properties and the occurrences of multiple failure modes.

Stabilities of back-failure cells on top of the bench can be determined from the probabilities of stability computed for simulated failure masses of a given failure mode. Several simulations of the bench produce the probabilities of retaining specified bench widths. The entire analytical procedure is repeated for different bench face angles to construct a bench stability graph for the given failure mode. The graphs for all failure modes present are then combined to yield a final bench stability graph for the design sector of interest.

Information from the final bench stability graph is used along with relationships between bench geometry and overall slope angle to produce a set of slope design charts. Important bench design parameters obtained from these charts, such as the probability of retaining zero bench width and the median retained bench width, are essential input for the selection of an overall slope angle. They are also useful for predicting bench and pit wall stability and for planning open pit mining operations.

References

Abramowitz, M. and Stegun, I., eds., 1965, Handbook of Mathematical Functions; Dover Publ., Inc., New York, 1046 p.

Andrew, M., 1981, Comparisons of the Normal Distribution with Log-normal and Gamma Distributions by Simulation Examples; unpubl. grad. seminar paper, Dept. of Statistics, Univ. of Wyoming, Laramie, WY.

Baker, E.J. and Lee, Y., 1975, Alternative Analysis of Geographical Contingency Tables; The Professional Geographer, v. 27, p. 179-188.

Blackman, R.B., and Tukey, J.W., 1958, The Measurement of Power Spectra; Dover Publ., Inc., New York, 190 p.

Borgman, L.E., 1973a, Spectrum Analysis of Random Data Including Procedures Based on the Fast Fourier Transform Algorithm; Publication No. STL-2008, Dept. of Statistics, Univ. of Wyoming, Laramie, WY, 360 p.

----------, 1973b, Statistical Properties of Fast Fourier Transform Coefficients Computed from Real-Valued, Covariance-Stationary, Periodic Random Sequences; Research Paper No. 23, Dept. of Statistics, Univ. of Wyoming, Laramie, WY 58 p.

----------, 1981, Geologic Sampling and Ore Reserve Estimation; unpubl. lecture notes, Dept. of Geology and Geophysics, Univ. of Wyoming, Laramie, WY.

----------, 1982, Techniques for Computer Simulation of Ocean Waves; Topics in Ocean Physics, from LXXX Corso, Soc. Italiana de Fisica, Bologna, Italy, p. 387-417.

Bremermann, H., 1965, Distributions, Complex Variables, and Fourier Transforms; Addison-Wesley Publ. Co., Reading, MA, 186 p.

Call, R.D. and Nicholas, D.E., 1978, Prediction of Step Path Failure Geometry for Slope Stability Analysis; paper presented at 19th U.S. Symp. on Rock Mechanics, Lake Tahoe, NV, 8 p.

----------, Savely, J.P., and Nicholas, D.E., 1976, Estimation of Joint Set Characteristics from Surface Mapping Data; Proc., 17th U.S. Symp. on Rock Mechanics, Salt Lake City, UT, p. 2B2.1-2B2.9.

Chapman, D.G. and Schaufele, R.A., 1970, Elementary Probability Models and Statistical Inference; Ginn-Blaisdell, Waltham, MA, p. 276.

Cochran, W.G., 1954, Some Methods for Strengthening the Common χ^2 Tests; Biometrics, v. 10, p. 417-451.

Cooley, J.W. and Tukey, J.W., 1965, An Algorithm for the Machine Calculation of Complex Fourier Series; Math. of Computations, v. 19, p. 297-301.

----------, Lewis, P.A.W., and Welch, P.D., 1967, Application of the FFT to Computation of Fourier Integrals, Fourier Series, and Convolution Integrals; IEEE Trans. on Audio and Electroacoustics, V. AU-15, no. 2, p. 79-84.

Draper, N.R. and Smith, H., 1981, Applied Regression Analysis, 2nd Edition; John Wiley & Sons, Inc., New York, 709 p.

Feller, W., 1966, An Introduction to Probability Theory and Its Applications, Vol. II; John Wiley & Sons, Inc., New York, 626 p.

Fisz, M., 1963, Probability Theory and Mathematical Statistics; John Wiley & Sons, Inc., New York, 677 p.

Goodman, R.E., 1976, Methods of Geological Engineering in Discontinuous Rocks; West Publ. Co., St. Paul, MN, 472 p.

Goodman, R.E. and Taylor, R.L., 1967, Methods of Analysis for Rock Slopes and Abutments; Proc., 8th U.S. Symp. on Rock Mechanics, Minneapolis, MN, p. 303-320.

Haldane, J.B.S., 1939, The Mean and Variance of χ^2, when Used as a Test of Homogeneity, when Expectations are Small; Biometrika, v. 31, p. 346-355.

Hoeg, K. and Murarka, R.P., 1974, Probabilistic Analysis and Design of a Retaining Wall; Jour. of the Geotech. Div., ASCE, GT3, p. 349-366.

Hoek, E. and Bray, J.W., 1977, Rock Slope Engineering, Revised 2nd ed.; The Institution of Mining and Metallurgy, London, 402 p.

Jaeger, J.C., 1971, Friction of Rocks and Stability of Rock Slopes; Geotechnique, v. 21, no. 2, p. 97-134.

Jenkins, G.M. and Watts, D.G., 1968, Spectral Analysis and Its Applications; Holden-Day, San Francisco, CA, 525 p.

John, K.W., 1968, Graphical Stability Analysis of Slopes in Jointed Rock; Jour. Soil Mech. and Found. Div., ASCE, v. 94, no. SM2, p. 497-526.

Journel, A.G., 1974, Geostatistics for Conditional Simulation of Ore Bodies; Economic Geology, v. 69, p. 673-687.

Kim, Y.C. and Wolff, S.F., 1978, Optimization of Coal Recovery from Open Pits (revised), report prepared for the Canada Centre for Mineral and Energy Technology; Dept. of Mining and Geological Engineering, Univ. of Arizona, Tucson, AZ, October, 250 p.

Lancaster, H.O., 1969, The Chi-squared Distribution; John Wiley & Sons, Inc., New York, 356 p.

La Pointe, P.R., 1980, Analysis of the Spatial Variation in Rock Mass Properties Through Geostatistics; Proc., 21st U.S. Symp. on Rock Mechanics, Rolla, MO, p. 570-580.

Londe, P., Vigier, G., and Vormeringer, R., 1970, Stability of Slopes -- Graphical Methods; Jour. Soil Mech. and Found, Div., ASCE, v. 96, No. SM4, p. 1411-1434.

Marek, J.M. and Savely, J.P., 1978, Probabilistic Analysis of the Plane Shear Failure Mode; Proc., 19th U.S. Symp. on Rock Mechanics, Lake Tahoe, NV, v. II, p. 40-44.

Mihram, G.A., 1972, Simulation: Statistical Foundations and Methodology; Academic Press, New York, 526 p.

Miller, S.M., 1979, Determination of Spatial Dependence in Fracture Set Characteristics by Geostatistical Methods; unpubl. M.S. thesis, Univ. of Arizona, Tucson, AZ, 111 p.

----------, 1981, Statistical Analysis of Rock Shear Strength; unpubl. research paper, Dept. of Civil Engrg., Univ. of Wyoming, Laramie, WY, July, 38 p.

----------, 1982a, A Statistical Method to Evaluate Homogeneity of Structural Populations; Proc., First MGUS Conf. on the Management, Analysis, and Display of Geoscience Data, Golden, CO; in press, Jour. Math. Geology.

----------, 1982b, Statistical and Fourier Methods for Probabilistic Design of Rock Slopes; unpubl. Ph.D. dissertation, Dept. of Geology and Geophysics. Univ. of Wyoming, Laramie, WY.

Miller, I. and Freund, J.E., 1977, Probability and Statistics for Engineers, Prentice-Hall, Inc., Englewood Cliffs, NJ, 529 p.

Savely, J.P., 1980, Personal communication; Inspiration Consolidated Copper Co., Inspiration, AZ.

Taheri, S.M., 1980, Data Retrieval and Multidimensional Simulation of Mineral Resources; unpubl. Ph.D. dissertaion, Dept. of Statistics, Univ. of Wyoming, Laramie, WY, 265 p.

Terzaghi, R.D., 1965, Sources of Error in Joint Surveys; Geotechniques, v. 15, no. 3, p. 287-304.

Wittke, W.W., 1965, Method to Analyze the Stability of Rock Slopes with and without Additional Loading (in German), Rock Mech. and Engrg. Geol., Suppl. II, v. 30, p. 52-79. Engl. trans. in Rock Mech. Res. Rep. No. 6, July, 1971, Imperial College, London.

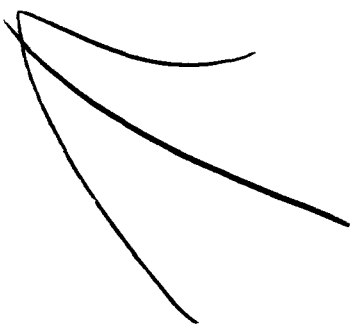

LIST OF PARTICIPANTS

SEMINAR ON PROBABILISTIC METHODS IN GEOTECHNICAL ENGINEERING

SEPTEMBER 21, 1982

Professor Loren Anderson
Department of Civil Engineering
University of Utah
Logan, UT 84322
(801) 750-1000

Professor Gregory Baecher
Department of Civil Engineering
Massachusetts Institute of Technology
Cambridge, MA 02139
(617) 253-8435

Dr. Don C. Banks
Chief, Engineering Geology and
Rock Mechanics Division
Waterways Experiment Station
PO Box 631
Vicksburg, MS 39180
(601) 634-2630 (FTS 542-2630)

Mr. Robert D. Bennett
Research Civil Engineer
Engineering Geology and
Rock Mechanics Division
Waterways Experiment Station
PO Box 631
Vicksburg, MS 39180
(601) 634-3974 (FTS 542-3974)

Dr. David S. Bowles
Engineering Manager
Law Engineering Testing Company
181 Inverness Drive W, Suite 100
Englewood, CO 80112
(303) 771-8641

Ms. Linda L. Buege
Civil Engineer
Earthquake Engineering and
Geophysics Division
Waterways Experiment Station
PO Box 631
Vicksburg, MS 39180
(601) 634-3917 (FTS 542-3917)

Mr. Dwain K. Butler
Research Geophysicist
Earthquake Engineering and
Geophysics Division
Waterways Experiment Station
PO Box 631
Vicksburg, MS 39180
(601) 634-2127 (FTS 542-2127)

Mr. Richard Davidson
Chief, Soil Mechanics Section
(DAEN-CWE-SS)
Department of the Army
Washington, DC 20314
(202) 272-0207 (FTS 272-0207)

Dr. G. Wendell Deer
Mathematician
Earthquake Engineering and
Geophysics Division
Waterways Experiment Station
PO Box 631
Vicksburg, MS 39180
(601) 634-3551 (FTS 542-3551)

Mr. James Erwin
Chief, Geotechnical Branch
US Army Engineer Division
South Atlantic
510 Title Building
30 Pryor Street, SW
Atlanta, GA 30303
(404) 221-4256 (FTS 242-4256)

Mr. Paul R. Fisher
Chief, Geology Section (DAEN-CWE-SG)
Department of the Army
Washington, DC 20314
(202) 272-0207 (FTS 272-0207)

Dr. A. G. Franklin
Chief, Earthquake Engineering and
Geophysics Division
Waterways Experiment Station
PO Box 631
Vicksburg, MS 39180
(601) 634-2658 (FTS 542-2658)

Professor Dimitri A. Grivas
Department of Civil Engineering
Rensselaer Polytechnic Institute
Troy, NY 12181
(518) 270-6360

Professor Atchintya Haldar
School of Civil Engineering
Georgia Institute of Technology
Atlanta, GA 30332
(404) 894-2236

Mr. Gene P. Hale
Chief, Soils Research Center
Soil Mechanics Division
Waterways Experiment Station
PO Box 631
Vicksburg, MS 39180
(601) 634-2219 (FTS 542-2219)

Mr. David Hammer
Chief, Geotechnical Branch
US Army Engineer Division, Ohio River
PO Box 1159
Cincinnati, OH 45202
(513) 684-3001 (FTS 684-3027)

Ms. Mary Ellen Hynes-Griffin
Research Civil Engineer
Earthquake Engineering and
Geophysics Division
Waterways Experiment Station
PO Box 631
Vicksburg, MS 39180
(601) 634-2280 (FTS 542-2280)

Mr. Robert James
Chief, Geotechnical Branch
US Army Engineer Division,
Southwestern
Main Tower Building
1200 Main Street
Dallas, TX 75202
(214) 767-2376 (FTS 729-2376)

Professor Edward Kavazanjian, Jr.
Department of Civil Engineering
Stanford University
Sanford, CA 94305
(415) 497-0236

Dr. George Kiersch
Geological Consultant
4750 N. Camino Luz
Tucson, AX 85718
(602) 299-3776

Mr. Edward Kovanic
Chief, Geotechnical Branch
US Army Engineer Division
Missouri River
PO Box 103 Downtown Station
Omaha, NE 68101
(402) 221-3020 (FTS 864-7340)

Dr. Ellis Krinitzsky
Geophysicist
Engineering Geology and
Rock Mechanics
Waterways Experiment Station
PO Box 631
Vicksburg, MS 39180
(601) 634-3329 (FTS 542-3329)

Dr. William F. Marcuson III
Chief, Geotechnical Laboratory
Waterways Experiment Station
PO Box 631
Vicksburg, MS 39180
(601) 634-2234 (FTS 542-2234)

Mr. LeRoy McAnear
Chief, Soil Mechanics Division
Waterways Experiment Station
PO Box 631
Vicksburg, MS 39180
(601) 634-2228 (FTS 542-2228)

Mr. Eugene McCoy
Chief, Geotechnical Branch
US Army Engineer Division,
North Pacific
PO Box 2870
Portland, OR 97208
(503) 221-3867 (FTS 423-3867)

Dr. Stanley M. Miller
2569 Kennedy Avenue
Laramie, WY 82070
(307) 766-6194

Dr. Paul F. Mlakar
Research Civil Engineer
Structural Mechanics Division
Structures Laboratory
Waterways Experiment Station
PO Box 631
Vicksburg, MS 39180
(601) 634-3365 (FTS 542-3365)

Mr. John F. Peters
Research Civil Engineer
Soil Mechanics Engineer
Waterways Experiment Station
PO Box 631
Vicksburg, MS 39180
(601) 634-2590 (FTS 542-2590)

Mr. Edward C. Pritchett
Chief, Geotechnical Branch
(DAEN-CWE-S)
Department of the Army
Washington, DC 20314
(202) 272-0207 (FTS 272-0207)

Professor Charles W. Schwartz
Department of Civil Engineering
University of Maryland
College Park, MD 20742
(301) 454-2438

Mr. W. E. Strohm, Jr.
Research Civil Engineer
Soil Mechanics Division
Waterways Experiment Station
PO Box 631
Vicksburg, MS 39180
(601) 634-2604 (FTS 542-2604)

Mr. Richard Thompson
Engineer, Geotechnical Branch
US Army Engineer Division,
South Pacific
630 Sansome Street
San Francisco, CA 94111
(415) 556-5710 (FTS 556-5710)

Professor Erik Vanmarcke
Department of Civil Engineering
Massachusetts Institute of Technology
Cambridge, MA 02139
(617) 253-1000

Mr. Frank Weaver
Chief, Geotechnical Branch
US Army Engineer Division,
Lower Mississippi Valley
PO Box 80
Vicksburg, MS 39180
(601) 634-5896 (FTS 542-5896)

Mr. Thomas D. White
Chief, Pavement Systems Division
Waterways Experiment Station
PO Box 631
Vicksburg, MS 39180
(601) 634-2209 (FTS 542-2209)

END

FILMED

2-84

DTIC